Self-Assembly of Metallo-Supramolecular Architectures and Mass Spectrometry of Bismuth-Oxido Clusters

Dissertation zur Erlangung des akademischen Grades des
Doktors der Naturwissenschaften
(Dr. rer. nat.)

eingereicht im Fachbereich Biologie, Chemie, Pharmazie
der Freien Universität Berlin

vorgelegt von
Ralf Wilhelm Troff
aus Leer

August 2011

Die vorliegende Arbeit wurde im Zeitraum von Januar 2007 bis April 2011 unter der Anleitung von Herrn Prof. Dr. Christoph A. Schalley am Institut für Chemie und Biochemie des Fachbereiches Biologie, Chemie, Pharmazie der Freien Universität Berlin angefertigt.

1. Gutachter: Prof. Dr. Christoph A. Schalley

2. Gutachter: Prof. Dr. Rainer Haag

Disputation am 07.12.2011

Für meine Familie

Indes sie forschten, röntgten, filmten, funkten, entstand von selbst die köstlichste Erfindung: der Umweg als die kürzeste Verbindung zwischen zwei Punkten.

(Erich Kästner, 1899 – 1974, deutscher Schriftsteller)

Table of Contents

0. Summary / Zusammenfassung

0.1 Summary

In the first part of this thesis, the principles of metallo-supramolecular self-assembly and self-sorting were studied. Depending on the properties of the building blocks used, many different metallo-supramolecular complexes were obtained and their properties were investigated using a combination of several analytic methods.

In order to get functionalized complexes which can interact with guest molecules, several bispyridyl-urea ligands have been synthesized and used for self-assembly. Due to their ability to act as hydrogen-bond donor and acceptor and their dipole moment in the urea groups, these ligands are promising candidates for molecular recognition. Unfortunately, the solubility of the complexes was very low which hampers their use for molecular recognition.

In many systems equilibria between two complexes were observed, which are based on a sensitive balance between enthalpy and entropy that can be influenced by the properties of their building blocks as well as by their environment. In principle, the larger complexes were favored at low temperatures and high concentrations, while the corresponding smaller complexes were favored vice versa. A drastic solvent effect was observed for the self-assembly of flexible divalent ligands with (en)Pd$(NO_3)_2$ in water. The formation of M_2L_2 complexes in equilibrium with their corresponding M_4L_4 catenanes was discovered, while the entropically more favorable M_3L_3 complexes were not observed. This can be assigned to hydrophobic effect which favors the formation of catenanes.

Interestingly, 1:1:1 mixtures of 4,4´-bis(pyridine-4-ylethynyl)-2,2´-bipyridin with the metal centers (dppp)M$(OTf)_2$ and (dppe)M$(OTf)_2$ (M = Pd^{2+}, Pt^{2+}) showed self-sorting behavior. While (dppp)M$(OTf)_2$ preferred coordination at the pyridine binding sites of the ligand, (dppe)M$(OTf)_2$ showed no preference. This was used for the self-sorting of homo- and heterometallic M_4L_2 complexes and nicely shows the influence an additional CH_2-group can have on self-assembly processes.

Kinetic studies of the formation of several Pt(II) and Pd(II) complexes revealed that the coordination of the ligands to the metal centers is fast, whereas the error correction

process is slower than that. Thus, some kinetically formed complexes were observed which convert into the thermodynamically favored complexes over time. Mixed-flow on-line mass spectrometry was successfully used to monitor fast self-assembly processes and identify intermediates of the self-assembly processes including the initial coordination. For the self-assembly reactions many different intermediates were observed and thus the process is rather unspecific, whereas self-sorting processes were found to be pathway-selective.

Comparing the assemblies of isomeric ligands with each other shows that the constitution of the ligand has a drastic effect on the resulting assemblies. The complexes formed can be isomeric to each other or totally different. It was discovered, that the behavior of isomeric complexes depends highly on their constitution. For example, tandem MS experiments showed that isomeric complexes can undergo fragmentation using totally different pathways.

The second part of the thesis deals with the analysis of bismuth-oxido clusters using ESI MS. Several bismuth-oxido clusters bearing different cluster cores as well as different ligands have been analyzed successfully. Tandem MS experiments confirmed their structure and enabled to investigate their stability. ESI MS has been shown to be a suitable analytical method to examine bismuth-oxido clusters.

0.2 Zusammenfassung (German)

Im ersten Teil dieser Arbeit wurden die Grundlagen metallo-supramolekularer Selbst-Assemblierung und Selbst-Sortierung untersucht. Die Kombination verschiedener Baueinheiten führte zur Ausbildung einer Vielzahl unterschiedlicher Komplexe, deren Eigenschaften durch die Kombination mehrerer analytischer Methoden untersucht wurden.

Um funktionalisierte Komplexe zu erhalten, welche in der Lage sind Gast-Moleküle zu erkennen, wurden mehrere Bispyridylharnstoff-Liganden hergestellt. Harnstoffe besitzen ein relativ hohes Dipolmoment und können bei der Ausbildung von Wasserstoff-Brücken sowohl als Donor als auch als Akzeptor fungieren, was sie zur molekularen Erkennung prädestiniert. Leider verhindert die geringe Löslichkeit der resultierenden Komplexe ausführliche Studien.

In vielen Systemen wurden Gleichgewichte zwischen unterschiedlichen Komplexen gefunden, die auf einem empfindlichen Zusammenspiel von Enthalpie und Entropie beruhen, das sowohl durch die Eigenschaften der einzelnen Baueinheiten als auch durch die Umgebung beeinflusst wird. Generell sind größere Komplexe bei niedrigen Temperaturen und hohen Konzentrationen bevorzugt, während sich die kleineren Komplexe entgegengesetzt verhalten. Ein drastischer Lösungsmittel-Effekt wird für die Selbst-Assemblierung flexibler divalenter Liganden mit $(en)Pd(NO_3)_2$ in Wasser beobachtet. Hier werden Gleichgewichte zwischen M_2L_2-Komplexen und ihren M_4L_4-Catenanen beobachtet, während die entropisch bevorzugten M_3L_3-Komplexe nicht auftreten. Dies kann mit Hilfe des hydrophoben Effekts erklärt werden, welcher die Ausbildung der Catenane bevorzugt.

Wenn 4,4´-Bis(pyridin-4-ylethynyl)-2,2´-bipyridin in einem 1:1:1-Verhältnis mit den Metallzentren $(dppp)M(OTf)_2$ und $(dppe)M(OTf)_2$ ($M = Pd^{2+}$, Pt^{2+}) kombiniert wird, werden Selbst-Sortierungs-Prozesse beobachtet. $(dppp)M(OTf)_2$ koordiniert bevorzugt an die Pyridine des Liganden, während $(dppe)M(OTf)_2$ keine Präferenz zeigt. Dies konnte für die Darstellung von homo- und heterometallischen M_4L_2-Komplexen über Selbst-Sortierungs-Prozesse genutzt werden.

Durch zeitabhängige Untersuchungen der Bildung verschiedener Pt(II)- und Pd(II)-Komplexe konnte gezeigt werden, dass die Koordination der Liganden an die Metallzentren sehr schnell erfolgt, während die anschließende Fehler-Korrektur langsamer verläuft. Auf Grundlage dessen konnten verschiedene kinetisch gebildete Komplexe identifiziert werden, welche sich mit der Zeit in die thermodynamisch bevorzugten Strukturen umwandelten. Schnelle Selbst-Assemblierungs-Prozesse wurden erfolgreich mit Hilfe der „Mixed-Flow online Massenspektrometrie“ untersucht, wodurch neben verschiedenen Intermediaten selbst die sehr schnelle Koordination beobachtet werden konnte. Während sich bei Selbst-Assemblierungs-Prozessen eine Vielzahl an Intermediaten ausbildete und die Prozesse daher eher unspezifisch sind, scheint die Bildung von Komplexen in Selbst-Sortierungs-Prozessen spezifisch zu sein.

Vergleicht man die Selbst-Assemblierungs-Prozesse isomerer Liganden mit denselben Metallzentren miteinander, so zeigt sich, dass die Konstitution der Liganden die Bildung der resultierenden Komplexe teils drastische beeinflusst. Hierbei können diese Komplexe sowohl isomer zueinander sein als auch völlig verschiedene Strukturen besitzen. Die Eigenschaften isomerer Komplexe unterscheiden können sich ebenfalls, so konnte zum Beispiel über MS/MS-Experimente gezeigt werden, dass isomere Komplexe völlig unterschiedliche Zerfallsmechanismen besitzen können.

Der zweite Teil dieser Arbeit beschäftigt sich mit der Analyse von Bismut-Oxido-Clustern mittels ESI-MS. Die untersuchten Cluster unterschieden sich dabei in ihrem Cluster-Kern und in der Art ihrer Liganden. Tandem MS-Experimente ermöglichten sowohl die Strukturaufklärung der Cluster als auch Untersuchungen bezüglich deren Stabilität. Es wurde gezeigt, dass ESI-MS eine gute analytische Methode ist, um solche Cluster zu untersuchen.

1. Introduction to Supramolecular Chemistry

Supramolecular chemistry is a fast emerging field of chemical research.[1, 2] Due to its diversity, it is quite difficult to find a definition for "supramolecular chemistry" which fits to all of its different aspects. Lehn[1] described it as "*chemistry beyond the molecule*", because it deals with intermolecular interactions. A more precise definition is given by the *International Union of Pure and Applied Chemistry* (IUPAC): *"A field of chemistry related to species of greater complexity than molecules, that are held together and organized by means of intermolecular interactions. The objects of supramolecular chemistry are supermolecules and other polymolecular entities that result from the spontaneous association of a large number of components into a specific phase (membranes, vesicles, micelles, solid state structures, etc.)."*[3, 4]

The roots of supramolecular chemistry can be traced back to the last decade of the 19th century. Alfred Werner published his *coordination theory* in 1893 (see chapter 3.1),[5] directly followed by Emil Fischer introducing his *lock-and-key concept* in 1894 which postulated a specificity in the binding of substrates to enzymes.[6] The enzymes and the substrates have complementary geometric shapes which fit exactly into each other and thereby produce certain specificity in their interaction. These were the first considerations of *molecular recognition* which became a very important part of (bio-) chemical, pharmaceutical and medical research.[2, 7] One reason for the evoking interest in *molecular recognition* and intermolecular interactions was the discovery of Paul Ehrlich, that a molecule can only have an effect on the human body, if it somehow interacts with it.[8] The concepts of supramolecular chemistry were revised and adjusted when more data and knowledge of chemistry became available. However, supramolecular chemistry really began evolving as an independent field of research in the 1960ies. This can be explained by the lack of appropriate analytic methods to characterize and describe supramolecular systems before the 1960ies. Also, a paradigm shift occurred. Before the 1960ies, chemical research was focused on the intrinsic properties of a molecular system and intermolecular interactions have somehow been neglected. It changed when the number of examples increased, whose properties could not be explained with the intrinsic properties of the molecules alone. Based on this paradigm shift, the interest in non-

covalent interactions increased immediately and the basis of supramolecular chemistry was formed.[1, 2, 9] In 1987, Cram, Lehn and Pedersen were awarded the noble prize for their work in supramolecular chemistry. This underlines the importance of intermolecular interactions for chemistry.

Table 1.1: *Several interactions and their typical bond energies are shown.*[10]

interaction	bond energy in kJ / mol
covalent CC bond	160-500
coordinative bond	40-340
hydrogen bond	4-65
ion-ion interaction	40-370
ion-dipole interaction	40-210
dipole-dipole interaction	4-40
cation-π interaction	4-80
π-π interaction	4-20
van-der-Waals interaction	<4-20

Intermolecular forces are relatively weak interactions[10] (Table 1.1) and thus normally allow the bonds between two or more molecules to form reversibly. In many different areas of (supramolecular) chemistry, biology or medicine, the reversibility of an intermolecular bond is mandatory or at least helpful. For example, molecular recognition, molecular machines, self-organization, template synthesis and even life itself were not possible without weak interactions between molecules. Thus, the understanding of intermolecular forces and their influences on microscopic systems is a fundamental requirement to understand macroscopic systems and their properties. Until now, the vast variety of possibilities emerging from supramolecular interactions for chemistry and other sciences is just partly reflected by the many projects performed in supramolecular chemistry.[1, 2]

2. Aim of this Study

This thesis is divided into two parts that are connected through the topic of coordination chemistry: The self-assembly of metallo-supramolecular complexes and the analysis of bismuth-oxido clusters using ESI mass spectrometry.

Self-assembly offers an interesting way to form complex structures from rather simple building blocks. This synthetic strategy is used to form metallo-supramolecular complexes with interesting properties and behaviors. In order to generate different types of structures, several differently programmed building blocks have to be synthesized and mixed with each other in an appropriate way. The resulting metallo-supramolecular architectures are then analyzed by several analytical methods like nuclear magnetic resonance spectroscopy (NMR) or electrospray ionization mass spectrometry (ESI MS). The properties of these metallo-supramolecular systems such as their kinetic and thermodynamic behavior, possible equilibria between two or more complexes, ligand-exchange reactions or even self-sorting are paving the way for new insights into metallo-supramolecular chemistry. Furthermore, the self-assembly processes of metallo-supramolecular complexes themselves should be analyzed. For slow self-assembly processes, common NMR spectroscopic and mass spectrometric techniques are sufficient enough, but for fast processes, other analytical tools have to be found. On-line mass spectrometry, for example, uses a micro-reactor and offers the ability to monitor fast self-assembly processes down to a time-scale of 0.2 seconds. Altogether, these aspects of metallo-supramolecular self-assembly result in an interesting and challenging field of chemical research that will be dealt with in these studies.

The second part of this thesis deals with the mass spectrometric characterization of bismuth-oxido clusters, which are of interest for materials science as well as medical applications. However, the analysis of heavy bismuth-oxido clusters that can have molecular masses up to 15.000 Da with ESI MS is a challenging task. The characterization of these clusters will be the basis for further experiments. In order to obtain information about their stability, tandem MS experiments of several different BiO clusters should be performed as well as ligand-exchange reactions between two different

clusters. The information about these clusters and their stability will help to understand their formation as well as their interesting properties.

3. Theoretical Background

3.1 Coordination Chemistry

In 1893 Alfred Werner published his *coordination theory* which allocates an oxidation number and a coordination number (*CN*) to every central atom in a complex and thereby to various elements of the periodic table.[5] The *CN* of a central particle (very often a metal ion) reveals the number of its coordination sites and by this also the maximum number of its coordination partners. Due to the specific composition of the coordination sites of the central particle and its *CN*, different coordination geometries can be achieved using different metal ions and ligands.[11] Based on this concept, coordination chemistry rapidly developed into an independent field of chemical research. All of those early coordination compounds had *CN*s of 2-6. In 1964/1965 the conceivable valences were extended beyond six.[11] When Hoard and co-workers reported the crystal structures of complexes containing 2,2´,2´´,2´´´-(ethane-1,2-diyldinitrilo)-tetraacetic acid (EDTA) coordinated to large cations revealing *CN*s of seven and ten.[12] In general, the *CN* is increasing with: (i) increasing size of the metal(-ion); (ii) decreasing size of the coordinating ligands. Transition metals have coordination numbers of 2-9, while lanthanides and actinides even have *CN*s up to 12.[13]

According to the *frontier molecular orbital theory*[14] today's knowledge defines a coordinative bond between a ligand and a metal(-ion) as an exchange of electronic density between the coordination partners. Electron density is transferred from the *highest occupied molecular orbital* (HOMO) of the ligand into the *lowest unoccupied molecular orbital* (LUMO) of the metal(-ion). On the one hand, σ bonds or electron deficient bonds are formed, if main group metals are coordinated by several ligands. On the other hand, transition metals can form σ and π bonds in order to coordinate ligands. The early transition metal ions have usually high oxidation states and are therefore electron poor. They normally form σ bonds with the ligands transferring electron density from the ligand to the metal ion (donor-acceptor bond). Nevertheless, in most cases such donor bonds have a partial π bonding as well (Figure 3.1). Those σ- and π-donor bonds between ligands and metal centers are common if hard ligands like alkoxy ligands, amido ligands, aryloxy ligands, imido ligands and/or oxo ligands are used.[15]

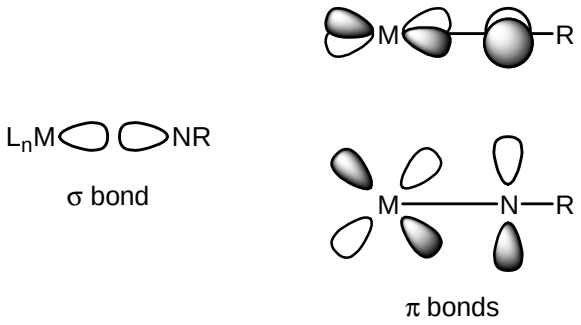

Figure 3.1: *Simplified scheme of the frontier molecular orbitals of an imido-metal bond.*[11]

The late transition metals are electron rich. When coordinating to ligands, σ-donor bonds and π-donor bonds and π-acceptor bonds (π-donor backbonds) are formed (Figure 3.2). The σ-donor bonds transfer electrons from the ligand to the metal center (see above). The π-donor bonds donate electrons from the filled π orbital or lone electron pair orbital of the ligand into an empty orbital of the metal center. This process cooperates with a back donation of electrons from a d-orbital of the metal into the empty π*-antibonding orbital of the ligand. To achieve this kind of backbonding, the d-orbital of the metal has to have certain π symmetry with respect to the metal-ligand axis and the orbitals have to fit in size.[15]

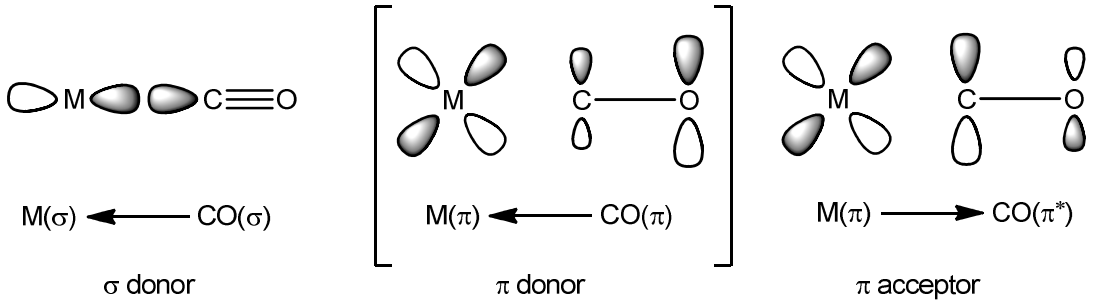

Figure 3.2: *Schematic drawing of the σ-donor bond, the π-donor bond (can normally be ignored) and the π-acceptor bond illustrated for transition metal CO bonding.*[11]

Two other interesting effects have to be taken into account, if the binding situation between metal ions and ligands is discussed. The *thermodynamic trans-effect* (called *trans-influence*) and the *kinetic trans-effect* (also called *trans-effect*) have certain effects on the metal-ligand bonds in metal-ligand complexes. They are well examined for

complexes containing square-planar and octahedral metal centers.[16] The *thermodynamic trans-effect* occurs, if two ligands with different π-acceptor strength are coordinating *trans* to each other. Due to its stronger π-acceptor bond, the better π-acceptor ligand is bound more strongly to the metal center than the ligand in the *trans* position. This yields in a weakening of the bond between the metal center and latter ligand. Based on this, the *thermodynamic trans-effect* was defined as 'the tendency of a ligand to selectively weaken the bond *trans* to itself'.[17] According to the *frontier molecular orbital theory* the two ligands *trans* to each other try to form a ligand-metal bond using the same orbital of the metal center. Therefore they weaken the ligand-metal bond *trans* to their own, respectively.[11, 18]

The *kinetic trans-effect* has been defined as 'the effect of a coordinated group on the rate of substitution reactions of ligands *trans* to itself'.[19] In a ligand-exchange experiment in ligand-metal complexes, the incoming ligand always coordinates most quickly at the position *trans* of the ligand with the biggest *trans-influence*. This does not always result in the thermodynamically favored complex. It was found that good π-acceptor ligands result in strong *kinetic trans-effects* whereas hard σ-donor ligands bear weak *kinetic trans-effects*. An exception of this is the hydride ion, which indeed is a strong σ-donor ligand but as well shows a strong *kinetic trans-effect*. However, the previously discussed rivalry of the ligands binding to the orbitals of the metal center holds for the *kinetic trans-effect* as well, if it is extended to σ-bonds.[11, 20]

If a ligand has more than one coordination site, it can bind to metal centers in two different ways. First, the binding sites of the ligands can coordinate to different metal centers leading to the formation of multi-nuclear complexes. Therefore, each metal-ligand interaction can be described like that for monodentate ligands coordinating to a metal center (see above). Second, a ligand can coordinate to a metal center using more than one of its binding sites. This is called *chelation* and "*the molecular entity in which there is chelation (and the corresponding chemical species) is called chelate.*"[4, 21] One chelating ligand bounds stronger to a metal center than one monodentate ligand. A reason for the stability of chelate complexes is the fact, that chelating ligands are bound to the metal ions by more than one coordinative bond. If one for example wants to replace a divalent chelating ligand A with another divalent chelating ligand B, it has to be

considered, that two bonds have to be broken to exchange the ligands. After the first bond between ligand A and the metal center is broken, two things can happen: (i) ligand B can coordinate to the empty coordination site of the metal center or (ii) ligand A can again coordinate to it. The same two choices can be made, if ligand B is coordinated to the metal center in the first place.[11] In contrast, monodentate ligands form only one coordinative bond to a metal center and can therefore be exchanged more easily.

The resulting complex is build by fewer building blocks when chelating ligands are used instead of analogous monodentate ligands. The metal ions have a sphere of solvent molecules around them, which interact with the metal ions in solution. These interactions are normally not very strong and can be overcompensated by ligand-metal coordination. Nevertheless, they have an influence on the entropic balance during the complexation. Whereas monodentate ligands normally can only replace one coordinating solvent molecule, one multidentate ligand can replace more than that. This leads to entropically favored chelate complexes. Interestingly, one chelate ligand with n donor atoms binds less strongly than n monodentate ligands containing the same donor atoms. This is due to a higher strain in the chelate ligands coordinating to metal centers when compared to the coordination of analogous monodentate ligands to the same metal centers.[22]

The use of bidentate, tridentate or even multidentate ligands created the field of what is nowadays called *metallo-supramolecular chemistry* (see Chapter 3.3).[1, 2]

3.2 Self-Processes

3.2.1 Self-Assembly and Self-Organization

Self-assembly[23] and *self-organization*[24] are two general, differing concepts which at first sight seem to be very similar to each other and therefore they are often mixed up in literature.[1, 2, 25] However, they are not similar to each other and describe two rather different processes. In *self-assembly*, molecular units organize themselves spontaneously into ordered structures using reversible intermolecular interactions (see Table 1.1). The system does this without any active help from outside (e.g. from a designer or scientist). Thus, in a self-assembled system the resulting structure is formed by itself. Nevertheless, the units of a self-assembled system can be programmed prior and thus the outcome of a

self-assembly process can be influenced by pre-organizing its building blocks. As far as *Self-assembly* is a process leading to a system in the thermodynamic equilibrium, some of the self-assembled structures possible are thermodynamically preferred compared to others. Nevertheless, also structures can be observed, which are kinetically but not thermodynamically preferred. Due to the reversibility of the structures formed, kinetically originated species can transform into the thermodynamically preferred ones. This error correction process enables self-assembled systems to correct errors as well as to react directly at changes in their environment (e.g. temperature, solvent). *Self-assembly* processes require mobility; otherwise error correction could not proceed.

In contrast to *self-assembly*, *self-organization* is a process which does not reflect the thermodynamic equilibrium. The term *self-organization* describes systems which spontaneously order far away from the thermodynamic minimum. The organization of the particles is a property of the whole system which appears without any guidance from outer sources. *Self-organization* can only happen in open systems with a constant energy flow through it. The organization in self-organized systems breaks down as soon as the energy flow stops. *Self-organization* processes are present in living organisms and in their social organizations (e.g. fish schools, ant colonies, and bee hives).[24] In contrast to this, *self-assembly* processes also can be observed in closed systems and do not need constant energy flows.

In self-organized systems, every change of the organization directly leads to new changes in system, because all the building blocks of a self-organized system interact with each other. The system reacts on every influence from outside the system as well as on internal influences. All changes of the system can in principle be the starting point for a new change of the system. Hence, the behavior of a self-organized system is always tracing back to the system itself. This feedback is very important for all self-organized systems, because it enables the system to react on changes in its organized structure. These feedback loops seem to be familiar to the error correction proceeding in *self-assembly* processes, but, in contrast to *self-assembly*, complex self-organized systems do not have a desired status. Therefore the terms error and error correction cannot be defined for *self-organization* processes. However, a self-organized system is much more stable against

influences from outside, when it exhibits many different (and complex) ways of feedback. Based on all these arguments, a self-organized system is defined by itself.[24]

Most self-ordering processes in chemistry are *self-assembly* processes, because the organization of these systems reflects the situation of their thermodynamic minima.[1, 2, 26]

Supramolecular chemists use the phenomena of self-assembly processes as an alternative synthetic route to obtain complex chemical structures.[1, 2, 27] Self-assembly is widely used to receive rather complicated supramolecular structures and architectures from a defined number of small relatively simple building blocks. The synthesis of such complex structures would require multi-step organic syntheses otherwise. Self-assembly reduces the synthetic effort for rather complex structures significantly. In order to influence the resulting self-assembled structures, the building blocks can be pre-organized by their geometric and electronic properties. This can be influenced during the synthesis of the building blocks (e.g. shape, number and position of binding sites). The synthesis of a supramolecule based on self-assembly has to be thermodynamically controlled, as otherwise no error correction can take place. Even if kinetic products are formed in the beginning and error correction is very slow at room temperature, self-assembly is always a thermodynamic process.[28]

Intermolecular interactions play an important role in self-assembly. They are relatively weak and reversible (see Table 1.1). For example, hydrogen bonds (binding energy = 4 - 65 kJ/mol) are directional which enables scientists to design self-assembled structures easily. Therefore, they are often used in self-assembled systems.[29] For example, benzene-1,3,5-tricarboxylic acid (trimesic acid) **1** forms crystals which contain large two-dimensional honeycomb-like networks (Figure 3.3).[30] These networks are folded and the free space in each of those contains units of neighboring networks, when pure trimesic acid **1** is used.[31] In contrast to this, open two-dimensional networks are obtained, when trimesic acid **1** is crystallized in the presence of alkanes.[32]

Self-assembly is the main synthetic route to form metallo-supramolecular complexes (see chapter 3.3).[1, 2, 33-35] These complexes are formed by the coordination of ligands to metal centers. Based on the properties of these building blocks, different complex metallo-supramolecular structures can be achieved. Depending on the building blocks used, metallo-supramolecular assemblies can be very stable and robust. Thus, metallo-

supramolecular self-assembly is a highly potent alternative to multi-step organic synthesis.

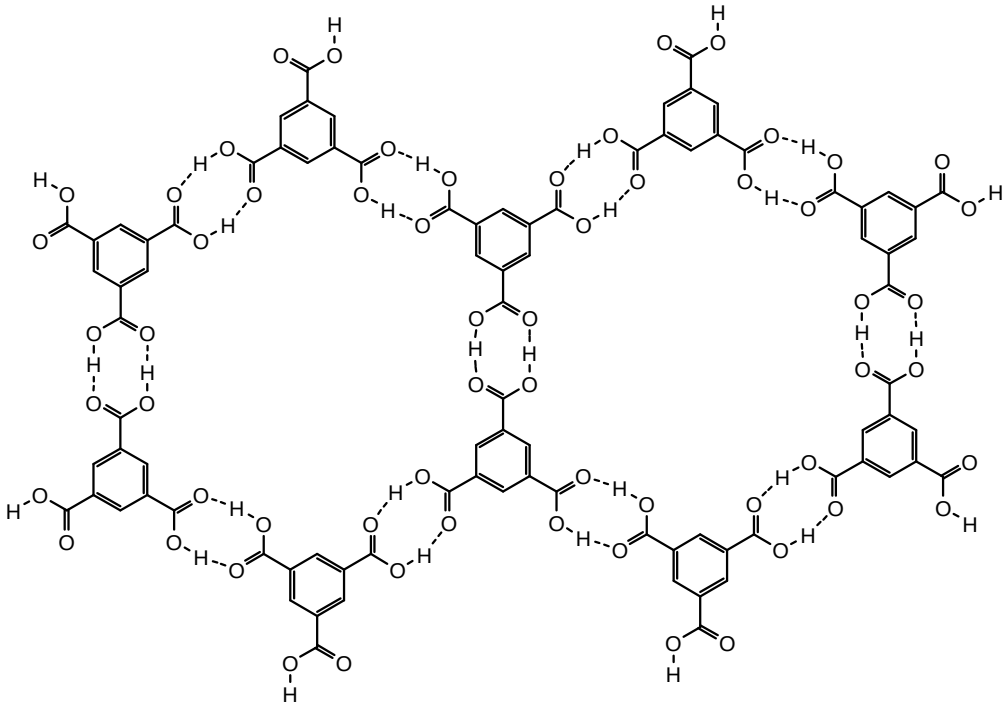

Figure 3.3: *Self-assembly of benzene-1,3,5-tricarboxylic acid* ***1*** *into two-dimensional honeycomb-like networks.*[30]

If different binding sites with different binding strength are used in the self-assembly process, "multi-step" self-assembly can occur. In these cases, the stronger interactions between the building blocks lead to an initial organization. After that, the weaker interactions can participate in the organization process. This phenomenon is called *hierarchical self-assembly.*[36, 37] The self-assembly of helical dinuclear titanium(IV) complex **4** reported by Albrecht and co-workers is a nice example for metallo-supramolecular hierarchical self-assembly (Figure 3.4).[38] The interaction between the catechol units of ligand **2** and the titanium(IV) ions is the strongest in this system. The carbonyl groups could in principle interact with the titanium ions as well, but their interactions not that strong. Thus, the catechol units and not the carbonyl groups coordinate to the titanium ions. Finally, also interactions between the lithium ions and the catechol groups and/or the carbonyl groups are observed, but both are also weaker. First, the monomeric structure **3** containing one titanium(IV) ion, three catecholate ligands and

two lithium ions each is formed. In a second step the lithium ions start to interact with the carbonyl groups of the monomeric complex **3**. Thus, the dimeric complex **4** is formed.

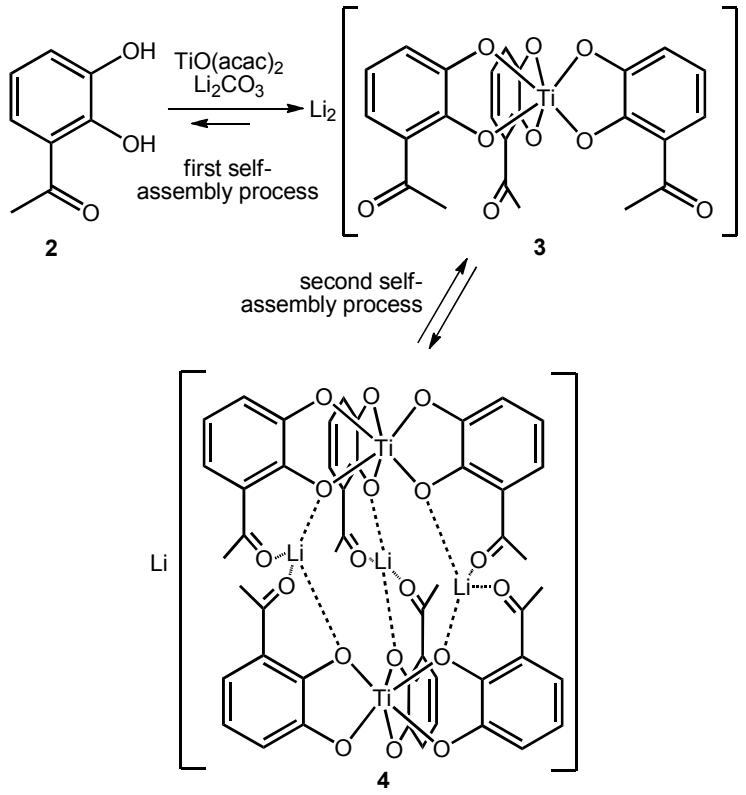

Figure 3.4: *The hierarchical self-assembly of the helical dinuclear titanium(IV) complex* ***4****.*[38]

Besides artificial self-assembled systems, (hierarchical) self-assembly plays an important role in nature as well (e.g. membrane formation, quaternary protein structures).[39] One famous example for self-assembly in nature is the building of the tobacco mosaic virus wherein protein units are arranged around a RNA strand.[40] The RNA strand has the function of a template for the arrangement of the proteins. These protein building blocks have to arrange themselves into the correct tertiary structure before they can assemble around the RNA strand and form a protective shell around it. When all different hierarchical levels of self-assembly are organized correctly, the tobacco mosaic virus is built by 2131 building blocks, which interact only by relatively weak non-covalent forces.

3.2.2 Self-Sorting

The phenomenon of *self-sorting* was defined and described in several ways. In the beginning, Wu and Isaacs gave the narcissistic description of self-sorting as the differentiation between "self" and "not self" (*narcissistic self-sorting*).[41] On the contrary, also *social self-sorting* exists, wherein the members of a mixture recognize other members and aggregate with them.[42] Two types of social self-sorting can be differentiated: (i) When two different hosts (A and B) are mixed with two different guests (C and D), host A can selectively recognize guest C whereas host B recognizes guest D selectively. (ii) In a similar mixture, both hosts A and B can have a high affinity to guest C and a low affinity to guest D. If the affinity of host A to guest C is significantly higher than that of host B, guest C will selectively bind to host A. C binds only to host B, when host A is consumed completely – otherwise host B will bind to guest D.

This was refined by Böhmer, who extended the definition of self-sorting and included the self-sorting of complementary systems.[43] Self-sorting is the sorting of a system by itself without any external stimulation. If many similar and complementary compounds which can interact with each other are mixed and just one out of many possible assemblies is realized by the system, this is called complete self-sorting. Non-complete self-sorting is observed, when more than one supramolecular assembly is formed out of a big library of possible assemblies, but still many possibilities are not realized.[44] This includes the definition given by Wu and Isaacs as one special case of self-sorting. Self-sorting phenomena meanwhile have been observed for several different artificial supramolecular systems like molecular clips,[45] cucurbiturils,[46] tetraurea calixarenes[43, 47] and crown ether/ammonium ion pseudo-rotaxanes.[48]

In metallo-supramolecular chemistry, self-sorting has been shown to be an interesting tool to form exclusively only one complex or just several complexes out of a big molecular library of possible metallo-supramolecular complexes.[49, 50] Stang *et al.* studied the influence of several parameters (e.g. temperature, solvent, polarity and geometry of the ligands) on the results of several self-sorting processes.[51] They for example reported the exclusive formation of a heteroleptic complex **8** which looks like a bow tie (Figure 3.5).[52] The combination of the tetravalent ligand **5** with four equivalents of the divalent

ligand **6** and six equivalents of the linear dinuclear metal center **7** results in the formation of metallo-supramolecular complex **8** quantitatively. Other possible homo- and heteroleptic complexes or metal-organic frameworks were not observed.

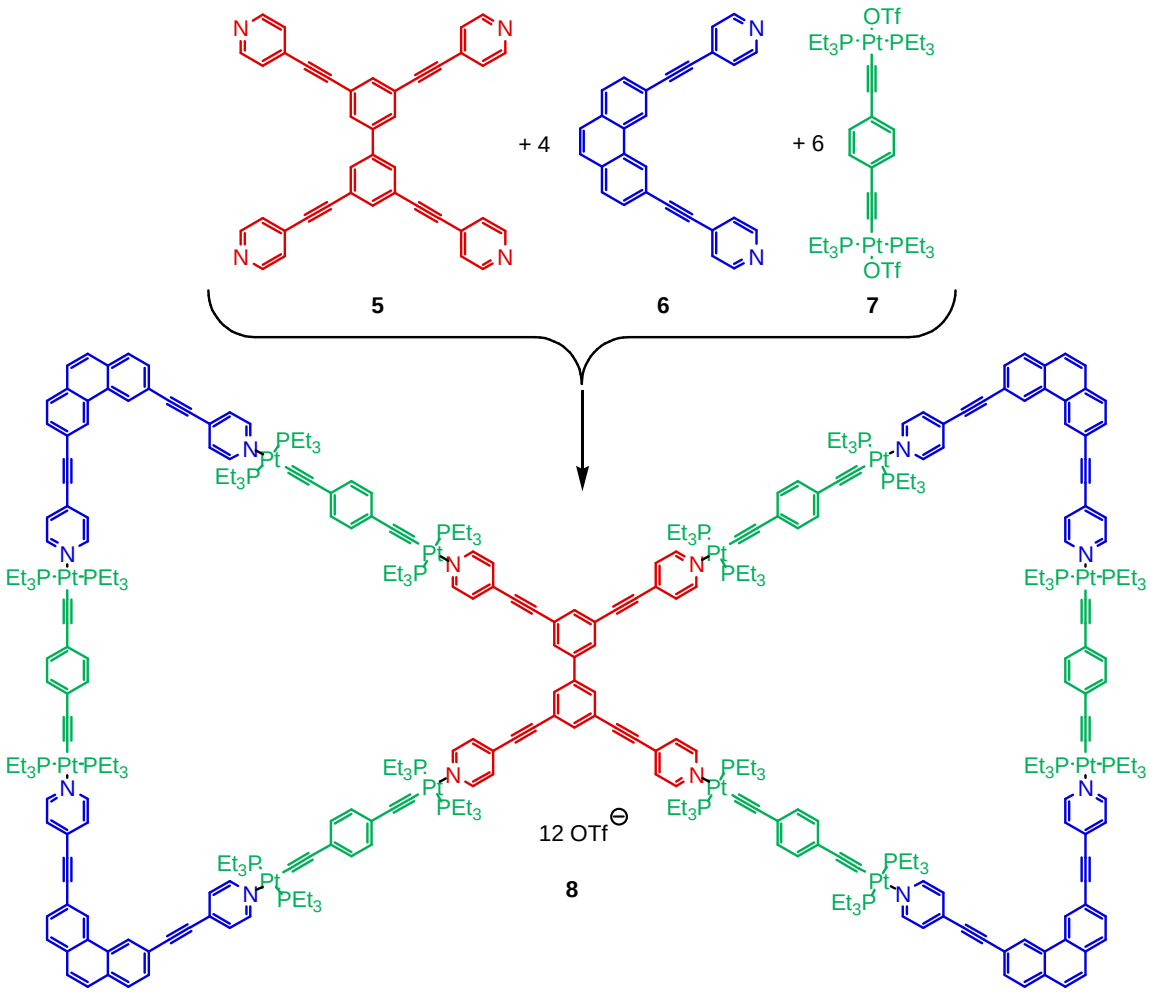

Figure 3.5: *A metallo-supramolecular bow tie formed by the interplay of self-assembly and self-sorting.* [52]

Another excellent example for metallo-supramolecular self-sorting is the selective self-assembly of the metallo-supramolecular trapezoid **14** reported by Schmittel and co-workers (Figure 3.6).[44] An equimolar mixture of the divalent chelate ligands **9** and **10** with two equivalents of the divalent chelate ligand **11** and two equivalents of tetrakis(acetonitrile)-copper(I) hexafluorophosphate **12** and zinc(II) trifluoromethane-sulfate **13** results in the formation of the trapezoid **14**. The exclusive formation of **14** can

be explained by steric effects, electrostatic interactions, π-π interactions and the different coordination spheres of Cu^{+} and Zn^{2+} ions. Schmittel and co-workers also reported the self-sorting of heterometallic metallo-supramolecular triangles.[53]

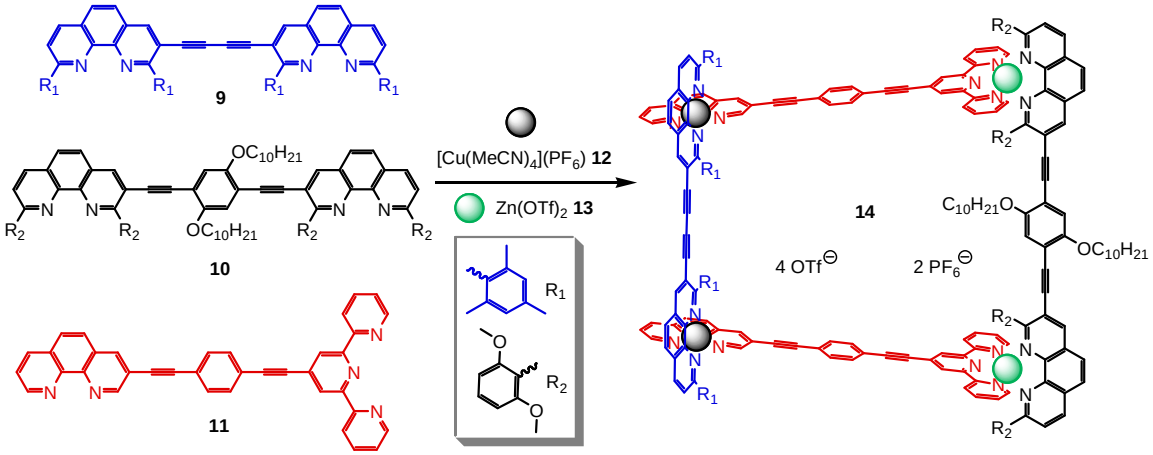

Figure 3.6: *Selective self-sorting of a heteroleptic bimetallic metallo-supramolecular trapezoid* ***14****.*[44]

3.3 Metallo-Supramolecular Self-Assembly: A Brief Overview

3.3.1 Introduction into Metallo-Supramolecular Self-Assembly

Metallo-supramolecular self-assembly is a mixture of coordination chemistry and supramolecular chemistry. It deals with metal centers and ligands which self-assemble and form complex metallo-supramolecular architectures. In order to influence the structure of the resulting metallo-supramolecular complexes, the building blocks used have to be well-designed. The self-assembly/self-organization process itself cannot be influenced easily. However, three different routes have been established to form metallo-supramolecular complexes.[35]

The most common strategic route to obtain metallo-supramolecular complexes is the thermodynamically controlled *Directional-Bonding Strategy*[35] which is also called *Molecular-Library Strategy*.[34] It enables the formation of many different metallo-supramolecular structures containing one or more metal centers. Using this strategy, relatively small dinuclear metallo-supramolecular macrocycles can be obtained as well as

rather big three-dimensional architectures. In the *Directional-Bonding Strategy*, the directionality of the pre-organized building blocks used is mandatory for the resulting complexes. In order to achieve this directionality, the building blocks need to be more or less rigid, because increasing flexibility of the building blocks results in decreasing directionality. In the *Directional-Bonding Strategy*, the metal centers as well as the ligands have a defined number of coordination sites and defined angles between them. In order to get appropriate angles at the metal centers, auxiliary ligands are used to block some coordination sites of the metal centers. The combination of rigid bidentate ligands with metal centers containing two binding sites is a simple example to gain a molecular library of metallo-supramolecular complexes (Figure 3.7).[34, 35] For example, the combination of a metal center with a ligand which both have a bite angle of 90° results in a dinuclear square-like complex, whereas the combination of a metal center with the same bite angle (90°) with a linear ligand which has a bite angle of 180° self-assembles into a tetranuclear metallo-supramolecular square. In this metallo-supramolecular square, the corners are represented by the metal centers and the ligands form the sides of the square. A similar tetranuclear metallo-supramolecular square can be achieved, when a divalent metal center with a bite angle of 180° is combined with a bidentate ligand which has a bite angle of 90°. In here, the ligands represent the corners of the square whereas the metal centers are located at the sides of it. Many other two- and three-dimensional metallo-supramolecular structures are available using the *Directional-Bonding Strategy*.

The number of defined binding sites and bite angles of ligands and metal centers as well as their geometry allows a chemist to predict and form metallo-supramolecular architectures by choosing appropriate ligands and metal centers. Nevertheless, the self-assembly of these ligands and metal centers can still result in metallo-supramolecular structures which contradict the initial prediction.

This strategy has many of advantages, but also limitations. The most important limitation is the need of relatively rigid building blocks. Flexibility is important for many functional supramolecular systems like molecular shuttles, molecular switches or molecular machines, as flexible movement is necessary for these devices to work. Due to the lack of flexibility, the use of the *Directional-Bonding Strategy* for the formation of supramolecular devices requiring flexibility is limited.

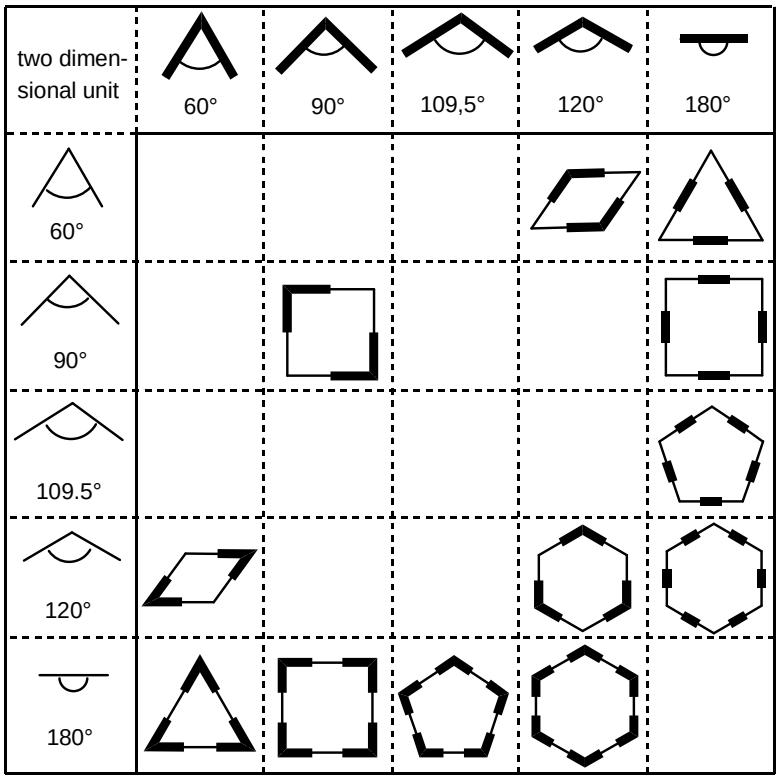

Figure 3.7: *The schematic drawing of a molecular library of metallo-supramolecular macrocycles which can be obtained by the combination of divalent building blocks with different bite angles.*[34]

The *Symmetry-Interaction Strategy* is a second strategic route to obtain metallo-supramolecular assemblies.[54] In contrast to the *Directional-Bonding Strategy*, no auxiliary ligands are used to block potential coordination sites at the metal centers. Within this strategy, highly symmetric coordination clusters are formed by a template effect[55] of the transition metals used. The ligands often are chelate ligands with two or more binding sites. They do not have to be rigid like in the *Directional-Bonding Strategy*. Due to the chelate effect, relatively stable complexes with high formation constants are formed. Similarly to the *Directional-Bonding Strategy*, in the *Symmetry-Interaction Strategy* the symmetry, the geometry, the number of binding sites and the relative position of the binding sites of metal centers and ligands define the structure of the resulting metallo-supramolecular complexes. The coordination geometry of the metal ion interacts with the symmetry of the chelate ligands used which yields complexes of high

symmetry (Figure 3.8). The coordination of the first ligand to the metal center pre-organizes the resulting intermediate complex for further coordination by other ligands to the same metal center.

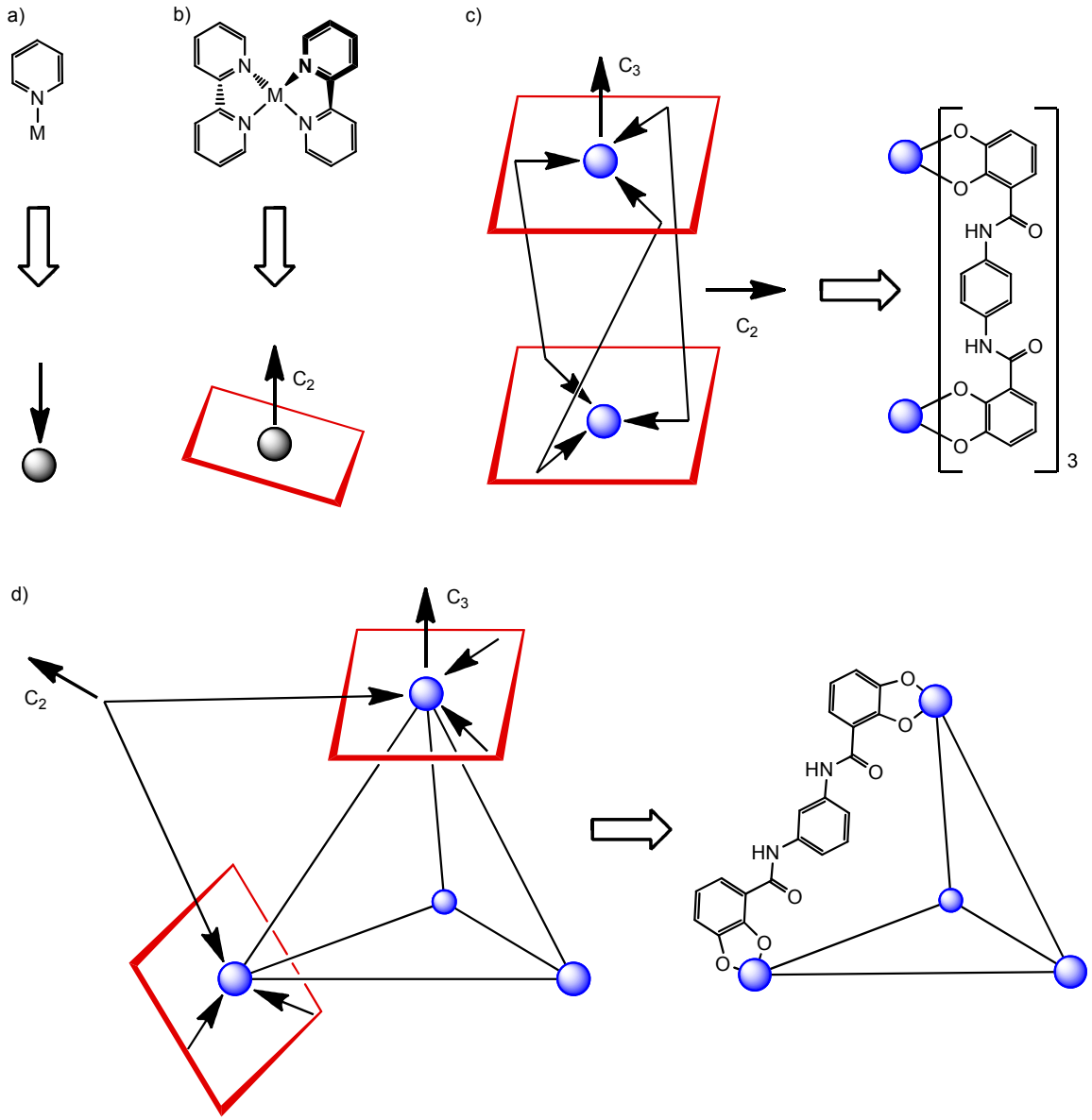

Figure 3.8: *a) The coordination vector shows from the coordinating atoms of the ligand into the direction of the metal center. b) Complexes containing chelate ligands have a "chelate plain" which is orthogonal to the main axis of rotation. c) The formation of a triple-stranded helicate is shown. d) A slight change in the ligand geometry (compared to Figure 3.8c) results is a C_3-symmetric tetrahedron.* [34]

The coordination of a ligand to a metal center can be described by a coordination vector (Figure 3.8). If a monodentate ligand is used, the coordination vector points from the coordinating atom of the ligand to the metal center. For chelate ligands like 2,2´-bipyridine or 1,2-dihydroxybenzene the coordination vectors are located in the "chelate plain" which is perpendicular to the main axis of symmetry of the metal fragment. Based on this concept, every symmetrical polyhedron can be described by the chelate plains and their relationship to each other. In order to generate new metallo-supramolecular polyhedra via the *Symmetry-Interaction Strategy*, appropriate buildings blocks have to be well-chosen, because symmetry has a much higher relevance in this strategic route than in the others (Figure 3.8). This strategy is thermodynamically controlled. Therefore always the thermodynamically favored metallo-supramolecular complex is formed. The *Symmetry-Interaction Strategy* can be used for the formation of many different metallo-supramolecular structures like helicates,[56] tetrahedra,[57] grids[58] and cage-like complexes.[59]

A third strategic route to get self-assembled metallo-supramolecular complexes is the *Weak-Link Strategy* that does not need auxiliary ligands at the metal centers, similar to the *Symmetry-Interaction Strategy*.[35, 60] In this strategy, flexible hemilabile ligands are used which coordinate to transition metal centers (Figure 3.9). The hemilabile ligands normally have two or more chelate binding sites, wherein the coordinating atoms of these chelate binding sites may be of the same kind or not. These ligands coordinate to the metal centers used and often quantitatively form the favored dinuclear M_2L_2 complexes **A**. The preference of these dinuclear complexes compared to often also possible mononuclear complexes can be explained by the higher ring strain in the mononuclear M_1L_1 complexes. Also, the formation of five- and six-membered chelate rings in case of the M_2L_2 complexes **A** is preferred energetically. In respect to the ligands used, also π-π interactions between the bridging spacers connecting the chelate binding sites of the hemilabile ligands can stabilize the dinuclear complexes **A**. However, the coordination of four coordinating atoms of the hemilabile ligands to the metal center decreases the bond strength of each of the four coordinative bonds (see chapter 3.1). The weakening of the coordinative bonds between the chelate ligands and the metal centers is used as a weak link to generate more stable metallo-supramolecular structures. If a ligand **L** which binds

stronger to the metal center than the coordinating atoms of the hemilabile ligands in complex **A** is added, the metallo-supramolecular complex **B** is formed. In many cases complex **B** is formed in quantitative yield.

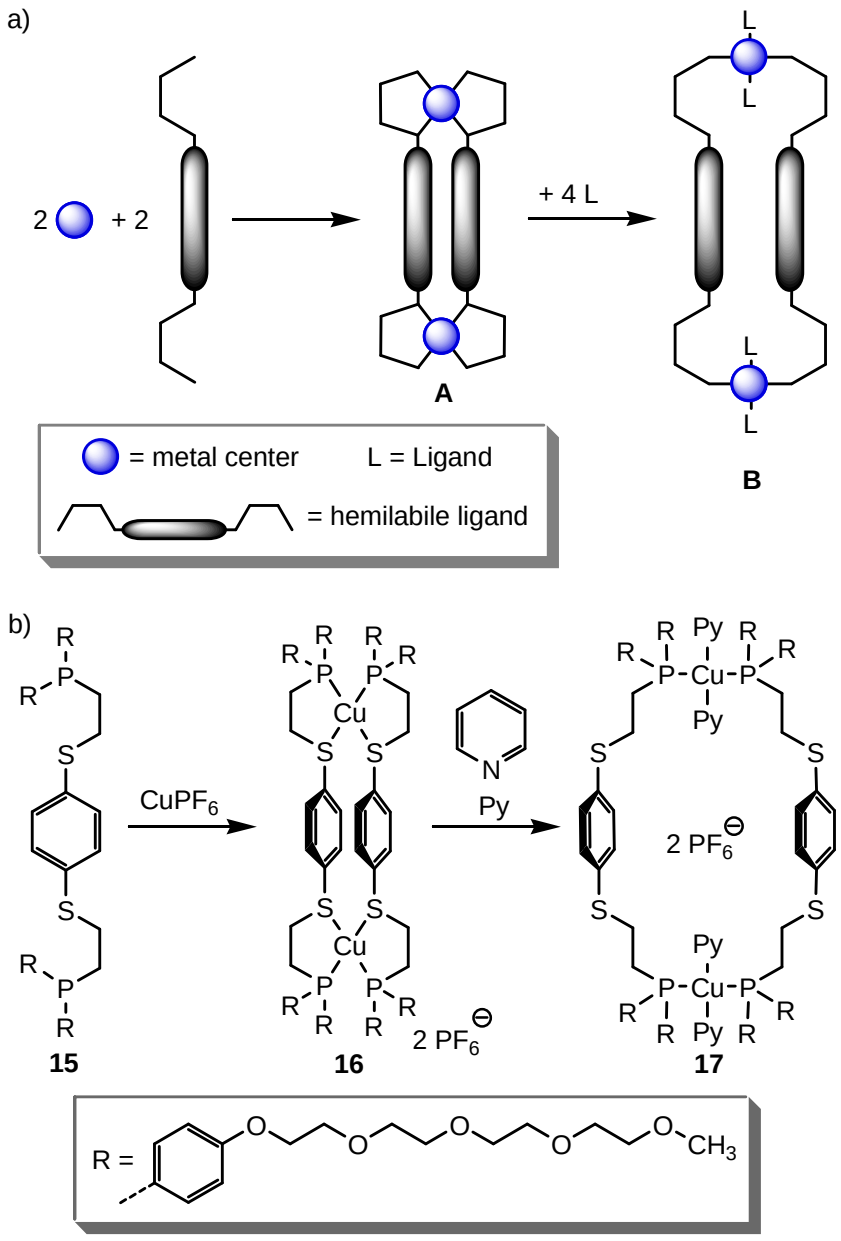

Figure 3.9: *The Weak-Link Strategy: a) Schematic drawing of the Weak-Link Strategy.*[35] *b) The formation of a water-soluble dinuclear Cu(I) complex using the Weak-Link Strategy.*[61]

The use of weakly coordinating hemilabile ligands offers an interesting way to gain two- and three-dimensional metallo-supramolecular structures. In contrast to the other two strategies, kinetically controlled complexes are obtained which have a certain thermal lability. Anyway, the energetic barriers between the kinetic and the thermodynamic metallo-supramolecular products are often very high. Therefore, no transformation of the kinetic into the thermodynamic products is observed.[62]

In comparison, every strategic route has positive and negative aspects. They have to be taken into account when a new metallo-supramolecular compound is synthesized. A large library of metallo-supramolecular complexes is available and can be realized, if these three strategies are used separately or in combination with each other.

3.3.2 Structural Insights into Metallo-Supramolecular Assemblies: From Small Dinuclear Macrocycles to Large Three-Dimensional Architectures

Dinuclear macrocycles of the type M_2L_2 (M = metal center, L = ligand) are some of the smallest metallo-supramolecular complexes. One of the first examples of a self-assembled dinuclear metallo-supramolecular macrocycle was published in 1984 by Maverick and co-workers.[63] This M_2L_2 complex **18** was made via the *Symmetry-Interaction Strategy* and contained copper(II) as metal centers and β-diketone based ligands (Figure 3.10a). It was used as a host that was binding to several different guest molecules like for example 1,4-diazabicyclo[2.2.2]octane (DABCO). In the beginning of the 1990ies, Fujita and co-workers used (ethylene diamine-*N*,*N*´)palladium(II) nitrate ((en)Pd(NO_3)$_2$) **19** as metal center to form dinuclear M_2L_2 complexes like **22** (Figure 3.10b).[64] Complexes like this are designed by the principles of the *Directional-Bonding Strategy*. Metal center **19** shows a very good solubility in water and later on became one of the most used metal centers in metallo-supramolecular chemistry. Due to the hydrophobic effect, the dinuclear metallo-supramolecular M_2L_2 macrocyles often exist in concentration-dependent equilibria with their corresponding M_4L_4 catenanes (Figure 3.10b), when water is used as the solvent.[65] In a catenane, the holes of the metallo-supramolecular macrocycles are filled by another macrocycle. Thus, the interphase

between the hydrophobic ligands and water is minimized. Due to the kinetically inert Pt-N bond in the complexes,[11] the conversion of the catenanes into their corresponding M_2L_2 complexes is relatively slow. Thus, the Pt-containing catenanes were also observed after the reaction mixture was diluted to low concentrations.[66] In a mixture of two different ligands with (en)M(NO_3)$_2$ two homoleptic and one heteroleptic M_2L_2 macrocycles can be formed as well as the equivalent catenanes of these. Interestingly, the comparably selective formation of a specific heteroleptic metallo-supramolecular catenane was observed which can be explained by an optimized fit of a ligand of one of the metallo-supramolecular macrocycles into the hole of the other one and *vice versa*.[67]

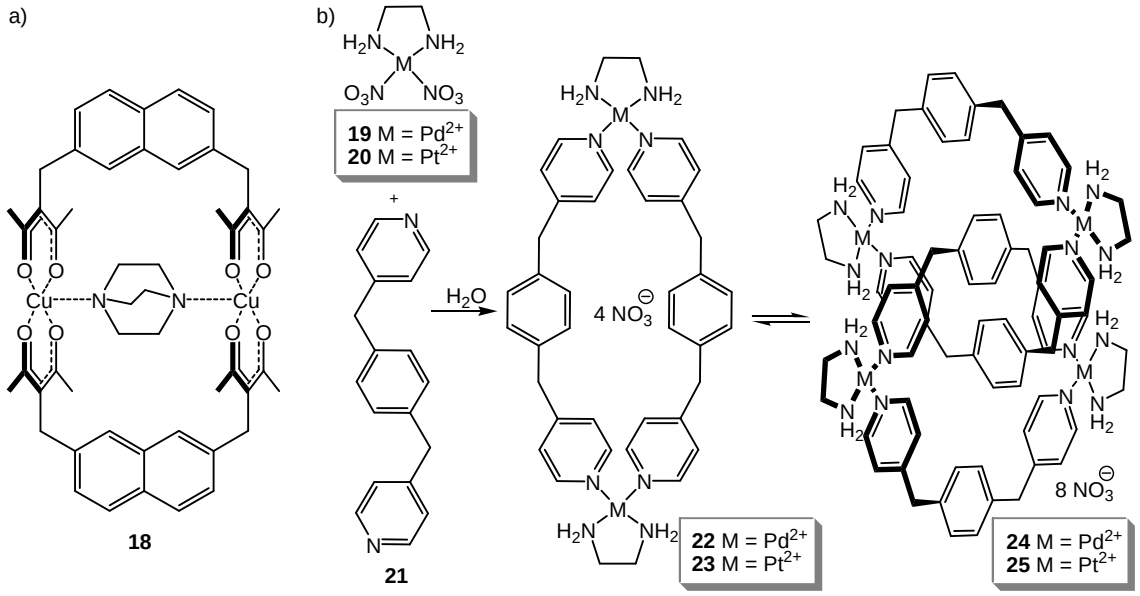

Figure 3.10: *a) A copper-based metallo-supramolecular M_2L_2 complex **18** as a host for DABCO. The complex was formed via the Symmetry-Interaction Strategy.*[63] *b) The self-assembly of [2]catenanes based on the hydrophobic effect.*[65]

Later on, Fujita,[68] Hosseini,[69] Hong[70] and Stang[71] published similar M_2L_2 complexes using the same or similar metal centers. In contrast to Fujita, Stang used metal centers which were soluble in organic solvents. Based on the two different types of metal centers, metallo-supramolecular macrocycles could be studied in water as well as in organic solvents. Due to solvent effects, the results of self-assembly reactions can differ significantly from each other. For example, no formation of catenanes was observed for

complexes formed in organic solvents.[71] However, many other homometallic dinuclear M_2L_2 complexes containing *cis*-blocked square-planar metal centers[72-74] other metal centers[75] as well as heterometallic ones[76] have been reported. Also some equilibria between M_2L_2 and their corresponding M_3L_3 complexes were observed.[64, 70, 77]

When more rigid linear ligands are combined with *cis*-blocked square-planar metal centers, metallo-supramolecular triangles and squares can be achieved easily. Thus, the first metallo-supramolecular squares were reported in the 1990ies by Fujita[78] and Stang.[79] Both used rigid linear ligands like 4,4´-bipyridine **26** and *cis*-blocked square-planar metal centers with a coordination angle of 90° to form similar metallo-supramolecular squares. Fujita used the relatively small (en)M(II)$(NO_3)_2$ (M = Pd^{2+} **19** or Pt^{2+} **20**) and Stang used the bigger (dppp)M(II)$(OTf)_2$ (M = Pd^{2+} **27** or Pt^{2+} **28**) as metal centers (Figure 3.11). Due to the different metal centers and the different counter anions, Fujitas complexes are highly soluble in water, whereas Stangs complexes show a very good solubility in most organic solvents. Complexes using one of these specific metal centers are also called Fujita-type or Stang-type complexes.[80-83] M_4L_4 squares of these types are some of the best characterized and analyzed species in metallo-supramolecular chemistry. For example, their nanometer-sized structures were visualized using scanning tunneling microscopy after the complexes were adsorbed to metal surfaces.[84, 85] Based on these first examples, many different metallo-supramolecular squares using *cis*-blocked square-planar metal centers have been reported.[50, 86-91]

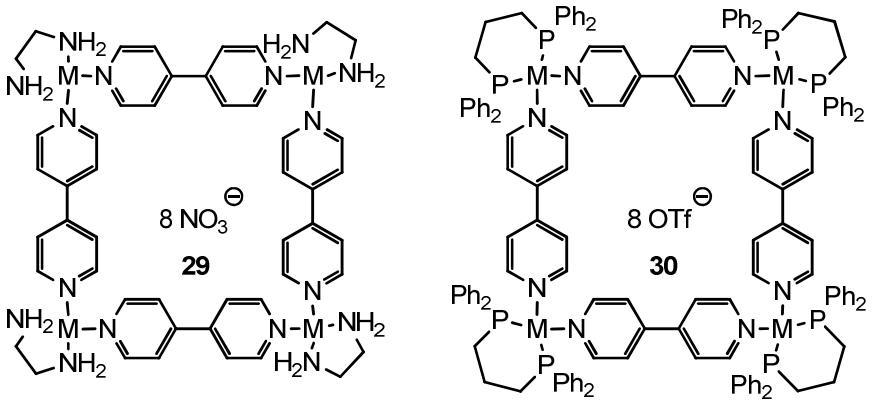

Figure 3.11: *Metallo-supramolecular squares from Fujita*[78] ***29*** *and Stang*[79] ***30****.*

Besides *cis*-blocked square-planar metal centers, also other metal centers like rhenium-[92] or molybdenum-based [93] metal centers were used to form homometallic supramolecular squares. Lees and co-workers reported the formation of a heterometallic square containing palladium and rhenium metal centers.[94] They used 4,4´-diazobipyridine as ligand which can be switched between its *cis* and *trans* conformation, when it is irradiated with light of a suitable wavelength. Based on this conformational switching, the square can be transferred into the analogous heterometallic M_2L_2 complex which can be returned into the square when it is heated. However, besides the complexes described in here, also some metallo-supramolecular squares were published that have their metal centers at the sides and the ligands at the corners.[95]

When less rigid linear ligands are used, the formation of triangles occurs following the same principles described for metallo-supramolecular squares.[68, 96-98] In order to achieve an appropriate angle to form metallo-supramolecular triangles, many triangular M_6L_3 structures have been reported which contain the metal centers at their sides instead of the corners (Figure 3.12). [99-102]

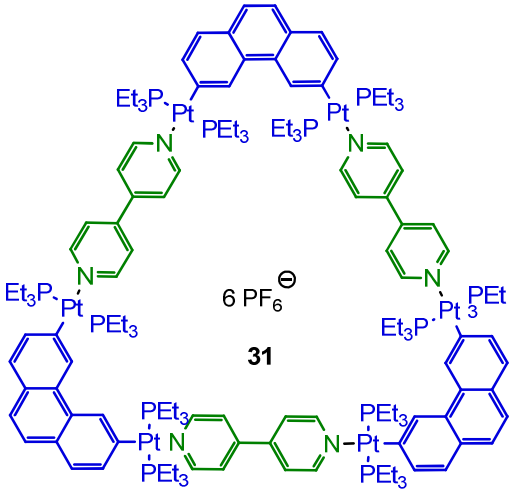

Figure 3.12: *A metallo-supramolecular M_6L_3 triangle* ***31*** *with ligands at the corners and metal centers at its sides.* [102]

Often metallo-supramolecular triangles and squares exist in thermodynamic equilibria with each other.[103] Due to many different examples, the equilibria between triangles and squares of the Fujita- and Stang-type are among the most extensively studied equilibria in

metallo-supramolecular chemistry. Like most equilibria between metallo-supramolecular complexes, the equilibria between the triangles and squares are generally based on a sensitive balance between enthalpy and entropy which is influenced by many different parameters.[104] These balances are influenced by the character of the metal centers (kind of metal, coordination number, coordination geometry, auxiliary ligands, counter ions), the ligands (shape, number of binding sites, flexibility) and other parameters (solvent, temperature, concentration).[104-106] In general, entropy favors smaller complexes because more of them can be formed of the same number of building blocks. In most cases, the smaller complexes have a higher strain than the larger ones, which favors the formation of the larger complexes enthalpically.[104] Thus, the triangles are entropically favored, while the analogue squares are enthalpically favored. The ring strain can be compensated by the ligands which can bend or by metal centers with a relatively flexible coordination sphere. When longer and/or more flexible linear divalent ligands are used, the resulting metallo-supramolecular triangles are favored, whereas short and rigid ligands favor the formation of squares.[104] Some reports exist, wherein the smaller complexes are entropically disfavored against the corresponding larger complexes.[107, 108] For example, von Zelewsky and co-workers observed an equilibrium between a hexanuclear silver complex and its tetranuclear analogue. The hexanuclear complex was entropically favored whereas the tetranuclear complex was enthalpically favored at low temperatures.[107]

Interestingly, Fujita and co-workers reported systems which contained equilibria between three different metallo-supramolecular species (Figure 3.13).[109] The self-assembly of the divalent ligands 1,4-bis(3-pyridyl)benzene **32** and 4,4´-bis(3-pyridyl)biphenyl **33** with the divalent metal center (en)Pd(NO_3)$_2$ **19** (en = ethylene diamine) results in the formation of dinuclear M_2L_2 **34 / 35**, trinuclear M_3L_3 **36 / 37**, and tetranuclear M_4L_4 complexes **38 / 39**. These equilibria are highly influenced by solvent and concentration effects. At low concentrations the formation of M_2L_2 complexes is favored while at high concentrations the M_4L_4 and at medium concentrations the M_3L_3 complexes are favored.[109]

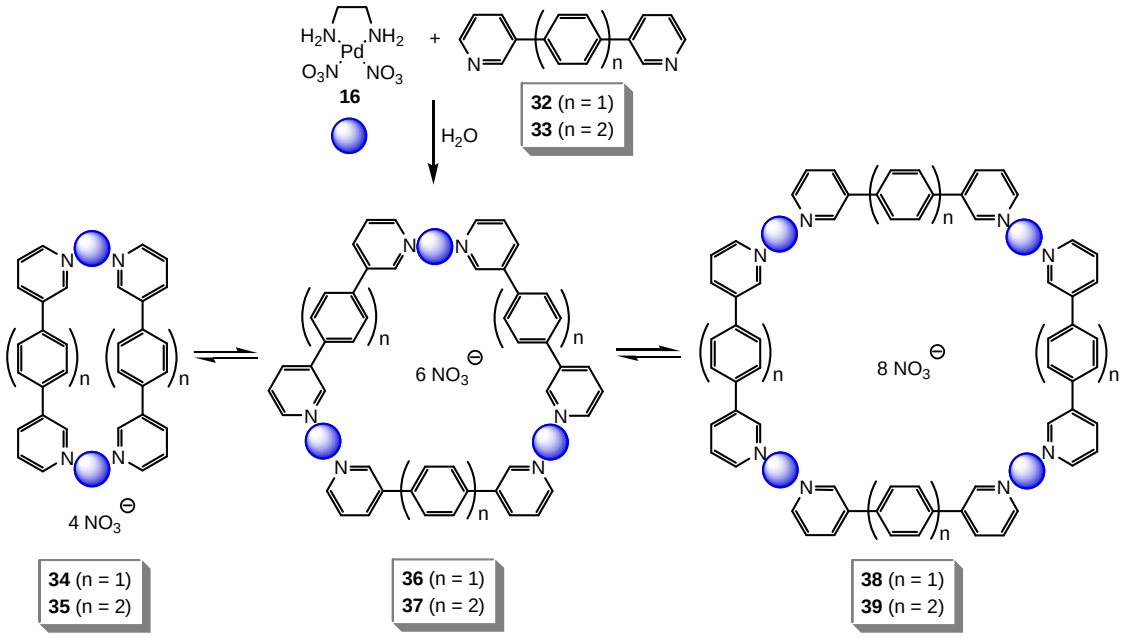

Figure 3.13: *Systems containing equilibria between three different metallo-supramlecular macrocycles reported by Fujita and co-workers.*[109]

The structure of metallo-supramolecular complexes can also be influenced by molecules or assemblies that act as templates for the complex formed. For example, Lehn and co-workers published a metallo-supramolecular pentagon **40** which was formed from iron(II) chloride **41** and trisbipyridyl ligands **42**.[110] When iron(II) sulfate **43** was used instead of iron(II) chloride **41**, analogue metallo-supramolecular hexagons **44** were observed.[111] These results can be explained by a template effect of the counter anion. The smaller chloride anions favor the formation of the pentagon **40** while the bigger sulfate anions favor the larger hexagonal complex **44**.

However, many other examples of large two-dimensional metallo-supramolecular complexes[112] and their equilibria[113] were published. Enhancing the concepts discussed to extended 2D and 3D structures, metallo-supramolecular grids[58] and metal-organic frameworks (MOFs)[114] are available. They play an important role on the way to functional materials since their various properties can be easily altered. Grids are two-dimensional metallo-supramolecular complexes which are normally formed from linear chelate ligands and tetrahedral or octahedral metal ions.[58] Metal-organic frameworks (MOFs) can be one-, two- and three-dimensional depending on the ligands and metal centers used.[114]

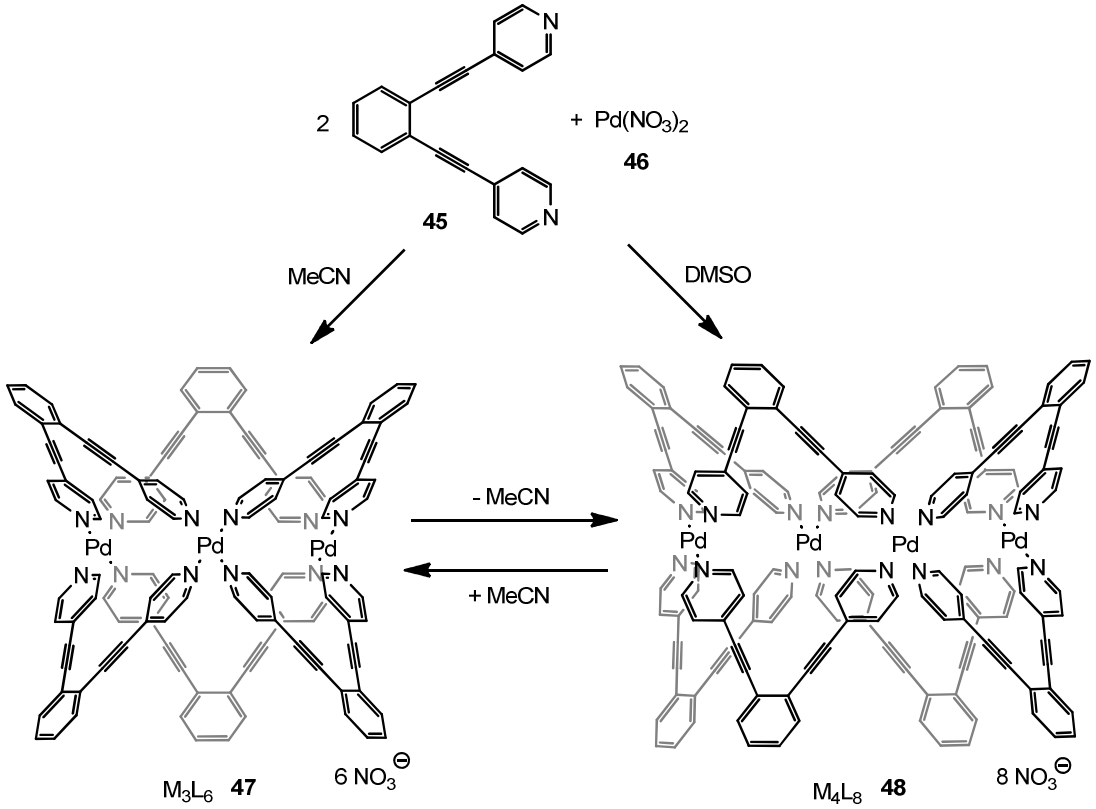

Figure 3.14: *An equilibrium between metallo-supramolecular M_3L_6* ***47*** *and M_4L_8 complexes* ***48*** *which can be switched by the solvents used.*[116]

The structural concepts and their variations that have been discussed for two-dimensional metallo-supramolecular complexes are in principle the same for three-dimensional complexes.[33-35, 115] In order to gain three-dimensional metallo-supramolecular architectures, the metal centers and/or the ligands have to be varied in an appropriate way. For example, the combination of square-planar Pd(II) as metal center with a rigid, linear and divalent ligand will form a two-dimensional metal-organic framework. Instead, when a bended divalent ligand like 1,2-bis[2-(pyridin-4-yl)ethynyl]benzene **45** is combined with palladium(II) nitrate **46**, small metallo-supramolecular boxes like the M_3L_6 **47** and M_4L_8 **48** complexes are formed (Figure 3.14). [116] When the building blocks were dissolved in DMSO, the exclusive formation of the M_4L_8 complex **48** is observed. In contrast to this, the smaller M_3L_6 complex **47** is exclusively formed, when acetonitrile is used instead of DMSO. In mixtures of both solvents, both complexes are in equilibrium. Thus, the equilibrium can be shifted to one side or the other by varying the amount of acetonitrile

in the solvent mixture.[116] In general, the equilibria observed for three-dimensional metallo-supramolecular architectures are based on the same balance of enthalpy and entropy discussed for two-dimensional complexes.

However, the influence of the building blocks used at the structure and size of the resulting complexes can be explained nicely for M_nL_{2n} complexes containing square-planar metal centers with four coordination sites. When relatively rigid, non-linear and divalent ligands are used in the self-assembly process, the coordination angles of those ligands as well as their flexibility have a direct influence on the structure of the resulting three-dimensional complex. Ligands with a relatively narrow coordination angle and/or a high flexibility form small complexes while rigid ligands containing a relatively large coordination angle form large spherical complexes. Based on these principles, many small M_2L_4, M_3L_6 and M_4L_8 boxes[109, 116-118] have been realized as well as large M_6L_{12} octahedra, [119, 120] $M_{12}L_{24}$ cuboctahedra[121-124] (Figure 3.15) and $M_{24}L_{48}$ spheres.[125] The latter ones are the largest discrete metallo-supramolecular architectures realized up to now.

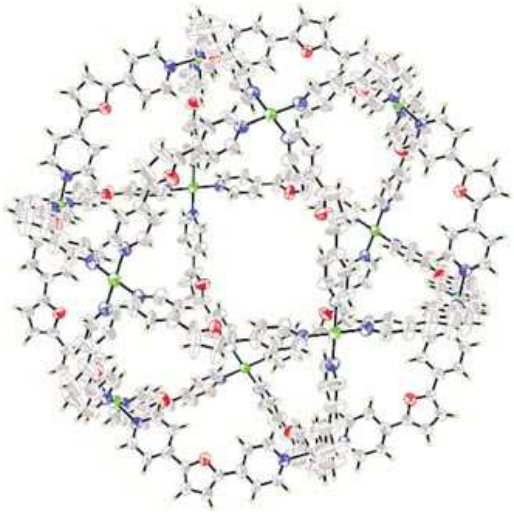

Figure 3.15: *Crystal structure of a metallo-supramolecular cuboctahedron by Fujita and co-workers.*[121] *The atoms are marked with different colors (green: Pd; red: O; blue: N; grey: C and white: H). The counter anions and solvent molecules are not shown. Reproduced from reference 121 with kind permission of John Wiley & Sons, © 2004.*

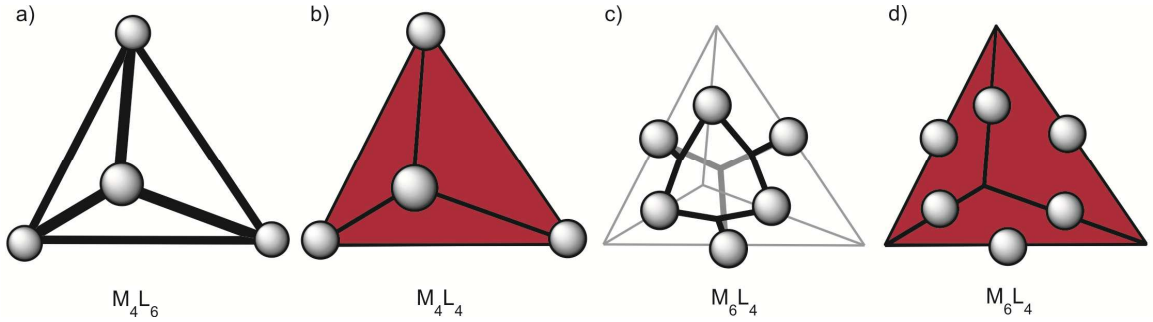

Figure 3.16: *The four possible ways to form a metallo-supramolecular tetrahedron: a) M_4L_6, b) M_4L_4, c) M_6L_4 and d) another M_6L_4 complex.*[126]

In order to gain esthetical metallo-supramolecular architectures, symmetry plays an important role, which is indicated by the complexes discussed above. Certainly, metallo-supramolecular tetrahedra, octahedra and cubes are some of the most esthetical structures achieved by supramolecular chemists.[126] In principle, metallo-supramolecular polyhedra like tetrahedra can be formed in four different ways which are similar to those discussed for two-dimensional complexes (Figure 3.16). M_4L_6[127-132] and M_4L_4[133] tetrahedra contain their metal centers at the corners which are bridged by linear ligands at the edges (M_4L_6) or by trigonal ligands at the sides (M_4L_4) of the tetrahedra (Figure 3.16a and b). On the contrary, two types of M_6L_4 tetrahedra exist, wherein the metal centers are located in the middle of the edges of the tetrahedra connected by two different types of ligands. Depending on the ligands used, the resulting M_6L_4 tetrahedron is truncated and bears large holes (Figure 3.16c) [134-139] or has a relatively closed structure (Figure 3.16d).[140] Many of these tetrahedra have been realized with a large variety of different metal centers.[126]

In contrast to metallo-supramolecular tetrahedra, octahedra with a real octahedral shape are relatively rare. Shionoya and co-workers designed ten metallo-supramolecular M_6L_8 octahedra **50a-j** combining a triangular disk-like ligand **49** with ten different metal centers (Figure 3.17a).[141] The cationic octahedra were able to include anionic guest molecules. However, several other metallo-supramolecular octahedral M_6L_{12} complexes and others have been published, but they often do not have a nice octahedral shape.[119, 120] Thomas and co-workers reported the formation of a metallo-supramolecular M_8L_{12} cube **53** from a combination of 4,4´-bipyridine **26** and tris(acetonitrilo)(1,4,7-trithiacyclo-

nonane-κ^3*S*)ruthenium(II) chloride **51** and silver(I) trifluoromethanesulfonate **52** (Figure 3.17b).[142] Several other cubes have been reported[143] which for example contain cyanide ions[144] or tetradentate molecules as ligands.[145]

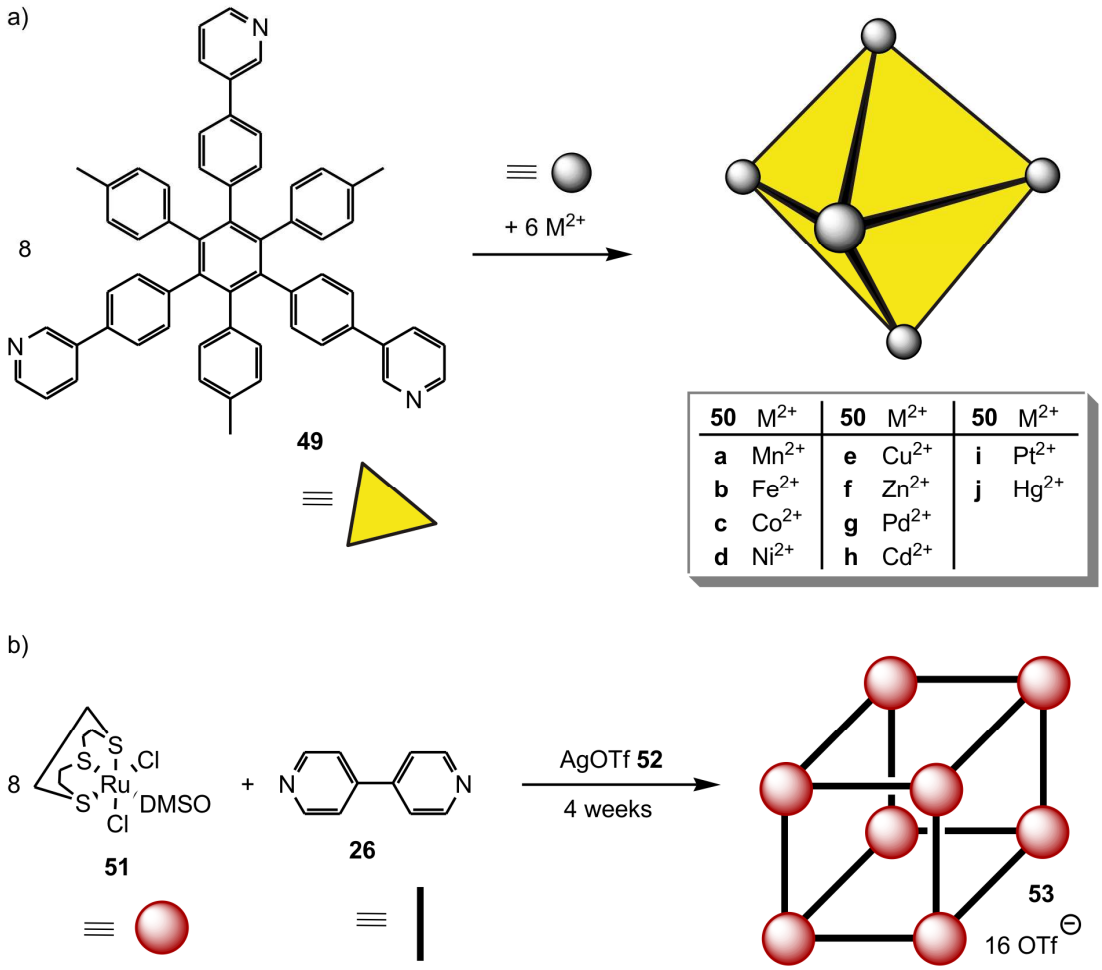

Figure 3.17: *a) Metallo-supramolecular octahedral **50a-j** by Shionoya and co-workers*[141] *and b) a metallo-supramolecular cube **53** by Thomas and co-workers.*[142]

Besides the structures discussed in here, many other metallo-supramolecular architectures like cuboctahedra,[146] dodecahedra,[147] isocahedra[148] or capsules based on ligands like resorcinarenes,[149] cycloveratrylenes[150] or pyrogallerenes[151] have been reported.

3.3.3 Functionalized Metallo-Supramolecular Systems

The properties of metallo-supramolecular assemblies can be influenced by the building blocks used. Thus, functionalization of those building blocks can be used to tune the properties of the resulting assemblies. Nevertheless, the properties of the complexes formed can be totally different to those implemented by the (functionalized) building blocks. However, often the functionalities introduced by the building blocks maintain in the final complexes and can be used for further studies.

Metallo-supramolecular building blocks can be functionalized in different ways.[152, 153] At first, the function is implemented in the basic structure of the building blocks and can influence their bite angles as well as their coordination behavior. Thus, the funtionalization directly influences the self-assembly process and the structure of the complexes formed. Another way to functionalize metallo-supramolecular assemblies is the substitution of the building blocks with functional groups. Here, the substituents used should not directly influence the bite angles or the coordination behavior of the functionalized building blocks. Two different ways exist to substitute a building block in the latter way. First, the functional group of a building block is positioned in a way that it is pointing into the inner space of the resulting metallo-supramolecular assembly. This is called *endo*-functionalization. Second, the functional group of a building block can also be performed at a position pointing outwards of the resulting metallo-supramolecular assembly. In these cases, the functional groups also show into the outer sphere of the final assembly which is called *exo*-functionalization.[152, 153]

Many metallo-supramolecular assemblies have been reported which implement functional groups in the structure of their building blocks.[33] In principle, both, metal centers and ligands can be functionalized with functional moieties (e.g. crown ethers; Figure 3.18).[154, 155] Nevertheless, the amount of metallo-supramolecular assemblies having functional moieties in their ligands is much larger compared to those containing functionalized metal centers. The variety of possible functionalizations in combination with a reasonable synthetic effort is higher for the ligands. Additionally, the functionlization of the metal centers decreases their number of coordination sites and thus limit the amount of complexes to that formed by the *Directional-Bonding Strategy*.[33]

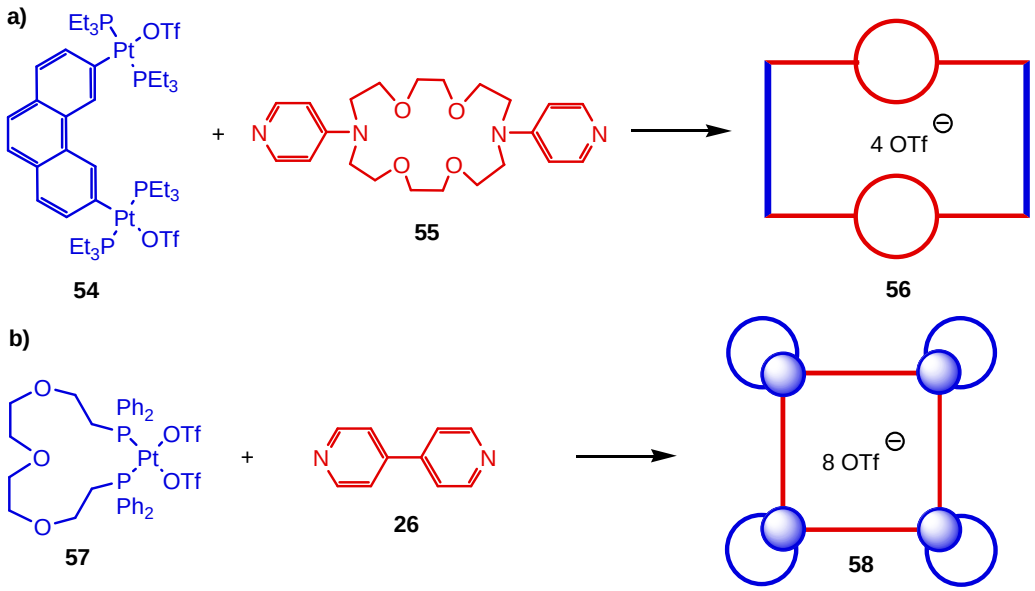

Figure 3.18: *The self-assembly of complexes containing crown ether moieties implemented in their ligands*[154] *(a) and metal centers*[155] *(b).*

When ligands bear different coordinative moieties, these can be used for the coordination of additional metal centers. Thus, different homo- and heterometallic structures can be formed using this kind of ligands.[156-159] For example, Stang and co-workers reported the formation of a metallo-supramolecular rectangle **61** which was formed by the combination of a dinuclear platinum(II) metal center **59** with linear dipyridyl ligand **60** wherein the two pyridine units were bridged by a phenanthroline moiety (Figure 3.19).[156] The pyridine units of the ligands **60** coordinated to the platinum metal centers **59** whereas the phenanthroline moieties were used to coordinate to other metal ions like Ni^{2+}, Cd^{2+} and Cr^{3+} (**62a-c**). Due to its optical properties, complex **61** could be used as a chemosensor for different metal ions in solution.[156]

Würthner and co-workers published several large metallo-supramolecular squares containing rigid perylene bisimide ligands.[86] The squares showed interesting photo- and electrochemical properties which can be influenced by the substitution of the ligands and thus their properties can be modified. When those ligands are substituted with fluorescent dyes like pyrenes or aminonaphthalimides, the metallo-supramolecular squares show light-harvesting behavior. These squares are artificial models for the cyclic light-harvesting complexes in purple bacteria and could be used to gain advanced materials. [86]

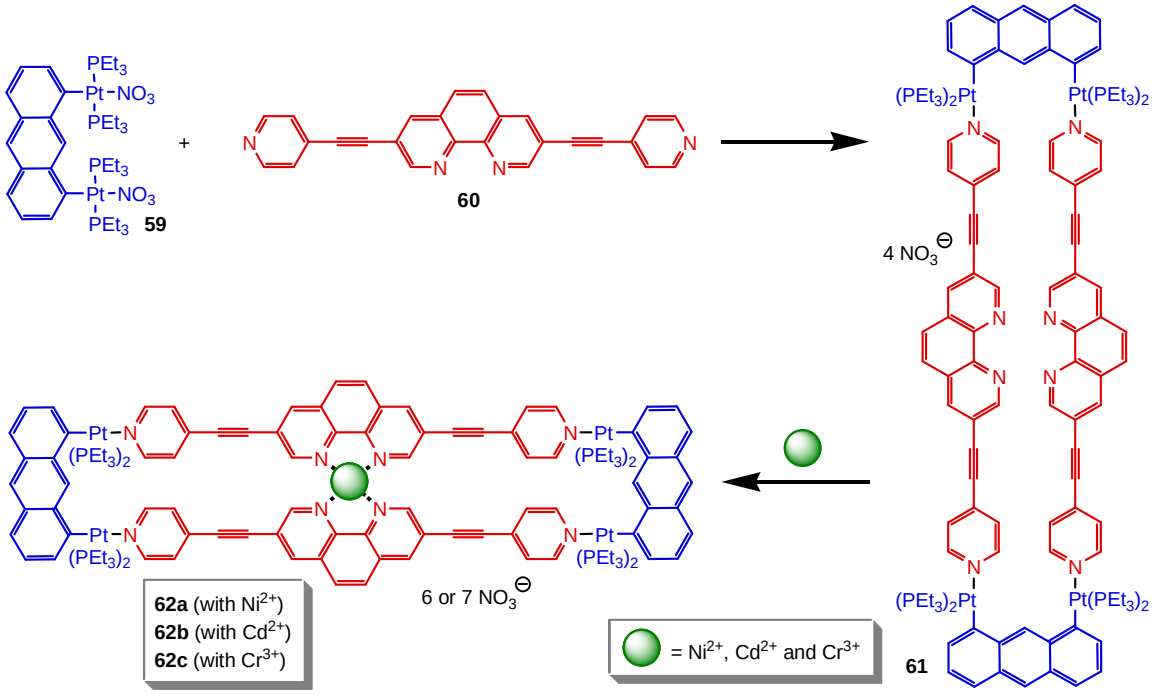

Figure 3.19: *The self-assembly of a metallo-supramolecular rectangle* ***61*** *with phenanthroline moieties that can be used to coordinate additional metal ions.*[156]

Recently, Fujita and co-workers formed *endo*-functionalized $M_{12}L_{24}$ cuboctahedra **64a-c** containing glucose units as functional substituents which point into the inner space of the spherical complexes (Figure 3.20a).[160] The inner space of the complexes **64a** and **64c** can be used to synthesize monodisperse silicon oxide nanoparticles with a size of 2-4 nm. Variation of the functionalized ligands yields in SiO nanoparticles of different sizes. The cuboctahedra **64a** and **64c** are acting as concave templates for the formation of SiO nanoparticles. This example shows just one of many other applications possible, which the inner cavity of *endo*-functionalized complexes can be used for. Thus, several other *endo*-functionalized metallo-supramolecular complexes containing different functional groups have been reported.[122]

On the contrary to the latter complexes described above, *exo*-functionalized metallo-supramolecular complexes can be tuned in a way to interact with other particles using their functionalized outer sphere. For example, a metallo-supramolecular macrocycle **66** which bears crown ether moieties in its outer sphere can be used to bind protonated guest molecules (**67**) and form pseudorotaxanes (complex **68**; Figure 3.20b).[161] In general, the

outer sphere of a metallo-supramolecular complex is much larger than its inner sphere. Thus, a large variety of functionalizations is available and many *exo*-functionalized complexes containing different functionalities have been reported.[50, 90, 122, 123, 162]

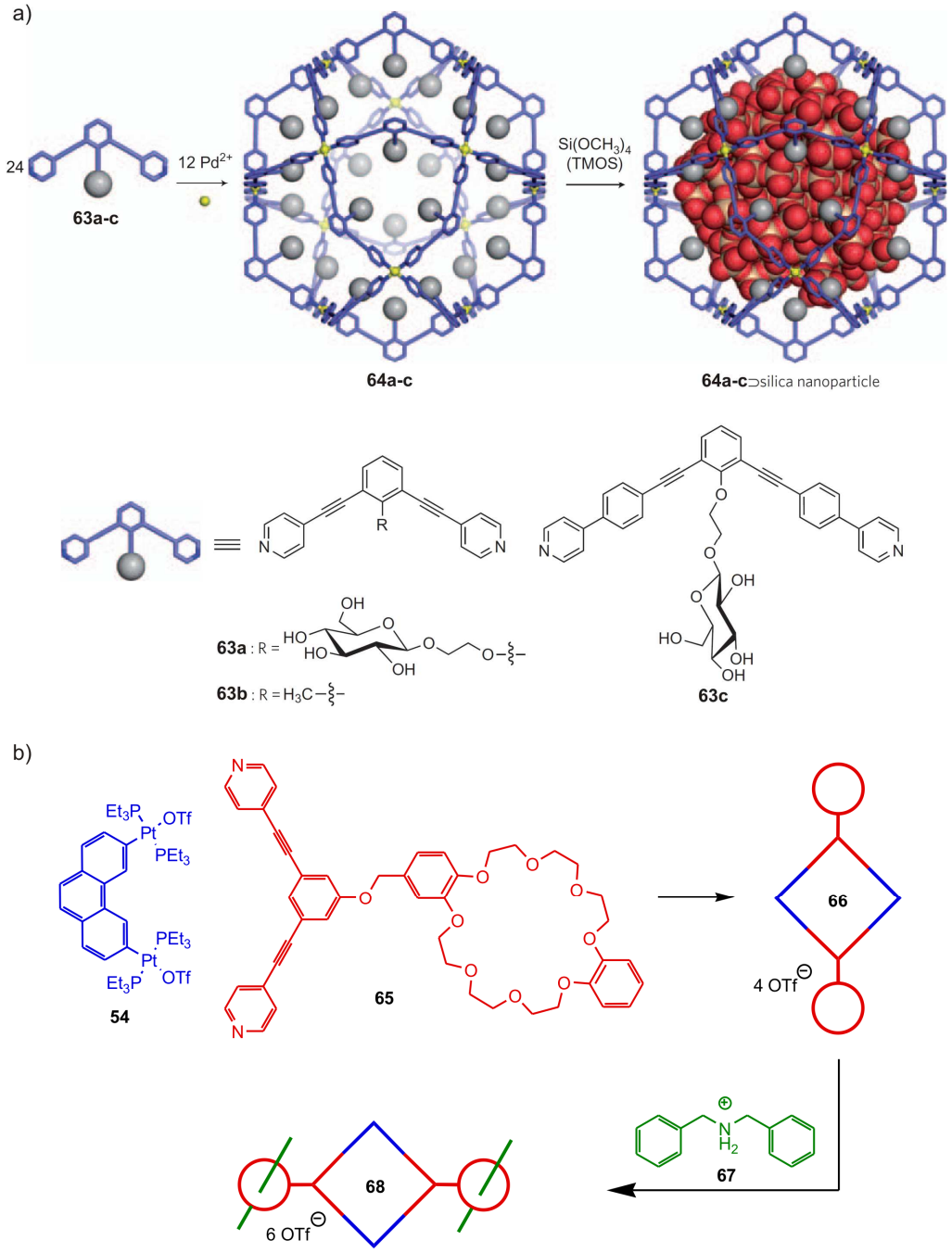

Figure 3.20: *Examples for a) endo- and b) exo-functionalized metallo-supramolecular complexes.*[160, 161] *Part a) was adapted from reference 160 by permission from Macmillan Publishers Ltd, © 2010.*

Since chirality plays an important role in nature, chemists tried to form chiral complexes on the basis of the knowledge described above.[163] Similar to the functionalization described above, chirality can be introduced into metallo-supramolecular complexes by modifying the building blocks used. For example, ligands containing chiral moieties like BINOL derivates,[164] Trögers base,[73] or amino acids,[50b] as well as axially chiral ligands[50] have been examined in respect to their influence at the formation of the resulting metallo-supramolecular complexes. According to the preferred coordination behavior, the complexes formed can be chiral[164] or achiral.[165] However, using the *symmetry-interaction strategy*, chiral complexes can also be formed of achiral building blocks. Based on the coordination geometry of the metal centers and ligands used, helical chiral complexes can be formed (Figure 3.21).[54, 56, 166, 167] The ligands used contain chelate binding sites like cathecholate and/or 2,2´-bipyridyl units that can coordinate to metal centers and form helicates. When these chelate ligands are combined with tetrahedral metal centers, double stranded helicates are formed (Figure 3.21a). Triple stranded helicates are formed, when octahedral metal centers are used (Figure 3.21b). The self-assembly of helicates using chiral ligands has been intensively studied.[168, 169]

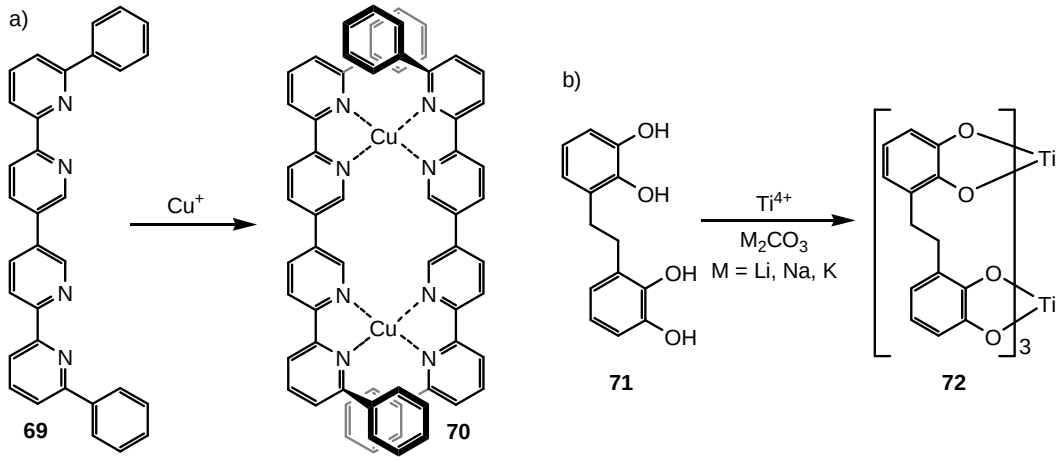

Figure 3.21: *Examples of the formation of double (a) and triple (b) stranded metallo-supramolecular helicates using chelate ligands and tetrahedral or octahedral metal centers.* [56b, 167]

3.3.4 Metallo-Supramolecular Complexes Acting as Micro-Reactors

Metallo-supramolecular complexes can act as host complexes and bind several different guest molecules. [130, 131, 134, 141, 172, 170] For example, Raymond and coworkers published a water-soluble M_4L_6 tetrahedron which selectively included small alkanes like *n*-pentane whereas bigger alkanes like *n*-decane were not incorporated.[171] This is a nice example for the size-selective inclusion of guest molecules into metallo-supramolecular hosts. The inclusion of the guests was driven by the hydrophobic effect and weak *CH-π* interactions. The hydrophobic effect is a powerful tool for the inclusion of guests into the inner space of (metallo-supramolecular) hosts (see also chapter 3.3.4) and has been widely used. In combination with the hydrophobic effect, large aromatic guest molecules can template the formation of heteroleptic $M_6(L_A)_2(L_B)_3$ host complexes. These heteroleptic complexes contain *cis*-blocked square-planar metal centers combined with trigonal and tridentate ligands (A) and bidentate and linear ligand (B).[172] The shape of the hydrophobic aromatic molecule enables the selective formation of the heteroleptic host complexes around the guest molecules.[173, 174] Interestingly, metallo-supramolecular host complexes can also be used as molecular containers, which protect their included guests against the environment. For example, oxygen-sensitive white phosphorus was shown to be air-stable as well as water-soluble, when it was included into the inner cavity of a metallo-supramolecular tetrahedron. [175] This is an interesting example, wherein the host complex does not stabilize the guest by totally separation from the outer space, because the host complex has rather big holes. The transition state for the reaction of oxygen with P_4 is too large for the inner space of the host complex.[175]

Metallo-supramolecular complexes are also able to influence reactions. They can be used to catalyze reactions as well as to influence them in a way which leads to different products. In most cases, the reactions take place in the inner space of cage-like metallo-supramolecular complexes – like already discussed for the size-selective formation of silica nanoparticles inside a cuboctahedron.[160] The metallo-supramolecular complexes used act as molecular micro-reactors and thus they are an interesting tool for synthetic chemistry.[176]

The M_4L_6 tetrahedra established by Raymond and co-workers were able to catalyze several organic reactions.[177] For example, the M_4L_6 tetrahedron **74** catalyzes the hydrolysis of *ortho*-esters of formic acid and accelerates the reaction up to 3900 times (Figure 3.22).[178] Due to the hydrophobic effect, the *ortho*-ester is included into the M_4L_6 tetrahedron **74**. Then hydrolysis of the *ortho*-ester is catalyzed by **74**. Charge repulsion favors the exclusion of the negatively charged product out of the negatively charged tetrahedral complex **74**. Based on this, product inhibition does not take place and the complex can undergo the next catalytic cycle. The inclusion of guests into the host **74** is size-selective. The hydrolysis of small *ortho*-esters is catalyzed whereas no catalytic reaction is observed for pentyl or phenyl esters of formic acid. The catalytic behavior of **74** can be stopped by addition of a strong binding guest like Et_4N^+ to the reaction mixture.

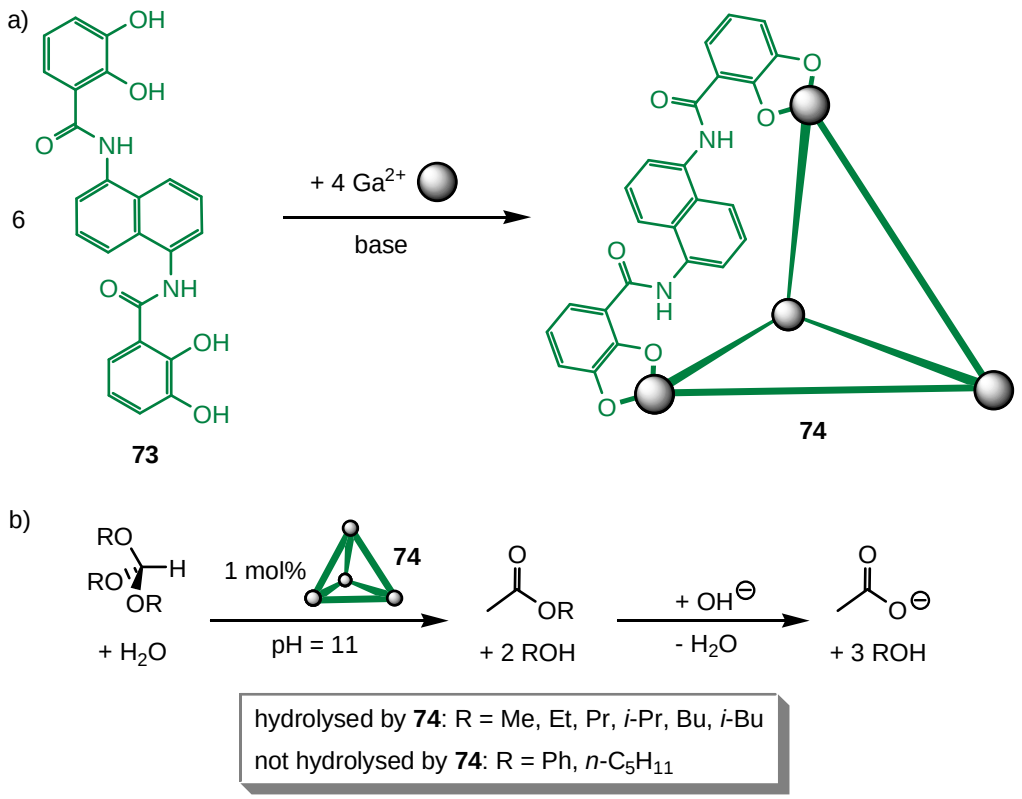

Figure 3.22: *a) The self-assembly of the metallo-supramolecular M_4L_6 tetrahedron **74**. b) The hydrolysis of ortho-esters of formic acid can be catalyzed by the M_4L_6 tetrahedron **74**.*[178]

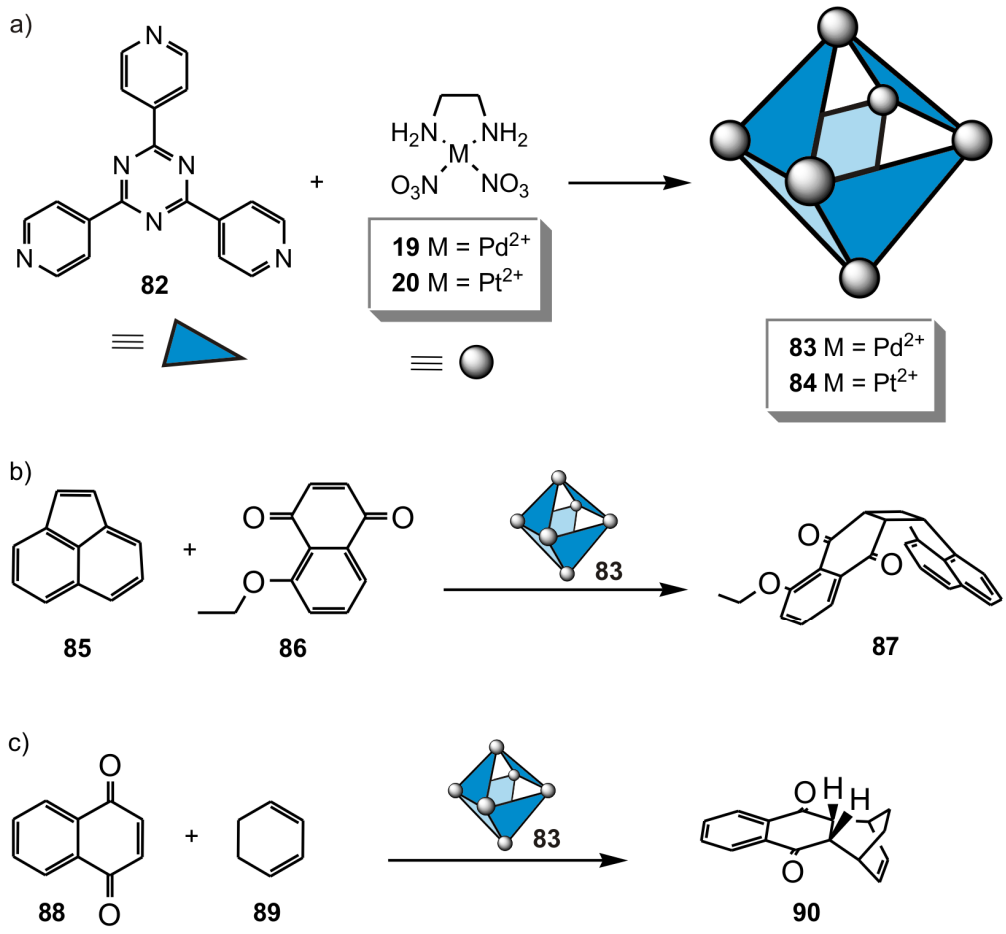

Figure 3.23: *a) The self-assembly of the metallo-supramolecular M_6L_4 complexes **83** and **84**.[134] b+c) Examples of reactions inside of metallo-supramolecular cage **83**: b) [2+2] cross-photodimerization of acenaphthylene **85** and 5-ethoxynaphthoquinone **86**[179] and c) Diels-Alder reaction of 1,4-naphthoquinone **88** with 1,3-cyclohexadiene **89**.[180]*

Fujita and co-workers published interesting pseudo-octahedral metallo-supramolecular M_6L_4 boxes (**83** and **84**) which contain the trigonal 2,4,6-tris(4-pyridyl)-1,3,5-triazine **82** as ligand and (en)$M(NO_3)_2$ (M = Pd^{2+} **19** or Pt^{2+} **20**) as metal centers (Figure 3.23a). The complexes have a very good solubility in water and bear a hydrophobic inner cavity which enables them to incorporate molecular guests.[134, 136] Based on this, the M_6L_4 box **83** was used to influence several organic reactions (Figure 3.23b and c).[176]

The inclusion of reactants into the complex **83** is based on the hydrophobic effect. The guest molecules can enter and leave the host complex through its relatively big holes. Nevertheless, the host complex **83** shows a certain size-selectivity for the inclusion of

guests. However, when two reactants react in a host complex like **83**, two different types of reactions can take place. On the one hand, only two different guests favorably enter the host which is called “AND-recognition”. On the other hand, two different guests as well as two identical guests can enter the host complex which is called “OR-recognition”. Complex **83** shows a relative preference for “AND-recognition”.[181] For example, in a mixture of *cis*-decaline and perylene only both molecules are included at the same time in complex **83**, but no inclusion of two *cis*-decaline or two perylene molecules is observed.[181] This selectivity has been used for a selective [2+2] photodimerization of two molecules like acenaphthylene **85** and 5-ethoxynaphthoquinone **86** resulting in the cross-dimers (here **87**) which otherwise would not be available in high yields (Figure 3.23b). Another example for “AND-recognition” is the Diels-Alder reaction of 1,4-naphthoquinone **88** with 1,3-cyclohexadiene **89** in a metallo-supramolecular M_6L_4 complex (Figure 3.23b).[180] The reaction was accelerated by 113 times and the product **90** could be extracted from the host complex using organic solvents. Due to their high solubility in water and their hydrophobic inner cavity, the M_6L_4 complexes established by Fujita and co-workers can also be used for the catalysis of phase-transfer reactions like Wacker-type oxidations.[135, 182] They could clearly show, that both, metal center **19** and ligand **82**, are necessary to gain a catalytic effect and the reaction takes place in the inner cavity of complex **83**.

However, besides the examples shown in here, several other metallo-supramolecular complexes[183, 184] have been tested as reaction vessels and as catalysts for many different reactions.[176, 185]

4. Mass Spectrometry

4.1 Mass Spectrometry in Supramolecular Chemistry: Ionization and Detection

Mass spectrometry (MS) can help chemists in many different ways to analyze their molecules, complexes or clusters. The most common way is to simply determine the mass over charge ratio (*m/z*) of a compound, because every different elemental composition results in a differing mass. Another asset is the isotopic pattern of an ion. It also reflects the elemental composition which thereby can be derived from the mass spectrum. Tandem mass spectrometry and gas-phase experiments offer several other analytical methods which can help to analyze chemical compounds and their behaviour (see below).[186]

However, mass spectrometry is an invasive analytical method. In order to examine a (supra-) molecular assembly by mass spectrometry, it has to be ionized. Many different ionization methods have been established, but most of them are not suitable to analyze supramolecular ensembles:[9, 187]

- Electron ionization (EI), chemical ionization (CI), atmospheric pressure chemical ionization (APCI), fast atom bombardment (FAB), secondary ion mass spectrometry (SIMS) and field desorption (FD) hardly or not at all useful to analyze supramolecules. They use high energies to ionize the substances or need other parameters which hamper the examination of supramolecules. High ionization energies would immediately destroy weakly aggregated supramolecules and thus these would not be detected. Nevertheless, some examples exist in which FAB or FD was used to analyze supramolecular assemblies.[187]
- In matrix-assisted laser desorption/ionization (MALDI) the sample is co-crystallized with a matrix which afterwards is irradiated by a laser. Ionization occurs by the attachment of H^+ or alkali metal ions. In many instances, MALDI is an adequate technique to analyze supramolecules. Nevertheless, sometimes the choice of less common, non-polar matrices together with special ion-labeling strategies[188] is required to keep the complexes intact.

- Electrospray ionization (ESI) and coldspray ionization (CSI) are soft ionization methods which are useful and often used techniques to analyze supramolecules (see the following chapters).
- Laser-induced liquid beam ionization/desorption (LILBID) and resonance-enhanced multiphoton ionization (REMPI) are relatively soft ionization techniques. These techniques are relatively new and their availability is limited. Nevertheless, first results on supramolecular systems using these ionization techniques are promising.[189, 190]

The mass analyzer is another integral part of every mass spectrometer.[187, 186] It separates the ions by their *m/z* value (m = mass, z = charge) utilizing electric and magnetic fields. Many different mass analyzers have been established during the last decades. They differ in their mass detection limits, their resolution and their mass accuracy. Many of them are capable of tandem MS experiments. The most common used analyzers in supramolecular chemistry are:[187]

- Quadrupoles (Q) and ion traps (IT) are low-cost analyzers with relatively low resolution and low mass accuracy. They have a certain use to analyze supramolecules but are limited by their properties. Ion traps can be used to store and manipulate ions. Thus, tandem MS experiments can be performed with IT.
- Time-of-flight (TOF) mass analyzers have the largest *m/z* range (modern linear TOFs have an *m/z* range of up to 40.000), the mass accuracy and the resolution of modern instruments are good as well. Tandem MS experiments can be performed using TOF/TOF instruments. Due to their high mass detection range, TOF analyzers are often combined with MALDI.
- Ion-cyclotron resonance (ICR) analyzers have a very good mass accuracy and the highest possible resolution. In principle, they are special versions of ion traps (IT). The *m/z* range of FTICR-MS instruments normally is somewhat limited (2000-8000 Da). ICR instruments are very expensive and therefore often not available. ICR analyzers can be used to store and

manipulate (MS^n) ions and are ideal to examine supramolecules (see next chapters).

- Orbitrap mass analyzers are suitable for the characterization of supramolecules as well. They have a high mass accuracy and resolution, but similar to ICR cells, the m/z range is limited to < 6000 Da. Tandem MS experiments are available, when the orbitrap is coupled to an ion trap.

4.2 ESI-FTICR Mass Spectrometry

Due to its soft ionization conditions, ESI mass spectrometry is the most common used technique to examine supramolecular systems.[187] Often, it is coupled with TOF, quadrupole, ion trap or ICR mass analyzers of which the ICR offers the largest variety of possible gas phase experiments. Most of the mass spectrometric experiments within this thesis were performed on an ESI-FTICR mass spectrometer. Thus, the principles of electrospray ionization (ESI) and the ion cyclotron resonance analyzer are explained here. The principles of electrospray ionization (ESI) allow the direct transfer of molecules from solution into the gas phase.[191, 192] The solutions have to be diluted to an appropriate concentration (normally 1-300 µmol/L). Within the instrumental setup of the mass spectrometer used within this thesis, the solution is injected into the ESI source using accurate syringes and a syringe pump. The injected solution is sprayed into the ESI source using an electric field (Figure 4.1). Due to the high electric potential at the end of the spray needle, a Taylor cone is formed. Depending on the electric field used, cations or anions are formed which are attracted by the counter electrode at the entrance of the mass spectrometer which has the opposite polarity of the attracted ions. Small positively or negatively charged droplets, respectively, are ejected from the Taylor cone. The droplets repulse each other and thus spread (Coulomb repulsion). Due to desolvation, often assisted by a heated gas flow, the droplets shrink and the charged particles in one droplet get closer to each other. When the Coulomb repulsion in a droplet is too high, the droplet splits in two or more parts, which occurs at the Rayleigh limit (equation 4.1). Thus, the limiting diameter *d* of a charged droplet is directly related to its charge *q*, the permittivity

ε_o of the environment around the droplet and the surface tension γ of the liquid (equation 4.2).

$$q = 8\pi^2 \varepsilon_0 \gamma d^2 \tag{4.1}$$

$$d = \sqrt[3]{\frac{q^2}{8\pi^2 \varepsilon_0 \gamma}} \tag{4.2}$$

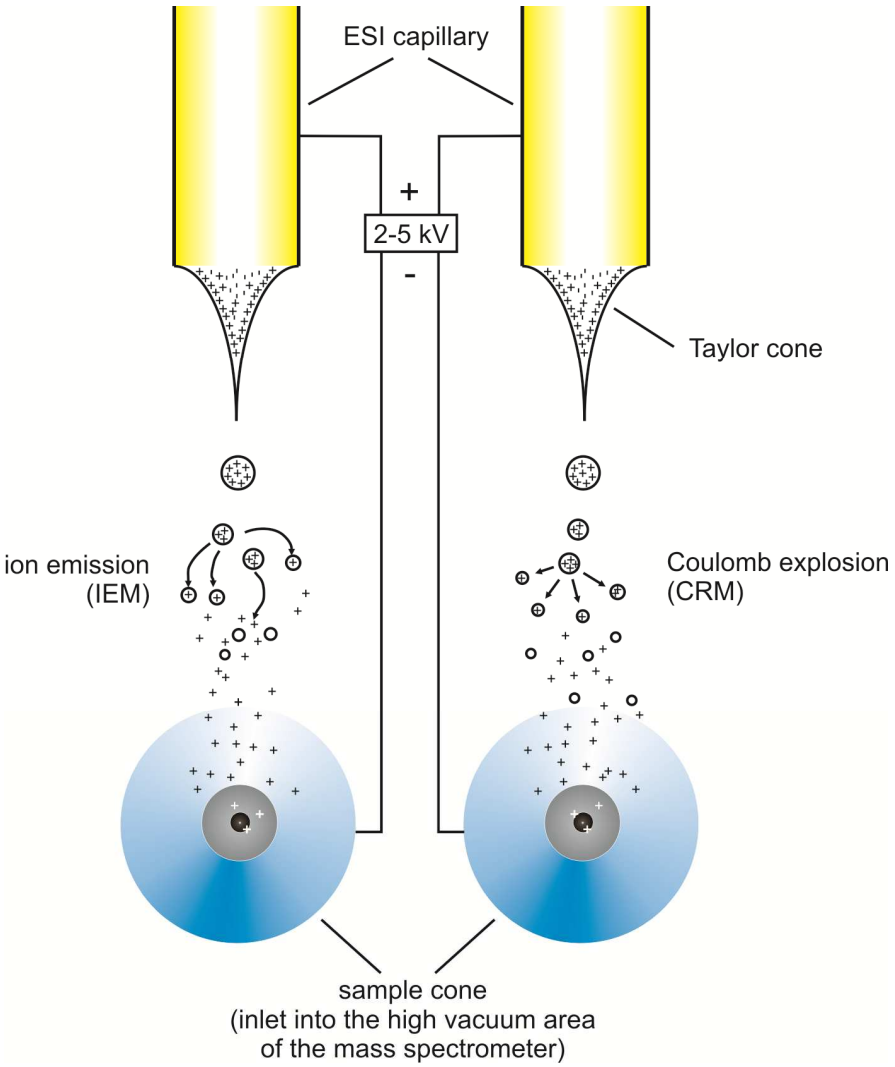

Figure 4.1: *The principles of the ESI process. The two most important electrospray ionization models are shown: the ion-evaporation model (IEM, on the left) and the Coulomb- explosion model (CRM, on the right).*[193]

Among others, two models exist to describe the formation of completely desolvated ions that enter the mass spectrometer:[9, 187, 186]

- The ion evaporation model (IEM) supposes that a single ion can "evaporate" from the surface of a droplet when the Coulomb repulsion is too high (Figure 4.1, left side).[194]
- The charge residue model (CRM) supposes that the splitting of the droplets goes on until the resulting droplets contain just single ions and some solvent molecules. The last solvent molecules can be easily evaporated and the "naked" ions are formed (Figure 4.1, right side).[191, 195]

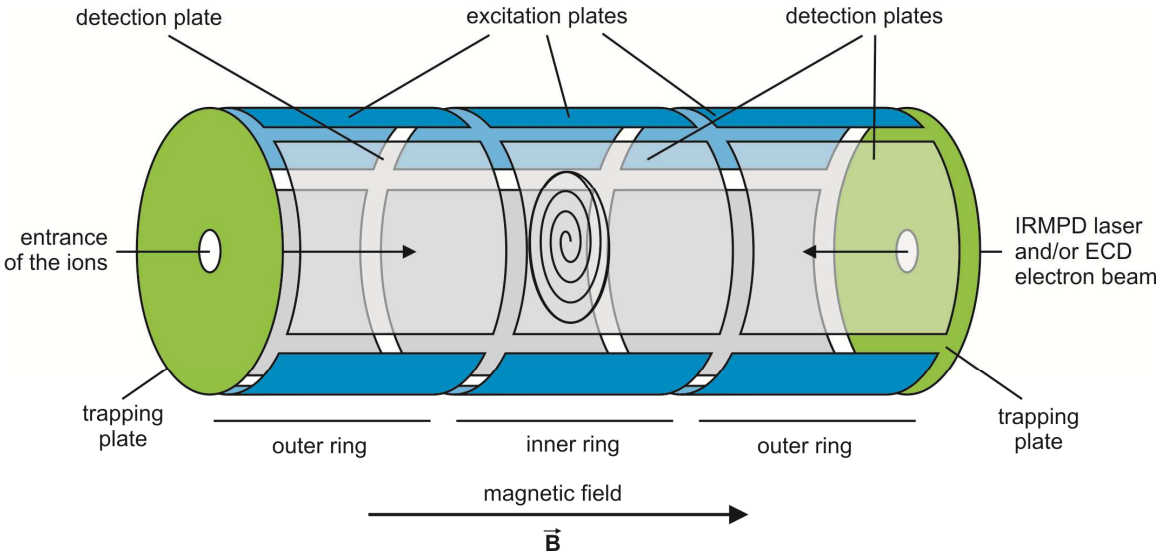

Figure 4.2: *Schematic overview of an ICR cell and its three different opposing sets of electrode plates: trapping plates (green), excitation plates (blue) and detection plates (grey).*[187, 193]

When the ions enter the mass spectrometer, they are collected and sent into the ICR cell (Figure 4.2) as ion packages. The technical basics of the ion cyclotron resonance analyzer can be traced back to the work of Lawrence and Livingston in 1932.[196] Besides some first examples,[197] Marshall and co-workers successfully introduced the ICR technique to mass spectrometry.[198] In a FTICR mass spectrometer, the cylindrical ICR cell is placed in the magnetic field of a superconducting magnet. The ions have a charge q and a velocity $\vec{v}$,

when they enter the ICR cell in z direction of the magnetic field $\vec{B}$. The magnetic field is perpendicular to the direction of the moving ions. The high magnetic field is used to bring the ions on a small orbit which is defined by the kinetic energy of the ions. During its circular movement, an ion is influenced by the Lorentz force F_L which equals its corresponding centrifugal force F_C (equation 4.3; m is the mass of the ion, r_m is the radius of the orbit an ion has in the ICR cell)).

$$\vec{F}_L = q\vec{v}\vec{B} = \frac{m\vec{v}^2}{r_m} = \vec{F}_C \tag{4.3}$$

Due to the strength of the Lorentz force, the ions stay at their orbits and do not escape from the cell in x and y directions. In order to keep the ions in the ICR analyzer and prevent their escape in z direction, the trapping plates are charged with the same potential as the ions under study and thus coulomb repulsion hinders the ions to escape.

The orbit of an ion perpendicular to the vector of the magnetic field $\vec{B}$ is depending on the mass m of the ion and its number z of elemental charges e (equation 4.4).

$$r_m = \frac{m\vec{v}}{q\vec{B}} = \frac{m\vec{v}}{ze\vec{B}} \tag{4.4}$$

When $\vec{v}$ is substituted with $r_m\omega_c$, the angular frequency ω_c becomes:

$$\omega_c = \frac{ze\vec{B}}{m} \tag{4.5}$$

Equation 4.5 shows that the angular frequency ω_c is a function of the constant magnetic field, the mass m and the charge z of the ion, but does not depend on the velocity of the ions. Thus, the angular frequency correlates directly with the m/z value of the ions under study and can be used to detect the ions.

The excitation plates can be used to manipulate the ions *via* radio frequency pulses. During the excitation with a transverse alternating high-frequency electrical field, the

ions accelerate and thus the radius r_m of their orbit in the ICR cell increases, but the angular frequency ω_c is not affected. The ions are shifted to larger orbits close to the detection plates. When the excitation ends, all ion packages are moving on their characteristic cyclotron orbits that have certain angular frequencies ω_c. Due to the circular motion of the charged ions, image currents are induced at the detection plates. These image currents are detected and enhanced. The resulting image current is the product of many superimposing frequencies. This current decreases over time, because the ions can collide with residual gas. Additionally, the coalescence of ion packages with similar *m/z* ratios plays an important role. Thus, the ion packages become incoherent. The resulting signal is called Free-Induction-Decay (FID) and is transformed into a frequency spectrum by means of Fourier-Transformation (FT). The frequencies correlate to *m/z* values and the amplitude of the signal provides information about the abundance of the ions.

Due to the extremely precise measurement of the frequencies as well as the continuous induction of image currents, very high resolutions and mass accuracies are available with FTICR instruments. The excitation of ions can be used to kick ions out of their orbits and neutralize them at the walls of the ICR cell. This ability enables a mass spectrometrist to isolate ions that are interesting for tandem MS or gas phase experiments.

4.3 Manipulation of Ions in the Gas Phase: Tandem Mass Spectrometry and Gas-Phase Chemistry

In order to perform experiments that can manipulate ions in the gas phase, one should think of the situation of the ions in the gas phase first. The transition of an ion from solution into the gas-phase represents a change of the environment. In solution, the intermolecular interactions between molecules compete with interactions between those molecules and the solvent, while the ions are isolated in the gas phase and no competition with solvent molecules exists anymore.

Binding enthalpies of non-covalent complexes usually increase upon transition into the gas phase: Electrostatic interactions are not attenuated anymore by the dielectricity constant ε of the solvent (vacuum: ε = 1, benzene: ε = 2.3, acetone: ε = 20.7, water: ε = 78.4). For example, the binding energy of two oppositely charged particles at a distance of 200 pm is 694 kJ/mol in vacuum, while it amounts only to 8.9 kJ/mol in water. The mere absence of competing solvent molecules already strengthens hydrogen bonding in the gas-phase. A particularly strong effect is however found for proton- or cation-bridged complexes. Charged hydrogen bonds such as that in the proton-bridged acetone dimer or in the phenol-phenolate hydrogen bond have binding energies up to 130 kJ/mol.[199] Solvophobic forces such as the hydrophobic effect do not exist in the gas-phase because of the absence of solvent. Entropic effects may counterbalance the increase in binding enthalpy to some extent. For example, the binding pocket of the host molecule is not empty in solution. Upon release of the guest, the pocket can be filled by one or even more solvent molecules so that the entropy remains constant or sometimes even decreases when the complex dissociates. In the gas phase, complex dissociation always leads to an entropically favorable increase in particle number.[200]

These differences between the gas-phase and the condensed phase may have drastic effects. A recent gas-phase study[201] showed unspecific binding of a carbohydrate to a protein to be even stronger than specific binding to the native binding site. Consequently, these effects have to be taken into account in data evaluation and interpretation of mass spectrometric results. Often, control experiments such as a test of the concentration dependence of complex formation are helpful to distinguish unspecific and specific binding.

It also has to be considered, that the temperature of isolated particles is ill-defined, because it is a macroscopic property of an ensemble of particles. Furthermore, no energy exchange can take place between the ions in the absence of collision partners. The ions thus are prone to have a non-Boltzmann distribution of internal energies. However, the internal energy distributions determine how many ions fragment and thus are directly connected to the appearance of a mass spectrum.[202] Ions only change their internal energies, if one of the following processes occurs: i) Collisions with gases, ii) IR photon exchange with the instrument walls,[203] and iii) fragmentation which distributes the ion´s

internal energy over the two fragments relative to their masses. Some of the excess internal energy is converted into the kinetic energy required to separate the two fragments.[204]

All of these considerations have to be taken into account, when (tandem) mass spectrometric experiments are performed. Now another question arises: What is tandem MS and how can ions be manipulated in the gas phase?

Tandem MS, MS/MS and MS^n are expressions referring to gas-phase experiments involving one (MS/MS or MS^2) or more (MS^n) mass-selection steps that are followed by a gas-phase experiment and either the next mass selection of one of the new fragments or a product ion scan. With tandem MS-capable instruments, mass spectrometry provides a whole laboratory to conduct ion chemistry in the gas phase. Once an ion is generated, many experiments are available which allow examining these ions under environment-free conditions. Before all these experiments can be performed, the ion of interest has to be mass-selected by removing all undesired ions from the ion beam or ion cloud. Soft ionization methods, in particular ESI, usually generate ions with a relatively low internal energy; therefore it is necessary to activate the ions under study in order to fragment them in a particular tandem-MS experiment.[205,206] Fragmentation reactions of the isolated ions can be induced by several different methods. In a collision-induced dissociation (CID) experiment, the ions are accelerated and then collided with an inert gas. Ion excitation can also be accomplished in an infrared multi-photon dissociation experiment (IRMPD) by irradiating them with an IR laser (10.6 µm). Electron-capture dissociation (ECD) and electron-transfer dissociation (ETD) are relatively new methods to induce fragmentation reactions. Single electrons derived from an electron-emitting cathode (ECD) or from a separately generated anion-radical (ETD) react with multiply charged cations. The electrons are transferred to the ion and not only reduce the charge state by one, but also induce radical-mediated fragmentation reactions. Besides fragmentation reactions, bimolecular reactions like H/D exchanges[207] can be carried out in ion trap or FTICR instruments.[187]

4.4 The Use of a Micro-Reactor - Online Mass Spectrometry

In many cases, common analytical methods are hampered by the fact that they cannot monitor fast processes in an appropriate way. It takes as well a certain time to prepare a sample as to put the sample into the analytical instrument. For fast reactions, these times maybe already too long to get sufficient information about them. However, mass spectrometry offers a way to observe intermediates of chemical reactions on-line.[208,209] This mass spectrometric method uses a mixed-flow micro-reactor, which is coupled to an ESI FTICR mass spectrometer (Figure 4.3). The reactants are separately dissolved in the same or different solvent(s). These solutions are placed in different syringes and transferred into the micro-reactor with a defined flow rate. The reactants mix in the micro-reactor and the mixed solution is transported through a capillary to the ESI source of a mass spectrometer. The use of defined flow rates and capillaries of defined length and diameter enables the investigation of reactions in the mixed sample solutions at defined reaction times. This is essential to identify different mechanistic steps and intermediates. Changing the flow rate or the length or diameter of the laminar flow tube influences the reaction time.[187]

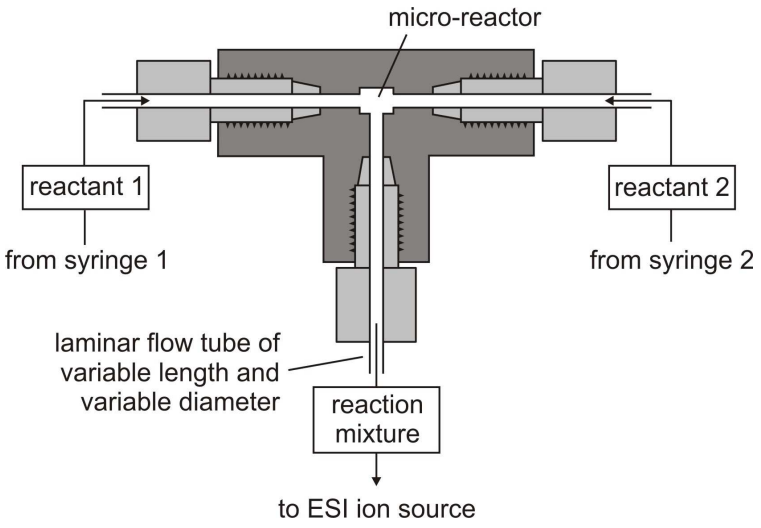

Figure 4.3: *A micro-reactor for mass spectrometric experiments.*[187]

4.5 ESI MS as a Tool in Metallo-Supramolecular Chemistry

Mass spectrometry and especially ESI MS (and CSI MS) has been shown to be a very helpful analytical tool in (metallo-)supramolecular chemistry.[9, 187] For example, the structures of interlocked molecules like catenanes and rotaxanes can be derived from a comparison of MS/MS spectra of the interlocked molecules with those of the corresponding non-interlocked aggregated structures.[210] Besides many other interesting application areas like ion recognition,[211] the characterization of dendrimers[212] or H/D exchanges in the gas phase,[207] ESI FTICR mass spectrometry has even been successfully used to characterize self-sorted supramolecular systems like pseudo-rotaxanes.[48]

However, in metallo-supramolecular chemistry ligand-exchange processes play an important role and mass spectrometry is the analytical tool of choice when differently composed ligands are used.[9, 187] Recently, Stang and co-workers reported about dynamic ligand-exchange processes of platinum-based metallo-supramolecular complexes (Figure 4.4).[213] They designed a metallo-supramolecular rectangle and a triangle containing 4,4´-bipyridines **26** or deuteratet 4,4´-bipyridines **91** as ligands. Both rectangles (**92a** and **92b**) and both triangles (**93a** and **93b**) were mixed and an exchange of ligands **26** and **91** was observed (Figure 4.4a and b). The ligand-exchange processes were monitored and after several days, a statistical distribution of the mixed complexes appeared when the thermodynamic equilibrium was reached. In another experiment, rectangle **92a** containing ligand **26** was mixed with triangle **93b** containing ligand **91** (Figure 4.4c). After several days, the thermodynamic equilibrium was reached and all possible rectangles and triangles were observed in the mass spectrum. Astonishingly, no complexes containing both metal centers (**54** and **59**) were detected.[213] However, these experiments nicely show that metallo-supramolecular systems are based on relatively weak intermolecular interactions that allow the exchange of building blocks although the complexes have already formed. Due to the similarity of ligands **26** and **91**, the intensities of the peaks in the mass spectra can be used to get quantitative information of the ligand-exchange processes.[213]

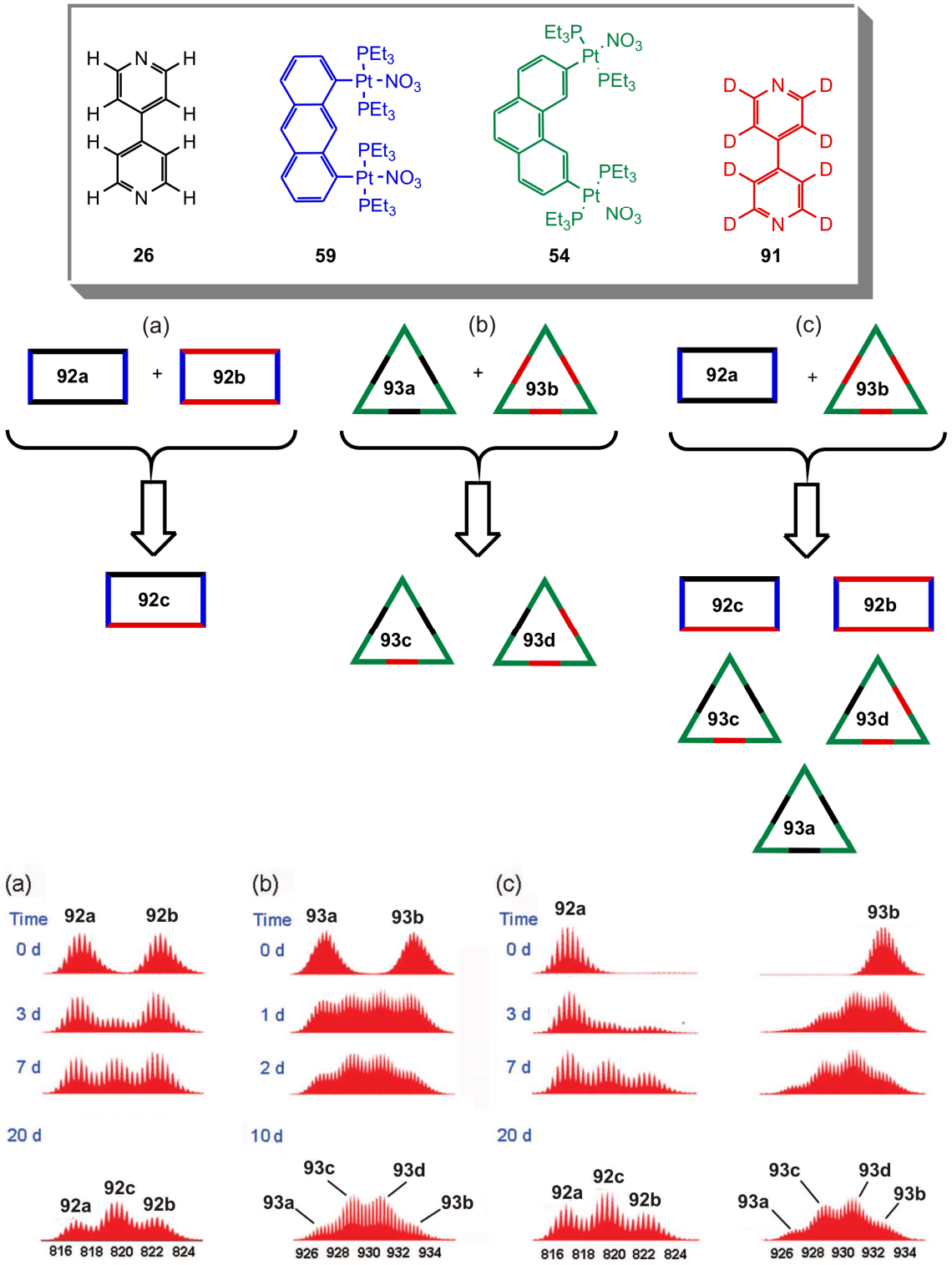

Figure 4.4: *Ligand-exchange experiments monitored by ESI mass spectrometry. Three different mixed systems are shown (a-c).*[213] *The Figure was adapted from Reference 213 with the kind permission of the American Chemical Society, © 2009.*

Another interesting aspect of metallo-supramolecular complexes is their behaviour in the gas phase when they are excited using IRMPD, CID or ECD to perform MS^n experiments.[9, 187] The fragmentation pattern of metallo-supramolecular species in the gas phase gives more evidence of the structures of these species. Interestingly, some examples of metallo-supramolecular polygons[105, 214] and cages[139] exist wherein an intramolecular nucleophilic substitution in the gas phase takes place. Due to a supramolecular neighbour-group effect, in the gas phase metallo-supramolecular squares can be transformed into the corresponding triangles induced by IR irradiation using an IRMPD laser.[105, 214] Similar processes take place in an IRMPD tandem MS experiment performed on ions of a metallo-supramolecular M_6L_4 cage. This cage undergoes a double cage contraction and ends up as a small M_3L_2 cage.[139] These are just some examples of the interesting possibilities mass spectrometry offers for (metallo-) supramolecular chemistry.[187]

5. Self-Assembly of Metallo-Supramolecular Architectures

5.1 Synthesis of Stang-Type Metal Centers

The Stang-type *cis*-blocked square-planar palladium(II) and platinum(II) metal centers containing 1,2-bis(diphenylphosphino)ethane **94** (dppe) or 1,3-bis(diphenylphosphino)-propane **95** (dppp) as auxiliary ligands, are some of the most frequently used metal centers in metallo-supramolecular chemistry.[1, 2, 80-83] Due to their precisely defined ligand-metal-ligand angle of 90° and their high solubility in organic solvents, these metal centers are interesting for the formation of many different two- and three-dimensional metallo-supramolecular architectures. Furthermore, the pre-organization of the metals using the auxiliary ligands supports the formation of discrete instead of polymeric structures.[80-83]

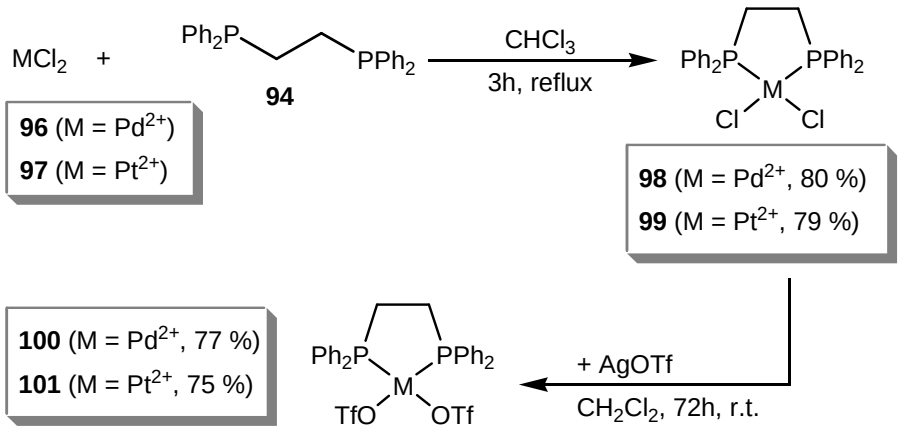

Figure 5.1: *Syntheses of the dppeM(OTf)$_2$ metal centers **100** (M = Pd^{2+}) and **101** (M = Pt^{2+}).*[215]

The two-step syntheses of the dppeM(OTf)$_2$ metal centers **100** (M = Pd^{2+}) and **101** (M = Pt^{2+}) start from palladium(II) chloride **96** or platinum(II) chloride **97**, respectively (Figure 5.1). Within the first step, palladium(II) chloride **96** or platinum(II) chloride **97** were mixed with equimolar amounts of 1,2-bis(diphenylphosphino)ethane **94** and the mixtures were dissolved in dry chloroform. After refluxing these mixtures for three hours, the products were isolated and purified. (1,2-bis(diphenylphosphino)ethane)palladium(II)

chloride **98** and (1,2-bis(diphenylphosphino)ethane)platinum(II) chloride **99** could be obtained in good chemical yields of 80 % and 79 %, respectively.

In the second step of the synthesis, the metal chlorides **98** and **99** were mixed with eight equivalents of silver(I) trifluoromethanesulfonate and suspended in dry dichloromethane. These mixtures were put into darkness and stirred for 72 hours at room temperature. After isolation and purification steps, (1,2-bis(diphenylphosphino)ethane)-palladium(II) trifluoromethanesulfonate **100** and (1,2-bis(diphenylphosphino)ethane)-platinum(II) trifluoromethanesulfonate **101** were isolated in good chemical yields of 77 % and 75 %, respectively.

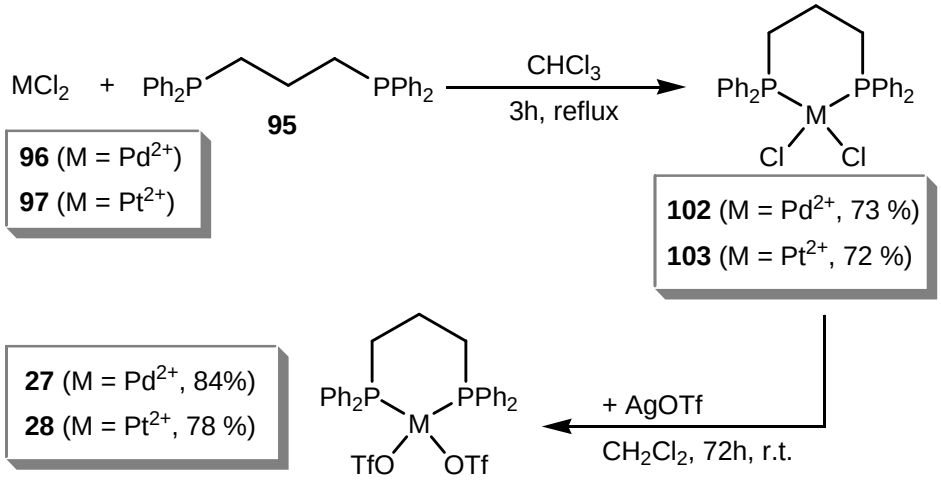

Figure 5.2: *Syntheses of the dpppM(OTf)$_2$ metal centers **27** (M = Pd^{2+}) and **28** (M = Pt^{2+}).*[215]

The syntheses of the dpppM(OTf)$_2$ metal centers (M = Pd^{2+}) and **27** (M = Pt^{2+}) **28** is analogous to that of dppeM(OTf)$_2$ (Figure 5.2). At first, (1,3-bis(diphenylphosphino)-propane)palladium(II) chloride **102** and (1,3-bis(diphenylphosphino)propane)platinum(II) chloride **103** were obtained in yields of 73 % and 72 %, respectively. In the second synthetic step, (1,3-bis(diphenylphosphino)propane)palladium(II) trifluoromethane-sulfonate **27** and (1,3-bis(diphenylphosphino)propane)platinum(II) trifluoromethane-sulfonate **28** were obtained in yields of 84 % or 78 %, respectively.

5.2 Self-Assembly as a Tool to Form Metallo-Supramolecular Complexes

5.2.1 The Self-Assembly of Metallo-Supramolecular M_2L_2 Complexes and Their Corresponding M_4L_4 Catenanes

The environment has a strong influence at the formation of metallo-supramolecular complexes. When cis-blocked square-planar metal centers are combined with flexible divalent ligands in organic solvents, normally the formation of metallo-supramolecular M_2L_2 macrocycles is preferred. On the contrary, the formation of catenanes can be observed, when the self-assembly occurs in water. This can be explained by the hydrophobic effect (see chapter 3.3.2).[63-77] In order to study the influence of the solvent at the formation of metallo-supramolecular macrocycles, several different divalent bis-pyridyl ligands (**104-112**) were combined with the (en)Pd$(NO_3)_2$ **19** and (dppp)Pd$(OTf)_2$ **27**, respectively. While complexes containing metal center **27** are soluble in organic solvents and rather insoluble in water, the behavior is completely opposite to that, when metal center **19** is used.[63-77] The project was performed in cooperation with Maurice Taszarek form the group of Professor H.-U. Reißig.[216]

In separate experiments, the ligands **104-111** were mixed with equimolar amounts of (en)Pd$(NO_3)_2$ **19** or (dppp)Pd$(OTf)_2$ **27**, respectively (Figure 5.3). When ligands **104-111** were combined with (dppp)Pd$(OTf)_2$ **27** and dissolved in DMSO or DMSO-d_6, respectively, the exclusive formation of M_2L_2 complexes **112-119** was observed. The situation is more complex, when the ligands are combined with (en)Pd$(NO_3)_2$ **19** in water or deuterated water, respectively. The self-assembly of ligands **104-107** with metal center **19** forms M_2L_2 complexes (**120-123**) as well, while equilibira between M_2L_2 complexes and their corresponding M_4L_4 catenanes (**124a/b-127a/b**) are observed for the combination of metal center **19** with ligands **108-111**. However, the mixtures were sonicated for 30 minutes at room temperature, in order to guarantee that the thermodynamic equilibria are monitored. This time is adequate, because normally palladium(II) complexes are kinetically labile and therefore the thermodynamic equilibrium is reached on a minute time-scale.[11] The solutions used for NMR experiments had a building block concentration of ca. 5 mM. For ESI mass spectrometry, the solutions were diluted with acetonitrile (systems **112-119**) or a 1:1 mixture of

acetonitrile and water (systems **120-127a/b**) to achieve a building block concentration of 100 µM. The self-assembled complexes **112-127a/b** were analyzed by NMR spectroscopy and mass spectrometry. All trials to crystallize one of these complexes failed and thus the structure assignment cannot be supported by crystal structure data.

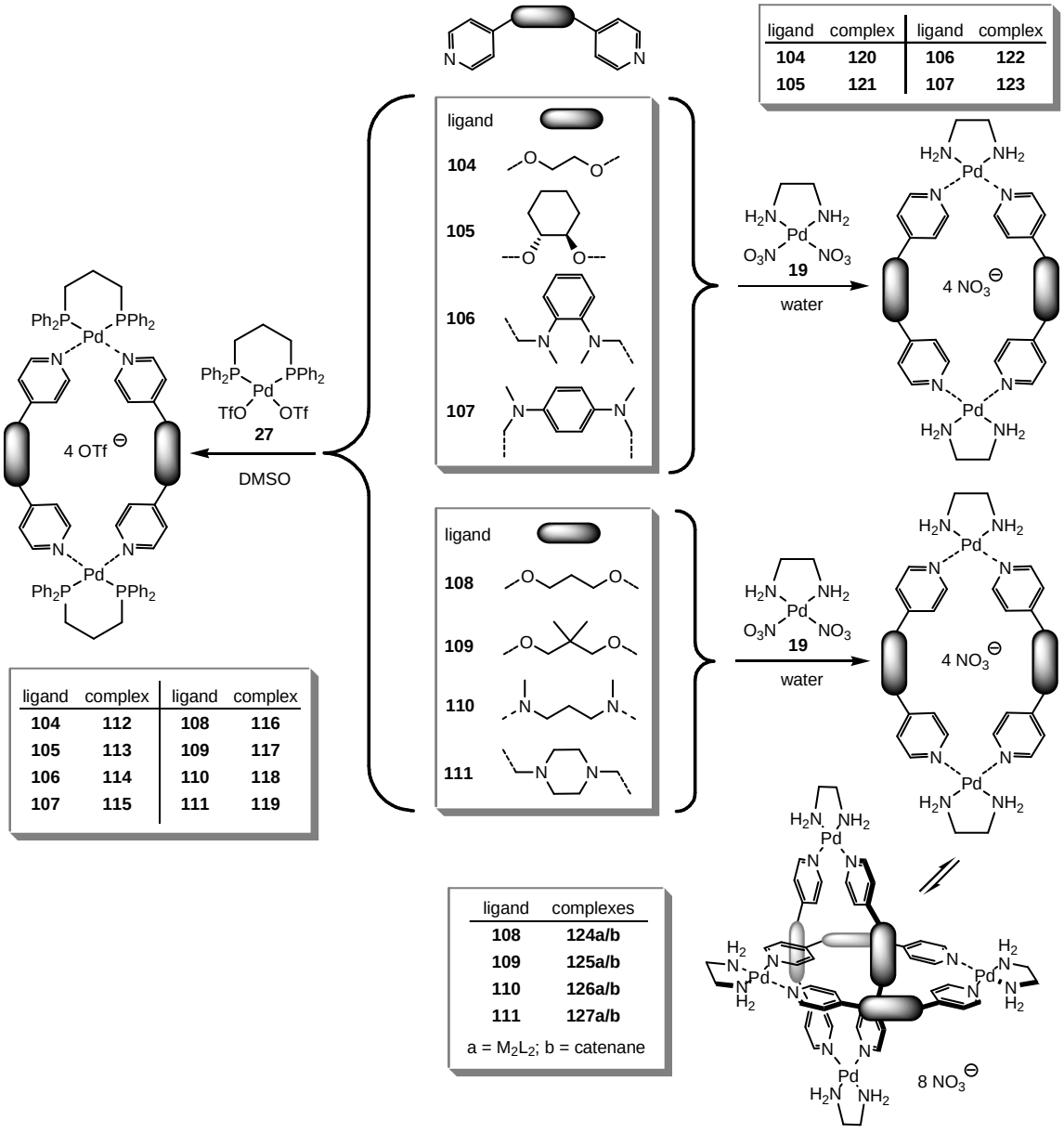

Figure 5.3: *Self-assembly of M_2L_2 complexes* ***112-123*** *and the equilibira between M_2L_2 complexes* ***124a-127a*** *and their corresponding M_4L_4 catenanes* ***124b-127b****.*

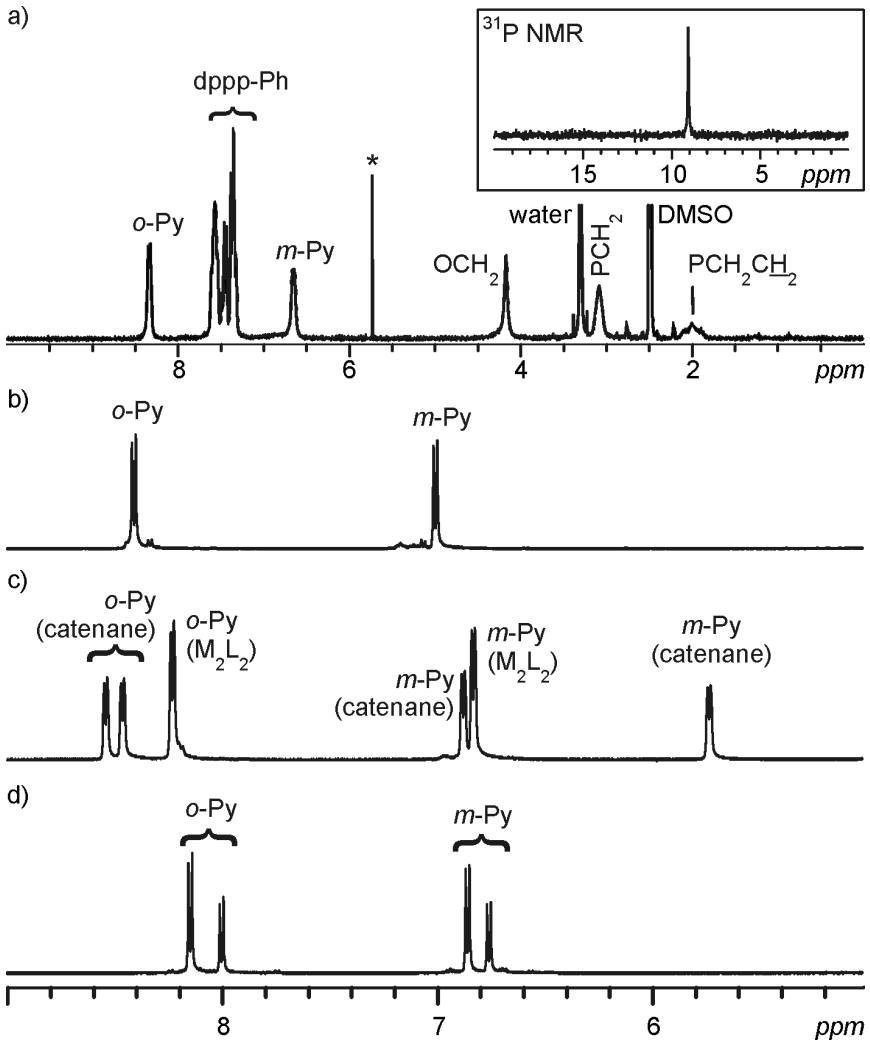

Figure 5.4: *a) The ^{1}H NMR and ^{31}P NMR spectra of the M_2L_2 complex **112** in DMSO-d_6 at room temperature. The signal marked with an asterix (*) can be assigned to traces of DCM. b-d) Partly ^{1}H NMR spectra of the M_2L_2 complex **120** (b), the equilibrium between M_2L_2 complex **124a** and M_4L_4 catenane **124b** (c) and the isomers of M_2L_2 complex **121** (d). The spectra shown in b-d were performed in D_2O at room temperature.*

The analysis of the assemblies by ^{1}H NMR spectroscopy clearly shows that the coordination of the ligands **104-111** to the metal centers **19** and **27** was successful. For all assemblies containing the Stang-type metal center **27** (**112-119**) as well as for complexes **120**, **122** and **123**, which bear the Fujita-type metal center **19**, only one set of signals was observed, respectively. The ^{1}H NMR spectra of the M_2L_2 complexes **112** and **120** are shown exemplarily (Figure 5.4a and b). For complexes **112-119**, also ^{31}P NMR

spectroscopy was performed. Due to the significant high-field shifts ($\Delta\delta \approx 8$ ppm) of the ^{31}P signals in coordination complexes (δ = 8-11 ppm) compared to (dppp)Pd(OTf)$_2$ **27**, the ^{31}P NMR spectra of the complexes are highly sensitive indicators for coordinating or non-coordinating (dppp)Pd(II) metal centers ($\delta \approx 18$ ppm).[106] Thus, the ^{31}P NMR spectra of the complexes **112-119** prove successful coordination and indicate the exclusive formation of one species in solution.

This situation has to be discussed in more detail for the assemblies containing ligand **105**. The chirality of ligand **105** has an influence at the complexes formed. A racemic mixture of the ligand was used in the self-assembly processes. Theoretically three different stereoisomers (two enantiomers (A and B) and one meso form (C)) of ligand **105** exist. When just the two enantiomers of **105** are present, two homoleptic (AA and BB) and one heteroleptic (AB) metallo-supramolecular M_2L_2 complexes should be observed. The two homoleptic complexes should be enantiomers and the heteroleptic meso-complex is a diastereomer of the homoleptic ones. Thus, two sets of signals should appear in the NMR spectra of the corresponding metallo-supramolecular systems **113** and **121**. Due to statistical distribution, the sets of signals should appear in a 1:1 ratio ({AA & BB}:{2 AB}). If also the meso-form of ligand **105** would be present, the number of possible complexes would increase (AA, BB, CC, AB, AC, BC) and thus the corresponding NMR spectra would be more complex.

However, the pyridine signals in the ^{1}H NMR spectrum of system **113** are broad and cannot be assigned to specific complexes. The ^{31}P NMR spectrum of **113** shows only one single peak. Based on that, the isomeric complexes can not be identified. Temperature-dependent NMR spectroscopy could help to solve this problem, because exchange processes between the isomeric complexes will slow down at low temperatures.

Interestingly, two sets of signals appear in a ratio of 10:3 when the chiral ligand **105** is combined with (en)Pd(NO$_3$)$_2$ **19** (Figure 5.4d). Concentration-dependent ^{1}H NMR spectra of system **121** showed no changes in the ratio of the sets of signals (Figure 5.5b). Thus, a possible equilibrium between a M_2L_2 complex and a M_3L_3 complex can be excluded as well as the presence of a M_4L_4 catenane. This gives evidence that these two sets of signals belong to at least two different isomers in system **121**. The ratio of 10:3 differs significantly from the expected ratio of 1:1, when both enantiomers of ligand **105** are

present and the corresponding complexes are formed in a statistical distribution. In order to get an appropriate characterization of the complexes in the systems **113** and **121**, the results have to be compared in future experiments with complexes which only contain one of the possible isomers of ligand **105**.

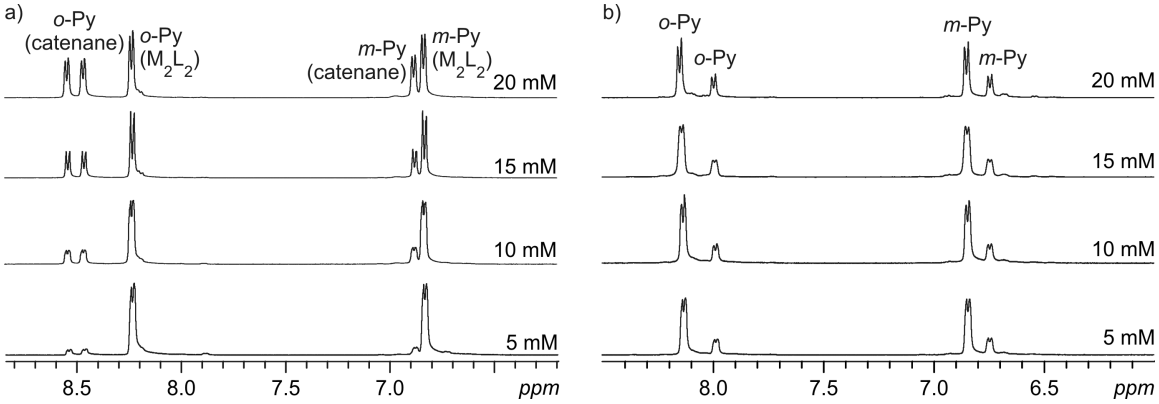

Figure 5.5: *Concentration-dependent ^{1}H NMR spectra of a) complexes **124a/b** and b) system **121**. The spectra show that the formation of catenanes like **124b** is concentration-dependent while the ratio of isomers in system **121** is not affected by changes of the concentration.*

In contrast to most of the metallo-supramolecular systems described before, two sets of signals were observed for the combination of ligands **108-111** with (en)Pd(NO_3)$_2$ **19** (Figure 5.4c). The signals were assigned to M_2L_2 complexes **124a-127a** and their corresponding M_4L_4 catenanes **124b-127b**. Due to the interlocked structure of the catenanes **124b-127b**, the chemical environment of the ligand-hydrogen atoms pointing inside the catenane is different from that of the ligand-hydrogen atoms pointing outwards. For example, the hydrogen atoms in *ortho* position to the pyridine-nitrogen atoms in system **124a/124b** show one sharp peak in case of the M_2L_2 complex **124a**, because all those hydrogen atoms have the same chemical environment. On the contrary, each pyridine unit of the catenane **124b** contains one hydrogen atom in *ortho* position to the pyridine-nitrogen atom pointing inside the catenane-structure while the other one points into the outer sphere. Thus, they have a different chemical environment and their ^{1}H NMR signal splits into two for catenane **124b** (Figure 5.4b). However, the presence of M_2L_2 complexes **124a-127a** and their corresponding catenanes **124b-127b** were

supported by concentration-dependent ^{1}H NMR experiments (Figure 5.5a) and ^{1}H, ^{1}H COSY NMR spectroscopy (Figure 5.6).

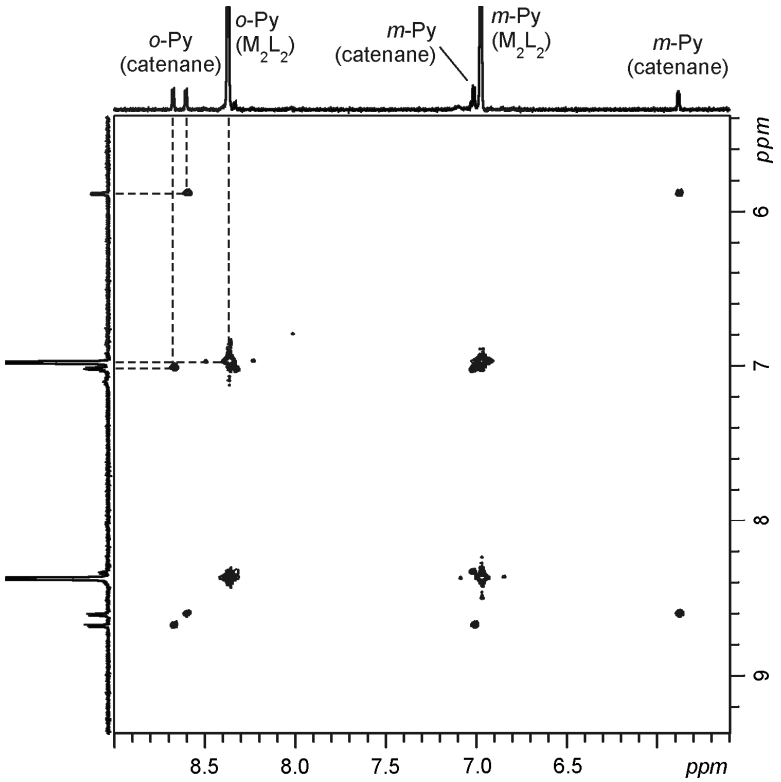

Figure 5.6: *The ^{1}H,^{1}H COSY NMR spectrum shows the relevant part of the system* ***124a/b****. The correlations between the peaks are shown by dashed lines.*

The equilibrium between the M_2L_2 complexes and their corresponding M_4L_4 catenanes is easily influenced by the concentration of the building blocks. At low concentration (5 mM), the smaller M_2L_2 complexes **127a-130a** are preferred while with increasing building block concentration the larger catenanes **127b-130b** are favored (Figure 5.5a). This can simply be explained by the different number of building blocks needed for the two types of complexes and their availability for complex formation. However, also the hydrophobic effect plays an important role in these equilibria. Starting from the M_2L_2 complexes, at higher concentrations M_4L_4 catenanes are formed instead of the entropically more reasonable M_3L_3 complexes. This can be ascribed to the hydrophobic effect, because in a catenane, the rings of two M_2L_2 complexes are filled. Thus the contact surfaces of the complexes with water are reduced compared to two M_2L_2 complexes or a possible M_3L_3 complex. The hydrophobic effect directs the self-assembly

process into the formation of catenanes and at the same time inhibits the formation of M_3L_3 complexes.

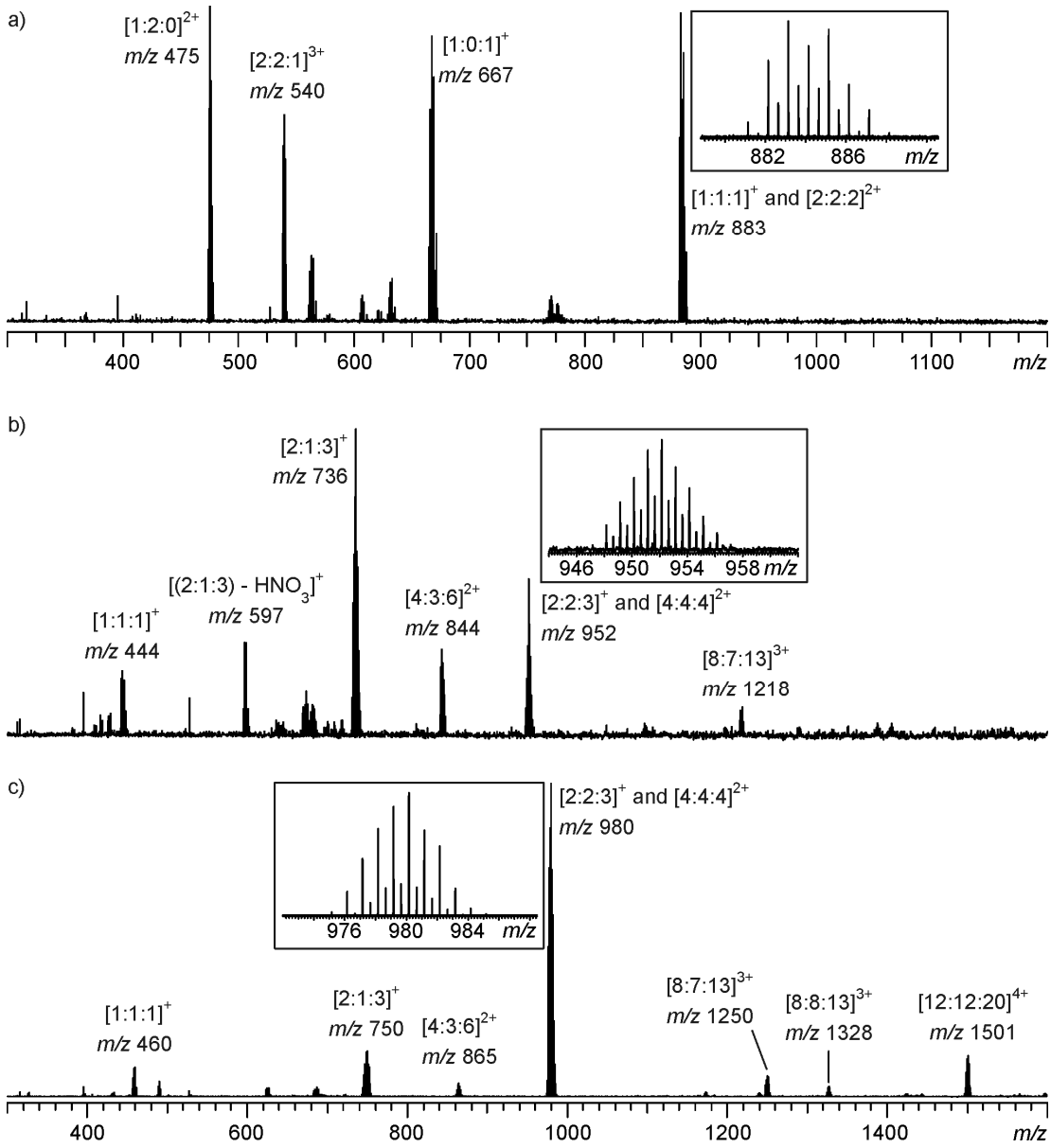

Figure 5.7: *The ESI mass spectra of a) the M_2L_2 complex **112**, b) the M_2L_2 complex **121** and c) system **124a/b**. The systems were measured with a building block concentration of 100 µmol/L.*

In order to identify the species under study, ESI FTICR mass spectrometry was used. In the ESI mass spectra, the following nomenclature is used: $[m:l:c]^{q+}$ (*m* stands for the

number of metal corners, *l* for the number of ligands, *c* for the number of counterions, and *q* for the number of charges). For all systems, M_2L_2 complexes (**112-127a**) were observed in the mass spectra (Figure 5.7). For example, the ESI mass spectrum of M_2L_2 complex **112** shows some peaks, which can be assigned directly to complex **112** (*m/z* 540 ($[2:2:1]^{3+}$) and *m/z* 883 ($[2:2:2]^{2+}$); Figure 5.7a). Due to partial fragmentation during the ionization process, other peaks refer to fragments of complex **112** (*m/z* 475 ($[1:2:0]^{2+}$), *m/z* 667 ($[1:0:1]^{+}$) and *m/z* 883 ($[1:1:1]^{+}$)). Similar results were observed for all other systems (**112-127a/b**). In many cases, also peaks were observed that correspond to oligomers of the M_2L_2 complexes. Interestingly, these peaks were mainly observed for systems containing Fujita-type metal centers (**120-127a/b**; Figure 5.7b and c). These oligomeric structures can be explained by the aggregation of two or more M_2L_2 complexes or fragments of them, which is known for ESI MS.[187] The presence of those peaks corresponding to oligomeric aggregates of the M_2L_2 complexes is no evidence for the formation of catenanes.

In conclusion, the coordination-driven self-assembly of relatively flexible divalent ligands (**104-111**) with (dppp)Pd$(OTf)_2$ **27** in DMSO results in the formation of small metallo-supramolecular M_2L_2 complexes **112-119**. When (en)Pd$(NO_3)_2$ **19** is used and the complexes are dissolved in water, the hydrophobic effect enables the formation of catenanes from M_2L_2 complexes (**124a/b-127a/b**). The catenanes are in equilibrium with their corresponding dinuclear complexes and no trinuclear complexes were observed. If the formation of catenanes in water is favored by the hydrophobic effect, it has to be considered, why no catenane formation was observed when ligands **104-107** were used. The only reasonable explanation for this observation is that the inner cavities of these M_2L_2 complexes are not large enough to support the formation of catenanes. Additionally, the metallo-supramolecular systems (**113** and **121**) containing chiral ligands offered interesting results which can be used for further studies. In order to get a better insight at the influence of chirality on the self-assembly of metallo-supramolecular complexes, it will be necessary to use the pure isomers of ligand **105** instead of a racemic mixture.

However, this study offered an interesting view into metallo-supramolecular self-assembly and the way the formation of the complexes can be influenced by their environment.

5.2.2 Equilibria between Metallo-Supramolecular Triangles and Squares

The equilibria between metallo-supramolecular triangles and squares are probably the best understood equilibria in metallo-supramolecular chemistry. The ratio between triangles and squares is determined by a sensitive balance between enthalpy and entropy. While entropy favors the formation of triangles, since a larger number of particles are formed from the same number of building blocks, enthalpy favors the formation of squares because ring strain is then minimized.[103-106] However, the characterization of these equilibria often raises analytical problems. In respect to the complexity of the equilibria between two or more metallo-supramolecular complexes, all common analytical methods are somehow limited. Thus, just the interplay of different analytic methods allows an appropriate characterization of those equilibria.[106]

In cooperation with Dr. Torsten Weilandt, Dr. Heidi Saxell and Professor Kari Rissanen, the equilibria between several metallo-supramolecular M_3L_3 triangles and their corresponding M_4L_4 squares were examined (Figure 5.8). The results presented in here have been published in *Inorganic Chemistry* in **2008**.[106]

All assemblies have been made by mixing stoichiometric amounts of the edge ligands **128**, **129**, **130**, or **131** and the corner complexes (dppp)Pd$(OTf)_2$ **27** or (dppp)Pt$(OTf)_2$ **28** in DMSO or DMF (Figure 5.8). These two solvents had to be used for solubility reasons, when the edge ligands contained either urea or amide groups. Furthermore, a wide temperature range is accessible for variable-temperature NMR experiments in DMF. The mixtures were thus stirred for a couple of hours at room temperature before analysis in order to make sure that the equilibrium situation is monitored. For NMR experiments, solutions with a building block concentration of 20 mM were used. The solutions for mass spectrometric analysis were prepared by dissolving the complexes in DMSO followed by dilution with acetone to a concentration of ca. 300 μM.

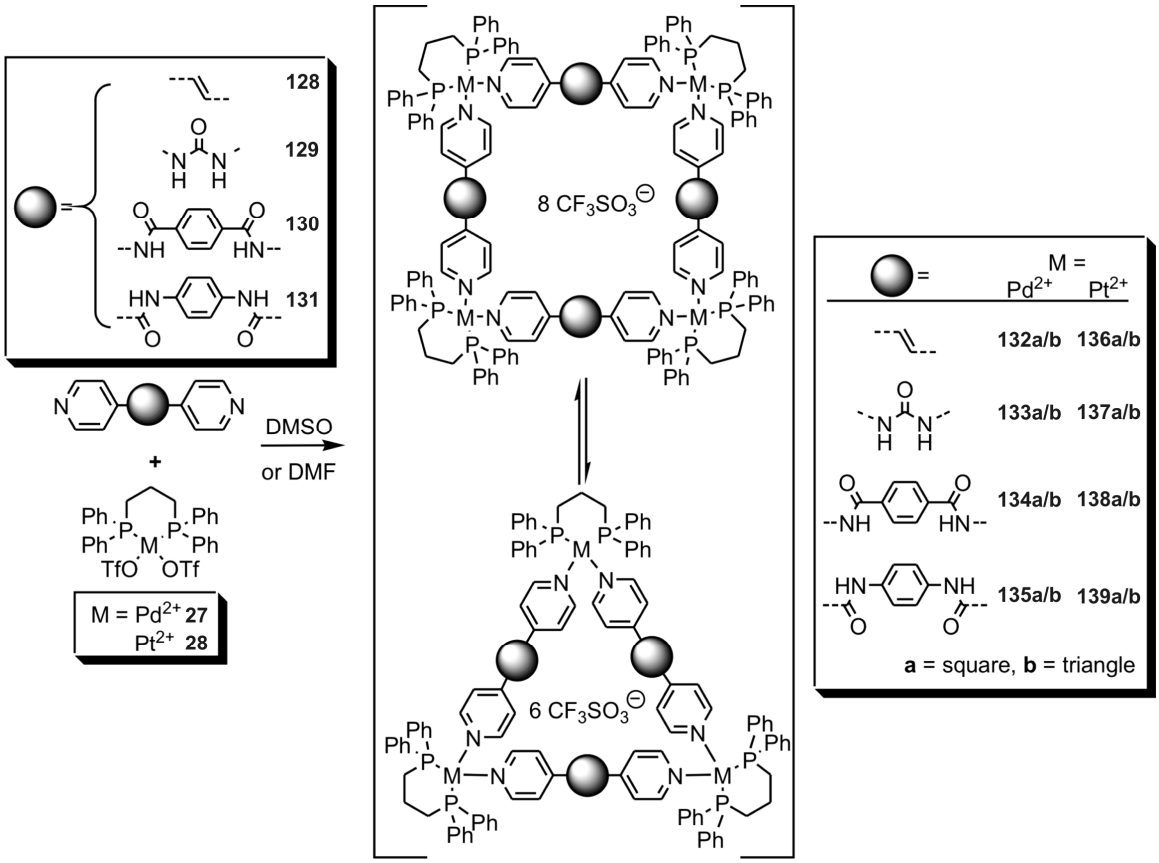

Figure 5.8: *The self-assembly of several Stang-type metallo-supramolecular triangles (**132a-139a**) and squares (**132b-139b**).*

The complexation of the pyridine nitrogens to the metal centers can be deduced from the complexation-induced signal shifts to higher field typically observed in the ^{31}P NMR spectra. A particularly reliable indicator of complex formation is the ^{195}Pt-P coupling constant of the pyridine complexes ($^{1}J_{Pt\text{-}P}$ = 3022-3045 Hz), which significantly differs from that of precursor **28** ($^{1}J_{Pt\text{-}P}$ = 3657 Hz). Clearly, two species exist in solution for **136a/b** and **140a/b** (Figure 5.9) as indicated by the ^{31}P NMR spectra. A comparison of the ^{1}H NMR signals of the building blocks with those of the complexes reveals that small but significant chemical shift changes occur. A closer inspection of the ^{1}H NMR spectra also reveals two different sets of signals, some of which are superimposed. The ^{1}H NMR signals of the platinum complexes are sharper at room temperature than those of the palladium analogues (Figure 5.9). This can be rationalized by dynamic ligand-exchange processes whose rates depend on the metal centers and the ligands used (see below).

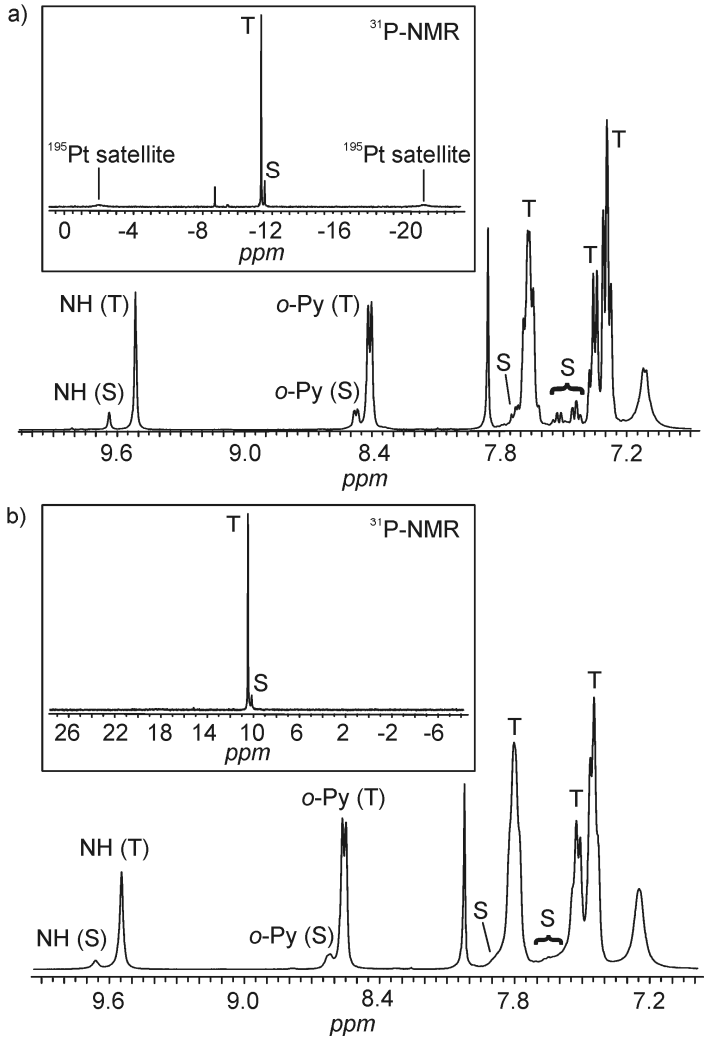

Figure 5.9: *^{1}H NMR and ^{31} P NMR spectra of a)* ***137a/b*** *and b)* ***133a/b*** *(S = square, T = triangle).*

To prove the simultaneous existence of squares and triangles in solution, Pulsed Field-Gradient Spin-Echo NMR (PGSE) experiments were performed. By measuring the diffusion coefficients, it is possible to determine the sizes of supramolecular compounds experimentally. The diffusion coefficients correlate with the size and the shape of the compounds. As a rough approximation, the different species under study were approximated as spheres, assuming that the fast rotation of the "discoidal" compounds on average leads to a sphere. With this approximation, the size of the different species can be calculated from the measured diffusion coefficients by the Stokes-Einstein equation

(equation 5.1), where T is the absolute temperature, k_B the Boltzmann constant, r the hydrodynamic radius, and η the solvent viscosity at temperature T.[217]

$$D = k_B T/6\pi\eta r \quad (5.1)$$

As representative examples, only the results of the ^{1}H DOSY NMR spectra of **133a/b** and **137a/b** will be discussed in detail. In all mixtures under study, the NH and *o*-pyridine protons are sufficiently separated from other signals so that they can easily be used for the DOSY measurements. Large structures have smaller diffusion coefficients than small ones. If squares and triangles coexist, two different sets of signals should thus be observed in the DOSY NMR spectra. Figure 5.10a shows the DOSY spectrum of **133a/b** at room temperature in DMSO-d_6. In the ^{1}H and ^{31}P NMR spectra, two sets of signals are clearly visible – a smaller one, which is tentatively assigned to the square, and a more intense one for the triangle. However, both sets of signals appear in the DOSY NMR spectrum with the same diffusion coefficient. This finding can be traced back to the three different time scales in the ^{1}H, ^{31}P, and DOSY NMR experiments. While the ligand exchange is slow on the ^{1}H and ^{31}P NMR experiments, it is fast on the DOSY time scale which works with a diffusion delay in its pulse sequence. At 273 K in DMF-d_7, the exchange becomes significantly slower so that two different diffusion coefficients for square and triangle can be determined for **133a/b** (Figure 5.10b). The diffusion coefficients calculated from the latter spectrum confirm the assignment of the square to the less intense signal and identifies the more intense signal with the triangle.

For the analogous platinum complexes **137a/b**, two different diffusion coefficients were already observed in DMSO-d_6 at room temperature (Figure 5.10c). Clearly, the exchange between **137a** and **137b** is slow even on the DOSY NMR time scale under these conditions. This confirms the triangle-square exchange to be faster for the Pd than for the Pt compounds. Again, the less intense signal corresponds to the square. Qualitatively, the other complexes under study yield similar results. The experimental data of the ^{1}H DOSY NMR measurements of **132a/b** to **139a/b** are summarized in Table 5.1.

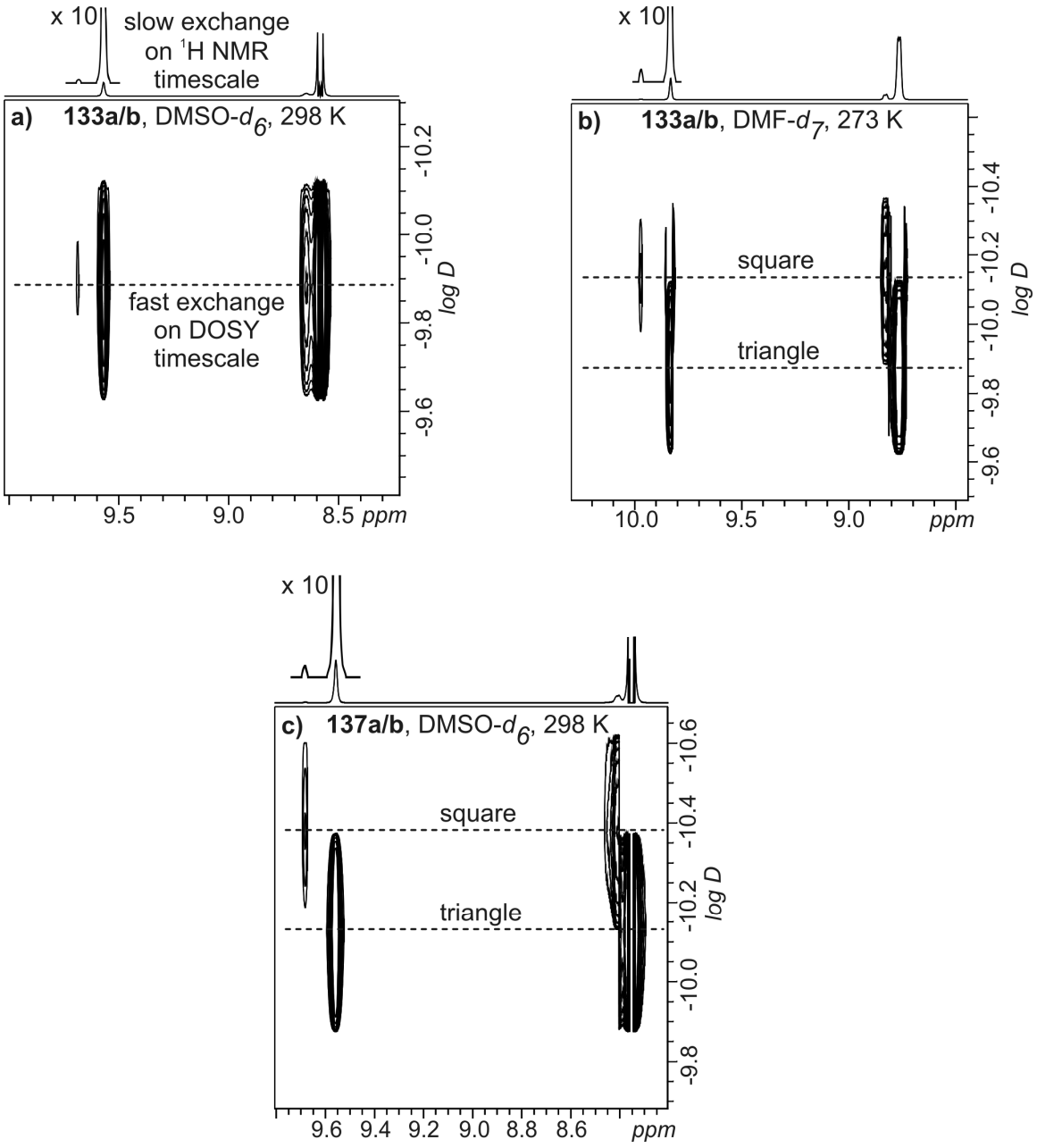

Figure 5.10: *The 2D DOSY NMR spectra of a)* ***133a/b*** *recorded at 298 K in DMSO-d_6 (fast exchange), b)* ***133a/b*** *recorded at 273 K in DMF-$_{d7}$ (slow exchange), and c)* ***137a/b*** *recorded at 298 K in DMSO-d_6.*

For a comparison with the experimental radii obtained from the DOSY NMR experiments, the geometries of triangles and squares were optimized with the MM2 forcefield implemented in the Cache program.[218] Different conformers have been explicitly considered in the calculations, although they have similar energies and

geometry parameters (defined in Figure 5.11 for **133a/b**). Consequently, we chose only the smallest conformer as a representative for determining the calculated geometry data summarized in Table 5.1. Ligand **129** is slightly bent because of the central urea unit. Nevertheless, triangles and squares form rather than M_2L_2 complexes because the two pyridines at each metal corner prefer to adopt a geometry perpendicular to the M-M-M-M plane. The ligand bending thus does not help to reduce strain in **133a/b** and **137a/b**.

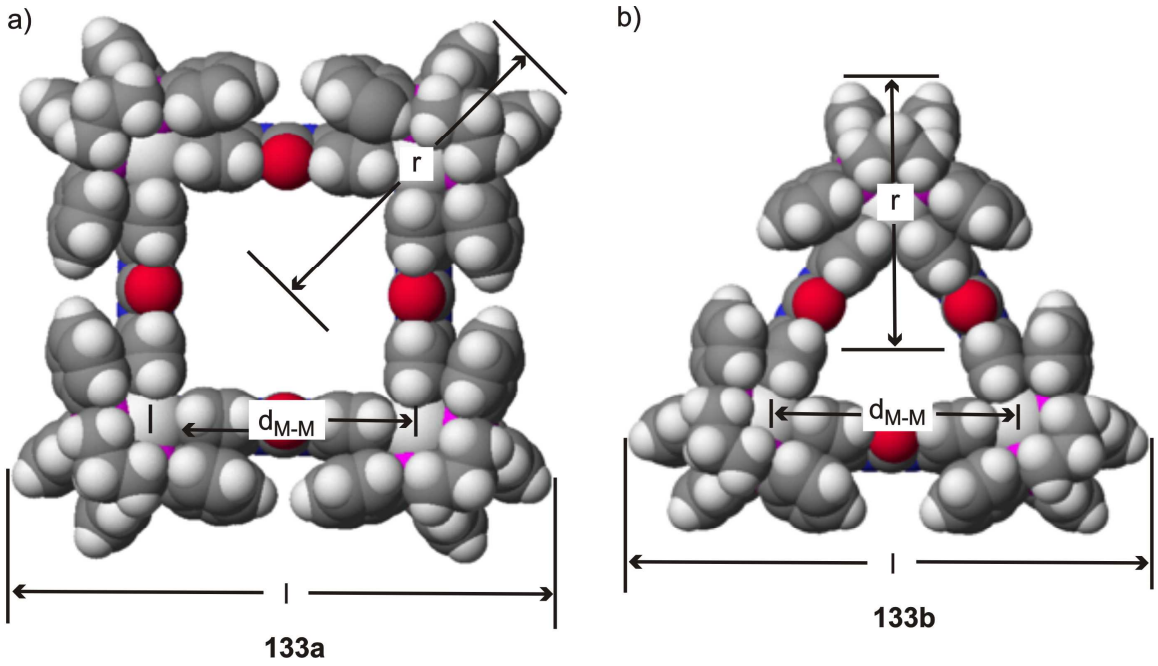

Figure 5.11: *MM2 force-field-optimized structures of* ***133a/b*** *in space-filling representation. Only the largest of the different conformers is shown.*

In good agreement with the X-ray crystal structure data of triangle **132b** below, the calculated N-M-N angles of triangle **133b** are between 86.4° to 88.7° and thus are close to the expected value of 90°. This shows most of the triangle strain to be compensated by ligand bending (also see crystallography part below). The rigidity of the ligand plays thus an important role for the triangle-square equilibrium. In both structures in Figure 5.11, π-π interactions between each pyridine ring and one of the dppp phenyl rings are visible.

Table 5.1: *Diffusion coefficients D experimentally determined from DOSY NMR experiments, radii r_{exp} calculated from them based on the Stokes-Einstein equation, and geometry parameters r_{calc}, $d_{M\text{-}M}$, and l (Figure 5.11) obtained from molecular modeling calculations with the augmented MM2 force field.*

Compound	***T*** [K]	***D*** [m^2s^{-1}]	r_{exp} [nm]	r_{calc} [nm]	$d_{M\text{-}M}$ [nm]	***l*** [nm]
132a	298[a]	$2.42 \cdot 10^{-10}$	1.036	1.64	1.34	2.71
132b	298[a]	$2.42 \cdot 10^{-10}$	1.036	1.40	1.32	2.79
132a	273[a]	$1.36 \cdot 10^{-10}$	1.252	1.64	1.34	2.71
132b	273[a]	$1.41 \cdot 10^{-10}$	1.209	1.40	1.32	2.79
132a	243[a]	$4.19 \cdot 10^{-11}$	2.044	1.64	1.34	2.71
132b	243[a]	$4.73 \cdot 10^{-11}$	1.809	1.40	1.32	2.79
133a	298[a]	$2.06 \cdot 10^{-10}$	1.328	1.63	1.43	2.66
133b	298[a]	$2.17 \cdot 10^{-10}$	1.267	1.36	1.41	2.67
133a	273[a]	$1.30 \cdot 10^{-10}$	1.303	1.63	1.43	2.66
133b	273[a]	$1.41 \cdot 10^{-10}$	1.203	1.36	1.41	2.67
134a	273[a]	$9.32 \cdot 10^{-11}$	1.861	2.08	1.96	3.36
134b	273[a]	$9.68 \cdot 10^{-11}$	1.791	1.68	1.93	3.37
134a	243[a]	$5.07 \cdot 10^{-11}$	1.774	2.08	1.96	3.36
134b	243[a]	$5.64 \cdot 10^{-11}$	1.595	1.68	1.93	3.37
135a	273[a]	$1.21 \cdot 10^{-10}$	1.455	2.08	1.96	3.34
135b	273[a]	$1.23 \cdot 10^{-10}$	1.427	1.71	1.93	3.43
135a	243[a]	$5.86 \cdot 10^{-11}$	1.766	2.08	1.96	3.34
135b	243[a]	$6.51 \cdot 10^{-11}$	1.590	1.71	1.93	3.43
136a	298[b]	$1.79 \cdot 10^{-10}$	1.535	1.66	1.35	2.71
136b	298[b]	$2.03 \cdot 10^{-10}$	1.350	1.40	1.33	2.79
137a	298[b]	$7.18 \cdot 10^{-11}$	1.524	1.64	1.44	2.66
137b	298[b]	$8.34 \cdot 10^{-11}$	1.311	1.36	1.42	2.70
138a	298[b]	$1.60 \cdot 10^{-10}$	1.709	2.10	1.96	3.43
138b	298[b]	$1.91 \cdot 10^{-10}$	1.439	1.70	1.93	3.37
139a	298[a]	$1.54 \cdot 10^{-10}$	1.779	2.09	1.97	3.35
139b	298[a]	$1.85 \cdot 10^{-10}$	1.478	1.72	1.94	3.43

[a] Experiment performed in DMF-d_7 ($\eta_{243\,K}$ = 1.979 g $m^{-1}s^{-1}$, $\eta_{273\,K}$ = 1.154 g $m^{-1}s^{-1}$, $\eta_{298\,K}$ = 0.811 g $m^{-1}s^{-1}$). The viscosity for 243 K is extrapolated from literature data.[219]

[b] DMSO-d_6 with $\eta_{298\,K}$ = 1.996 g $m^{-1}s^{-1}$

Three conclusions can be drawn from a comparison of the experimental and calculated radii. (i) The two species present in solution are triangles and squares. Even if the absolute, but approximate, experimental radii do not perfectly fit the calculation, the calculated radii of other possible species such as pentameric or hexameric complexes give a much worse agreement with the experimental data. (ii) Except for the lowest temperature (243 K), the experimentally determined radii are always somewhat smaller than the calculated ones. This can be attributed to the approximation of the rather discoidal complexes as spherical ones and the cavity in the complex, which reduces the effective diffusion coefficient additionally. At 243 K, the experimental radii are larger than the calculated ones, likely because the viscosity of the solvent had to be extrapolated to this temperature. (iii) Irrespective of the solvent, the temperature, or the metal used, the squares always give smaller diffusion coefficients and therefore larger experimental radii than the corresponding squares.

Because of the weak coordinative bonds of the supramolecular assemblies, ESI is used as a soft ionization method. The compounds under study can be ionized in the ESI ion source by stripping off some counterions, thus generating complexes in different charge states. Figure 5.12a shows the electrospray ionization Fourier transform ion-cyclotron resonance (ESI-FTICR) mass spectrum of **133a/b**. In addition to smaller peaks resulting from fragmentation of larger complexes, two major peaks are observed: (i) Signals for a singly charged $[2:2:3]^{+}$ fragment are superimposed with signals for doubly charged $[4:4:6]^{2+}$ (squares) and triply charged $[6:6:9]^{3+}$ (dimer of triangles) complex ions at *m*/*z* 1911 (in our $[m:l:c]^{q+}$-nomenclature, *m* stands for the number of *m*etal corners, *l* for the number of *l*igands, *c* for the number of *c*ounterions, and *q* for the number of charges). The $[4:4:6]^{2+}$ signals are quite weak indicating a small fraction of squares to be present. (ii) The other main peak at *m*/*z* 1396 corresponds to the superposition of quite abundant $[3:3:4]^{2+}$ complexes (triangle) and less abundant $[6:6:8]^{4+}$ complexes (dimer of triangles). Unspecific aggregation, which is the reason for the 6:6 complexes, is very typical for ESI-MS experiments of salts, and it is found for many similar species.[105] One can think of these ions as anion-bridged dimers of cationic triangles mainly held together by electrostatic forces. In good qualitative agreement with the NMR spectra, the mass spectrum thus clearly exhibits more intense signals for triangles than for squares.

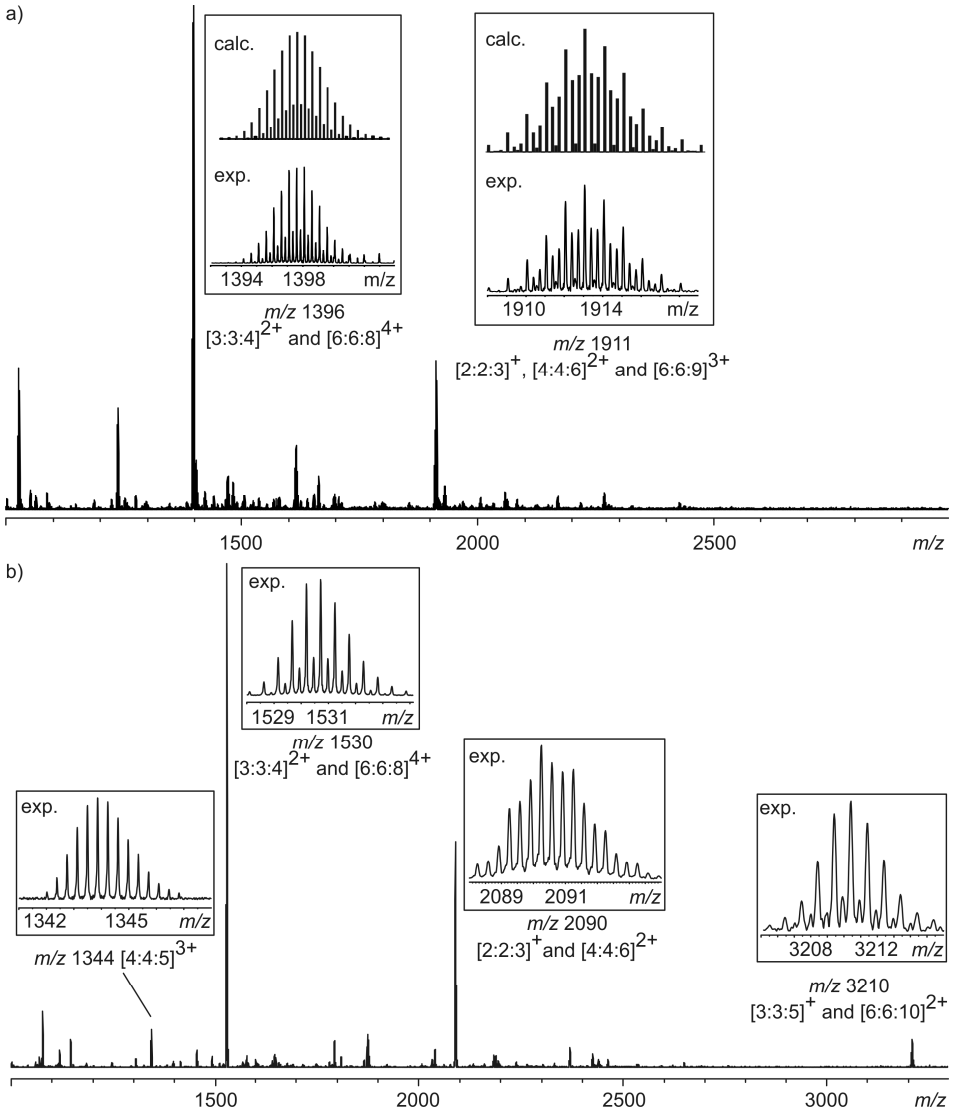

Figure 5.12: *The ESI mass spectra of a)* ***133a/b*** *and b)* ***137a/b****.*

A similar mass spectrum (Figure 5.12b) is observed for the analogous Pt compounds. The peak at *m*/*z* 1344 corresponds to a $[4{:}4{:}5]^{3+}$ square, which is not superimposed by other signals. Again, the signals for the triangles at *m*/*z* 1530 ($[3{:}3{:}4]^{2+}$) and *m*/*z* 3210 ($[3{:}3{:}5]^{+}$) are more intense than those for the squares and superimposed by unspecific dimer ions. Fragmentation, however, is less pronounced for the Pt complexes as compared to the Pd complexes.

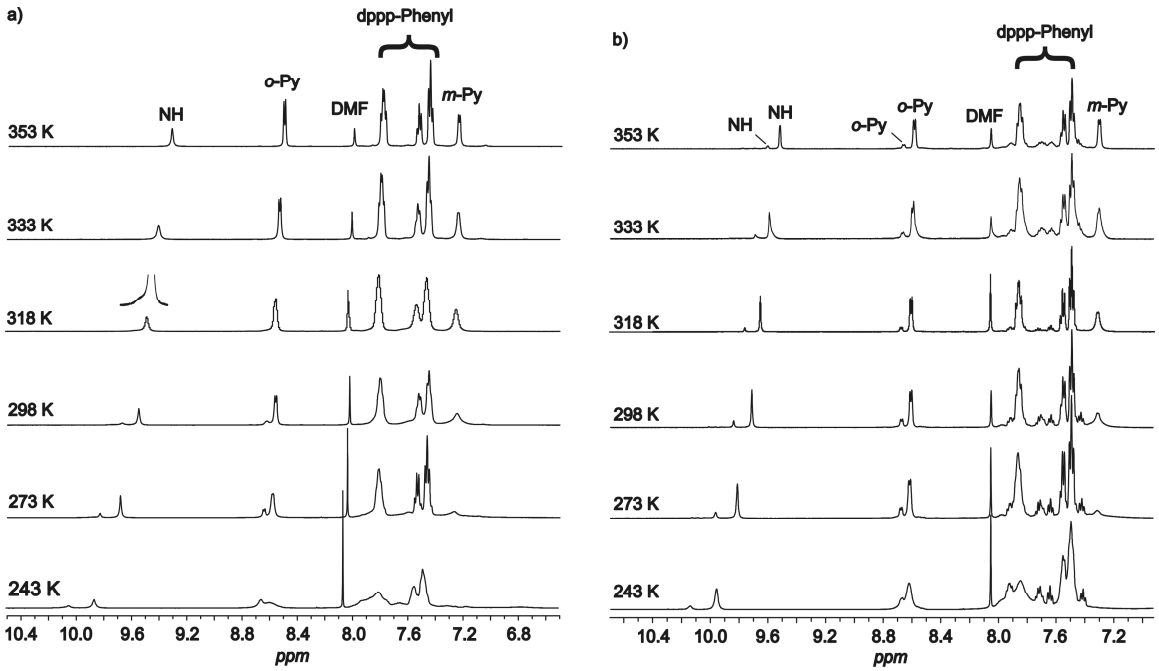

Figure 5.13: *Aromatic regions of the variable-temperature ^{1}H NMR spectra of a)* ***133a/b*** *and b)* ***137a/b*** *in DMF-d_7.*

Equilibria can be influenced significantly by changing temperature, concentration, or solvent. Similarly, the kinetics of the exchange processes may be altered by both parameters. Therefore, an examination of these effects is important to get a more complete picture of the complexes under study.

At 353 K, only one set of sharp, well resolved signals is observed in the NMR spectra of **133a/b** (Figure 5.13a), while two sets of signals appear at 273 K. The NH and *o*-pyridine protons are well separated, while most other signals are superimposed. Above the coalescence temperature is Tc ≈ 325 K (500 MHz), the equilibration of squares and triangles is fast on the NMR time scale for the Pd complexes. In the spectrum at 243 K, the signals are broader than those at higher temperatures. This can be traced back to the existence of different conformers which interconvert slowly at this temperature. Different conformers exist because of the chair-chair interconversion of the diphosphametalla-cyclohexane rings at each corner. At the same time, the dppp phenyl groups that stack with the pyridines hamper ligand rotation along the M-M axis. Both processes likely are slow on the NMR time scale now.

For the analogous platinum complexes **137a/b** (Figure 5.13b) no coalescence is observed even at 353 K. Consequently, the triangle-square equilibration is significantly faster for the Pd complexes in agreement with common knowledge that Pt(II) complexes are kinetically more stable than the Pd(II) analogues. In analogy to **133a/b**, broader signals are observed for **137a/b** at 243 K, which we again attribute to slow conformer equilibria. Similar behavior was detected for the other metal complexes generated by self-assembly with ligands **128**, **130**, and **131**. In all cases, the triangle-square equilibration is faster for the Pd complexes as indicated by the coalescence of NMR signals into one set at temperature clearly below 350 K. For the Pt complexes no coalescence up to 353 K is observed.

Because the *o*-pyridine protons appear separately for triangles and squares, quantitative data on the triangle-square equilibrium can be derived from their integration ratios and the initial concentration of the building blocks used. Because three squares can be converted into four triangles without changing the number of building blocks, equation 5.2 describes the equilibrium constant, from which the free enthalpies ΔG_{eq} for the equilibrium can be calculated. As this can easily be done at different temperatures, the enthalpic and entropic contributions can be obtained from a van't Hoff plot of ln K over $1/T$ (Figure 5.14, equation 5.3).

$$K = \frac{[triangle]^4}{[square]^3} \tag{5.2}$$

$$\ln K = -\frac{\Delta G_{eq}}{RT} = -\frac{\Delta H_{eq}}{RT} + \frac{\Delta S_{eq}}{R} \tag{5.3}$$

This thermodynamic analysis was performed for **139a/b** (Table 5.2) because the available temperature range was too small for the other equilibria. At lower temperatures, the rather long equilibration times limit the experiment; for the Pd complexes, the temperature range is limited at the upper end through the coalescence discussed above. In the accessible temperature range, the triangles and squares were allowed to equilibrate until no integral changes were observed anymore. The data for **139a/b** is clearly consistent with the above discussion of enthalpic and entropic factors: The enthalpy for the conversion of three squares **139a** into four triangles **139b** is positive (ΔH_{eq} = 35.1 kJ

mol-1) reflecting the strain in the triangle structure. The entropic contribution is quite large and positive (ΔS_{eq} = 113 J mol-1 K-1) and thus at elevated temperatures overcompensates the reaction enthalpy through a large $-T\Delta S_{eq}$ term. The positive entropy indicates that the reaction profits from the larger number of particles, when triangles are formed from squares.

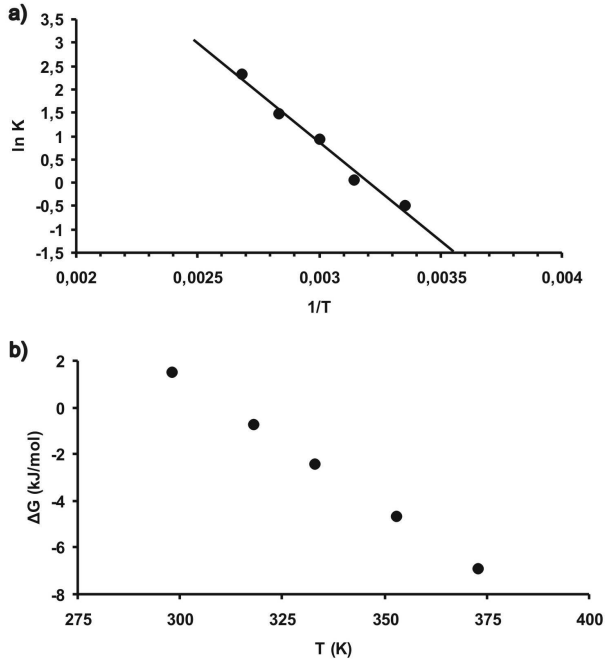

Figure 5.14: *a) Van't Hoff plot of ln K over 1/T for the equilibrium of* ***139a/b****. b) Plot of free enthalpy ΔG_{eq} over temperature T.*

Table 5.2: *Thermodynamic data for the* ***139a/b*** *equilibrium (experimental errors ca. ± 20%).*

T [K]	c(triangle) [mmol l^{-1}]	c(square) [mmol l^{-1}]	K [mol l^{-1}]	ΔG_{eq} [kJ mol^{-1}]
298	15.5	4.5	0.62	1.5
318	16.0	4.0	1.06	-0.7
333	16.8	3.2	2.56	-2.4
353	17.3	2.7	4.42	-4.7
373	17.9	2.1	10.33	-6.9
ΔH_{eq} = 35.1 kJ mol^{-1}; ΔS_{eq} = 113 J mol^{-1} K^{-1}				

The square/triangle ratio is also influenced by the building block concentration. For **133a/b** and **137a/b**, ^{1}H NMR spectra were recorded for solution concentrations between 2.5 mM and 20 mM. These two values limit the available concentration range because the signal-to-noise ratio decreases too much below 2.5 mM and the solubility of the urea squares prohibits examining solutions more concentrated than 20 mM. In this concentration range, a small but clearly visible shift of the square/triangle ratio is observed. For **133a/b**, it is <2:98 at 2.5 mM and 14:86 at 20 mM; for **137a/b**, we obtain 6:94 at 2.5 mM and 17:83 at 20 mM concentration (Figure 5.15). The triangle is thus dominating the spectra over the whole concentration range.

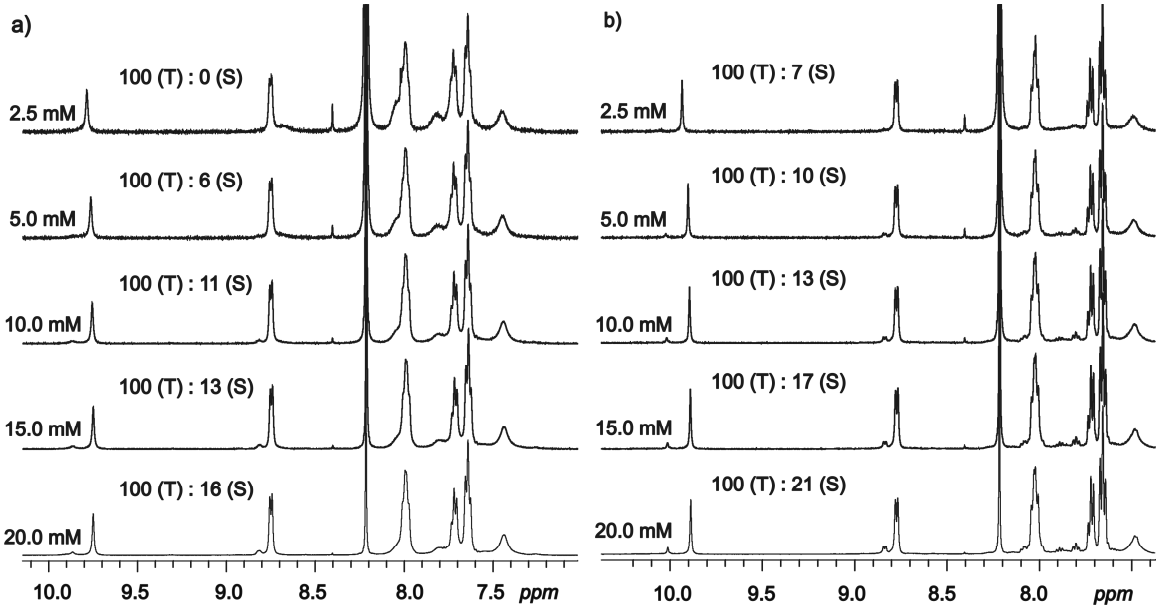

Figure 5.15: *Square/triangle ratios at different concentrations obtained for* ***133a/b*** *(a) and* ***137a/b*** *(b).*

Besides the temperature and concentration, the solvent is an important factor which influences the thermodynamics of the triangle-square equilibrium. For the NMR experiments reported so far, dipolar aprotic DMF-d_7 or DMSO-d_6 has been used as the NMR solvent. If more non-polar solvents such as tetrachloroethane-d_2 (TCE) are added, the equilibrium shifts toward the triangles. Figure 5.16 shows this for the **132a**/**b** equilibrium. Again, the *o*-pyridine protons provide the clearest picture. With stepwise increase of the TCE fraction, the signal assigned to the square decreases in favor of the

triangle signal. A similar effect has been observed for the corresponding Pt complexes **136a/b**. The solvent mixture changes also the kinetic behavior in that the exchange processes proceed at lower rates with increasing TCE content of the sample. This is confirmed by coalescence temperatures increasing with TCE/DMF ratio. We attribute this finding to DMF molecules which support metal-ligand bond cleavages through their ability to donate an electron-pair into the empty coordination site formed in the intermediates.

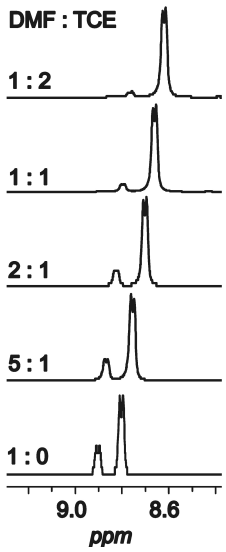

Figure 5.16: *Partial ^{1}H NMR spectra (o-pyridine proton signals) of* ***132a/b*** *in various mixtures of DMF-d_7 and tetrachloroethane-d_2 at 298 K. The same 20 mmol l^{-1} concentration was kept constant.*

Finally, X-ray analysis provides direct information about the structure of particles in the solid phase. Thus, it is a helpful tool for the structure assignment of metallo-supramolecular complexes.

Colorless, highly solvent-dependent single crystals suitable for X-ray analysis were grown by slowly diffusing benzene into an acetonitrile solution of a 1:1 mixture of the *cis*-coordinated platinum(II) corners **28** with *trans*-bis(4-pyridyl)ethene **128**. The X-ray crystal structure confirmed the formation of Pt triangles **132b** (Figure 5.17). It should be

noted that NMR spectroscopy confirms both the triangles and squares to be present in acetonitrile as well (Figure 5.18).

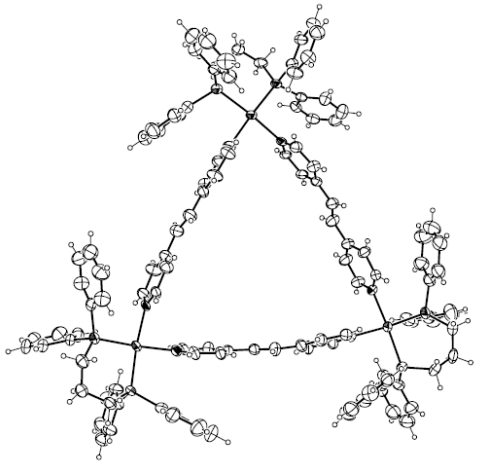

Figure 5.17: *Oak Ridge Thermal Ellipsoid Plot (ORTEP; 50%-probability) of triangle* ***132b****. Anions and solvent molecules are omitted for clarity.*

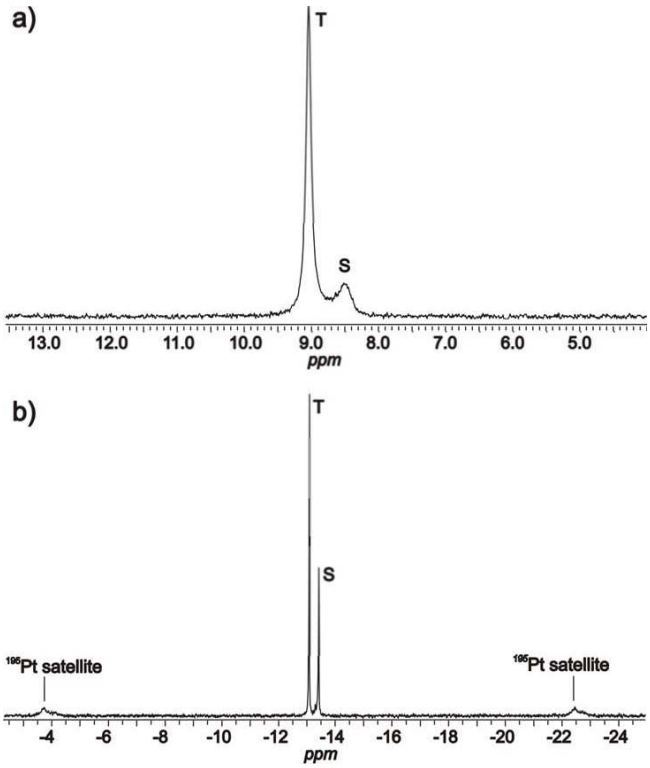

Figure 5.18: *For comparison:* ^{31}*P NMR spectra of* ***132a/b*** *(a) and* ***136a/b*** *(b) in acetonitrile. Both spectra clearly show two different species existing in solution.*

The lattice of the crystal structure of **132b** includes five acetonitrile molecules for each triangle in addition to the triangle itself and the six triflate counterions. In the structure analysis, some electron density remained unassigned because of high disorder. The packing of the triangles is shown in Figure 5.19. The cationic triangles form sheets that are further stacked on each other so that the disordered triflate anions are in between the cationic layers. Interestingly, the acetonitrile molecules are ordered to form a solvent cluster that runs through two stacked triangles belonging to upper and lower triangle sheets (Figure 5.19e).

The Pt-N bonds are all ~0.21 nm long, and each N-Pt-N bond angle falls in the range of 83-85º. The bidentate phosphine bite angle is ~92-93º. The angles around the Pt ion do not differ much from the ideal 90º and, as predicted by molecular modeling (see above), the ring strain of the triangle is mostly neutralized by bending the bis-pyridyl ethene ligands. Two planes defined by the two pyridine rings of each one of the ligands appear in the crystal structure with angles of 166º to 157º and thus deviate significantly from the expected, unstrained 180º. The Pt-Pt distances are 1.34 nm. The conformation and distances are similar to the previously reported triangle by Schweiger et al.[220] which bears trimethylphosphine platinum(II) corners. Schweiger et al. described that squares crystallized when the crystals were grown in the presence of small triflate counterions and that triangles were observed in the crystal when the mixture was crystallized in the presence of larger cobalticarborane anions. Unlike Schweiger et al., we never got crystals of the squares with our corners **27** and **28** that are definitively present in the solution equilibria. We attribute this to packing effects that are dominated by the nature of the corners. In addition to the crystal structure of **136b**, an analogous isomorphic structure of **132b** was obtained.

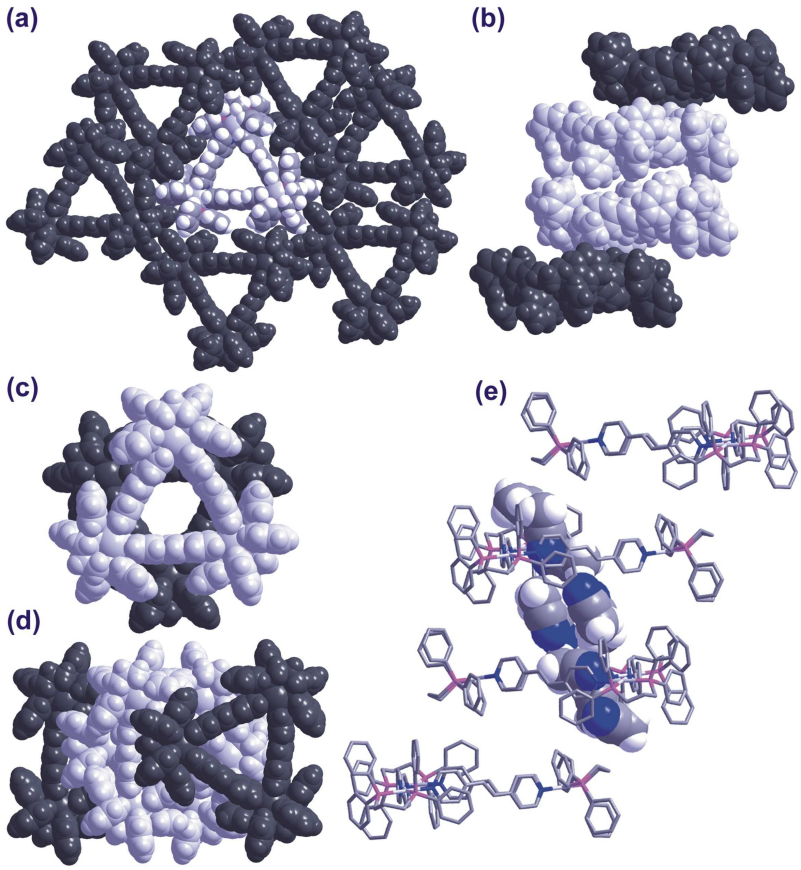

Figure 5.19: *(a) Space-filling representation of a single triangle sheet in the crystal structure of* ***136b****. Each triangle is surrounded by six others by multiple* $\pi\cdots\pi$ *– interactions. The packing of the triangles is similar in the structure of* ***132b****. (b) The sheets pack on top of each other so that a cavity is formed by four triangles where the walls of the cavity are defined by two triangles (light grey) and it is further closed by the corners of upper and lower triangles (dark grey). (c) A picture about how the cavity forming triangles are stacked on each other (light and dark). (d) The cavity (light grey) is closed by the corners of the upper and lower triangles (dark grey). (e) The cavity is filled by a cluster of ten acetonitrile molecules. The disordered anions are omitted for clarity.*

Three important conclusions can be drawn from the results presented here. (i) A thorough analytical characterization of metallo-supramolecular complexes which can quickly interconvert requires the application of a number of different methods. From simple NMR experiments, we can only conclude that two different, highly symmetrical species

are present but it remains unclear which ones. Mass spectrometry adds some information here but because of the formation of unspecific aggregates and fragments may lead to misinterpretations. Only the addition of DOSY NMR results on the diffusion coefficients and approximate radii of the complexes under study provides coherence here - at best, in combination with molecular modeling. On the basis of crystallography, one would arrive at the conclusion that triangles are formed exclusively, even for **132a/b** and **137a/b**, for which the amount of squares in solution is significant. Crystallization may prefer one component; the equilibrium readjusts the solution concentrations.

(ii) In this study, we presented bis-pyridyl ligands of different lengths and flexibility. Molecular modeling and crystallography agree that ligand bending is the major contribution to accommodate the strain. Consequently, the size of metallo-supramolecular squares cannot be increased easily by just extending the length of the ligands connecting the metal corners. When the ligand becomes long enough and therefore sufficiently flexible, triangles are entropically favored. The generation of larger squares thus would require a different strategy that takes into account the rigidity requirements that would prevent triangle formation. Simple squares formed according to Stang's self-assembly approach are thus limited to ligands not significantly longer than 4,4´- bipyridine itself.

(iii) The thermodynamic and kinetic behavior of the complexes discussed here is interesting in several respects. The equilibrium is affected by temperature in that entropy-favored triangles become more prominent at higher temperatures. It is also affected significantly by solvent polarity. Increasing amounts of nonpolar solvents result in an increased preference for triangle formation. For both, the Pd and Pt complexes, exchange reactions are observed which interconvert squares into triangles and vice versa. These processes depend on the nature of the metal. Pd complexes exchange more quickly than the Pt analogues. They also depend on solvent polarity. More polar solvents promote the exchange processes so that lower coalescence temperatures are observed in the temperature-dependent NMR spectra.

5.2.3 The Influence of Small Constitutional Changes at the Formation of Metallo-Supramolecular Boxes

The combination of divalent ligands with divalent cis-blocked square-planar metal centers results in the formation of various two-dimensional metallo-supramolecular macrocycles (see above).[72] In order to achieve three-dimensional cage-like metallo-supramolecular complexes, the valency of at least one building block has to be increased.[33-35] Thus, the combination of bent divalent ligands with square-planar palladium(II) salts has been used to form a large variety of three-dimensional metallo-supramolecular structures, which includes small M_2L_4 cages as well as large metallo-supramolecular spheres.[109, 116-125] The constitution of a ligand plays an important role for the structure of the resulting metallo-supramolecular complex. For example, the self-assembly of 4-(4-(pyridin-4-yl)phenyl)pyridine with (en)Pd(NO_3)$_2$ **19** results in an equilibrium of metallo-supramolecular triangles and squares.[221] On the contrary, equilibria between metallo-supramolecular M_2L_2, M_3L_3 and M_4L_4 complexes have been observed, when 3-(4-(pyridin-3-yl)phenyl)pyridine **32** was combined with (en)Pd(NO_3)$_2$ **19**.[109] Both ligands used differ only in the position of their pyridine-nitrogen atoms.

In order to study the direct influence of such small constitutional changes on the formation of three-dimensional metallo-supramolecular complexes, the self-assembly of ligands **145-148** with [Pd(MeCN)$_4$(BF_4)$_2$] **149** was studied. This project was performed in cooperation with Dr. Boris Brusilowskij and Egor V. Dzyuba.

The ligands used within this study were synthesized according to literature-known procedures. Ligands **145** and **146** were achieved in a two-step synthesis including a Bestmann-Ohira reaction and a subsequent Sonogashira cross coupling reaction.[157, 159] However, ligands **147** and **148** have been synthesized in two steps as well (Figure 5.20). At first, nicotinic acid **140** or isonicotinic acid **142**, respectively, were mixed with thionyl chloride and catalytic amounts of DMF and were refluxed for one hour. The corresponding acid chlorides (**141** and **143**) formed and were isolated in very good chemical yields of 95 % or 96 %, respectively. In the second step, an amide-formation was performed. In the presence of triethylamine, Hunter´s diamine (1,1-bis(4-amino-3,5-dimethylphenyl)cyclohexane) **144** reacted with three equivalents of nicotinoyl chloride

141 or isonicotinoyl chloride **143**, respectively.[37] The ligands *N*,*N*'-(4,4'-(cyclohexane-1,1-diyl)-bis-(2,6-dimethyl-4,1-phenylene)) dinicotinamide **145** and *N*,*N*'-(4,4'-(cyclohexane-1,1-diyl)-bis-(2,6-dimethyl-4,1-phenylene)) diisonicotinamide **146** were obtained in acceptable chemical yields of 72 % or 70 %, respectively.

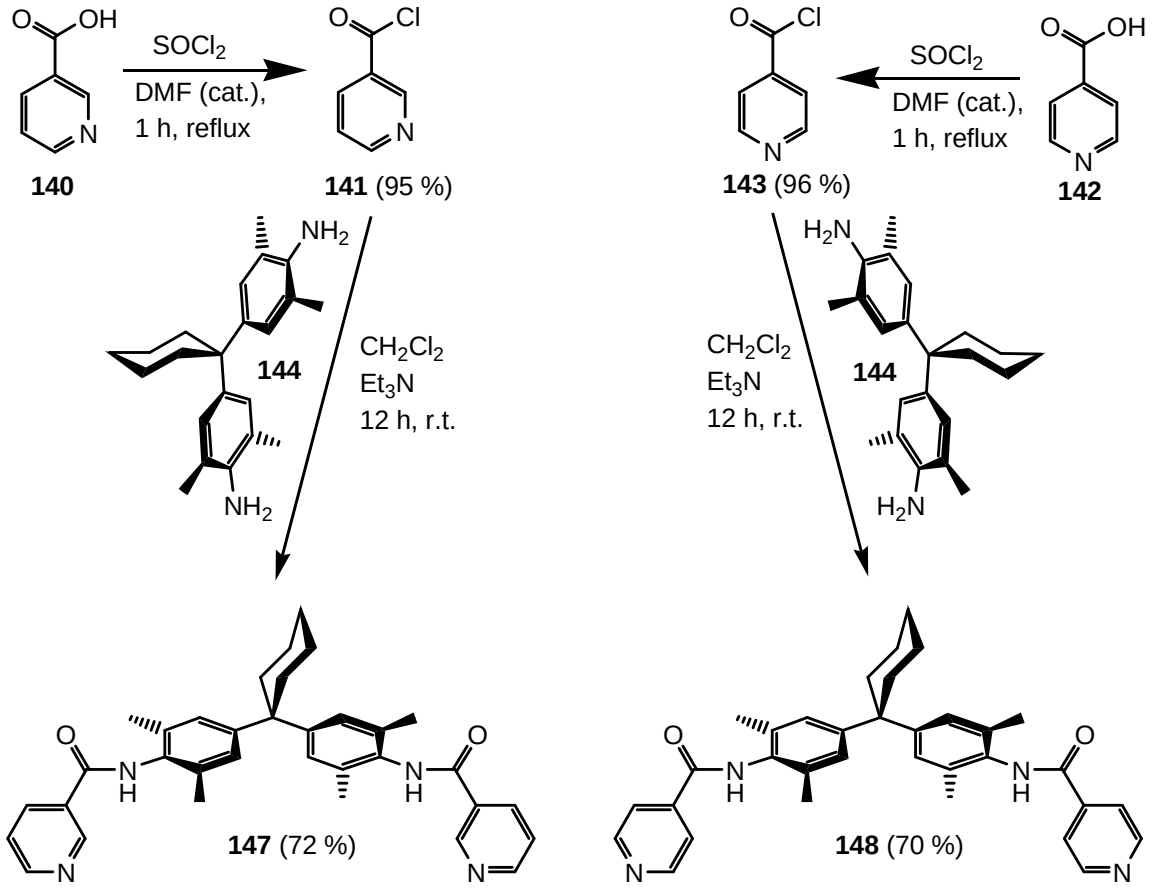

Figure 5.20: *The Syntheses of the long divalent ligands **147** and **148**.*[37]

For self-assembly reactions, the metal center **149** was mixed with two equivalents of ligands **145-148**, respectively. In order to obtain a good solubility, all systems were dissolved in DMSO or DMF. The samples were stirred for four hours at room temperature, to ensure that the thermodynamic equilibria were analyzed. The NMR experiments were performed in DMSO-d_6 or DMF-d_7 using ligand-concentrations of 15 mM. For ESI mass spectrometry, the solutions were diluted with acetonitrile to result in a ligand-concentration of ca. 100 µM. According to the constitution of the ligands used, different metallo-supramolecular systems have been achieved (Figure 5.21).

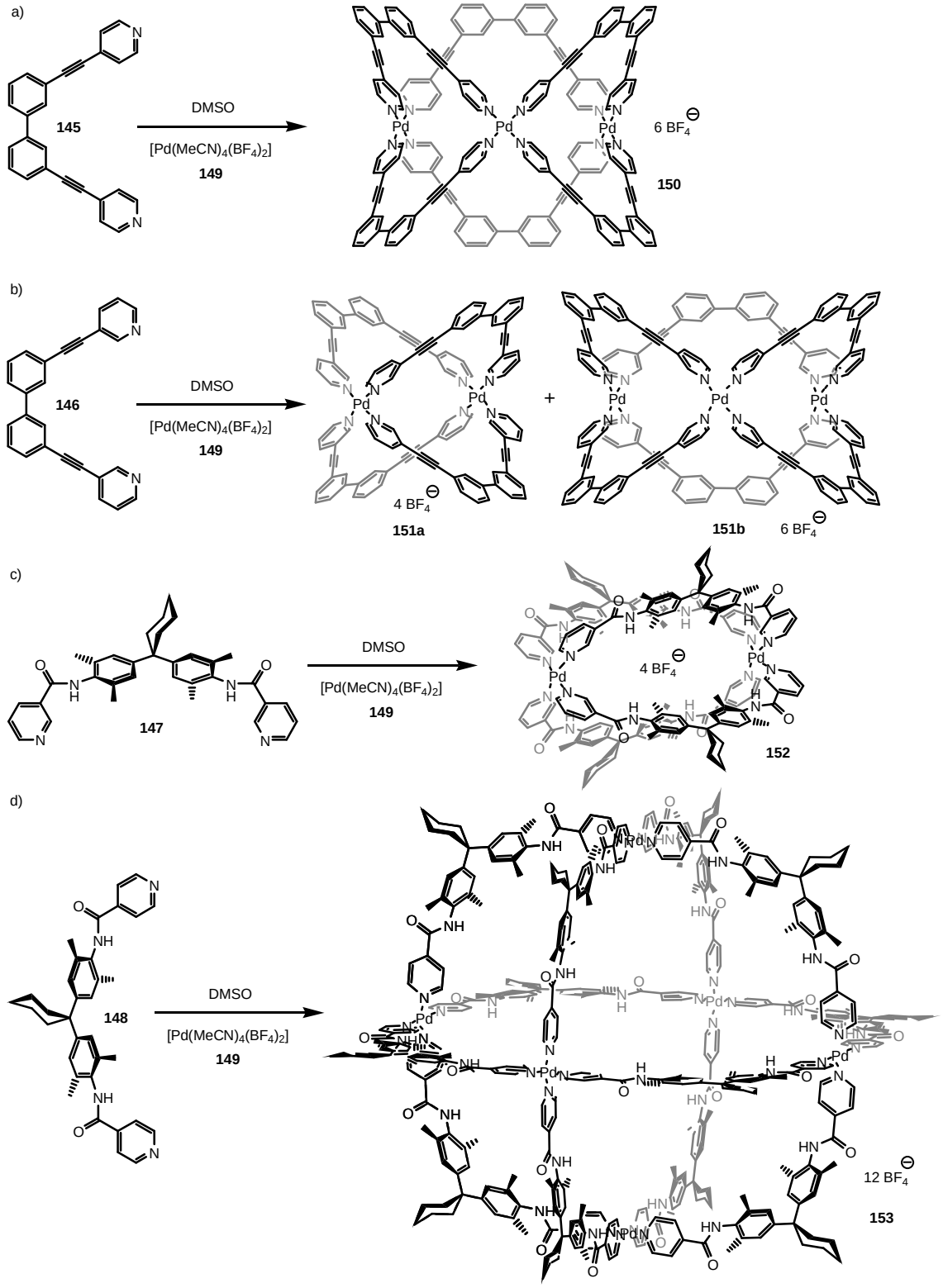

Figure 5.21: *The self-assembly of different metallo-supramolecular cages: a) M_3L_6 complex **150**, b) an equilibrium between M_2L_4 complex **151a** and M_3L_6 complex **151b**, c) M_2L_4 complex **152** and d) the octahedral M_6L_{12} complex **153**.*

At first, the self-assembly reactions of the isomeric ligands **145** and **146** with metal center **149** will be discussed. A comparison of the ^{1}H NMR spectra of ligands **145** and **146** with their corresponding metallo-supramolecular systems **150** and **151a/b** reveals that the coordination of the ligands at the metal center **149** was successful (Figure 5.22 a-d). For the self-assembly of ligand **145** with metal center **149** only one set of signals is observed, indicating that only one metallo-supramolecular species (**150**) is present in solution. On the contrary, two sets of signals are observed, when metal center **149** is combined with ligand **146**. The presence of two metallo-supramolecular complexes in solution is supported by H,H-COSY NMR spectroscopy (Figure 5.22e). Due to a precise assignment of the two sets of signals appearing in the ^{1}H NMR spectra of system **151a/b**, additional experiments like ^{1}H-DOSY NMR spectroscopy have to be performed.

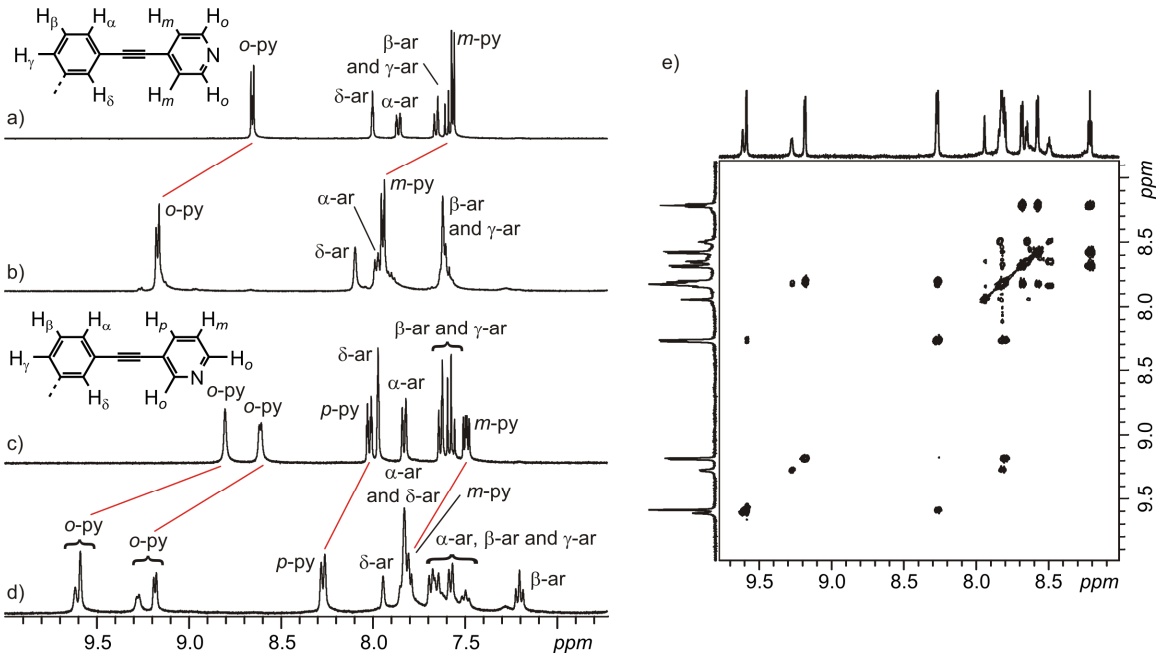

Figure 5.22: *The ^{1}H NMR spectra of a) ligand **145**, b) the metallo-supramolecular M_3L_6 complex **150**, c) ligand **146** and d) the equilibrium between metallo-supramolecular M_2L_4 complex **151a** and metallo-supramolecular M_3L_6 complex **151b**. The shifting of the pyridine hydrogens is marked by red lines. The H,H-COSY of **151a/b** supports shows two species to be present (e).*

ESI mass spectrometry was performed to identify the metallo-supramolecular complexes under study (Figure 5.23). The ESI mass spectrum of the mixture of ligand **145** with metal center **149** shows only two peaks at *m/z* 906 ($[1:2:1]^{+}$ and $[3:6:3]^{3+}$) and *m/z* 1402 ($[3:6:4]^{2+}$) which can be assigned to a metallo-supramolecular M_3L_6 complex **150** and fragments of it (Figure 5.23a). Thus, the combination of ligand **145** with metal center **149** exclusively leads to the formation of M_3L_6 complex **150**.

For the self-assembly reaction of metal center **149** with ligand **146**, the situation is more complex. The ESI mass spectrum of system **151a/b** shows many different peaks (Figure 5.23b). Some of the observed peaks can be assigned to a metallo-supramolecular M_2L_4 complex **151a** (*m/z* 410 ($[2:4:0]^{4+}$), *m/z* 575 ($[2:4:1]^{3+}$), *m/z* 906 ($[2:4:2]^{2+}$) and *m/z* 1899 ($[2:4:3]^{+}$)) while other peaks can be associated to the corresponding M_3L_6 complex **151b** (*m/z* 410 ($[3:6:0]^{6+}$), *m/z* 509 ($[3:6:1]^{5+}$), *m/z* 658 ($[3:6:2]^{4+}$), *m/z* 906 ($[3:6:3]^{3+}$) and *m/z* 1402 ($[3:6:4]^{2+}$)). These results clearly identify the two complexes observed by NMR spectroscopy as M_2L_4 complex **151a** and M_3L_6 complex **151b**.

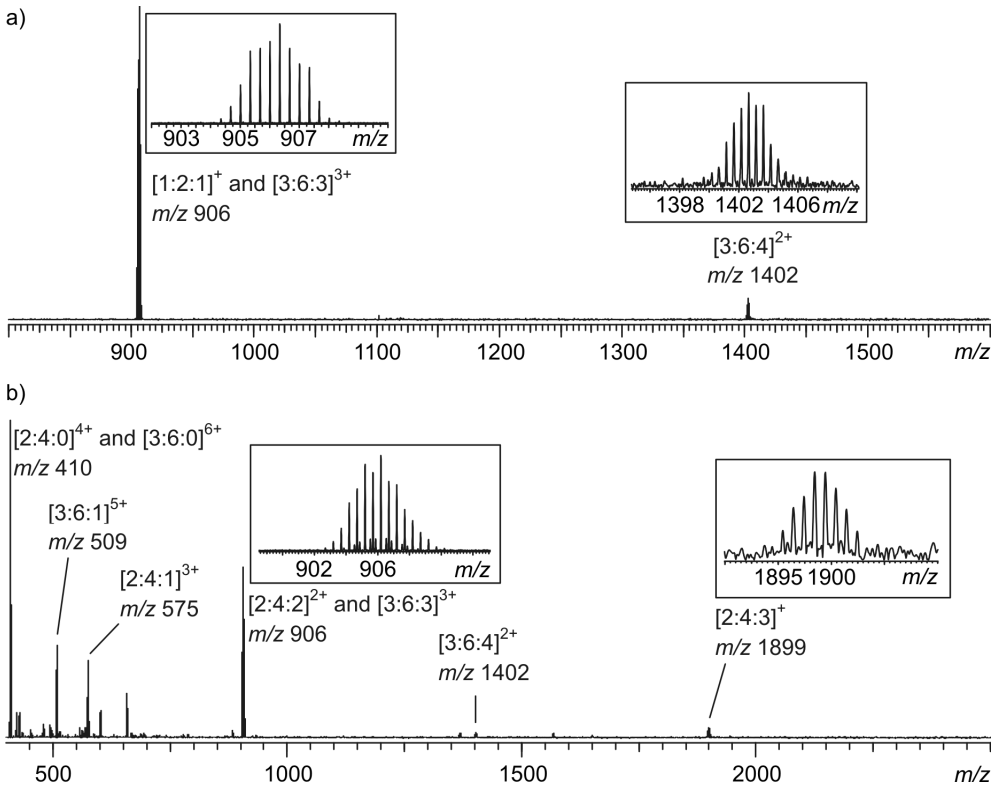

Figure 5.23: *ESI mass spectra of a) M_3L_6 complex **150** and b) the equilibrium of M_2L_4 complex **151a** and M_3L_6 complex **151b**.*

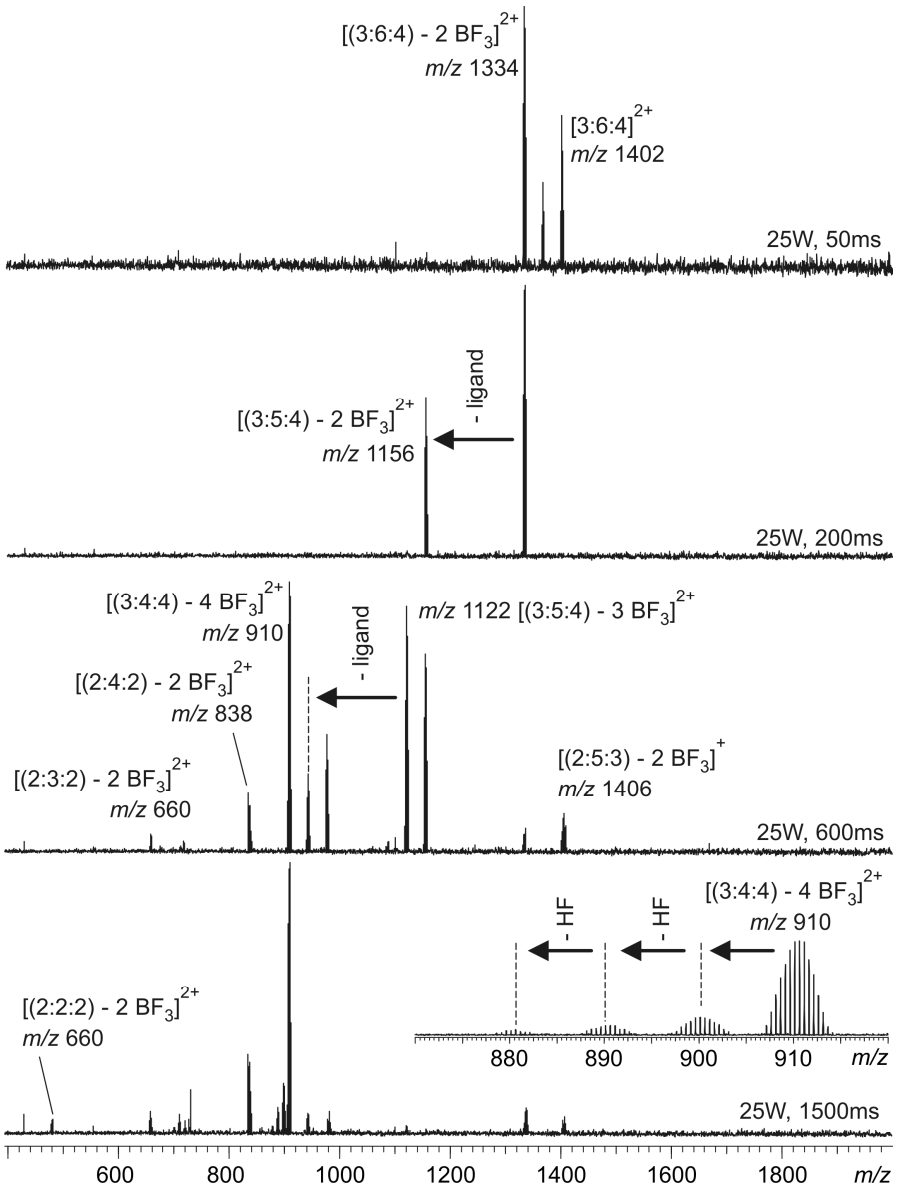

Figure 5.24: *IRMPD tandem-MS spectra of the peak at m/z 1402 ($[3:6:4]^{2+}$) corresponding to M_3L_6 complex **150**. The spectra were performed using a 25W IR-laser with different irradiation times.*

In order to confirm the structures observed, infra-red multi-photon dissociation (IRMPD) tandem mass spectrometry of the different metallo-supramolecular complexes under study was performed using a 25W IR laser at different irradiation times. For M_3L_6 complex **150**, the peak at *m/z* 1402 ($[3:6:4]^{2+}$) was isolated and fragmented afterwards (Figure 5.24). At an irradiation time of 50 ms, the subsequent loss of two BF_3 fragments was observed which are formed of the BF_4^- anions. Additionally to the loss of BF_3 units,

at larger irradiation times also the subsequent loss of ligands is observed (e.g. *m/z* 1156 ($[(3:5:4) - 2\ BF_3]^{2+}$)). After the loss of one or two ligands, the remaining fragments lose one metal center (e.g. *m/z* 838 ($[(2:4:2) - 2\ BF_3]^{2+}$) and *m/z* 1406 ($[(2:5:3) - 2\ BF_3]^{+}$). At increasing irradiation times, these fragments decompose by the subsequental loss of ligands. Interestingly, at irradiation times of 1500 ms the subsequent loss of neutral HF units was observed. However, the tandem-MS experiments support the structure of M_3L_6 complex **150**.

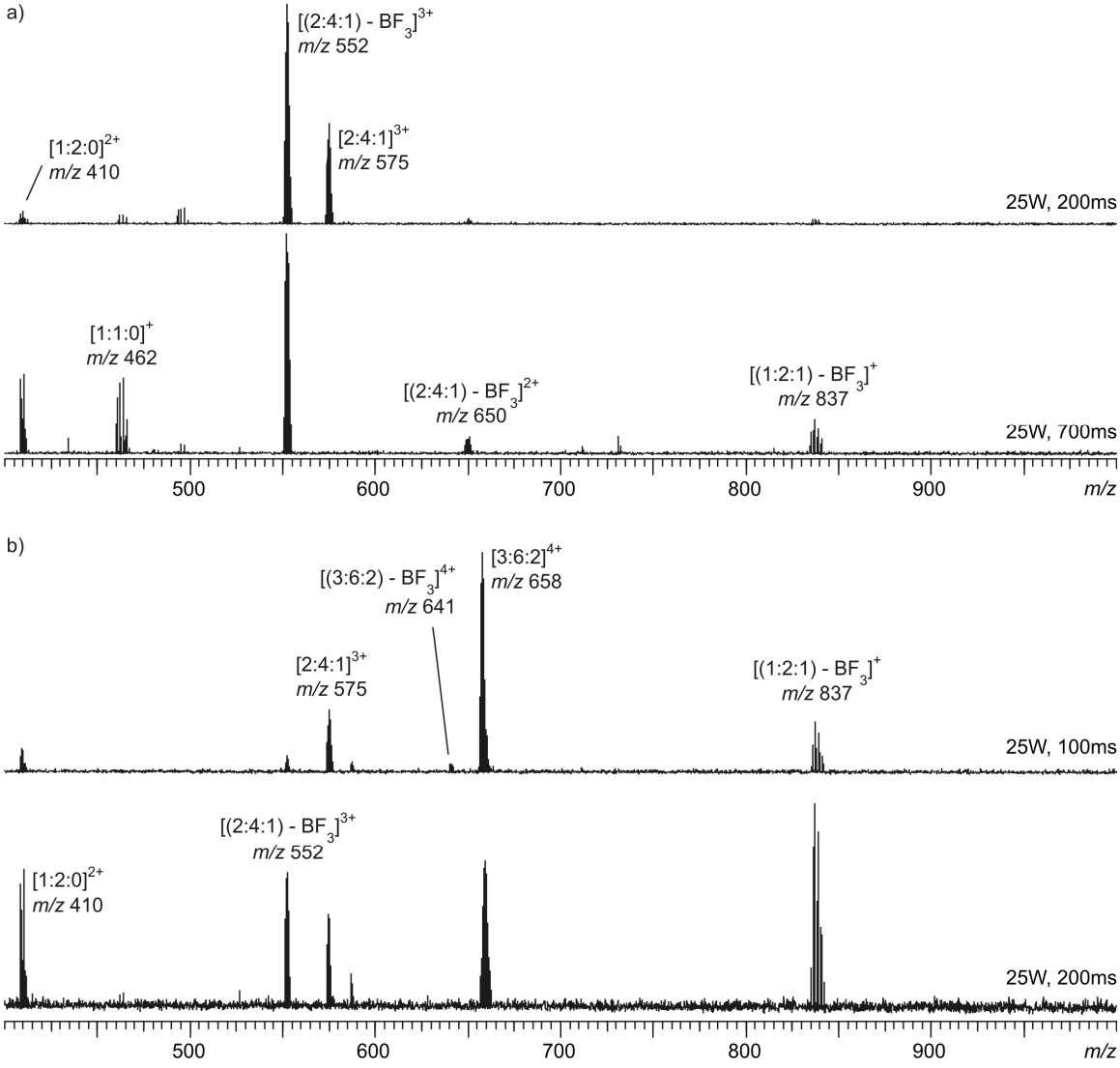

Figure 5.25: *IRMPD tandem-MS spectra of a) M_2L_4 complex **151a** (m/z 575 ($[2:4:1]^{3+}$)) and b) M_3L_6 complex **151b** (m/z 658 ($[3:6:2]^{4+}$)). The spectra were performed using a 25W IR-laser with different irradiation times.*

For system **151a/b**, the peaks at *m/z* 575 ($[2:4:1]^{3+}$) and *m/z* 658 ($[3:6:2]^{4+}$) have been chosen for IRMPD tandem mass spectrometry (Figure 5.25). For both complexes (**151a** and **151b**) the loss of BF_3 units was observed as well. After the loss of one BF_3 fragment, the corresponding fragment of M_2L_4 complex **151a** (*m/z* 552 ($[(2:4:1) - BF_3]^{3+}$)) decomposes into $[1:2:0]^{2+}$ (*m/z* 410) and $[(1:2:1) - BF_3]^{+}$ (*m/z* 837) (Figure 5.25a). At larger irradiation times additional peaks are observed, which can just be explained by a reduction of their parent ions (*m/z* 462 ($[1:1:0]^{+}$) and *m/z* 650 ($[(2:4:1) - BF_3]^{2+}$)).

However, the fragmentation pattern of M_3L_6 complex **151b** (*m/z* 658 ($[3:6:2]^{4+}$)) is similar to that of its corresponding M_2L_4 complex **151a** (Figure 5.25b). After the loss of one BF_3 unit, the quadruply charged ion at *m/z* 641 ($[(3:6:2) - BF_3]^{4+}$) exclusively decomposes into $[(1:2:1) - BF_3]^{+}$ (*m/z* 837) and $[2:4:1]^{3+}$ (*m/z* 575). These ions undergo further fragmentation similar to that observed for M_2L_4 complex **151a**. This shows that even in the gas phase the M_2L_4 complex **151a** can be formed from its corresponding M_3L_6 complex **151b** by fragmentation which can be explained by the support of an intramolecular "neighbor-group effect".[105, 139]

A comparison of the fragmentation pathways of the M_3L_6 complexes **150** and **151b** exhibits that the fragmentation of both complexes is completely different. While the fragmentation of complex **150** shows the subsequent loss of building blocks, the fragmentation of complex **151b** leads exclusively to the formation of complex **151a**. Thus, the two isomeric complexes **150** and **151b** can be distinguished by tandem mass spectrometry. Nevertheless, it has to be mentioned, that the charge of the ions chosen for the tandem-MS experiments differs from each other. Due to charge repulsion, the charge of the parent ion plays an important role for its fragmentation pathway. However, the ions used in the tandem-MS experiments have been chosen due to appropriate intensities and lack of superposition with other ions.

Inspired by these first remarkable results, the self-assembly reactions of metal center **149** with the isomeric ligands **147** and **148** have been examined. In both cases, a comparison of the ^{1}H NMR spectra of the ligands **147** and **149** with their corresponding assemblies **152** and **153** showed a chemical shifting of the peaks (Figure 5.26). Thus, the coordination of the ligands to metal center **149** was successful. Furthermore, both

metallo-supramolecular systems (**152** and **153**) show only one set of signals, indicating the exclusive formation of one metallo-supramolecular complex, respectively.

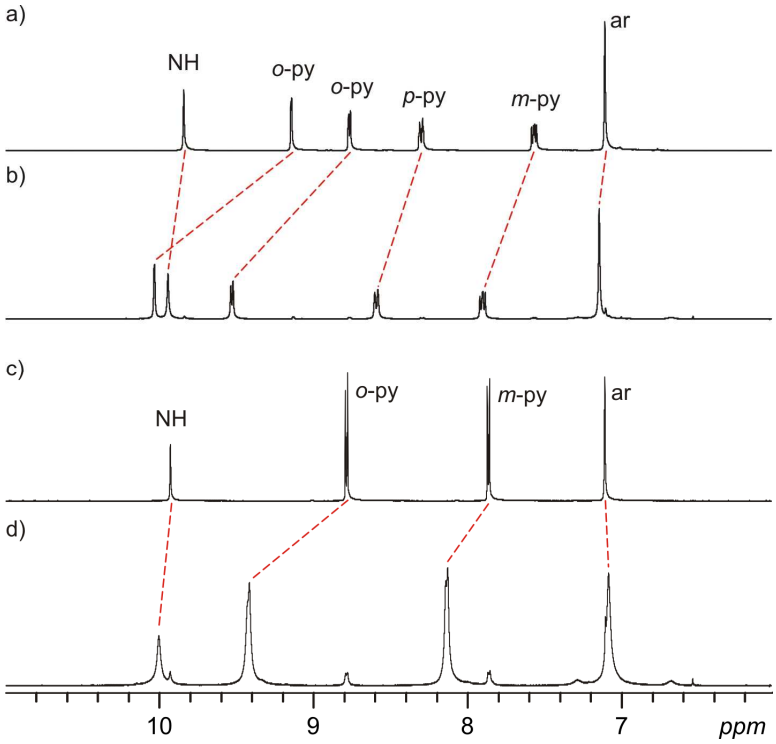

Figure 5.26: *The aromatic region of the ^1H NMR spectra of a) ligand **147**, b) M_2L_4 complex **152**, c) ligand **148** and d) M_6L_{12} complex **153**. The chemical shifting of the aromatic hydrogens is marked by red lines.*

ESI mass spectrometry was performed to identify the metallo-supramolecular complexes formed. The mass spectrum of the mixture of ligand **147** with metal center **149** showed three prominent peaks which can be assigned to doubly, triply and quadruply charged ions of M_2L_4 complex **152** (*m/z* 586 ($[2:4:0]^{4+}$), *m/z* 810 ($[2:4:1]^{3+}$) and *m/z* 1259 ($[2:4:2]^{2+}$); Figure 5.27a). Other peaks observed in the mass spectrum represent aggregates of one of the ions of **152** and one extra ligand. However, the structure of M_2L_4 complex was confirmed by IRMPD tandem-MS experiments performed with the peak at *m/z* 586 ($[2:4:0]^{4+}$) (Figure 5.27b). At irradiation times of 150 ms, the $[2:4:0]^{4+}$ ion loses one protonated ligand (*m/z* 533 ($[\text{ligand} + H]^+$)) and thus, fragment $[(2:3:0) - H]^{4+}$ (*m/z* 603) is observed. After the loss of another protonated ligand, fragment $[(2:2:0) - 2\ H]^{2+}$ (*m/z* 603) is formed which decomposes into two singly charged $[(1:1:0) - H]^+$ (*m/z* 603)

fragments. The protons attached to the ligands probably originate from the amide NH hydrogen atoms of other ligands. The loss of protonated ligands is favored by charge repulsion.

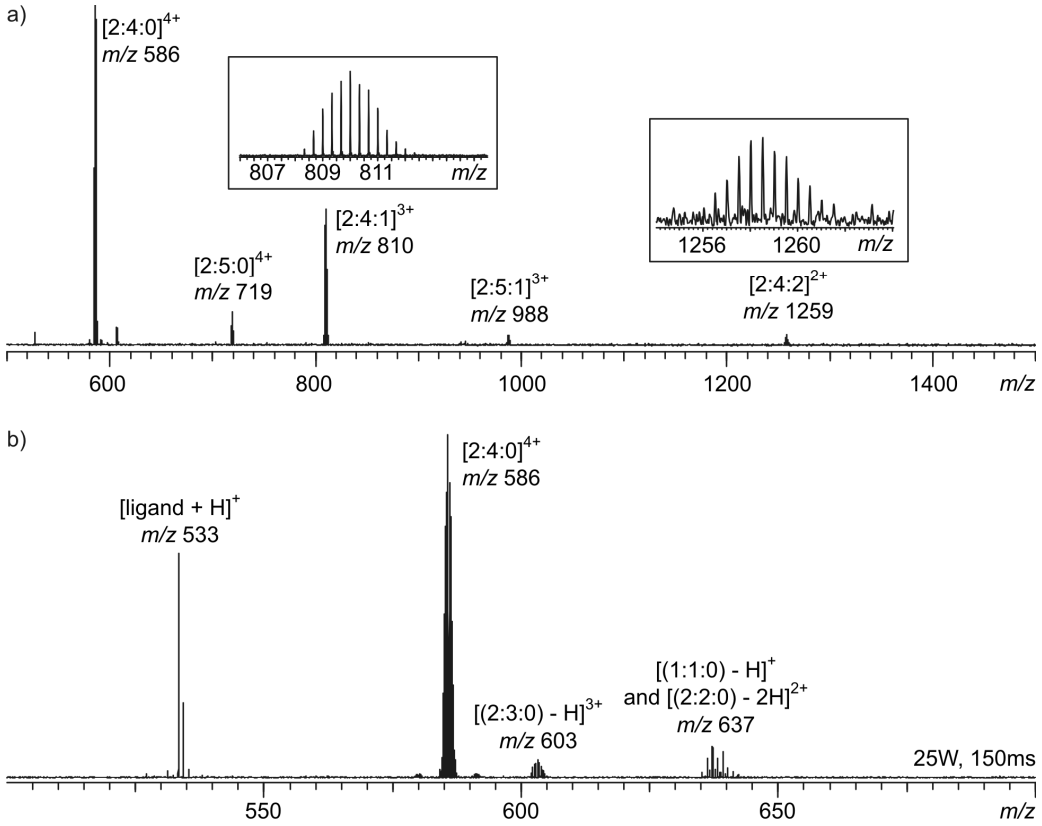

Figure 5.27: *a) ESI mass spectrum of M_2L_4 complex **152** and b) the IRMPD mass spectrum of the $[2:4:0]^{4+}$ ion (m/z 586). The tandem mass spectrum was performed using an IR-laser at a laser power of 25W and an irradiation time of 150 ms.*

The ESI mass spectrum of the mixture of ligand **148** with metal center **149** shows a different situation (Figure 2.28a). In here, differently charged ions of M_6L_{12} complex **153** (*m/z* 923 ($[6:12:4]^{8+}$), *m/z* 1066 ($[6:12:5]^{7+}$) and *m/z* 1258 ($[6:12:6]^{6+}$)) are observed as well as fragments of these (*m/z* 533 ($[\text{ligand} + H]^{+}$), *m/z* 585 ($[1:2:0]^{2+}$), *m/z* 787 ($[(2:4:0) - BF_3]^{3+}$) and *m/z* 852 ($[1:3:0]^{2+}$)). The structure of the metallo-supramolecular M_6L_{12} complex **153** was confirmed by IRMPD tandem mass spectrometry of the peak at *m/z* 1066 ($[6:12:5]^{7+}$). At short irradiation times, the loss of one BF_3 unit was observed as well as the loss of protonated ligands. Interestingly, the fragments corresponding to the

loss of protonated ligands could not be observed within the tandem mass spectra. However, with increasing irradiation times, small fragments like $[1:2:0]^{2+}$ (*m/z* 585), $[1:3:0]^{2+}$ (*m/z* 852) and $[(2:3:0) - 2\ H]^{2+}$ (*m/z* 904) appear in the mass spectra. Their corresponding counter-fragments have not been observed in the mass spectra as well. The lack of these counter-fragments indicates that they have a short life-time and undergo fast fragmentation themselves. Additionally, the increasing intensity of peak for $[ligand + H]^{+}$ indicates, that further fragmentation of all other ions observed in the IRMPD experiments takes place. However, the structure of M_6L_{12} complex **153** could be confirmed by ESI MS and IRMPD tandem mass spectrometry.

Two conclusions can be drawn from the results presented within this chapter. First, the constitution of the ligands used in self-assembly processes is mandatory for the resulting metallo-supramolecular complexes. While the combination of metal center **149** with ligand **145** exclusively forms M_3L_6 complex **150**, an equilibrium between an M_2L_4 complex **151a** and its corresponding M_3L_6 complex **151b** is observed, when **149** is combined with ligand **146**. The influence of the position of the pyridine-nitrogen atoms is even more drastically when the self-assembly processes of **149** with ligands **147** and **148**, respectively, are compared. On the one hand, the small M_2L_4 complex **152** is formed while on the other hand the large M_6L_{12} **153** complex is observed.

Second, IRMPD tandem mass spectrometry has been shown to be an interesting tool to examine metallo-supramolecular complexes. Even isomeric metallo-supramolecular complexes like **150** and **151b** can be distinguished by their different fragmentation patterns.

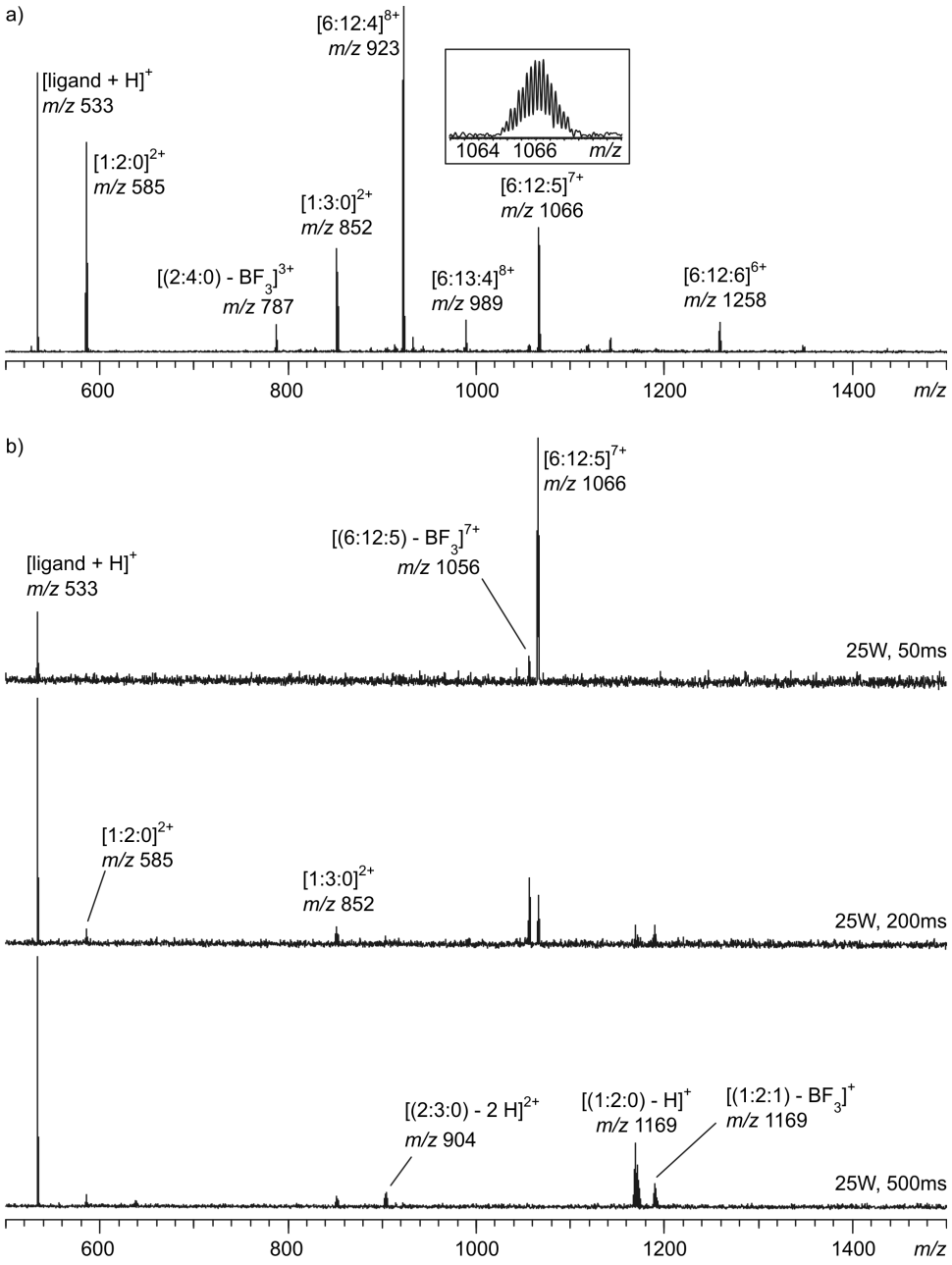

Figure 5.28: *a) ESI mass spectrum of M_6L_{12} complex **153** and b) the IRMPD mass spectra of the $[6:12:5]^{7+}$ ions (m/z 1066). The tandem mass spectra were performed using an IR-laser at a laser power of 25W and increasing irradiation times.*

5.3 The Self-Assembly of Urea-Functionalized Metallo-Supramolecular Complexes

5.3.1 Bispyridyl-Urea Ligands – Synthesis and Structure

Many pyridine-based ligands bear additional functional groups, which enable them to interact with each other, with guest molecules or with their environment. Most of these groups have just one interesting function (e.g. electron donor, electron acceptor, hydrogen donor, hydrogen acceptor). Nevertheless, some functional groups like ureas also have more than just a single functionality.[1, 2] An urea group can for example act as a hydrogen donor and acceptor at the same time. Due to their dipole moment, urea groups can also interact with other dipoles. All of its properties are very interesting for the studies of intermolecular interactions and thus, it is of interest to implement urea groups into ligands for metallo-supramolecular self-assembly. In order to use the properties of urea groups to gain functionalized metallo-supramolecular complexes which can be used for molecular recognition, the bispyridyl-urea ligands **162-168** have been synthesized.

Substituted urea compounds are often synthesized using isocyanates, phosgene or phosgene analogues as starting materials.[222, 223] Thus, the phosgene analogue *N,N´*-carbonyl diimidazole **161** was used to synthesize the bispyridyl-urea ligands **162-168** from the amino-pyridines **154-158** or aminomethyl pyridines **159** and **160**.[106] The dipyridylurea ligands **162-168** were obtained in acceptable chemical yields (55 – 93%; Figure 5.29).

The solubility of the urea ligands is rather poor in most organic solvents. On the one hand, this is an advantage during the syntheses of the ligands 162-168. The bispyridyl-urea ligands precipitate in toluene, while the starting materials as well as the side products are soluble in toluene. On the other hand, the analysis of bispyridyl-urea ligands is limited to the use of highly polar aprotic solvents such as DMSO and DMF. For example, 1,3-bis(6-methylpyridin-3-yl)urea **166** was only soluble in DMSO or DMF at $T \geq 60$ °C.

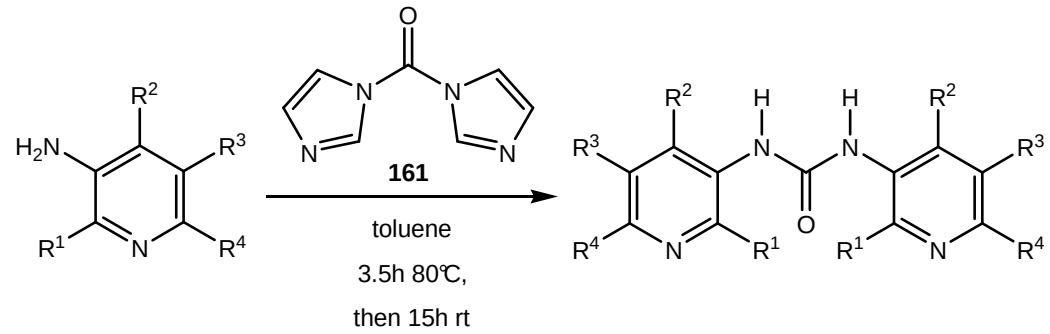

	R^1	R^2	R^3	R^4
154	H	H	H	H
155	Me	H	H	H
156	H	Me	H	H
157	H	H	Me	H
158	H	H	H	Me

	R^1	R^2	R^3	R^4	%
162	H	H	H	H	85
163	Me	H	H	H	60
164	H	Me	H	H	62
165	H	H	Me	H	75
166	H	H	H	Me	93

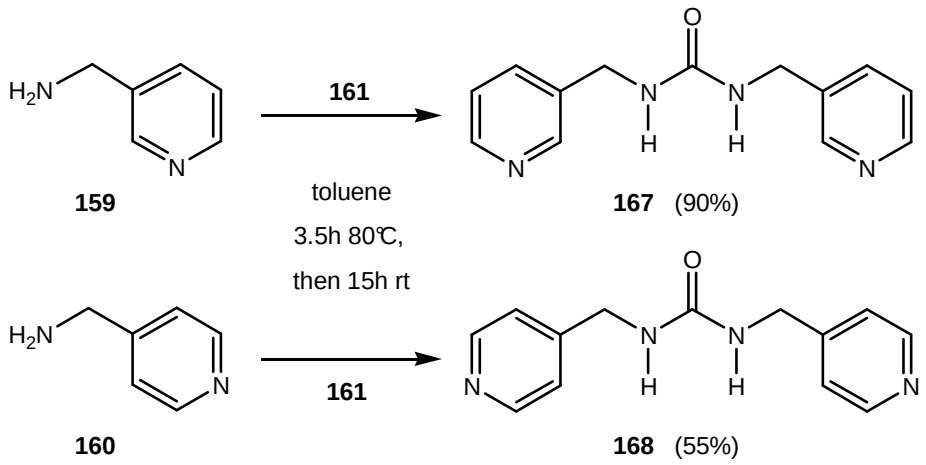

159 **167** (90%)

160 **168** (55%)

Figure 5.29: *Syntheses of the different bispyridyl-urea ligands* ***162-168****.*[106]

For the ability of the final assemblies to recognize guests or to be influenced by templates, it will be of great importance to control the orientation of the urea groups as well as that of the pyridines. Since for ligands **162-166** the C-H bonds *ortho* and *para* to the pyridine nitrogen atom are the most polarized positions, they are able to form intramolecular C-H•••O contacts with the carbonyl oxygen. These contacts flatten the molecule, considerably affect the angle defined by the two lines through the pyridine nitrogens and the *para*-carbon atoms, and may even be important to establish a certain orientation of the urea units connecting the two pyridine rings. Replacing one of these hydrogens by methyl groups may be expected to change this

behaviour significantly. These changes would likely also affect the formation of coordination complexes with the dipyridylurea ligands incorporated in this study. In total, three different planar structures can be drawn which consider these aspects (Figure 5.30). In a *syn-syn* conformarion both pyridine nitrogen atoms show into the same direction as the carbonyl oxygen atom. The opposite of this would be an *anti-anti* conformation wherein both pyridine nitrogen atoms show into the opposite direction of the carbonyl oxygen atom. A mixed isomer of these is called *syn-anti* isomer.

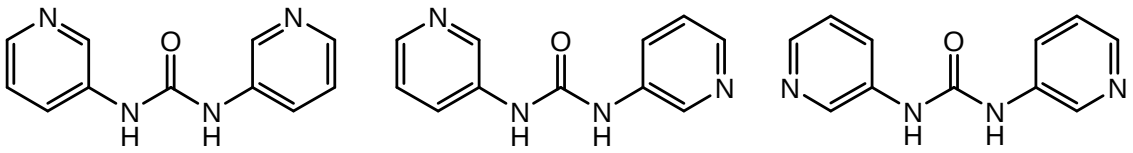

Figure 5.30: *The three different orientations of the bispyridyl-urea ligands are shown for ligand* ***162****.*

In order to get some experimental evidence, the orientations of the ligands in solution were established by 1D NOESY experiments which provided information about those aromatic and methyl C-H atoms which are close to the urea NH protons (Figure 5.31). For ligand **162** the NOE experiments in DMF-d_7 show a slight preference of the *anti-anti* isomer. Due to the increased steric hinderance introduced by the methyl group in *ortho*-position of the pyridine-nitrogen atomss, ligand **163** strongly prefers the *anti-anti* conformation. No NOE between the NH and the *p*-pyridine CH is observed. Based on the same steric effects, ligand **164** clearly exhibits a *syn-syn* conformation. In contrast to **163** and **164**, no conformation seems to be clearly preferred over the other by ligand **165**. Due to its very low solubility in any solvent at appropriate temperatures, no comparable NOESY spectra could be obtained for ligand **166**, but one may consider an analogous behaviour as observed for **162** and **165**. Similar to ligand **162**, rotation of the pyridines is not sterically hindered for ligands **165** and **166** and thus, they can easily switch between the different conformations. The equilibrium between these three different possible conformations is known to be highly solvent

dependent and thus, it may change for ligands **162**, **165** and **166**, if other solvents are used.[224] For ligands **163** and **164** every solvent effect should be overcompensated by the steric effect of their methyl groups.

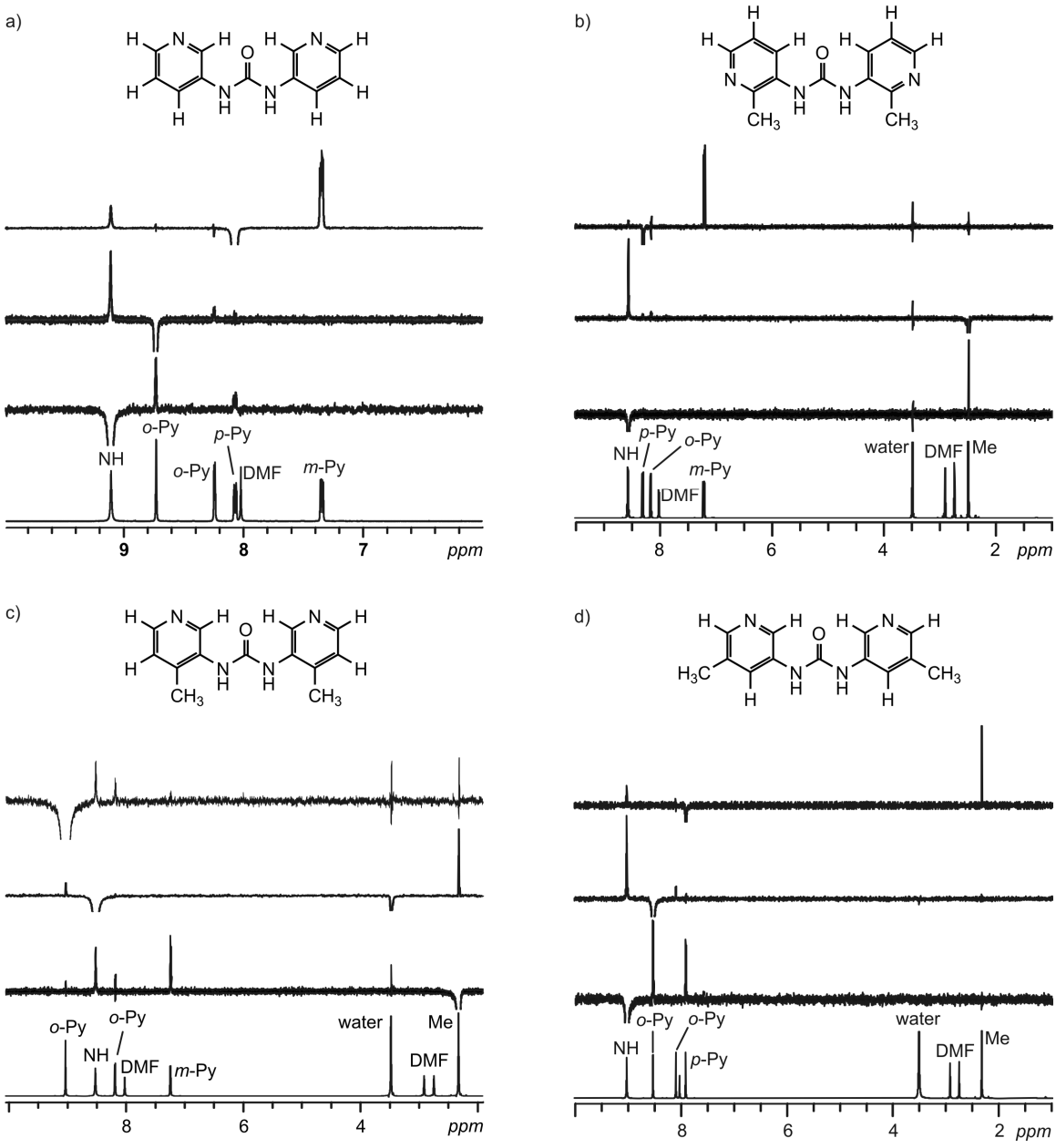

Figure 5.31: *The 1D ^{1}H NOESY NMR spectra of ligands a)* ***162****, b)* ***163****, c)* ***164*** *and d)* ***165****. All spectra were recorded in DMF-d_7 at 298 K. Due to its low solubility; no NOESY NMR spectra of ligand* ***166*** *could be recorded at 298 K.*

The analysis of the crystal structures of ligands **162-166** can support the information on the orientation of the gained from NOESY NMR experiments. The crystal structure of ligand **162** is known,[224, 225] but none of those of the corresponding dimethyl analogues. Crystals of ligands **162-165** could be obtained by diffsion of diethylether into a solution of these ligands in DMF. In contrast to this, ligand **166** was crystallized by slow cooling of a hot DMSO solution of **166**. Interestingly, crystals of **164** were only obtained when it was crystallized in the presence of minor impurities of imidazole.

Some X-ray structures of ligand **162** show the *syn-syn* isomer while others show the *anti-anti* isomer – depending on solvent and crystallization effects. The molecules are essentially planar due to the C-H•••O=C interactions which locks their overall conformation, and the pyridine rings are twisted only slightly with respect to the urea moiety. The values of the dihedral angles between the urea moiety non-hydrogen atoms and the pyridine rings are between 11.27(16) and 11.56(10)°. However, the different orientations of ligand **162** in its crystal structures support the results observed by NOESY NMR spectroscopy.

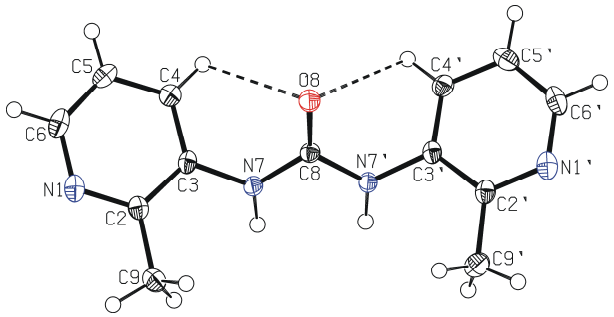

Figure 5.32: *The solid-state structure of **163** containing the atom-numbering scheme. The displacement ellipsoids for non-hydrogen atoms are drawn at the 50 % probability level. The intramolecular hydrogen bonds are shown in dashed lines.*

Ligand **163** (Figure 5.32) is structurally very similar to the non-methylated analogue **162**. However, introducing the methyl groups at the 2-position of pyridine rings causes deviation from planarity. The two pyridine rings, N1-C6 (Py) and N1'-C6' (Py'), form an angle of 26.95(7)°, and the angles between the Py and Py' rings and the

N7/C8/O8/N7' urea moiety atoms are 44.86(8) and 49.20(8)^{o}, respectively. Although this ligand is slightly bent, and the rings are twisted relatively to the urea moiety, its conformation still allows C-H•••O intramolecular hydrogen-bond formation (Figure 5.32; Table 5.3). Because of steric reasons, *i.e.* a repulsion between the carbonyl oxygen atom and the methyl groups, the molecule adops the *anti-anti* conformation.

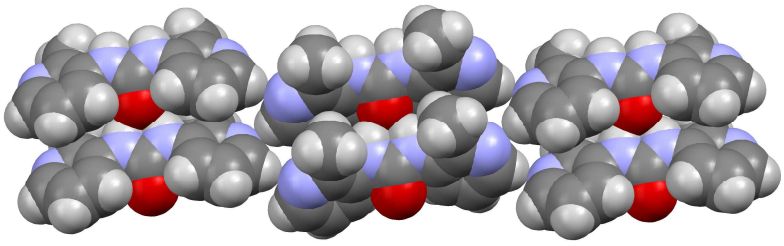

Figure 5.33: *CPK plot of the packing of* ***163****, showing hydrogen-bonded molecules running in opposite directions.*

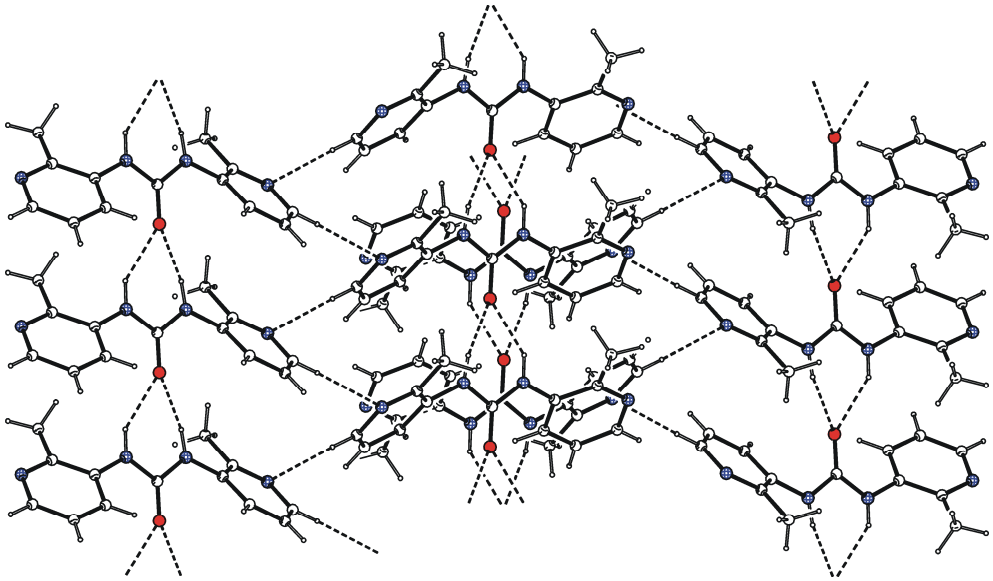

Figure 5.34: *A part of the crystal structure of* ***163****, showing the α–network and the double chains formed by N–H···O and C–H···N hydrogen bonds. The hydrogen bonds are indicated by dashed lines.*

In the crystal, adjacent molecules are held together by two N-H•••O hydrogen bonds involving both urea nitrogen atoms and the carbonyl oxygen atom, so forming α-network (Table 5.3). The hydrogen-bonded chains built of bifurcated N-H•••O hydrogen bonds run in opposite directions (Figure 5.33). Two C–H•••π interactions participate also in chain formation as methyl hydrogen atoms point to the pyridine rings of neighbouring molecules (Table 5.4). Finally, these chains are mutually linked by C-H•••N hydrogen bonds forming double chains and hydrogen-bonded sheets (Figures 5.34 and 5.35).

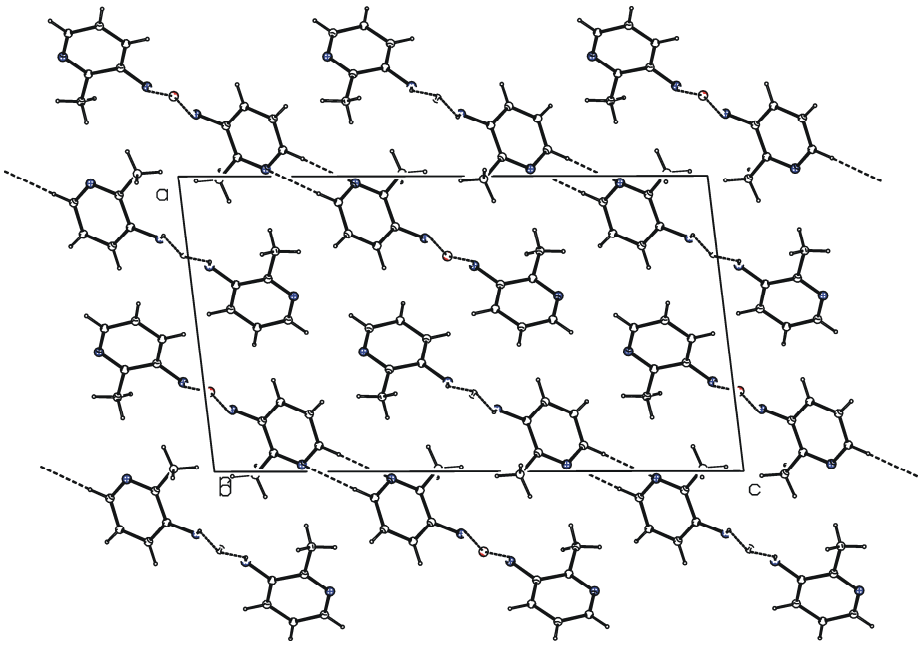

Figure 5.35: *A crystal packing diagram of* ***163****, viewed down the b axis, showing hydrogen-bonded sheets. Hydrogen bonds are indicated by dashed lines.*

Table 5.3: *Hydrogen-bonding geometry for* ***163-166****.*

	D–H•••A	D–H (Å)	H•••A (Å)	D•••A (Å)	D–H•••A (°)	Symmetry codes
163	C4–H4•••O8	0.95	2.58	2.9409(18)	103	
	C4'–H4'•••O8	0.95	2.64	2.9452(18)	99	
	N7–H7•••O8	0.88	2.08	2.8638(16)	148	x, -1+y, z
	N7'–H7'•••O8	0.88	2.11	2.8793(17)	145	x, -1+y, z
	C6'–H6'•••N1'	0.95	2.61	3.556(2)	178	2-x, 1/2+y, 1/2-z
164	C2–H2•••O8	0.95	2.27	2.845(4)	118	
	C2'–H2'•••O8	0.95	2.22	2.834(4)	122	
	N7–H7•••N10	0.88	2.18	3.011(4)	157	
	N7'–H7'•••N10	0.88	2.18	3.010(4)	158	
	N12–H12•••O15	0.88	1.96	2.802(4)	159	
	O15–H15A•••N1'	0.96(2)	1.84(2)	2.784(3)	169(4)	x, -1+y, z
	O15–H15B•••N1	0.95(3)	1.99(3)	2.898(4)	158(3)	1+x, -1/2-y, 1/2+z
	C14–H14•••O8	0.95	2.53	3.376(4)	149	-x, -y, 1-z
165	C2–H2•••O8	0.95	2.26	2.890(5)	123	
	C4'–H4'•••O8	0.95	2.39	2.948(5)	117	
	N7–H7•••N1	0.88	2.09	2.936(5)	162	1-x, y, 1/2+z
	N7'–H7'•••N1	0.88	2.23	3.044(5)	154	1-x, y, 1/2+z
	C6–H6•••O8	0.95	2.47	3.318(5)	149	1-x,-1/2+y,1-z
166	C4–H4•••O8	0.95	2.30	2.864(3)	117	
	C4'–H4'•••O8	0.95	2.28	2.872(3)	120	
	N7–H7•••N1'	0.88	2.19	2.965(3)	147	1-x, -1/2+y, 1/2-z
	N7'–H7'•••N1	0.88	2.17	2.944(3)	146	-x, 1/2+y, 1/2-z
	C2'–H2'•••N1	0.95	2.57	3.342(4)	139	-x, 1/2+y, 1/2-z

Table 5.4: *The geometry of C–H•••π interactions for* ***163-166****.*

	D–H•••Cg	D–H (Å)	H•••Cg (Å)	D•••Cg (Å)	D–H•••Cg (°)	Symmetry codes
163	C9–H9C•••Py[a]	0.98	2.73	3.4593(16)	132	x, -1+y, z
	C9'–H91'•••Py'	0.98	2.71	3.5799(18)	148	x, -1+y, z
164	C13–H13•••Py	0.95	2.80	3.554(4)	137	x, -1/2-y, 1/2+z
165	C9'–H92'•••Py	0.98	2.80	3.683(5)	150	-1+x, 1/2+y, 3/2-z
166	C9–H9C•••Py'	0.98	2.82	3.582(3)	135	-1+x, -1+y, z
	C9'–H93'•••Py	0.98	2.82	3.552(3)	132	1+x, 1+y, z

[a] Py denotes the N1/C2/C3/C4/C5/C6 ring, and Py' the N1'/C2'/C3'/C4'/C5'/C6' pyridine ring

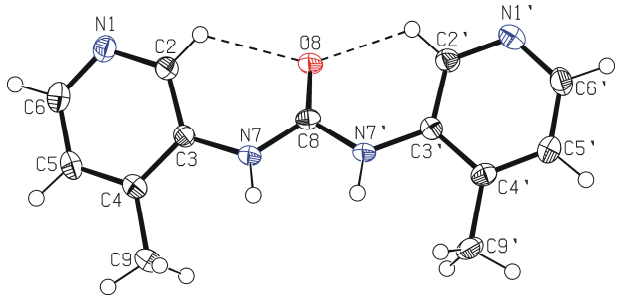

Figure 5.36: *Solid-state structure of* ***164****, with the atom-numbering scheme. The water and imidazole molecules have been omitted for clarity. The displacement ellipsoids for non-hydrogen atoms are drawn at the 50 % probability level. Intramolecular hydrogen bonds are shown dashed.*

In the crystal structure of ligand **164** (Figure 5.36), the nitrogen atoms have the same orientation with respect to the carbonyl oxygen atom (*syn-syn*). Although the methyl groups are in the same position with respect to the urea moiety as in **163**, *i.e.* they are close to the hydrogen atoms of the N7 and N7´atoms, the molecule is more flattened. The values of the dihedral angles between the urea moiety and two pyridine rings are significantly smaller (21.9(2)° for Py and 16.2(2)° for Py') and the angle between the pyridine rings is only 12.9(2)°. This more planar orientation of the pyridine rings and the urea carbonyl group compared with ligand **163** enables significantly shorter H•••O contacts (Table 5.3) and is probably caused by intermolecular interactions.

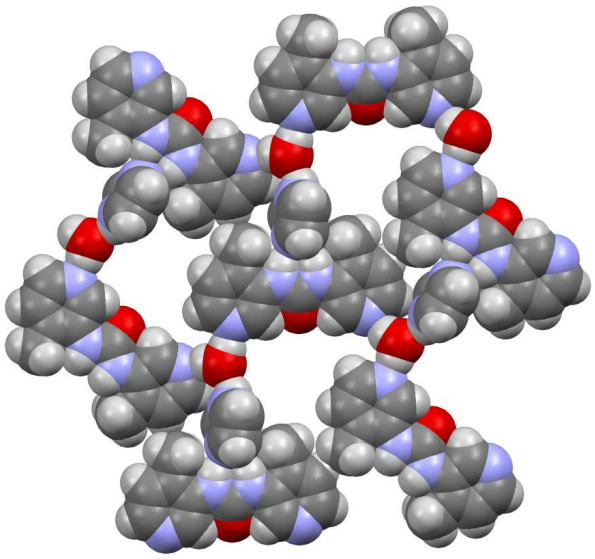

Figure 5.37: *CPK plot of packing of* ***164****, showing the hydrogen-bonded circle made of ligands, water and imidazole molecules.*

The supramolecular architecture of **164** is completely different since water and imidazole molecules play a significant role in molecular packing (Table 5.3). Both nitrogen atoms of the urea moiety are linked to the neighbouring imidazole molecule, which are further linked to the water molecule. Both hydrogen atoms of the water molecule form hydrogen bonds with the Py nitrogen atoms closing a hydrogen-bonded circle and forming a two-dimensional network (Figure 5.37). One C–H•••O hydrogen bond participates also in the network formation. Finally, the hydrogen atom of the imidazole molecule is directed towards pyridine ring of neighbouring network, and thus, one C–H•••π interaction (Table 5.4) completes the three-dimensional network (Figure 5.38).

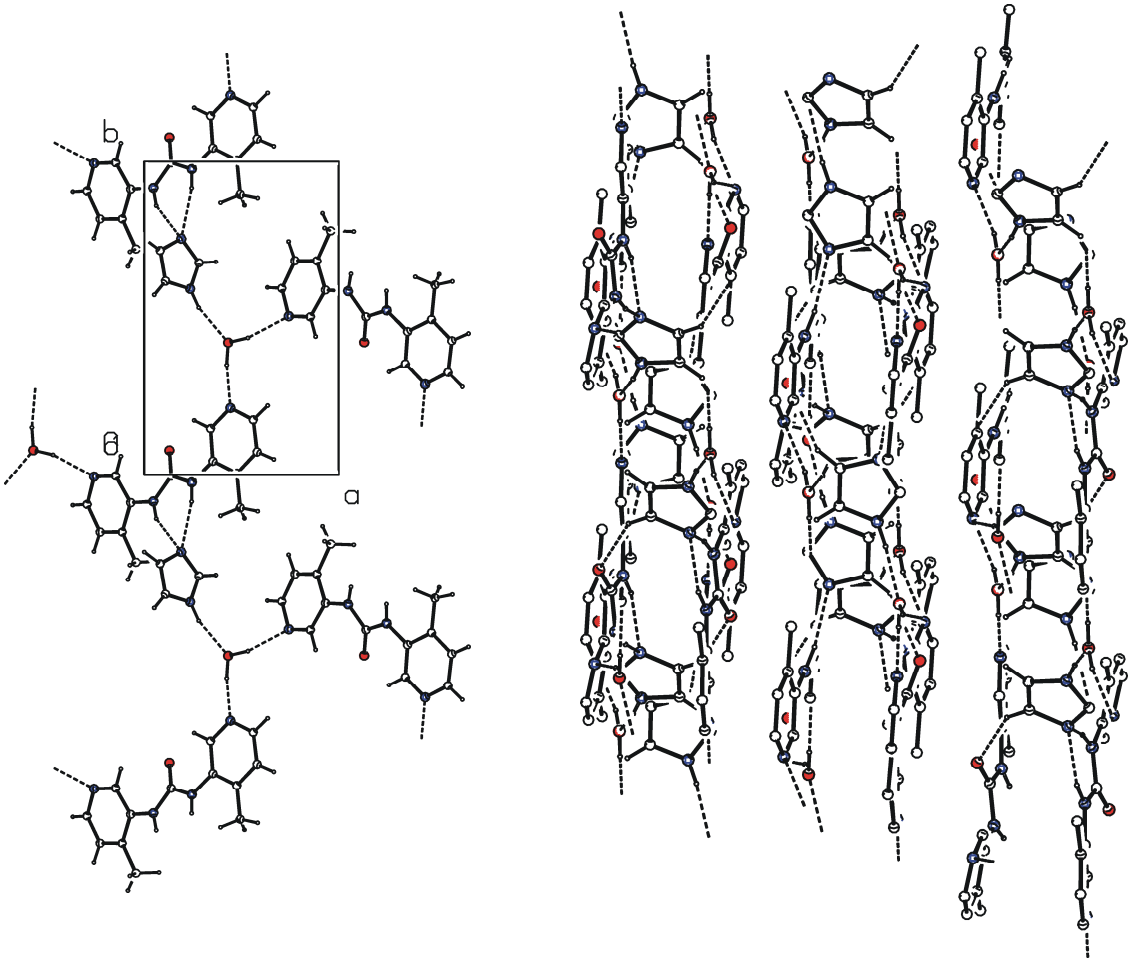

Figure 5.38: *Left) A crystal packing diagram of* ***164*** *viewed down the c axis, showing the two-dimensional network formed by N–H···N, N–H···O and O–H···N hydrogen bonds. The hydrogen bonds are indicated by dashed lines. Right) A part of the crystal structure of* ***164****, showing the two-dimensional network and hydrogen atoms of the imidazole molecules pointing to the pyridine rings of the neighboring molecules. The hydrogen bonds are indicated by dashed lines and the hydrogen atoms which not involved in intermolecular interactions have been omitted for clarity.*

As there is no steric hindrance of the ring methyl groups with the urea moiety atoms, **165** is almost planar (Figure 5.39). The pyridine ring (Py) forms a dihedral angle of only 4.3(2)^{o} with respect to the urea moiety (C–N–C–O angle), while the dihedral angle between this moiety and Py' ring is slightly bigger 14.8(2)^{o}. The pyridine nitrogen atoms in **165** have two different orientations with respect to the carbonyl oxygen atom defined as syn-anti-molecular conformation. Consequently, two

different pyridyl carbon atoms, C2 and C4', are intramolecular hydrogen-bond donors (Table 5.3). The dihedral angle between the rings is 14.3(2)°.

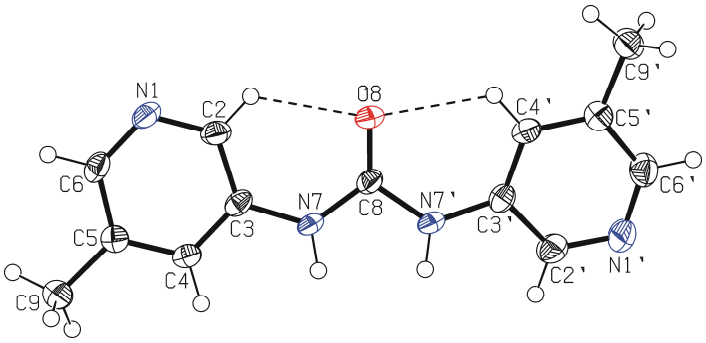

Figure 5.39: *Solid-state structure of* ***165****, with the atom-numbering scheme. The displacement ellipsoids for non-hydrogen atoms are drawn at the 50 % probability level. Intramolecular hydrogen bonds are shown dashed.*

As in **163**, the main hydrogen-bonded motif in **165** is an *α*-network, but the molecules are disposed in a zig-zag manner (Figure 5.40) and a chain is formed by two N–H•••N hydrogen bonds (Table 5.3). One C–H•••O hydrogen bond links the neighbouring chains into a two-dimensional network (Figure 5.41, left). One C–H•••π interaction and two π•••π interactions (Table 5.4; Figure 5.41, right) participate also in the supramolecular assembly and thus generate a three-dimensional network.

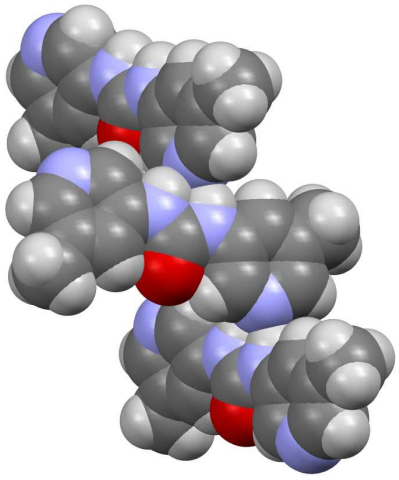

Figure 5.40: *CPK plot of packing of ligand* ***165****, showing the zigzag chains of the molecules.*

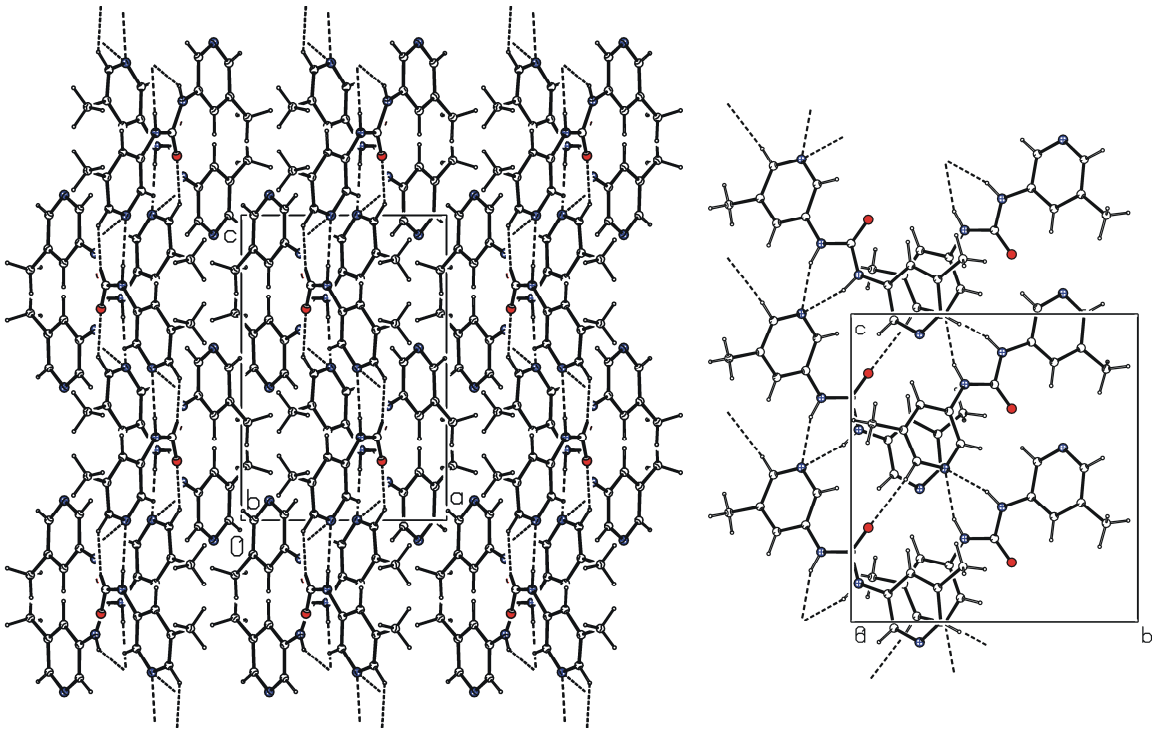

Figure 5.41: *Left) A crystal packing diagram of* ***165*** *viewed down the b axis, showing a two-dimensional network formed by N–H···N and C–H···O hydrogen bonds. The hydrogen bonds are indicated by dashed lines. Right) A crystal packing diagram of* ***165*** *viewed down the a axis, showing the stacking of the molecules and π···π interactions.*

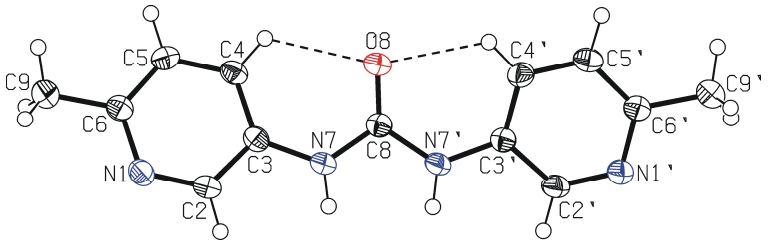

Figure 5.42: *Solid-state structure of* ***166****, with the atom-numbering scheme. The displacement ellipsoids for non-hydrogen atoms are drawn at the 50 % probability level. Intramolecular hydrogen bonds are shown dashed.*

The molecule of compound **166** is also planar, with similar values of the dihedral angles as in **165** (Figure 5.42). The angle between the pyridyl rings is 18.91(12)°, and the angles between the urea moiety and the rings are approximately equal (8.26(14)°

for Py; 11.19(14)^{o} for Py'). The molecule shows an anti-orientation of the pyridine nitrogens and the carbonyl oxygen, and its conformation is locked by C4•••O8 and C4'•••O8 hydrogen bonds (Table 5.3).

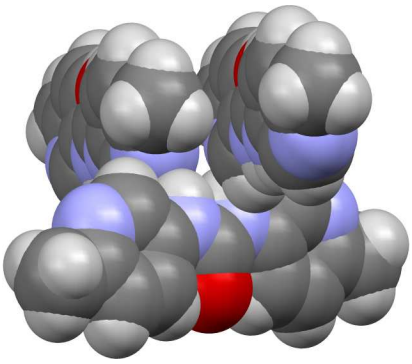

Figure 5.43: *CPK plot of packing of* ***166****, showing two N–H•••N hydrogen bonds and the molecules disposed in the herringbone fashion.*

The molecules of **166** are linked by two N–H•••N hydrogen bonds between the nitrogen atoms of the urea moiety and the pyridine rings. Compared to **165**, two N–H bonds are directed to pyridine rings of two different molecules (Figure 5.43). One C–H•••N hydrogen bond connects the molecules disposed in the herringbone fashion and form a two-dimensional network (Figure 5.44). This network is extended to a three-dimensional network by two C–H•••π interactions (Table 5.4). It should be also added that the arrangement of the molecules does not provide pyridine rings' stacking and π•••π interactions (Table 5.5).

The information about the conformation of the ligands derived from the crystal structure data analysis supports the results obtained by NOESY NMR spectroscopy.

Table 5.5: *The geometry of π•••π interactions for ligand* ***166****.*

	Cg•••Cg	Cg•••Cg (Å)	α (^{o})	CgI•••Perp (Å)	Slippage (Å)	Symmetry codes
117	Py•••Py'[a]	3.795(2)	5.3(2)	3.5084(17)	*ca*. 1.45	x, -1/2+y, 3/2-z
	Py'•••Py	3.795(2)	5.3(2)	3.5061(17)	*ca*. 1.45	x, 1/2+y, 3/2-z

[a] Py denotes the N1/C2/C3/C4/C5/C6 ring, and Py' the N1'/C2'/C3'/C4'/C5'/C6' pyridine ring

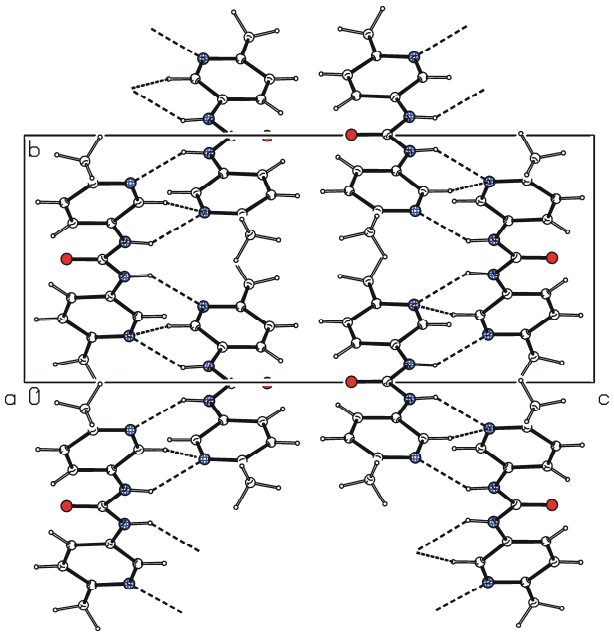

Figure 5.44: *A crystal packing diagram of* ***166*** *viewed down the a axis, showing the two-dimensional network formed by N–H···N and C–H···N hydrogen bonds. The hydrogen bonds are indicated by dashed lines.*

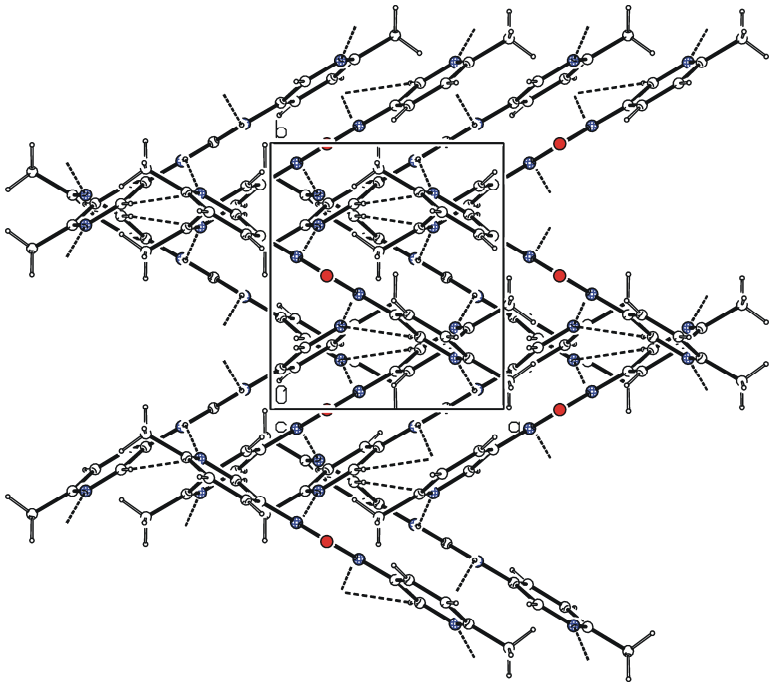

Figure 5.45*: A crystal packing diagram of* ***166*** *viewed down the c axis, showing the hydrogen-bonded molecules disposed in herringbone fashion. The hydrogen bonds are indicated by dashed lines.*

5.3.2 The Self-Assembly of Bispyridyl-Urea based M_2L_2 Complexes and their Equilibria with the corresponding M_3L_3 Complexes

It is well known, that the self-assembly of linear divalent ligands with *cis*-blocked square-planar metal centers results in the formation of metallo-supramolecular M_4L_4 squares and their corresponding M_3L_3 triangles (see chapter 5.2.2).[78-91] When non-linear and/or flexible divalent ligands are used instead, smaller M_2L_2 complexes can be achieved (see chapter 5.2.1).[72] Astonishingly, not many examples of equilibria between M_2L_2 and M_3L_3 complexes have been reported up to now.[64, 70, 77, 109] In general, the equilibrium between two metallo-supramolecular assemblies like M_2L_2 and M_3L_3 complexes is based on a sensitive balance between enthalpy and entropy which is influenced by many different parameters (see chapter 3.3.2).[104-106] However, when functionalized non-linear divalent ligands are combined with *cis*-blocked square-planar metal centers, the functional groups of the resulting complexes can interact with other molecules and thus these complexes could be used for molecular recognition. Furthermore, the guest molecules used might also act as templates which influence equilibria between different metallo-supramolecular complexes one way or the other.

In order to obtain small functionalized metallo-supramolecular macrocycles, the self-assembly of bispyridyl-urea ligands **162-168** together with metal centers **19**, **27** and **28** has been studied. The study was performed in cooperation with Dr. Torsten Weilandt, Rainer Hovorka, Dr. Mario Cetina, Dr. Martin Nieger, Prof. Dr. Kari Rissanen and Prof. Dr. Dieter Lentz.

The metallo-supramolecular assemblies under study have been formed from the bispyridyl-urea ligands **162-168** by mixing stoichiometric amounts of the ligands with metal centers (en)Pd$(NO_3)_2$ **19**, (dppp)Pd$(OTf)_2$ **27** or (dppp)Pt$(OTf)_2$ **28** in water or in polar aprotic DMSO or DMF (Figure 5.46). If the Fujita-type metal center **19** was used, M_2L_2 complexes were observed. Instead of this, equilibria between M_2L_2 and M_3L_3 complexes were observed, if the Stang-type metal centers **27** and **28** were used. Unfortunately, no defined assemblies like M_2L_2 could be observed using ligands **163** and **166**.

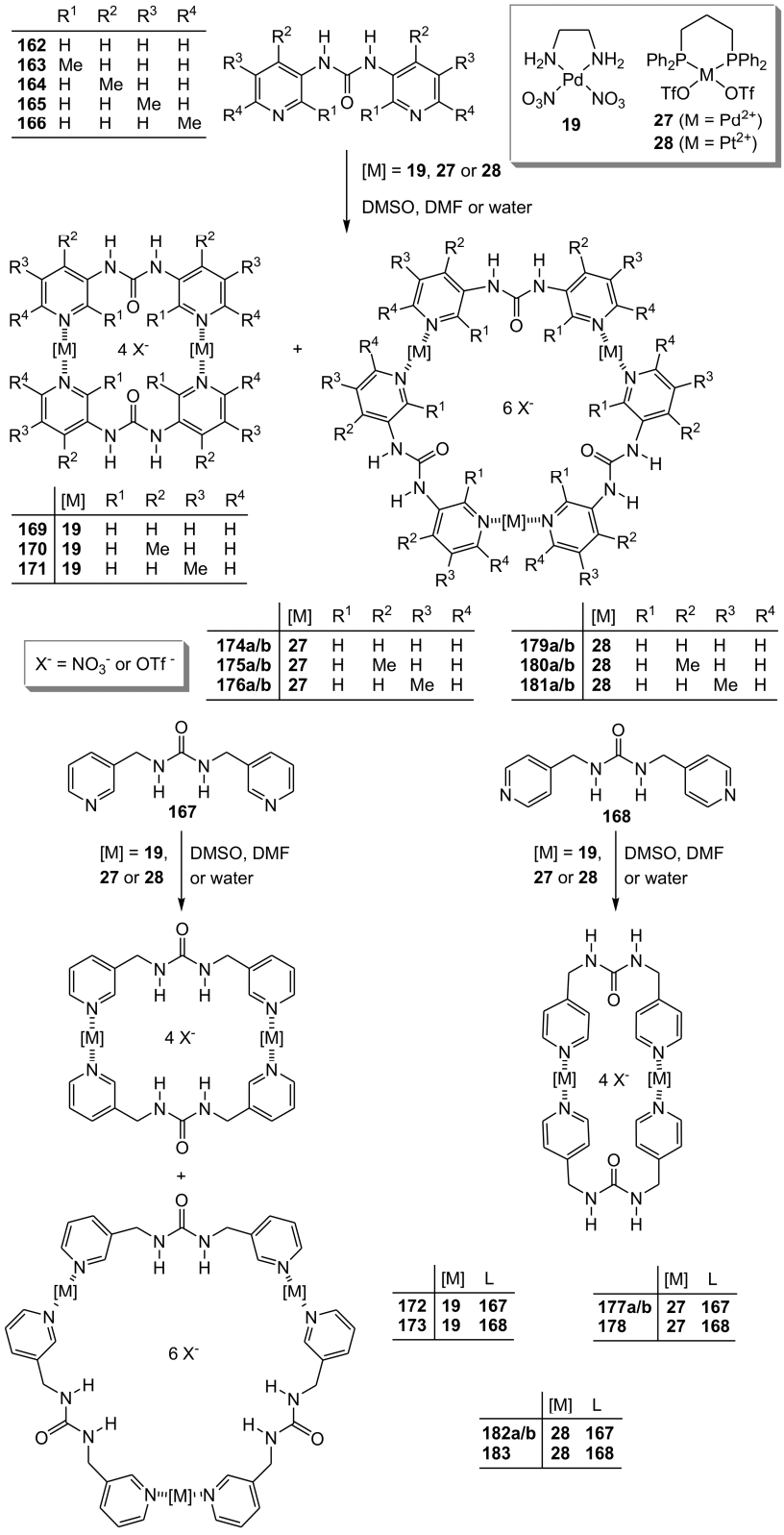

	R1	R2	R3	R4
162	H	H	H	H
163	Me	H	H	H
164	H	Me	H	H
165	H	H	Me	H
166	H	H	H	Me

	[M]	R1	R2	R3	R4
169	**19**	H	H	H	H
170	**19**	H	Me	H	H
171	**19**	H	H	Me	H

	[M]	R1	R2	R3	R4
174a/b	**27**	H	H	H	H
175a/b	**27**	H	Me	H	H
176a/b	**27**	H	H	Me	H

	[M]	R1	R2	R3	R4
179a/b	**28**	H	H	H	H
180a/b	**28**	H	Me	H	H
181a/b	**28**	H	H	Me	H

	[M]	L
172	**19**	**167**
173	**19**	**168**

	[M]	L
177a/b	**27**	**167**
178	**27**	**168**

	[M]	L
182a/b	**28**	**167**
183	**28**	**168**

Figure 5.46: *Self-assembly of the complexes* ***169-183*** *wherein* ***a*** *represents the* M_2L_2 *complexes and* ***b*** *the* M_3L_3 *complexes.*

The equilibria of the self-assembled complexes are usually reached within several minutes. Nevertheless, the mixtures were stirred for one hour at room temperature before analysis in order to make sure that the equilibria are monitored. For NMR experiments, 1:1 mixtures of metal centers **19, 27** or **28**, respectively, and ligands **162-168** were dissolved in 0.5 ml of deuterated water, DMSO or DMF to prepare a solution with a building block concentration of 20 mM. Due to solubility reasons, DMSO and DMF had to be used, furthermore in the case of DMF, a wide temperature range for variable temperature NMR experiments is accessible. However, neither of them is well-suited as a spray solvent for electrospray mass spectrometric experiments due to their high boiling points and low vapour pressures. The solutions for mass spectrometric analysis were therefore prepared by mixing metal center and ligand in DMSO followed by dilution with acetone to a concentration of ca. 200 μM.

If the ligands coordinate to the metal centers or not, can easily be observed by the chemical shifts of the protons in ^{1}H NMR spectroscopy. Especially the protons of the ligand-pyridines undergo significant chemical shifts to lower field, when a successful coordination occurred. However, a comparison of the experimental ^{1}H NMR data of the ligands with their corresponding metallo-supramolecular assemblies revealed successful coordination. On the one hand, only one set of signals is observed for all systems containing **19** as metal center. On the other hand, two different sets of signals are observed for the systems **174a/b-177a/b** and **179a/b-182a/b** containing metal centers **27** or **28** (Figure 5.47). Unlike Ballester and co-workers, just one set of signals was observed for the metallo-supramolecular systems containing ligand **168** (systems **178** and **183**). The use of Stang-type metal centers (**27**, **28**) discloses ^{31}P NMR spectroscopy as a well known and very sensitive analytical method for coordination complexes. Instead of systems **178** and **183**, all systems with metal centers **27** and **28** show two ^{31}P NMR signals, which is perfectly in line with the results from ^{1}H NMR spectroscopy of these systems. In these cases two species are present in solution. Another reliable indicator of complex formation is the ^{195}Pt-P coupling constant of the pyridine complexes ($^{1}J_{\text{Pt-P}}$ = 3000-3036 Hz), which is significantly different from that of the metal center **27** ($^{1}J_{\text{Pt-P}}$ = 3657 Hz). If ligands **163** and **166** are combined with metal centers **19**, **27** or **28**, no complexation could be observed.

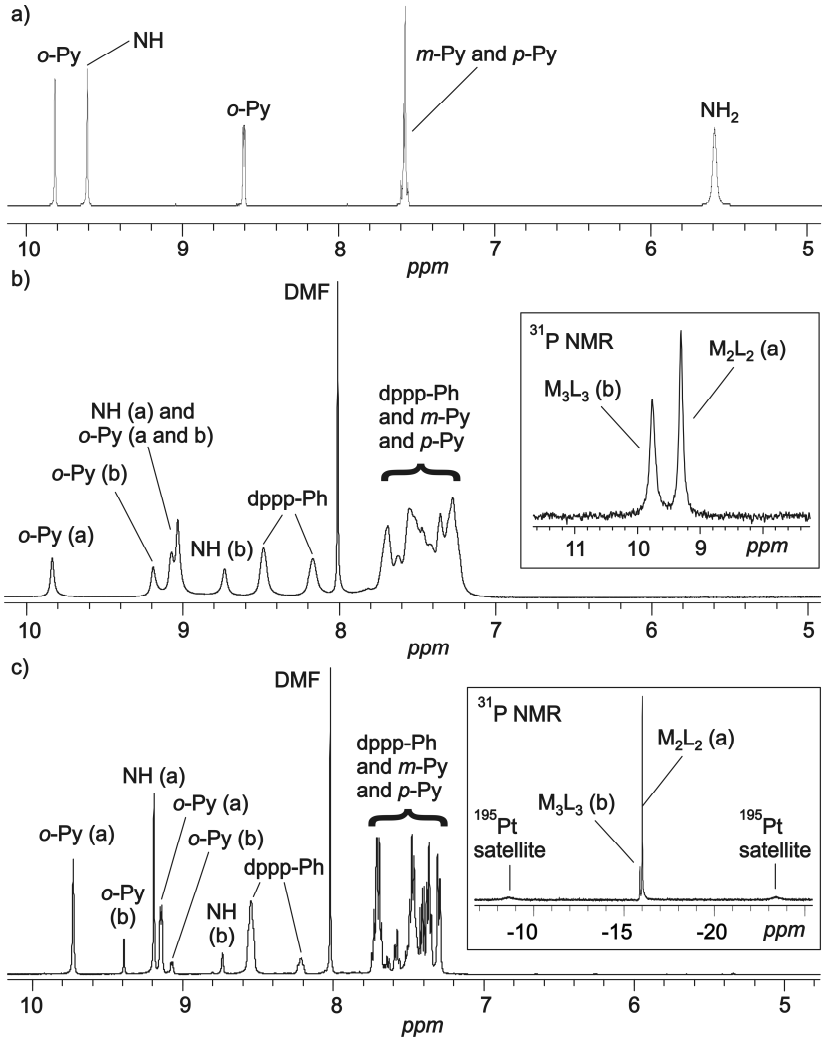

Figure 5.47: *NMR spectra of the systems with ligand* ***162****: a)* ^{1}H *NMR spectrum of system* ***169*** *(298 K, DMSO-*d_6*); b)* ^{1}H *and* ^{31}P *NMR spectra of system* ***174a/b*** *(303 K, DMF-*d_7*) and c)* ^{1}H *and* ^{31}P *NMR spectra of system* ***179a/b*** *(298 K, DMF-*d_7*). The different complexes in b) and c) are assigned with a (*M_2L_2*) and b (*M_3L_3*).*

Single crystals were successfully obtained of four metallo-supramolecular M_2L_2 assemblies. Three of those contain (dppp)Pd$(OTf)_2$ **27** as metal center and the fourth contained (en)Pd$(NO_3)_2$ **19**. The single crystals of the M_2L_2 complexes **174a**, **175a** and **178** were obtained via diffusion of diethylether into a solution of the complexes in DMF, respectively. In contrast, complex **171** crystallized from a solution in water.

Complex **174a** (Figure 5.48) crystallized with two independent cationic M_2L_2 complexes and correspondingly eight triflate anions in the asymmetric unit, while the crystal

structure of complex **175a** (Figure 5.49) besides the M_2L_2 cationic complex and four triflate counter-anions also includes three molecules of *N,N*-dimethylformamide, one diethyl ether molecule and one crystal lattice water.

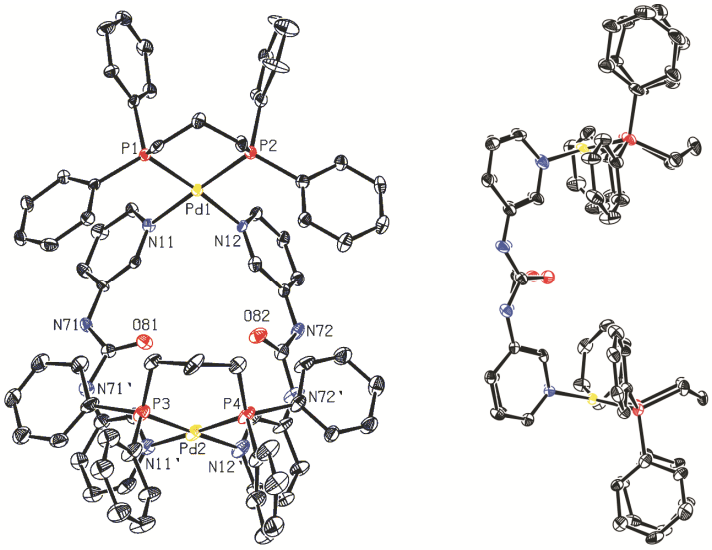

Figure 5.48: *Solid-state structure of the independent cationic complex* ***174a*** *containing the atom-numbering scheme. The displacement ellipsoids for non-hydrogen atoms are drawn at the 20 % probability level. The hydrogen atoms have been omitted for clarity. Selected bond lengths (Å) and angles (°): Pd1–N11 = 2.106(7), Pd1–N12 = 2.100(7), Pd1–P1 = 2.275(2), Pd1–P2 = 2.281(2), Pd2–N11' = 2.078(9), Pd2–N12' = 2.113(9), Pd2–P3 = 2.274(3), Pd2–P4 = 2.262(3), Pd3–N13 = 2.106(8), Pd3–N14 = 2.102(7), Pd3–P5 = 2.263(3), Pd3–P6 = 2.277(3), Pd4–N13' = 2.088(10), Pd4–N14' = 2.119(9), Pd4–P7 = 2.269(4), Pd4–P8 = 2.273(3); N12–Pd1–N11 = 85.7(3), P1–Pd1–P2 = 90.54(9), N11'–Pd2–N12' = 86.3(4), P4–Pd2–P3 = 89.97(12), N14–Pd3–N13 = 85.7(3), P5–Pd3–P6 = 90.49(9), N13'–Pd4–N14' = 86.2(4), P7–Pd4–P8 = 89.62(13).*

The palladium atoms have a distorted square planar geometry in both complexes. Two *cis* positions of the Pd(II) atoms are occupied by two phosphorous atoms of the dppp ligand while the remaining binding sites are coordinated by two pyridyl nitrogens atoms from 1,3-bis(3-pyridyl)urea **162**. The N–Pd–N angles in two independent cationic complexes of **174a** are narrowed and fall in the range of 85.7(3)-86.3(4)°. The deviation from ideal square planar geometry is probably caused by steric reasons. In **175a** the N11–Pd1–N12

bond angle of 86.22(16)^{o} is in the same range as in **174a** but the N11'–Pd2–N12' angle value of 88.59(17)^{o} is closer to the value for an ideal square planar geometry. The bidentate phosphine bite angles range from 89.62(13)-90.54(9)^{o} in complex **174a** and amount 89.36(5) and 92.28(5)^{o} in complex **175a** while the distances between the Pd(II) atoms are 8.81 Å in both cations of **174a** and 8.83 Å in **175a**. Side view on a cation of **174a** reveals that both ligands, dppp and **162**, are almost perfectly overlapped (Figure 5.48). The bispyridylurea moiety is slightly bent and the dihedral angles between pyridyl rings are in the very short range, from 13.4(5) to 17.2(5)^{o}.

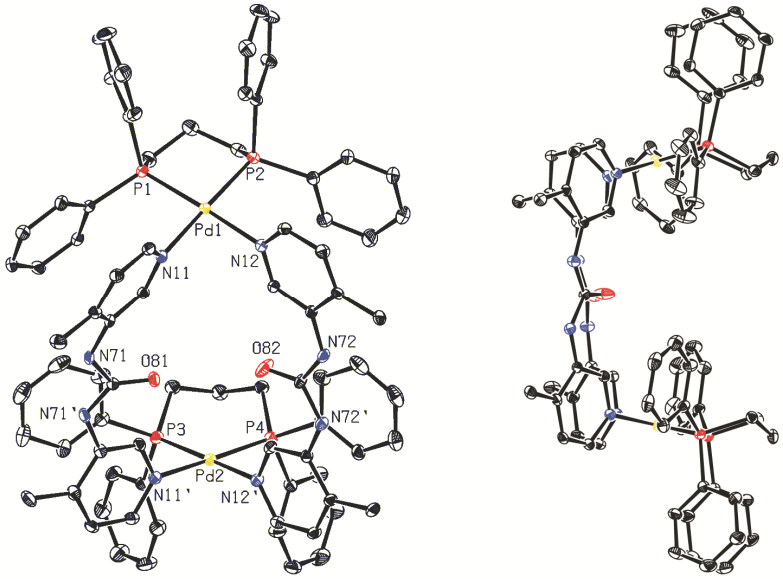

Figure 5.49: *Solid-state structure of the cation of complex* ***176a*** *containing the atom-numbering scheme. The displacement ellipsoids for non-hydrogen atoms are drawn at the 20 % probability level. The hydrogen atoms have been omitted for clarity. Selected bond lengths (Å) and angles (^{o}): Pd1–N11 = 2.100(4), Pd1–N12 = 2.107(4), Pd1–P1 = 2.2745(14), Pd1–P2 = 2.2787(14), Pd2–N11' = 2.095(5), Pd2–N12' = 2.106(4), Pd2–P3 = 2.2818(14), Pd2–P4 = 2.2714(15); N11–Pd1–N12 = 86.22(16), P1–Pd1–P2 = 89.36(5), N11'–Pd2–N12' = 88.59(17), P4–Pd2–P3 = 92.28(5).*

Although the molecular structure of **175a** is very similar to that of **174a**, the ligands are not so well overlapped (Figure 5.49). One bispyridylurea moiety is almost flattened, with a dihedral angle between the pyridyl rings of 7.8(3)^{o} (N11–C61/N11'–C61'), and the

second one is highly bent with the corresponding angle of 28.3(3)° (N12–C62/N12'–C62'). This deviation is probably a consequence of the geometric arrangement of the ligands during complex formation. Probably, it is not caused by repulsion between the methyl groups attached to the 4-position of the pyridine rings in ligand **164** and the neighbouring phenyl rings of the dppp ligand.

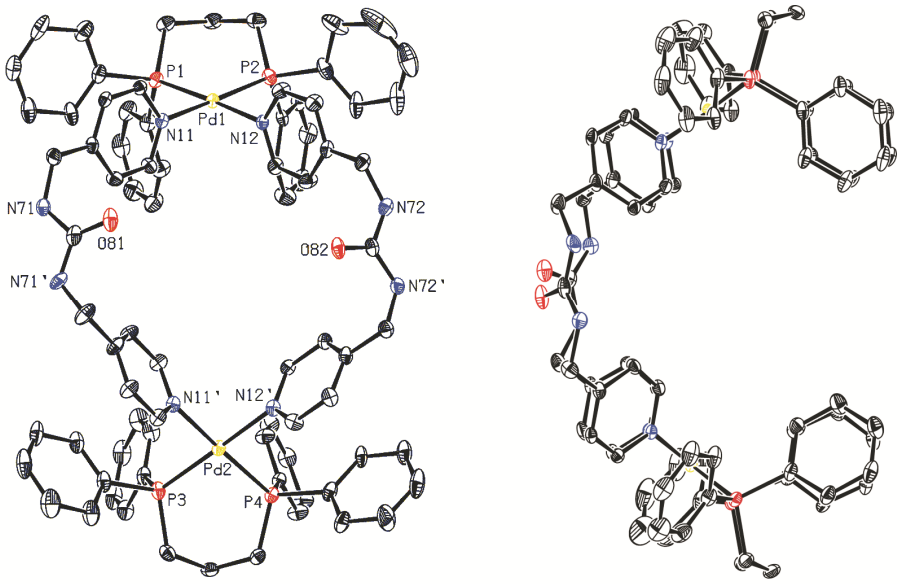

Figure 5.50: *The solid-state structure of the cation of complex* ***178*** *containing the atom-numbering scheme. The displacement ellipsoids for non-hydrogen atoms are drawn at the 20 % probability level. The hydrogen atoms have been omitted for clarity. Selected bond lengths (Å) and angles (°): Pd1–N11 = 2.087(6), Pd1–N12 = 2.099(6), Pd1–P2 = 2.275(2), Pd1–P1 = 2.275(2), Pd2–N11' = 2.087(7), Pd2–N12' = 2.103(6), Pd2–P4 = 2.273(2), Pd2–P3 = 2.281(2); N11–Pd1–N12 = 86.0(2), P2–Pd1–P1 = 90.36(8), N11'–Pd2–N12' = 85.8(3), P4–Pd2–P3 = 90.55(8).*

In complex **178**, 1,3-bis(4-pyridylmethyl)urea **168** was used for complex preparation (Figure 5.50). A survey of the Cambridge Structural Database[226] revealed that the structure of this compound is already published[77] and that the compound crystallizes in the orthorhombic space group $P\ 2_12_12_1$. However, we obtained a monoclinic $P\ 2_1/n$ polymorph of this compound, which includes also three dichloromethane and water molecules in the asymetric unit. The methylene spacers that link the pyridyl units with

the urea moiety result in a higher flexibility of the ligands. Thus, a C-shape of the cation is observed (Figure 5.50). Methylene group incorporation resulted in much a longer distance between the Pd atoms of 10.20 Å. The N–Pd–N angles are 86.0(2) and 85.8(3)^{o} and the P–Pd–P angles are 90.36(8) and 90.55(8)^{o}, so defining the same, a distorted square planar geometry of the palladium atoms is observed. This is similar to the structures found for complexes **174a** and **175a**.

In all three structures discussed above, one of the triflate counter-anions is located in the center of the cation, but in completely different positions. Thus, in **174a** (Figure 5.51) and **175a** the triflate is situated at the edge of the cation. On the contrary, the longer ligand **168** in complex **178** enables encapsulation of one of the triflates inside the cavity of the cation (Figure 5.51). Two other triflates in these complexes are displaced at the sides of the metallo-macrocycles, each of them interacting with one palladium center. However, in **178** one Pd atom interacts with a water oxygen atom instead of triflate, with the Pd1•••O3W distance of 3.035(7) Å.

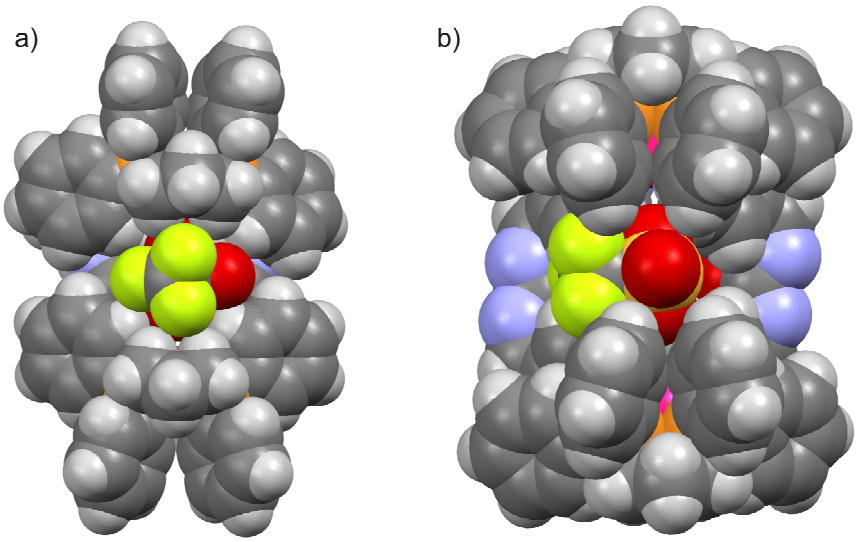

Figure 5.51: *Spacefilling model of complex* ***174a*** *(a) and complex* ***178*** *(b), showing the position of one triflate counter-anion, which is located in the center of cation. Other triflate counter-anions in* ***174a*** *and* ***178****, as well as solvent molecules in complex* ***178*** *have been omitted for clarity. Only the major component of the disordered triflate atoms in* ***178*** *is shown.*

The crystallization of ligand **165** with the (en)Pd(NO_3)$_2$ **19** resulted in a dinuclear complex with a completely different overall geometry. Metal center **19** is much less sterically demanding as (dppp)Pd(OTf)$_2$ **27**. Thus, complex **171** does not have a similar cavity as in the (dppp)Pd(OTf)$_2$ complexes (**174a**, **175a** and **178**) and does not show any inclusion of anions or solvent molecules (Figures 5.52 and 5.53).

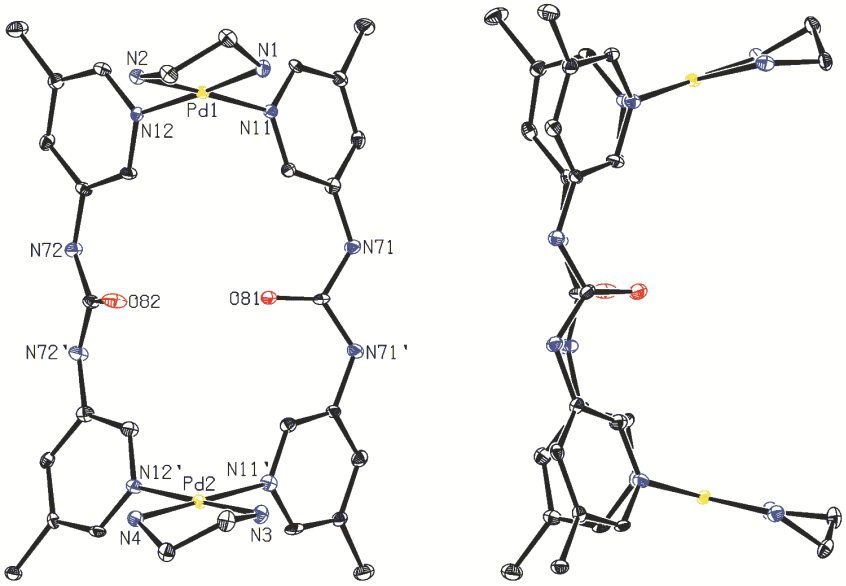

Figure 5.52: *Solid-state structure of the cation of complex* ***171*** *containing the atom-numbering scheme. The displacement ellipsoids for non-hydrogen atoms are drawn at the 30 % probability level. The hydrogen atoms have been omitted for clarity. Selected bond lengths (Å) and angles (°): Pd1–N11 = 2.038(7), Pd1–N12 = 2.036(7), Pd1–N1 = 2.030(6), Pd1–N2 = 2.042(7), Pd2–N11' = 2.051(7), Pd2–N12' = 2.044(7), Pd2–N3 = 2.028(7), Pd2–N4 = 2.025(7); N11–Pd1–N12 = 90.8(2), N1–Pd1–N2 = 84.5(3), N11'–Pd2–N12' = 91.4(3), N3–Pd2–N4 = 84.4(3).*

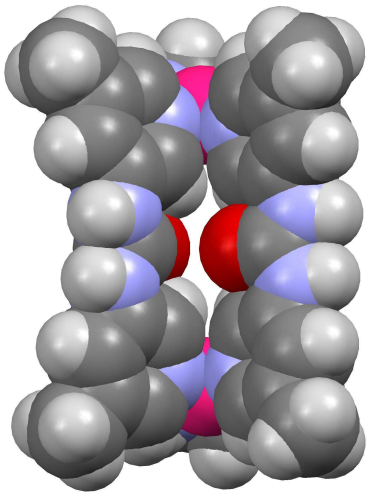

Figure 5.53: *Spacefilling model of the cation of complex **171**, showing space between two bispyridylurea ligands which are too small for counter-anion encapsulation. Counter-anions and solvent molecules have been omitted for clarity.*

In order to examine the simultaneously existence of M_2L_2 and M_3L_3 complexes in solution, *Pulsed Field-Gradient Spin-Echo NMR* (PGSE) experiments were performed. The diffusion coefficients of the complexes correlate with their size and shape. Due to this, the sizes of the compounds can be assigned experimentally from the diffusion coefficients of these complexes. As a rough approximation, the different species under study were approximated as spheres, assuming that the fast rotation of the "discoidal" compounds on average leads to a sphere. Based on this approximation, the size of the species can be calculated from the measured diffusion coefficients by the Stokes-Einstein equation (equation 5.1).

As representative examples, only the results of the ^{1}H DOSY NMR spectra of **174a/b** and **179a/b** will be discussed. Large structures have smaller diffusion coefficients than small ones. If M_2L_2 and M_3L_3 complexes coexist, two different sets of signals should be observed in the DOSY NMR spectra. Indeed two sets of signals are observed in the spectra of **174a/b** and **179a/b** (Figure 5.54). In these systems two different species coexist in solution, which supports the results form ^{1}H and ^{31}P NMR spectroscopy. The DOSY NMR spectra of the Stang-type complexes **174a/b-177a/b** and **179a/b-182a/b** show two species to exist in solution as well. For the systems **178** and **183** only one set of DOSY signals is observed.

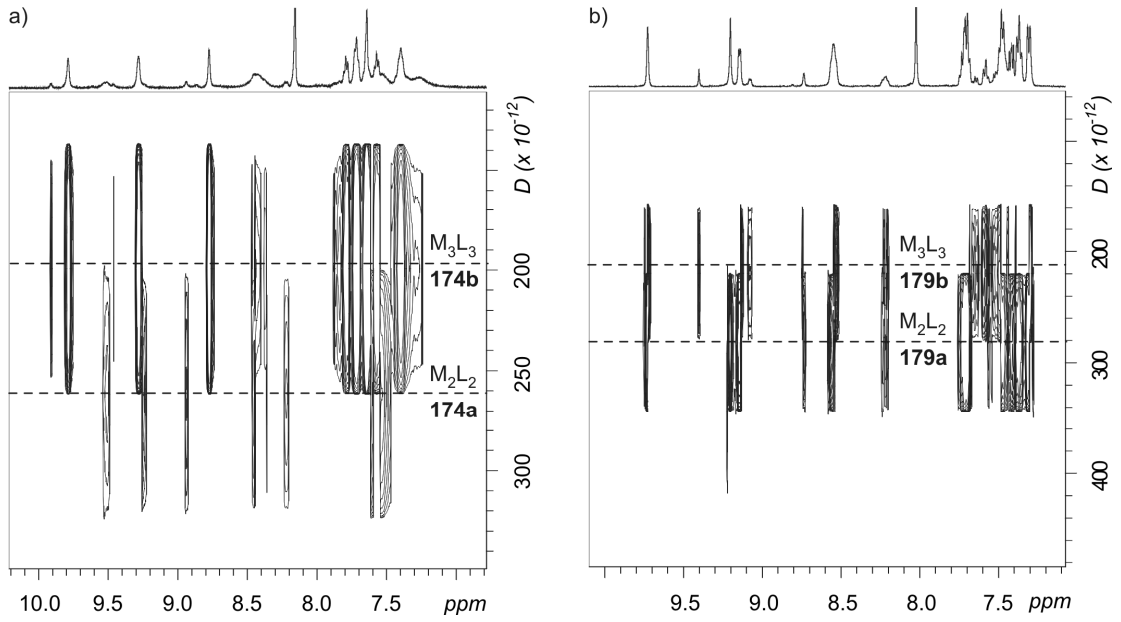

Figure 5.54: *DOSY NMR spectra of a)* ***174a/b*** *recorded at 243K in DMF-d_7 and c)* ***179a/b*** *recorded at 298 K in DMF-d_7.*

For a comparison with the experimental radii obtained from the DOSY NMR experiments, the geometries of the M_2L_2 and M_3L_3 complexes were optimized with the MM2 force-field implemented in the Cache program.[227] Different conformers have been explicitly considered in the calculations. i) The ligands can have a *syn-syn*, a *syn-anti* or an *anti-anti* conformation, which can also be possible in the complexes. In all cases, those complexes were energetically favored, wherein all ligands have a *syn-syn* conformation. Based on this and the results derived from the crystal structures of the complexes (see above), it can be assumed that this ligand conformation is favored in the complexes as well. ii) In case of the Stang-type complexes **174a/b-183**, the dppp-phenyl groups of the metal centers can point into the cavity of the M_2L_2 and M_3L_3 complexes (small conformers) or they can point away from it (large conformers). These conformers differ a lot in their size, but not too much in their calculated energies. Thus, the small conformer can easily convert into the bigger one by a conversion of the six-membered ring of dppp. Probably, both conformers (small and large) exist in solution, but the conversion into each other should be fast enough to observe average experimental radii for those complexes. iii) Other conformers than those discussed before are neglected, because they do not affect the size of the complexes under study.

Table 5.6: *The experimental data of the ^{1}H NMR DOSY experiments compared to the calculated radii of the complexes under study. The radii were obtained from calculated structures which were geometry-optimized using the MM2 force field method.*[227]

Compound	solvent	T [K]	D [m^2s^{-1}]	$r_{exp.}$ [nm]	$r_{cal.}$ [nm]
169	DMSO	298	$1.41 \cdot 10^{-10}$	0.778	0.879
170	DMSO	298	$1.30 \cdot 10^{-10}$	0.840	0.905
171	DMSO	298	$1.32 \cdot 10^{-10}$	0.829	0.992
172	DMSO	298	$1.21 \cdot 10^{-10}$	0.907	0.967
173	DMSO	298	$1.32 \cdot 10^{-10}$	0.831	1.045
174a	DMF	243	$1.19 \cdot 10^{-10}$	0.759	1.048
174b	DMF	243	$8.43 \cdot 10^{-11}$	1.188	1.098
175a	DMF	273	$2.10 \cdot 10^{-10}$	0.826	1.066
175b	DMF	273	$1.84 \cdot 10^{-10}$	0.942	1.093
176a	DMF	243	$8.88 \cdot 10^{-11}$	1.013	1.065
176b	DMF	243	$8.43 \cdot 10^{-11}$	1.066	1.100
177a	DMF	233	$7.03 \cdot 10^{-11}$	1.002	1.190
177b	DMF	233	$6.69 \cdot 10^{-11}$	1.053	1.307
178	DMF	243	$7.83 \cdot 10^{-11}$	1.149	1.271
179a	DMF	298	$2.93 \cdot 10^{-10}$	0.918	1.052
179b	DMF	298	$2.64 \cdot 10^{-10}$	1.019	1.102
180a	DMF	298	$2.71 \cdot 10^{-10}$	0.992	1.075
180b	DMF	298	$2.54 \cdot 10^{-10}$	1.060	1.097
181a	DMF	298	$2.81 \cdot 10^{-10}$	0.958	1.068
181b	DMF	298	$2.59 \cdot 10^{-10}$	1.038	1.104
182a	DMF	298	$2.92 \cdot 10^{-10}$	0.921	1.193
182b	DMF	298	$2.47 \cdot 10^{-10}$	1.089	1.317
183	DMF	298	$2.65 \cdot 10^{-10}$	1.014	1.276

Viscosity coefficients used for DMF at different temperatures: $\eta_{233\,K}$ = 2.420 g $m^{-1}s^{-1}$ $\eta_{243\,K}$ = 1.979 g $m^{-1}s^{-1}$, $\eta_{273\,K}$ = 1.154 g $m^{-1}s^{-1}$, $\eta_{298\,K}$ = 0.811 g $m^{-1}s^{-1}$. The viscosities for 233 K and 243 K were extrapolated from literature data.[228] The viscosity coefficient for DMSO at 298 K is: $\eta_{298\,K}$ = 1.996 g $m^{-1}s^{-1}$

Comparing the experimental and the calculated radii of the complexes **169-183**, four different conclusions can be drawn: i) The species observed in solution are metallo-supramolecular M_2L_2 and M_3L_3 complexes. The experimental radii do not perfectly reflect the calculated ones, but the calculated radii of all other possible metallo-supramolecular species would fit even worse. ii) All experimental radii are smaller as the calculated ones. This can be ascribed to the approximation that the complexes under study are spherical instead of cylindrical or discoidal. Additionally, the M_2L_2 and M_3L_3 complexes bear small cavities which influence the diffusion of the complexes. iii) The experimental radius of a metallo-supramolecular M_2L_2 complex is always smaller than that of its corresponding M_3L_3 complex. iv) The size of the complexes depends on the metal centers used. A metallo-supramolecular M_2L_2 complex with $(en)Pd(NO_3)_2$ is always smaller than an analogous complex containing $(dppp)Pt(OTf)_2$ or $(dppp)Pd(OTf)_2$. Additionally, a M_2L_2 or M_3L_3 complex bearing $(dppp)Pd(OTf)_2$ is always smaller than its analogue with $(dppp)Pt(OTf)_2$.

In order to verify the results from NMR spectroscopy and crystal structure data analysis, electrospray ionization mass spectrometric (ESI MS) experiments of the complexes were performed. The complexes under study can be ionized in the ESI ion source by stripping off some counterions, thus generating complexes in different charge states. In here we will discuss the electrospray ionization ESI-FTICR mass spectrum of system **174a/b** as a representative example (Figure 5.55). Four major peaks are observed in for **174a/b**: i) The first peak at *m/z* 882 can be explained by a superposition of a doubly charged $[2:2:2]^{2+}$ complex (M_2L_2) and a singly charged $[1:1:1]^{+}$ fragment. ii) A second peak shows a singly charged $[1:2:1]^{2+}$ fragment at *m/z* 1095. iii) The triply charged $[4:4:5]^{3+}$ complex at *m/z* 1226 can be explained by unspecific aggregation of two M_2L_2 complexes. Unspecific aggregation is very typical for ESI-MS experiments of salts, and it is found for many similar species. iv) The fourth peak at *m/z* 1913 can be assigned to a superposition of a singly charged $[2:2:3]^{+}$ complex (M_2L_2) and a doubly charged $[4:4:6]^{2+}$ aggregate, which can as well be explained by unspecific aggregation. It is remarkable that no M_3L_3 complex is observed in the ESI mass spectrum. Similar results are observed for the other Stang-type complexes (**175a/b-183**) as well. For the corresponding Fujita-type complexes **169-173** the formation of M_2L_2 complexes was confirmed by ESI MS.

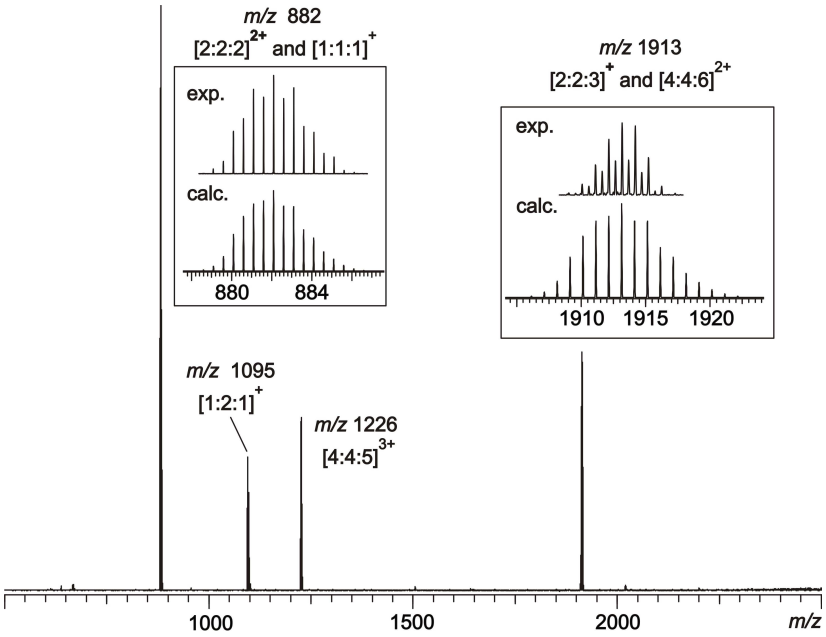

Figure 5.55: *The ESI-FTICR mass spectrum of* ***174a/b****.*

Changing the temperature can significantly influence the equilibria of metallo-supramolecular complexes. Similarly, the kinetics of the exchange processes may be altered by all of these parameters. The effects of these parameters on the equilibria of the complexes under study were examined to get a more complete picture of those complexes. The experiments to examine the equilibria were performed exemplarily with the systems **174a/b**.

The temperature-dependent ^{1}H and ^{31}P NMR spectra of system **175a/b** are shown in Figure 5.56. At 293 K two sharp sets of signals are clearly visible in the ^{1}H and ^{31}P NMR spectra. Both species (M_2L_2 and M_3L_3) exist more or less in a 1:1 ratio. Starting from 233 K, three effects are observed with increasing temperature: i) A conversion of the M_3L_3 complex (**174b**) into the M_2L_2 complex (**174a**) is observed. On the one hand, M_3L_3 is the favored complex at lower temperatures. On the other hand, at higher temperatures the signals of M_2L_2 complex (**174a**) are increasing. ii) The ligand-exchange between the two species becomes faster with increasing temperature. Between 333 K and 353 K it is too fast to separate the two species via ^{1}H and ^{31}P NMR spectroscopy and coalescence appears at a temperature of $T_c \approx 343$ K. iii) The NMR spectra at 233 K contain broader signals than those at higher temperatures. This

can be explained by the existence of different conformers (see above) which interconvert slowly at this temperature.

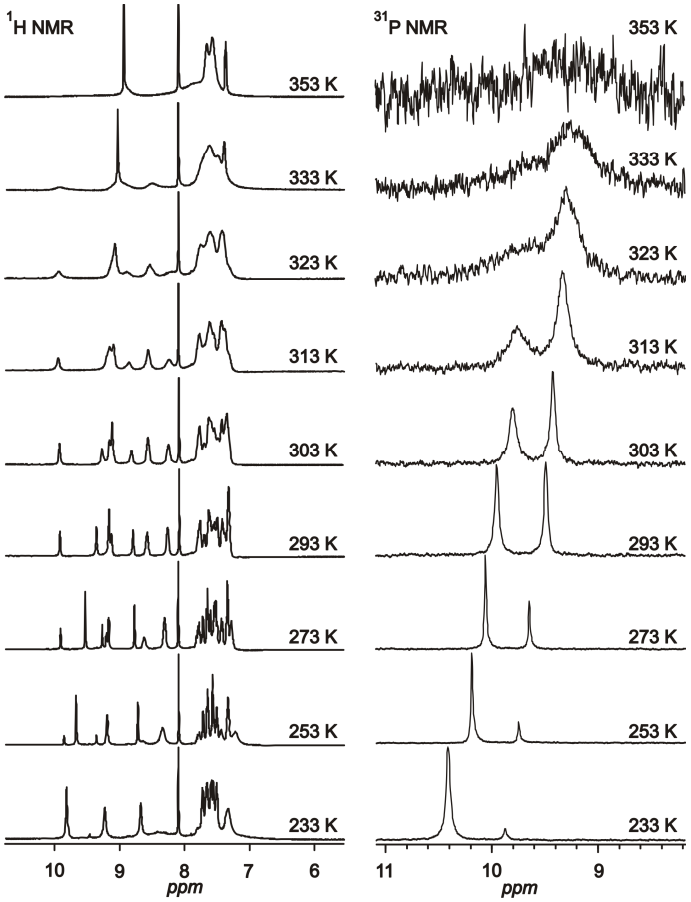

Figure 5.56: *Temperature-dependent ^1H and ^{31}P NMR spectra of system* ***174a/b*** *(monitored in DMF-d_7).*

The two signals in the ^{31}P NMR spectra of system **174a/b** are suitable to get quantitative data on the equilibrium of M_2L_2 and M_3L_3. The data can be calculated from the ratios of the integrals of both signals and the initial concentration of the building blocks used. Equation 5.4 describes the equilibrium constant *K*, from which the free enthalpies ΔG_{eq} for the equilibrium can be calculated. The basis of this is formed by the possible conversion of three M_2L_2 complexes into two M_3L_3 complexes, which happens without changing the number of building blocks involved. This calculation can easily be done at different temperatures, thus the enthalpic and

entropic contributions can be obtained from a van't Hoff plot of ln *K* over 1/*T* (Figure 5.57a, Equation 5.3 – repeated from chapter 5.2.2).

$$K = \frac{[M_2L_2]^3}{[M_3L_3]^2} \tag{5.4}$$

$$\ln K = -\frac{\Delta G_{eq}}{RT} = -\frac{\Delta H_{eq}}{RT} + \frac{\Delta S_{eq}}{R} \tag{5.3}$$

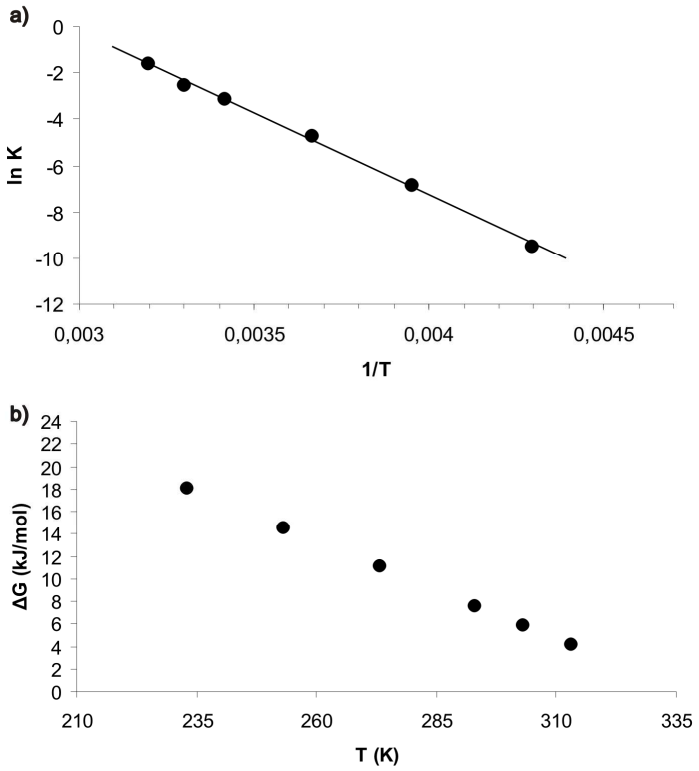

Figure 5.57: *a) Van't Hoff plot of ln K over 1/T for the equilibrium of* ***174a/b*** *and b) plot of free enthalpy* ΔG_{eq} *over temperature T.*

The temperature range of system **174a/b** was well suited to perform this thermodynamic analysis (Table 5.7). In the accessible temperature range, the complexes were allowed to equilibrate until no integral changes were observed anymore.

Table 5.7: *Thermodynamic data for the equilibrium of* ***175a/b*** *(experimental errors: ca. 20 %).*

T [K]	$c(M_2L_2)$ [mmol l^{-1}]	$c(M_3L_3)$ [mmol l^{-1}]	K [mmol l^{-1}]	ΔG_{eq} [kJ mol^{-1}]
233	5.1	41.6	0.075	18.08
253	11.2	35.6	1.099	14.60
273	19.8	27.6	9.231	11.12
293	26.2	20.5	43.129	7.64
303	29.2	17.5	81.089	5.90
313	33.2	13.5	200.777	4.16

ΔH_{eq} = 58.6 kJ mol^{-1}; ΔS_{eq} = 174.0 J mol^{-1} K^{-1}

The positve enthalpy (ΔH_{eq} = 58.6 kJ mol^{-1}) for the conversion of two M_3L_3 complexes **174b** into three M_2L_2 complexes **174a** can be assigned to three different factors: i) The M_2L_2 complex has a higher strain compared to the M_3L_3 complex. ii) In a M_2L_2 complex, both bispyridyl-urea ligands necessarily have the same orientation including the orientation of the dipole moments of their urea groups. Thus, a disfavorable repulsion between both dipoles appears. Due to their larger inner cavity, this repulsion is less important in M_3L_3 complexes. iii) In the complexes under study, the metal cations are shielded by bispyridyl-urea ligands and the dppp auxiliary ligand. Nevertheless, the M_3L_3 complexes are more open compared to their M_2L_2 analogues. Thus, the interaction between the metal cations and their counter anions should be better for the larger M_3L_3 complexes.

The quite large entropic term (ΔS_{eq} = 174.0 J mol^{-1} K^{-1}) is positive as well, reflecting the conversion of two M_3L_3 complexes into three M_2L_2 complexes. Due to the entropic term, at higher temperatures the equilibrium is shifted towards the formation of M_3L_3 complexes.

The solvent is also known to influence metallo-supramolecular equilibria. ^{1}H NMR and ^{31}P NMR spectroscopy of system **174a/b** in different mixtures of DMF-d_7 and acetone-d_6 at room temperature reveal a drastic influence of the solvents on the

equlibrium between M_2L_2 complexes **174a** and M_3L_3 complexes **174b** (Figure 5.58). While both complexes appear in more or less equal amounts in pure DMF-d_7, M_2L_2 complex **174a** is clearly preferred in the presence of acetone. The signals assigned to M_3L_3 complex **174b** nearly vanish when the amount of acetone-d_6 is increased. Due to the low solubility of **174a/b**, the situation in pure acetone-d_6 could not be monitored.

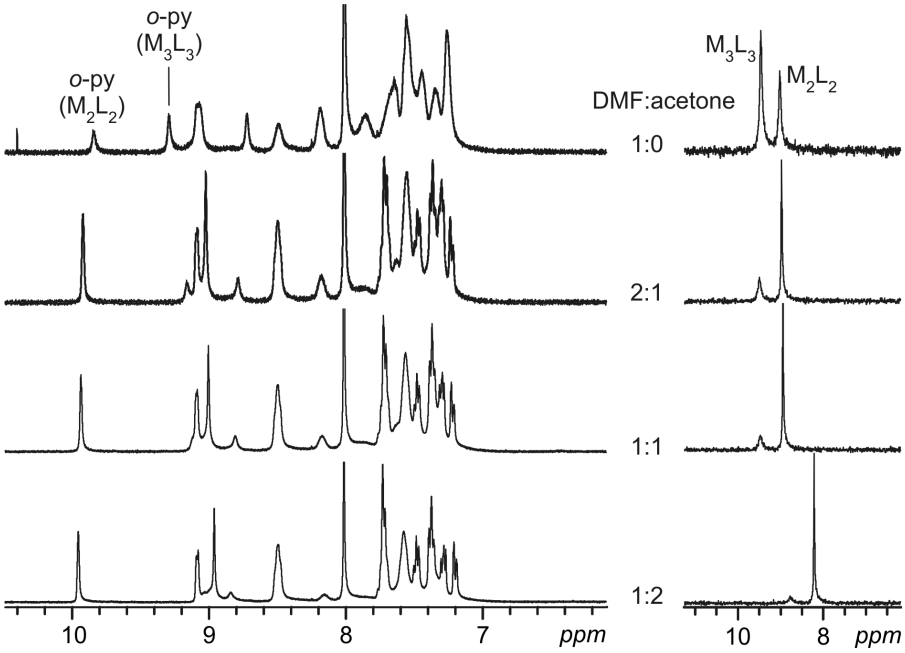

Figure 5.58: *^{1}H NMR and ^{31}P NMR spectra of **174a/b** in different solvent mixtures of DMF-d_7 and acetone-d_6.*

The low solubility of the complexes under study in appropriate non-polar aprotic solvents like dichloromethane or chloroform hampers the chances of the complexes **169**-**183** to use the capabilities of their urea groups for a directed interaction with other molecules. Thus, the M_2L_2 and M_3L_3 complexes cannot act as host complexes for guest inclusion, because the competition with solvent molecules is too high in polar solvents. Nevertheless, acids can affect metallo-supramolecular complexes.[77]

In a titration experiment, increasing equivalents (based on the concentration of ligand **162**) of $N(Bu)_4H_2PO_4$ **184** were added system **174a/b** (Figure 5.59). The titration was performed in DMSO-d_6 and monitored by ^{1}H NMR and ^{31}P NMR spectroscopy. With increasing amount of $N(Bu)_4H_2PO_4$ **184**, a broadening of the ^{1}H NMR signals occurs.

At the same time, the peaks assigned to the complexes **174a** and **174b** decrease, while a new set of signals appears. When four equivalents of **184** have been added to system **174a/b**, the signals belonging to the complexes **174a** and **174b** vanish. Only one set of signals remains which gets sharper with incresing amounts of **184**. These results are supported by ^{31}P NMR spectroscopy. The two ^{31}P NMR signals observed for M_2L_2 complex **174a** and M_3L_3 complex **174b** decrease with increasing amount of $N(Bu)_4H_2PO_4$ **184**, while a new ^{31}P NMR signal appears. When one equivalent of **184** has been added only the new signal was observed in the ^{31}P NMR spectrum. At higher amounts of **184**, the latter signal vanishes as well and two new peaks at 13.8 ppm and 1.7 ppm appear which can be assigned to non-coordinated metal center **27** and PO_4^{3-}, respectively.

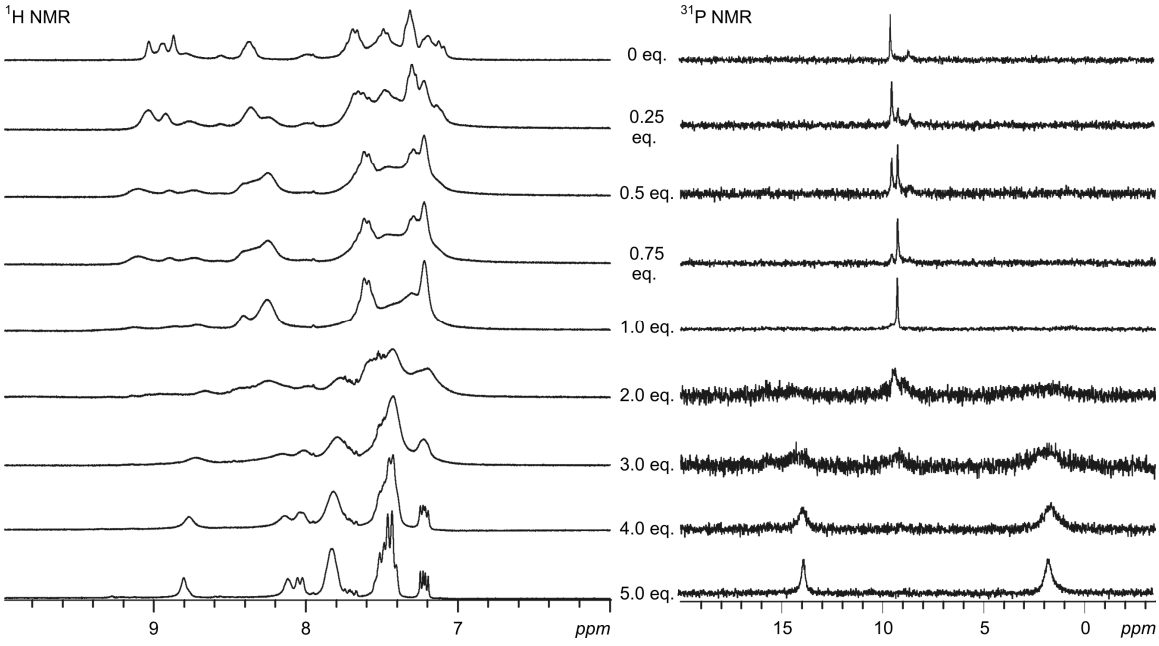

Figure 5.59: *^{1}H and ^{31}P NMR spectra of system **174a/b** monitored during the titration with increasing amounts of $N(Bu)_4H_2PO_4$ **184**. The equivalents of **184** were calculated according to the concentration of ligand **162** ([ligand] = 10 mM).*

These results can be explained by the formation of the preferential formation of one species as well as by a sequential protonation of of the pyridine nitrogen atoms. Thus, the signals observed for the complexes **174a/b** vanish and new signals are observed.

In order to identify the processes happening during the titration, the discussion will be parted in two parts. At first, the results obtained for adding less than one equivalent of $N(Bu)_4H_2PO_4$ **184** will be discussed. With increasing amount of **184** a new species appears, which is the only species left when 1 eq. of **184** was added. Due to its signal in the ^{31}P NMR spectra, the new species has to be symmetrically. All unsymmetrically species produced by partly protonation of the ligands pyridine units can be excluded. The only symmetric protonated species would contain one metal center coordinating to two mono-protonated ligands ($[M(ligand+H)_2]^{2+}$) which can be excluded as well. The partly protonation would result in non-coordinating metal centers which are not observed in the NMR spectra monitored below an amount of 1 eq. of **184**. Therefore, the new peaks can only be explained by the interaction of the $H_2PO_4^-$ ions with the M_2L_2 and M_3L_3 complexes in solution. i) An anion exchange is observed and $H_2PO_4^-$ replaces the triflate counter anions. Thus, the signals observed for the complexes should undergo some chemical shifting. Nevertheless, it does not explain the formation of only one new signal in the ^{31}P NMR spectra. ii) The $H_2PO_4^-$ anion can bind to the urea groups at the ligands.[229] Thereby the anions act as templates and the M_2L_2 complex is formed preferrably. This induces a chemical shift in the ^{31}P NMR spectra and thus can explain the results observed.

However, the situation changed, when more than one equivalent of $N(Bu)_4H_2PO_4$ **184** were added. Due to sequential protonation, the signals relating to the complexes decrease and signals for the non-coordinated metal center (13.8 ppm) and PO_4^{3-} (1.7 ppm) can be observed in the ^{31}P NMR spectra. Similar results have been reported by Ballester and co-workers.[77]

It has been shown that bispyridyl-urea ligands **162-168** can form metallo-supramolacular M_2L_2 and M_3L_3 complexes (**169-183**), when they are combined with cis-blocked square-planar metal centers like $(en)Pd(NO_3)_2$ **19**, $(dppp)Pd(OTf)_2$ **27** or $(dppp)Pt(OTf)_2$ **28**. Due to sterical hindrence, no complex-formation has been observed for ligands **163** and **165**. While just M_2L_2 complexes (**169-173**) have been observed with metal center **19**, equilibria between M_2L_2 and M_3L_3 complexes (**174a/b-177a/b** and **179a/b-182a/b**) occur when metal centers **27** or **28** are used. When ligand **168** was combined with metal centers **27** and **28**, only the formation of

M_2L_2 complexes (**178** and **183**) was observed.

The complexes and their equilibria were characterized by the interplay of different analytical methods like ^{1}H and ^{31}P NMR spectroscopy, DOSY NMR spectroscopy, ESI mass spectrometry and crystal data analysis. The influence of the environment on the equilibria has nicely been shown by changing the temperature, the solvent and the pH value of the systems under study.

Unfortunately, the low solubility of the complexes hinder their abilities to act as host complexes for molecular recognition. Nevertheless, bispyridyl-urea ligands and their metallo-supramolecular complexes remain interesting candidates for molecular recognition, when their solubility is increased.

5.3.3 The Self-Assembly of Small Functionalyzed Metallo-Supramolecular Cages

Metallo-supramolecular cages can be used as host complexes to encapsulate guest molecules and influence reactions performed inside their inner cavity.[176] However, most of these systems use the hydrophobic effect for encapsulation of guests. Nevertheless, it would be interesting to influence reactions in organic solvents as well. Thus, functionalized building blocks are important to enable interactions between the host complexes and the guest molecules. These interactions have to be strong enough to bind the guest molecules which can be achieved by the interplay of more interactions at the same time.

Inspired by the metallo-supramolecular macrocycles **169-183** containing bispyridyl-urea ligands **162-168** described in the last chapter, several metallo-supramolecular cages (**185a/b-189**) were obtained combining of $(MeCN)_4Pd(BF_4)_2$ **149** with ligands **162-169** (Figure 5.60). The properties of these complexes were studied in cooperation with Johannes Poppenberg and Prof. Kari Rissanen.[246a]

The structure of the smaller bispyridyl-urea ligands **162-166** can in principle have three different orientations (*syn-syn*, *syn-anti* and *anti-anti*; see chapter 5.3.1). The self-assembly of ligands **162-166** with cis-blocked square-planar metal centers revealed, that the *syn-syn* conformation of the ligands seems to be favored in the resulting complexes (see chapter 5.3.2). Nevertheless, the *anti-anti* conformations cannot be ruled out, whereas the *syn-anti* conformations do not play a role in the final assemblies. Thus, the orientation of the urea groups in the complexes is fixed to two different isomeric structures. Due to the structure of the complexes and the orientation of the ligands therein, all oxygen atoms or all NH groups of the bispyridyl-urea ligands point into the inner cavity of the complexes formed. Based on the polarity of the urea groups, the polarity of the inner cavity of a resulting complex differs from that of its outer sphere. Even more important, many hydrogen-bond acceptors or donors originating from the urea groups turn into the inner cavity of the complexes and thus can interplay with each other and strengthen the interactions between the host complexes and guest molecules. For complexes containing the more flexible ligands **167** and **168**, this effect is probably not as strong as for the rigid ligands **162-166**.

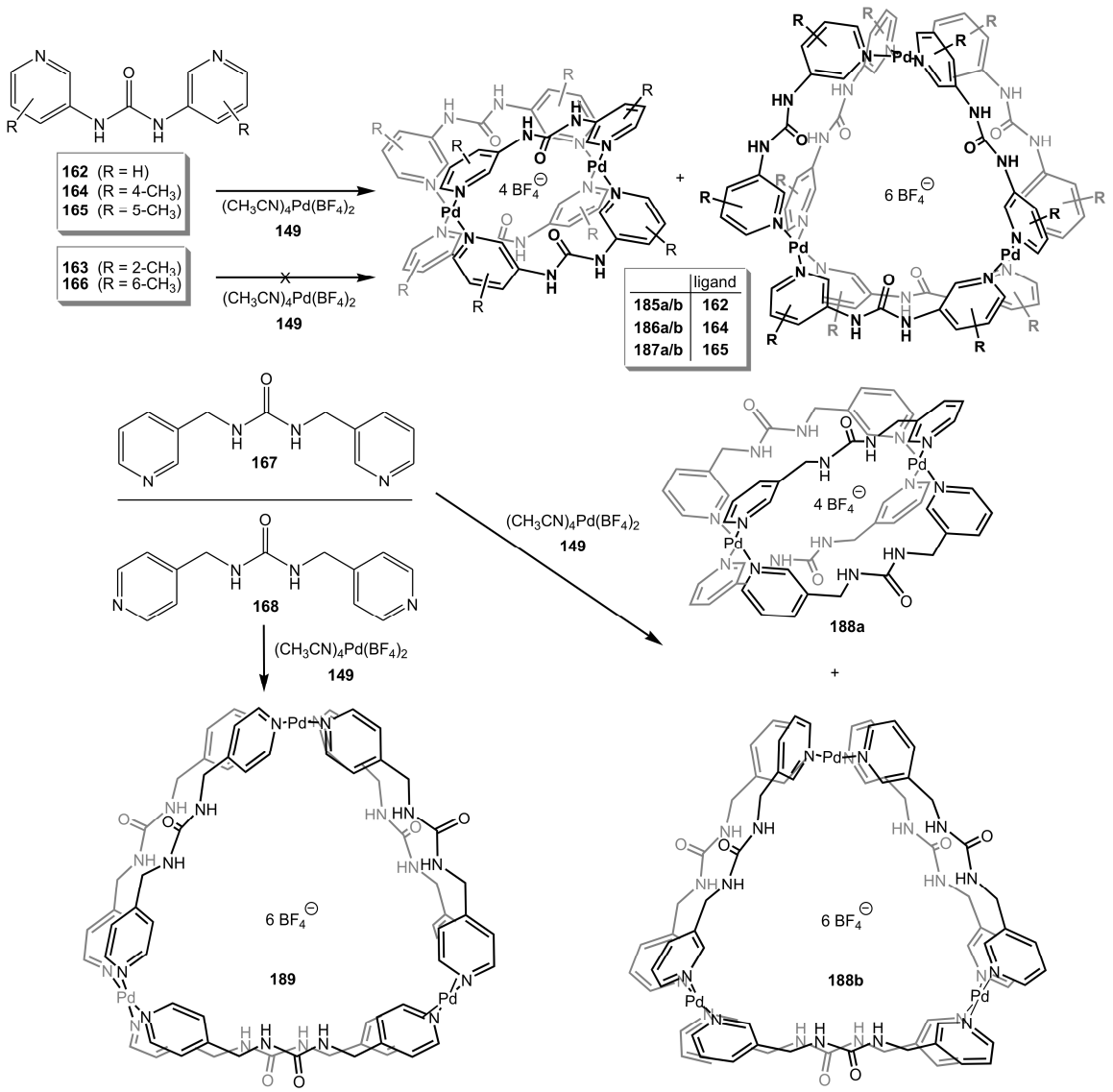

Figure 5.60: *Self-assembly of metallo-supramolecular M_2L_4 and M_3L_6 cages* ***185a/b-189*** *(a = M_2L_4 and b = M_3L_6).*

Metal center $(MeCN)_4Pd(BF_4)_2$ **149** was mixed with two equivalents of ligands **162-169**, respectively (Figure 5.60). The mixture was dissolved in DMSO or DMF and stirred for one hour at room temperature in order to ensure coordination to be completed. DMSO and DMF had to be used as solvents due to the low solubility of the complexes. For NMR experiments, samples with a ligand concentration of 15 mM were analyzed in DMSO-d_6 or DMF-d_7. Due to get an appropriate ligand concentration of 100 µM for the ESI mass

spectrometric experiments, the systems under study were dissolved in DMSO and diluted with acetonitrile.

A successful coordination of the ligands **162**, **164**, **165**, **167** and **168** was proven by comparing the ^{1}H NMR spectra of the ligands with those of their corresponding assemblies (Figure 5.61). Due to coordination, chemical shifting of the ^{1}H NMR signals for the ligands was observed. While the ^{1}H NMR spectra of the systems **185a/b-188a/b** two sets of signals, only one set of signals is observed for system **189**. Unfortunately, no coordination was observed, when ligands **163** and **166** were used. This can be assigned to the steric hindrance of the methyl group in ortho-position to the pyridine-nitrogen atoms in ligands **163** and **166**.

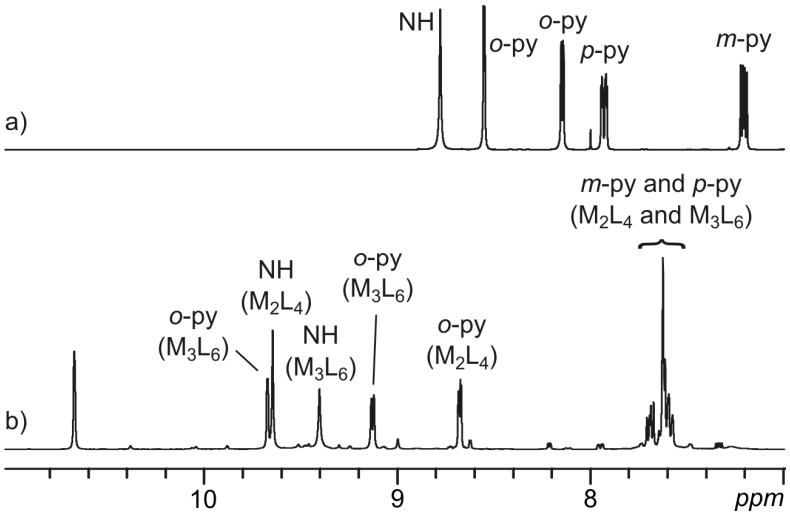

Figure 5.61: *^{1}H NMR spectra of a) ligand **162** and b) the equilibrium between metallo-supramolecular M_2L_4 complex **185a** and M_3L_6 complex **185b**.*

The final prove for the coexistence of two species in systems **185a/b-188a/b** can be derived from DOSY NMR spectroscopy. The size and shape of the complexes is directly correlated to their diffusion coefficients and thus their size can be calculated from the diffusion coefficients monitored. Due to fast rotation in solution, the different cylindrical M_2L_4 and discoidal M_3L_6 complexes **185a/b-189** were approximated to be spherical. This rough approximation enables the calculation of the hydrodynamic radii of the individual species using the Stokes-Einstein equation (equation 5.1).

The DOSY spectrum of system **185a/b** is exemplarily shown in Figure 5.62. It clearly shows two different metallo-supramolecular species to be present in solution. Additionally some excess of ligand **162** can be observed in the DOSY spectrum of **185a/b**. The DOSY spectrum explicitly shows that the diffusion coefficients of the metallo-supramolecular complexes **185a/b** are larger than that of the non-coordinated ligand **162**. This supports a successful coordination. However, the DOSY spectra of **186a/b**-**188a/b** also contain two differently sized species while that for **189** only shows one set of signals.

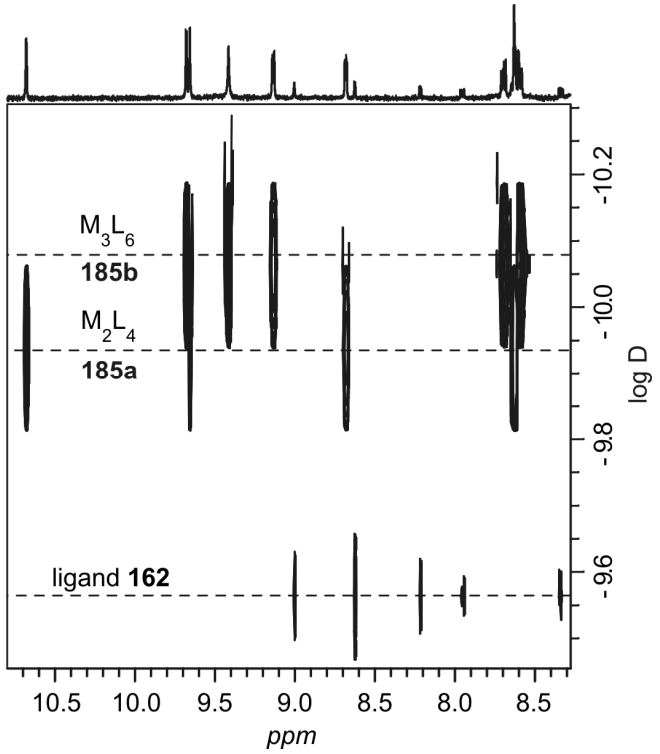

Figure 5.62: *The DOSY NMR spectra of system* ***185a/b****.*

In order to identify the metallo-supramolecular species observed in solution, the experimentally calculated radii of complexes **185a/b**-**189** were compared with calculated ones (Table 5.8). The calculations were performed using the MM2 force field method for geometry-optimization of the M_2L_4 and M_3L_6 complexes under study. Complexes containing both reasonable isomers of ligands **162**-**166** (*syn*-*syn* and *anti*-*anti*) have been considered and thus, the average radii were used for comparison.

For complexes **185a/b-187a/b**, the experimental radii reflect their corresponding calculated radii very well. Thus, these species can clearly be identified as M_2L_4 and M_3L_6 complexes **185a/b-187a/b**. The experimental radii of systems **188a/b** and **189** differ significantly from the calculated ones. This can be explained by three reasons: i) Due to the flexibility of the ligands, the calculation of geometry-optimized structures is difficult and can easily result in misleading calculations. ii) The approximated spherical structure of the complexes is reflecting the real situation of the rather discoidal complexes. iii) Based on the flexibility of the ligands, the interaction of the complexes with the counter anions as well as with solvent molecules increased compared to that of the complexes bearing less flexible ligands. Nevertheless, the species observed for the systems containing ligands **167** or **168** can still be identified as M_2L_4 and M_3L_6 complexes, because the calculated radii of all other possible complexes would fit worse.

Table 5.8: *The experimental data of the ^{1}H NMR DOSY experiments compared with the calculated radii of complexes **185a/b-189**. The calculated radii were obtained from geometry-optimized structures using the MM2 force field method.*[227]

Compound	solvent	T	D	$r_{exp.}$	$r_{cal.}$
185a	DMSO	298	$1.22 \cdot 10^{-10}$	0.896	0.872
185b	DMSO	298	$9.86 \cdot 10^{-11}$	1.140	1.025
186a	DMF	298	$1.84 \cdot 10^{-10}$	0.947	0.925
186b	DMF	298	$1.37 \cdot 10^{-10}$	1.134	1.112
187a	DMF	298	$1.92 \cdot 10^{-10}$	0.921	0.932
187b	DMF	298	$1.38 \cdot 10^{-10}$	1.132	1.186
188a	DMF	298	$1.53 \cdot 10^{-10}$	1.758	0.954
188b	DMF	298	$1.21 \cdot 10^{-10}$	2.228	1.099
189	DMF	298	$1.95 \cdot 10^{-10}$	1.385	0.954

ESI mass spectrometry supported the existence of two species in systems **185a/b-188a/b**. The mass spectrum of system **185a/b** will be discussed as representative example (Figure 6.63a). Two peaks were observed which could directly be assigned to ions of the metallo-supramolecular M_2L_4 complex **185a** and M_3L_6 complex **185b** (*m/z* 622 ($[1:2:1]^+$ and $[2:4:2]^{2+}$ and $[3:6:3]^{3+}$) and *m/z* 976 ($[3:6:4]^{2+}$)). Additionally, also fragments of both

complexes have been observed as well as unspecific aggregates. However, the loss of HBF_4 is a prominent fragmentation observed for system **185a/b**. It has been proven by deuteration experiments that the proton in HBF_4 is stripped off from one of the urea-NH groups implemented in the ligands.[246a] No other metallo-supramolecular complexes like M_4L_8 have been observed in the mass spectrum. Similar results have been observed in the mass spectra of systems **186a/b-188a/b**.

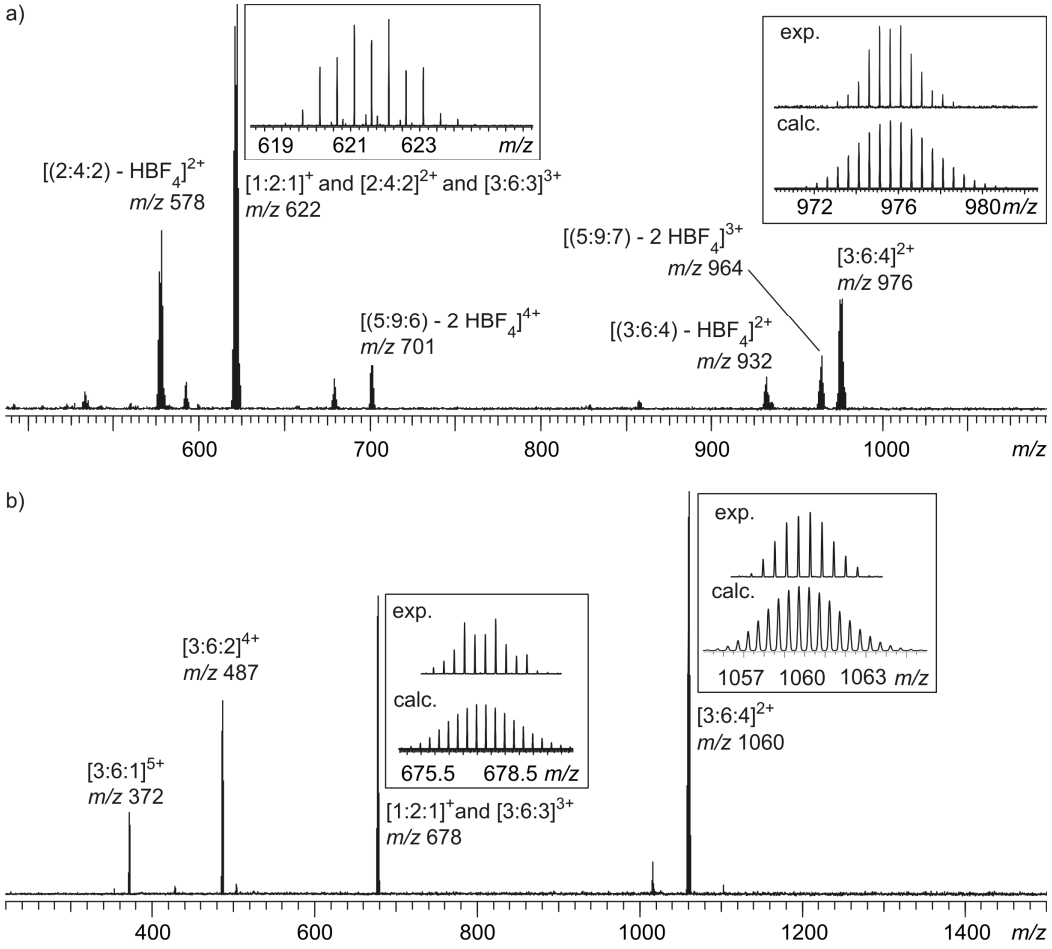

Figure 5.63: *ESI mass spectra of a) the equilibrium between metallo-supramolecular M_2L_4 complex **185a** and M_3L_6 complex **185b**, and b) the metallo-supramolecular M_3L_6 complex **189**.*

On the contrary, the mass spectrum of the combination of metal center **149** with ligand **168** bears just peaks which can directly be related to ions of M_3L_6 complex **189** (Figure 5.63b). Besides one fragment ion (*m/z* 678 $[1:2:1]^+$), only doubly (*m/z* 1060 ($[3:6:4]^{2+}$)),

triply (*m/z* 678 ($[3:6:3]^{3+}$), quadruply (*m/z* 487 ($[3:6:2]^{4+}$)) and quintuply (*m/z* 372 ($[3:6:1]^{5+}$)) charged ions of complex **189** were observed in ESI mass spectrometry. The results obtained by mass spectrometry support the information gained from ^{1}H NMR and DOSY NMR spectroscopy.

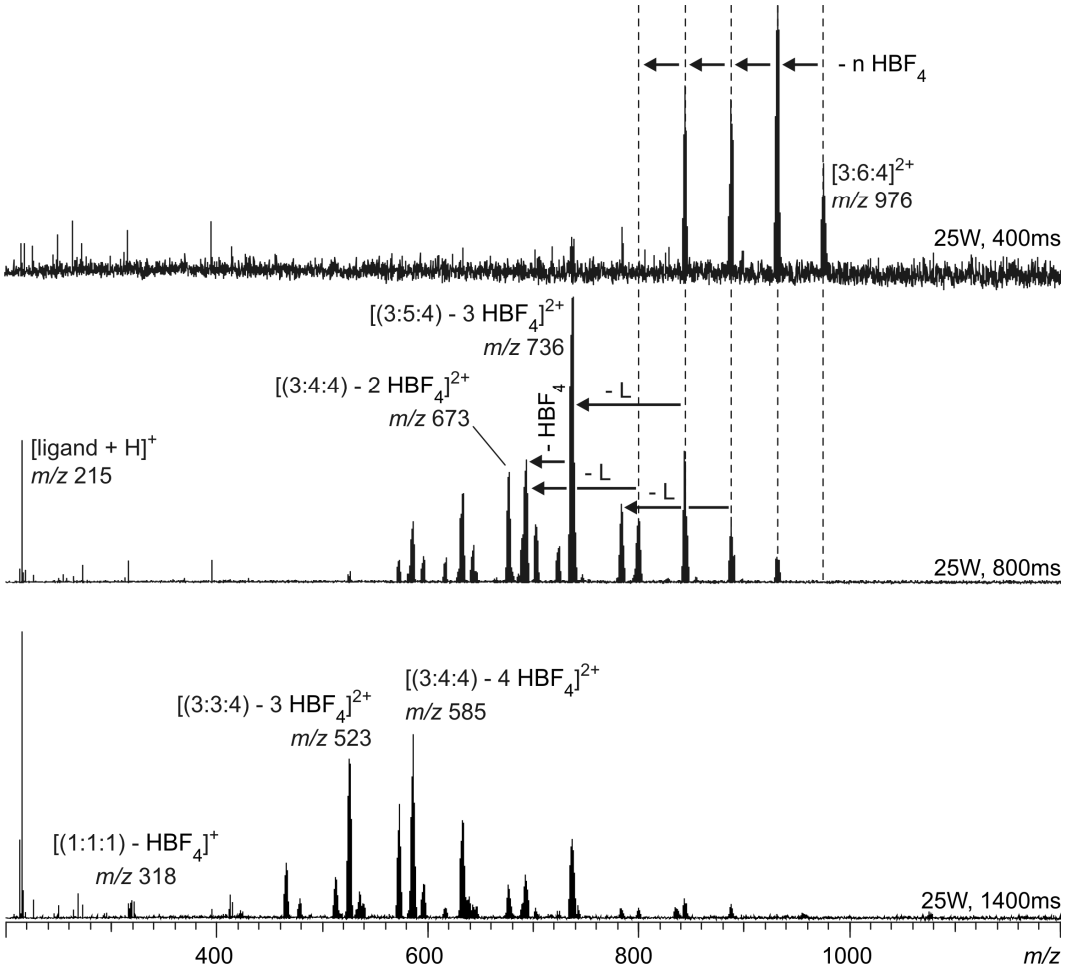

Figure 5.64: *IRMPD tandem mass spectra of M_3L_6 complex **185b**. The peak at m/z 976 ($[3:6:4]^{2+}$) was irradiated with an IR-laser with a laser power of 25 W at different irradiation times.*

Tandem mass spectrometry was performed to get a better understanding of the stability and the fragmentation of the complexes under study. The fragmentation of M_3L_6 complex **185b** is discussed in detail (Figure 5.64); similar results were observed for all other complexes under study. The peak at *m/z* 976 ($[3:6:4]^{2+}$) was mass-selected and irradiated

with an IR-laser (25 W) at different irradiation times. At short irradiation times, the sequential loss of neutral HBF_4 molecules was observed. At longer irradiation times, also the loss of ligands was observed. All peaks appearing in the tandem mass spectra of complex **185b** can be explained by a sequential loss of HBF_4 molecules and ligands. In the end, the resulting fragments (e.g. $[(3:3:4) - 3\ HBF_4]^{2+}$ (*m/z* 523)) decompose into fragments like $[(1:1:1) - HBF_4]^+$ (m/z 318). However, with increasing irradiation times also a prominent peak for the protonated ligand appears. Due to the lack of counter-fragments, the peak can probably be assigned to the simultaneous loss of $[L+H]^+$ and BF_4^-. The results obtained from the tandem MS experiments support the structural assignment of the complexes under study.

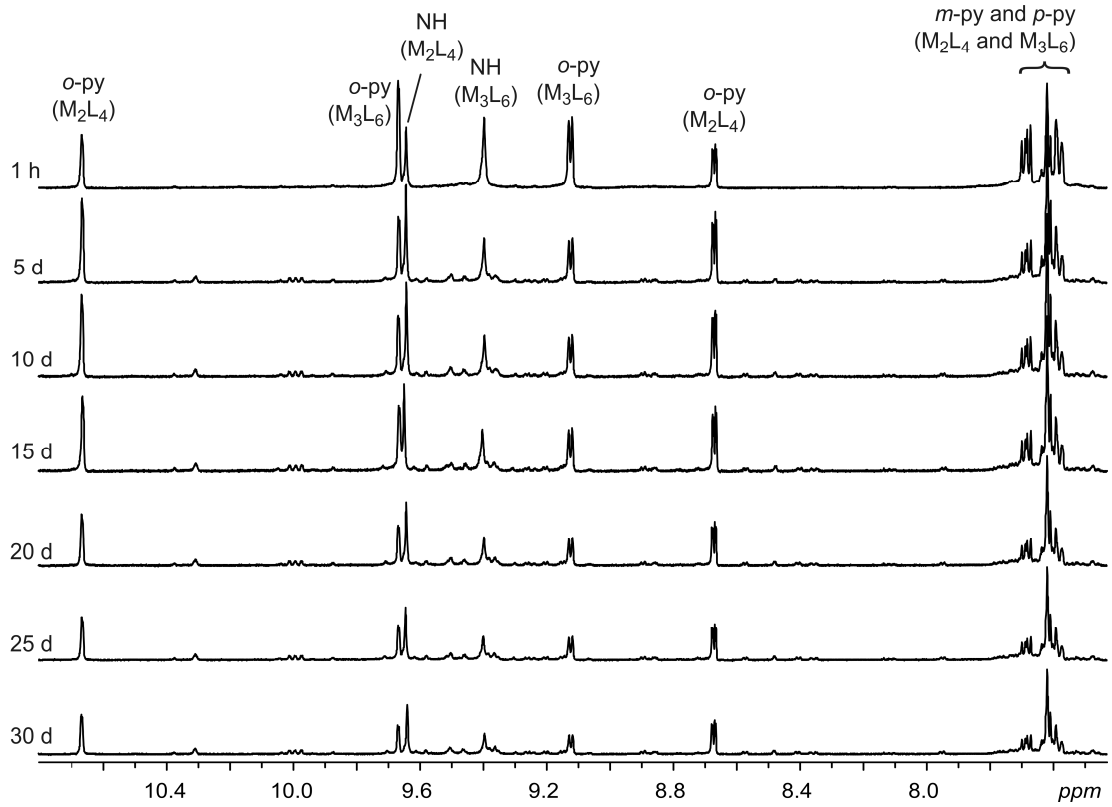

Figure 5.65: *Time-dependent ^1H NMR spectra of system **185a/b**.*[246a]

The stability of the complexes was studied using time-dependent ^1H NMR spectroscopy (Figures 5.65 and 5.66). For system **185a/b** a slow decrease of the signals attributed to the M_3L_6 complex **185b** was observed. In the beginning, the peaks for the larger M_3L_6

complex **185b** are more prominent, while the smaller M_2L_4 complex **185a** is the minor compound. With increasing time, complex **185a** becomes the major compound. This can be explained by a slow conversion of M_3L_6 complex **185b** into M_2L_4 complex **185a**. Thus, complex **185b** is a kinetic product, while **185a** is thermodynamically favored. However, after several days another set of signals appears with a very low intensity which could not be assigned. This may as well have an effect on the ratio of M_2L_4 and M_3L_6 complexes in solution.

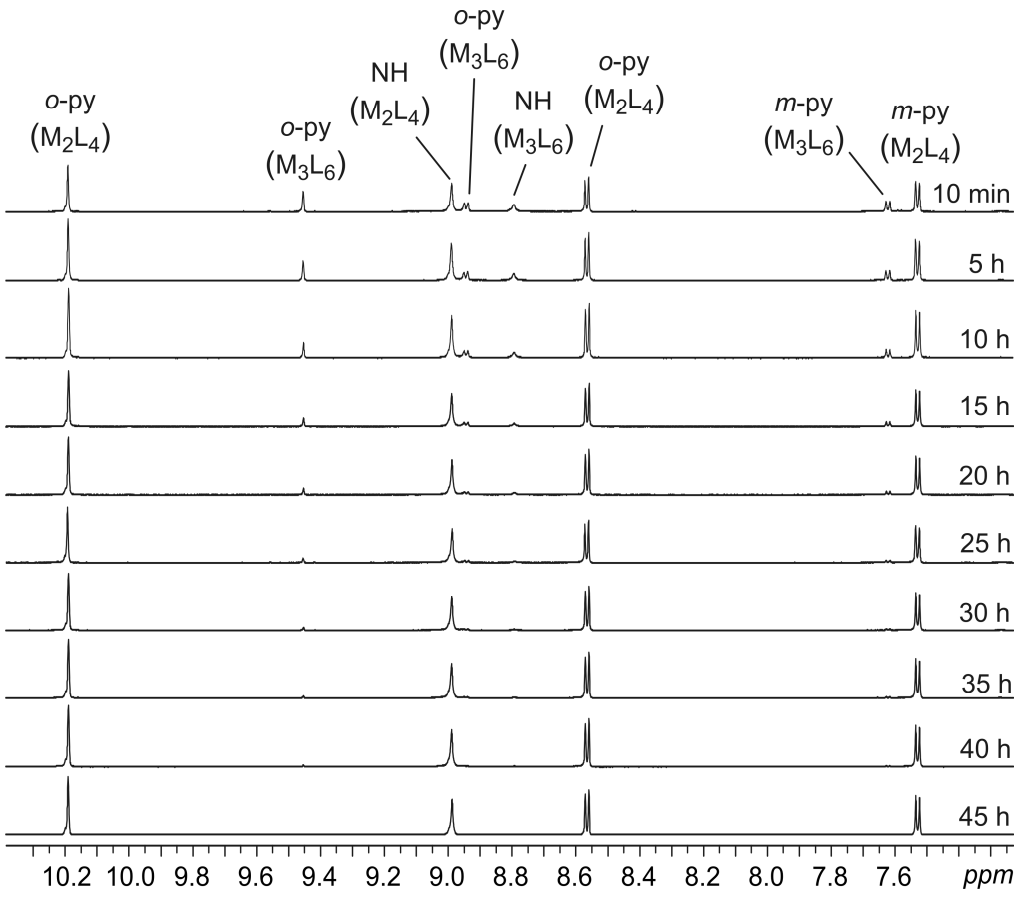

Figure 5.66: *Time-dependent ^{1}H NMR spectra of system **186a/b**.*[246a]

A similar situation was observed for system **186a/b**. In the beginning, the major compound observed is M_2L_4 complex **186a** and M_3L_6 complex **186b** coexists as the minor complex. With increasing time, complex **186b** converts into the smaller complex **186a** and the peaks related to complex **186b** vanish after 40 hours. Thus, **186b** can be clearly identified as kinetic product whereas **186a** is the thermodynamic one.

Interestingly, the conversion of the larger M_3L_6 complex **186b** into the smaller M_2L_4 complex **186a** appears to be much faster than that of complex **185b** into **185a**. This can be assigned to the methyl group in *para*-position to the pyridine-nitrogen atoms implemented in ligand **164**. ^{1}H NOESY NMR experiments and X-ray analysis revealed, that ligand **164** prefers the *syn-syn* orientation, while ligand **162** does not show a significant preference (see chapter 5.3.1). Additionally, a methyl-group is more space-demanding than a hydrogen atom and thus, the methyl-group has a direct influence on the flexibility of ligand **164**. Ligand **162** is flexible enough to form M_3L_6 complexes as well as M_2L_4 complexes. Due to the methyl-group in *para*-position to its pyridine-nitrogen atoms and their steric interference with the NH-groups, ligand **164** is less flexible and thus the strain of M_3L_6 complexes containing **164** increases compared to that containing ligand **162**. Therefore the formation of M_3L_6 complex **186b** is thermodynamically disfavored.

However, this clearly shows that small changes in the structure of one building block can have a significant effect on the properties of the resulting metallo-supramolecular complexes.

Ligand-exchange experiments were performed, in order to check whether the size of the ligands plays a role in the self-assembly process or not. Ligand **162** was mixed with equimolar amounts of metal center **149** and ligands **165**, **167** or **168**, respectively. The mixtures were dissolved in DMSO and stirred for 5 days to ensure that the mixing process was completed. Due to this long period of time, no mixing experiments were performed with ligand **164**, because no M_3L_6 complexes would be present anymore. After dilution with acetonitrile to a concentration of 100 µM, ESI mass spectrometry of the mixed systems was performed (Figure 5.67). The ligand-exchange will be discussed for the resulting M_3L_6 complexes, because the peaks observed for the corresponding M_2L_4 complexes were superimposed by other peaks.

First, the mixture of metal center **149** with ligands **162** and **165** shows a statistical distribution which would be expected for a complete ligand-exchange. Every ligand-position of ligand **162** in the homoleptic M_3L_6 complex **185b** can be exchanged by a ligand **164** (Figure 5.67a). So the methyl-groups in ligand **165** do not influence the exchange process.

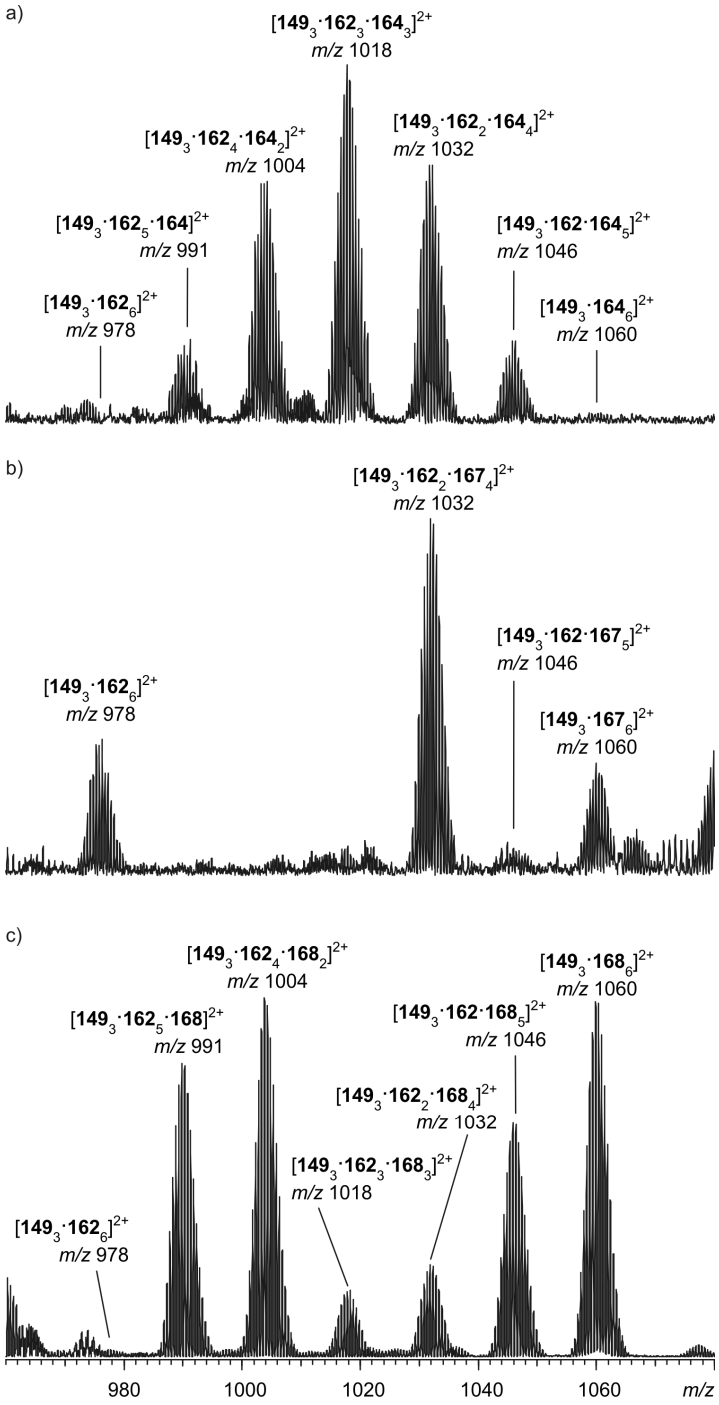

Figure 5.67: *Mixing-experiments monitored by ESI mass spectrometry: a) mixing of metal center **149** with ligands **162** and **165**, b) mixing of **149** with ligands **162** and **167** and c) mixture of **149** with ligands **162** and **168**.*

On the contrary, the mixture of **149** with ligands **162** and **165** shows no statistical distribution (Figure 5.67b). Besides both homoleptic M_3L_6 complexes **185b** (*m/z* 978)

and **188b** (*m/z* 1060), only two mixed species can be observed in the mass spectrum. These peaks can be assigned to the heteroleptic complexes $[\mathbf{149}_3\cdot\mathbf{162}_2\cdot\mathbf{167}_4]^{2+}$ (*m/z* 1032) and $[\mathbf{149}_3\cdot\mathbf{162}\cdot\mathbf{167}_5]^{2+}$ (*m/z* 1046). The latter one has a very low intensity, while the peak at *m/z* 1032 is the major peak observed. Obviously, a M_3L_6 complex bearing four small and rigid ligands **162** and two large and flexible ligands **167** is the most favored heteroleptic species, while all other possible heteroleptic species are far less favorable. This can be explained by the differences in size and flexibility of ligands **162** and **167**:

i) Due to the different sizes of ligands **162** and **167**, the introduction of a large ligand **167** into a ligand-position which bridges two metal centers **149** wherein the other bridging ligand-position is blocked by a short ligand **162** results in a relatively high strain. When two ligands are exchanged, the situation is different. These ligands can bridge different metal centers or they can both bridge the same metal centers. Due to less strain, the latter one should be preferred. Therefore, the exchange of an odd number of ligands is less favored and would cause much more strain than the exchange of an even number of ligands. This reflects the lack of intense peaks related to exchanges of an odd number of ligands.

ii) Ligand **167** is flexible and thus two ligands **162** can be implemented in a heteroleptic metallo-supramolecular M_3L_6 complex. On the contrary, no complex containing four ligands **162** and two ligands **167** is observed. Ligands **162** and **167** are not flexible enough to form such a complex.

Interestingly, the 1:1:1 mixture of metal center **149** and the ligands **162** and **168** again showed a completely different situation. In the ESI mass spectrum of this mixture, all possible homo- and heteroleptic M_3L_6 species were observed, but their distribution was not statistically (Figure 5.67c). The intensity of the peak assigned to the homoleptic M_3L_6 complex **185b** is very low, while the peak related to the homoleptic M_3L_6 complex **189** is one of the major peaks. This can be explained by two reasons: i) The low intensity of the peak for **185b** is due to improper ionization during the ESI process. ii) Ligand **162** can easily be implemented into heteroleptic M_3L_6 complexes, while the introduction of the larger ligands **168** is less favorable.

The intensities for the peaks at *m/z* 991 ($[\mathbf{149}_3\cdot\mathbf{162}_5\cdot\mathbf{168}]^{2+}$) and *m/z* 1004 ($[\mathbf{149}_3\cdot\mathbf{162}_4\cdot\mathbf{168}_2]^{2+}$) are very high. Therefore, the exchange of one and two ligands **162**

by ligands **168** is easily accessible. On the contrary, the exchange of three or four ligands **162** by **168** seems to be less favorable, because their relating peaks have lower intensities. The M_3L_6 complex containing five ligands **168** and one ligand **162** is again prominent.

This situation is complex and has to be discussed in detail: i) The system – especially ligand **168** – is flexible enough to compensate the size-difference of the ligands and thus, all possible homo- and heteroleptic M_3L_6 complexes can be observed. ii) The heteroleptic complexes $[\mathbf{149}_3\cdot\mathbf{162}_3\cdot\mathbf{168}_3]^{2+}$ (*m/z* 1018) and $[\mathbf{149}_3\cdot\mathbf{162}_2\cdot\mathbf{168}_4]^{2+}$ (*m/z* 1032) are less favored compared to other heteroleptic complexes. For both complexes, the strain caused by the different sizes of the ligands cannot be compensated very well. iii) The system is flexible enough to compensate the introduction of one ligand **162** into complex **189** resulting in $[\mathbf{149}_3\cdot\mathbf{162}_5\cdot\mathbf{168}]^{2+}$. Nevertheless, this species is less favored than complex **189** itself. iv) The introduction of one and two ligands **168** into complex **185b** seems to reduce the strain in the system.

Taking everything into account, it can be claimed that starting from complex **189** the successive exchange of ligands **168** by **162** causes more strain in the resulting system and therefore the probability to form such complexes decreases in the same manner. This drastically changes for complexes $[\mathbf{149}_3\cdot\mathbf{162}_4\cdot\mathbf{168}_2]$ and $[\mathbf{149}_3\cdot\mathbf{162}_5\cdot\mathbf{168}]$ which can be explained by a strain-compensation of the introduced ligands **168**. The strain in the latter complexes seems to be even less than in complex **185b**.

In conclusion, the self-assembly of functionalized metallo-supramolecular cages **185a/b-189** revealed the formation of kinetically formed M_3L_6 complexes which convert over time into thermodynamically favored M_2L_4 complexes. The structure of the complexes and their properties were characterized by the cooperation of several analytical methods. Ligand-exchange experiments revealed a size-selective formation of heteroleptic complexes which partly can be compensated by the flexibility of the ligands used. Due to the low solubility in appropriate solvents, the systems could not be used as host complexes to bind molecular guests.

5.4 Thermodynamically Controlled Self-Sorting of Homo- and Hetero-Bimetallic Metallo-Supramolecular Macrocycles

The project described within this chapter was performed in cooperation with Dr. Boris Brusilowskij and Egor V. Dzyuba. The results have been published in *Chemical Communications* in 2011.[158]

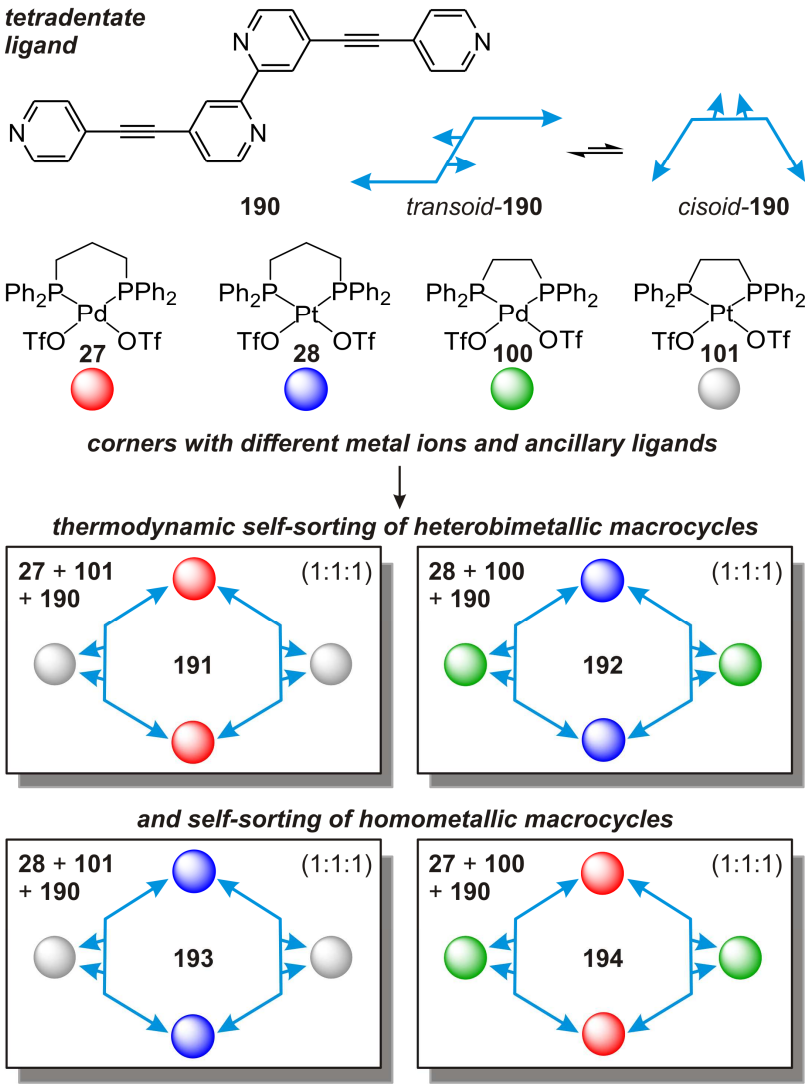

Figure 5.68: *Tetradentate ligand* ***190****, metal centers* ***27*** *(red),* ***28*** *(blue),* ***100*** *(green) and* ***101*** *(gray) and the four self-sorted hetero-bimetallic metallo-supramolecular macrocycles* ***190-194****.*

The "complex-as-a-ligand" concept has been widely employed to construct hetero-bimetallic complexes.[89b, 230] It roots in the formation of a kinetically inert metal complex bearing ligands that carry suitable binding sites to assemble in a subsequent step with a different metal complex into larger metallo-supramolecular complexes.[231] Assemblies, however, in which *both* metals are incorporated non-statistically under thermodynamic control rely on self-sorting phenomena and are still quite rare.[44, 53, 232] Hetero-bimetallic coordination has been based on denticity[233] as well as geometric[234] and electronic discrimination.[235]

In the present study, the self-sorting capability of complexes based on the tetradentate ligand **190** (Figure 5.68) and (dppp)M(II) and/or (dppe)M(II) triflates[236] **27**, **28**, **100** and **140** (M = Pd, Pt; dppp = bis-1,3-(diphenylphosphanyl)-propane, dppe = bis-1,2-(diphenylphosphanyl)-ethane) was explored. The synthesis of the ligand, which bears a bidentate 2,2'-bipyridine core and two terminal monodentate pyridine coordination sites, has recently been reported together with the formation of homometallic M_4L_2 complexes.[157] Interestingly, the addition of only one equivalent of **27** resulted in a strongly preferred binding of the metal to the pyridine sites: In marked contrast to a previously reported quaterpyridyl ligand lacking the ethinylene spacers,[237] M_2L_2 metallo-macrocycles form in a 1:1 mixture of **190** and **27**.[238]

The metal complexes **27**, **28**, **100** and **101** bear two d^8-square planar metal centers (Pd(II) and Pt(II)) at which two coordination sites are blocked by dppp and dppe ancillary ligands. These ligands differ by one CH_2 group, which causes slightly different angles between the phenyl groups attached to the diphosphametallacycle. Based on these steric differences, self-sorting may occur and provide the basis for the formation of hetero-bimetallic macrocycles.

Since the interpretation of the ^{1}H NMR spectra (Figure 5.69) is less straightforward due to signal overlap, the much more clear-cut ^{31}P NMR spectra of the complexes under study are shown in Figure 5.41. In order to evaluate the preference of metal centers **27**, **28**, **100** and **101** for either the pyridine or the bipyridine sites, **190** was assembled separately with each of the four metal complexes in CD_2Cl_2 at room temperature. After an equilibration period of twelve hours, the results were monitored by ^{31}P NMR spectroscopy (Figure 5.70A). Clearly, the two (dppp)M(II) complexes **27**

and **28** bind exclusively to the pyridine site. The positions of the signals corresponding to coordination to the bipyridine sites can easily be determined by addition of a second equivalent of the metal complex.[157] They are indicated in Figure 5.70A by the brackets on top and are absent in the spectrum of the 1:1 mixture. In contrast to this marked selectivity of **27** and **28** for the pyridine sites, the dppe complexes **100** and **101** do not show a strong preference for either one of the binding sites. Consequently, two signals are observed in the corresponding ^{31}P NMR spectra. Thus, the first conclusion is that only the (dppp)M(II) complexes can mediate self-sorting, while the (dppe)M(II) triflates do not provide support for such a process.

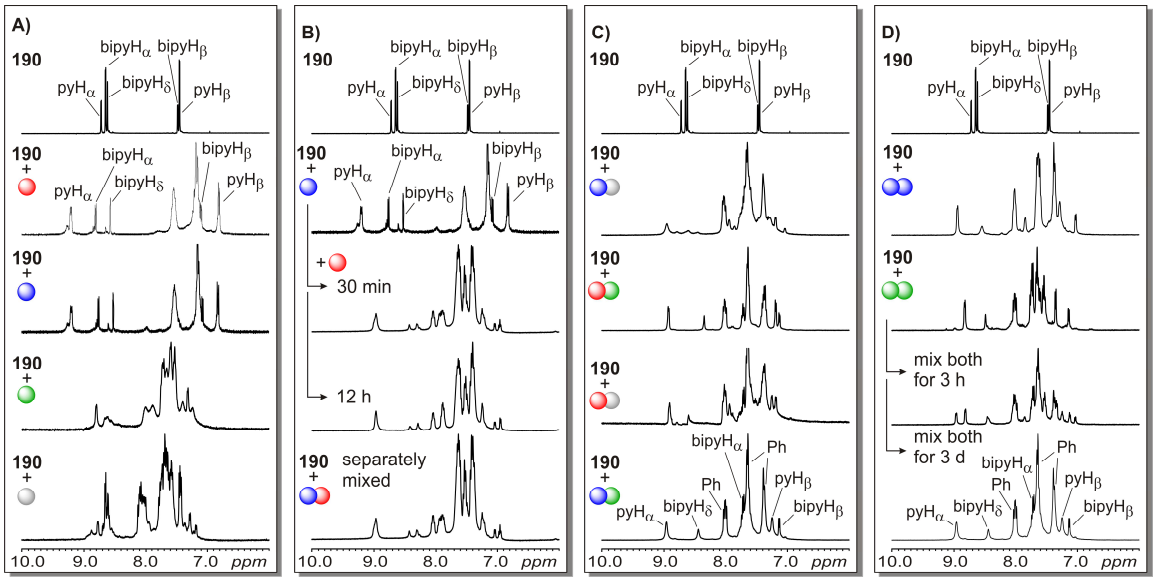

Figure 5.69: *Room-temperature ^{1}H NMR spectra in CD_2Cl_2: A) separate 1:1 mixtures of* ***190*** *and* ***27***, ***28***, ***100*** *or* ***101***, *respectively. B) 1:1 mixture of* ***190*** *and* ***28*** *(top), to which 1 eq. of* ***27*** *is added (recorded after 30 min and 12 h (center)), and* ***190*** *added to a 1:1 mixture of* ***27*** *and* ***28*** *directly. C) mixtures of* ***190*** *with pairwise mixtures of* ***27***, ***28***, ***100*** *and* ***101*** *(1:1:1 each) showing the self-sorting based on the anchillary ligands. D) Heterobimetallic self-sorting of metal corners between two preformed homometallic M_4L_2 macrocycles.*

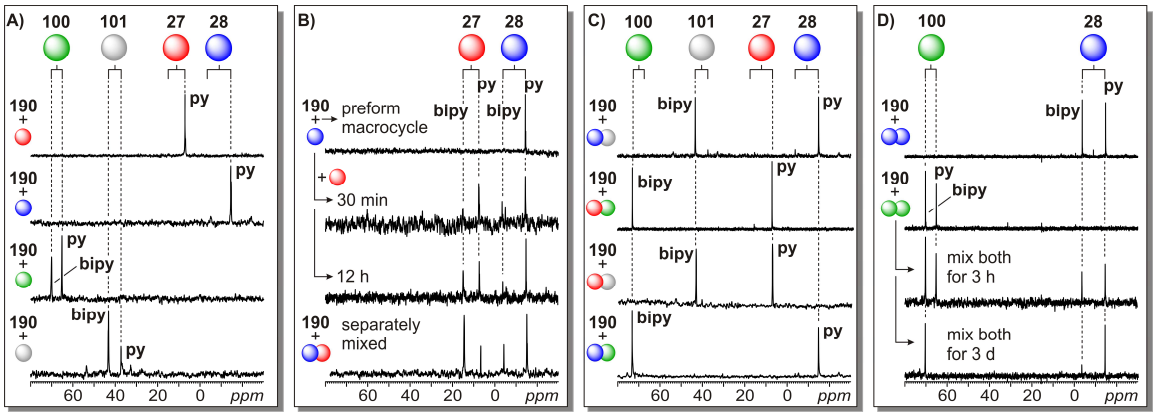

Figure 5.70: *Room-temperature ^{31}P NMR spectra in CD_2Cl_2: A) separate 1:1 mixtures of* ***190*** *and* ***27***, ***28***, ***100*** *or* ***101***, *respectively. B) 1:1 mixture of* ***190*** *and* ***28*** *(top), to which 1 eq. of* ***27*** *is added (recorded after 30 min and 12 h (center)), and* ***190*** *added to a 1:1 mixture of* ***27*** *and* ***28*** *directly. C) mixtures of* ***190*** *with pairwise mixtures of* ***27***, ***28***, ***100*** *or* ***101*** *(1:1:1 each) showing the self-sorting based on the anchillary ligands. D) Heterobimetallic self-sorting of metal corners between two preformed homometallic M_4L_2 metallo-macrocycles.*

Figure 5.70B shows an experiment, in which a M_2L_2 metallocycle incorporating **190** and **28** was preformed. After equilibration, 1 eq. of **27** was added to occupy the bipyridine binding sites. A ^{31}P NMR spectrum recorded 30 min after the addition of **27** already showed an exchange of the metal complexes to occur. Two additional signals for the coordination of the two metal complexes to the bipyridine sites grow over time. Since the Pt-N bond is kinetically more stable than the Pd-N bond, the exchange is slow.[11] The spectrum obtained after 12 hours resembles very much a spectrum which was obtained after adding **190** to a 1:1 mixture of **27** and **28**. Consequently, a mixture of all possible coordination isomers is obtained finally.

ESI mass spectrometry confirmed this result. Except for the $[Pd_4L_2\text{-}n\text{OTf}]^{n+}$ ions, all $[Pd_xPt_{4-x}L_2\text{-}n\text{OTf}]^{n+}$ complexes (x = 0 - 4) appear in their +2 (n = 2) and +3 (n = 3) charge states (Figure 5.71). The second conclusion is therefore that two different metal ions with the same dppp ancillary ligand do not induce any sorting. This experiment is important as a control which shows that the major differences between the Pd and the Pt complexes are kinetic in nature. The equilibrium is thus reached quite slowly, but the differences in bipyridine vs. pyridine bond dissociation energy

differences of the two metal ions ($\Delta\Delta BDE = \Delta BDE_{bpy\text{-}py}(Pd) - \Delta BDE_{bpy\text{-}py}(Pd)$) are small and do not significantly affect thermodynamics.

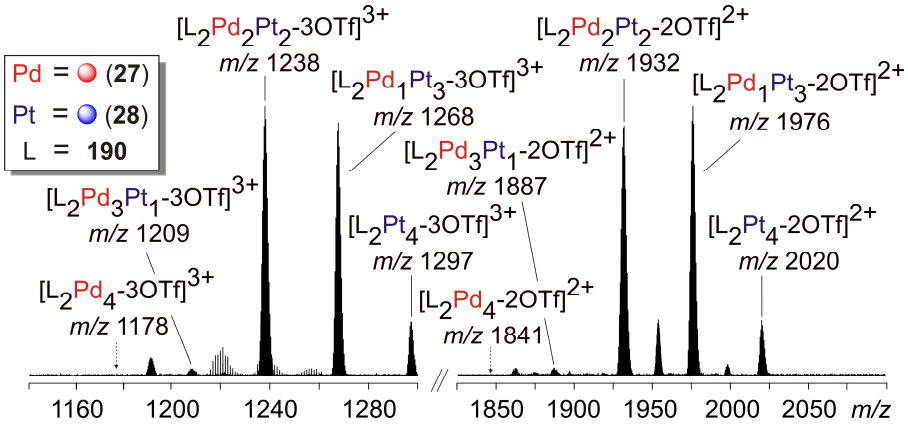

Figure 5.71: *ESI mass spectrum of the mixture of ligand **190** after combination with metal centers **27** and **28** and stirring for 12 h. In this mixture, the two (dppp)M(II) (M = Pd, Pt) complexes compete with each other for both binding sites. Since both bear the same ancillary ligand, no self-sorting can occur. In this case, a distribution of both metal centers over both binding sites is observed implying that stoichiometries other than M_{bpy}:M_{py}:L = 2:2:2 can form. The ESI mass spectra shown here nicely confirm this conjecture. The different complexes are observed in their +2 (right) and +3 (left) charge states. The lower abundance of Pd-rich complexes may result either from different ESI response factors or from a faster fragmentation of the kinetically less inert Pd complexes.*

The following NMR experiments (Figure 5.70C) aimed at probing whether the additional methylene group in the dppp complexes would be capable of inducing a self-sorting process - even though the dppe complexes do not contribute to it. All four possible combinations of ligand **190** with one dppp and one dppe complex were prepared and equilibrated for three days to ensure that equilibrium is reached. All four ^{31}P NMR spectra exhibit only two signals, which can easily be assigned as labeled in Figure 5.69C. Very clearly, a high-fidelity self-sorting occurs. Two self-sorted hetero-bimetallic and two homometallic[238] metallo-macrocycles (**191-194**; Figure 5.68) result. Consequently, the difference of merely one methylene group incorporated in the ancillary ligands suffices to induce high-fidelity self-sorting. In all four product complexes, the (dppp)M(II) complex coordinates to the pyridines. The (dppe)M(II) is

displaced from the pyridine and binds exclusively to the bipyridine sites when thermodynamic equilibrium is achieved.

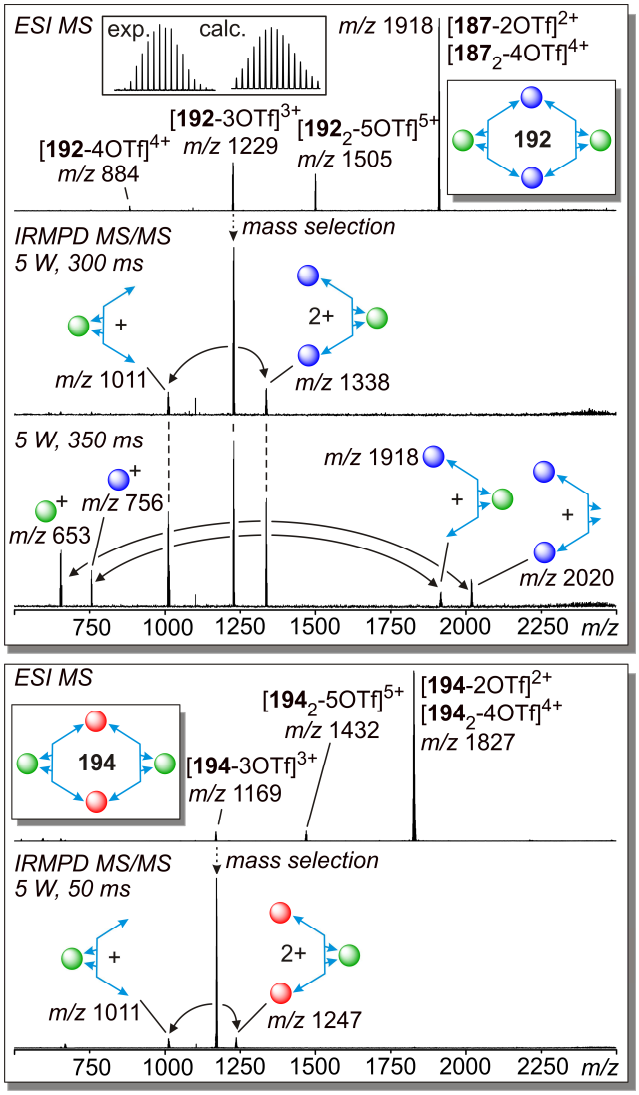

Figure 5.72: *ESI-FTICR and IRMPD tandem mass spectra. Top: Hetero-bimetallic metallo-macrocycle* ***192****. Bottom: Pd homometallic macrocycle* ***194*** *bearing (dppp)Pd(II) at the pyridines and (dppe)Pd(II) at the bipyridines.*

The last set of experiments is again a control. When two M_4L_2 complexes are preformed separately (Figure 5.70D) and then mixed, one would expect to initially observe all four signals in the ^{31}P NMR spectra. Over time, the mixture would self-sort finally reaching the same equilibrium situation as the mixture in which all three

components are just mixed simultaneously. This is indeed the case. After equilibrating the mixture of the two preformed metallo-macrocycles for three hours, all four ^{31}P NMR signals are observed. After three days, the (dppp)Pt(II) complex has almost completely occupied all pyridine units, while the (dppe)Pd(II) center is bound to the bipyridines. These experiments confirm the complete self-sorting observed here to occur under thermodynamic control.

Electrospray ionization Fourier-transform ion-cyclotron-resonance mass spectrometric experiments fully support the conclusions drawn from the ^{31}P NMR spectra. Figure 5.72 shows the ESI mass spectra obtained for hetero-bimetallic complex **192** and Pd homometallic complex **194** in which both ancillary ligands are present. All ESI mass spectra are similar in that the metallo-macrocycles are ionized by stripping away two or three counterions. In addition, some ions corresponding to dimers $\mathbf{192}_2$ or $\mathbf{194}_2$ are observed in their +4 and +5 charge states. Such dimers have been observed before for other metallo-supramolecular assemblies and can be attributed to "unspecific" complexation common in ESI mass spectrometry.[105, 106]

The fact that only 2:2:2 complexes (M_{py}:M_{bpy}:L), but no assemblies with other stoichiometries such as 1:3:2 or 3:1:2 are observed is already a first indication for self-sorting (see Figure 5.71 for a non-sorted mixture of **190**, **27** and **28**). Nevertheless, tandem MS experiments have been performed in order to induce fragmentation. The fragmentation patterns often provide structural information and one may be able to deduce the positions to which the dppp and dppe complexes are bound in the assemblies under study. The triply charged complex ions were thus mass-selected by removing all other ions from the FTICR analyzer cell. Subsequently, a CO_2 laser (10.6 µm) was employed in an infrared multi-photon dissociation (IRMPD) experiment to increase the ions' internal energy until they fragment. The initial fragmentation reaction is similar in both cases: The triply charged ions undergo a fragmentation reaction driven by charge separation. A singly charged M_{bpy}:L = 1:1 complex is formed concomitand with a doubly charged M_{py}:M_{bpy}:L = 2:1:1 fragment. If both metal complexes were randomly distributed over the two binding sites, one would expect to find both possible M_{bpy}:L = 1:1 complexes. This is, however, not the case. The only 1:1 fragment formed is that bearing the dppe metal complex.

Consequently, ESI mass spectrometry together with fragmentation experiments nicely confirm the conclusions drawn from the ^{31}P NMR experiments described above.

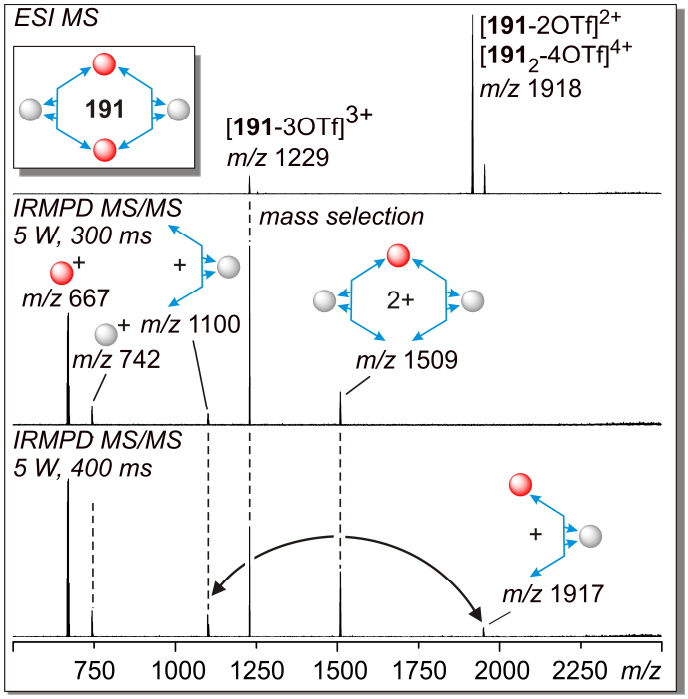

Figure 5.73: *ESI-FTICR mass spectrum (top) and the IRMPD tandem MS experiments at different irradiation times (middle and bottom) of metallo-macrocycle* ***191****. The M_{bpy}:L = 1:1 fragment ion at m/z = 1100 unambiguously confirms the position of the metal ions and supports the conclusions drawn from the ^{31}P NMR experiments.*

The heterobimetallic metallo-macrocycle **192** (Figure 5.72) bears the kinetically more inert Pt centers at the pyridine coordination sites. Thus one might expect the preferential loss of a (dppe)Pd(II) ion from the bipyridine sites. The chelate effect, however, compensates for that and structure-indicative fragments are formed as described above. The second heterobimetallic metallo-macrocycle **191** fragments differently (Figure 5.73). It bears the kinetically more labile Pd centers at the pyridine sites so that both effects, the more inert Pt-N bond and the chelate effect now cooperate to keep the (dppe)Pt(II) fragment at the bipyridine sites. Consequently, the loss of a singly charged (dppp)Pd(II) fragment leaves the doubly charged M_{bpy}:M_{py}:L = 2:1:2 fragment at *m/z* 1509 which is not structure indicative. However, the subsequent fragmentation at longer irradiation times (Figure 5.73, bottom spectrum)

yields only one 1:1 fragment. A random distribution of metal centers should result in the formation of two different 1:1 fragments. As this is not the case, the mass spectrometric experiments provide evidence for successful self-sorting for **191** as well. The ESI mass spectrum of the remaining homometallic macrocycle **193** as well as the results of the tandem MS experiments performed (Figure 5.74) are analogue to those of the homometallic complex **194**. Thus, the self-sorting of the metal centers is also confirmed for complex **193**.

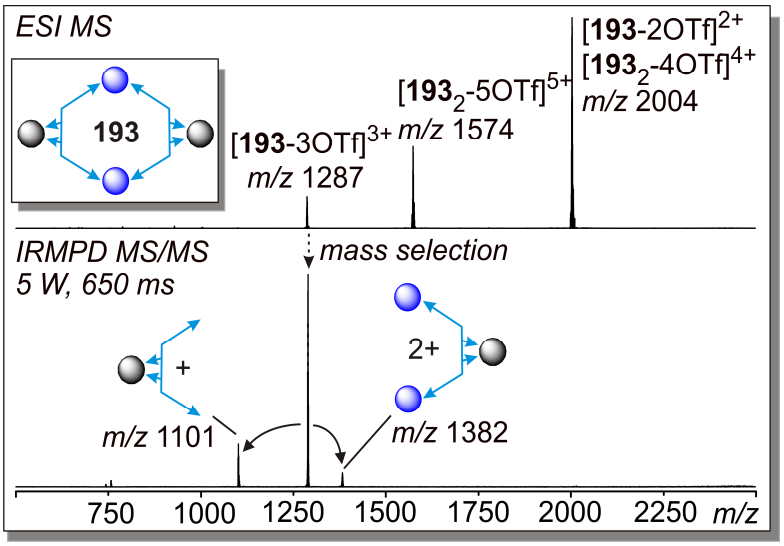

Figure 5.74: *ESI-FTICR mass spectrum (top) and the IRMPD tandem MS experiment (bottom) of metallo-macrocycle* ***193****. The* M_{bpy}*:L = 1:1 fragment ion at m/z = 1100 unambiguously confirms the position of the metal ions and supports the conclusions drawn from the* ^{31}*P NMR experiments.*

In conclusion, convincing evidence was obtained for a thermodynamically controlled self-sorting process leading to hetero-bimetallic metallo-macrocycles - merely because of one additional CH_2 group in one of the ancillary ligands. It is important to note that the preference of the dppp complexes for the pyridine rather than the bipyridine binding site overrides the lack of preference of the dppe complexes in a high-fidelity self-sorting process. Consequently, one can expect that this effect would also direct other metal complexes to the bipyridine coordination site - as long as the other metal complex is a square-planar (dppp)M(II) complex. This is to be confirmed in future studies.

5.5 Investigation into the Mechanisms of Self-Assembly Reactions

5.5.1 Kinetic and Structural Investigation of the Self-Assembly of Metallo-Supramolecular Pt(II) Complexes

Similar to the project presented in the last chapter, this project was performed in cooperation with Dr. Boris Brusilowskij and Egor V. Dzyuba as well. The results of this study have been accepted for publication in *Dalton Transactions* in 2011.[159]

Usually, self-assembly involves quickly reversible exchange processes, which guarantee error correction and thus the formation of one specific assembly out of much simpler, suitably programmed building blocks (see chapter 3).[33-35] However, a number of examples exist, in which one ligand/metal pair assembles into two or more discrete assemblies that coexist in thermodynamic equilibrium.[64, 70, 77, 109, 103] Those equilibria reflect a sensitive balance of enthalpic and entropic effects originating from different features of the ligands (shape, number and orientation of binding sites, flexibility), the metal centers (metal, coordination number, coordination geometry, auxiliary ligands, counter ions) and others (solvent, temperature, concentration).[104-106]

Recently, the self-assembly of (dppp)Pd(OTf)$_2$ **27** with tetradentate ligands which contained two pyridines and one 2,2´-bipyridine as the binding sites was examined.[157] Due to the steric demand of the dppp-phenyl groups, the pyridine sites were coordinated first to yield an M_2L_2 polygon. Only when all pyridine binding sites were occupied, the chelating bipyridine site coordinates to an additional metal center. Based on this preference of the dppp metal complex for the pyridine sites, the heterobimetallic metallo-supramolecular assemblies **191-194** self-sorted under thermodynamic control mediated by the auxiliary ligands ring size (see chapter 5.4).[158]

In here, the self-assembly of (dppp)Pt(OTf)$_2$ **28** with ligands **190**, **190-192** is discussed (Figure 5.75). Since Pt(II) complexes are known to be kinetically much more stable than the corresponding Pd complexes,[11, 104-106, 239] the error correction in the self-assembly processes of these complexes is slow. This allows us to examine the kinetic behaviour qualitatively with ^{1}H and ^{31}P NMR spectroscopy and electrospray ionization mass spectrometry (ESI-MS). Also, assemblies that are formed under kinetic control, but which are not present in thermodynamic equilibrium can be

identified as intermediates of the self-assembly process. Furthermore, the four ligands **190**, **190-192** are selected with the aim to study the constitutional effects of the pyridine N-atom position (*meta* vs. *para* with respect to the ethynyl substituent on the pyridine ring). The comparison of ligands with biphenyl and bipyridin cores allows us also to explore conformational aspects on the assembly process. While the biphenyl is folded along the aryl-aryl bond, the free bipyridine exists in a transoid conformation. Metal coordination to the bipyridine will enforce a cisoid presentation of the two pyridylethynyl substituents.

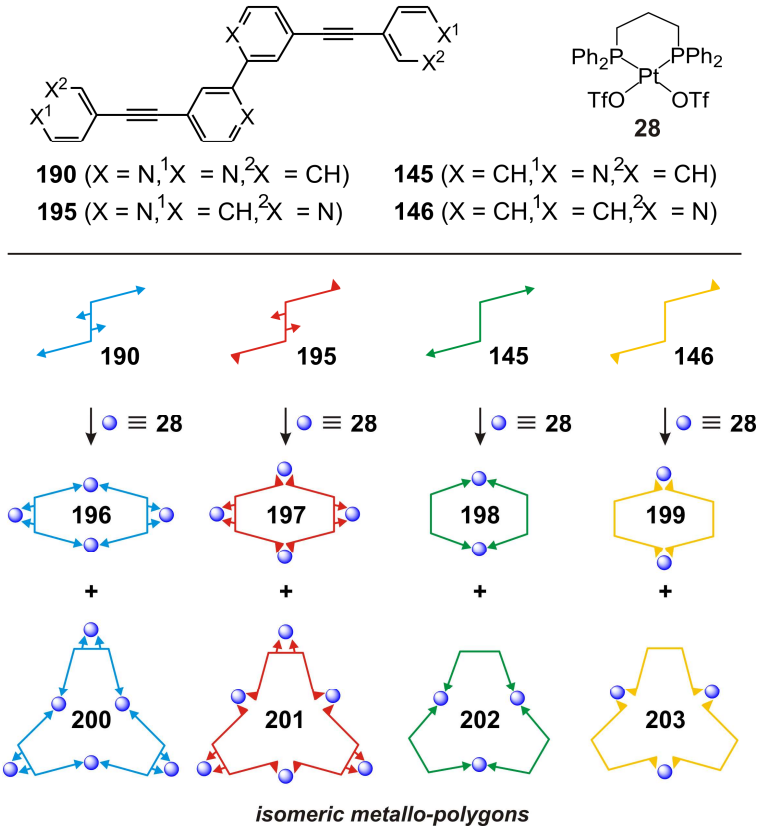

Figure 5.75: *The self-assembly of ligands **145**, **146**, **190** and **195** with (dppp)Pt(OTf)$_2$ **28** results in four pairs of constitutional isomers of metallo-supramolecular polygons: **196** and **197**, **198** and **199**, **200** and **201**, and finally **202** and **203**.*

Ligands **145**, **146**, **190** and **195** were synthesized according to established literature procedures from the corresponding bipyridine dialdehyde or biphenyl dialdehyde, respectively.[157, 240] Self-assembly was achieved by mixing metal center **28** with either

0.5 (**190** and **195**) or 1.0 equivalent (**145** and **146**) of the ligands in CD_2Cl_2 at room temperature. The samples were analyzed by NMR spectroscopy without isolating and purifying the assembly products in order to be able to examine the species formed without any bias. For mass spectrometric analysis, the NMR samples were diluted with CH_2Cl_2/acetone (1:1, v/v). The acetone is necessary to obtain reliable and constant spray conditions in the electrospray ion source. Since the measurement was done directly after diluting and since the exchange processes are slow, when (dppp)Pt(II) is used as the metal, it can be safely assumed that no major changes occur during the MS experiment.

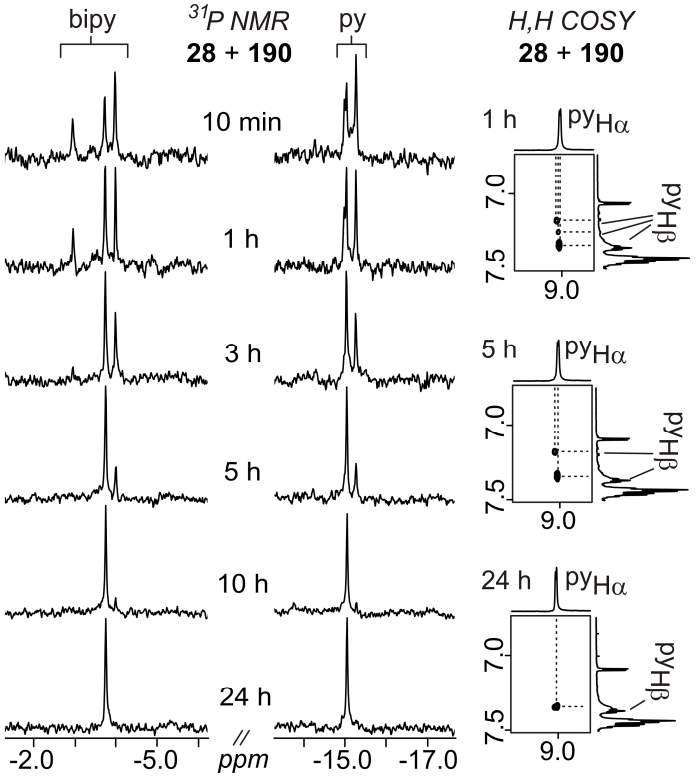

Figure 5.76: *Time-dependent ^{31}P NMR spectra of the mixture of ligand **190** with metal center **28** ([**28**] = 4.9 mM, left). Right: Partial $^{1}H,^{1}H$ COSY NMR spectra showing three, two and one cross peak of $py_{H\alpha}$ and $py_{H\beta}$ protons indicating the presence of three, two and finally only one product in the mixture.*

While the initial coordination of the ligands to the metal centers is fast for (dppp)Pd(II) as well as (dppp)Pt(II), there is a large rate difference for the ligand

exchange processes which finally correct any assembly intermediates that are formed under kinetic control,[28, 241] but that are not present when the equilibrium is achieved. The slow ligand exchanges at the (dppp)Pt(II) centers can be explained by the kinetical inert behaviour of Pt(II) complexes[11] which has been shown in many substitution experiments at Pt(II) complexes.[242] Recently, Stang and co-workers showed that ligand exchange processes in metallo-supramolecular Pt(II) complexes can tlast several days until the thermodynamic equilibrium is reached.[213] These slow ligand exchanges therefore allow to follow the error correction processes and to identify kinetic intermediates along the assembly pathway.

Time-dependent ^{31}P NMR spectra of the mixture of **28** and **190** clearly show the kinetic behavior of this system (Figure 5.76, left). The signals for coordination of (dppp)Pt(OTf)$_2$ to the bipyridine binding site are observed at ca. -5 ppm, while the signals for the coordination to the pyridine appear in at around -15 ppm. This is in line to analogous complexes studied before (see chapter 5.4).[158] Ten minutes after mixing, three different signals can be observed for both coordination sites, two of which overlap for the pyridine site. The intensities of two of the three different sets of signals decrease with increasing time, while the intensity of the third one is increasing. After three hours, the first set of signals almost vanishes within the noise and after five hours only two sharp sets of signals are observed. The second set of signals which was initially the most prominent one vanishes more slowly, but is not present anymore in the spectrum obtained after 24 hours. The thermodynamic minimum is characterized by only one sharp set of signals is left. It should be noted that each of the three species initially observed is characterized by only two signals, one for the pyridine-coordinated (dppp)Pt(II) center, one for that at the bipyridine. This points to a quite high symmetry of each of the species with both P atoms at each metal being identical all metal centers in each of the two coordination sites also being equivalent. This rules out the presence of a significant amount of linear oligomers, which would be expected to exhibit lower symmetry.

The time-dependent ^{1}H NMR spectra of this system are difficult to evaluate, because their signals are strongly superimposed (Figure 5.77). However, the ^{1}H NMR spectra become clear with increasing time and after 5 hours the ^{1}H NMR spectrum shows two discrete metallo-supramolecular assemblies to be present in solution in agreement with

the interpretation of the ^{31}P NMR spectra. These results are also supported by $^{1}H,^{1}H$ COSY NMR spectra (Figure 5.76, right). After one hour of mixing time, three cross-peaks for the coupling between the $py_{H\alpha}$ and the $py_{H\beta}$ protons are observed, while after five hours only two of them are left. In the thermodynamic minimum after 24 hours, only one cross peak remains visible.

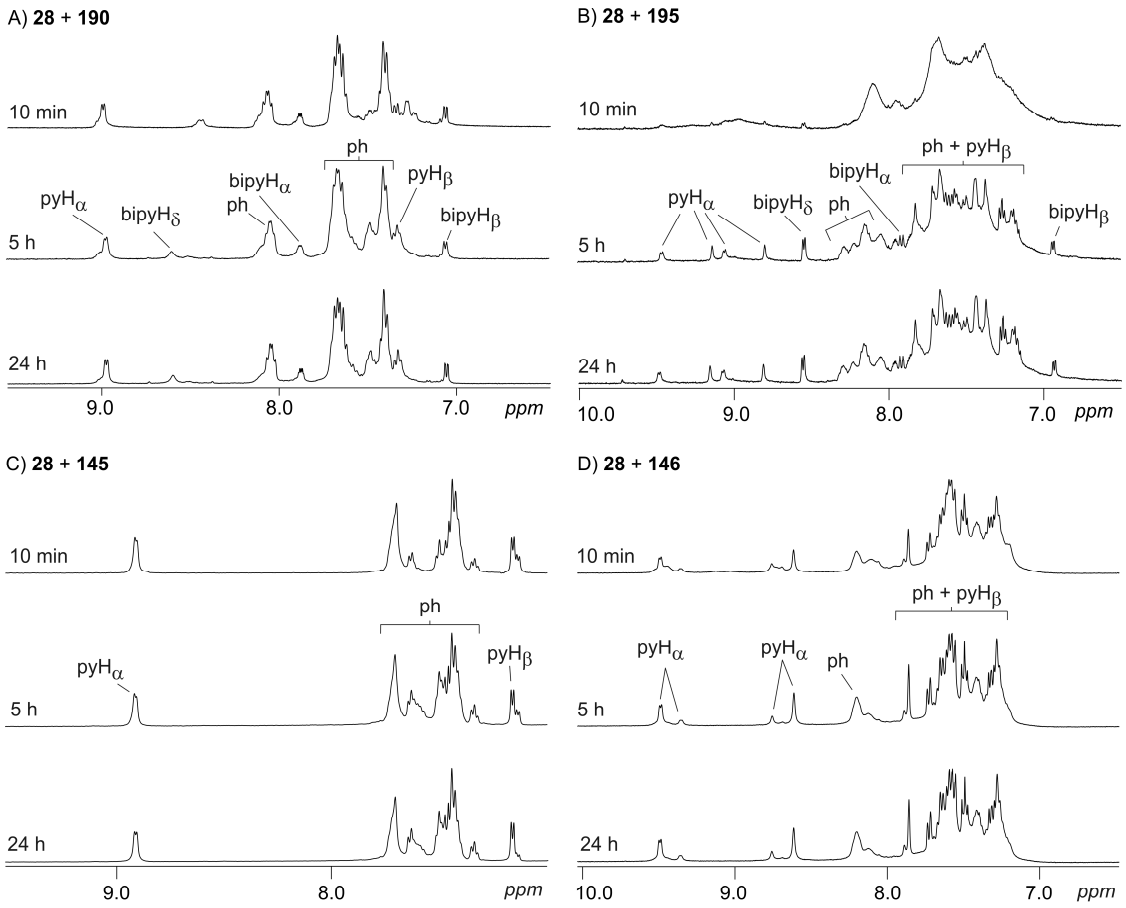

Figure 5.77: *^{1}H NMR spectra of the aromatic region for the separate mixtures of ligand A)* ***190****, B) ligand* ***195****, C) ligand* ***145*** *or D) ligand* ***146*** *with Pt metal center* ***28*** *([**28**] = 4.9 mM) after 10 min, 5 h and 24 h stirring at room temperature.*

To determine the stoichiometry of the species present at different times, ESI mass spectra were recorded (Figure 5.78). The ionization occurs through stripping away some of the triflate counterions so that the charge state indicates how many triflate ions are lost during ionization. The ESI mass spectrum recorded 10 minutes after mixing exhibits a

number of peaks, which can be assigned to several metallo-supramolecular complexes some of which may be formed by fragmentation during the ESI process. The peaks at *m/z* 1297 ([**196**]$^{3+}$) and *m/z* 2020 ([**196**]$^{2+}$) correspond to the M_4L_2 complex **196**. The peaks at *m/z* 1478 ([**200**]$^{4+}$) and *m/z* 2020 ([**200**]$^{3+}$) can clearly be assigned to M_6L_3 complex **200**. Both complexes are also observed in the mass spectrum recorded after 5 hours, so that these two complexes, **196** and **200** can unambiguously be identified as the last two remaining species. The third component observed in the early NMR spectra, however, remains somewhat unclear. An M_8L_4 macrocycle would be in line with the high symmetry indicated by the NMR data. It also agrees with the signal at *m/z* 1586 in the ESI mass spectra, which is not present anymore in the later spectra and thus likely does not correspond to an unspecific dimer [(**196**)$_2$]$^{5+}$. After 24 hours, only peaks for the M_4L_2 complex **196** are found so that we can conclude the smaller macrocycle **196** to be the thermodynamic product, while **200** is an intermediate formed under kinetic control.

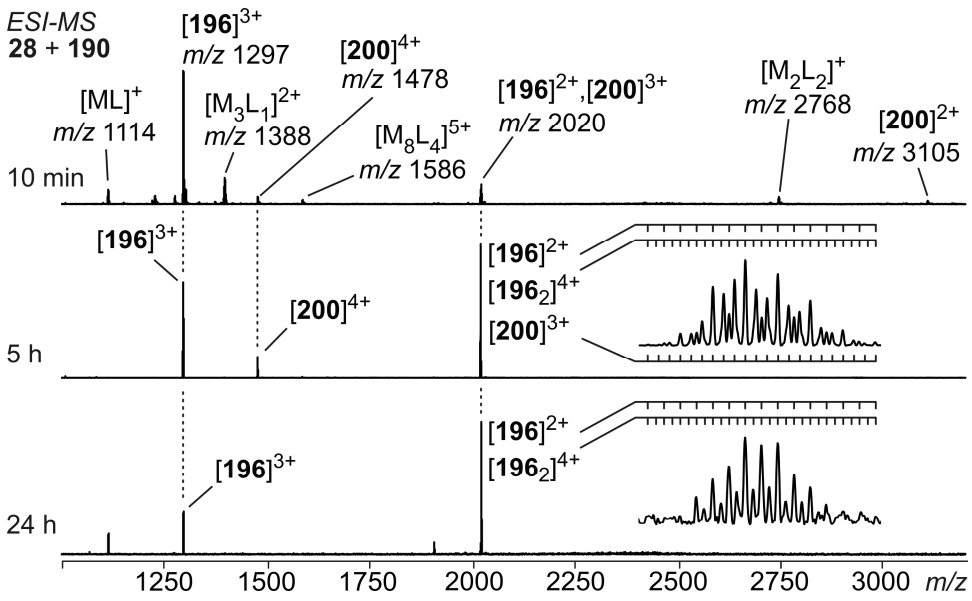

Figure 5.78: *ESI mass spectra of the mixture of **190** and **28** after 10 min, 5 h und 24 h. Isotope pattern analysis indicates a significant contribution of [**200**]$^{3+}$ still to be present after 5 h reaction time, while it has vanished after 24 h. The dimer [**196**$_2$]$^{4+}$ is a typical unspecific complex formed during electrospray ionization.*

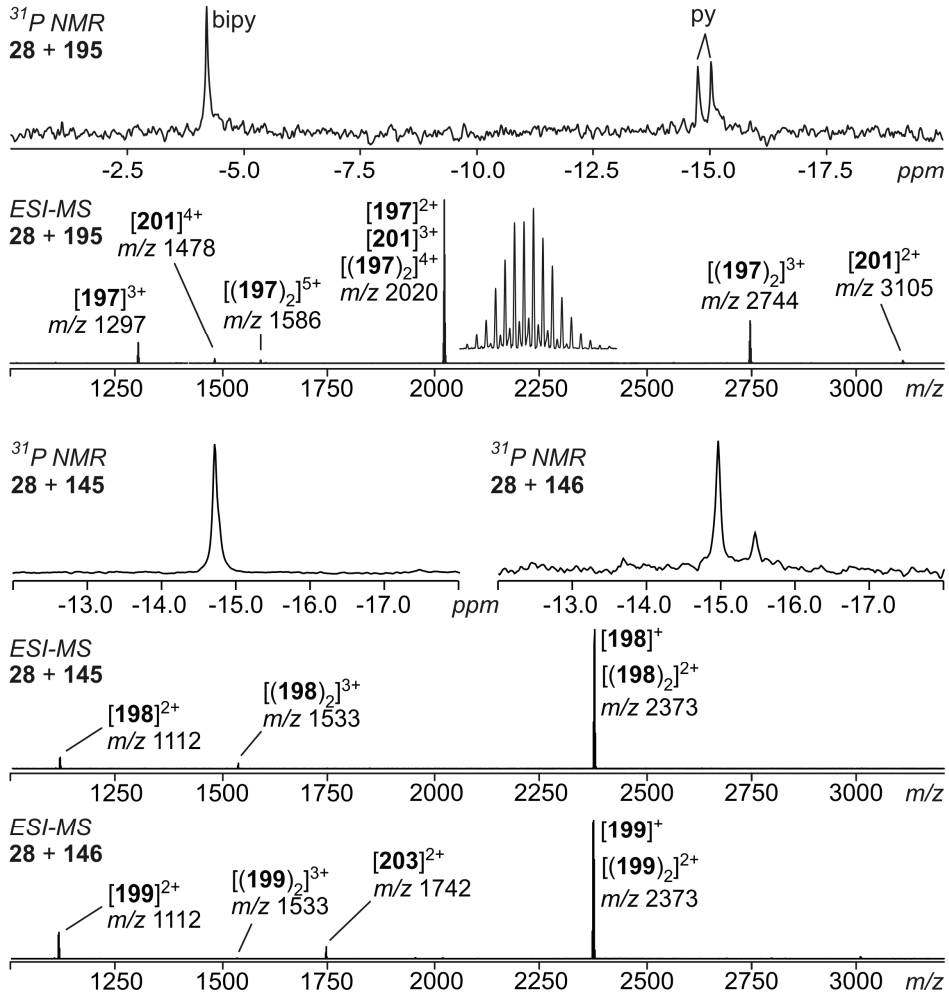

Figure 5.79: *^{31}P NMR and ESI mass spectra of the mixtures of **28** + **195**, **28** + **145**, and **28** + **146** recorded 24 h after mixing. The spectra do not change anymore at longer reaction times. They indicate the exclusive formation of the smaller metallo-macrocycle from ligands with 4-ethynyl-substituted pyridine binding sites. In contrast, **197** and **201** or **199** and **203**, respectively, co-exist in equilibrium with each other when the pyridine rings are substituted at C(3).*

Figure 5.79 shows the ^{31}P NMR and ESI mass spectra recorded after 24 hours equilibration time for the mixtures **28** + **195**, **28** + **145**, and **28** + **146**. In all three cases, the equilibrium is reached and no further changes in the spectra are observed. Comparing the mixture of **28** and **190** with that of **28** and **195** yields to quite different results. For the latter self-assembly reaction, two species are observed in the NMR and mass spectra

which equilibrate with each other (see also Figure 5.80). ESI mass spectrometry helps to identify these species as the M_4L_2 complex **197**, which appears in charge states +2 and +3 at *m/z* 1297 ([**197**]$^{3+}$), and *m/z* 2020 ([**197**]$^{2+}$) and the M_6L_3 complex **201** at *m/z* 1478 ([**201**]$^{4+}$), *m/z* 2020 ([**201**]$^{3+}$), and *m/z* 3105 ([**201**]$^{2+}$). The [**201**]$^{3+}$ ion is only visible as small shoulders in the isotope pattern at *m/z* 2020 that appear between the signals of [**197**]$^{2+}$ and its unspecific dimer [**197**$_2$]$^{4+}$.

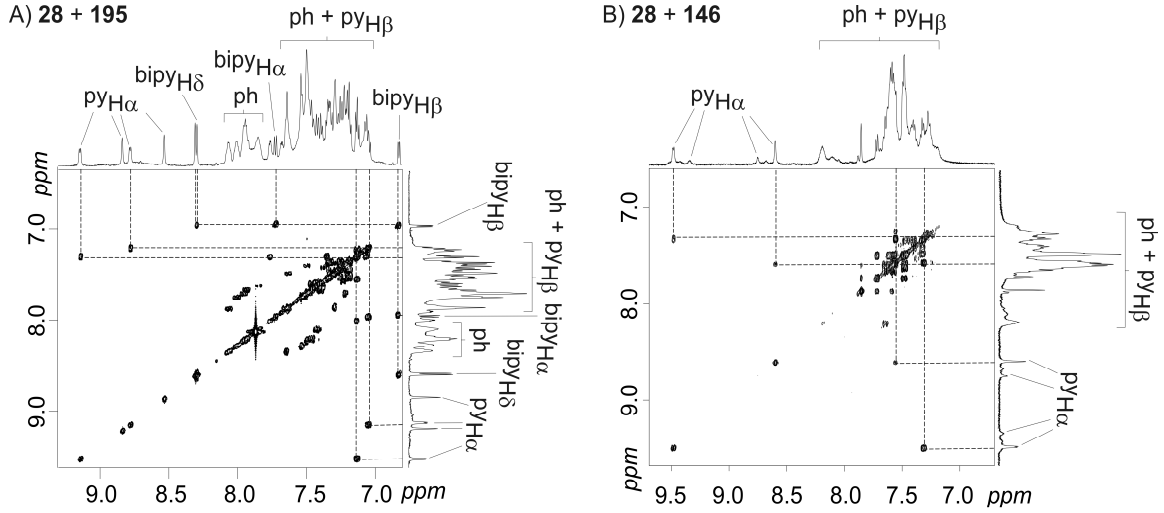

Figure 5.80: *^{1}H,^{1}H COSY NMR spectra of the aromatic region for the separate mixtures of ligand A)* ***195*** *and B) ligand* ***146*** *with Pt metal center* ***28*** *([**28**] = 4.9 mM) after 24 h stirring at room temperature.*

Very similar results are obtained for the second pair of constitutionally different ligands. Ligand **145** assembles with **28** into only one product which is identified by mass spectrometry to be **198**. In marked contrast, **28** and **146** form again two equilibrating assemblies which can be identified as **199** (the major product) and **203** (the minor product). Consequently, the position of the pyridine N-atom has a clearly visible effect on the assemblies that are present in the thermodynamic equilibrium.

The fact that **196** and **198** are the only thermodynamic products, when the 4-ethynyl-substituted ligands **190** and **145** are reacted with **28**, while **197**/**201** and **199**/**203** equilibrate with each other, when 3-ethynyl-substituted ligands **195** and **146** are used, indicates **197** and **199** to be more strained than **196** and **198** due to the altered pyridine N

atom position. This strain obviously disfavors the smaller polygons and shifts the delicate equilibrium to the larger macrocycles.

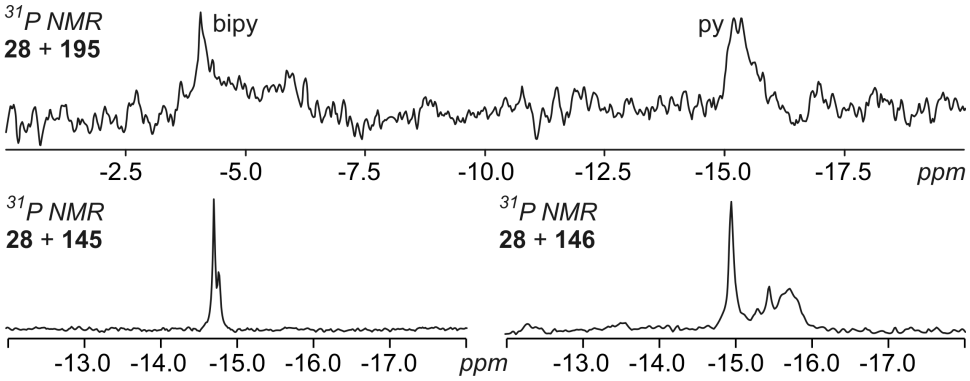

Figure 5.81: *^{31}P NMR spectra of the mixtures **28** + **195**, **28** + **145** and **28** + **146** recorded 10 minutes mixing. The corresponding spectrum of **28** + **190** is shown in Figure 5.76 (top row).*

It is also interesting to compare the ^{31}P NMR spectra of the four mixtures that are obtained 10 minutes after mixing each of the four ligands with **28** (Figure 5.76, top row, and Figure 5.81). Again, the two ligands carrying the ethynyl group at the pyridine C(4)-atom have in common that only few sets of sharp signals are visible. The two mixtures **28** + **190** and **28** + **145** are thus already quite well defined after 10 minutes. In marked contrast, the **28** + **195** and **28** + **146** mixtures yield ^{31}P NMR spectra with broad signals that appear to be structured to some extent. These spectra indicate the formation of many more assemblies, if the ethynyl-substituent is located at the pyridine C(3)-atom. A comparison of the ESI mass spectra performed after a reaction time of 10 minutes with those after 24 hours supports these observations (Figures 5.78, 5.79 and 5.82). Although all assembly reactions finally converge into a rather simple product distribution, the assembly pathways quite significantly differ depending on the position of the pyridine N-atom. The reason for these differences is likely the higher conformational freedom of the 3-ethynyl pyridines. Rotation of the pyridine rings allows the ligand to adjust to many different orientations just as required for the formation of any of the assemblies present in the mixture. In contrast, the 4-ethynyl pyridine bears the pyridine N-atom on the axis defined by the ethynyl

group. Irrespective of any pyridine rotation, the direction of the coordinative bond is thus fixed. Therefore, **195** and **146** are able to form a much greater variety of assemblies with **28**, while the selection of possible assemblies is limited for **190** and **145**.

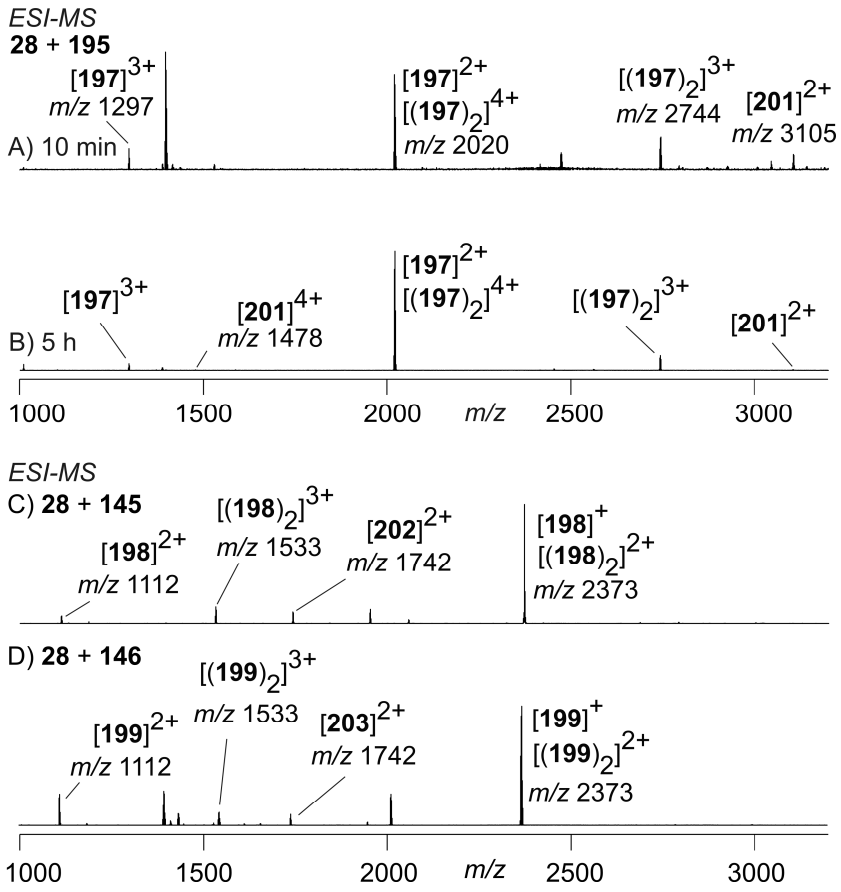

Figure 5.53: *ESI mass spectra of the mixture of ligand **190** with Pt metal center **28** after A) 10 min and B) 24 h stirring at room temperature. Furthermore, the ESI mass spectra of the mixtures of C) ligand **145** and D) ligand **146** with Pt metal center **28** after stirring at room temperature for 10 min is shown.*

The ^{31}P NMR spectra of the **28** + **190** and **28** + **145** mixtures recorded after 10 minutes exhibit yet another difference. The most prominent product initially formed from **28** + **190** is **200**, while the thermodynamic product **196** is a minor component. In addition, a larger M_8L_4 macrocycle is generated. The major signal in the ^{31}P NMR spectrum of the **28** + **145** mixture, however, is the smaller macrocycle **198**, while **201** is the minor product and no larger M_4L_4 macrocycle is observed.

This difference can be explained by the higher conformational flexibility of system **28** + **145**. According to molecular modelling,[157] ligand **145** with its biphenyl core is not planar and can exist in two conformations with dihedral angles along the central aryl-aryl bond of either 40^{o} or 139^{o}. Since the barrier between both is presumably small, these ligands can adjust quite easily to the requirement of any assembly formed. Consequently, the smaller macrocycle **198** forms quite easily from a linear M_2L_2 precursor. The situation is, however, very different for ligand **190** with its bipyridine core. The uncoordinated bipyridine prefers a coplanar *transoid* conformation with the two pyridyl sites pointing away from each other.[243] The corresponding *cisoid* conformation is less stable by 23.8 kJ/mol.[244] With (dppp)M(II) (M = Pd, Pt), it was observed that the bipyridine coordination site is occupied only after the pyridine sites have coordinated to the first equivalent of the metal complexes.[158, 157] This is important here, because this means that **190** forms macrocycles with its pyridine sites first and thus reacts initially in its transoid conformation. This explains why larger macrocycles are preferred for this ligand. After that, the bipyridine sites are occupied and thereby forced into the *cisoid* form. The macrocycles then refold into another conformation containing only cisoid bipyridines. Consequently, not only ligand constitution, but also ligand conformation has a notable effect on the self-assembly pathways. Although the conformational differences do not affect the thermodynamic product distribution, they change the kinetic intermediates formed on the way to the final equilibrium.

Above, it was hypothesized that **197** and **199** would be more strained than **196** and **198** due to the position of the pyridine N-atom. With this argument, it was rationalized that the equilibrium shifted more towards the larger macrocycles **201** and **203**. Of course, another possible explanation would be that **201** and **203** are more favorable in energy than **200** and **202**. In order to be able to provide more convincing evidence for our strain hypothesis, macrocycles **196-199** were investigated by tandem mass spectrometry. After mass-selection of the desired ions, the parent ions were irradiated with a CO_2 laser at 10.6 µm wavelength which is tunable between 0 and 25 W laser power. In this infrared multiphoton dissociation (IRMPD) experiment, the parent ions absorb IR photons until they fragment.

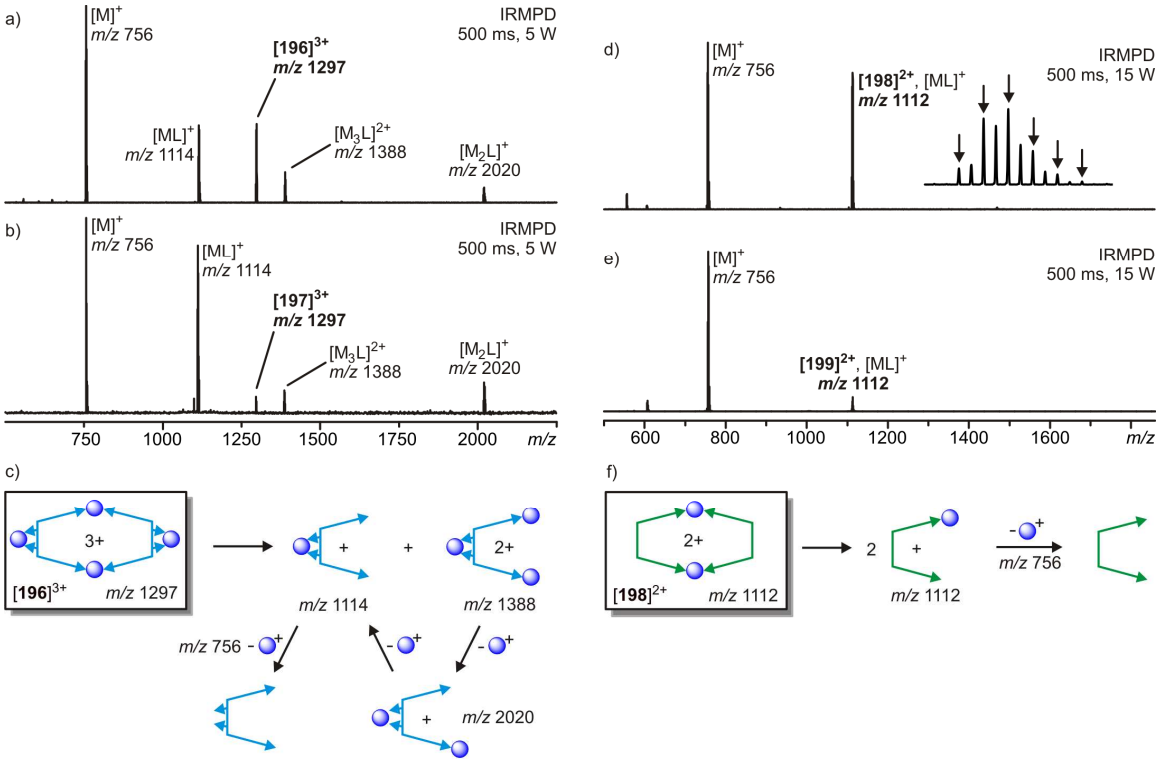

Figure 5.83: *IRMPD mass spectra of mass-selected* ***[196]***$^{3+}$ *(a),* ***[197]***$^{3+}$ *(b),* ***[198]***$^{2+}$ *(d), and* ***[199]***$^{2+}$ *(e) and fragmentation mechanisms shown representatively for* ***[196]***$^{3+}$ *(c) and* ***[198]***$^{2+}$ *(f). Mass-selected parent ions are assigned in bold. Isotope pattern analysis confirms the symmetrical cleavage of* ***[198]***$^{2+}$ *and* ***[199]***$^{2+}$ *giving rise to singly charged product ions (arrows) with the same mass-to-charge ratio as the doubly charged parent ions. The unsymmetrical cleavage of* ***[196]***$^{3+}$ *and* ***[197]***$^{3+}$ *can be attributed to the +3 charge state, which requires an uneven distribution of charges over the two primary product ions.*

Figure 5.83 shows the MS/MS spectra obtained together with the fragmentation pathways. Primary product ions and consecutive fragments can be distinguished by repeating the IRMPD experiment with different irradiation intervals. The fragmentation mechanisms can thus be determined. They depend on the charge state. A triply charged ion such as **[196]**$^{3+}$ or **[197]**$^{3+}$ undergoes an unsymmetric charge-separating cleavage leaving two charges on an $[M_3L]^{2+}$ fragment and one charge on the remaining $[ML]^{+}$ ion. Doubly charged ions such as **[198]**$^{2+}$ or **[199]**$^{2+}$ undergo a

clean charge-separating fragmentation into two identical halves. Consecutive fragmentations involve losses of $[(dppp)Pt^{II}(OTf)]^{+}$. Interestingly, [**196**]$^{3+}$ and [**197**]$^{3+}$ fragment qualitatively through the same pathways as do [**198**]$^{2+}$ and [**199**]$^{2+}$. In both cases, however, the fragmentation is significantly more efficient, when the complexes contain 3-ethynyl pyridine subunits. The [**197**]$^{3+}$ and [**199**]$^{2+}$ parent ions vanish more quickly than [**196**]$^{3+}$ and [**198**]$^{2+}$, respectively, under exactly the same experimental conditions. This behaviour nicely agrees with the hypothesis that **197** and **199** are more strained than **196** and **198** due to the pyridine constitution.

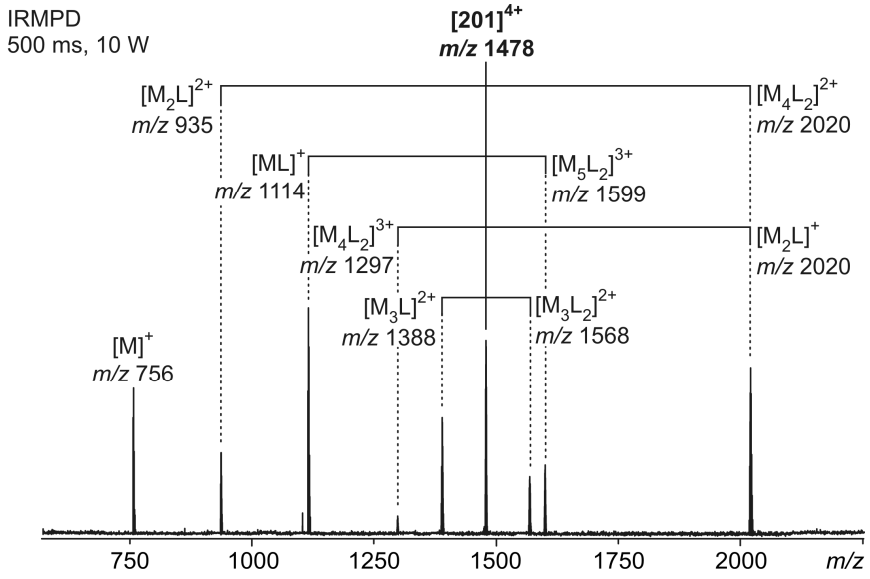

Figure 5.84: *IRMPD tandem mass spectrum of mass-selected [**201**]$^{4+}$ cations. The tetracation undergoes very unspecific charge-separating dissociation into four competing fragmentation pathways each one of which yields two complementary fragment ions.*

Tandem mass spectrometric experiments can be used to investigate the unimolecular fragmentation processes of supramolecules.[245] In contrast to solution studies, a very important difference of these gas-phase experiments is that no exchange processes are possible, since the ions of interest are isolated species without any environment. Such experiments have provided insight into mechanistic details of the fragmentation of metallo-supramolecular squares which undergo a ring contraction from a square to a

triangle during fragmenatation.[187, 105, 214] Similarly, cage contraction reactions have been observed for 3D metallo-supramolecular complexes.[139] Both processes proceed through a "backside-attack" mechanism. After opening the first Pt-N bond, the free pyridine nitrogen can attack a different metal center. An intramolecular ligand exchange which proceeds through a trigonal bipyramid leads to the contracted macrocycle or cage and releases a fragment by cleaving another Pt-N bond.

Since the ligand exchanges at the (dppp)Pt(II) centers are slow, all four M_6L_3 and M_3L_3 metallo-macrocycles **200**-**203** can be subjected to tandem mass spectrometry - even when they are only kinetic intermediates. Both **200** and **201** tend to be ionized in higher charge states than **202** and **203** due to the additional metal centers bound to the bipyridine sites. Figure 5.84 shows the IRMPD mass spectrum of [**201**]$^{4+}$ as a representative example for the laser-induced decomposition. Four pairs of complementary fragments are observed which can clearly be assigned to charge-separating fragmentation reactions. The charges are distributed over the two fragments in each channel more or less according to the sizes of the two fragments and thus, decompositions into +1 and +3 ions are equally possible as the formation of two +2 daughter ions of almost equal size. The fragmentation pattern is thus quite unspecific and best compatible with the following scenario: The first step is ring cleavage resulting in the formation of linear coordination oligomers. These oligomers then fragment at any of the Pt-N bonds along the chain. Mass-selected [**200**]$^{4+}$ ions behave similarly (Figure 5.85), but the number of different, competing fragmentation channels is somewhat reduced. Nevertheless, the fragmentation is not specific for one channel alone. In view of the high charge state, this behaviour may not seem surprising, but earlier, a highly specific fragmentation of a metallo-supramolecular square even in its +5 charge state was reported,[214] which exclusively decomposed into a +4 triangle and a singly charged 1:1 complex of (dppp)Pt(OTf)$^+$ and 4,4'-bipyridine through the above-mentioned backside-attack mechanism.

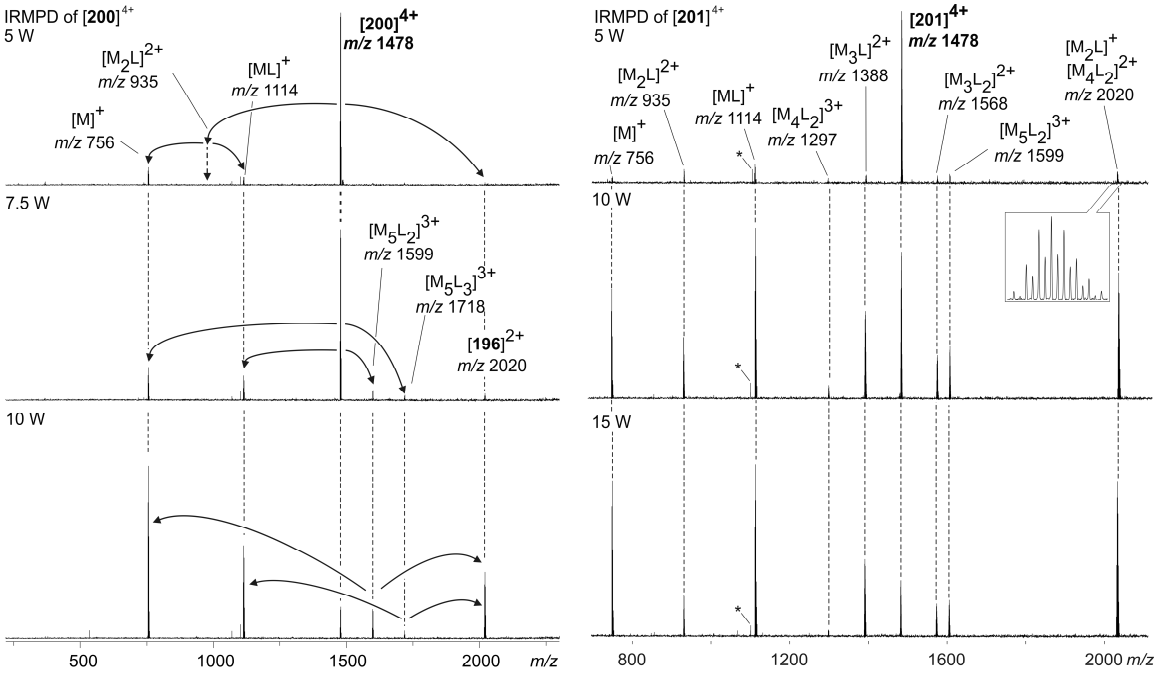

Figure 5.85: *Tandem ESI mass experiments of the* $[\mathbf{200}]^{4+}$ *and* $[\mathbf{201}]^{4+}$ *ions with different IRMPD laser intensities for 500 ms (* = artefact due to stray radiation).*

A look at the IRMPD mass spectra of mass-selected $[\mathbf{201}]^{2+}$ (Figure 5.86) and $[\mathbf{203}]^{2+}$ (Figure 5.87) reveals these two ions to fragment through the same pathways, but in a much more specific way than $[\mathbf{200}]^{4+}$ and $[\mathbf{198}]^{4+}$. Only one primary fragmentation channel is observed, which gives rise to a 1:1 $[ML]^{+}$ and a $[M_2L_2]^{+}$ fragment. No fragmentation in, e.g. $[ML_2]^{+}$ and $[M_2L]^{+}$ is observed, which would be an alternative route. As in the earlier reports discussed above, this quite specific fragmentation can be explained by a backside-attack mechanism (Figure 5.57): After ring cleavage at the first Pt-N bond, the free pyridine N-atom can form a bond with the second rather than the most distant metal center. Cleavage of a Pt-N bond, which connects the 1:1 piece to the rest of the complex then leads to the fragmentation. This process is energetically more favourable, because the new bond is formed while the old one is broken. The backside-attack mechanism is therefore more or less thermoneutral. Other fragmentation reactions, which do not involve the formation of the smaller macrocycles, are more energy demanding, because the bond dissociation energy required for the second bond cleavage is not compensated for.

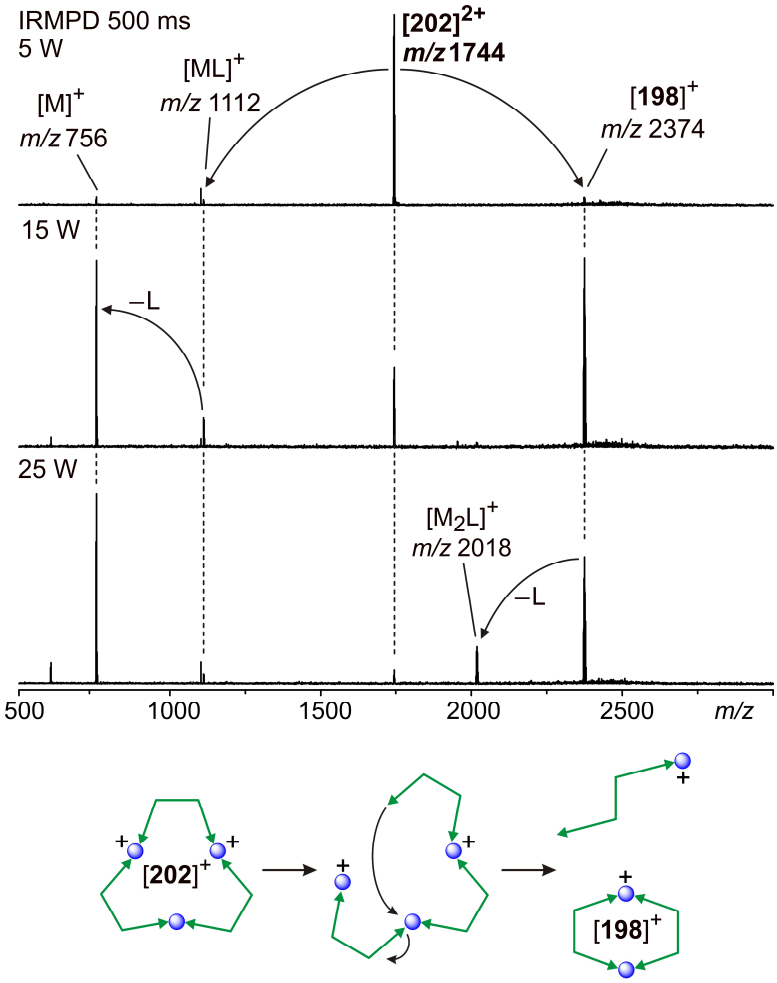

Figure 5.86: *IRMPD tandem mass spectra of mass-selected* ***[202]***$^{2+}$ *cations with different laser flux densities. Only one charge-separating primary fragmentation channel is populated which can be interpreted as a ring contraction of the parent ion to yield the smaller 2:2 macrocycle* ***[198]***$^{+}$ *(mechanism shown below). At higher laser flux densities, consecutive ligand losses are observed.*

To explain the significantly different fragmentation behaviour of [**200**]$^{4+}$ and [**201**]$^{4+}$ on one hand and [**202**]$^{2+}$ and [**203**]$^{2+}$ on the other, one might of course invoke charge repulsion. The higher charge state then would fragment less specifically. In addition, however, the conformational flexibility of the biphenyl core in [**202**]$^{2+}$ and [**203**]$^{2+}$ might also be favourable, while the bipyridyl core is fixed in a cisoid conformation by the coordinating metal. Both effects together may thus cause the observed differences.

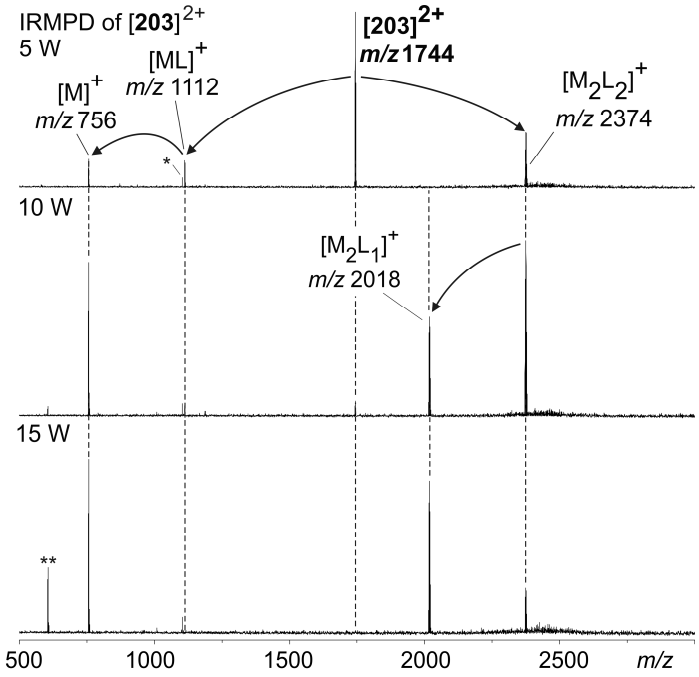

Figure 5.87: *Tandem mass spectra of the* $[\mathbf{203}]^{2+}$ *ion with different IRMPD laser intensities for 500 ms.*

Two pairs of pyridine-based ligands, one pair with bipyridine core (**190** and **195**), one with biphenyl core (**145** and **146**) have been examined with respect to their self-assembly behaviour with ((dppp)Pt(OTf)$_2$. Insight has been gained into the thermodynamic assembly products: Only one product - i.e. an M_4L_2 complex from **190** and an M_2L_2 complex from **145** - is obtained, when the pyridine rings are ethynyl-substituted at C(4). Two equilibrating macrocycles of different sizes represent the thermodynamic equilibrium, when the ethynyl-substituent is located at C(3).

The kinetics of the ligand exchange at the (dppp)Pt(II) centers is slow enough to monitor the error correction by NMR spectroscopy and mass spectrometry. The intermediate M_6L_3 and M_3L_3 macrocycles, which form under kinetic control for ligands **190** and **145**, can thus be examined without any problems. For example, tandem MS experiments demonstrate an interesting fragmentation mechanism to occur for doubly charged ions $[\mathbf{201}]^{2+}$ and $[\mathbf{203}]^{2+}$, which does not operate for quadruply charged ions $[\mathbf{200}]^{4+}$ and $[\mathbf{202}]^{4+}$. The present study furthermore shows the significant changes to the assembly behaviour of the four ligands with (dppp)Pt(OTf)$_2$ induced by subtle differences in the constitution and conformation of the ligands.

5.5.2 Online Mass Spectrometry: The Use of a Micro-Reactor to Examine Fast Metallo-Supramolecular Self-Assembly Processes

The following project was performed in cooperation with Johannes Poppenberg and Sebastian Richter, who helped to develop the micro-reactor technique for metallo-supramolecular systems.[246]

Self-assembly of metallo-supramolecular complexes is a very well known concept to achieve highly complex structures from simple building blocks.[33] Several studies on the thermodynamics, kinetics and mechanisms of the self-assemly of metallo-supramolecular complexes exist.[247, 248] Within the last chapters, several different details of self-assembled metallo-supramolecular systems have been discussed. For example, the self-assembly of the (dppp)Pt(II) containing complexes **193-200** revealed that error correction can be monitored for relatively slow self-assembly processes.[158] Nevertheless, it is challenging to get information about fast self-assembly processes like Pd(II)-based self-assembly reactions.

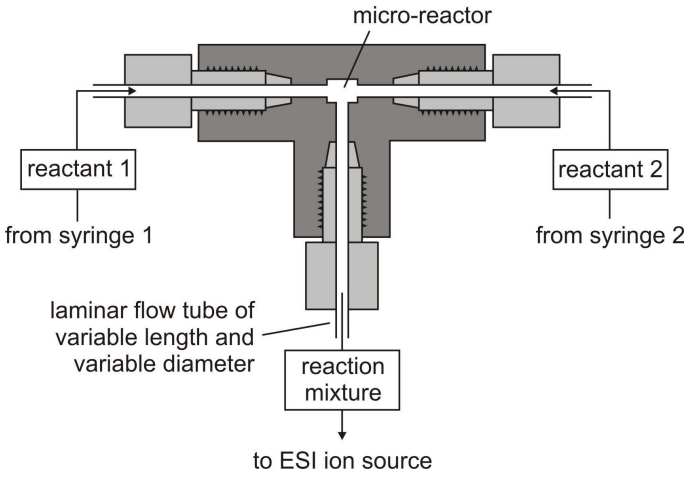

Figure 5.88: *The mixed-flow technique using a micro-reactor coupled to an ESI-FTICR mass spectrometer.*[187]

Mass spectrometry offers an interesting tool to observe intermediates of (fast) chemical reactions on-line.[208, 209] This mass spectrometry method uses a micro-reactor, which is coupled to an ESI FT-ICR mass spectrometer (Figure 5.88; see also chapter 4.4). The

building blocks of the self-assembly reactions are separately dissolved in appropriate solvents and these solutions are transferred separately into the micro-reactor with a defined flow rate. The building blocks mix in the micro-reactor. The reaction mixture is then transferred through a laminar flow tube into the ESI source of the mass spectrometer. Using defined flow rates of the solvents and capillaries of defined length and diameter enables the investigation of the reactions at defined reaction times. This is essential to identify different mechanistic steps and intermediates. The reaction time can be influenced by changing the flow rate of the solvents or the length or diameter of the laminar flow tube.

Within these studies, three different metallo-supramolecular systems were examined using a micro-reactor to investigate self-assembly as well as self-sorting phenomena on-line.

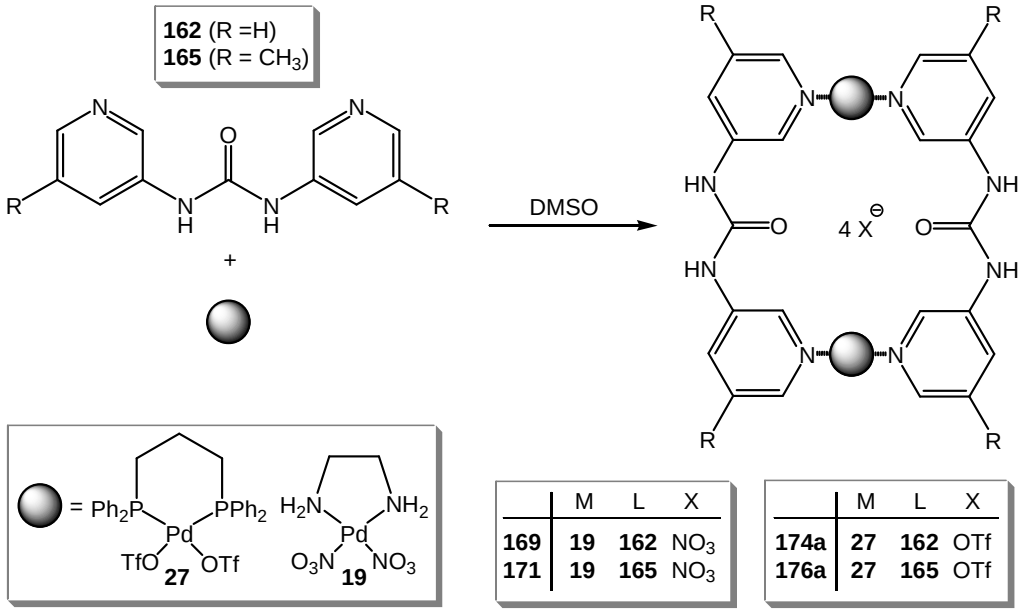

Figure 5.89: *Self-assembly of small dinuclear M_2L_2 complexes. In solution, also M_3L_3 complexes are observed, when metal center **27** is used. However, these are not observed in ESI mass spectrometry.*

First, the self-assembly process of small metallo-supramolecular M_2L_2 complexes was studied. The self-assembly of equimolar amounts of 1,3-di(pyridin-3-yl)urea **162** or 1,3-bis(5-methylpyridin-3-yl)urea **165** and the metal centers **27** ((dppp)Pd(OTf)$_2$; (1,3-bis-

(diphenylphosphino)-propane)palladium(II) trifluoromethanesulfonate) or **19** ((en)Pd(NO_3)$_2$, (ethylenediamine-*N,N'*)-palladium(II) nitrate) in DMSO result in the formation of the M_2L_2 complexes (Figure 5.89). If metal center **27** is used, also the analogous M_3L_3 complexes are observed by NMR spectroscopy, but they were not observed in the corresponding mass spectra. This is probably due to dilution. However, as far as the M_3L_3 complexes were not observed in ESI MS, just the formation of M_2L_2 complexes can be described.

Equimolar amounts of all building blocks were separately dissolved in DMSO and then diluted with acetonitrile to a building-block concentration of 150 µmol/L. The solutions were used for the mass spectrometric experiments as described above.

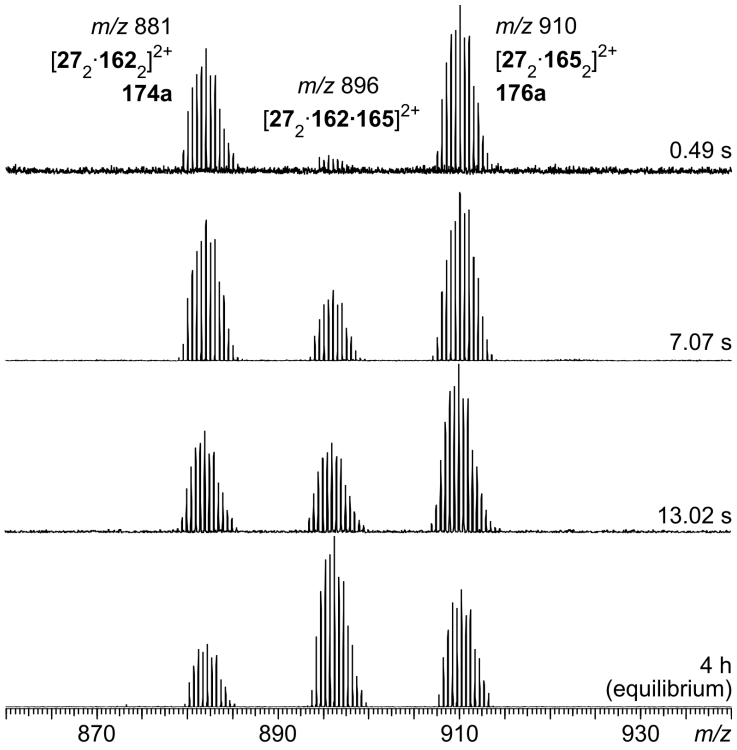

Figure 5.90: *Time-dependent Mass spectra of a mixture of **174a** and **176a** (1:1).*

In order to prove the abilities of the mixed-flow technique, the ligand exchange between complexes **174a** and **176a** was examined (Figure 5.90). The reaction time was controlled by the use of mixing capillaries of different length, while the other parameters (diameter, flow rate) were fix. Surprisingly, already at a reaction time of 0.49 s three different

species are observed by ESI MS. On the one hand, the two preformed homodimeric complexes **174a** and **176a** are observed. On the other hand, already a heterodimeric complex [**27**$_2$·**162**·**165**] is observed as a minor species. This proves the ligand-exchange process to be very fast for the systems under study. With increasing reaction time, the intensities of the peaks for the homodimers **174a** and **176a** are decreasing while the intensities of the peaks for the heterodimer [**27**$_2$·**162**·**165**] is increasing. The ligand-exchange process ends in an equilibrium between all species, wherein a statistical mixture (1:2:1) is observed for the complexes in this system (Figure 5.90).

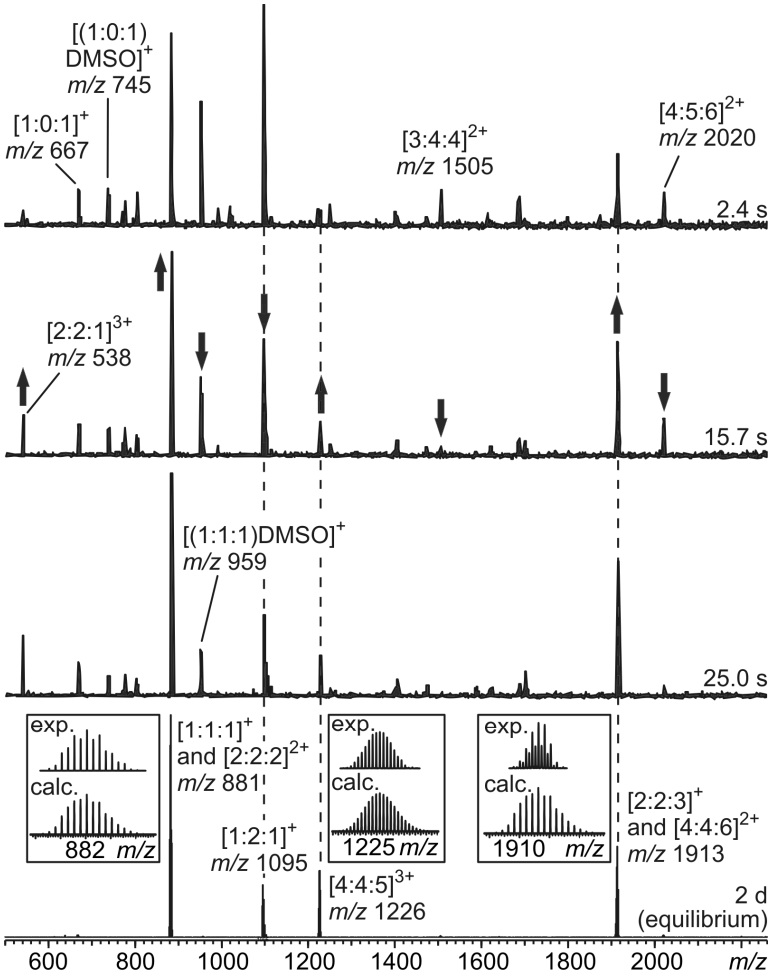

Figure 5.91: *The time-dependent mass spectra of system **174a**. The arrows indicate the intensity increase or decrease of the peaks with increasing time.*

Since it was proven that the mixed-flow micro-reactor technique is a suitable tool to investigate in fast metallo-supramolecular self-assembly reaction, the self-assembly of M_2L_2 complex **174a** was examined (Figure 5.91). The reaction time was controlled by using capillaries of different length with a fixed diameter and a constant flow rate of 40 µL/min in the laminar flow tube.

The time-dependent spectra show that the self-assembly of **174a** is very fast. Peaks related to **174a** (*m/z* 881 ($[2:2:2]^{2+}$) and *m/z* 1913 $[2:2:3]^{+}$)) could already be observed at a reaction time of 2.4 s (Figure 5.91). The intensities of these peaks rose with increasing reaction times. Some other species like the $[1:2:1]^{+}$ ion at *m/z* 1095 and the $[1:1:1]^{+}$ ion at *m/z* 881 can clearly be identified as intermediates in the self-assembly process of the M_2L_2 complex **174a**. The relative intensities of these peaks decreased with increasing reaction time. Besides those, also some peaks are observed which can be assigned to the metal center **27** (*m/z* 667 ($[1:0:1]^{+}$) and *m/z* 745 ($[(1:0:1)DMSO]^{+}$)). In here, DMSO coordinates to **27** indicating that the solvent influences the self-assembly process. Interestingly, several peaks were observed which can be assigned to ions bearing a systematic structure (e.g. *m/z* 1095 ($[1:2:1]^{+}$), *m/z* 1505 ($[3:4:4]^{2+}$), *m/z* 2020 ($[4:5:6]^{2+}$)). All of them contain exactly one ligand more than metal centers (M_XL_{X+1}) and their intensities decrease with increasing reaction time. They are intermediates in the self-assembly process. The structure of the M_XL_{X+1} species has to be open, because metal center **27** and ligand **162** have two coordination sites each. Assuming the metal centers in the M_XL_{X+1} species to be completely coordinated, no ring-closed macrocycle structures can exist for these intermediates. Interestingly, no species are observed containing more metal centers than ligands – instead of the peaks for **27** alone (M:L = 1:0). However, during the fast self-assembly process no larger species containing a ring-like structure (e.g. M_3L_3) were observed. The presence of [4:4] ions in the equilibrated system can probably be explained by aggregation of two M_2L_2 species which is known for ESI MS of salts.[187, 106]

For comparison of the self-assembly processes of $(dppp)Pd(OTf)_2$ **27** containing Stang-type complexes with Fujita-type complexes containing $(en)Pd(NO_3)_2$ **19**, the self-assembly of ligand **162** and metal center **19** was studied (Figure 8.92). In here, the reaction time was again controlled by using capillaries of different lenghts with

the same diameter and a constant flow rate of 120 µL/min in the laminar tube. This higher flow rate was chosen to achieve even shorter reaction times as for system **174a**.

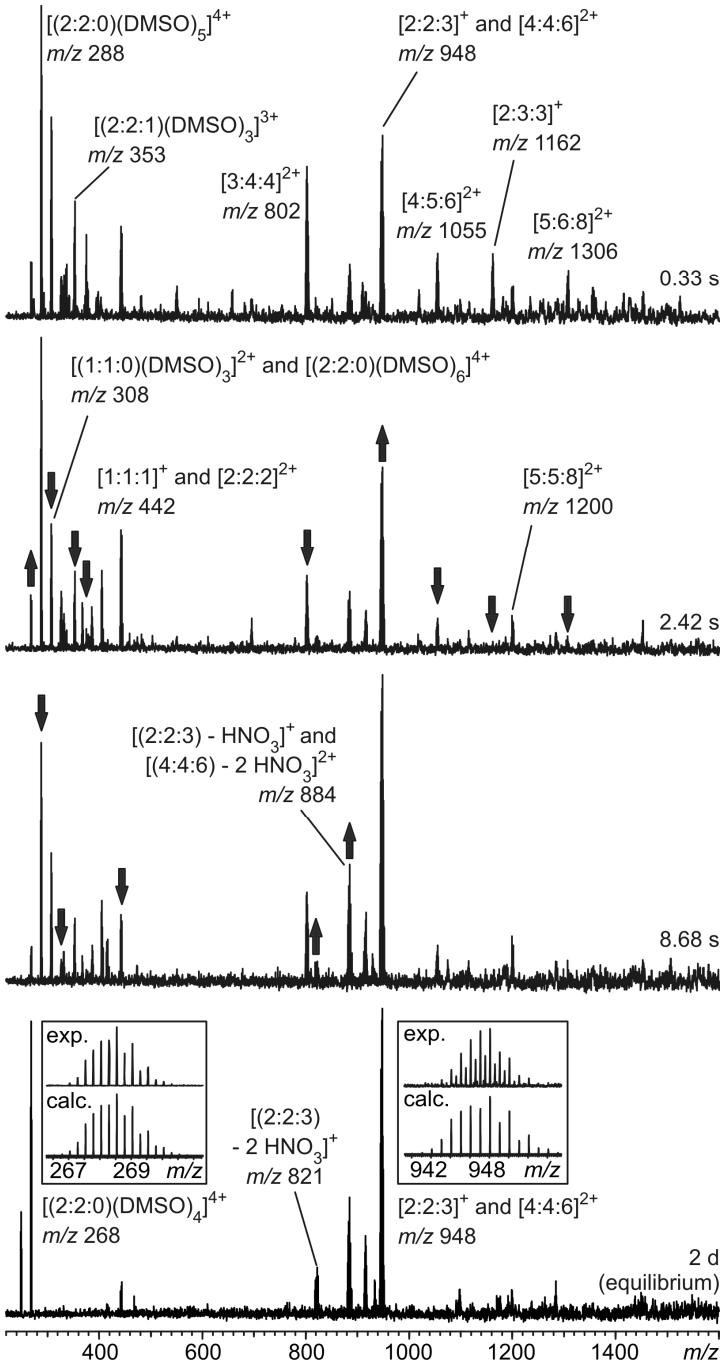

Figure 5.92: *The time-dependent mass spectra of system* ***169****. The arrows indicate the intensity increase or decrease of the peaks with increasing reaction time.*

Intermediates of the self-assembly process of **169** were already observed at a very short reaction time of 0.33 s. Even signals of the M_2L_2 complex **169** were observed after 0.33 s (*m/z* 442 ($[2:2:2]^{2+}$) and *m/z* 948 ($[2:2:3]^{+}$)). The intensities of these two peaks increase at longer reaction times. Another increasing peak was identified as $[(2:2:2)\text{-}H]^{+}$ (*m/z* 885). The loss of an H^{+} was already observed for other complexes with metal center **19**.[164] All other peaks decrease in their intensities with longer reaction times. Similar key intermediates like for the self-assembly process of **174a** were found for the self-assembly of **169** ((*m/z* 288 ($[(1:1:0)(DMSO)_2]^{2+}$) and *m/z* 308 ($[(1:1:0)(DMSO)_2CH_3CN]^{2+}$)). Additionally to these, the peak at m/z 442 can be assigned tyo a superposition of a $[(1:1:1]^{+}$ and a $[2:2:2]^{2+}$ species. It increases first and decreases at longer reaction times, which can be explained by the formation of the M_1L_1 species in the beginning which at longer times converts into **169** or other species. Several other peaks can be assigned to ions bearing a M_XL_{X+1} structure (e.g. *m/z* 802 ($[3:4:4]^{2+}$), *m/z* 1055 ($[4:5:6]^{2+}$), *m/z* 1162 ($[2:3:3]^{+}$)). Analogous to the M_XL_{X+1} species found for **174a**, these should also have an open structure. The peak at *m/z* 353 can be assigned to a M_2L_2 species aggregated with three DMSO molecules ($[(2:2:1)(DMSO)_3]^{3+}$). This species can be a ring-closed or an open-chained M_2L_2 complex. The DMSO molecules are somehow coordinating to the metal centers or the urea groups of the ligand which indicates an open-chained structure. However, the intensity of this peak is decreasing with increasing reaction time. Again, no bigger ring-closed structures like a M_3L_3 species could be detected.

Based on the results of these mass spectrometric experiments, some mechanisms of the self-assembly processes of **174a** and **169** can be drawn (Figure 5.93). Starting from the building blocks, a [1:1] species (M:L) should be the first complex formed. The [1:1] complex itself can react with another ligand or another metal center and result in a [1:2] or a [2:1] complex, respectively. When this is repeated several times, one can assume every possible complex to be formed like this. Due to entropic reasons, not every possible species forms.

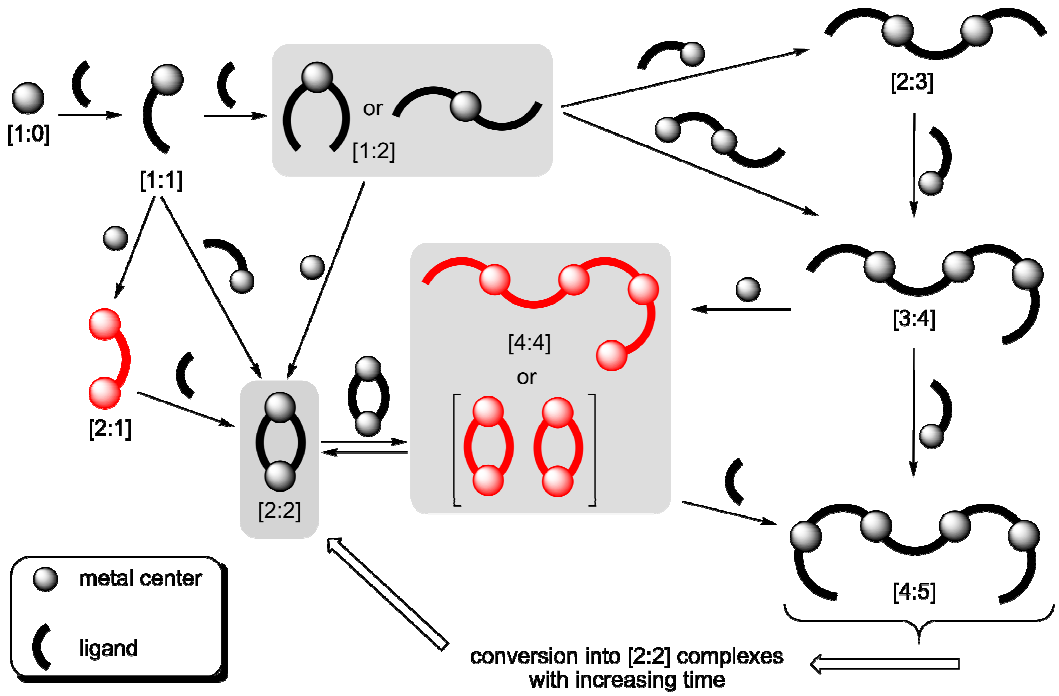

Figure 5.93: *A first mechanistic insight into the self-assembly of M_2L_2 complexes derived from the data of complexes* ***169*** *and* ***174a****. The assignment of the species is shown in a [M:L] nomenclature. Some key intermediates are highlighted within grey frames, while the species shown in red color were not observed in the mass spectra of* ***169*** *and* ***174*** *or can be explained by unspecific aggregation.*

The [1:1] and the [1:2] complex seem to be the most importat intermediates in the self-assembly of [2:2] complexes. Both of them can directly react with other building blocks to form a [2:2] complex. Another possible key intermediate would be a [2:1] species, which is not observed in the ESI MS experiments. Probably, this can be explained by charge repulsion between two cationic (dppp)Pd(II) metal centers which is not compensated by their simultaneously coordination to only one ligand. However, some larger species than the [2:2] complexes are observed as well. All of these have the structure M_XL_{X+1} and due to this, they should be open-chained. These intermediates can be formed by consecutive addition of metal centers or ligands as well. Additionally, the smaller intermediates can react with the building blocks or other small species to result in larger intermediates. In respect to the experimental data, all of these bigger intermediates have to undergo some kind of conversion into

[2:2] complexes (M_2L_2). This conversion can be explained by nucleophilic substitution at the Pd(II) metal centers supported by a supramolecular neighbor-group effect.[105, 139, 214] The M_XL_{X+1} complexes rearrange themselves in a way that they split into a [2:2] complex and a fragment which itself is again an intermediate in the self-assembly process. It is also possible, that a [4:4] species plays a role in this process. A [4:4] species could convert into two [2:2] complexes at once. Nevertheless, the minor peaks according to a [4:4] species can also belong to the aggregation of two [2:2] complexes.

These first mechanistic insights into fast self-assembly reactions at Pd(II) metal centers clearly show, that error correction plays an important role in self-assembly processes. All building blocks in the self-assembly of the M_2L_2 complexes are equal and the coordination of the ligands to the metal centers is a very fast process. Thus, many kinetically favored intermediates are formed. Without any error correction steps, all of these species would "survive" and not only the observed M_2L_2 complexes would be present in the thermodynamic equilibrium. However, error correction exists and only the M_2L_2 complexes are observed in the mass spectra of the thermodynamic equilibrium situation.

Inspired by these results, the self-sorting / self-assembly process of ligand **190** with (dppp)Pd(OTf)$_2$ **27** and (dppe)Pd(OTf)$_2$ **100** forming the homometallic complex **194** was examined (Figure 5.94). In here, the metal centers **27** and **100** are competing about the two different coordination sites of ligand **190**.

Equimolar amounts of metal centers **27** and **100** were mixed and dissolved in dichloromethane and diluted to a building block concentration of 150 µM. An equimolar amount of ligand **190** was dissolved in dichloromethane with a concentration of 150 µM as well. These solutions were separately injected into the micro-reactor and the self-sorting of the building blocks was monitored by ESI FTICR mass spectrometry. Analogue to the experiments discussed above, the length of the laminar flow tube was varied and the flow rate of the solutions (20 µL/min in the laminar flow tube) was kept constant.

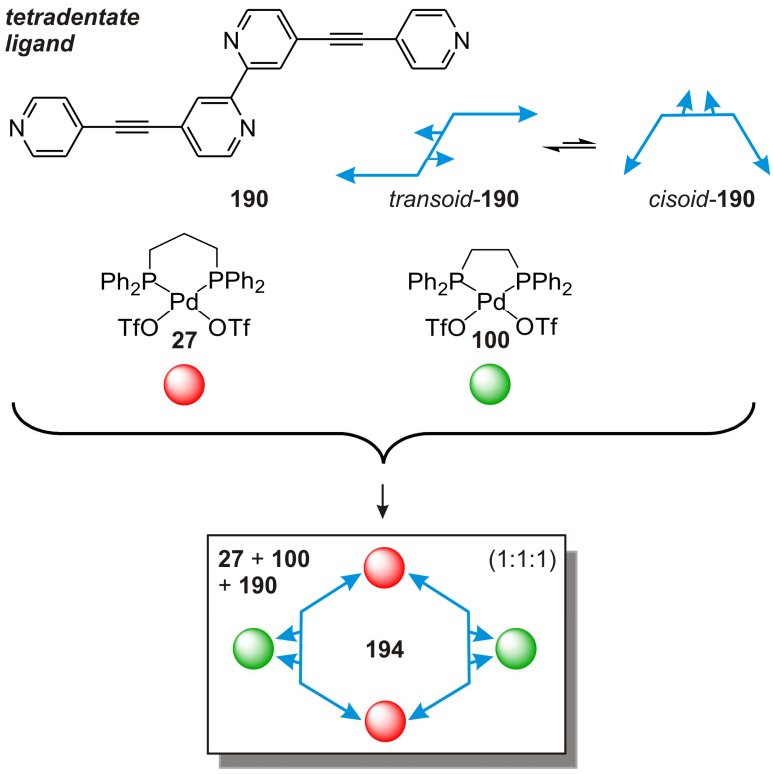

Figure 5.94: *Self-assembly / self-sorting of the homometallic metallo-supramolecular* M_4L_2 *complex* ***194****.*

The ESI mass spectrum recorded at a reaction time of 1.8s obtains peaks for the non-coordinated metal centers (*m/z* 653 ([**100**]$^+$) and *m/z* 667 ([**27**]$^+$)) as well as intermediate [1:1] complexes (*m/z* 1011 ([**100**·**190**]$^+$) and *m/z* 1025 ([**27**·**190**]$^+$)). Interestingly, the intensity of the peak at *m/z* 1011 ([**100**·**190**]$^+$) is much higher than that of the corresponding peak containing metal center **27**. This reflects the result observed before (see chapter 5.4), wherein (dppp)Pd(II) prefers to bind to the pyridine binding sites and not to the bipyridine binding site, while (dppe)Pd(II) shows no preferences. Thus, one (dppe)Pd(II) has three possible positions to bind to ligand **190**, whereas (dppp)Pd(II) has just two. Statistically, the intensities of the peaks at *m/z* 1011 and *m/z* 1025 should have a ratio of 3:2. Nevertheless, the intensity of the peak at *m/z* 1011 ([**100**·**190**]$^+$) is much higher then expected from the statistical distribution. Due to the chelate effect, the coordination of the metal center is stronger to the bipyridine binding site compared to the one pyridine binding site. Thus, the relatively high intensity of the peak at *m/z* 1011 ([**100**·**190**]$^+$) reflects that the

(dppe)Pd(II) metal center is mainly coordinated to the bipyridine binding site. This is a first hint on the self-sorting process within the self-assembly reaction of complex **194**. Additionally, a first peak relating to the final assembly **194** is observed at 1.8 s (*m/z* 1170 ($[\mathbf{27}_2\cdot\mathbf{100}_2\cdot\mathbf{190}_2]^{3+}$)).

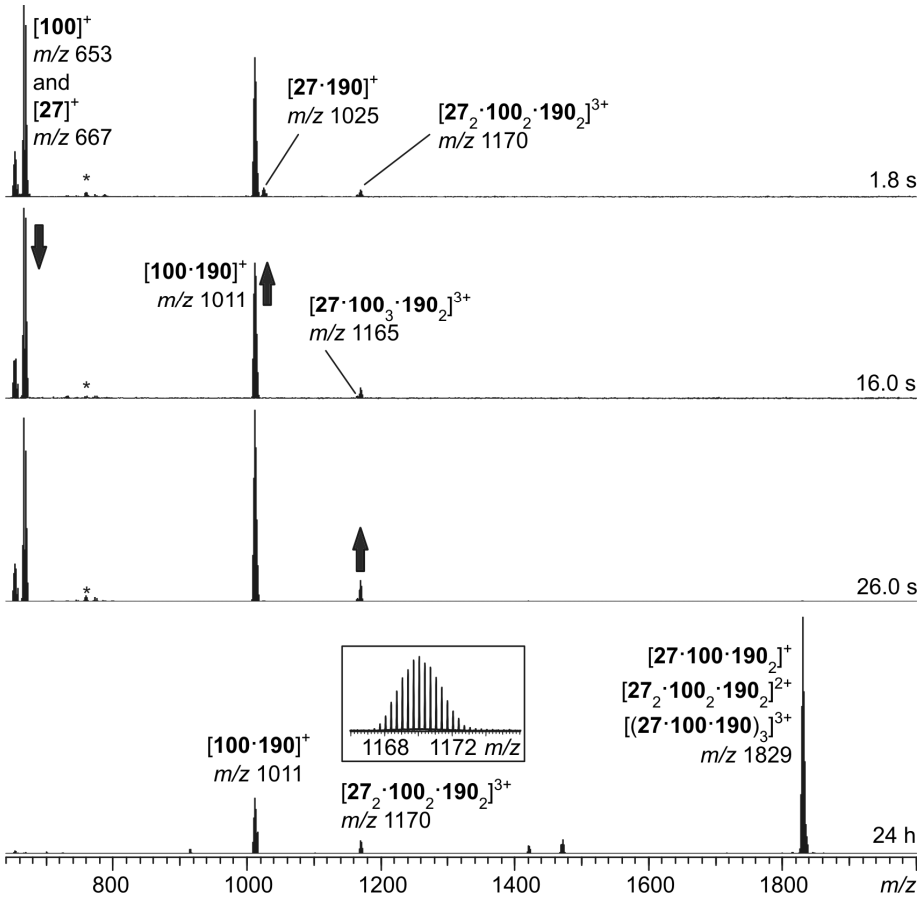

Figure 5.95: *Time-dependent mass spectra of the self-sorting of complex **194**. The arrows indicate the time-dependent increase or decrease of the peaks observed. For clarity, the counteranions of the observed species are not shown in the assignment. The peaks marked with an asterix (*) can be assigned to salt clusters which do not belong to the self-assembly process.*

With increasing reaction time, the peaks relating to the non-coordinated metal centers **27** and **100** decrease. At the same time, the intermediate [1:1] complex containing (dppp)Pd(II) vanishes. On the contrary, the [1:1] intermediate bearing (dppe)Pd(II) increases with increasing reaction time which is another hint for a stronger binding of

(dppe)Pd(II) to ligand **190** compared to (dppp)Pd(II). When the reaction time is elongated further, the intermediates are consumed and assembly **194** is formed. However, also a peak relating to $[\mathbf{27}\cdot\mathbf{100}_3\cdot\mathbf{190}_2]^{3+}$ can be observed at *m/z* 1165. In here, an error occured during the formation of **194**. Due to the error correction process in self-assembly processes, the peak vanishes and is not observed in the thermodynamic equilibrium situation.

The self-sorting process of complex **194** has been monitored by time-dependent ESI mass spectrometry. The [1:1] species $[\mathbf{100}\cdot\mathbf{190}]^{+}$ is the key intermediate for this self-sorting / self-assembly process. When the results obtained for the formation of system **194** are compared to those gained from the self-assembly reactions of the M_2L_2 complexes **169** and **174a**, the lack of many different intermediates for the formation of **194** is peculiar. In the self-assembly of the M_2L_2 complexes **169** and **174a**, all binding sites of the building blocks are equal and thus, the fast coordination of the ligands to the metal centers results in many different intermediates. On the contrary, ligand **190** has different binding sites – two pyridine binding sites and one bipyridine binding site. Due to the chelate effect, the binding sites are not equal anymore. The same conclusion can be drawn for the metal centers **27** and **100**. Due to their different sterical properties, they show a different preference in coordinating to the binding sites of ligand **194**. The building blocks are not equal anymore. This leads to the selective formation of the key intermediate ($[\mathbf{100}\cdot\mathbf{190}]^{+}$) which can undergo further coordination to other building blocks and this finally results in the formation of complex **194**. Thus, complex **194** is formed on a selective pathway.

In order to validate the information obtained for the fast self-assembly processes of palladium-based metallo-supramolecular macrocycles on the formation process of metallo-supramolecular cages, the self-assembly of the metallo-supramolecular cages **185a** and **185b** was studied (Figure 5.96).

Metal center **149** and two equivalents of ligand **162** were separately dissolved in DMSO and diluted with acetonitrile to a concentration 100 µM (metal center **149**) and 200 µM (ligand **162**), respectively. Both solutions were separately injected into the micro-reactor with a constant flow rate of 20 µL/min in the laminar flow tube. The length of the laminar flow tube was varied to achieve time-dependent data.

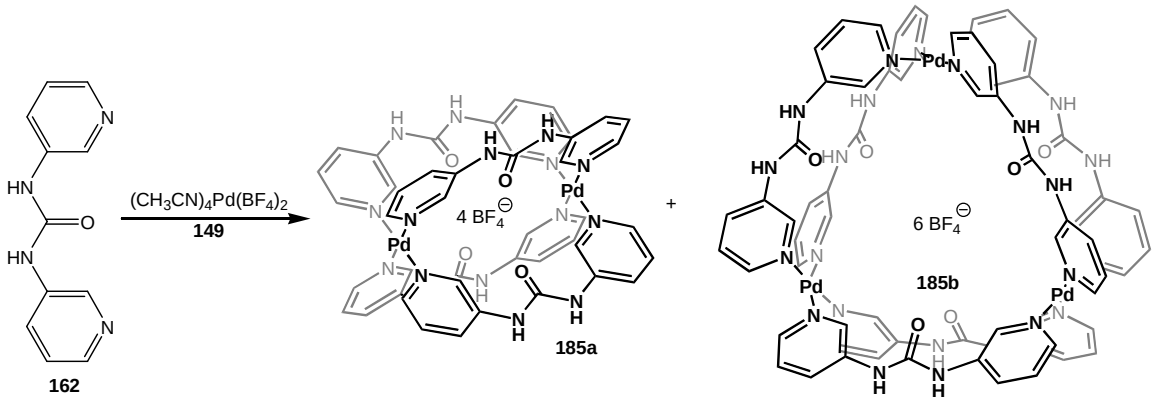

Figure 5.96: *Self-assembly of the metallo-supramolecular complexes* ***185a*** *(M_2L_4) and* ***185b*** *(M_3L_6).*

Similar to the systems described above, a fast self-assembly process was observed (Figure 5.97). Even at short reaction times of 2.3 seconds, a peak according to the M_2L_4 complex **185a** aggregating to two DMSO molecules was observed (*m/z* 669 $[(2:4:2)(DMSO)_2]^{2+}$). The aggregation of solvent molecules to the ions is very prominent for this system (Figure 5.97). This is due to coordination of the solvent molecules to the Pd(II) metals as well as to the urea groups of the ligands. Thus, the aggregation of the DMSO molecules can be a hint, that this M_2L_4 species is not a cage and has an open structure. Several other peaks observed could be assigned to intermediates (e.g. *m/z* 547 ($[3:2:4]^{2+}$), *m/z* 592 ($[(2:3:2)(DMSO)_2]^{2+}$) and *m/z* 654 ($[3:3:4]^{2+}$). In here, also intermediates containing more metal centers than ligands were observed (e.g. m/z 547 ($[3:2:4]^{2+}$) and m/z 806 ($[(4:3:4)(MeCN)(DMSO)_2]^{2+}$). Unfortunately, no peak corresponding to the M_3L_6 complex **185b** was observed in the time-dependent mass spectra. Nevertheless, **185b** is present in the thermodynamic equilibrium. M_3L_6 complex **185b** probably forms during the error correction process which due to the instrumental setup could not be monitored completely. According to the experimental data, the complexes **185a/b** are formed in a stepwise formation process similar to that observed for the metallo-supramolecular macrocycles **169** and **174a**. With increasing reaction time, the intermediates undergo a conversion into the metallo-supramolecular cages **185a** and **185b**.

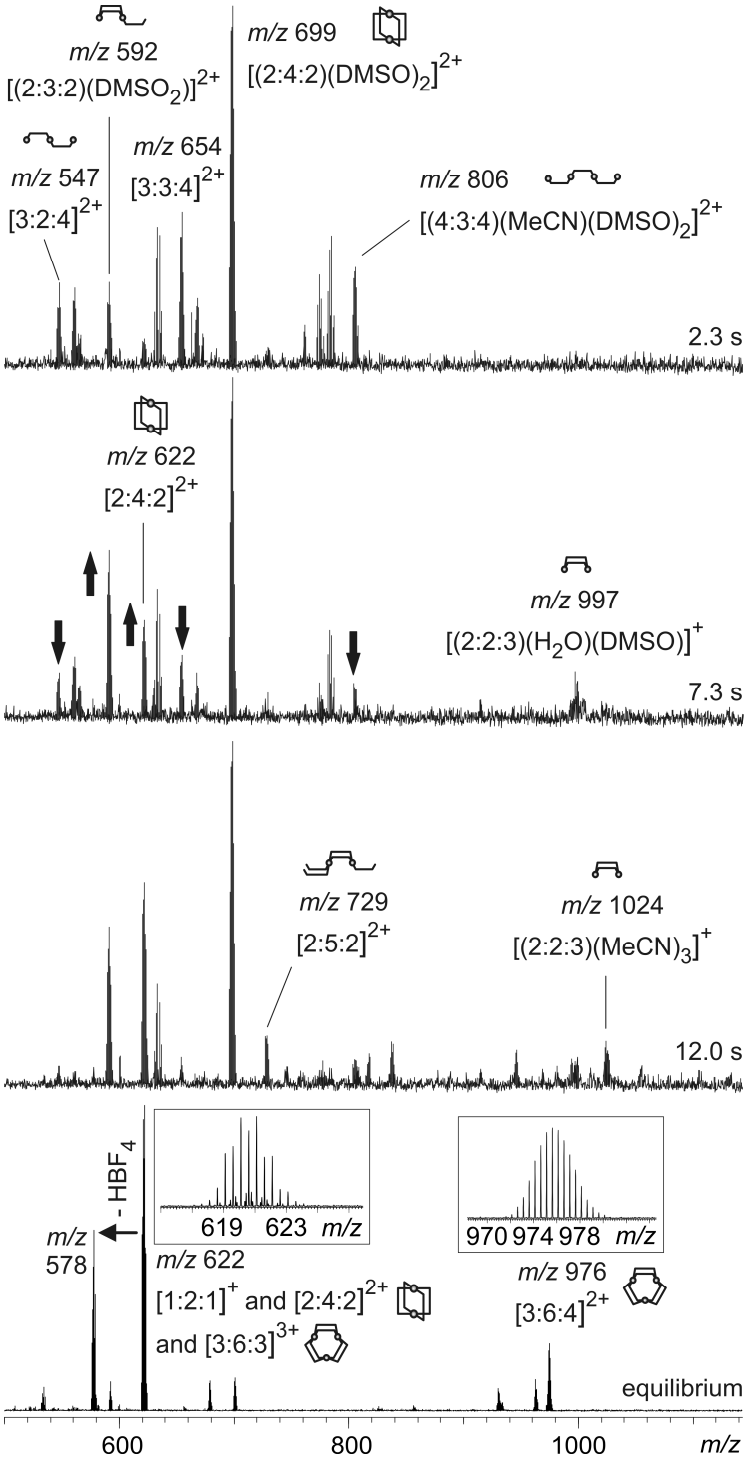

Figure 5.97: *Time-dependent mass spectra of the self-assembly of complexes* ***202a*** *and* ***202b****. The arrows indicate the time-dependent increase or decrease of the peaks observed.*

Taking all results into account, the mass spectrometric mixed-flow technique using a micro-reactor is a good tool to investigate self-assembly processes. Some important intermediates of the self-assembly of M_2L_2, M_2L_4 and M_3L_6 complexes could be found and based on this, first mechanistical insights into the self-assembly processes of metallo-supramolecular complexes could be drawn. In the beginning many different complexes formed and with increasing time most of them converted into their most favored corresponding complexes. This clearly shows the error-correction process based on the reversibility of these systems. Due to their possible coordination to the metal centers and/or ligands, solvent molecules can influence the self-assembly process and the complexes which are built in there.

Additionally, the self-sorting of the metallo-supramolecular complex **194** was successfully examined by the mixed-flow technique. Interestingly, not many intermediates were observed which can be related to the pathway-selective self-sorting within this system.

6. ESI Mass Spectrometry of Bismuth-Oxido Clusters

Since the 18th century, bismuth compounds are known to have some medical use. They were used as agents for the treatment of diarrhea, gastric and duodenal ulcer.[249] These bismuth compounds are suggested to cover the stomach mucosa and thereby protect it.[250] However, bismuth containing compounds have a low toxicity. Hence, these compounds are interesting for medical and materials science.[251, 252]

In cooperation with the groups of Professor Michael Mehring from the TU Chemnitz and Professor Dirk Zahn from the University of Erlangen/Nürnberg, several bismuth oxidoclusters and their properties were studied. The investigations by ESI mass spectrometry were performed in our working group.[253] Parts of the results presented in here have been published in *Chemistry – A European Journal* in 2011.[254]

Within this project, the formation of solid-state bismuth oxide starting from simple bismuth compounds like $Bi(NO_3)_3$ is examined. Bismuth-oxido clusters probably are representative compounds to identify intermediates of that nucleation process. Therefore, several bismuth-oxido clusters containing different nuclear sizes as well as coordinating ligands have been synthesized.[255] These clusters were analyzed by the combination of suitable techniques like X-ray crystal structure analysis and ESI mass spectrometry.

Due to the monoisotopic bismuth, mass spectrometry of bismuth oxide compounds is challenging. It is very difficult to assign the peaks appearing in ESI MS without an isotopic pattern and any information about the charge of the observed ions. Therefore, mass spectrometry was seldom used to examine large bismuth oxide compounds.[256] Nevertheless, ESI mass spectrometry was successfully used to analyze other metal oxide clusters.[257] However, when the bismuth oxide clusters bear anionic ligands which can be stripped off during the ESI process, also large bismuth-oxido clusters should be detectable using ESI mass spectrometry.

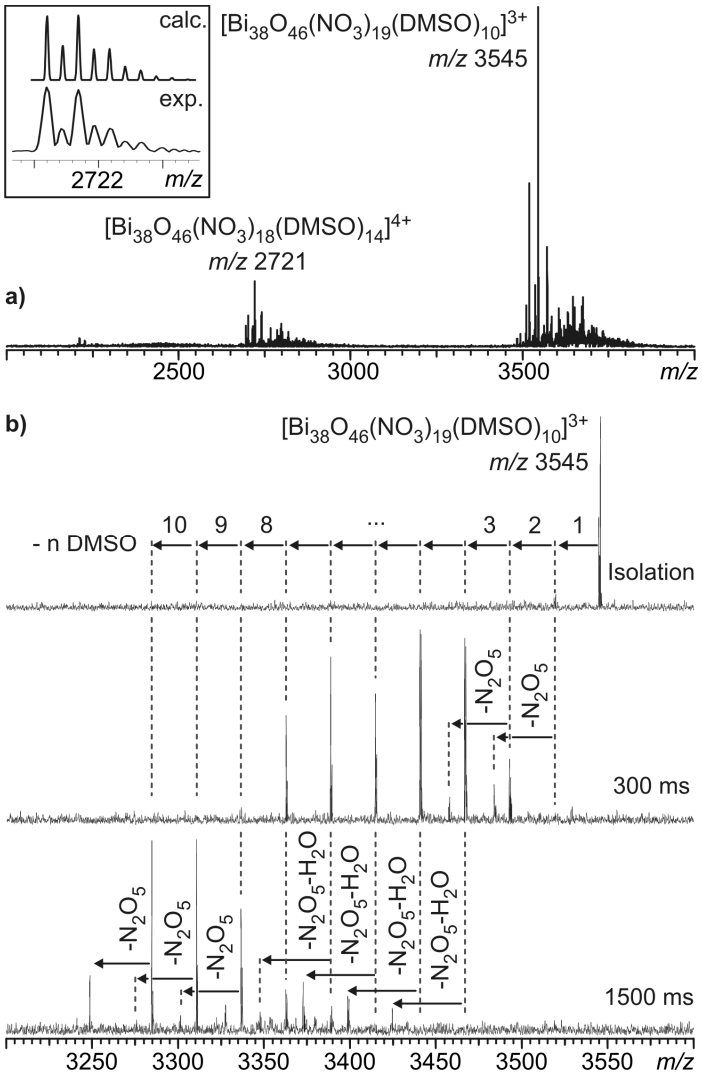

Figure 6.1: *a) ESI mass spectrum of* $[Bi_{38}O_{45}(NO_3)_{20}(DMSO)_{28}](NO_3)_4(DMSO)_4$ ***204*** *(for the assignment of all peaks see experimental part) and b) MS/MS fragmentation pattern of m/z = 3545 (*$[Bi_{38}O_{46}(NO_3)_{19}(DMSO)_{10}]^{3+}$*) using an IRMPD laser at a laser power of 2.5 W and different irradiation times.*

First, the bismuth-oxido cluster $[Bi_{38}O_{45}(NO_3)_{20}(DMSO)_{28}](NO_3)_4(DMSO)_4$ **204** was examined. The structure of **204** was revealed by X-ray crystal structure analysis. Due to the bad solubility of bismuth-oxido clusters in general, it was suspended into DMSO and heated for five minutes at 70 °C. Afterwards, the resulting solution was allowed to cool down to room temperature and it was diluted with acetonitrile to a concentration of ca. 100 µM.

The ESI MS analysis of cluster **204** revealed that its core structure is stable in solution and in the gas phase (Figure 6.1). The peaks of major intensity observed in the mass spectrum can be assigned to threefold (*m/z* 3450-3800) and fourfold charged (*m/z* 2650-2850) ions of **204** (Figure 6.1a). The assignments of all peaks observed in the mass spectrum of **204** are reported in Table 8.2. These peaks indicate the preservation of the bismuth oxido core $\{Bi_{38}O_{45}\}$ and the cleavage of mainly three and four nitrate groups as well as DMSO molecules from **204**. IRMPD experiments were performed to get some information about the behavior of **204** in the gas phase. The prominent peak at *m/z* 3545 ($[Bi_{38}O_{46}(NO_3)_{19}(DMSO)_{10}]^{3+}$) was isolated and fragmented using an IR laser with a laser power of 2.5 W at different irradiation times (Figure 6.1b). A stepwise cleavage of all ten DMSO molecules can be observed with increasing irradiation times. At longer irradiation times also the dissociation of N_2O_5 as well as the simultaneously loss of N_2O_5 and H_2O are observed. The loss of N_2O_5 molecules can be explained by the reaction of two nitrates to N_2O_5 and O^{2-} which remains at the bismuth oxide cluster and therefore the ions do not change their charge. Due to the lack of other hydrogen-containing units, the loss of water molecules can just be explained by partial deprotonation of the remaining DMSO molecules. The experiment has shown that all coordinating DMSO molecules can be removed from $[Bi_{38}O_{46}(NO_3)_{19}(DMSO)_{10}]^{3+}$ to get $[Bi_{38}O_{46}(NO_3)_{19}]^{3+}$. Depending on the irradiation period and intensity of the laser, it seems to be possible to generate a bare bismuth oxido core in the gas phase.

Depending on the crystallization method, different shaped crystals were obtained of **204**. Unfortunately, not all of these crystals were suitable for crystal data analysis. Thus, ESI mass spectrometry of all fractions (**204a-c**) was performed and compared with the results of **204**. The three compounds **204a-c** were dissolved in DMSO at 70 °C and diluted with acetonitrile to an approximated concentration of 100 µM. The ESI mass spectra of **204a-c** clearly show that all three fractions contain the same clusters (see tables 8.3-8.5). Hence, the different shapes of the crystals are due to crystallization effects and do not reflect the presence of different clusters.

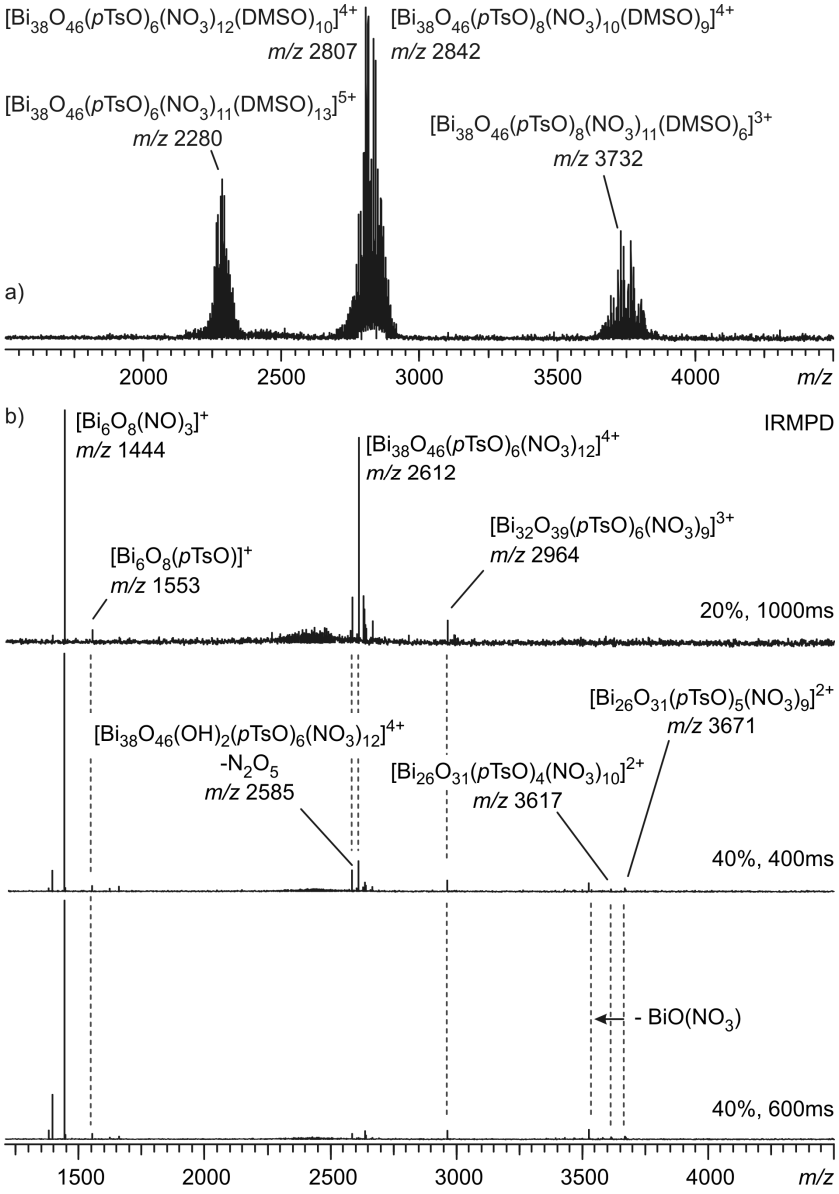

Figure 6.2: *a) ESI mass spectrum of $[Bi_{38}O_{45}(OH)_2(pTsO)_8(NO_3)_{12}(DMSO)_{24}](NO_3)_2$-$(DMSO)_4(H_2O)$* ***205*** *(for the assignment of all peaks see Table 8.6) and b) MS/MS fragmentation pattern of m/z 2807 ($[Bi_{38}O_{46}(pTsO)_6(NO_3)_{12}(DMSO)_{10}]^{4+}$) using an IRMPD laser (25 W) at different laser powers and irradiation times. The spectra shown in here begin with a laser power of 5 W and an irradiation time of 1s, which shows the fragmentation after all 10 DMSO molecules were already stripped of the cluster. The loss of DMSO molecules is shown in Figure 6.3.*

When $[Bi_6O_4(OH)_4](NO_3)_6 \cdot H_2O$ as starting material was treated with *para*-toluene sulfonic acid (pTsOH), $[Bi_{38}O_{45}(OH)_2(pTsO)_8(NO_3)_{12}(DMSO)_{24}](NO_3)_2(DMSO)_4(H_2O)_2$ **205** crystallized. **205** contains two anionic ligands and thus it is interesting to analyze its behavior in the gas phase. For ESI mass spectrometry, a solution of compound **205** in DMSO/acetonitrile (100 $\mu molL^{-1}$) was prepared similarly to that of **204**. The resulting mass spectrum of **205** shows peaks that can be assigned to triply (*m/z* 3600-3900), quadruply (*m/z* 2700-2950) and quintuply charged (*m/z* 2150-2400) species (Figure 6.2a). It perfectly confirms the presence of Bi_{38}-oxido clusters in solution. However, due to the elimination of water, an additional oxygen atom is inserted at the bismuth-oxido core which results in a core structure of $\{Bi_{38}O_{46}\}$. The assignments of all peaks are reported in Table 8.6. Similar to **204**, IRMPD-MS/MS experiments have been performed of $[Bi_{38}O_{46}(pTsO)_6(NO_3)_{12}(DMSO)_{10}]^{4+}$ (*m/z* 2807) demonstrating the fragmentation mechanism of this prominent species (Figures 6.2b and 6.3). Analogous to **204**, the stepwise loss of all DMSO molecules and N_2O_5 was observed (Figure 6.3). After cleavage of ten DMSO molecules and one N_2O_5 molecule, cluster peaks assigned to $[Bi_6O_8(NO_3)]^+$ and $[Bi_6O_8(OTs)]^+$, respectively, occur. As a result a peak at *m/z* 2964 ($[Bi_{32}O_{39}(pTsO)_6(NO_3)_9]^{3+}$) appears. However, a peak assigned to $[Bi_{32}O_{39}(pTsO)_5(NO_3)_{10}]^{3+}$ (*m/z* 2929) was not observed – probably due to its low intensity in the mass spectrum. An additional cleavage of both, $[Bi_6O_8(NO_3)]^+$ and $[Bi_6O_8(pTsO)]^+$, from the $\{Bi_{32}O_{39}\}$ clusters induce the formation of $[Bi_{26}O_{31}(pTsO)_5(NO_3)_9]^{2+}$ (*m/z* 3671) and $[Bi_{26}O_{31}(pTsO)_4(NO_3)_{10}]^{2+}$ (*m/z* 3617). In a last fragmentation step, the loss of neutral $BiO(NO_3)$ from $[Bi_{26}O_{31}(pTsO)_5(NO_3)_9]^{2+}$ (*m/z* 3671) and a peak at *m/z* 3528 ($[Bi_{25}O_{30}(pTsO)_5(NO_3)_8]^{2+}$) occurs. However, no further fragmentation is observed.

The fragmentation pattern of **205** shows the destruction of its core structure, wherein the prominent loss of $[Bi_6O_8(X)]^+$ ($X = NO_3^-$ or $pTsO^-$) indicates that this structure is a relatively stable part of the original cluster core. Interestingly, the synthesis of **205** started from a Bi_6-cluster ($[Bi_6O_4(OH)_4](NO_3)_6 \cdot H_2O$). As far as a $\{Bi_{38}O_{45}(OH)_2\}$ core cannot simply be formed by the aggregation of several units of $\{Bi_6O_4(OH)_4\}$, a comparison of the fragmentation with the formation process can only happen when the formation

process of Bi_{38}-clusters from Bi_6-clusters is analyzed properly. This will be an interesting task for future experiments.

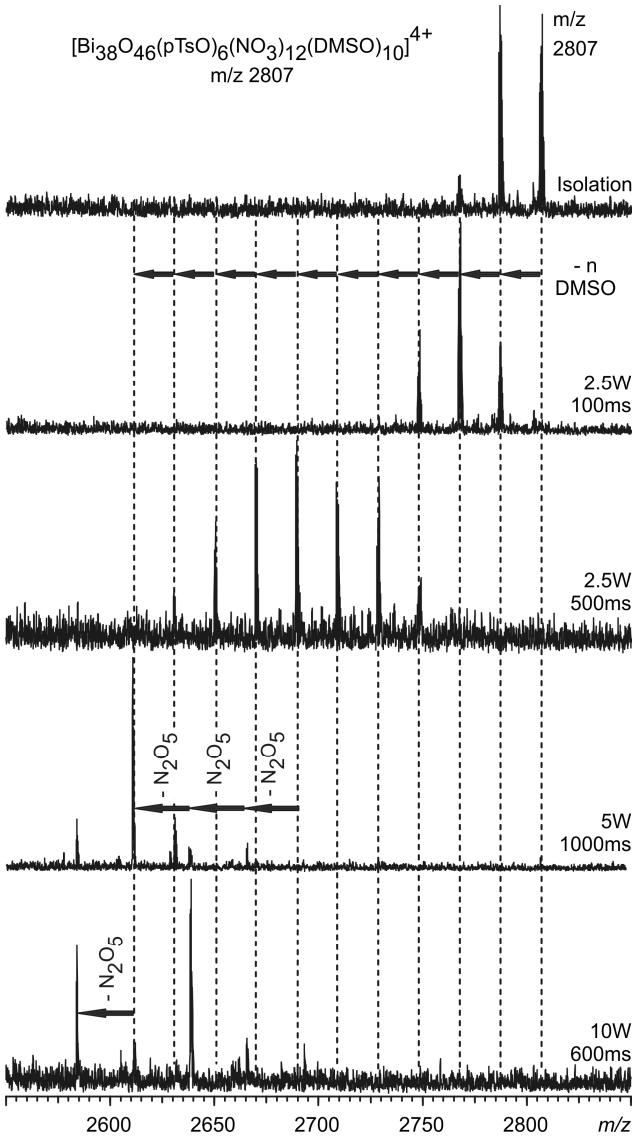

Figure 6.3: *IRMPD MS/MS experiments of* ***205*** *performed at different irradiation times using an IR laser with laser powers of 2.5 to 10 W.*

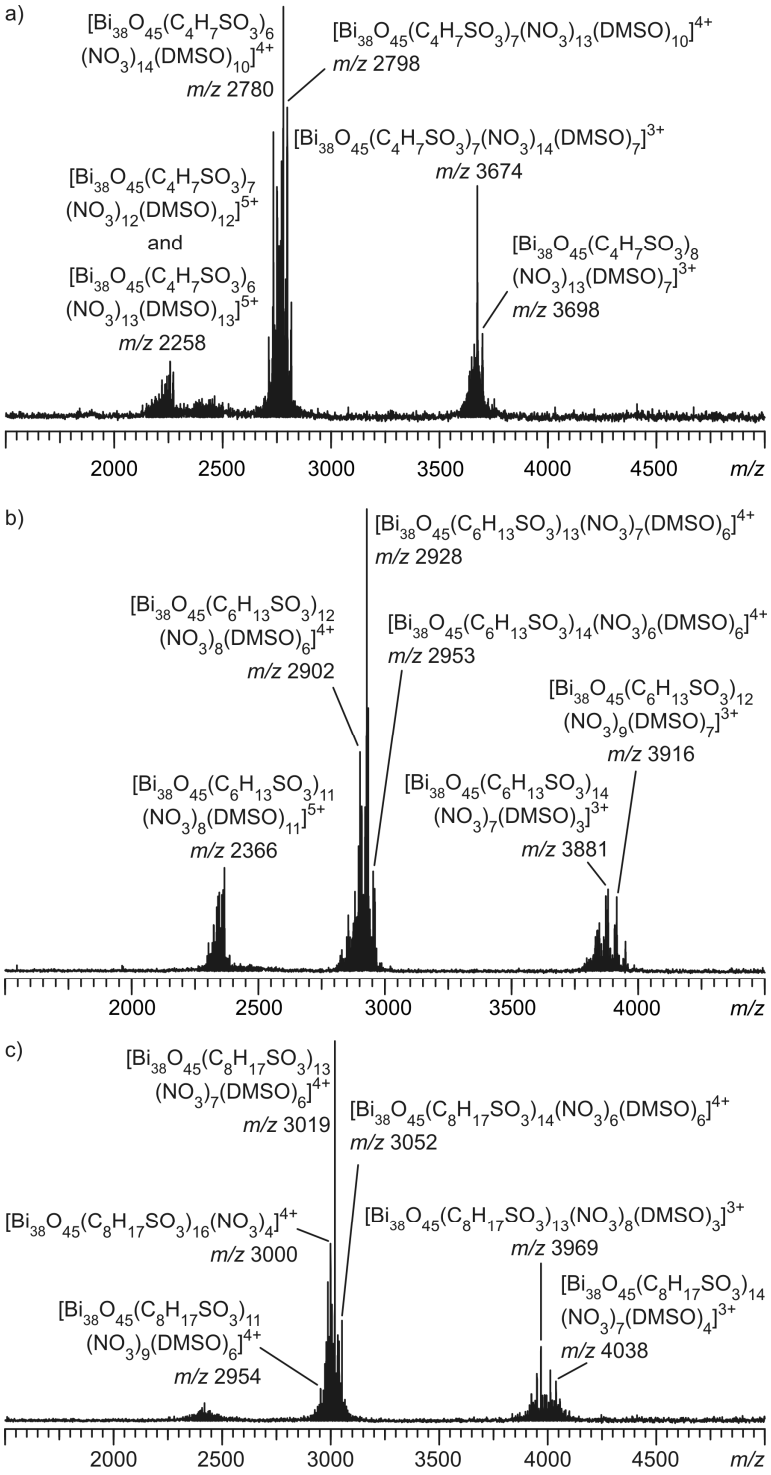

Figure 6.4: *ESI mass spectra of a) $[Bi_{38}O_{45}(C_4H_7SO_3)_x(NO_3)_y(DMSO)_z]$* ***206****, b) $[Bi_{38}O_{45}(C_6H_{13}SO_3)_x(NO_3)_y(DMSO)_z]$* ***207*** *and c) $Bi_{38}O_{45}(C_8H_{17}SO_3)_x(NO_3)_y(DMSO)_z]$* ***208*** *($x + y = 24$). The assignments of all peaks are reported in Tables 8.7-8.9.*

The successful implementation of different ligands at a bismuth-oxido cluster inspired us to perform ligand-exchange experiments with other ligands. Thus, $[Bi_{38}O_{45}(C_4H_7SO_3)_x(NO_3)_y(DMSO)_z]$ **206**, $[Bi_{38}O_{45}(C_6H_{13}SO_3)_x(NO_3)_y(DMSO)_z]$ **207** and $Bi_{38}O_{45}(C_8H_{17}SO_3)_x(NO_3)_y(DMSO)_z]$ **208** (x + y = 24) were synthesized similar to **205** using differently substituted sulfonate ligands for the ligand exchange. In order to analyze the resulting clusters **206**-**208**, they were dissolved in DMSO at 70 °C and diluted with acetonitrile to a concentration of approximately 100 µM.

For all three clusters, triply charged (*m/z* 3640 - 3960 (**206**), *m/z* 3790 - 3960 (**207**) and *m/z* 3880 - 4080 (**208**)) and quadruply charged ions (*m/z* 2700 - 2820 (**206**), *m/z* 2800 - 2970 (**207**) and *m/z* 2950 - 4080 (**208**)) were observed in the ESI mass spectra, respectively (Figure 6.4). Additionally, also quintuply charged ions were observed for clusters **206** and **207** (*m/z* 2200 - 2300 (**206**) and *m/z* 2290 - 2370 (**207**)). The assignments of all peaks are reported in Tables 8.7-8.9. ESI MS confirms the successful ligand-exchange for bismuth-oxido clusters **206**-**208**. Due to superimposed peaks in the mass spectra of these clusters, no suitable tandem MS experiments could be performed.

Besides sulfonates, also amino acids and salicylic acid have been implemented as ligands during the formation of bismuth-oxido clusters. The ionization and detection of the clusters containing BOC-protected amino acids ($[Bi_{38}O_{45}(BOC\text{-}Val)_{22}(OH)_2]$ **209** and $[Bi_{38}O_{45}(BOC\text{-}Phe)_{22}(OH)_2]$ **210**) was somehow problematic and thus the peaks observed in the mass spectra were of low intensities and showed a bad resolution. Nevertheless, the clusters **209** and **210** could be identified, but no tandem MS experiments could be performed (Tables 8.10 and 8.11). Thus, no information about the stability and the fragmentation process of those clusters was obtained.

On the contrary, the clusters containing anionic salicylate ligands ($[Bi_{22}O_{26}(HSal)_{14}]$ **211**, $[Bi_{34}O_{40}(HSal)_{22}]$ **212** and $[Bi_{38}O_{46}(HSal)_{22}(OH)_2]$ **213**) could be clearly identified by ESI mass spectrometry. Interestingly, the ESI MS analysis of $[Bi_{22}O_{26}(HSal)_{14}]$ **211** revealed two species to be present in solution. The mass spectrum of 211 shows doubly (*m/z* 3490 - 3740), triply (*m/z* 2290 - 2640) and quadruply charged peaks (*m/z* 1820 - 1960) which can be assigned to ions of $[Bi_{22}O_{26}(HSal)_{14}]$ **211**. Additionally, quadruply charged peaks were observed in the range of *m/z* 2690 - 2910 which could be assigned to $[Bi_{34}O_{40}(HSal)_{22}]$ **212** (Figure 6.5 and Table 8.12). This is the first time that a $\{Bi_{34}O_{40}\}$

cluster has been observed. Due to superimposing signals and low intensities, no tandem MS experiments could be performed to confirm the structure of $[Bi_{34}O_{40}(HSal)_{22}]$ **212** and analyze its fragmentation pathway. Nevertheless, the presence of **212** is astonishing, because the sample originally just contained $[Bi_{22}O_{26}(HSal)_{14}]$ **211**. Thus, the formation of **212** had occurred after the preparation of **211** and is probably an intermediate in the formation process of larger bismuth-oxido clusters like $\{Bi_{38}O_{46}\}$ clusters. However, this has to be evaluated in further experiments.

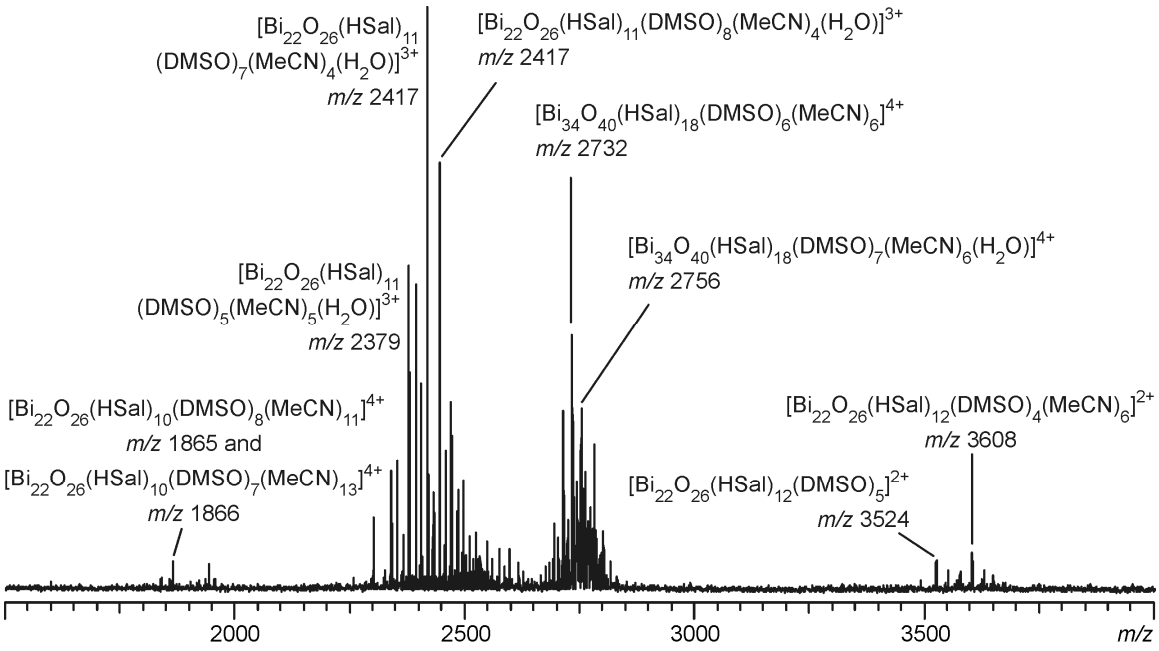

Figure 6.5: *ESI mass spectrum of $[Bi_{22}O_{24}(HSal)_{14}]$ **(211)** containing a new bismuth oxide species $[Bi_{34}O_{40}(HSal)_{22}]$ **(212)**. In order to give an overview of the species observed, some of the major peaks in the spectrum are assigned to their fragments.*

On the contrary to the clusters discussed above, relatively few peaks are observed in the ESI mass spectrum of $[Bi_{38}O_{46}(HSal)_{22}(OH)_2(DMSO)_{16.5}]$ **213** (Figure 6.6 and Table 8.13). Only triply charged peaks were observed in the mass spectrum (*m/z* 2540 - 3720, Figure 6.6a). Interestingly, all peaks observed are related to fragments of **213** which lost one molecule of water and several neutral molecules of salicylic acid (H_2Sal). The structure of the fragments observed was confirmed by IRMPD tandem mass spectrometry using an IR laser at a laser power of 25 W at different irradiation times (Figure 6.6b). At

first, the fragment at m/z 3576 ($[Bi_{38}O_{46}(HSal)_{19}(DMSO)_2$ - H_2O, - 5 $H_2Sal]^{3+}$) loses both DMSO molecules. At longer irradiation times the successive loss of three water molecules is observed followed by an additional loss of H_2Sal. The loss of water can be explained by the condensation of two salicylate anions (2 $HSal^- \rightarrow (Sal\text{-}O\text{-}Sal)^{2-} + H_2O$). However, no further fragmentation was observed. Nevertheless, the composition of the peaks observed in the ESI mass spectrum was confirmed by the tandem MS experiments.

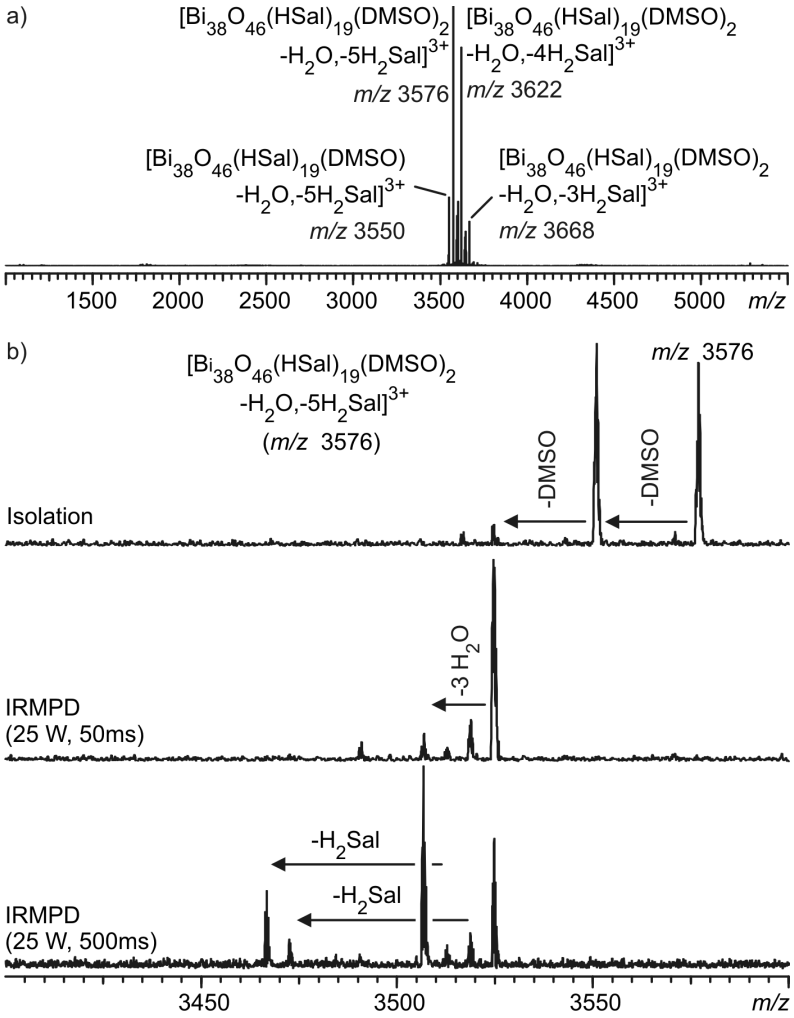

Figure 6.6: *ESI mass spectrum of* $[Bi_{38}O_{46}(HSal)_{22}(OH)_2]$ ***213*** *(a) and IRMPD tandem MS spectra of m/z 3576 (*$[Bi_{38}O_{46}(HSal)_{19}(DMSO)_2$ - H_2O, - 5 $H_2Sal]^{3+}$*) (b). For the tandem MS experiments, an IR laser with a laser power of 25 W was used at different irradiation times.*

Three different conclusions can be drawn: i) ESI mass spectrometry is a useful method to analyze the structure of bismuth-oxido clusters. ii) Tandem mass spectrometry can be used to gain information about the stability of the clusters in the gas phase. It has been shown that “naked” cluster cores can be produced by stripping off ligands and solvent molecules. The fragmentation of the cluster cores can help to identify stable structures like Bi_6-species which are known to be intermediates in the formation process of these clusters. iii) Reactions of the clusters like ligand exchanges can be analyzed by mass spectrometry as well as new intermediates in the formation process of bismuth-oxido clusters. In further experiments, using the mass spectrometric mixed-flow technique described above can help to get insights into the nucleation process of these clusters and their reactions.

7. Outlook

Many different aspects of metallo-supramolecular self-assembly have been examined within this thesis. Similar to the work of Schmittel and co-workers,[44, 53] future experiments could focus on the use of self-sorting processes to form heterometallic heteroleptic metallo-supramolecular architectures which otherwise would just be available in mixtures with other metallo-supramolecular complexes. In order to achieve those complexes, ligands bearing different binding sites have to be used as well as metal centers with different coordination geometries. For example, when a ligand containing two sterically hindered 2,2´-bipyridine units like **9** and a ligand containing a 2,2´-bipyridine and two pyridine units like **190** or **214** are combined with (dppp)M(OTf)$_2$ (M = Pd^{2+} **27** or Pt^{2+} **28**) and Cu(OTf) **215**, metallo-supramolecular complexes like **216** could be achieved (Figure 7.1). The building blocks used for those self-sorting processes can be functionalized in a way that different functional groups show into the inner cavity or the outer sphere of the resulting complexes. Thus, a library of metallo-supramolecular complexes functionalized with a combination of different functional groups is accessible which can be used for molecular recognition studies of different guest molecules.

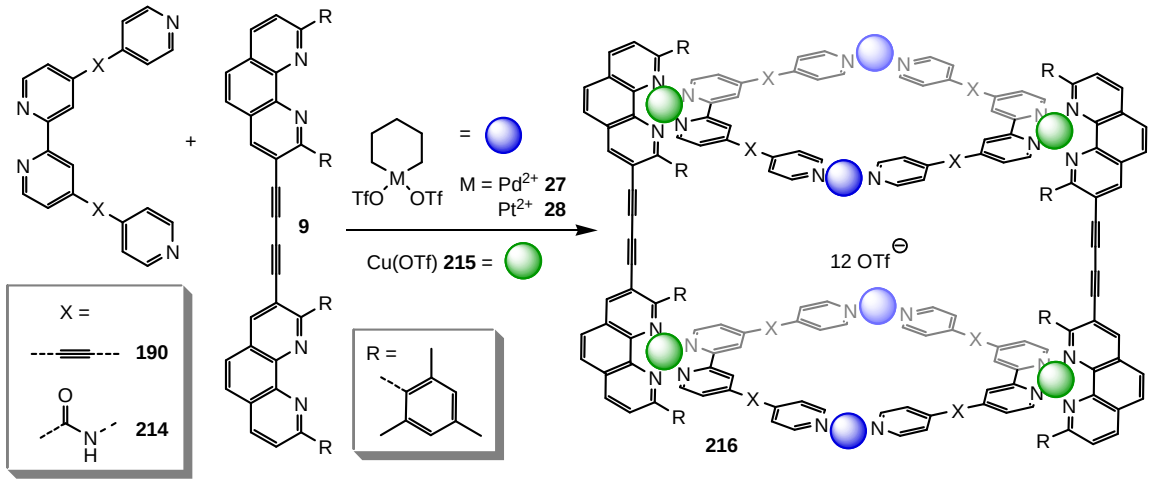

Figure 7.1: *A possible self-sorting reaction of a metallo-supramolecular complex* ***216****.*

Ligands similar to **214** could be used to form axially chiral building blocks with free coordination sites. When ligands **217** or **218** would be combined with metal centers

bearing octahedral coordination geometry like ruthenium (II), the axially chiral complexes **219** and **220** would form (Figure 7.2). Similar to analogous complexes containing phenyl groups instead of pyridine groups, these complexes should be able to recognize anions. [258] However, these complexes could also be used for further coordination with other metal centers bearing a different number of free coordination sites. Due to the chirality and photochemical properties of the ruthenium containing building blocks **219** and **220**, the resulting complexes or metal-organic frameworks should have interesting properties as well. Therefore the final metallo-supramolecular architectures could be interesting materials for solar energy conversion [259] or photocatalysis.[260]

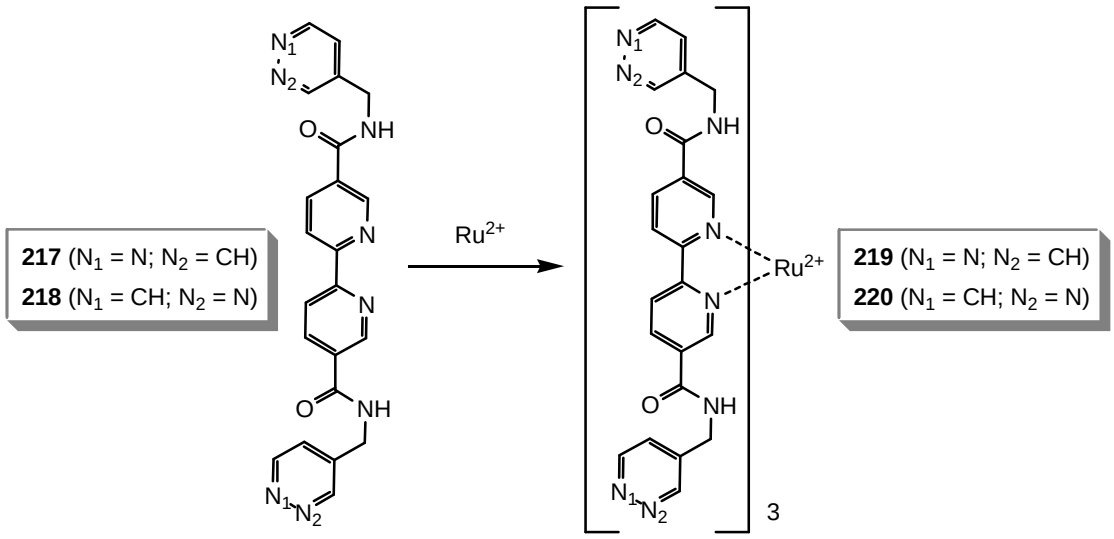

Figure 7.2: *The Self-assembly of the axial chiral metallo-supramolecular ruthenium(II) complexes* ***219*** *and* ***220****.*

8 Experimental Part

8.1 General Techniques and Materials

Molecular Modeling

The theoretically calculated structures shown in this thesis were calculated on the MM2 force field level to achieve an optimized geometry. These calculations were done with the CaChe 5.0 program package for Windows systems provided by Fujitsu Ltd. from Krakow / Poland in 2001.

Melting Points

The melting points were measured with a Büchi 510 Melting Point apparatus and are not corrected. Due to the properties of the silicon oil used in this apparatus, only melting points up to 250°C could be measured.

NMR Spectroscopy

^{1}H NMR, ^{13}C NMR, ^{31}P NMR, ^{1}H-^{1}H COSY NMR, ^{1}H-^{1}H NOESY NMR, ^{1}H 2D DOSY NMR and time- and temperature-dependent NMR spectra were recorded on Joel ECX 400 MHz, Joel ECP 500 MHz, Bruker AC 250 MHz, Bruker AC 500 MHz, Bruker DMX 500 MHz and Bruker DRX 500 MHz NMR spectrometers. The chemical shifts are reported in ppm. In ^{1}H and ^{13}C NMR spectra, the residual solvents were used as internal standards. For ^{31}P NMR spectra 85% phosphoric acid was used as external standard. The ^{13}C and ^{31}P NMR spectra were measured with decoupled broadband for ^{1}H. The coupling constants (*J*) are given in Hz. The abbreviations used for the signal multiplicities are: s = singlet; d = doublet; t = triplet; m = multiplet and br for broad signals.

Mass Spectrometry

The EI mass spectra were measured with a MAT 711 EI mass spectrometer from Varian MAT in Bremen (Germany) or with a HP 5989 A EI mass spectrometer from HEWLETT-PACKARD in Palo Alto (CA, USA). Standard ionization energies of 80 eV or 70 eV were used.

The ESI TOF mass spectra were recorded using an Agilent 6210 ESI TOF mass spectrometer from Agilent Technologies in Santa Clara (CA, USA). The flow rate was set to 4 µL/min and the spray voltage was adjusted to 4 kV. The desolvation gas was used with a pressure of 15 psi (1 bar). All other parameters were optimized to get the maximal abundance for the respective $[M+H]^+$.

Most mass spectrometric experiments were performed at an Ionspec QFT-7 ESI FTICR mass spectrometer from Agilent Technologies (former Varian Inc.) in Walnut Creek (CA, USA). The ESI FTICR mass spectrometer was equipped with a 7 T superconducting magnet and a Micromass Z-spray ESI source from Waters Co. in Saint-Quentin (France) which had a stainless steel capillary with an inner diameter of 0.65 mm. In regular experiments, the solvent flow rate of the integrated syringe pump was set to 4 µL/min and the spray voltage was 3.8 kV. All other parameters were optimized to get the maximum abundance of the peaks of the systems under study. Both, the temperatures of the ESI source and the steel needle, were set to 40 °C. No nebulizer gas was used throughout the experiments.

IRMPD MS/MS experiments were performed at the ESI FTICR mass spectrometer using a 25 W CO_2 IR-laser (10.6 µm wavelength). After isolation of the ions in the ICR cell, the laser was used for fragmentation. In order to get appropriate data, the laser intensity as well as the irradiation times of the laser was varied.

For the on-line mass spectrometric experiments, a Micro Static Mixing Tee from Upchurch Scientific in Oak Harbor (WA, USA) was used. This micro reactor contains a mixing frit and has an inner volume of 0.95 µL. For these experiments, the flow rates were varied between 4 and 40 µL/min. Mixing capillaries with various lengths were used to obtain the different reaction times. For further information see chapter 10.7.

Chemicals, Reagents and Solvents

The reagents, chemicals and solvents used were bought from ABCR, ACROS, ALDRICH, ALFA AESAR, FLUKA, GRÜSSING, LANCASTER, MERCK, STREM, TCI and WAKO. The reagents were used without further purification. The solvents were dried and purified using appropriate procedures. The deuterated solvents for the NMR spectroscopic experiments were bought from DEUTERO and used without further purification.

8.2 List of Abbreviations

BOC	*tert*-butoxycarbonyle group
br	broad (NMR)
d	doublet (NMR)
dd	doublet of doublets (NMR)
dppp	1,3-bis(diphenylphopshino)propane
d_x	order of deuteration in deuterated solvents
calc.	calculated (data)
CID	Collision Induced Decay
CN	Coordination Number
CSI	Coldspray Ionization
c.y.	chemical yield
Da	Dalton
DMF	*N,N´*-dimethylformamide
DMSO	dimethylsulfoxide
EI	Electron Ionization
en	1,2-diaminoethane
ESI	Electrospray Ionization
eq.	equivalent(s)
Et_3N	triethylamine
EtOH	ethanol
exp.	experimental (data)

FAB	Fast Atom Bombardment
FT	Fourier-Transformation
h	hour(s)
Hz	Hertz
ICR	Ion Cyclotron Resonance
IRMPD	Infra-Red Multi-Photon Dissociation
IUPAC	International Union of Pure and Applied Chemistry
J	coupling constant (NMR)
L	ligand (in a complex)
m	multiplet (NMR)
m	*meta*
M	metal center (in a complex)
$M^{\cdot+}$	molecular radical cation
MALDI	Matrix Assisted Laser Desorption Ionization
MeCN	acetonitrile
min	minute(s)
MeOH	methanol
MHz	megahertz
m.p.	melting point
MS	Mass Spectrometry
m/z	mass per charge
NMR	Nuclear Magnetic Resonance
o	*ortho*
p	*para*
ppm	parts per million
Ph	phenyl
Phe	phenylalanine
Py	pyridine
pTsO	*para*-toluene sulfonic acid
q	quartet (NMR)
r	radius

r.t.	room temperature
t	time
t	triplet (NMR)
T	temperature
THF	tetrahydrofurane
s	singlet (NMR)
Sal	salicylate
v	velocity
V	volume
Val	valine

8.3 Syntheses of Organic Ligands

Syntheses of dipyridylurea ligands **129** and **162-168**

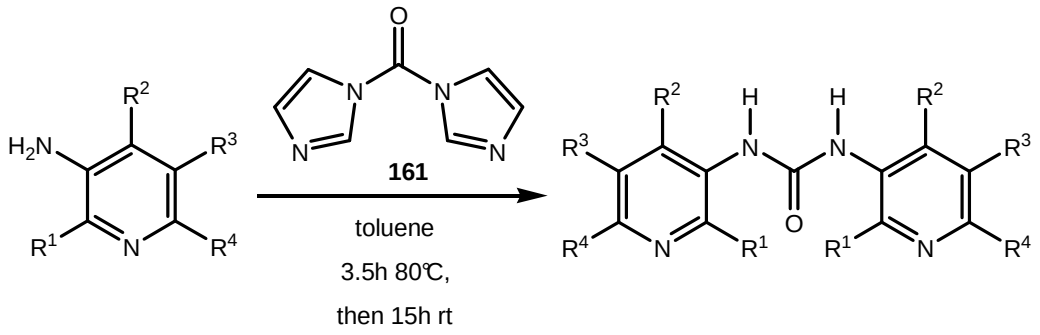

	R^1	R^2	R^3	R^4
154	H	H	H	H
155	Me	H	H	H
156	H	Me	H	H
157	H	H	Me	H
158	H	H	H	Me

	R^1	R^2	R^3	R^4	%
162	H	H	H	H	85
163	Me	H	H	H	60
164	H	Me	H	H	62
165	H	H	Me	H	75
166	H	H	H	Me	93

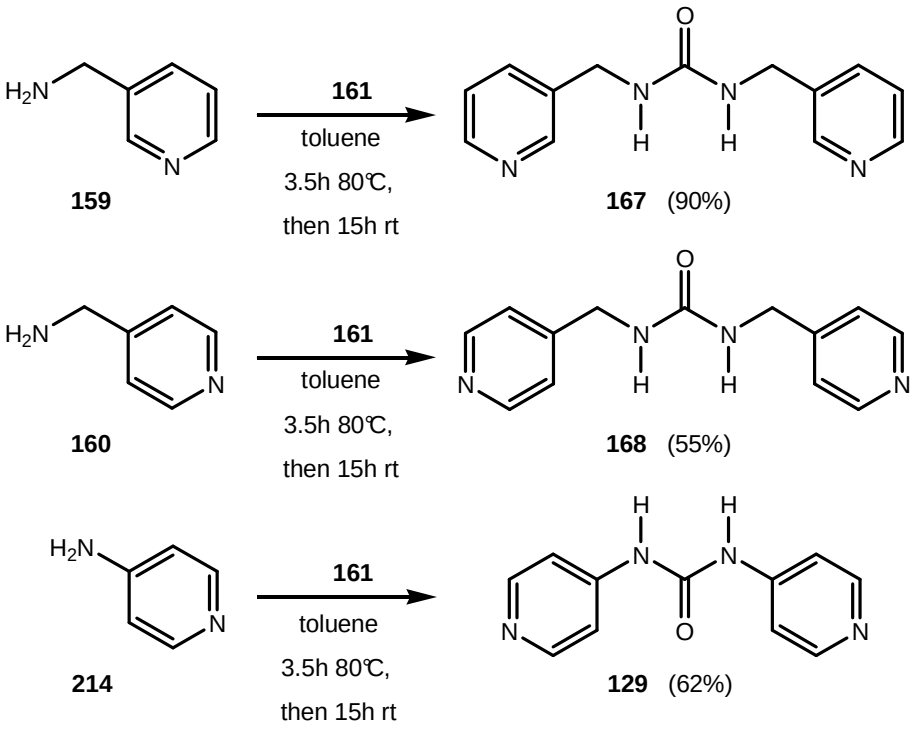

General Synthetic Route:[81, 106]

500 mg of the aminopyridine or (aminomethyl)pyridine and 0.6 equivalents of *N,N´*-carbonyldiimidazole were dissolved in 80 mL dry toluene. The solution was heated to 80 °C for 3.5 h. Now a second portion 0.1 equivalents of *N, N´*-carbonyl-diimidazole was added to the hot solution. After 30 more minutes of heating, the mixture was cooled down and stirred for 15 hours at room temperature. The resulting precipitate was collected by filtration and washed with toluene and diethyl ether.

1,3-di(pyridin-4-yl)urea **129**

Starting materials:

500.00 mg	(5.31 mmol)	4-aminopyridine **214**
474.00 mg	(2.92 mmol, 0.55 eq.)	*N, N´*-carbonyldiimidazole **161** (1. dose)
86.00 mg	(1.59 mmol, 0.1 eq.)	*N, N´*-carbonyl-diimidazole **161** (2. dose)

Using the general synthesis route, 398.92 mg (1.86 mmol, 62 % c.y.) of 1,3-di(pyridin-3-yl)urea **129** were obtained as white powder.

$C_{11}H_{10}N_4O$ 214.22 g/mol

^{1}H NMR (300 MHz, DMSO-d_6) δ = 9.39 (s, 2 H, NH); 8.39 (dd, 4 H, $^3J_{HH}$ = 4.91 Hz, $^4J_{HH}$ = 1.42 Hz, H-2) 7,45 (dd, 4 H, $^3J_{HH}$ = 4.81 Hz, $^4J_{HH}$ = 1.51 Hz, H-3) ppm.

^{13}C NMR (75.5 MHz, DMSO-d_6) δ = 152.22 (CO); 150.56 (C-2); 146.50 (C-4); 122.93 (C-3) ppm.

EI-MS (EI^+, 70 eV) m/z (%) = 214.1 ($[M]^{+\cdot}$, 100); 121.1 ($[M - PyNH]^{+\cdot}$, 30); 120.1 ($[M - PyNH_2]^{+\cdot}$, 18); 94.1 ($[PyNH_2]^{+\cdot}$, 44); 78.1 ($[Py - H]^{+\cdot}$, 10); 67.1 ($[C_4H_5N]^{+\cdot}$, 12).

m.p. > 250 °C

1,3-di(pyridin-3-yl)urea **162**

Starting materials:

500.00 mg	(5.31 mmol)	3-aminopyridine **154**
474.00 mg	(2.92 mmol, 0.55 eq.)	*N*, *N´*-carbonyldiimidazole **161** (1. dose)
86.00 mg	(1.59 mmol, 0.1 eq.)	*N*, *N´*-carbonyl-diimidazole **161** (2. dose)

Using the general synthesis route, 546.93 mg (2.55 mmol, 85 % c.y.) of 1,3-di(pyridin-3-yl)urea **162** were obtained as white powder.

$C_{11}H_{10}N_4O$ 214.22 g/mol

^{1}H NMR (400 MHz, DMSO-d_6, 298 K): δ = 8.77 (s, 2 H, NH), 8.55 (d, 2 H, $^4J_{HH}$ = 2.39 Hz, H-2), 8.14 (dd, 2 H, $^3J_{HH}$ = 4.66 Hz, $^4J_{HH}$ = 1.51 Hz, H-6), 7.93 (ddd, 2 H, $^3J_{HH}$ = 8.31 Hz, $^4J_{HH}$ = 2.64 Hz, $^4J_{HH}$ = 1.51 Hz, H-4), 7.20 (dd, 2 H, $^3J_{HH}$ = 8.31 Hz, $^3J_{HH}$ = 4.66 Hz, H-5) ppm.

^{13}C NMR (100 MHz, DMSO-d_6, 298 K): δ = 151.72 (CO), 142.05 (C-2), 39.28 (C-6), 135.25 (C-4), 124.36 (C-3), 122.39 (C-5) ppm.

EI-MS (EI^+, 70 eV): m/z (%) = 214.1 ($[M]^{+\cdot}$, 100), 121.1 ($[M - PyNH]^{+\cdot}$, 25), 120.1 ($[M - PyNH_2]^{+\cdot}$, 14), 94.1 ($[PyNH_2]^{+\cdot}$, 78), 78.1 ($[Py - H]^{+\cdot}$, 14), 67.1 ($[C_4H_5N]^{+\cdot}$, 15).

m.p. > 250 °C

1,3-bis(2-methylpyridin-3-yl)urea **163**

Starting materials:

500.00 mg	(4.62 mmol)	3-amino-2-methylpyridine **155**
413.00 mg	(2.92 mmol, 0.55 eq.)	*N*, *N´*-carbonyldiimidazole **161** (1. dose)
75.00 mg	(1.59 mmol, 0.1 eq.)	*N*, *N´*-carbonyl-diimidazole **161** (2. dose)

Using the general synthesis route, 336.06 mg (1.39 mmol, 60 % c.y.) of 1,3-bis(2-methylpyridin-3-yl)urea **163** could be obtained as white powder.

$C_{13}H_{14}N_4O$ 242.28 g/mol

^{1}H NMR (250 MHz, DMSO-d_6, 303 K): δ = 8.59 (s, 2 H, NH), 8.18 (d, 2 H, $^3J_{HH}$ = 8.25 Hz, H-6), 8.13 (d, 2 H, $^3J_{HH}$ = 4.73 Hz, H-4), 7.23 (dd, 2 H, $^3J_{HH}$ = 8.25 Hz and $^3J_{HH}$ = 4.72 Hz, H-5), 2.50 (s, 6 H, CH_3) ppm.

^{13}C NMR (63 MHz, DMSO-d_6, 303 K): δ = 152.95 (CO), 148.22 (C-2), 142.81 (C-6), 133.60 (C-3), 127.93 (C-4) 121.35 (C-5), 21.18 (CH_3) ppm.

EI-MS (EI^+, 80 eV): m/z (%) = 241.9 ($[M]^{+\cdot}$, 40), 134.7 ($[M + H - C_6H_8N_2]^{+\cdot}$, 16), 133.7 ($[M - C_6H_8N_2]^{+\cdot}$, 22), 108.0 ($[C_6H_8N_2]^{+\cdot}$, 100), 92.2 ($[C_6H_6N]^{+\cdot}$, 8), 80.2 ($[Py + H]^{+\cdot}$, 20).

m.p. > 250 °C

1,3-bis(4-methylpyridin-3-yl)urea **164**

Starting materials:

500.00 mg	(4.62 mmol)	3-amino-4-methylpyridine **156**
413.00 mg	(2.92 mmol, 0.55 eq.)	*N*, *N´*-carbonyldiimidazole **161** (1. dose)
75.00 mg	(1.59 mmol, 0.1 eq.)	*N*, *N´*-carbonyl-diimidazole **161** (2. dose)

Using the general synthesis route, 347.18 mg (1.43 mmol, 62 % c.y.) of 1,3-bis(4-methylpyridin-3-yl)urea **164** could be obtained as white powder.

$C_{13}H_{14}N_4O$ 242.28 g/mol

^{1}H-NMR (300 MHz, DMSO-d_6, 298 K): δ = 8.88 (s, 2 H, NH), 8.45 (s, 2 H, H-2), 8.15 (d, 2 H, $^3J_{HH}$ = 4.91 Hz, H-6), 7.23 (d, 2 H, $^3J_{HH}$ = 4.72 Hz, H-5), 2.28 (s, 6 H, CH_3) ppm.

^{13}C-NMR (75.5 MHz, DMSO-d_6, 298 K): δ = 152.79 (CO), 143.99 (C-2), 143.45 (C-6), 137.42 (C-3), 134.35 (C4) 125.14 (C-5), 7.28 (CH_3) ppm.

EI-MS (EI^+, 70 eV): m/z (%) = 243.1 ($[M + H]^{+\cdot}$, 8), 242.1 ($[M]^{+\cdot}$, 48), 135.1 ($[M + H - C_6H_8N_2]^{+\cdot}$, 30), 134.1 ($[M - C_6H_8N_2]^{+\cdot}$, 26), 108.1 ($[C_6H_8N_2]^{+\cdot}$, 100), 92.1 ($[C_6H_6N]^{+\cdot}$, 7), 80.1 ($[Py + H]^{+\cdot}$, 12).

m.p. > 250 °C

1,3-bis(5-methylpyridin-3-yl)urea **165**

Starting materials:

500.00 mg	(4.62 mmol)	3-amino-5-methylpyridine **157**
413.00 mg	(2.92 mmol, 0.55 eq.)	*N*, *N´*-carbonyldiimidazole **161** (1. dose)
75.00 mg	(1.59 mmol, 0.1 eq.)	*N*, *N´*-carbonyl-diimidazole **161** (2. dose)

Using the general synthesis route, 419.84 mg (1.73 mmol, 75 % c.y.) of 1,3-bis(5-methylpyridin-3-yl)urea **165** were obtained as white powder.

$C_{13}H_{14}N_4O$ 242.28 g/mol

^{1}H-NMR (250 MHz, DMSO-d_6, 303 K): δ = 8.91 (s, 2 H, NH), 8.41 (s, 2 H, H-2), 8.05 (s, 2 H, H-6), 7.79 (s, 2 H, H-4), 2.28 (s, 6 H, CH_3) ppm.

^{13}C-NMR (63 MHz, DMSO-d_6, 303 K): δ = 152.59 (CO), 143.39 (C-2), 137.38 (C-6), 135.77 (C-3), 132.84 (C4) 125.68 (C-5), 17.88 (CH_3) ppm.

EI-MS (EI^+, 80 eV): m/z (%) = 241.9 ($[M]^{+\cdot}$, 16), 134.9 ($[M + H - C_6H_8N_2]^{+\cdot}$, 14), 133.8 ($[M - C_6H_8N_2]^{+\cdot}$, 61), 108.0 ($[C_6H_8N_2]^{+\cdot}$, 100), 92.2 ($[C_6H_6N]^{+\cdot}$, 5), 80.2 ($[Py + H]^{+\cdot}$, 27).

m.p. > 250 °C

1,3-bis(6-methylpyridin-3-yl)urea **166**

Starting materials:

500.00 mg	(4.62 mmol)	3-amino-5-methylpyridine **158**
413.00 mg	(2.92 mmol, 0.55 eq.)	*N*, *N´*-carbonyldiimidazole **161** (1. dose)
75.00 mg	(1.59 mmol, 0.1 eq.)	*N*, *N´*-carbonyl-diimidazole **161** (2. dose)

Using the general synthesis route, 520.43 mg (2.15 mmol, 93 % c.y.) of 1,3-bis(6-methylpyridin-3-yl)urea **166** were obtained as white powder.

$C_{13}H_{14}N_4O$ 242.28 g/mol

^{1}H-NMR (500 MHz, DMSO-d_6, 303 K): δ = 8.61 (s, 2 H, NH), 8.47 (d, 2 H, $^4J_{HH}$ = 2.50 Hz, H-2), 7.78 (dd, 2 H, $^3J_{HH}$ = 8.35 Hz and $^4J_{HH}$ = 2.69 Hz, H-4), 7.15 (d, 2 H, $^3J_{HH}$ = 8.44 Hz, H-5), 2.41 (s, 6 H, CH_3) ppm.

^{13}C-NMR (126 MHz, DMSO-d_6, 303 K): δ = 152.49 (CO), 150.87 (C-2), 139.43 (C-6), 133.29 (C-3), 126.00 (C4) 122.16 (C-5), 22.76 (CH_3) ppm.

EI-MS (EI^+, 80 eV): m/z (%) = 242.1($[M]^{+\cdot}$, 17), 134.9 ($[M + H - C_6H_8N_2]^{+\cdot}$, 13), 133.8 ($[M - C_6H_8N_2]^{+\cdot}$, 76), 108.0 ($[C_6H_8N_2]^{+\cdot}$, 100), 92.2 ($[C_6H_6N]^{+\cdot}$, 4), 80.2 ($[Py + H]^{+\cdot}$, 38).

m.p. > 250 °C

1,3-bis((pyridin-3-yl)methyl)urea **167**

Starting materials:

500.00 mg	(4.62 mmol)	3-aminomethylpyridine **159**
413.00 mg	(2.92 mmol, 0.55 eq.)	*N*, *N´*-carbonyldiimidazole **161** (1. dose)
75.00 mg	(1.59 mmol, 0.1 eq.)	*N*, *N´*-carbonyl-diimidazole **161** (2. dose)

Using the general synthesis route, 503.64 mg (2.08 mmol, 90 % c.y.) of 1,3-bis((pyridin-3-yl)methyl)urea **167** were obtained as white powder.

$C_{13}H_{14}N_4O$ 242.28 g/mol

^{1}H-NMR (400 MHz, DMSO-d_6, 298 K): δ = 8.47 (s, 2 H, H-2), 8.42 (d, 2 H, $^3J_{HH}$ = 4.78, H-6), 7.63 (d, 2 H, $^3J_{HH}$ = 7.68 Hz, H-4), 7.32 (dd, 2 H, $^3J_{HH}$ = 7.55 Hz, $^3J_{HH}$ = 4.78 Hz, H-5), 6.63 (t, 2 H, $^3J_{HH}$ = 5.85 Hz, NH), 4.24 (d, 4 H, $^3J_{HH}$ = 6.04 Hz, CH_2) ppm.

^{13}C-NMR (100 MHz, DMSO-d_6, 298 K): δ = 158.11 (CO), 148.60 (C-2), 147.88 (C-6), 136.31 (C-3), 134.89 (C-4), 123.42 (C-5), 40,73 (CH_2) ppm.

EI-MS (EI^+, 70 eV): m/z (%) = 243.2 ($[M + H]^{+\cdot}$, 16), 242.1 ($[M]^{+\cdot}$, 100), 150.1 ($[M - C_6H_6N]^{+\cdot}$, 10), 135.0 ($[M + H - C_6H_8N_2]^{+\cdot}$, 13), 134.0 ($[M - C_6H_8N_2]^{+\cdot}$, 7), 107.0 ($[C_6H_7N_2]^{+\cdot}$, 59), 93.0 ($[C_6H_7N]^{+\cdot}$, 24), 92.0 ($[C_6H_6N]^{+\cdot}$, 27), 80.0 ($[Py + H]^{+\cdot}$, 16), 79.0 ($[Py]^{+\cdot}$, 9), 65.0 ($[C_5H_5]^{+\cdot}$, 11).

m.p. > 250 °C

1,3-bis((pyridin-4-yl)methyl)urea **168**

Starting materials:

500.00 mg	(4.62 mmol)	4-aminomethylpyridine **160**
413.00 mg	(2.92 mmol, 0.55 eq.)	*N*, *N*´-carbonyldiimidazole **161** (1. dose)
75.00 mg	(1.59 mmol, 0.1 eq.)	*N*, *N*´-carbonyl-diimidazole **161** (2. dose)

Using the general synthesis route, 307.52 mg (1.27 mmol, 55 % c.y.) of 1,3-bis((pyridin-4-yl)methyl)urea **168** were obtained as white powder.

$C_{13}H_{14}N_4O$ 242.28 g/mol

^{1}H-NMR (300 MHz, DMSO-d_6, 298 K): δ = 8.49 (d, 4 H, $^{3}J_{HH}$ = 6.04 Hz, H-2 and H-6), 7.24 (d, 4 H, $^{3}J_{HH}$ = 5.66 Hz, H-3 und H-5), 6.73 (t, 2 H, $^{3}J_{HH}$ = 6.04 Hz, NH), 4.26 (d, 4 H, $^{3}J_{HH}$ = 6.23 Hz, CH_2) ppm.

^{13}C-NMR (75.5 MHz, DMSO-d_6, 298 K): δ = 158.09 (CO), 150.04 (C-4), 149.39 (C-2 and C-6), 121.89 (C-3 and C-5), 42.05 (CH_2) ppm.

EI-MS (EI^+, 70 eV): m/z (%) = 243.2 ($[M + H]^{+\cdot}$, 16), 242.1 ($[M]^{+\cdot}$, 100), 150.1 ($[M – C_6H_6N]^{+\cdot}$, 3), 135.0 ($[M + H – C_6H_8N_2]^{+\cdot}$, 12), 134.0 ($[M – C_6H_8N_2]^{+\cdot}$, 12), 107.0 ($[C_6H_7N_2]^{+\cdot}$, 35), 93.0 ($[C_6H_7N]^{+\cdot}$, 13), 92.0 ($[C_6H_6N]^{+\cdot}$, 15), 80.0 ($[Py + H]^{+\cdot}$, 15), 79.0 ($[Py]^{+\cdot}$, 12), 65.0 ($[C_5H_5]^{+\cdot}$, 6).

m.p. > 250 °C

Syntheses of "Hunter-ligands" **147** and **148**[37]

nicotinoyl chloride hydrochloride **141**

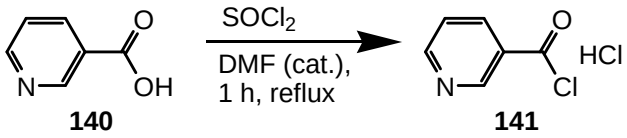

140 **141**

500.00 mg (3.53 mmol) nicotinic acid **140** were suspended in 5 ml (6.89 mmol) thionyl chloride. After adding 0.1 ml of DMF, the reaction mixture was refluxed and stirred for one hour. The excess of thionyl chloride was removed carefully using a water aspirator pump. The resulting white powder was suspended into 20 mL of dry diethyl ether and filtered using a glass filter. After washing with another 20 mL of dry diethyl ether, the product was dried under vacuum and 573.15 mg (3.19 mmol, 95 % c.y.) of a white powder (**141**) were obtained.

$C_6H_5Cl_2NO$ 178.02 g/mol

The nicotinoyl chloride hydrochloride **141** was used without further characterization. It was indirectly characterized by the results of the reactions it was used in.

N,*N*'-(4,4'-(cyclohexane-1,1-diyl)-bis-(2,6-dimethyl-4,1-phenylene)) dinicotinamide **147**

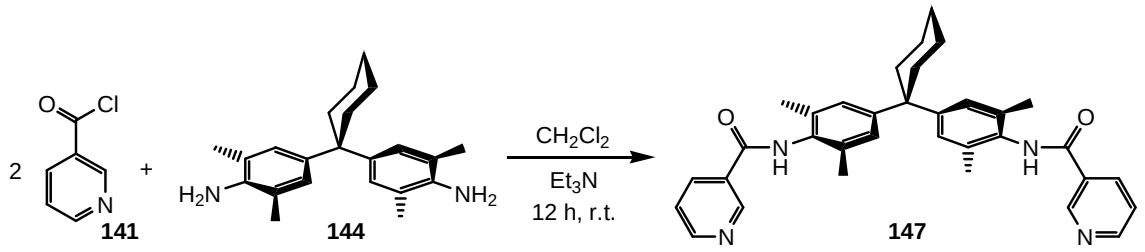

141 **144** **147**

The reaction was performed in an argon atmosphere. 100 mg (0.31 mmol) of 1,1-bis(4-amino-3,5-dimethylphenyl)cyclohexane (Hunter´s diamine) **144** was dissolved in 50 mL of dry dichloromethane and mixed with 0.13 mL (3 eq., 0.94 mmol) triethylamine. Within one hour, 133 mg (3 eq., 0.94 mmol) nicotinoyl chloride **141** were added stepwise. The reaction mixture was stirred for 12 hours at room temperature. Afterwards, the mixture was transferred into an extraction funnel and washed two times with 50 mL ammonia water and three times with 100 mL of destilled water. The organic phase was dried with anhydrous magnesium sulfate which afterwards was removed by filtration. The dichloromethane was removed in the vacuum. The residue was isolated by column chromatography (silica) using CH_2Cl_2/MeOH (22:1) as the eluent (R_f = 0.46). The product was dried in vacuum and 120.00 mg (0.25 mmol, 72 %) of **147** were obtained as white powder.

$C_{34}H_{36}N_4O_2$ 532.68 g/mol

^{1}H-NMR (400 MHz, DMSO-d_6, 293 K): δ = 9.84 (s, 2 H, NH); 9.14 (d, 2 H, $^4J_{HH}$ = 1.88 Hz, $H_{o\text{-pyridine}}$); 8.76 (dd, 2 H, $^3J_{HH}$ = 4.78 Hz, $^4J_{HH}$ = 1.58 Hz, $H_{o\text{-pyridine}}$); 8.30 (dd, 2 H, $^3J_{HH}$ = 8.22 Hz, $^4J_{HH}$ = 1.97 Hz, $H_{p\text{-pyridine}}$); 7.56 (dd, 2 H, $^3J_{HH}$ = 6.38 Hz, $^3J_{HH}$ = 6.38 Hz, $H_{m\text{-pyridine}}$); 7.11 (s, 4 H, H_{phenyl}); 2.28 (br, 4 H, CCH_2); 2.16 (s, 12 H, CH_3); 1.53-1.45 (m, 6 H, $CCH_2C\underline{H_2}$ and $CCH_2CH_2C\underline{H_2}$) ppm.

^{13}C-NMR (100 MHz, DMSO-d_6, 293 K): δ = 163.54; 152.13; 148.51; 146.80; 135.23; 135.04; 132.13; 129.96; 126.17; 123.66; 44.80; 36.13; 25.79; 22.63; 18.47 ppm.

ESI-MS (ESI$^+$, MeOH): *m/z* = 533.29 ([M+H]$^+$); 555.27 ([M+Na]$^+$); 571.25 ([M+K]$^+$). HRMS (ESI): found: *m/z* 533.2905 ([M+H]$^+$), calc.: 533.2911.

m.p. 184 °C

isonicotinoyl chloride hydrochloride **143**

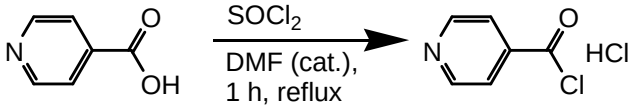

142 **143**

500.00 mg (3.53207 mmol) isonicotinic acid **142** were suspended in 5 ml (6.89249 mmol) thionyl chloride. After adding 0.1 ml of DMF, the reaction mixture was refluxed and stirred for one hour. The excess of thionyl chloride was removed carefully using a water aspirator pump. The resulting white powder was suspended into 20 mL of dry diethyl ether and filtered using a glass filter. After washing with another 20 mL of dry diethyl ether, the product was dried under vacuum and 567.19 mg (3.21958 mmol, 96 % c.y.) of a white powder (**143**) were obtained.

$C_6H_5Cl_2NO$ 178.02 g/mol

The isonicotinoyl chloride hydrochloride **143** was used without further characterization. It was indirectly characterized by the results of the reactions it was used in.

N,*N*'-(4,4'-(cyclohexane-1,1-diyl)bis-(2,6-dimethyl-4,1-phenylene)) diisonicotinamide **148**

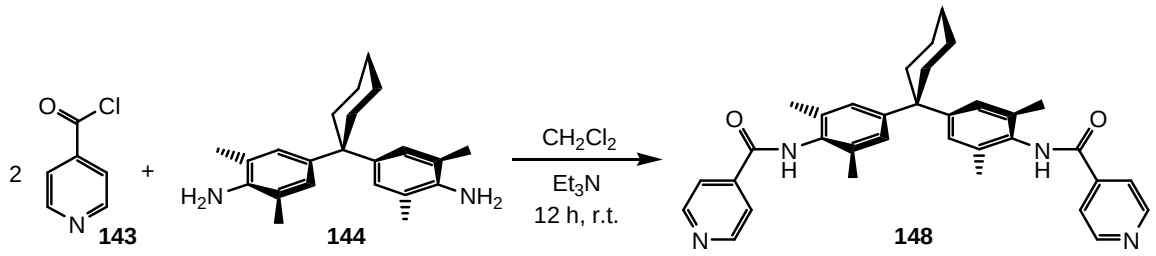

The reaction was performed in an argon atmosphere. 100 mg (0.31 mmol) of 1,1-bis(4-amino-3,5-dimethylphenyl)cyclohexane (Hunter´s diamine) **144** was dissolved in 50 mL of dry dichloromethane and mixed with 0.13 mL (3 eq., 0.94 mmol) triethylamine. Within one hour, 133 mg (3 eq., 0.94 mmol) isonicotinoyl chloride **143** were added stepwise. The reaction mixture was stirred for 12 hours at room temperature. Afterwards, the mixture was transferred into an extraction funnel and washed two times with 50 mL ammonia water and three times with 100 mL of destilled water. The organic phase was dried with anhydrous magnesium sulfate which afterwards was removed by filtration. The dichloromethane was removed in the vacuum. The residue was isolated by column chromatography (silica) using CH_2Cl_2/MeOH (9:1) as the eluent (R_f = 0.55). The product was dried in vacuum and 116.43 mg (0.24 mmol, 70 %) of **148** were obtained as white powder.

$C_{34}H_{36}N_4O_2$ 532.68 g/mol

^{1}H-NMR (400 MHz, DMSO-d_6, 295 K): δ = 9.92 (s, 2 H, NH); 8.78 (dd, $^3J_{HH}$ = 4.40 Hz, $^5J_{HH}$ = 1.68 Hz, $H_{o\text{-pyridine}}$); 7.86 (dd, 4 H, $^3J_{HH}$ = 4.41 Hz, $^5J_{HH}$ = 1.66 Hz, $H_{m\text{-pyridine}}$); 7.11 (s, 4 H, H_{phenyl}); 2.29 (br, 4 H, CCH_2); 2.15 (s, 12 H, CH_3); 1.48 (br, 6 H, $CCH_2C\underline{H_2}$ and $CCH_2CH_2C\underline{H_2}$) ppm.

^{13}C-NMR (100 MHz, DMSO-d_6, 295 K): δ = 163.46; 150.38; 146.90; 141.36; 134.96; 131.89; 126.18; 121.40; 44.80; 36.09; 22.61; 21.20; 18.40 ppm.

ESI-MS (ESI$^+$, MeOH): *m/z* = 533.29 ([M+H]$^+$); 555.27 ([M+Na]$^+$); 571.25 ([M+K]$^+$). HRMS (ESI): found: *m/z* 533.2905 ([M+H]$^+$), calc.: 533.2911.

m.p. 185 °C

8.4 Syntheses of Metal Centers

The metal centers synthesized within this thesis are literature-known.[215] Thus, just ^{1}H and ^{31}P NMR data is reported to characterize them.

(1,2-bis(diphenylphosphino)ethane)palladium(II) chloride **98**

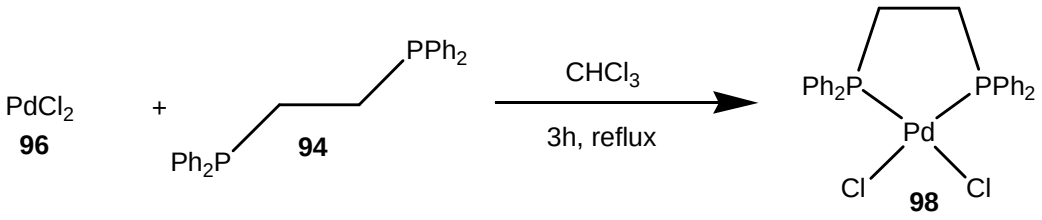

This Synthesis was performed in an argon atmosphere. 300.00 mg (1.69176 mmol) palladium(II) chloride **96** and 741.44 mg (1.86094 mmol, 1.1 eq.) 1,2-bis(diphenylphosphino)ethane **94** were suspended in 100 mL of dry chloroform. The suspension was refluxed and stirred for three hours. After this, 280 mL of *n*-hexane were added to the hot solution and the resulting precipitate was immediately filtered using a glass filter. The solid was washed with 100 mL of *n*-hexane. In order to isolate the product from palladium(II) chloride **96** which did not react, the solid mixture in the glass filter was washed with 180 mL of dichloromethane. The dichloromethane was removed and the product was dried under vacuum. 779.20 mg (1.35341 mmol, 80 % c.y.) of a yellowish powder (**98**) were obtained.

$C_{26}H_{24}Cl_2P_2Pd$ 575.74 g/mol

^{1}H NMR (400 MHz, DMSO-d_6, 294 K): δ = 7.87 (m, 8 H, $H_{dppp\text{-}phenyl}$); 7.62 (m, 4 H, $H_{dppp\text{-}phenyl}$); 7.56 (m, 8 H, $H_{dppp\text{-}phenyl}$); 2.69 (d, $^{3}J_{PH}$ = 24.38 Hz, 4 H, PCH_2) ppm.

^{31}P NMR (162 MHz, DMSO-d_6, 294 K): δ = 67.28 (s, P_{dppp}) ppm.

(1,2-bis(diphenylphosphino)ethane)palladium(II) trifluoromethanesulfonate **100**

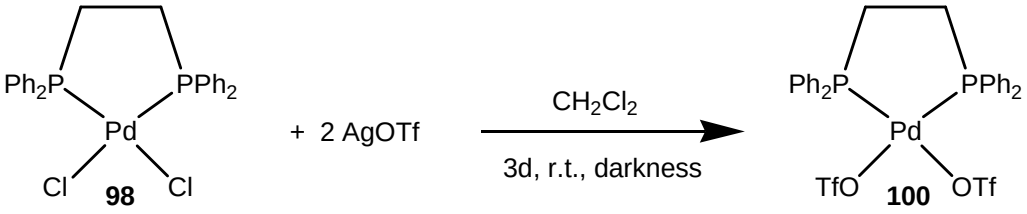

This Synthesis was performed in an argon atmosphere. 300 mg (0.52107 mmol) (1,2-bis(diphenylphosphino)ethane)palladium(II) chloride **98** were mixed with 1071.10 mg (4.16855 mmol, 8 eq.) silver(I) trifluoromethanesulfonate. The mixture was suspended in 30 mL of dry dichloromethane and stirred in darkness at room temperature for 72 h. Afterwards, the suspension was filtered with a glass filter and the filtrate was reduced to a volume of 5 mL. 30 mL of diethyl ether were mixed with the filtrate and the suspension was cooled in the fridge for four hours. The precipitate was isolated by filtration with a glass filter, washed with 30 mL of diethyl ether and the product was dried in vacuum. 330.55 mg (0.41165 mmol, 79 % c.y.) of a light yellow powder (**100**) were obtained.

$C_{28}H_{24}F_6O_6P_2PdS_2$ 802.97 g/mol

^{1}H NMR (400 MHz, DMSO-d_6, 294 K): δ = 7.89 (dd, 8 H, $^{3}J_{HH}$ = 7.18 Hz, $^{3}J_{PH}$ = 12.89 Hz, $H_{o\text{-}phenyl}$); 7.78 (dd, 4 H, $^{3}J_{HH}$ = 8.33 Hz, $^{3}J_{HH}$ = 6.46 Hz, $H_{p\text{-}phenyl}$); 7.67 (m, 8 H, $H_{m\text{-}phenyl}$); 2.95 (d, 4 H, $^{3}J_{PH}$ = 24.23 Hz, PCH_2) ppm.

^{31}P NMR (162 MHz, DMSO-d_6, 294 K): δ = 72.27 (s, P_{dppp}) ppm.

(1,2-bis(diphenylphosphino)ethane)platinum(II) chloride **99**

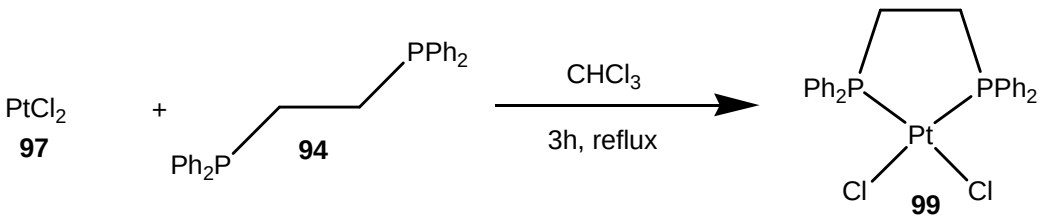

This Synthesis was performed in an argon atmosphere. 300.00 mg (1.12790 mmol) platinum(II) chloride **97** and 494.30 mg (1.24069 mmol, 1.1 eq.) 1,2-bis(diphenylphosphino)ethane **94** were suspended in 100 mL of dry chloroform. The suspension was refluxed and stirred for three hours. After this, 280 mL of *n*-hexane were added to the hot solution and the resulting precipitate was immediately filtered using a glass filter. The solid was washed with 100 mL of *n*-hexane. In order to isolate the product from palladium(II) chloride **97** which did not react, the solid mixture in the glass filter was washed with 180 mL of dichloromethane. The dichloromethane was removed and the product was dried under vacuum. 577.14 mg (0.86849 mmol, 77 % c.y.) of a white powder (**99**) were obtained.

$C_{26}H_{24}Cl_2P_2Pt$ 664.40 g/mol

^{1}H NMR (400 MHz, DMSO-d_6, 294 K): δ = 7.84 (m, 8 H, $H_{dppp\text{-}phenyl}$); 7.57 (m, 12 H, $H_{dppp\text{-}phenyl}$); 2.55 (d, $^3J_{PH}$ = 19.39 Hz, 4 H, PCH_2) ppm.

^{31}P NMR (162 MHz, DMSO-d_6, 294 K): δ = 43.22 (s, $^1J_{Pt\text{-}P}$ = 3609.79 Hz, P_{dppp}) ppm.

(1,2-bis(diphenylphosphino)ethane)platinum(II) trifluoromethanesulfonate **101**

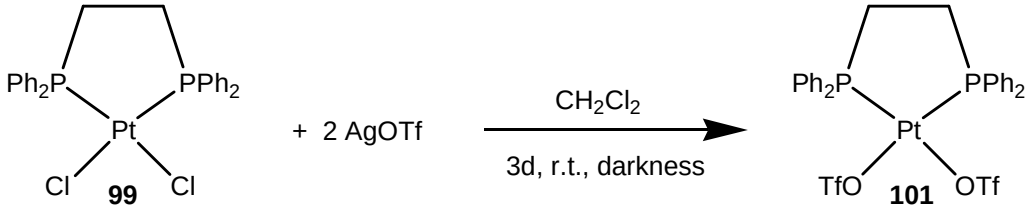

This Synthesis was performed in an argon atmosphere. 300 mg (0.45154 mmol) (1,2-bis(diphenylphosphino)ethane)platinum(II) chloride **99** were mixed with 928.14 mg (3.61228 mmol, 8 eq.) silver(I) trifluoromethanesulfonate. The mixture was suspended in 20 mL of dry dichloromethane and stirred in darkness at room temperature for 72 h. Afterwards, the suspension was filtered with a glass filter and the filtrate was reduced to a volume of 5 mL. 30 mL of diethyl ether were mixed with the filtrate and the suspension was cooled in the fridge for four hours. The precipitate was isolated by filtration with a glass filter, washed with 30 mL of diethyl ether and the product was dried in vacuum. 301.90 mg (0.533865 mmol, 75 % c.y.) of a white powder (**101**) were obtained.

$C_{28}H_{24}F_6O_6P_2PtS_2$ 891.63 g/mol

^{1}H NMR (400 MHz, DMSO-d_6, 295 K): δ = 7.82 (dd, 8 H, $^3J_{HH}$ = 7.24 Hz, $^3J_{PH}$ = 12.75 Hz, $H_{o\text{-phenyl}}$); 7.76 (d, 4 H, $^3J_{HH}$ = 7.04 Hz, $H_{p\text{-phenyl}}$); 7.67 (m, 8 H, $H_{m\text{-phenyl}}$); 2.75 (d, 4 H, $^3J_{PH}$ = 18.91 Hz, CH_2) ppm.

^{31}P NMR (162 MHz, DMSO-d_6, 295 K): δ = 37.61 (s, P_{dppp}) ppm.

(1,3-bis(diphenylphosphino)propane)palladium(II) chloride **102**

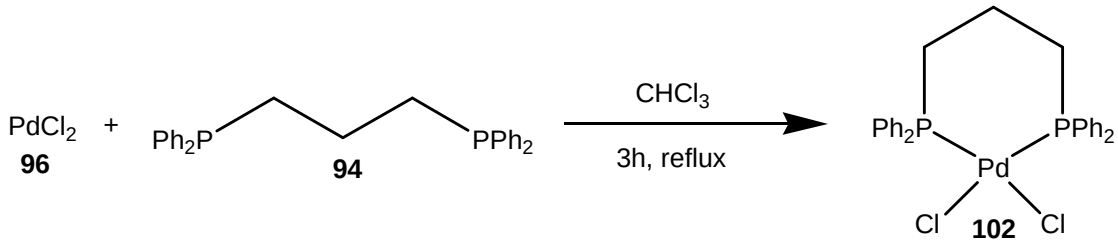

This Synthesis was performed in an argon atmosphere. 500.00 mg (2.81960 mmol) palladium(II) chloride **96** and 1280.00 mg (3.10348 mmol, 1.1 eq.) 1,3-bis(diphenylphosphino)propane **94** were suspended in 140 mL of dry chloroform. The suspension was refluxed and stirred for three hours. After this, 280 mL of *n*-hexane were added to the hot solution and the resulting precipitate was immediately filtered using a glass filter. The solid was washed with 100 mL of *n*-hexane. In order to isolate the

product from palladium(II) chloride **96** which did not react, the solid mixture in the glass filter was washed with 180 mL of dichloromethane. The dichloromethane was removed and the product was dried under vacuum. 1213.92 mg (2.05829 mmol, 73 % c.y.) of a yellow powder (**102**) were obtained.

$C_{27}H_{26}Cl_2P_2Pd$ 589.77 g/mol

^{1}H NMR (400 MHz, chloroform-d_1) δ = 7.79 (m, 8 H, $CH_{o\text{-phenyl}}$); 7.47 (m, 4 H, $CH_{p\text{-phenyl}}$); 7.40 (m, 8 H, $CH_{m\text{-phenyl}}$); 2.39 (m, 4 H, $PC\underline{H}_2$); 2.05 (m, 2 H, $PCH_2C\underline{H}_2CH_2P$) ppm.

^{31}P NMR (162 MHz, chloroform- d_1) δ = 11.85 ppm.

(1,3-bis(diphenylphosphino)propane)palladium(II) trifluoromethanesulfonate **27**

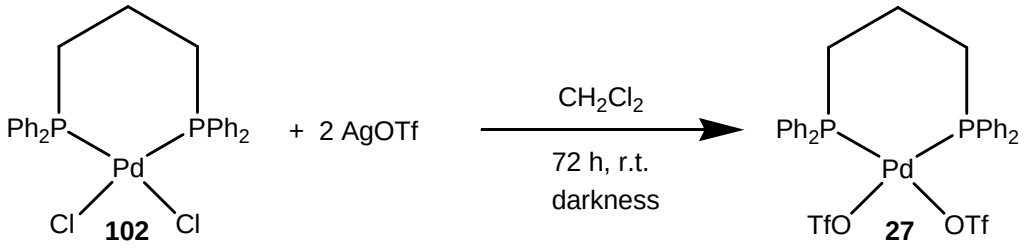

This Synthesis was performed in an argon atmosphere. 500 mg (0.84779 mmol) (1,3-bis(diphenylphosphino)propane)palladium(II) chloride **102** were mixed with 1742.65 mg (6.78232 mmol, 8 eq.) silver(I) trifluoromethanesulfonate. The mixture was suspended in 20 mL of dry dichloromethane and stirred in darkness at room temperature for 72 h. Afterwards, the suspension was filtered with a glass filter and the filtrate was reduced to a volume of 5 mL. 30 mL of diethyl ether were mixed with the filtrate and the suspension was cooled in the fridge for four hours. The precipitate was isolated by filtration with a glass filter, washed with 30 mL of diethyl ether and the product was dried in vacuum. 581.82 mg (0.71214 mmol, 84 % c.y.) of a light yellow powder (**27**) were obtained.

$C_{29}H_{26}F_6O_6P_2PdS_2$ 817.00 g/mol

^{1}H NMR (400 MHz, DMSO-d_6, 295 K): δ = 7.72 (m, 8 H, $H_{o\text{-phenyl}}$); 7.62 (m, 4 H, $H_{p\text{-phenyl}}$); 7.53 (m, 8 H, $H_{m\text{-phenyl}}$); 2.83 (m, 4 H, PCH_2); 1.87 (m, 2 H, $^3J_{PH}$ = 24.05 Hz, PCH_2CH_2) ppm.

^{31}P NMR (162 MHz, DMSO-d_6, 295 K): δ = 17.84 (s, P_{dppp}) ppm.

(1,3-bis(diphenylphosphino)propane)platinum(II) chloride **103**

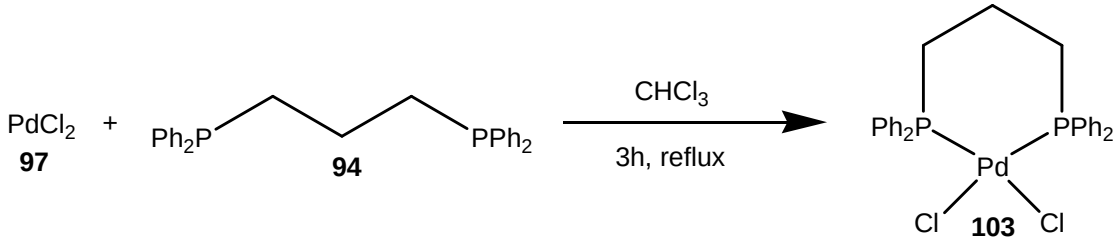

This Synthesis was performed in an argon atmosphere. 500.00 mg (1.87984 mmol) platinum(II) chloride **97** and 775.00 mg (1.87984 mmol, 1.1 eq.) 1,3-bis(diphenylphosphino)propane **94** were suspended in 140 mL of dry chloroform. The suspension was refluxed and stirred for three hours. After this, 280 mL of *n*-hexane were added to the hot solution and the resulting precipitate was immediately filtered using a glass filter. The solid was washed with 100 mL of *n*-hexane. In order to isolate the product from palladium(II) chloride **97** which did not react, the solid mixture in the glass filter was washed with 180 mL of dichloromethane. The dichloromethane was removed and the product was dried under vacuum. 916.94 mg (1.35156 mmol, 72 % c.y.) of a white powder (**103**) were obtained.

$C_{27}H_{26}Cl_2P_2Pt$ 678.43 g/mol

^{1}H NMR (400 MHz, DMSO-d_6) δ = 7.78 (m, 8 H, $CH_{o\text{-phenyl}}$); 7.49 (m, 12 H, $CH_{p\text{-phenyl}}$ and $CH_{m\text{-phenyl}}$); 2.78 (m, 4 H, $PC\underline{H}_2$); 1.74 (m, 2 H, $^{3}J_{P\text{-}H}$ = 22.98 Hz, $PCH_2C\underline{H}_2CH_2P$) ppm.

^{31}P NMR (162 MHz, DMSO-d_6, 293 K): δ = -3.42 (s, $^{1}J_{Pt\text{-}P}$ = 3405.76 Hz, P_{dppp}) ppm.

(1,3-bis(diphenylphosphino)propane)platinum(II) trifluoromethanesulfonate **43**

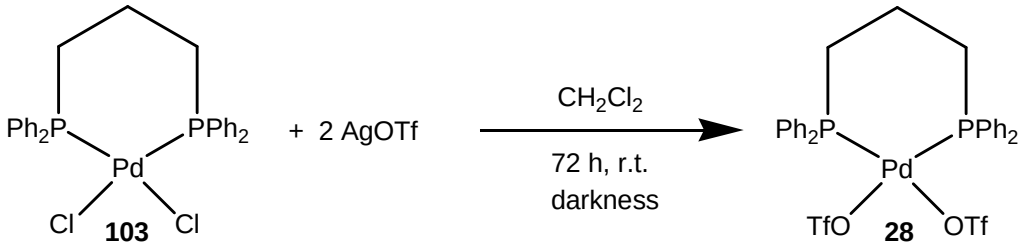

This Synthesis was performed in an argon atmosphere. 500 mg (0.73700 mmol) (1,3-bis(diphenylphosphino)propane)platinum(II) chloride **103** were mixed with 1514.92 mg (5.89600 mmol, 8 eq.) silver(I) trifluoromethanesulfonate. The mixture was suspended in 20 mL of dry dichloromethane and stirred in darkness at room temperature for 72 h. Afterwards, the suspension was filtered with a glass filter and the filtrate was reduced to a volume of 5 mL. 30 mL of diethyl ether were mixed with the filtrate and the suspension was cooled in the fridge for four hours. The precipitate was isolated by filtration with a glass filter, washed with 30 mL of diethyl ether and the product was dried in vacuum. 520.63 mg (0.57486 mmol, 78 % c.y.) of a white powder (**28**) were obtained.

$C_{29}H_{26}F_6O_6P_2PtS_2$ 905.66 g/mol

^{1}H NMR (400 MHz, DMSO-d_6, 293 K): δ = 7.75 (m, 8 H, $H_{dppp\text{-}phenyl}$); 7.61 (m, 4 H, $H_{dppp\text{-}phenyl}$); 7.54 (m, 8 H, $H_{dppp\text{-}phenyl}$); 2.94 (m, 4 H, $PC\underline{H}_2$); 1.81 (m, 2 H, $^{3}J_{P\text{-}H}$ = 24.74 Hz, $PCH_2C\underline{H}_2$) ppm.

^{31}P NMR (162 MHz, DMSO-d_6, 293 K): δ = -9.07 (s, $^{1}J_{Pt\text{-}P}$ = 3678.10 Hz, P_{dppp}) ppm.

8.5 Self-Assembly of Metallo-Supramolecular Complexes

8.5.1 Self-Assembly of M_2L_2 Complexes and their Catenanes

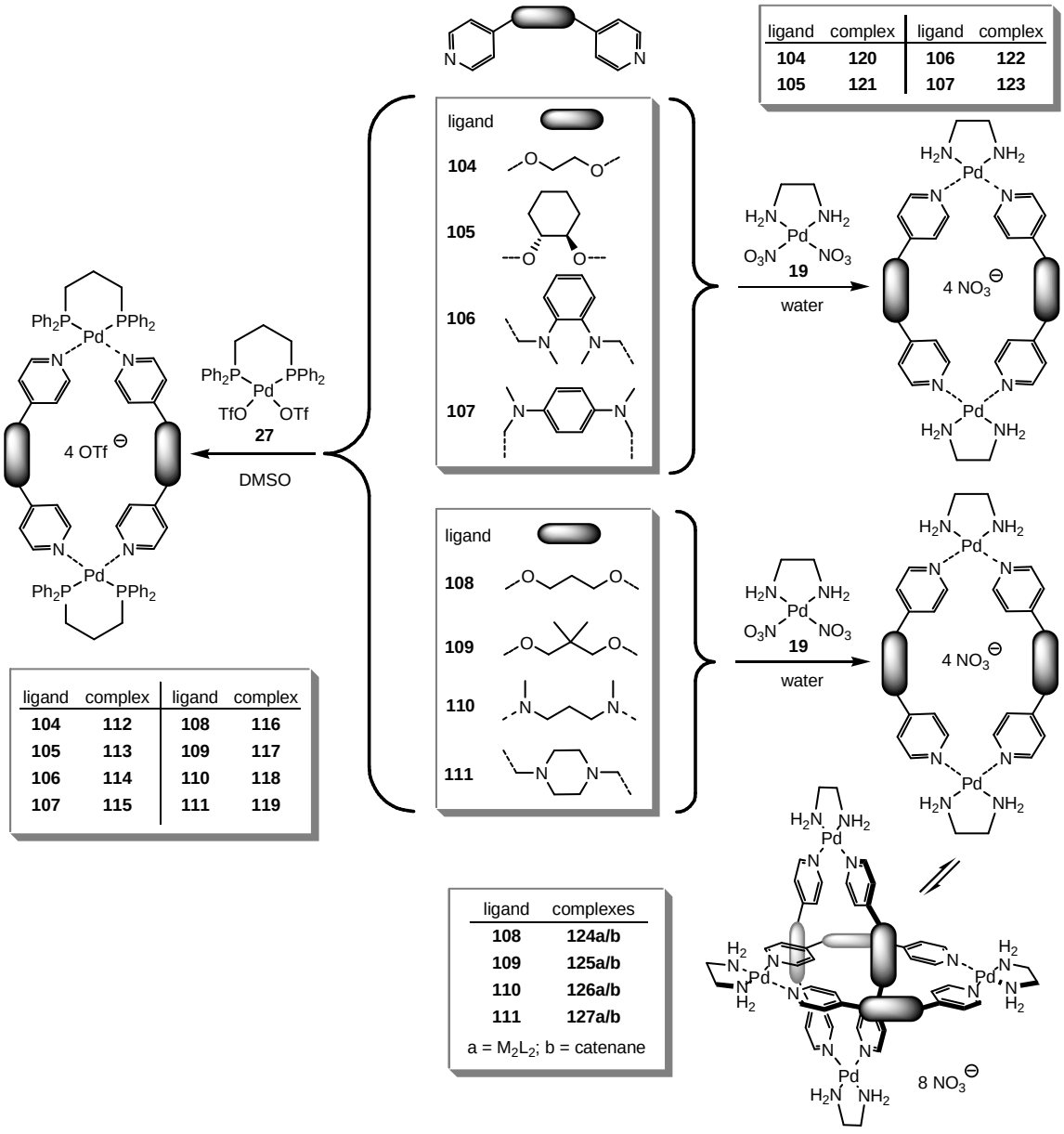

ligand	complex	ligand	complex
104	**120**	**106**	**122**
105	**121**	**107**	**123**

ligand	complex	ligand	complex
104	**112**	**108**	**116**
105	**113**	**109**	**117**
106	**114**	**110**	**118**
107	**115**	**111**	**119**

ligand	complexes
108	**124a/b**
109	**125a/b**
110	**126a/b**
111	**127a/b**

a = M_2L_2; b = catenane

M_2L_2 complexes with (dppp)Pd(OTf)$_2$ **112-119**

General Self-Assembly Procedure:

3 mg (0.00367 mmol) of (dppp)Pd(OTf)$_2$ **27** were mixed with an equimolar amount of ligands **104-111**. These mixtures were dissolved in DMSO or DMSO-d_6 and stirred for one day at room temperature. The solutions were then used to examine the systems under study.

M_2L_2 complex [((dppp)Pd)$_2$(**104**)$_2$](OTf)$_4$ **112**

Building blocks:

3.00 mg (0.00367 mmol)	(1,3-bis(diphenylphosphino)propane)palladium(II) trifluoro-methanesulfonate **27**
0.80 mg (0.00367 mmol)	1,2-bis(pyridin-4-yloxy)ethane **104**

$C_{82}H_{76}F_{12}N_4O_{16}P_4Pd_2S_4$ 2066.47 g/mol

^{1}H NMR (DMSO-d_6, 250 MHz, 303 K): δ = 8.35 (d, 8 H, $^3J_{HH}$ = 5.83 Hz, $H_{o\text{-pyridine}}$); 7.70-7.30 (m, 40 H, $H_{dppp\text{-phenyl}}$); 6.66 (d, 8 H, $^3J_{HH}$ = 4.93 Hz, $H_{m\text{-pyridine}}$); 4.18 (s, 8 H, $OCH_{2\ ligand}$); 3.09 (br., 8 H, PCH_2); 2.00 (m, $^3J_{P\text{-}H}$ = 24.18 Hz 4 H, $PCH_2C\underline{H}_2$) ppm.

^{31}P NMR (DMSO-d_6, 202 MHz, 303 K): δ = 9.05 (s, P_{dppp}) ppm.

ESI MS (ESI$^+$, DMSO/MeCN): *m/z* = 367 ([1:1:0]$^{2+}$); 475 ([1:2:0]$^{2+}$); 540 ([2:2:1]$^+$); 667 ([1:0:1]$^+$); 776 ([2:1:2]$^{2+}$); 883 ([2:2:2]$^{2+}$ and [1:1:1]$^+$); 1917 ([2:2:3]$^+$).

M_2L_2 complex [((dppp)Pd)$_2$(**105**)$_2$](OTf)$_4$ **113**

Building blocks:

3.00 mg (0.00367 mmol)	(1,3-bis(diphenylphosphino)propane)palladium(II) trifluoro-methanesulfonate **27**
0.99 mg (0.00367 mmol)	*trans*-1,2-di(pyridine-4-yloxy)cyclohexane **105**

$C_{90}H_{88}F_{12}N_4O_{16}P_4Pd_2S_4$ 2174.65g/mol

^{1}H NMR (400 MHz, DMSO-d_6, 293 K): δ = 8.28 (br, $H_{o\text{-pyridine}}$); 7.60-7.30 (m, $H_{dppp\text{-phenyl}}$); 6.90 (br, $H_{m\text{-pyridine}}$); 6.33 (br, $H_{m\text{-pyridine}}$); 4.46 (m, Py-OC<u>H</u>CH$_2$); 3.09 (m, PCH$_2$); 1.98 (m, $^3J_{PH}$ = 26.44 Hz, PCH$_2$C<u>H$_2$</u>); 1.83 (m, Py-OCHC<u>H$_2$</u>); 1.71 (m, Py-OCHC<u>H$_2$</u>); 1.32 (m, Py-OCHCH$_2$C<u>H$_2$</u>) ppm.

^{31}P NMR (162 MHz, DMSO-d_6, 293 K): δ = 9.21 (s, P_{dppp}) ppm.

ESI MS (ESI$^+$, DMSO/MeCN) *m/z* = 529 ([1:2:0]$^{2+}$); 576 ([2:2:0]$^{3+}$); 667 ([1:0:1]$^+$); 937 ([1:1:1]$^+$ and [2:2:2]$^{2+}$); 2025 ([2:2:3]$^+$ and [4:4:6]$^{2+}$).

M_2L_2 complex [((dppp)Pd)$_2$(**106**)$_2$](OTf)$_4$ **114**

Building blocks:

3.00 mg (0.00367 mmol)	(1,3-bis(diphenylphosphino)propane)palladium(II) trifluoro-methanesulfonate **27**
1.17 mg (0.00367 mmol)	*N*,*N*´-(1,2-phenylene-bis-(methylene))bis(*N*-methylpyridine-4-amine) **106**

$C_{98}H_{96}F_{12}N_8O_{12}P_4Pd_2S_4$ 2270.83 g/mol

^{1}H NMR (DMSO-d_6, 250 MHz, 303 K): δ = 7.98 (d, $^3J_{HH}$ = 4.57 Hz, $H_{o\text{-pyridine}}$); 7.90-7.20 (m, $H_{dppp\text{-phenyl}}$); 6.97 (br, H_{phenyl}); 6.50 (br, H_{phenyl}); 6.31 (d, $^3J_{HH}$

= 6.28 Hz, $H_{m\text{-pyridine}}$); 4.38 (br, CH_2); 4.21 (br, CH_2); 3.07 (m, PCH_2); 2.89 (s, CH_3); 2.61 (s, CH_3); 1.94 (m, $^3J_{PH}$ = 25.75 Hz, $PCH_2C\underline{H_2}$) ppm.

^{31}P NMR (DMSO-d_6, 202 MHz, 303 K): δ = 8.93 (s, P_{dppp}) ppm.

ESI MS (ESI^+, DMSO/MeCN): *m/z* = 419 ($[1:1:0]^{2+}$); 577 ($[1:2:0]^{2+}$); 607 ($[2:2:1]^{3+}$); 986 ($[1:1:1]^+$ and $[2:2:2]^{2+}$); 2121 ($[2:2:3]^+$).

$\underline{M_2L_2}$ complex $[((dppp)Pd)_2(\mathbf{107})_2](OTf)_4$ **115**

Building blocks:

3.00 mg (0.00367 mmol)	(1,3-bis(diphenylphosphino)propane)palladium(II) trifluoro-methanesulfonate **27**
1.17 mg (0.00367 mmol)	*N,N´*-(1,4-phenylene-bis(methylene))-bis(*N*-methyl-pyridine-4-amine) **107**

$C_{98}H_{96}F_{12}N_8O_{12}P_4Pd_2S_4$ 2270.83 g/mol

^{1}H NMR (DMSO-d_6, 250 MHz, 303 K): δ = 7.98 (d, $^3J_{HH}$ = 4.58 Hz, $H_{o\text{-pyridine}}$); 7.58 (m, $H_{dppp\text{-phenyl}}$); 7.50-7.20 (m, $H_{dppp\text{-phenyl}}$); 6.97 (s, H_{phenyl}); 6.03 (br, $H_{m\text{-pyridine}}$); 4.44 (br, NCH_2); 3.03 (m, PCH_2); 2.84 (br, CH_3); 2.76 (br, CH_3); 1.93 (m, $^3J_{PH}$ = 24.96 Hz, $PCH_2C\underline{H_2}$) ppm.

^{31}P NMR (DMSO-d_6, 202 MHz, 303 K): δ = 9.89 (s, P_{dppp}) ppm.

ESI MS (ESI^+, DMSO/MeCN): *m/z* = 418 ($[1:1:0]^{2+}$); 607 ($[2:2:1]^{3+}$); 985 ($[1:1:1]^+$ and $[2:2:2]^{2+}$).

$\underline{M_2L_2}$ complex $[((dppp)Pd)_2(\mathbf{108})_2](OTf)_4$ **116**

Building blocks:

3.00 mg (0.00367 mmol)	(1,3-bis(diphenylphosphino)propane)palladium(II) trifluoro-methanesulfonate **27**
0.85 mg (0.00367 mmol)	4-(3-(pyridine-4-yloxy)propoxy)pyridine **105**

$C_{84}H_{80}F_{12}N_4O_{16}P_4Pd_2S_4$ 2094.53 g/mol

^{1}H NMR (DMSO-d_6, 250 MHz, 303 K): δ = 8.36 (d, 8 H, $^3J_{HH}$ = 6.15 Hz, $H_{o\text{-pyridine}}$); 7.70-7.30 (m, 40 H, $H_{dppp\text{-phenyl}}$); 6.64 (d, 8 H, $^3J_{HH}$ = 6.65 Hz, $H_{m\text{-pyridine}}$); 3.83 (br., 8 H, $OCH_{2\ ligand}$); 3.09 (br., 8 H, PCH_2); 2.2-1.8 (m, 8 H, $OCH_2C\underline{H}_{2\ ligand}$ and $PCH_2C\underline{H}_2$) ppm.

^{31}P NMR (DMSO-d_6, 202 MHz, 303 K): δ = 9.21 (s, P_{dppp}) ppm.

ESI MS (ESI^+, DMSO/MeCN): *m/z* = 489 ($[1:2:0]^{2+}$); 667 ($[1:0:1]^+$); 897 ($[2:2:2]^{2+}$ and $[1:1:1]^+$).

$\underline{M_2L_2}$ complex $[((dppp)Pd)_2(\mathbf{109})_2](OTf)_4$ **117**

Building blocks:

3.00 mg (0.00367 mmol)	(1,3-bis(diphenylphosphino)propane)palladium(II) trifluoro-methanesulfonate **27**
0.95 mg (0.00367 mmol)	1,3-di(pyridine-4-yloxy)-2,2-di(methyl)propene **117**

$C_{88}H_{88}F_{12}N_4O_{16}P_4Pd_2S_4$ 2150.63 g/mol

^{1}H NMR (400 MHz, DMSO-d_6, 293 K): δ = 8.34 (d, 8 H, $^3J_{HH}$ = 6.00 Hz, $H_{o\text{-pyridine}}$); 7.57 (m, 16 H, $H_{dppp\text{-phenyl}}$); 7.46 (m, 8 H, $H_{dppp\text{-phenyl}}$); 7.36 (m, 16 H, $H_{dppp\text{-phenyl}}$); 6.64 (d, 8 H, $^3J_{HH}$ = 5.89 Hz, $H_{m\text{-pyridine}}$); 3.52 (s, 8 H, Py-OCH_2); 3.08 (m, 8 H, PCH_2); (m, 4 H, $^3J_{PH}$ = 24.61 Hz, $PCH_2C\underline{H}_2$); 0.96 (s, 12 H, CH_3) ppm.

^{31}P NMR (162 MHz, DMSO-d_6, 293 K): δ = 9.23 (s, P_{dppp}) ppm.

ESI MS (ESI^+, DMSO/MeCN): *m/z* = 388 ($[1:1:0]^{2+}$); 517 ($[1:2:0]^{2+}$); 568 ($[2:2:1]^{3+}$); 667 ($[1:0:1]^+$); 925 ($[1:1:1]^+$ and $[2:2:2]^{2+}$); 2001 ($[2:2:2]^+$).

M_2L_2 complex $[((dppp)Pd)_2(\mathbf{110})_2](OTf)_4$ **118**

Building blocks:

3.00 mg (0.00367 mmol)	(1,3-bis(diphenylphosphino)propane)palladium(II) trifluoro-methanesulfonate **27**
0.94 mg (0.00367 mmol)	*N*,*N*´-dimethyl-*N*,*N*´-di(pyridine-4-yl)propane-1,3-diamine **110**

$C_{88}H_{92}F_{12}N_8O_{12}P_4Pd_2S_4$ 2146.69 g/mol

^{1}H NMR ($DMSO$-d_6, 250 MHz, 303 K): δ = 7.94 (d, 8 H, $^3J_{HH}$ = 5.67 Hz, $H_{o\text{-pyridine}}$); 7.70-7.30 (m, 40 H, $H_{dppp\text{-phenyl}}$); 6.24 (br., 8 H, $H_{m\text{-pyridine}}$); 3.07 (br., 8 H, PCH_2); 2.76 (s, 12 H, CH_3); 1.95 (t, $^3J_{P\text{-}H}$ = 22.67 Hz 4 H, $PCH_2C\underline{H_2}$) ppm.

^{31}P NMR ($DMSO$-d_6, 202 MHz, 303 K): δ = 9.00 (s, P_{dppp}) ppm.

ESI MS (ESI^+, DMSO/MeCN): *m/z* = 515 ($[1:2:0]^{2+}$); 566 ($[2:2:1]^{3+}$); 924 ($[1:1:1]^+$ and $[2:2:2]^{2+}$); 1997 ($[2:2:3]^+$ and $[4:4:6]^{2+}$).

M_2L_2 complex $[((dppp)Pd)_2(\mathbf{111})_2](OTf)_4$ **119**

Building blocks:

3.00 mg (0.00367 mmol)	(1,3-bis(diphenylphosphino)propane)palladium(II) trifluoro-methanesulfonate **27**
0.98 mg (0.00367 mmol)	1,4-bis(pyridine-4-ylmethyl)piperazine **111**

$C_{90}H_{92}F_{12}N_8O_{12}P_4Pd_2S_4$ 2170.72 g/mol

^{1}H NMR ($DMSO$-d_6, 400 MHz, 293 K): δ = 8.53 (br, $H_{o\text{-pyridine}}$); 7.60-7.30 (m, $H_{dppp\text{-phenyl}}$); 7.05 (br, $H_{m\text{-pyridine}}$); 3.25 (br, Py-$C\underline{H_2}$N); 3.11 (m, PCH_2); 2.01 (m, N $C\underline{H_2}C\underline{H_2}$N and $PCH_2C\underline{H_2}$) ppm.

^{31}P NMR ($DMSO$-d_6, 162 MHz, 303 K): δ = 8.88 (s, P_{dppp}) ppm.

ESI MS (ESI$^+$, DMSO/MeCN): *m/z* = 394 ([1:1:0]$^{2+}$); 574 ([2:2:1]$^{3+}$); 667 ([1:0:1]$^+$); 935 ([1:1:1]$^+$ and [2:2:2]$^{2+}$).

M_2L_2 Complexes with (en)Pd(NO_3)$_2$ and the corresponding M_4L_4 Catenanes

General Self-Assembly Procedure:

2.00 mg (0.00344 mmol) of (en)Pd(NO_3)$_2$ **19** were mixed with an equimolar amount of ligands **104-111**. These mixtures were dissolved in water or deuterated water and stirred for one day at room temperature. The solutions were then used to examine the systems under study.

M_2L_2 complex [((en)Pd)$_2$(**104**)$_2$](NO_3)$_4$ **120**

Building blocks:

2.00 mg (0.00688 mmol) (ethylenediamine)palladium(II) nitrate **19**

1.49 mg (0.00688 mmol) 1,2-bis(pyridin-4-yloxy)ethane **104**

$C_{28}H_{40}N_{12}O_{16}Pd_2$ 1013.53 g/mol

^{1}H NMR (400 MHz, D_2O, 293 K): δ = 8.41 (d, 8 H, $^3J_{HH}$ = 7.04 Hz, $H_{o\text{-pyridine}}$); 7.01 (d, 8 H, $^3J_{HH}$ = 7.08 Hz, $H_{m\text{-pyridine}}$); 4.51 (s, 4 H, OC$\underline{H}_2$); 2.83 (s, 4 H, $NH_2C\underline{H}_2$) ppm.

ESI MS (ESI$^+$, water/acetone): *m/z* = 444 ([1:1:1]$^+$); 597 ([(2:1:3) – HNO_3]$^+$); 736 ([2:1:3]$^+$); 844 ([4:3:6]$^{2+}$); 952 ([2:2:3]$^+$ and [4:4:6]$^{2+}$); 1097 ([5:4:8]$^{2+}$); 1218 ([8:7:13]$^{3+}$); 1289 ([8:8:13]$^{3+}$).

M_2L_2 complex $[((en)Pd)_2(\mathbf{1105})_2](NO_3)_4$ **121**

Building blocks:

2.00 mg (0.00688 mmol) (ethylenediamine)palladium(II) nitrate **19**

1.86 mg (0.00688 mmol) *trans*-1,2-di(pyridine-4-yloxy)cyclohexane **105**

$C_{36}H_{52}N_{12}O_{16}Pd_2$ 1121.71 g/mol

Without further experiments, the peaks in the ^{1}H NMR spectrum of system **105** cannot be assigned to the different isomeric species in solution. Thus the peaks are just assigned to their corresponding hydrogen atoms of the building blocks.

^{1}H NMR (400 MHz, D_2O, 293 K): δ = 8.28 (d, $^3J_{HH}$ = 7.12 Hz, $H_{o\text{-pyridine}}$); 8.14 (d, $^3J_{HH}$ = 7.12 Hz, $H_{o\text{-pyridine}}$); 7.00 (d, $^3J_{HH}$ = 7.19 Hz, $H_{m\text{-pyridine}}$); 6.90 (d, $^3J_{HH}$ = 7.20 Hz, $H_{m\text{-pyridine}}$); ca. 4.80 ($OC\underline{H}CH_2$, superimposed by the solvent peak); 2.84 (s, $NH_2C\underline{H}_2$); 2.81 (s, $NH_2C\underline{H}_2$); 2.18 (m, $H_{cyclohexyl}$); 1.81 (m, $H_{cyclohexyl}$); 1.60 (m, $H_{cyclohexyl}$); 1.42 (m, $H_{cyclohexyl}$) ppm.

ESI MS (ESI^+, water/MeCN): *m/z* = 498 ($[1:1:1]^+$); 790 ($[2:1:3]^+$); 924 ($[4:3:6]^{2+}$); 1060 ($[2:2:3]^+$ and $[4:4:6]^{2+}$ and $[6:6:9]^{3+}$).

M_2L_2 complex $[((en)Pd)_2(\mathbf{106})_2](NO_3)_4$ **122**

Building blocks:

2.00 mg (0.00688 mmol) (ethylenediamine)palladium(II) nitrate **19**

2.19 mg (0.00688 mmol) *N*,*N*´-(1,2-phenylene-bis-(methylene))bis(*N*-methylpyridine-4-amine) **106**

$C_{44}H_{60}N_{16}O_{12}Pd_2$ 1217.89 g/mol

^{1}H NMR (400 MHz, D_2O, 295 K): δ = 7.98 (d, 8 H, $^3J_{HH}$ = 6.84 Hz, $H_{o\text{-pyridine}}$); 7.26 (dd, 4 H, $^3J_{HH}$ = 5.54 Hz, $^4J_{HH}$ = 3.38 Hz, H_{phenyl}); 7.04 (dd, 4 H, $^3J_{HH}$ = 5.24 Hz, $^4J_{HH}$ = 3.64 Hz, H_{phenyl}); 6.63 (d, 8 H, $^3J_{HH}$ = 6.52 Hz, $H_{m\text{-pyridine}}$); 4.47 (s, 8 H, CH_2); 2.96 (s, 12 H, NCH_3); 2.71 (s, 8 H, $NH_2C\underline{H_2}$) ppm.

ESI MS (ESI$^+$, water/MeCN): *m/z* = 485 ((1:1:1) – $HNO_3]^+$); 546 ([1:1:1]$^+$ and [2:2:2]$^{2+}$); 851 ([3:3:4]$^{2+}$); 864 ([1:2:1]$^+$); 1156 ([2:2:3]$^+$ and [4:4:6]$^{2+}$).

$\underline{M_2L_2}$ complex $[((en)Pd)_2(\underline{\mathbf{107}})_2](NO_3)_4$ **123**

Building blocks:

2.00 mg (0.00688 mmol) (ethylenediamine)palladium(II) nitrate **19**

2.19 mg (0.00688 mmol) *N*,*N*´-(1,4-phenylene-bis(methylene))-bis(*N*-methyl-pyridine-4-amine) **123**

$C_{44}H_{60}N_{16}O_{12}Pd_2$ 1217.89 g/mol

^{1}H NMR (400 MHz, D_2O, 295 K): δ = 7.93 (d, 8 H, $^3J_{HH}$ = 6.44 Hz, $H_{o\text{-pyridine}}$); 7.16 (s, 8 H, H_{phenyl}); 6.69 (d, 8 H, $^3J_{HH}$ = 6.72 Hz, $H_{m\text{-pyridine}}$); 4.62 (s, 8 H, CH_2); 3.05 (s, 12 H, NCH_3); 2.71 (s, 8 H, $NH_2C\underline{H_2}$) ppm.

ESI MS (ESI$^+$, water/MeCN): *m/z* = 485 ((1:1:1) – $HNO_3]^+$); 546 ([1:1:1]$^+$ and [2:2:2]$^{2+}$); 1156 ([2:2:3]$^+$ and [4:4:6]$^{2+}$).

$\underline{M_2L_2}$ complex $[((en)Pd)_2(\underline{\mathbf{108}})_2](NO_3)_4$ **124a** and catenane $[((en)Pd)_4(\underline{\mathbf{108}})_4](NO_3)_8$ **124b**

Building blocks:

2.00 mg (0.00688 mmol) (ethylenediamine)palladium(II) nitrate **19**

1.58 mg (0.00334 mmol) 1,3-bis(pyridin-4-yloxy)propane **108**

$C_{29}H_{42}N_{12}O_{16}Pd_2$ 1027.55 g/mol (M_2L_2)

$C_{58}H_{84}N_{24}O_{32}Pd_4$ 2055.11 g/mol (catenane)

^{1}H NMR (400 MHz, D_2O, 293 K): δ = 8.55 (d, $^3J_{HH}$ = 6.72 Hz, $H_{o\text{-pyridine}}$ (M_4L_4 catenane)); 8.48 (d, $^3J_{HH}$ = 6.76 Hz, $H_{o\text{-pyridine}}$ (M_4L_4 catenane)); 8.24 (d, $^3J_{HH}$ = 6.72 Hz, $H_{o\text{-pyridine}}$ (M_2L_2)); 6.89 (m, $H_{m\text{-pyridine}}$ (M_4L_4 catenane)); 6.84 (d, $^3J_{HH}$ = 6.96 Hz, $H_{m\text{-pyridine}}$ (M_2L_2)); 5.75 (d, $^3J_{HH}$ = 6.64 Hz, $H_{m\text{-pyridine}}$ (M_4L_4 catenane)); 4.09 (t, $^3J_{HH}$ = 5.23 Hz, OCH_2 (M_2L_2)); 3.93 (t, $^3J_{HH}$ = 5.02 Hz, OCH_2 (M_4L_4 catenane)); 2.75 (m, OCH_2 (M_4L_4 catenane)); 2.69 (s, $NH_2C\underline{H_2}$); 2.12 (m, $OCH_2C\underline{H_2}$ (M_4L_4 catenane) and $OCH_2C\underline{H_2}$ (M_2L_2)) ppm.

ESI MS (ESI^+, water/acetone): *m/z* = 460 ($[1:1:1]^+$); 750 ($[2:1:3]^+$); 865 ($[4:3:6]^{2+}$); 980 ($[2:2:3]^+$ and $[4:4:6]^{2+}$); 1174 ($[8:6:13]^{3+}$); 1250 ($[8:7:13]^{3+}$); 1328 ($[8:8:13]^{3+}$); 1501 ($[12:12:20]^{4+}$).

M_2L_2 complex $[((en)Pd)_2(\mathbf{109})_2](NO_3)_4$ **125a** and catenane $[((en)Pd)_4(\mathbf{109})_4](NO_3)_8$ **125b**

Building blocks:

2.00 mg (0.00688 mmol) (ethylenediamine)palladium(II) nitrate **19**

1.78 mg (0.00688 mmol) 1,3-di(pyridine-4-yloxy)-2,2-di(methyl)propene **109**

$C_{34}H_{52}N_{12}O_{16}Pd_2$ 1097.69 g/mol (M_2L_2)

$C_{68}H_{104}N_{24}O_{32}Pd_4$ 2195.37 g/mol (catenane)

^{1}H NMR (400 MHz, D_2O, 293 K): δ = 8.64 (d, $^3J_{HH}$ = 6.44 Hz, $H_{o\text{-pyridine}}$ (M_4L_4 catenane)); 8.56 (br, $H_{o\text{-pyridine}}$ (M_4L_4 catenane)); 8.35 (d, $^3J_{HH}$ = 6.84 Hz, $H_{o\text{-pyridine}}$ (M_2L_2)); 6.96 (d, $^3J_{HH}$ = 6.92 Hz, $H_{m\text{-pyridine}}$ (M_2L_2)); 6.92 (br, $H_{m\text{-pyridine}}$ (M_4L_4 catenane)); 5.55 (br, $H_{m\text{-pyridine}}$ (M_4L_4 catenane)); 3.94 (s, OCH_2 (M_2L_2)); 3.78 (s, OCH_2 (M_4L_4 catenane)); 2.87 (s, $NH_2C\underline{H_2}$ (M_4L_4 catenane)); 2.81 (s, $NH_2C\underline{H_2}$ (M_2L_2)); 1.08 (s, CH_3 (M_2L_2)); 1.00 (s, CH_3, (M_4L_4 catenane)); 0.96 (s, CH_3, (M_4L_4 catenane)) ppm.

ESI MS (ESI$^+$, water/acetone): *m/z* = 425 ((1:1:1) – HNO_3]$^+$); 488 ([1:1:1]$^+$); 1036 ([2:2:3]$^+$ and [4:4:6]$^{2+}$).

M_2L_2 complex [((en)Pd)$_2$(**110**)$_2$](NO_3)$_4$ **126a** and catenane [((en)Pd)$_4$(**110**)$_4$](NO_3)$_8$ **126b**

Building blocks:

2.00 mg (0.00688 mmol) (ethylenediamine)palladium(II) nitrate **19**

1.76 mg (0.00688 mmol) *N*,*N*´-dimethyl-*N*,*N*´-di(pyridine-4-yl)propane-1,3-diamine **110**

$C_{34}H_{56}N_{16}O_{12}Pd_2$ 1093.75 g/mol (M_2L_2)

$C_{68}H_{112}N_{32}O_{24}Pd_4$ 2187.50 g/mol (catenane)

^{1}H NMR (400 MHz, D_2O, 293 K): δ = 8.02 (d, $^3J_{HH}$ = 6.72 Hz, $H_{o\text{-pyridine}}$ (M_4L_4 catenane)); 7.98 (d, $^3J_{HH}$ = 6.49 Hz, $H_{o\text{-pyridine}}$ (M_4L_4 catenane)); 7.94 (d, $^3J_{HH}$ = 6.37 Hz, $H_{o\text{-pyridine}}$ (M_2L_2)); 6.48 (d, $^3J_{HH}$ = 6.37 Hz, $H_{m\text{-pyridine}}$ (M_2L_2)); 6.38 (d, $^3J_{HH}$ = 6.14 Hz, $H_{m\text{-pyridine}}$ (M_4L_4 catenane)); 3.26 (m, NC$\underline{H_2}$$CH_2$ (M_2L_2)); 3.09 (m, NC$\underline{H_2}$$CH_2$ (M_4L_4 catenane)); 2.85-2.58 (m, CH_3 (M_4L_4 catenane) and CH_3 (M_2L_2) and PdNC$\underline{H_2}$ (M_4L_4 catenane) and PdNC$\underline{H_2}$ (M_2L_2)); 1.68 (m, $NCH_2C\underline{H_2}$ (M_2L_2)); 1.47 (m, $NCH_2C\underline{H_2}$ (M_4L_4 catenane)) ppm.

ESI MS (ESI$^+$, water/MeCN): *m/z* = 423 ([(1:1:1) – HNO_3]$^+$); 484 ([1:1:1]$^+$ and [2:2:2]$^{2+}$); 713 ([(2:1:3) – HNO_3]$^+$); 757 ([3:3:4]$^{2+}$);1032 ([2:2:3]$^+$ and [4:4:6]$^{2+}$ and [6:6:9]$^{3+}$).

M_2L_2 complex $[((en)Pd)_2(\mathbf{111})_2](NO_3)_4$ **127a** and catenane $[((en)Pd)_4(\mathbf{111})_4](NO_3)_8$ **127b**

Building blocks:

2.00 mg (0.00688 mmol) (ethylenediamine)palladium(II) nitrate **19**

1.85 mg (0.00688 mmol) 1,4-bis(pyridine-4-ylmethyl)piperazine **111**

$C_{346}H_{56}N_{16}O_{12}Pd_2$ 1117.77 g/mol (M_2L_2)

$C_{72}H_{112}N_{32}O_{24}Pd_4$ 2235.54 g/mol (catenane)

^{1}H NMR (400 MHz, D_2O, 293 K): δ = 8.75 (d, $^3J_{HH}$ = 6.40 Hz, $H_{o\text{-pyridine}}$ (M_4L_4 catenane)); 8.59 (d, $^3J_{HH}$ = 6.60 Hz, $H_{o\text{-pyridine}}$ (M_4L_4 catenane)); 8.53 (d, $^3J_{HH}$ = 6.60 Hz, $H_{o\text{-pyridine}}$ (M_2L_2)); 7.43 (d, $^3J_{HH}$ = 6.73 Hz, $H_{m\text{-pyridine}}$ (M_4L_4 catenane)); 7.36 (d, $^3J_{HH}$ = 6.60 Hz, $H_{o\text{-pyridine}}$ (M_4L_4 catenane) and $H_{o\text{-pyridine}}$ (M_2L_2)); 4.11 (s, Py-C$\underline{H_2}$N (M_4L_4 catenane)); 3.75 (m, NC$\underline{H_2}$C$\underline{H_2}$N (M_4L_4 catenane)); 3.51 (s, Py-C$\underline{H_2}$N (M_4L_4 catenane)); 3.49 (s, Py-C$\underline{H_2}$N (M_2L_2); 2.71 (s, $NH_2C\underline{H_2}$); 2.70-1.90 (br, m, NC$\underline{H_2}$C$\underline{H_2}$N (M_4L_4 catenane) and NC$\underline{H_2}$C$\underline{H_2}$N (M_2L_2) ppm.

ESI MS (ESI^+, water/acetone): m/z = 435 ((1:1:1) – $HNO_3]^+$); 498 ($[1:1:1]^+$); 787 ($[2:1:3]^+$); 921 ($[4:3:6]^{2+}$); 1055 ($[2:2:3]^+$ and $[4:4:6]^{2+}$).

8.5.2 Self-Assembly Metallo-Supramolecular Triangles and Squares

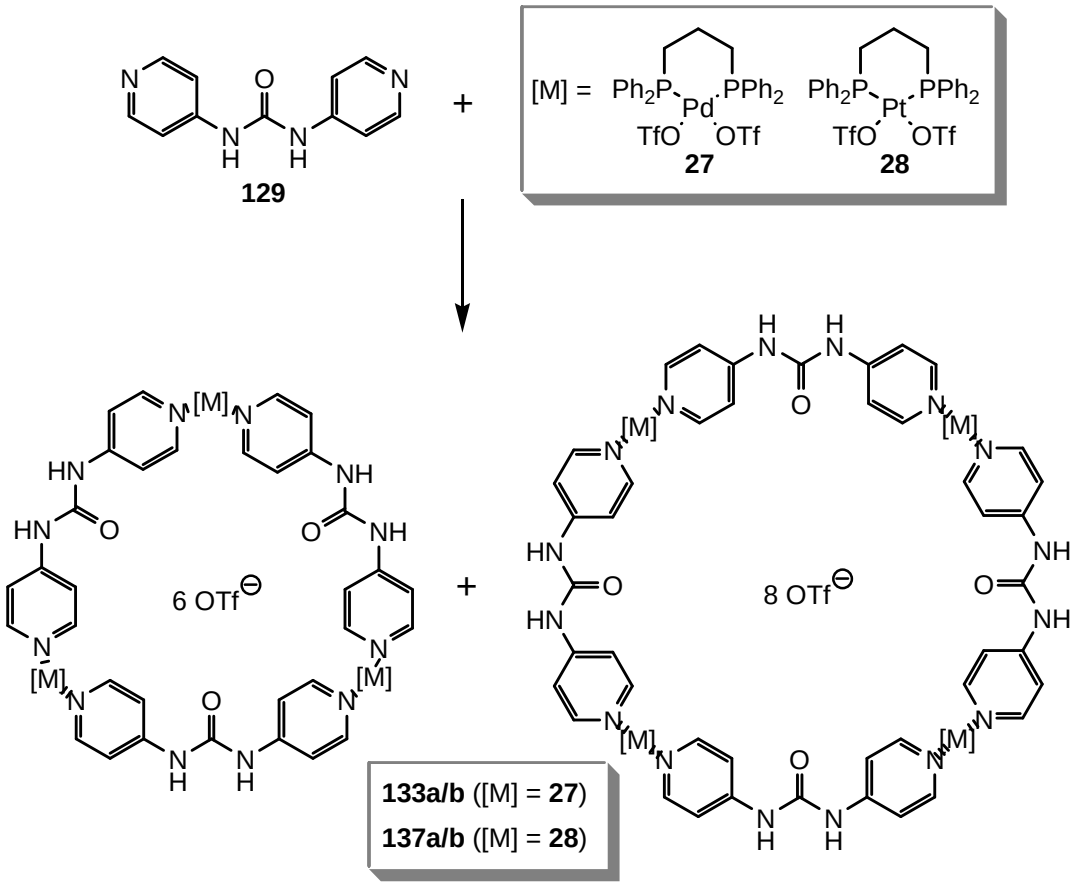

Self-Assembly Procedure[106]

5.00 mg (0.047 mmol) 1,3-di(pyridin-4yl)urea **129** were combined with equimolar amounts of (dppp)Pd(OTf)$_2$ or (dppp)Pt(OTf)$_2$, respectively. The mixtures were dissolved in DMSO, DMSO-d$_6$, DMF or DMF-d$_7$, respectively, and stirred fo 24 hours at room temperature. Afterwards the samples were used for NMR spectroscopic and mass spectrometric analyses.

triangle [((dppp)Pd)$_3$(**129**)$_3$](OTf)$_6$ **133a** and Square [((dppp)Pd)$_4$(**129**)$_4$](OTf)$_8$ **133b**

Building blocks:

5.00 mg (0.047 mmol) 1,3-di(pyridin-4yl)urea **129**

38.11 mg (0.047 mmol) (1,3-bis(diphenylphosphino)propane)palladium(II) trifluoromethanesulfonate **27**

$C_{120}H_{108}F_{18}N_{12}O_{21}P_6S_6Pd_3$ 3093.7 gmol^{-1} (triangle)
$C_{150}H_{144}F_{24}N_{16}O_{28}P_8S_8Pd_4$ 4004.8 gmol^{-1} (square)

^{1}H NMR (500 MHz, DMF-d_7, 298 K): δ = 9.67 (br, NH (square)); 9.41 (br, NH (triangle); 8.59 (s, $H_{o\text{-py}}$ (square)); 8.54 (s, $H_{o\text{-py}}$ (triangle)); 7.79 (m, $H_{dppp\text{-phenyl}}$); 7.51 (m, $H_{dppp\text{-phenyl}}$); 7.44 (m, $H_{dppp\text{-phenyl}}$); 7.23 (m, $H_{m\text{-py}}$); 3.29 (m, $PC\underline{H}_2$); 2.21 (m, $PCH_2C\underline{H}_2CH_2P$) ppm.

^{31}P NMR (202 MHz, DMF-d_7, 298 K): δ = 9.50 (s, P_{dppp} (square)); 9.82 (s, P_{dppp} (triangle)) ppm.

ESI MS (ESI$^+$, acetone) *m/z* = 2944 ([3:3:5]$^+$); 1913 ([4:4:6]$^{2+}$); 1398 ([3:3:4]$^{2+}$); 822 ([3:3:3]$^{3+}$).

<u>triangle [((dppp)Pt)$_3$(**129**)$_3$](OTf)$_6$ **137a** and square [((dppp)Pt)$_4$(**129**)$_4$](OTf)$_8$ **137b**</u>

5.00 mg (0.047 mmol) 1,3-di(pyridin-4yl)urea **129**
42.27 mg (0.047 mmol) (1,3-bis(diphenylphosphino)propane)platin(II) trifluoromethanesulfonate **28**

$C_{120}H_{108}F_{18}N_{12}O_{21}P_6S_6Pt_3$ 3359.6 gmol^{-1} (triangle)
$C_{150}H_{144}F_{24}N_{16}O_{28}P_8S_8Pt_4$ 4359.4 gmol^{-1} (square)

^{1}H-NMR (500 MHz, DMSO-d_6, 298 K): δ = 9.66 (s, NH (square)); 9.53 (s, NH (triangle)); 8.35 (d, $^3J_{HH}$ = 5.65 Hz, $H_{o\text{-py}}$ (square)); 8.32 (d, $^3J_{HH}$ = 6.26 Hz, $H_{o\text{-py}}$ (triangle)); 7.64 (m, $H_{dppp\text{-phenyl}}$); 7.46 (m, $H_{dppp\text{-phenyl}}$); 7.38 (m, $H_{dppp\text{-phenyl}}$); 7.09 (m, $H_{m\text{-py}}$); 3.20 (m, $PC\underline{H}_2$); 1.98 (m, $PCH_2C\underline{H}_2CH_2P$) ppm.

^{31}P NMR (202 MHz, DMSO-d_6, 298 K): δ = - 12.04 (s, $^3J_{Pt\text{-}P}$ = 3030 Hz, P_{dppp} (square)); - 11.81 (s, $^3J_{Pt\text{-}P}$ = 3030 Hz, P_{dppp} (triangle)) ppm.

ESI MS (ESI^+, acetone) *m/z* = 3210 ($[3:3:5]^+$ and $[6:6:10]^{2+}$); 2090 ($[2:2:3]^+$, $[4:4:6]^{2+}$ and $[6:6:9]^{3+}$); 1530 ($[3:3:4]^{2+}$ and $[6:6:8]^{4+}$); 1344 ($[4:4:5]^{3+}$); 971 ($[3:3:3]^{3+}$).

8.5.3 Self-Assembly of Small Metallo-Supramlecular Cages

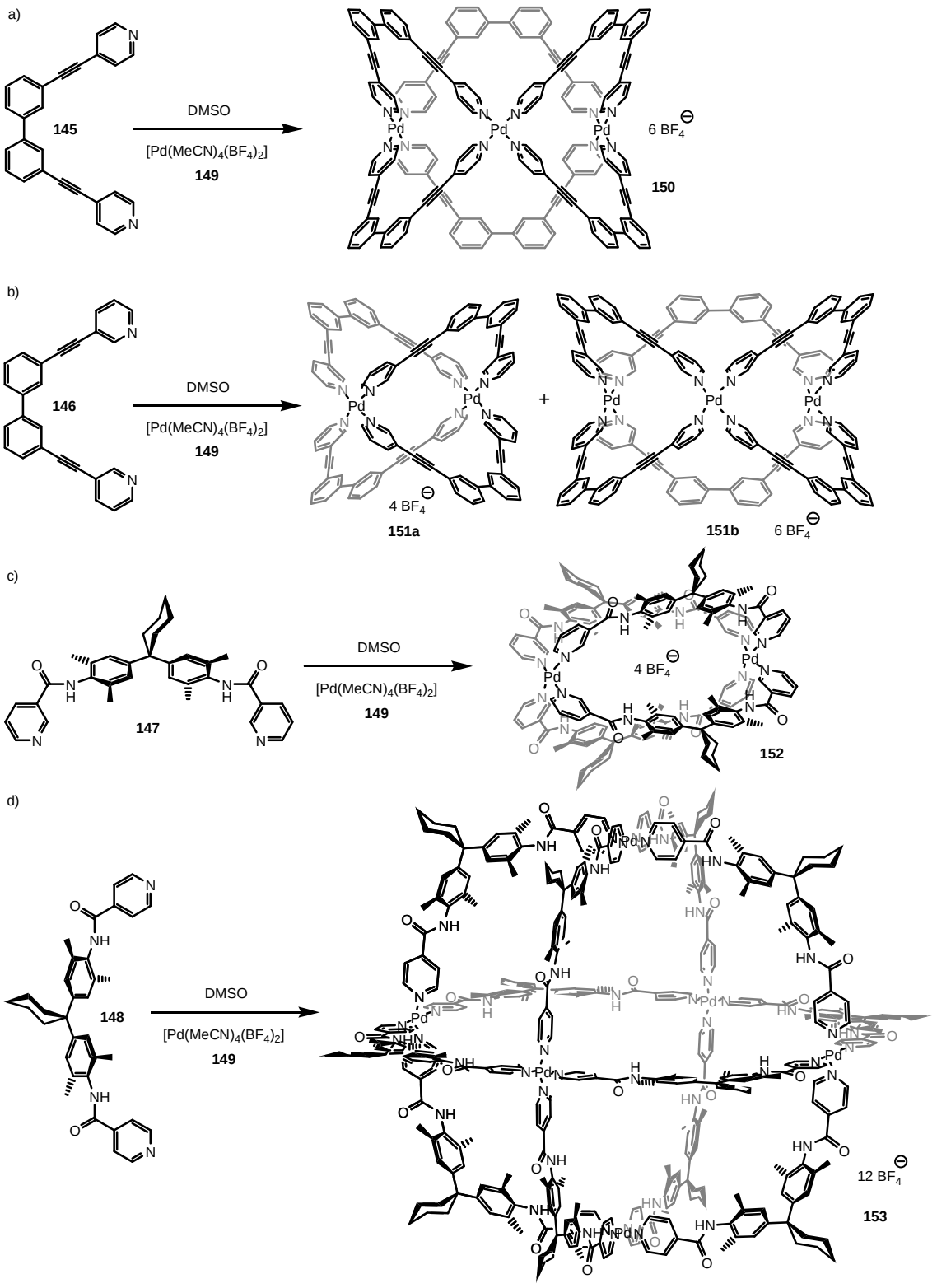

General Self-Assembly Procedure:

2.00 mg (0.0045 mmol) tetrakis(acetonitrilo)palladium(II) tetrafluoroborate **149** was mixed with two equivalents of the ligands **145-148** and dissolved in 0.6 mL of DMF, DMSO, DMF-d_7 or DMSO-d_7, respectively. These solutions were stirred for 15 min at room temperature and afterwards characterized with NMR spectroscopy and ESI mass spectrometry.

M_2L_4 complex $[Pd_2(\mathbf{145})_4](BF_4)_4$ **150**

Building blocks:

2.00 mg (0.00450 mmol) tetrakis(acetonitrilo)palladium(II) tetrafluoroborate **149**

4.80 mg (0.00900 mmol) 3,3'-bis(pyridin-4-ylethynyl)biphenyl **145**

$C_{156}H_{96}B_6F_{24}N_{12}Pd_3$ 2978.6 g/mol (M_3L_6)

^{1}H NMR (500 MHz, DMF-d_7, 298 K): δ = 9.17 (*AA´XX´*, $^3J_{HH}$ = 6.68 Hz, $H_{o\text{-pyridine}}$); 8.10 (s, $H_{\delta\text{-biaryl}}$); 7.98 (m, $^3J_{HH}$ = 6.68 Hz, $H_{\alpha\text{-biaryl}}$); 7.95 (*AA´XX´*, $^3J_{HH}$ = 6.76 Hz, $H_{m\text{-pyridine}}$); 7.61 (m, br., $H_{\beta\text{-biaryl}}$ and $H_{\gamma\text{-biaryl}}$) ppm.

ESI MS (ESI^+, DMSO/MeCN): *m/z* = 906 ($[1:2:1]^+$ and $[3:6:3]^{3+}$); 1402 ($[3:6:2]^{2+}$).

M_2L_4 complex $[Pd_2(\mathbf{146})_4](BF_4)_4$ **151a** and M_3L_6 complex $[Pd_3(\mathbf{146})_6](BF_4)_6$ **151b**

Building blocks:

2.00 mg (0.00450 mmol) tetrakis(acetonitrilo)palladium(II) tetrafluoroborate **149**

4.80 mg (0.00900 mmol) 3,3'-bis(pyridin-3-ylethynyl)biphenyl **146**

$C_{104}H_{64}B_4F_{16}N_8Pd_2$ 1985.73 g/mol (M_2L_4)

$C_{156}H_{96}B_6F_{24}N_{12}Pd_3$ 2978.6 g/mol (M_3L_6)

^{1}H NMR (400 MHz,DMSO-d_6, 298 K): δ = 9.61 (s, $H_{o\text{-pyridine}}$ (M_3L_6)); 9.59 (s, $H_{o\text{-pyridine}}$ (M_2L_4)); 9.27 (d, $^3J_{HH}$ = 4.06 Hz, $H_{o\text{-pyridine}}$ (M_3L_6)); 9.18 (d, $^3J_{HH}$ = 6.13 Hz, $H_{o\text{-pyridine}}$ (M_2L_4)); 8.27 (d, $^3J_{HH}$ = 7.66 Hz, $H_{p\text{-pyridine}}$ (M_2L_4 and M_3L_6)); 7.94 (s, $H_{\delta\text{-biaryl}}$ (M_3L_6)); 7.86-7.78 (m, $H_{m\text{-pyridine}}$ (M_2L_4 and M_3L_6) and $H_{\delta\text{-biaryl}}$ (M_2L_4) and $H_{\alpha\text{-biaryl}}$ (M_3L_6)); 7.68 (d, $^3J_{HH}$ = 7.63 Hz, $H_{\alpha\text{-biaryl}}$ (M_2L_4)); 7.65 (d, $^3J_{HH}$ = 7.42 Hz, $H_{\gamma\text{-biaryl}}$ (M_3L_6)); 7.58 (d, $^3J_{HH}$ = 7.35 Hz, $H_{\gamma\text{-biaryl}}$ (M_2L_4)); 7.49 (t, $^3J_{HH}$ = 7.84 Hz, $H_{\beta\text{-biaryl}}$ (M_3L_6)); 7.21 (t, $^3J_{HH}$ = 7.66 Hz, $H_{\beta\text{-biaryl}}$ (M_2L_4)) ppm.

ESI MS (ESI^+, DMSO/MeCN): *m/z* = 410 ($[2:4:0]^{4+}$ and $[3:6:0]^{6+}$); 422 ($[(3:6:0)DMSO]^{6+}$); 428 ($[(2:4:0)DMSO]^{4+}$); 509 ($[3:6:1]^{5+}$); 575 ($[2:4:1]^{3+}$); 601 ($[(2:4:1)DMSO]^{3+}$); 658 ($[3:6:2]^{4+}$); 883 ($[(3:6:3) – BF_3]^{3+}$); 906 ($[2:4:2]^{2+}$ and $[3:6:3]^{2+}$); 1402 ($[3:6:2]^{2+}$); 1899 ($[2:4:3]^{+}$).

M_2L_4 complex $[Pd_2(\mathbf{147})_4](BF_4)_4$ **152**

Building blocks:

2.00 mg (0.00450 mmol)	tetrakis(acetonitrilo)palladium(II) tetrafluoroborate **149**
4.80 mg (0.00900 mmol)	*N*,*N'*-(4,4'-(cyclohexane-1,1-diyl)-bis-(2,6-dimethyl-4,1-phenylene)) diisonicotinamide **147**

$C_{136}H_{144}B_4F_{16}N_{16}O_8Pd_2$ 8072.28 g/mol (M_2L_4)

^{1}H NMR (400 MHz, DMSO-d_6, 294 K): δ = 10.03 (d, $^4J_{HH}$ = 1.39 Hz, $H_{o\text{-pyridine}}$); 9.94 (s, NH); 9.52 (d, $^3J_{HH}$ = 5.68 Hz, $H_{o\text{-pyridine}}$); 8.59 (d, $^3J_{HH}$ = 8.00 Hz, $H_{p\text{-pyridine}}$); 7.90 (dd, $^3J_{HH}$ = 7.80 Hz, $^3J_{HH}$ = 5.91 Hz, $H_{m\text{-pyridine}}$); 7.14 (s, H_{phenyl}); 2.24 (m, CCH_2); 2.07 (s, CH_3); 1.43 (m, $CCH_2C\underline{H_2}$ and $CCH_2CH_2C\underline{H_2}$) ppm.

ESI MS (ESI^+, DMSO/MeCN): *m/z* = 586 ($[2:4:0]^{4+}$); 719 ($[2:5:0]^{4+}$); 810 ($[2:4:1]^{3+}$); 988 ($[2:5:1]^{3+}$); 1258 ($[2:4:2]^{2+}$).

M_6L_{12} complex $[Pd_6(\mathbf{148})_{12}](BF_4)_{12}$ **153**

Building blocks:

2.00 mg (0.00450 mmol)	tetrakis(acetonitrilo)palladium(II) tetrafluoroborate **149**
4.80 mg (0.00900 mmol)	*N*,*N*'-(4,4'-(cyclohexane-1,1-diyl)-bis-(2,6-dimethyl-4,1-phenylene)) dinicotinamide **148**

$C_{408}H_{432}B_{12}F_{48}N_{48}O_{24}Pd_6$ 8072.28 g/mol (M_6L_{12})

^{1}H NMR (400 MHz, DMSO-d_6, 294 K): δ = 10.00 (br, NH); 9.41 (*AA´-XX´*, $^3J_{HH}$ = 4.87 Hz, $H_{o\text{-pyridine}}$); 8.13 (*AA´-XX´*, $^3J_{HH}$ = 4.76 Hz, $H_{m\text{-pyridine}}$); 7.09 (br, H_{phenyl}); 2.25 (m, CCH_2); 2.02 (s, CH_3); 1.48 (m, $CCH_2C\underline{H_2}$ and $CCH_2CH_2C\underline{H_2}$) ppm.

ESI-MS (ESI^+, DMSO/MeCN): *m/z* = 533 ($[(0:1:0)+H]^+$) 585 ($[1:2:0]^{2+}$); 851 ($[1:3:0]^{2+}$); 922 ($[6:12:4]^{8+}$); 989 ($[6:13:4]^{3+}$); 1066 ($[6:12:5]^{7+}$); 1143 ($[6:13:5]^{7+}$); 1258 ($[6:12:6]^{6+}$).

8.5.4 Self-Assembly of M_2L_2 and M_3L_3 Complexes Based on Urea Ligands

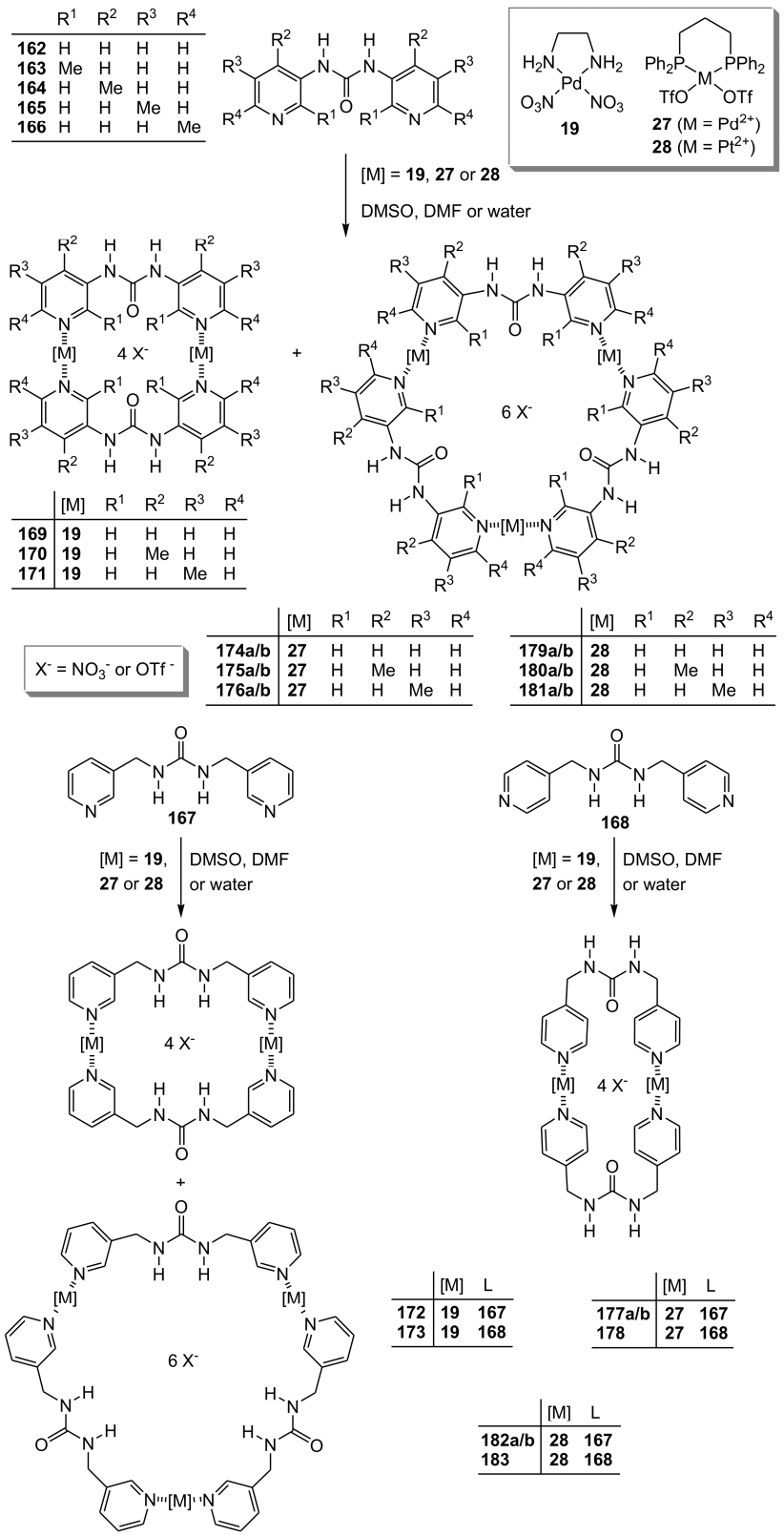

	R^1	R^2	R^3	R^4
162	H	H	H	H
163	Me	H	H	H
164	H	Me	H	H
165	H	H	Me	H
166	H	H	H	Me

	[M]	R^1	R^2	R^3	R^4
169	**19**	H	H	H	H
170	**19**	H	Me	H	H
171	**19**	H	H	Me	H

	[M]	R^1	R^2	R^3	R^4
174a/b	**27**	H	H	H	H
175a/b	**27**	H	Me	H	H
176a/b	**27**	H	H	Me	H

	[M]	R^1	R^2	R^3	R^4
179a/b	**28**	H	H	H	H
180a/b	**28**	H	Me	H	H
181a/b	**28**	H	H	Me	H

	[M]	L
172	**19**	**167**
173	**19**	**168**

	[M]	L
177a/b	**27**	**167**
178	**27**	**168**

	[M]	L
182a/b	**28**	**167**
183	**28**	**168**

M_2L_2 complexes **169-173** with (en)Pd(NO_3)$_2$

General Self-Assembly Procedure:

2 mg of the ligands **162-168** were mixed with an equimolar amount of (en)Pd(NO_3)$_2$ **19**. These mixtures were dissolved in H_2O, D_2O, DMSO or DMSO-d_6 and stirred for one day at room temperature. The solutions were then used to examine the systems under study.

No discrete complexes were observed using ligands **163** and **166** and an appropriate characterization of these mixtures was not possible.

M_2L_2 complex [((en)Pd)$_2$(**162**)$_2$](NO_3)$_4$ **169**

Building blocks:

2.71 mg (0.00934 mmol) (ethylenediamine)palladium(II) nitrate **19**

2.00 mg (0.00934 mmol) 1,3-di(pyridin-3-yl)urea **162**

$C_{26}H_{36}N_{16}O_{14}Pd_2$ 1008.07 g/mol (M_2L_2)

^{1}H NMR: (DMSO-d_6, 400 MHz, 298 K): δ = 9.82 (s, 4 H, $H_{o\text{-pyridine}}$); 9.61 (s, 4 H, NH_{urea}); 8.61 (dd, $^3J_{HH}$ = 4.76 Hz, $^4J_{HH}$ = 1.76 Hz, 4 H, $H_{o\text{-pyridine}}$); 7.58 (m, 8 H, $H_{m\text{-pyridine}}$ and $H_{p\text{-pyridine}}$); 5.59 (s, 8 H, NH_2); 2.69 (s, 8 H, CH_2) ppm.

ESI MS: (ESI$^+$, DMSO/acetonitrile): *m/z* = 948 ([2:2:3]$^+$); 443 ([2:2:2]$^{2+}$).

M_2L_2 complex [((en)Pd)$_2$(**164**)$_2$](NO_3)$_4$ **170**

Building blocks:

2.40 mg (0.00825 mmol) (ethylenediamine)palladium(II) nitrate **19**

2.00 mg (0.00825 mmol) 1,3-bis(4-methylpyridin-3-yl)urea **164**

$C_{30}H_{44}N_{16}O_{14}Pd_2$ 1064.13 g/mol (M_2L_2)

^{1}H NMR: (DMSO-d_6, 400 MHz, 298 K): δ = 9.58 (s, $H_{o\text{-pyridine}}$); 8.92 (s, NH_{urea}); 8.48 (d, $^3J_{HH}$ = 5.70 Hz, $H_{o\text{-pyridine}}$); 7. (d, $^3J_{HH}$ = 5.83 Hz, $H_{m\text{-pyridine}}$); 5.57 (s, NH_2); 2.89 (s, CH_2); 2.33 (s, CH_3) ppm.

ESI MS: (ESI^+, DMSO/acetonitrile): *m/z* = 1004 ($[2:2:3]^+$ and $[4:4:6]^{2+}$); 972 ($[(4:4:6) – HNO_3]^{2+}$); 472 ($[2:2:2]^{2+}$).

M_2L_2 complex $[((en)Pd)_2(\mathbf{165})_2](NO_3)_4$ **171**

Building blocks:

2.40 mg (0.00825 mmol) (ethylenediamine)palladium(II) nitrate **19**

2.00 mg (0.00825 mmol) 1,3-bis(5-methylpyridin-3-yl)urea **165**

$C_{30}H_{44}N_{16}O_{14}Pd_2$ 1064.13 g/mol (M_2L_2)

^{1}H NMR: (DMSO-d_6, 250 MHz, 303 K): δ = 9.65 (d, $^4J_{HH}$ = 2.03 Hz, $H_{o\text{-pyridine}}$); 9.53 (s, NH_{urea}); 8.49 (d, $^4J_{HH}$ = 1.03 Hz, $H_{o\text{-pyridine}}$); 7.36 (m, $H_{p\text{-pyridine}}$); 5.55 (br, NH_2); 2.68 (br, CH_2); 2.31 (s, CH_3) ppm.

ESI MS: (ESI^+, DMSO/acetonitrile): *m/z* = 1004 ($[2:2:3]^+$ and $[4:4:6]^{2+}$); 972 ($[(4:4:6) – HNO_3]^{2+}$); 941 ($[(4:4:6) – 2\ HNO_3]^{2+}$); 648 ($[4:4:5]^{3+}$); 472 ($[1:1:1]^+$ and $[2:2:2]^{2+}$).

M_2L_2 complex $[((en)Pd)_2(\mathbf{167})_2](NO_3)_4$ **172**

Building blocks:

2.40 mg (0.00825 mmol) (ethylenediamine)palladium(II) nitrate **19**

2.00 mg (0.00825 mmol) 1,3-bis((pyridin-3-yl)methyl)urea **167**

$C_{30}H_{44}N_{16}O_{14}Pd_2$ 1064.13 g/mol (M_2L_2)

^{1}H NMR: (DMSO-d_7, 500 MHz, 298 K): δ = 8.65 (d, $^3J_{HH}$ = 5.35 Hz, $H_{o\text{-pyridine}}$); 8.56 (s, $H_{o\text{-pyridine}}$); 7.86 (d, $^3J_{HH}$ = 7.70 Hz, $H_{p\text{-pyridine}}$); 7.86 (dd, $^3J_{HH}$ = 7.80 Hz, $^3J_{HH}$ = 5.60 Hz, $H_{m\text{-pyridine}}$); (t, $^3J_{HH}$ = 6.05 Hz, NH_{urea}); 5.58 (s, NH_2); 4.19 (d, $^3J_{HH}$ = 5.75 Hz, $(CH_2)_{urea}$); 2.67 (s, $NH_2C\underline{H_2}$) ppm.

ESI MS: (ESI^+, DMSO/acetonitrile): *m/z* = 1004 ($[2:2:3]^+$); 761 ($[2:1:3]^+$); 472 ($[1:1:1]^+$ and $[2:2:2]^{2+}$).

$\underline{M_2L_2}$ complex $[((en)Pd)_2(\mathbf{168})_2](NO_3)_4$ **173**

Building blocks:

2.40 mg (0.00825 mmol) (ethylenediamine)palladium(II) nitrate **19**

2.00 mg (0.00825 mmol) 1,3-bis((pyridin-4-yl)methyl)urea **168**

$C_{30}H_{44}N_{16}O_{14}Pd_2$ 1064.13 g/mol (M_2L_2)

^{1}H NMR: (DMSO-d_7, 500 MHz, 298 K): δ = 8.77 (d, $^3J_{HH}$ = 6.10 Hz, $H_{o\text{-pyridine}}$); 7.42 (d, $^3J_{HH}$ = 5.99 Hz, $H_{m\text{-pyridine}}$); 6.90 (t, $^3J_{HH}$ = 5.97 Hz, NH_{urea}); 5.56 (s, NH_2); 4.29 (d, $^3J_{HH}$ = 5.36 Hz, $(CH_2)_{urea}$); 2.67 (s, $NH_2C\underline{H_2}$) ppm.

ESI MS: (ESI^+, DMSO/acetonitrile): *m/z* = 1004 ($[2:2:3]^+$ and $[4:4:6]^{2+}$); 882 ($[4:3:6]^{2+}$); 761 ($[2:1:3]^+$); 472 ($[1:1:1]^+$ and $[2:2:2]^{2+}$).

$\underline{M_2L_2}$ and $\underline{M_3L_3}$complexes **174a/b-183** with $(dppp)Pd(OTf)_2$ and $(dppp)Pt(OTf)_2$

General Self-Assembly Procedure:

2 mg of the ligands **162-168** were mixed with an equimolar amount of the metal centers or $(dppp)Pd(OTf)_2$ (**27**) or $(dppp)Pt(OTf)_2$ (**28**), respectively. These mixtures were dissolved in DMSO, DMSO-d_6, DMF or DMF-d_7 and stirred for one day at room temperature. The solutions were then used to examine the systems under study.

No discrete complexes were observed using ligands **163** and **166** and an appropriate characterization of these mixtures was not possible.

M_2L_2 [((dppp)Pd)$_2$(**162**)$_2$](OTf)$_4$ and M_3L_3 complex [((dppp)Pd)$_3$(**162**)$_3$](OTf)$_6$ **174a/b**

Building blocks:

7.63 mg (0.00934 mmol)	(1,3-bis(diphenylphosphino)propane)palladium(II) trifluoro-methanesulfonate **27**
2.00 mg (0.00934 mmol)	1,3-bis(pyridin-3-yl)urea **162**

$C_{80}H_{72}F_{12}N_8O_{14}P_4Pd_2S_4$ 2062.45 g/mol (M_2L_2)

$C_{120}H_{108}F_{18}N_{12}O_{21}P_6Pd_3S_6$ 3093.67 g/mol (M_3L_3)

^{1}H NMR: (DMF-d_7, 500 MHz, 273 K): δ = 9.81 (s, $H_{o\text{-pyridine}}$, M_2L_2); 9.43 (s, $H_{o\text{-pyridine}}$, M_3L_3); 9.17 (s, NH, M_2L_2); 9.11 (d, $^3J_{HH}$ = 4.68 Hz, $H_{o\text{-pyridine}}$, M_2L_2); 9.07 (d, $^3J_{HH}$ = 4.61 Hz, $H_{o\text{-pyridine}}$, M_3L_3); 8.68 (s, NH, M_3L_3); 8.53 (b, $H_{m\text{-pyridine}}$, M_2L_2); 8.22 (m, $H_{m\text{-pyridine}}$ (M_3L_3) and $H_{p\text{-pyridine}}$ (M_2L_2)); 7.15-8.26 (m, $H_{p\text{-pyridine}}$ (M_3L_3) and $H_{dppp\text{-phenyl}}$, M_2L_2 and M_3L_3); 3.28 (br., PCH_2); 1.72 (m, PCH_2CH_2) ppm.

^{31}P NMR: (DMF-d_7, 202 MHz, 303 K): δ = 9.77 (s, P_{dppp}, M_3L_3); 9.32 (s, P_{dppp}, M_2L_2) ppm.

ESI MS: (ESI$^+$, DMSO/acetonitrile): *m/z* = 1913 ($[2:2:3]^+$ and $[4:4:6]^{2+}$); 1226 ($[4:4:5]^{3+}$); 1095 ($[1:2:1]^+$); 882 ($[1:1:1]^+$ and $[2:2:2]^{2+}$).

M_2L_2 [((dppp)Pd)$_2$(**164**)$_2$](OTf)$_4$ and M_3L_3 complex [((dppp)Pd)$_3$(**164**)$_3$](OTf)$_6$ **175a/b**

Building blocks:

6.74 mg (0.00825 mmol)	(1,3-bis(diphenylphosphino)propane)palladium(II) trifluoro-methanesulfonate **27**

2.00 mg (0.00825 mmol) 1,3-bis(4-methylpyridin-3-yl)urea **164**

$C_{84}H_{80}F_{12}N_8O_{14}P_4Pd_2S_4$ 2116.62 g/mol (M_2L_2)
$C_{126}H_{84}F_{18}N_{12}O_{21}P_6Pd_3S_6$ 3141.55 g/mol (M_3L_3)

^{1}H NMR: (DMF-d_7, 500 MHz, 298 K): δ = 9.70 (s, $H_{o\text{-pyridine}}$, M_2L_2); 9.17 (s, $H_{o\text{-pyridine}}$, M_3L_3); 8.96 (s, NH, M_2L_2); 8.81 (br, $H_{o\text{-pyridine}}$ (M_2L_2) and NH (M_3L_3)); 8.63 (s $H_{o\text{-pyridine}}$, M_3L_3); 8.41(br, $H_{dppp\text{-phenyl}}$, M_2L_2); 7.93 (br, $H_{dppp\text{-phenyl}}$, M_3L_3); 7.84-7.27 (m, $H_{p\text{-pyridine}}$ (M_3L_3) and $H_{dppp\text{-phenyl}}$, M_2L_2 and M_3L_3); 7.03 (s, $H_{p\text{-pyridine}}$, M_2L_2); 3.32 (br., $PC\underline{H_2}$); 2.29 (m, $PCH_2C\underline{H_2}$); 2.17 (s, CH_3) ppm.

^{31}P NMR: (DMF-d_7, 202 MHz, 298 K): δ = 10.07 (s, P_{dppp}, M_3L_3); 9.67 (s, P_{dppp}, M_2L_2) ppm

ESI MS: (ESI^+, DMSO/acetonitrile): *m/z* = 1968 ($[2:2:3]^+$); 910 ($[1:1:1]^+$ and $[2:2:2]^{2+}$).

$\underline{M_2L_2}$ $\underline{[((dppp)Pd)_2(\mathbf{165})_2](OTf)_4}$ and $\underline{M_3L_3}$ complex $\underline{[((dppp)Pd)_3(\mathbf{165})_3](OTf)_6}$ **176a/b**

Building blocks:

6.74 mg (0.00825 mmol) (1,3-bis(diphenylphosphino)propane)palladium(II) trifluoro-methanesulfonate **27**

2.00 mg (0.00825 mmol) 1,3-bis(5-methylpyridin-3-yl)urea **165**

$C_{84}H_{80}F_{12}N_8O_{14}P_4Pd_2S_4$ 2116.62 g/mol (M_2L_2)
$C_{126}H_{84}F_{18}N_{12}O_{21}P_6Pd_3S_6$ 3141.55 g/mol (M_3L_3)

^{1}H NMR: (DMF-d_7, 500 MHz, 298 K): δ = 9.70 (s, $H_{o\text{-pyridine}}$, M_2L_2); 9.17 (s, $H_{o\text{-pyridine}}$, M_3L_3); 8.97 (s, $H_{o\text{-pyridine}}$, M_2L_2); 8.81 (m, NH (M_2L_2) and $H_{o\text{-pyridine}}$ (M_3L_3)); 8.63 (s, $H_{p\text{-pyridine}}$, M_3L_3); 8.41 (br., NH, M_3L_3); 8.00-7.30 (m,

$H_{dppp\text{-}phenyl}$); 7.03 (s, $H_{p\text{-}pyridine}$, M_2L_2); 3.40-3.20 (m, $PC\underline{H_2}$, M_2L_2 and M_3L_3); 2.42-1.92 (m, CH_3 and $PCH_2C\underline{H_2}$, M_2L_2 and M_3L_3) ppm.

^{31}P NMR: (DMF-d_7, 202 MHz, 298 K): δ = 10.07 (s, P_{dppp}, M_3L_3); 9.67 (s, P_{dppp}, M_2L_2) ppm.

ESI MS: (ESI^+, DMSO/acetonitrile): *m/z* = 910 ($[1:1:1]^+$ and $[2:2:2]^{2+}$); 667 ($[1:0:1]^+$); 557 ($[2:2:1]^{3+}$); 501 ($[1:2:0]^{2+}$).

$\underline{M_2L_2}$ $\underline{[((dppp)Pd)_2(\mathbf{167})_2](OTf)_4}$ and $\underline{M_3L_3}$ complex $\underline{[((dppp)Pd)_3(\mathbf{167})_3](OTf)_6}$ **177a/b**

Building blocks:

6.74 mg (0.00825 mmol) (1,3-bis(diphenylphosphino)propane)palladium(II) trifluoro-methanesulfonate **27**

2.00 mg (0.00825 mmol) 1,3-bis((pyridin-3-yl)methyl)urea **167**

$C_{84}H_{80}F_{12}N_8O_{14}P_4Pd_2S_4$ 2116.62 g/mol (M_2L_2)

$C_{126}H_{84}F_{18}N_{12}O_{21}P_6Pd_3S_6$ 3141.55 g/mol (M_3L_3)

^{1}H NMR: (DMF-d_7, 500 MHz, 273K): δ = 9.09 (br., $H_{o\text{-}pyridine}$); 8.53 (s, $H_{o\text{-}pyridine}$); 8.33 (br., $H_{dppp\text{-}phenyl}$); 8.00-7.15 (br., m, $H_{dppp\text{-}phenyl}$ and NH); 6.78 (br., $H_{m\text{-}pyridine}$); 4.12 (br.,NCH_2); 3.76 (br., NCH_2); 3.36 (PCH_2); 1.79 ($PCH_2C\underline{H_2}$) ppm.

^{31}P NMR: (DMF-d_7, 202 MHz, 233 K): δ = 10.71 (s, P_{dppp}, M_3L_3); 10.52 (s, P_{dppp}, M_2L_2) ppm.

ESI MS: (ESI^+, DMSO/acetonitrile): *m/z* = 910 ($[1:1:1]^+$ and $[2:2:2]^{2+}$); 667 ($[1:0:1]^+$); 557 ($[2:2:1]^{3+}$); 501 ($[1:2:0]^{2+}$); 380 ($[1:1:0]^{2+}$).

M_2L_2 [((dppp)Pd)$_2$(**168**)$_2$](OTf)$_4$ **178**

Building blocks:

6.74 mg (0.00825 mmol)	(1,3-bis(diphenylphosphino)propane)palladium(II) trifluoro-methanesulfonate **27**
2.00 mg (0.00825 mmol)	1,3-bis((pyridin-4-yl)methyl)urea **168**

$C_{84}H_{80}F_{12}N_8O_{14}P_4Pd_2S_4$ 2116.62 g/mol (M_2L_2)

^{1}H NMR: (DMF-d_7, 500 MHz, 303 K): δ = 8.81 (d, $^3J_{HH}$ = 4.85 Hz, $H_{o\text{-pyridine}}$); 7.77 (m, $H_{dppp\text{-phenyl}}$); 7.60 (m, $H_{dppp\text{-phenyl}}$); 7.50 (m, $H_{dppp\text{-phenyl}}$); 7.07 (d, $^3J_{HH}$ = 4.85 Hz, $H_{m\text{-pyridine}}$); 6.88 (m, NH); 4.18 (d, $^3J_{HH}$ = 5.50 Hz, CH_2); 3.37 (br., P$C\underline{H}_2$); 1.72 (m, $PCH_2C\underline{H}_2$) ppm.

^{31}P NMR: (DMF-d_7; 202 MHz; 303 K): δ = 9.16 (s, P_{dppp}) ppm.

ESI MS: (ESI^+, DMSO/acetonitrile): *m/z* = 910 ($[1:1:1]^+$ and $[2:2:2]^{2+}$); 667 ($[1:0:1]^+$); 557 ($[2:2:1]^{3+}$); 501 ($[1:2:0]^{2+}$); 380 ($[1:1:0]^{2+}$).

M_2L_2 [((dppp)Pt)$_2$(**162**)$_2$](OTf)$_4$ and M_3L_3 complex [((dppp)Pt)$_3$(**162**)$_3$](OTf)$_6$ **179a/b**

Building blocks:

8.46 mg (0.00934 mmol)	(1,3-bis(diphenylphosphino)propane)platinum(II) trifluoro-methanesulfonate **28**
2.00 mg (0.00934 mmol)	1,3-bis(pyridin-3-yl)urea **162**

$C_{80}H_{72}F_{12}N_8O_{14}P_4Pt_2S_4$ 2239.76 g/mol (M_2L_2)

$C_{120}H_{108}F_{18}N_{12}O_{21}P_6Pt_3S_6$ 3359.65 g/mol (M_3L_3)

^{1}H NMR: (DMF-d_7, 500 MHz, 298 K): δ = 9.71 (br, NH, M_2L_2); 9.38 (s, $H_{o\text{-pyridine}}$, M_3L_3); 9.18 (s, $H_{o\text{-pyridine}}$, M_2L_2); 9.13 (d, $^3J_{HH}$ = 4.89 Hz, $H_{o\text{-pyridine}}$, M_2L_2); 9.07 (d, $^3J_{HH}$ = 4.89 Hz, $H_{o\text{-pyridine}}$ M_3L_3); 8.72 (br, NH, M_3L_3); 8.54 (m,

$H_{dppp\text{-}phenyl}$, M_2L_2); 8.20 (m, $H_{dppp\text{-}phenyl}$, M_3L_3); 7.76-7.26 (m, $H_{dppp\text{-}phenyl}$ and $H_{m\text{-}pyridine}$ and $H_{p\text{-}pyridine}$, M_2L_2 and M_3L_3); 3.71 (m, PCH_2); 3.37 (m, PCH_2); 2.95 (m, PCH_2CH_2) ppm.

^{31}P NMR: (DMF-d_7, 202 MHz, 298K): δ = -15.81 (s, P_{dppp}, $^1J_{Pt\text{-}P}$ = 3000 Hz, M_3L_3); -16.13 (s, P_{dppp}, $^1J_{Pt\text{-}P}$ = 3000 Hz, M_3L_3) ppm.

ESI MS: (ESI^+, DMSO/acetonitrile): *m/z* = 2146 ($[2:2:3]^+$); 1381 ($[4:4:5]^{3+}$); 999 ($[2:2:2]^{2+}$).

M_2L_2 $[((dppp)Pt)_2$**(164)**$_2](OTf)_4$ and M_3L_3 complex $[((dppp)Pt)_3$**(164)**$_3](OTf)_6$ **180a/b**

Building blocks:

7.48 mg (0.00825 mmol)	(1,3-bis(diphenylphosphino)propane)platinum(II) trifluoro-methanesulfonate **28**
2.00 mg (0.00825 mmol)	1,3-bis(4-methylpyridin-3-yl)urea **164**

$C_{84}H_{80}F_{12}N_8O_{14}P_4Pt_2S_4$	2295.87 g/mol (M_2L_2)
$C_{126}H_{84}F_{18}N_{12}O_{21}P_6Pt_3S_6$	3407.52 g/mol (M_3L_3)

^{1}H NMR: (DMF-d_7, 500 MHz, 298 K): δ = 9.58 (s, $H_{o\text{-}pyridine}$, M_2L_2); 9.07 (d, $^3J_{HH}$ = 5.86 Hz, $H_{o\text{-}pyridine}$, M_3L_3); 9.02 (d, $^3J_{HH}$ = 4.65 Hz, $H_{o\text{-}pyridine}$, M_2L_2); 8.56 (s, NH, M_3L_3); 8.49 (m, $H_{dppp\text{-}phenyl}$, M_2L_2); 8.41 (br, NH, M_2L_2); 8.24 (m, $H_{dppp\text{-}phenyl}$, M_3L_3); 8.22 (br, $H_{o\text{-}pyridine}$, M_3L_3); 7.76-7.12 (m, $H_{dppp\text{-}phenyl}$ and $H_{m\text{-}pyridine}$, M_2L_2 and M_3L_3); 3.27 (m, PCH_2); 2.62 (m, PCH_2CH_2); 2.29 (s, CH_3, M_3L_3); 2.08 (s, CH_3, M_2L_2) ppm.

^{31}P NMR (DMF-d_7, 121 MHz, 298K): δ = -12.57 (s, P_{dppp}, $^1J_{Pt\text{-}P}$ = 3021 Hz, M_2L_2); -12.63 (s, P_{dppp}, $^1J_{Pt\text{-}P}$ = 3021 Hz, M_2L_2) ppm.

ESI MS: (ESI^+, DMSO/acetone): *m/z* = 2146 ($[2:2:3]^+$); 1381 ($[4:4:5]^{3+}$); 999 ($[2:2:2]^{2+}$); 616 ($[2:2:1]^{3+}$).

M_2L_2 [((dppp)Pt)$_2$(**165**)$_2$](OTf)$_4$ and M_3L_3 complex [((dppp)Pt)$_3$(**165**)$_3$](OTf)$_6$ **181a/b**

Building blocks:

7.48 mg (0.00825 mmol) (1,3-bis(diphenylphosphino)propane)platinum(II) trifluoromethanesulfonate **28**

2.00 mg (0.00825 mmol) 1,3-bis(5-methylpyridin-3-yl)urea **165**

$C_{84}H_{80}F_{12}N_8O_{14}P_4Pt_2S_4$ 2295.87 g/mol (M_2L_2)

$C_{126}H_{84}F_{18}N_{12}O_{21}P_6Pt_3S_6$ 3407.52 g/mol (M_3L_3)

^{1}H NMR: (DMF-d_7, 500 MHz, 298K): δ = 9.56 (s, $H_{o\text{-pyridine}}$, M_2L_2); 9.27 (s, $H_{o\text{-pyridine}}$, M_3L_3); 9.05 (s, $H_{o\text{-pyridine}}$, M_2L_2); 8.90 (s, NH, M_2L_2); 8.80 (s, NH, M_3L_3); 8.66 (s, $H_{o\text{-pyridine}}$, M_3L_3); 8.50 (m, $H_{dppp\text{-phenyl}}$, M_2L_2); 7.94 (m, $H_{dppp\text{-phenyl}}$, M_3L_3); 7.77-7.33 (m, $H_{dppp\text{-phenyl}}$ (M_2L_2 and M_3L_3) and $H_{p\text{-pyridine}}$, M_3L_3); 7.07 (s, $H_{p\text{-pyridine}}$, M_2L_2); 3.71 (m, PC$\underline{H}_2$); 2.16 (s, CH_3); 2.08 (m, $PCH_2C\underline{H}_2$) ppm.

^{31}P NMR: (DMF-d_7, 202 MHz, 298 K): δ = -11.84 (s, P_{dppp}, $^1J_{Pt\text{-}P}$ = 3020 Hz, M_3L_3); -11.99 (s, P_{dppp}, $^1J_{Pt\text{-}P}$ = 3020 Hz, M_2L_2) ppm.

ESI MS: (ESI$^+$, DMSO/acetonitrile): *m/z* = 546 ([1:2:0]$^{2+}$); 566 ([(2:2:1) – HOTf]$^{3+}$); 616 ([2:2:1]$^{3+}$); 998 ([1:1:1]$^+$ and [2:2:2]$^{2+}$); 1120 ([2:3:2]$^{2+}$); 1381 ([4:4:5]$^{3+}$).

M_2L_2 [((dppp)Pt)$_2$(**167**)$_2$](OTf)$_4$ and M_3L_3 complex [((dppp)Pt)$_3$(**167**)$_3$](OTf)$_6$ **182a/b**

Building blocks:

7.48 mg (0.00825 mmol) (1,3-bis(diphenylphosphino)propane)platinum(II) trifluoromethanesulfonate **28**

2.00 mg (0.00825 mmol) 1,3-bis((pyridin-3-yl)methyl)urea **167**

$C_{84}H_{80}F_{12}N_8O_{14}P_4Pt_2S_4$ 2295.87 g/mol (M_2L_2)

$C_{126}H_{84}F_{18}N_{12}O_{21}P_6Pt_3S_6$ 3407.52 g/mol (M_3L_3)

^{1}H NMR: (DMF-d_7, 500 MHz, 273K): δ = 9.09 (s, $H_{o\text{-pyridine}}$, M_2L_2); 8.84 (s, $H_{o\text{-pyridine,}}$ M_3L_3); 8.51 (s, $H_{o\text{-pyridine}}$ M_2L_2); 8.00-7.15 (m, NH (M_3L_3) and $H_{dppp\text{-phenyl}}$ and $H_{o\text{-pyridine}}$ and $H_{o\text{-pyridine}}$, M_2L_2 and M_3L_3); 6.67 (t, NH, M_2L_2); 4.13 (br.,NCH_2); 3.77 (br., NCH_2); 3.41 (br., PCH_2); 1.77 (m, $PCH_2C\underline{H_2}$) ppm.

^{31}P NMR: (DMF-d_7, 202 MHz, 298K): -14.57 (s, P_{dppp}, $^{1}J_{Pt\text{-}P}$ = 3025 Hz, M_3L_3); -15.10 (s, P_{dppp}, $^{1}J_{Pt\text{-}P}$ = 3025 Hz, M_3L_3) ppm.

ESI MS: (ESI^+, DMSO/acetonitrile): *m/z* = 546 ($[1:2:0]^{2+}$); 616 ($[2:2:1]^{3+}$); 696 ($[2:3:1]^{3+}$); 998 ($[1:1:1]^{+}$ and $[2:2:2]^{2+}$).

$\underline{M_2L_2\ [((dppp)Pt)_2(\mathbf{168})_2](OTf)_4}$ **183**

Building blocks:

7.48 mg (0.00825 mmol)	(1,3-bis(diphenylphosphino)propane)platinum(II) trifluoro-methanesulfonate **28**
2.00 mg (0.00825 mmol)	1,3-bis((pyridin-4-yl)methyl)urea **168**

$C_{84}H_{80}F_{12}N_8O_{14}P_4Pt_2S_4$ 2295.87 g/mol (M_2L_2)

^{1}H NMR: (DMF-d_7, 500 MHz, 303 K): δ = 8.81 (d, $^{3}J_{HH}$ = 4.90 Hz, $H_{o\text{-pyridine}}$); 7.80 (m, $H_{dppp\text{-phenyl}}$); 7.61 (m, $H_{dppp\text{-phenyl}}$); 7.51 (m, $H_{dppp\text{-phenyl}}$); 7.09 (d, $^{3}J_{HH}$ = 6.00 Hz, $H_{m\text{-pyridine}}$); 6.95 (t, $^{3}J_{HH}$ = 5.72 Hz, NH); 4.19 (d, $^{3}J_{HH}$ = 5.67 Hz, CH_2); 3.46 (br., $PC\underline{H_2}$); 1.72 (m, $^{3}J_{P\text{-}H}$ = 24.20 Hz, $PCH_2C\underline{H_2}$) ppm.

^{31}P NMR: (DMF-d_7, 202 MHz, 298K): -15.47 (s, P_{dppp}, $^{1}J_{Pt\text{-}P}$ = 3036 Hz) ppm.

ESI MS: (ESI^+, DMSO/acetonitrile): *m/z* = 546 ($[1:2:0]^{2+}$); 616 ($[2:2:1]^{3+}$); 696 ($[2:3:1]^{3+}$); 998 ($[1:1:1]^{+}$ and $[2:2:2]^{2+}$).

8.5.5 Self-Assembly of Bispyridyl-Urea Based M_2L_4 and M_3L_6 Complexes

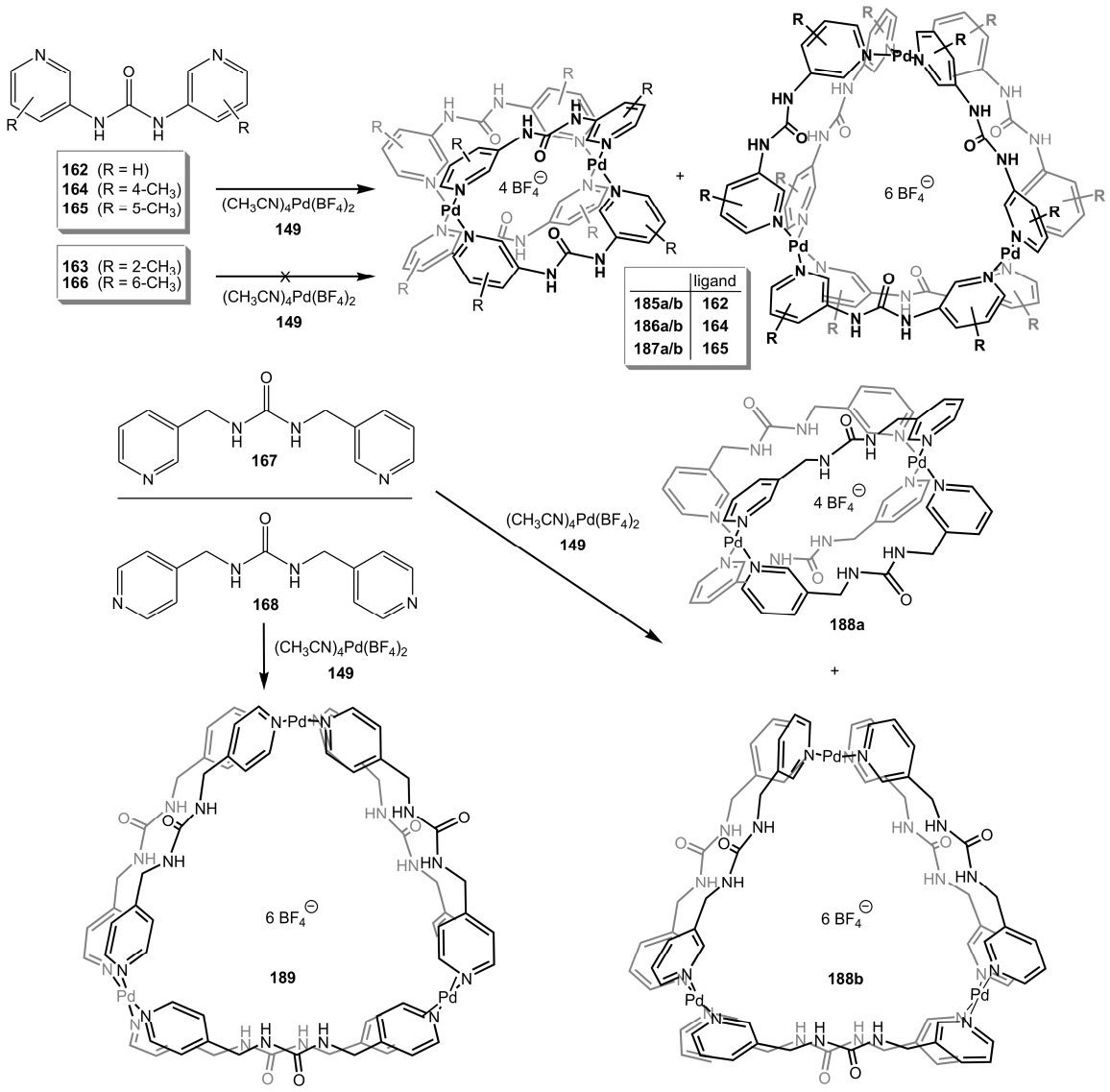

<u>General Self-Assembly Procedure:</u>

2.07 mg (0.0046 mmol) tetrakis(acetonitrilo)palladium(II) tetrafluoroborate **149** was mixed with two equivalents of the 1,3-bis(pyridine-3-yl)urea ligands **162-119** and dissolved in 1 mL of DMF, DMSO, DMF-d_7 or DMSO-d_7, respectively. These solutions were stirred for 15 min at room temperature and afterwards characterized with NMR spectroscopy and ESI mass spectrometry.

For the mixtures with ligands **163** and **117**, no formation of discrete complexes was observed.

M_2L_4 complex $[Pd_2(\mathbf{162})_4](BF_4)_4$ and M_3L_6 complex $[Pd_3(\mathbf{162})_6](BF_4)_6$ **185a/b**

Building blocks:

2.07 mg (0.00467 mmol) tetrakis(acetonitrilo)palladium(II) tetrafluoroborate **149**

2.00 mg (0.00934 mmol) 1,3-bis(pyridin-3-yl)urea **162**

$C_{44}H_{40}B_4F_{16}N_{16}O_4Pd_2$ 1416.95 g/mol (M_2L_4)

$C_{66}H_{60}B_6F_{24}N_{24}O_6Pd_3$ 2125.43 g/mol (M_3L_6)

^{1}H NMR (400 MHz, DMSO-d_6) δ = 10.67 (d, $^4J_{HH}$ = 1.01 Hz, $H_{o\text{-pyridine}}$ (M_2L_4)); 9,67 (d, $^4J_{HH}$ = 2.01 Hz, $H_{o\text{-pyridine}}$ (M_3L_6)); 9.64 (s, NH (M_2L_4)); 9.40 (s, NH (M_3L_6)); 9.12 (d, $^3J_{HH}$ = 5.41 Hz, $H_{o\text{-pyridine}}$ (M_3L_6)); 8.67 (dd, $^3J_{HH}$ = 4.59 Hz, $^4J_{HH}$ = 2.08 Hz, $H_{o\text{-pyridine}}$ (M_2L_4)); 7,62 (m, $H_{m\text{-pyridine}}$ and $H_{p\text{-pyridine}}$ (M_2L_4 and M_3L_6)) ppm.

ESI MS (ESI$^+$, DMSO/acetone): *m/z* = 533 ($[(2:4:2) - 2\ HBF_4]^{2+}$); 578 ($[(2:4:2) - HBF_4]^{2+}$); 622 ($[1:2:1]^+$ and $[2:4:2]^{2+}$ and $[3:6:3]^{3+}$); 679 ($[(5:9:6) - 3\ HBF_4]^{4+}$); 701 ($[(5:9:6) - 2\ HBF_4]^{4+}$); 857 ($[4:8:5]^{3+}$); 932 ($[(3:6:4) - HBF_4]^{2+}$); 935 ($[(5:9:7) - 3\ HBF_4]^{3+}$); 964 ($[(5:9:7) - 2\ HBF_4]^{3+}$); 976 ($[3:6:4]^{2+}$); 1330 ($[4:8:6]^{2+}$).

M_2L_4 complex $[Pd_2(\mathbf{164})_4](BF_4)_4$ and M_3L_6 complex $[Pd_3(\mathbf{164})_6](BF_4)_6$ **186a/b**

Building blocks:

2.07 mg (0.00467 mmol) tetrakis(acetonitrilo)palladium(II) tetrafluoroborate **149**

2.26 mg (0.00934 mmol) 1,3-bis(4-methylpyridin-3-yl)urea **164**

$C_{52}H_{56}B_4F_{16}N_{16}O_4Pd_2$ 1529.16 g/mol (M_2L_4)

$C_{78}H_{84}B_6F_{24}N_{24}O_6Pd_3$ 2293.75 g/mol (M_3L_6)

^{1}H NMR (500 MHz, DMF-d_7, 298 K): δ = 10.84 (d, $^4J_{HH}$ = 2.00 Hz, $H_{o\text{-pyridine}}$ (M_2L_4)); 9.85 (d, $^4J_{HH}$ = 2.00 Hz, $H_{o\text{-pyridine}}$ (M_3L_6)); 9.84 (s, NH (M_2L_4)); 9.81 (s, NH (M_3L_6)); 9.11 (s, $H_{o\text{-pyridine}}$ (M_3L_6)); 8.74 (s, $H_{o\text{-pyridine}}$ (M_2L_4)); 7.56 (m, $H_{m\text{-pyridine}}$ (M_2L_4) and $H_{o\text{-pyridine}}$ (M_3L_6)); 2.35 (s, CH_3 (M_3L_6)); 2.32 (s, CH_3 (M_2L_4)) ppm.

ESI-MS (ESI$^+$, DMSO/acetone): *m/z* = 1442 ([2:4:2]$^+$); 1060 ([3:6:4]$^{2+}$); 678 ([2:4:2]$^{2+}$).

M_2L_4 complex $[Pd_2(\mathbf{165})_4](BF_4)_4$ and M_3L_6 complex $[Pd_3(\mathbf{165})_6](BF_4)_6$ **187a/b**

Building blocks:

2.07 mg (0.00467 mmol) tetrakis(acetonitrilo)palladium(II) tetrafluoroborate **149**

2.26 mg (0.00934 mmol) 1,3-bis(5-methylpyridin-3-yl)urea **165**

$C_{52}H_{56}B_4F_{16}N_{16}O_4Pd_2$ 1529.16 g/mol (M_2L_4)

$C_{78}H_{84}B_6F_{24}N_{24}O_6Pd_3$ 2293.75 g/mol (M_3L_6)

^{1}H NMR (500 MHz, DMF-d_7, 298 K): δ = 10.84 (d, $^4J_{HH}$ = 2.00 Hz, $H_{o\text{-pyridine}}$ (M_2L_4)); 9.85 (d, $^4J_{HH}$ = 2.00 Hz, $H_{o\text{-pyridine}}$ (M_3L_6)); 9.84 (s, NH (M_2L_4)); 9.81 (s, NH (M_3L_6)); 9.11 (s, $H_{o\text{-pyridine}}$ (M_3L_6)); 8.74 (s, $H_{o\text{-pyridine}}$ (M_2L_4)); 7.56 (m, $H_{m\text{-pyridine}}$ (M_2L_4) and $H_{o\text{-pyridine}}$ (M_3L_6)); 2.35 (s, CH_3 (M_3L_6)); 2.32 (s, CH_3 (M_2L_4)) ppm.

ESI-MS (ESI$^+$, DMSO/acetone): *m/z* = 487 ([3:6:2]$^{4+}$); 506; 525 ([(3:7:2) – HBF_4]$^{4+}$);538 ([(3:5:3) – 2 HBF_4]$^{3+}$); 590 ([(2:4:2) – 2 HBF_4]$^{2+}$); 619 ([(3:6:3) – 2 HBF_4]$^{3+}$); 634 ([(2:4:2) – HBF_4]$^{2+}$); 648 ([(3:6:3) – HBF_4]$^{3+}$); 678 ([1:2:1]$^+$ and [2:4:2]$^{2+}$ and [3:6:3]$^{3+}$); 1016 ([(3:6:4) – HBF_4]$^{2+}$); 1059 ([3:6:4]$^{2+}$).

M_2L_4 complex $[Pd_2(\mathbf{167})_4](BF_4)_4$ and M_3L_6 complex $[Pd_3(\mathbf{167})_6](BF_4)_6$ **188a/b**

Building blocks:

2.07 mg (0.00467 mmol) tetrakis(acetonitrilo)palladium(II) tetrafluoroborate **149**

2.26 mg (0.00934 mmol) 1,3-bis((pyridin-3-yl)methyl)urea **167**

$C_{52}H_{56}B_4F_{16}N_{16}O_4Pd_2$ 1529.16 g/mol (M_2L_4)

$C_{78}H_{84}B_6F_{24}N_{24}O_6Pd_3$ 2293.75 g/mol (M_3L_6)

^{1}H NMR (500 MHz, DMF-d_7, 298 K): δ = 9.79 (s, $H_{o\text{-pyridine}}$ (M_2L_4)); 9.55 (s, $H_{o\text{-pyridine}}$ (M_2L_4)); 9.42 (s, $H_{o\text{-pyridine}}$ (M_3L_6)); 9.29 (m, (s, NH (M_2L_4)); 9.17 (m, $H_{o\text{-pyridine}}$ (M_3L_6)); 8.96 (d, $^3J_{HH}$ = 5.60 Hz, $H_{p\text{-pyridine}}$ (M_2L_4)); 7.98 (m, $H_{p\text{-pyridine}}$ (M_3L_6)); 7.65 (m, $H_{m\text{-pyridine}}$ (M_3L_6)); 7.51 (m, $H_{m\text{-pyridine}}$ (M_2L_4)); 7.04 (m, NH (M_3L_6)); 4.46 (m, $NHC\underline{H_2}$ (M_2L_4) and (M_3L_6)) ppm.

ESI MS (ESI^+, DMSO/acetone): *m/z* = 487 ($[3:6:2]^{4+}$); 538 ($[(3:5:3) - 2\ HBF_4]^{3+}$); 590 ($[(2:4:2) - 2\ HBF_4]^{2+}$); 619 ($[(3:6:3) - 2\ HBF_4]^{3+}$); 634 ($[(2:4:2) - HBF_4]^{2+}$); 648 ($[(3:6:3) - HBF_4]^{3+}$); 678 ($[1:2:1]^+$ and $[2:4:2]^{2+}$ and $[3:6:3]^{3+}$); 972 ($[(3:6:4) - 2\ HBF_4]^{2+}$); 1016($[(3:6:4) - HBF_4]^{2+}$); 1059 ($[3:6:4]^{2+}$).

M_3L_6 complex $[Pd_3(\mathbf{168})_6](BF_4)_6$ **189**

Building blocks:

2.07 mg (0.00467 mmol) tetrakis(acetonitrilo)palladium(II) tetrafluoroborate **149**

2.26 mg (0.00934 mmol) 1,3-bis((pyridin-4-yl)methyl)urea **168**

$C_{78}H_{84}B_6F_{24}N_{24}O_6Pd_3$ 2293.75 g/mol (M_3L_6)

^{1}H NMR (500 MHz, DMF-d_7, 298 K): δ = 9.28 (br., $H_{o\text{-pyridine}}$); 7.67 (br., $H_{m\text{-pyridine}}$); 7.08 (br., NH); 4.44 (br., $NHC\underline{H_2}$) ppm.

ESI MS (ESI^+, DMSO/MeCN) *m/z* = 487 ($[3:6:2]^{4+}$); 547 ($[3:7:2]^{4+}$); 678 ($[3:6:3]^{3+}$); 758 ($[3:7:3]^{3+}$); 1059 ($[3:6:4]^{2+}$).

8.5.6 Self-Assembly and Self-Sorting of Homo- and Heterometallic M_4L_2 complexes

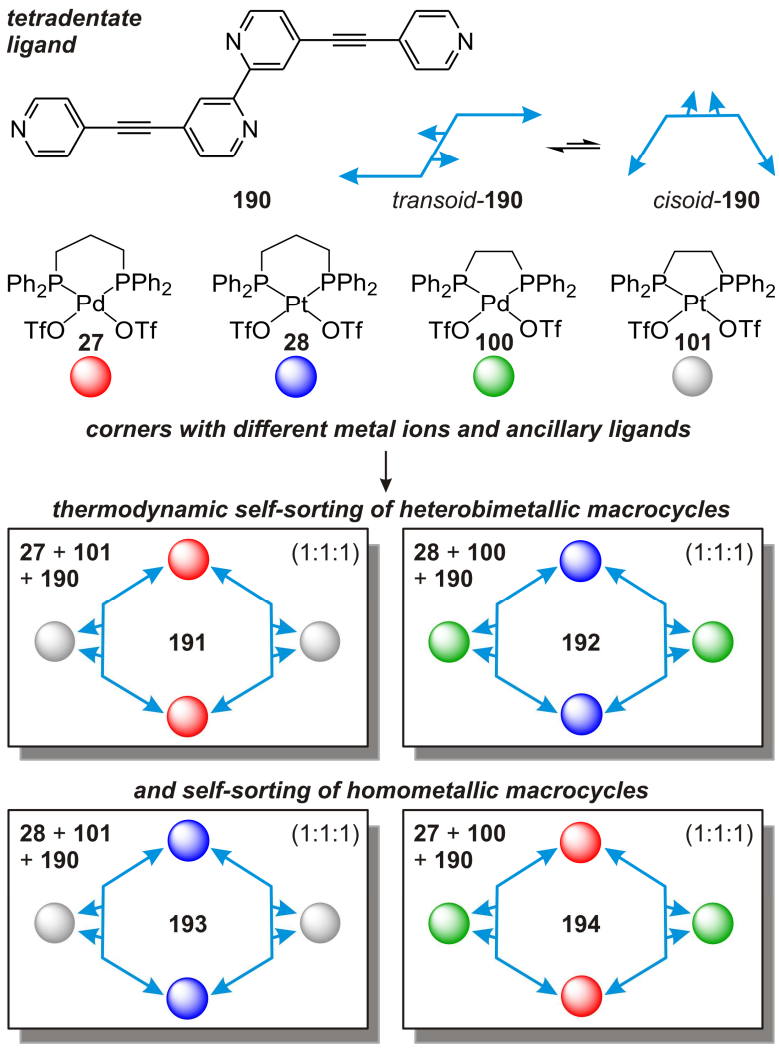

General Self-Assembly Procedure for the 1:1 (M:L) Mixtures:[158]

In separate glass vials, ligand **190** (0.88 mg, 2.46 µmol) was mixed in CD_2Cl_2 (0.25 ml) with metal centers Pd(dppp)OTf_2 **27** (2 mg, 2.46 µmol), Pt(dppp)OTf_2 **28** (2.22 mg, 2.46 µmol), Pd(dppe)OTf_2 **100** (1.98 mg, 2.46 µmol) or Pt(dppe)OTf_2 **101** (2.18 mg, 2.46 µmol) which were suspended in 0.25 ml CD_2Cl_2 each before mixing. The mixtures were stirred at r.t. for 12 h. The solutions were then transferred into NMR tubes for analysis and subsequently investigated with FTICR mass spectrometry.

General Self-Assembly Procedure for the 2:1 (M:L) Mixtures:

In separate glass vials, ligand **190** (0.44 mg, 1.23 μmol) was mixed in CD_2Cl_2 (0.25 ml) with two different metal centers Pd(dppp)OTf_2 **27** (2 mg, 2.46 μmol), Pt(dppp)OTf_2 **28** (2.22 mg, 2.46 μmol), Pd(dppe)OTf_2 **100** (1.98 mg, 2.46 μmol) or Pt(dppe)OTf_2 **101** (2.18 mg, 2.46 μmol) in CD_2Cl_2 (0.25 ml) which were suspended in 0.25 ml CD_2Cl_2 each before mixing. The mixtures were stirred at r.t. for 3 d to reach thermodynamic equilibrium. The solutions were transferred into NMR tubes for analysis and subsequently investigated with FTICR mass spectrometry.

M_4L_2 complex [((dppp)Pd)$_2$((dppe)Pt)$_2$ (**190**)$_2$$(OTf)_8$] **191**

Building blocks:

2.00 mg (0.00246 mmol)	(1,3-bis(diphenylphosphino)propane)palladium(II) trifluoromethanesulfonate **27**
2.18 mg (0.00246 mmol)	(1,3-bis(diphenylphosphino)ethane)platinum(II) trifluoromethanesulfonate **101**
0.44 mg (0.00123 mmol)	4,4'-bis(pyridine-4-ylethynyl)-2,2'-bipyridin **190**

$C_{162}H_{128}F_{24}N_8O_{24}P_8Pd_2Pt_2S_8$ 4143.06 g/mol (M_4L_2)

^{1}H NMR (400 MHz, CD_2Cl_2, 293 K): δ = 8.94 (br, $H_{o\text{-pyridine}}$); 8.62 (br, $H_{\delta\text{-bipyridine}}$); 8.04 (m, H_{phenyl}); 7.95-7.50 (m, H_{phenyl} and $H_{\alpha\text{-bipyridine}}$); 7.26 (br, $H_{m\text{-pyridine}}$); 7.19 (br, $H_{\beta\text{-bipyridine}}$); 3.21 (m, $PCH_{2\text{-dppp}}$); 2.59 (d, $^3J_{PH}$ = 22.92 Hz, $PCH_{2\text{-dppe}}$); 2.31 (m, $PCH_2C\underline{H}_{2\text{-dppp}}$) ppm.

^{31}P NMR (400 MHz, CD_2Cl_2, 293 K): δ = 43.32 (s, $P_{dppe\text{-bipyridine}}$); 7.39 (s, $P_{dppp\text{-pyridine}}$) ppm.

ESI MS (ESI^+, CH_2Cl_2): *m/z* = 922 ([dppePt)$_2$(**190**)$(OTf)_2]^{2+}$); 1100 ([dppePt)(**190**)$(OTf)]^+$); 1229 ([(dpppPd)$_2$(dppePt)$_2$(**190**)$_2$$(OTf)_5]^{3+}$); 1253 ([(dpppPd)(dppePt)$_3$(**190**)$_2$$(OTf)_5]^{3+}$); 1918 ([(dpppPd)$_2$(dppePt)$_2$(**190**)$_2$$(OTf)_6]^{2+}$ and

[(dpppPd)$_4$(dppePt)$_4$(**190**)$_4$(OTf)$_{12}$]$^{4+}$); 1955 ([(dpppPd)(dppePt)$_3$(**190**)$_2$(OTf)$_6$]$^{2+}$ and [(dpppPd)$_2$(dppePt)$_6$(**190**)$_4$(OTf)$_{12}$]$^{4+}$).

M_4L_2 complex [((dppp)Pt)$_2$((dppe)Pd)$_2$ (**190**)$_2$(OTf)$_8$] **192**

Building blocks:

2.22 mg (0.00246 mmol)	(1,3-bis(diphenylphosphino)propane)platinum(II) trifluoromethanesulfonate **28**
1.98 mg (0.00246 mmol)	(1,3-bis(diphenylphosphino)ethane)palladium(II) trifluoromethanesulfonate **100**
0.44 mg (0.00123 mmol)	4,4'-Bis(pyridine-4-ylethynyl)-2,2'-bipyridin **190**

$C_{162}H_{128}F_{24}N_8O_{24}P_8Pd_2Pt_2S_8$ 4143.06 g/mol (M_4L_2)

^{1}H NMR (400 MHz, CD_2Cl_2, 293 K): δ = 8.98 (br, $H_{o\text{-pyridine}}$); 8.47 (br, $H_{\delta\text{-bipyridine}}$); 8.03 (m, H_{phenyl}); 7.85-7.50 (m, H_{phenyl} and $H_{\alpha\text{-bipyridine}}$); 7.40 (m, H_{phenyl}); 7.28 (br, $H_{m\text{-pyridine}}$); 7.16 (d, $^3J_{HH}$ = 5.72 Hz, $H_{\beta\text{-bipyridine}}$); 3.31 (m, $PCH_{2\text{-dppp}}$); 2.76 (d, $^3J_{PH}$ = 24.14 Hz, $PCH_{2\text{-dppe}}$); 2.32 (m, $^3J_{PH}$ = 23.84 Hz, $PCH_2C\underline{H}_{2\text{-dppp}}$) ppm.

^{31}P NMR (400 MHz, CD_2Cl_2, 293 K): δ = 70.22 (s, $P_{dppe\text{-bipyridine}}$); -14.77 (s, $P_{dppp\text{-pyridine}}$) ppm.

ESI MS (ESI$^+$, CH_2Cl_2): *m/z* = 1229 ([(dpppPt)$_2$(dppePd)$_2$(**190**)$_2$(OTf)$_5$]$^{3+}$); 1501 ([(dpppPt)$_4$(dppePd)$_4$(**190**)$_4$(OTf)$_{11}$]$^{5+}$); 1917 ([(dpppPd)$_2$(dppePt)$_2$(**190**)$_2$(OTf)$_6$]$^{2+}$ and [(dpppPd)$_4$(dppePt)$_4$(**190**)$_4$(OTf)$_{12}$]$^{4+}$).

M_4L_2 complex $[((dppp)Pt)_2((dppe)Pt)_2(\mathbf{190})_2(OTf)_8]$ **193**

Building blocks:

2.22 mg (0.00246 mmol)	(1,3-bis(diphenylphosphino)propane)platinum(II) trifluoromethanesulfonate **28**
2.18 mg (0.00246 mmol)	(1,3-bis(diphenylphosphino)ethane)platinum(II) trifluoromethanesulfonate **101**
0.44 mg (0.00123 mmol)	4,4'-Bis(pyridine-4-ylethynyl)-2,2'-bipyridin **190**

$C_{162}H_{128}F_{24}N_8O_{24}P_8Pt_4S_8$ 4311.37 g/mol (M_4L_2)

^{1}H NMR (400 MHz, CD_2Cl_2, 293 K): δ = 8.98 (d, $^3J_{HH}$ = 4.84 Hz, $H_{o\text{-pyridine}}$); 8.54 (br, $H_{\delta\text{-bipyridine}}$); 8.06 (m, H_{phenyl}); 7.85-7.60 (m, H_{phenyl} and $H_{\alpha\text{-bipyridine}}$); 7.40 (m, H_{phenyl}); 7.28 (d, $^3J_{HH}$ = 6.14 Hz, $H_{m\text{-pyridine}}$); 7.21 (dd, $^3J_{HH}$ = 5.96 Hz, $^4J_{HH}$ = 1.63 Hz, $H_{\beta\text{-bipyridine}}$); 3.32 (m, $PCH_{2\text{-dppp}}$); 2.59 (d, $^3J_{PH}$ = 20.14 Hz, $PCH_{2\text{-dppe}}$); 2.29 (m, $^3J_{PH}$ = 24.35 Hz, $PCH_2C\underline{H}_{2\text{-dppp}}$) ppm.

^{31}P NMR (400 MHz, CD_2Cl_2, 293 K): δ = 43.28 (s, $P_{dppe\text{-bipyridine}}$); -14.77 (s, $P_{dppp\text{-pyridine}}$) ppm.

ESI MS (ESI^+, CH_2Cl_2): *m/z* = 1100 ([dppePt)(**190**)(OTf)]$^+$); 1114 ([dpppPt)(**190**)(OTf)]$^+$); 1288 ([(dpppPt)$_2$(dppePt)$_2$(**190**)$_2$(OTf)$_5$]$^{3+}$); 1575 ([(dpppPt)$_4$(dppePt)$_4$(**190**)$_4$(OTf)$_{11}$]$^{5+}$); 2006 ([(dpppPt)$_2$(dppePt)$_2$(**190**)$_2$(OTf)$_6$]$^{2+}$ and [(dpppPt)$_4$(dppePt)$_4$(**190**)$_4$(OTf)$_{12}$]$^{4+}$).

M_4L_2 complex [((dppp)Pd)$_2$((dppe)Pd)$_2$ (**190**)$_2$(OTf)$_8$] **194**

Building blocks:

2.00 mg (0.00246 mmol)	(1,3-bis(diphenylphosphino)propane)palladium(II) trifluoromethanesulfonate **27**
1.98 mg (0.00246 mmol)	(1,3-bis(diphenylphosphino)ethane)palladium(II) trifluoromethanesulfonate **100**
0.44 mg (0.00123 mmol)	4,4'-Bis(pyridine-4-ylethynyl)-2,2'-bipyridin **190**

$C_{162}H_{128}F_{24}N_8O_{24}P_8Pd_4S_8$ 3956.74 g/mol (M_4L_2)

^{1}H NMR (400 MHz, CD_2Cl_2, 293 K): δ = 8.95 (d, $^3J_{HH}$ = 5.73 Hz, $H_{o\text{-pyridine}}$); 8.37 (s, $H_{\delta\text{-bipyridine}}$); 8.04 (m, H_{phenyl}); 7.80-7.60 (m, H_{phenyl} and $H_{\alpha\text{-bipyridine}}$); 7.40 (m, H_{phenyl}); 7.21 (d, $^3J_{HH}$ = 6.23 Hz, $H_{m\text{-pyridine}}$); 7.15 (dd, $^3J_{HH}$ = 5.72 Hz, $^4J_{HH}$ = 1.55 Hz, $H_{\beta\text{-bipyridine}}$); 3.23 (m, $PCH_{2\text{-dppp}}$); 2.75 (d, $^3J_{PH}$ = 24.12 Hz, $PCH_{2\text{-dppe}}$); 2.29 (m, $^3J_{PH}$ = 24.08 Hz, $PCH_2C\underline{H}_{2\text{-dppp}}$) ppm.

^{31}P NMR (400 MHz, CD_2Cl_2, 293 K): δ = 70.08 (s, $P_{dppe\text{-bipyridine}}$); 7.37 (s, $P_{dppp\text{-pyridine}}$) ppm.

ESI MS (ESI^+, CH_2Cl_2): *m/z* = 1169 ($[(dpppPd)_2(dppePd)_2(\mathbf{190})_2(OTf)_5]^{3+}$); 1829 ($[(dpppPd)_2(dppePd)_2(\mathbf{190})_2(OTf)_6]^{2+}$).

8.5.7 Self-Assembly of Platinum-Containing Metallo-Supramolecular Macrocycles

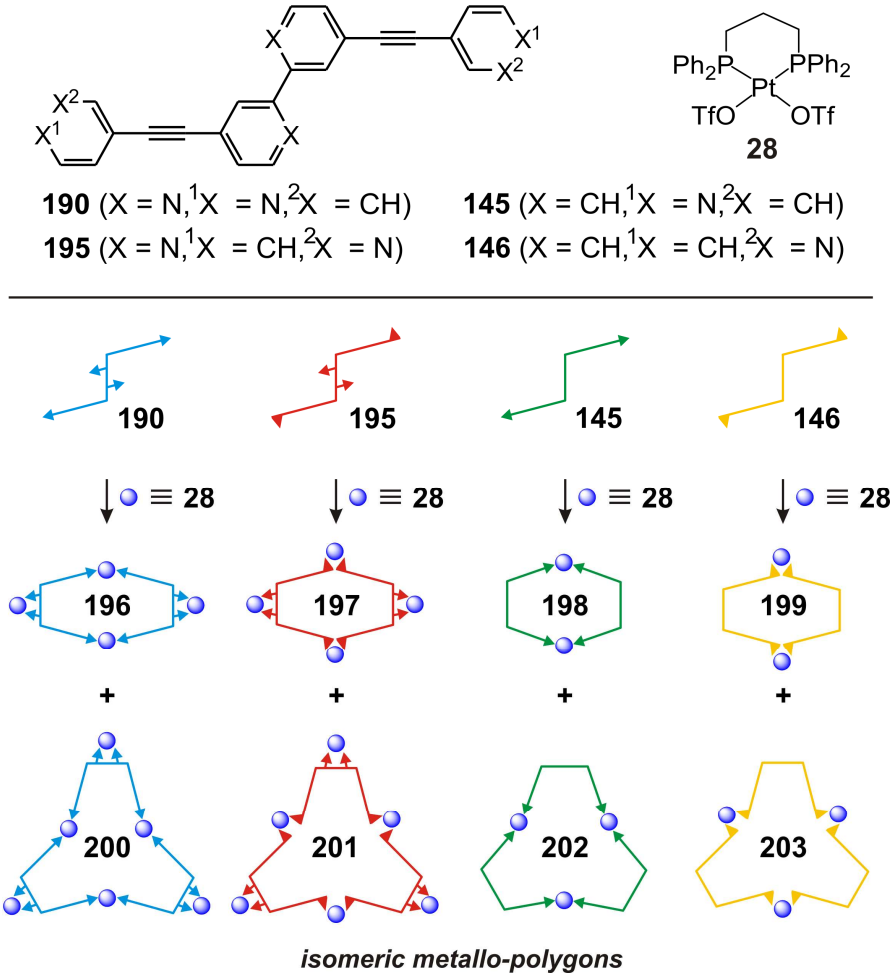

General Self-Assembly Procedure:

Ligand **190** (0.40 mg, 0.0011 mmol), ligand **194** (0.40 mg, 0.0011 mmol), ligand **145** (0.79 mg, 0.0022 mmol) or ligand **146** (0.79 mg, 0.0022 mmol), separately dissolved in CD_2Cl_2 (0.25 ml), were added to separate suspensions of Pt(dppp)OTf_2 **28** (2.00 mg, 0.0022 mmol) in CD_2Cl_2 (0.25 ml) in glass vials. The mixtures were stirred at room temperature and then transferred into NMR tubes for analysis. A sample for ESI-MS analysis was obtained from the NMR samples by diluting with a CH_2Cl_2 / acetone mixture.

M_4L_2 complex $[((dppp)Pt)_4(\mathbf{190})_2(OTf)_8]$ **196**

Building blocks:

2.00 mg (0.00221 mmol)	(1,3-bis(diphenylphosphino)propane)platinum(II) trifluoromethanesulfonate **28**
0.40 mg (0.00110 mmol)	4,4'-Bis(pyridine-4-ylethynyl)-2,2'-bipyridin **190**

$C_{164}H_{132}F_{24}N_8O_{24}P_8Pt_4S_8$ 4339.43 g/mol (M_4L_2)

^{1}H NMR (400 MHz, $CDCl_2$, 293 K): δ = 8.92 (d, $^3J_{HH}$ = 4.1 Hz, pyH_α); 8.44 (br, $bipyH_\delta$); 8.07 (m, $H_{dppp\text{-}phenyl}$); 7.87 (m, $bipyH_\alpha$); 7.75-7.20 (m, $H_{dppp\text{-}phenyl}$ and pyH_β); 7.06 (d, $^3J_{HH}$ = 6.2 Hz, $bipyH_\beta$); 3.32 (m, $PC\underline{H}_2$); 2.58 (m, $PCH_2C\underline{H}_2$); 2.29 (m, $PCH_2C\underline{H}_2$) ppm.

^{31}P NMR (202 MHz, $CDCl_2$, 293 K): δ = -3.76 (s, $P_{dppp\text{-}bipyridine}$); -14.78 (s, $P_{dppp\text{-}pyridine}$) ppm.

ESI MS (ESI^+, CH_2Cl_2): *m/z* = 1114 ($[1:1:1]^+$), 1297 ($[4:2:5]^{3+}$), 2020 ($[4:2:6]^{2+}$ and $[8:4:12]^{4+}$).

Equilibrium of M_4L_2 and M_6L_3 complexes $[((dppp)Pt)_4(\mathbf{[195]})_2(OTf)_8]$ **197** and $[((dppp)Pt)_6(\mathbf{[195]})_3(OTf)_{12}]$ **201**

Building blocks:

2.00 mg (0.00221 mmol)	(1,3-bis(diphenylphosphino)propane)platinum(II) trifluoromethanesulfonate **28**
0.40 mg (0.00110 mmol)	4,4'-Bis(pyridine-3-ylethynyl)-2,2'-bipyridin **195**

$C_{164}H_{132}F_{24}N_8O_{24}P_8Pt_4S_8$ 4339.43 g/mol (M_4L_2)

$C_{246}H_{198}F_{36}N_{12}O_{36}P_{12}Pt_6S_{12}$ 6509.14 g/mol (M_6L_3)

^{1}H NMR (400 MHz, $CDCl_2$, 293 K): δ = 9.53 (d, $^{3}J_{HH}$ = 1.5 Hz, pyH_{α}); 9.18 (s, pyH_{α}); 9.15 (d, $^{3}J_{HH}$ = 1.6 Hz, pyH_{α}); 8.88 (s, pyH_{α}); 8.61 (s, $bipyH_{\delta}$); 8.59 (s, $bipyH_{\delta}$); 8.32-7.22 (m, pyH_{β}, $pyH_{\gamma,}$ $bipyH_{\alpha}$ and $H_{dppp\text{-}phenyl}$); 6.97 (d, $^{3}J_{HH}$ = 2.2 Hz, $bipyH_{\beta}$); 3.36 (m, $H_{dppp\text{-}alkyl}$); 2.53 (m, $H_{dppp\text{-}alkyl}$); 2.31 (m, $H_{dppp\text{-}alkyl}$) ppm.

^{31}P NMR (202 MHz, CD_2Cl_2, 293 K): δ = -4.58 (s, $P_{dppp\text{-}bipy}$); -14.81 (s, $P_{dppp\text{-}py}$); -15.07 (s, $P_{dppp\text{-}py}$) ppm.

ESI MS (ESI^+, CH_2Cl_2): *m/z* = 1297 ($[4:2:5]^{3+}$), 1478 ($[6:3:8]^{4+}$), 1586 ($[8:4:11]^{5+}$), 2020 ($[4:2:6]^{2+}$ and $[6:3:9]^{3+}$ and $[8:4:12]^{4+}$), 2744 ($[8:4:13]^{3+}$), 3105 ($[6:3:10]^{2+}$).

M_2L_2 complex $[((dppp)Pt)_2(\mathbf{145})_2(OTf)_4]$ **198**

Building blocks:

2.00 mg (0.00221 mmol)	(1,3-bis(diphenylphosphino)propane)platinum(II) trifluoromethanesulfonate **28**
0.79 mg (0.00221 mmol)	3,3'-bis(pyridin-4-ylethynyl)biphenyl **145**

$C_{110}H_{84}F_{12}N_4O_{12}P_4Pt_2S_4$ 2524.16 g/mol (M_4L_2)

^{1}H NMR (400 MHz, $CDCl_2$, 293 K): δ = 8.91 (d, $^{3}J_{HH}$ = 6.3 Hz, pyH_{α}); 7.80-7.30 (m, $H_{dppp\text{-}phenyl}$ and H_{biaryl}); 7.15 (d, $^{3}J_{HH}$ = 6.7 Hz, pyH_{β}); 3.32 (m, $H_{dppp\text{-}alkyl}$); 2.26 (m, $H_{dppp\text{-}alkyl}$) ppm.

^{31}P NMR (202 MHz, CD_2Cl_2, 293 K): δ = -14.71 (s, P_{dppp}) ppm.

ESI MS (ESI^+, CH_2Cl_2): *m/z* = 1112 ($[2:2:2]^{2+}$), 1533 ($[4:4:5]^{3+}$), 2373 ($[2:2:3]^{+}$ and $[4:4:6]^{2+}$).

Equilibrium of M_2L_2 and M_3L_3 complexes $[((dppp)Pt)_2(\mathbf{146})_2(OTf)_4]$ **199** and $[((dppp)Pt)_3(\mathbf{146})_3(OTf)_6]$ **203**

Building blocks:

2.00 mg (0.00221 mmol)	(1,3-bis(diphenylphosphino)propane)platinum(II) trifluoromethanesulfonate **28**
0.79 mg (0.00221 mmol)	3,3'-bis(pyridin-3-ylethynyl)biphenyl **146**

$\mathbf{C_{110}H_{84}F_{12}N_4O_{12}P_4Pt_2S_4}$	2524.16 g/mol (M_4L_2)
$\mathbf{C_{165}H_{126}F_{18}N_6O_{18}P_6Pt_3S_6}$	3786.23 g/mol (M_6L_3)

^{1}H NMR (400 MHz, $CDCl_2$, 293 K): δ = 9.43 (d, $^3J_{HH}$ = 1.6 Hz, pyH_α); 9.39 (br, pyH_α); 8.76 (br, pyH_α); 8.59 (s, pyH_α); 8.23-7.34 (m, $H_{dppp\text{-}phenyl}$, H_{biaryl} and pyH_β); 3.27 (m, $H_{dppp\text{-}alkyl}$); 2.33 (m, $H_{dppp\text{-}alkyl}$) ppm.

^{31}P NMR (202 MHz, CD_2Cl_2, 293 K): δ = -14.99 (s, $P_{dppp\text{-}py}$); -15.51 (s, $P_{dppp\text{-}py}$) ppm.

ESI MS (ESI^+, CH_2Cl_2): *m/z* = 1112 ($[2:2:2]^{2+}$), 1533 ($[4:4:5]^{3+}$), 1742 ($[3:3:4]^{2+}$), 2373 ($[2:2:3]^+$ and $[4:4:6]^{2+}$).

8.6 Capillary Parameter for the Online Mass Spectrometric Experiments Using a Micro-reactor

The reaction time t of the starting materials within the micro-reactor can be calculated using equation 9.1 wherein V is the total volume of the micro-reactor, the mixing capillary and the ESI spray needle and v_p represents the velocity of the reaction mixture in the mixing capillary.

$$t = V/v_p \tag{9.1}$$

Table 9.1: *Reaction times of the self-assembly systems at different length of the mixing capillaries and at different flow-rates of the solvents in the mixing capillary. The total volumes of the mixing capillaries are given, including the ESI spray needle.*

capillary nr.	**length of the capillaries** in m	**volume** in m^3	**time (40 µL/min)** in s	**time (120 µL/min)** in s
spray capillary	----	3.27E-09	0.49	0.16
1	0.06	5.97E-09	0.90	0.30
2	0.09	7.59E-09	1.14	0.38
3	0.15	1.06E-08	1.59	0.53
4	0.20	1.32E-08	1.99	0.66
5	0.26	1.59E-08	2.39	0.80
6	0.31	1.84E-08	2.76	0.92
7	0.37	2.13E-08	3.20	1.07
8	0.43	2.42E-08	3.63	1.21
9	0.48	2.69E-08	4.03	1.34
10	0.61	3.33E-08	5.00	1.67
11	0.75	4.00E-08	6.01	2.00
12	0.89	4.71E-08	7.07	2.36
13	1.02	5.33E-08	8.00	2.67
14	1.16	6.04E-08	9.06	3.02
15	1.31	6.76E-08	10.14	3.38
16	1.43	7.33E-08	10.99	3.66
17	1.56	7.96E-08	11.94	3.98
18	1.70	8.68E-08	13.02	4.34

8.7 Mass Spectrometry of Bismuth-Oxido Clusters

The ESI mass spectra of the bismuth-oxido clusters studied were measured with similar parameters. Therefore, a general set of parameters given which was slightly varied for the individual measurements in order to get the best signal intensities:

ion guide	frequency: 962 kHz; amplitude: 160-175 V; width: 106 ms
arbitrary waveform	amplitude: 60-200 V; width: 32.768 ms; DAC rate: 2-4 MHz
collection time (Q3 exit)	50-10000 ms (highly depending on the sample)
sample cone DC	35-55 V
extractor cone DC	7-10 V
desolvation gas	0-3 V
spray voltage (probe HV)	3.5-4.2 kV
number of scans	1-100 scans (highly depending on the sample)
ion source temperature	T = 40 °C
spray capillary temperature	T = 40 °C
flow rate	2-10 µL/min (usually 4 µL/min)

In order to isolate ions for MS/MS experiments, the arbitrary waveform was modified with an ion isolation function. The IRMPD MS/MS experiments were performed with a 25 W IR laser (CO_2, wavelength: 10.6 µm) using different laser powers as well as different irradiation times.

$[Bi_{38}O_{45}(NO_3)_{20}(DMSO)_{28}](NO_3)_4(DMSO)_4$ **204**

3.00 mg (0.23717 mmol) $[Bi_{38}O_{45}(NO_3)_{20}(DMSO)_{28}](NO_3)_4(DMSO)_4$ **204** were suspended in 0.3 ml DMSO and heated for 5 min at 70 °C. The resulting solution was cooled to room temperature and diluted with 1.7 ml acetonitrile which yielded in a solution of **204** with a concentration of 120 µmol/L. This solution was used for the ESI MS experiments.

$C_{64}H_{192}O_{149}N_{24}S_{32}Bi_{38}$ 12649.2 g/mol

Table 8.2: *ESI-MS data of* $[Bi_{38}O_{45}(NO_3)_{20}(DMSO)_{28}](NO_3)_4(DMSO)_4$ ***204****.*

m/z	**Fragment**	*m/z*	**Fragment**
2695	$[Bi_{38}O_{45}(NO_3)_{20}(DMSO)_{11}(H_2O)]^{4+}$	3493	$[Bi_{38}O_{46}(NO_3)_{19}(DMSO)_8]^{3+}$
2702	$[Bi_{38}O_{46}(NO_3)_{18}(DMSO)_{13}]^{4+}$	3509	$[Bi_{38}O_{46}(NO_3)_{20}(DMSO)_7(MeCN)Na]^{3+}$
2712	$[Bi_{38}O_{46}(NO_3)_{18}(DMSO)_{13}(MeCN)]^{4+}$	3519	$[Bi_{38}O_{46}(NO_3)_{19}(DMSO)_9]^{3+}$
2714	$[Bi_{38}O_{45}(NO_3)_{20}(DMSO)_{12}(H_2O)]^{4+}$	3536	$[Bi_{38}O_{46}(NO_3)_{20}(DMSO)_8(MeCN)Na]^{3+}$
2721	$[Bi_{38}O_{46}(NO_3)_{18}(DMSO)_{14}]^{4+}$	3556	$[Bi_{38}O_{45}(NO_3)_{21}(DMSO)_9]^{3+}$
2729	$[Bi_{38}O_{45}(NO_3)_{20}(DMSO)_{13}]^{4+}$	3545	$[Bi_{38}O_{46}(NO_3)_{19}(DMSO)_{10}]^{3+}$
2741	$[Bi_{38}O_{46}(NO_3)_{18}(DMSO)_{15}]^{4+}$	3571	$[Bi_{38}O_{46}(NO_3)_{19}(DMSO)_{11}]^{3+}$
2760	$[Bi_{38}O_{46}(NO_3)_{18}(DMSO)_{16}]^{4+}$	3581	$[Bi_{38}O_{45}(NO_3)_{21}(DMSO)_{10}]^{3+}$
2768	$[Bi_{38}O_{45}(NO_3)_{20}(DMSO)_{15}]^{4+}$	3596	$[Bi_{38}O_{46}(NO_3)_{19}(DMSO)_{12}]^{3+}$
2778	$[Bi_{38}O_{45}(NO_3)_{20}(DMSO)_{15}(MeCN)]^{4+}$	3605	$[Bi_{38}O_{45}(NO_3)_{21}(DMSO)_{11}]^{3+}$
2787	$[Bi_{38}O_{45}(NO_3)_{20}(DMSO)_{16}]^{4+}$	3621	$[Bi_{38}O_{45}(NO_3)_{21}(DMSO)_{11}(MeCN)]^{3+}$
2791	$[Bi_{38}O_{46}(NO_3)_{18}(DMSO)_{17}(MeCN)]^{4+}$	3625	$[Bi_{38}O_{46}(NO_3)_{19}(DMSO)_{12}(MeCN)_2]^{3+}$
2797	$[Bi_{38}O_{45}(NO_3)_{20}(DMSO)_{16}(MeCN)]^{4+}$	3633	$[Bi_{38}O_{45}(NO_3)_{21}(DMSO)_{12}]^{3+}$
2801	$[Bi_{38}O_{45}(NO_3)_{20}(DMSO)_{17}]^{4+}$	3647	$[Bi_{38}O_{45}(NO_3)_{21}(DMSO)_{12}(MeCN)]^{3+}$
2807	$[Bi_{38}O_{46}(NO_3)_{18}(DMSO)_{17}(MeCN)_2]^{4+}$	3649	$[Bi_{38}O_{46}(NO_3)_{19}(DMSO)_{14}]^{3+}$
2817	$[Bi_{38}O_{45}(NO_3)_{20}(DMSO)_{17}(MeCN)]^{4+}$	3651	$[Bi_{38}O_{46}(NO_3)_{19}(DMSO)_{13}(MeCN)_2]^{3+}$
2819	$[Bi_{38}O_{46}(NO_3)_{18}(DMSO)_{19}]^{4+}$	3673	$[Bi_{38}O_{45}(NO_3)_{21}(DMSO)_{13}(MeCN)]^{3+}$
		3675	$[Bi_{38}O_{46}(NO_3)_{19}(DMSO)_{15}]^{3+}$
		3702	$[Bi_{38}O_{46}(NO_3)_{19}(DMSO)_{16}]^{3+}$

Different Crystals of $[Bi_{38}O_{45}(NO_3)_{20}(DMSO)_{28}](NO_3)_4(DMSO)_4$ **204a-c**

3.00 mg (0.23717 mmol) of the different crystals of $[Bi_{38}O_{45}(NO_3)_{20}(DMSO)_{28}](NO_3)_4(DMSO)_4$ **204a-c** were suspended in 0.3 ml DMSO and heated for 5 min at 70 °C. The resulting solution was cooled to room temperature and diluted with 1.7 ml acetonitrile which yielded in a solution of **204** with a concentration of 120 µmol/L. This solution was used for the ESI MS experiments.

$C_{64}H_{192}O_{149}N_{24}S_{32}Bi_{38}$ 12649.2 g/mol

Table 8.3: *ESI-MS data of the needle-like crystals of* $[Bi_{38}O_{45}(NO_3)_{20}(DMSO)_{28}]$-$(NO_3)_4(DMSO)_4$ ***204a*** *- crystallized by diffusion of THF into a DMSO solution of* ***204****.*

m/z	**Fragment**	*m/z*	**Fragment**
2173	$[Bi_{38}O_{45}(NO_3)_{19}(DMSO)_{10}(MeCN)_6]^{5+}$	2736	$[Bi_{38}O_{45}(NO_3)_{20}(DMSO)_{11}(MeCN)_4(H_2O)]^{4+}$
2195	$[Bi_{38}O_{45}(NO_3)_{19}(DMSO)_{14}(MeCN)]^{5+}$	2737	$[Bi_{38}O_{45}(NO_3)_{20}(DMSO)_{10}(MeCN)_6(H_2O)]^{4+}$
2205	$[Bi_{38}O_{45}(NO_3)_{19}(DMSO)_{11}(MeCN)_8]^{5+}$	2740	$[Bi_{38}O_{45}(NO_3)_{20}(DMSO)_{12}(MeCN)_3]^{4+}$
2208	$[Bi_{38}O_{45}(NO_3)_{19}(DMSO)_{13}(MeCN)_4(H_2O)]^{5+}$	2748	$[Bi_{38}O_{45}(NO_3)_{20}(DMSO)_{14}]^{4+}$
2211	$[Bi_{38}O_{45}(NO_3)_{19}(DMSO)_{14}(MeCN)_3]^{5+}$	2752	$[Bi_{38}O_{45}(NO_3)_{20}(DMSO)_{10}(MeCN)_8]^{4+}$
2224	$[Bi_{38}O_{45}(NO_3)_{19}(DMSO)_{13}(MeCN)_6(H_2O)]^{5+}$	2753	$[Bi_{38}O_{45}(NO_3)_{20}(DMSO)_{14}(H_2O)]^{4+}$
2227	$[Bi_{38}O_{45}(NO_3)_{19}(DMSO)_{15}(MeCN)_3]^{5+}$	2756	$[Bi_{38}O_{45}(NO_3)_{20}(DMSO)_{11}(MeCN)_6(H_2O)]^{4+}$
2242	$[Bi_{38}O_{45}(NO_3)_{19}(DMSO)_{16}(MeCN)_3]^{5+}$	2760	$[Bi_{38}O_{45}(NO_3)_{20}(DMSO)_{13}(MeCN)_3]^{4+}$
		2779	$[Bi_{38}O_{45}(NO_3)_{20}(DMSO)_{14}(MeCN)_3]^{4+}$
2583	$[Bi_{38}O_{45}(NO_3)_{20}(DMSO)_5(MeCN)]^{4+}$		
2602	$[Bi_{38}O_{45}(NO_3)_{20}(DMSO)_6(MeCN)]^{4+}$	3544	$[Bi_{38}O_{45}(NO_3)_{21}(DMSO)_7(MeCN)_3]^{3+}$
2622	$[Bi_{38}O_{45}(NO_3)_{20}(DMSO)_7(MeCN)]^{4+}$	3564	$[Bi_{38}O_{45}(NO_3)_{21}(DMSO)_7(MeCN)_4(H_2O)]^{3+}$
2623	$[Bi_{38}O_{45}(NO_3)_{20}(DMSO)_6(MeCN)_3]^{4+}$	3569	$[Bi_{38}O_{45}(NO_3)_{21}(DMSO)_9(MeCN)]^{3+}$
2641	$[Bi_{38}O_{45}(NO_3)_{20}(DMSO)_8(MeCN)]^{4+}$	3581	$[Bi_{38}O_{45}(NO_3)_{21}(DMSO)_{10}]^{3+}$
2642	$[Bi_{38}O_{45}(NO_3)_{20}(DMSO)_7(MeCN)_3]^{4+}$	3586	$[Bi_{38}O_{45}(NO_3)_{21}(DMSO)_6(MeCN)_8]^{3+}$
2662	$[Bi_{38}O_{45}(NO_3)_{20}(DMSO)_9(MeCN)]^{4+}$	3590	$[Bi_{38}O_{45}(NO_3)_{21}(DMSO)_8(MeCN)_4(H_2O)]^{3+}$
2674	$[Bi_{38}O_{45}(NO_3)_{20}(DMSO)_6(MeCN)_8]^{4+}$	3595	$[Bi_{38}O_{45}(NO_3)_{21}(DMSO)_{10}(MeCN)]^{3+}$
2693	$[Bi_{38}O_{45}(NO_3)_{20}(DMSO)_8(MeCN)_6]^{4+}$	3607	$[Bi_{38}O_{45}(NO_3)_{21}(DMSO)_{11}]^{3+}$
2694	$[Bi_{38}O_{45}(NO_3)_{20}(DMSO)_7(MeCN)_8]^{4+}$	3613	$[Bi_{38}O_{45}(NO_3)_{21}(DMSO)_{11}(H_2O)]^{3+}$
2697	$[Bi_{38}O_{45}(NO_3)_{20}(DMSO)_7(MeCN)_8(H_2O)]^{4+}$	3616	$[Bi_{38}O_{45}(NO_3)_{21}(DMSO)_9(MeCN)_4(H_2O)]^{3+}$
2703	$[Bi_{38}O_{45}(NO_3)_{20}(DMSO)_8(MeCN)_7]^{4+}$	3621	$[Bi_{38}O_{45}(NO_3)_{21}(DMSO)_{11}(MeCN)]^{3+}$
2710	$[Bi_{38}O_{45}(NO_3)_{20}(DMSO)_{12}]^{4+}$	3634	$[Bi_{38}O_{45}(NO_3)_{21}(DMSO)_{12}]^{3+}$
2713	$[Bi_{38}O_{45}(NO_3)_{20}(DMSO)_9(MeCN)_6]^{4+}$	3637	$[Bi_{38}O_{45}(NO_3)_{21}(DMSO)_9(MeCN)_6]^{3+}$
2714	$[Bi_{38}O_{45}(NO_3)_{20}(DMSO)_8(MeCN)_8]^{4+}$	3642	$[Bi_{38}O_{45}(NO_3)_{21}(DMSO)_{10}(MeCN)_4(H_2O)]^{3+}$
2717	$[Bi_{38}O_{45}(NO_3)_{20}(DMSO)_9(MeCN)_6(H_2O)]^{4+}$	3647	$[Bi_{38}O_{45}(NO_3)_{21}(DMSO)_{12}(MeCN)]^{3+}$
2720	$[Bi_{38}O_{45}(NO_3)_{20}(DMSO)_{12}(MeCN)]^{4+}$	3660	$[Bi_{38}O_{45}(NO_3)_{21}(DMSO)_{12}(MeCN)_2]^{3+}$
2721	$[Bi_{38}O_{45}(NO_3)_{20}(DMSO)_{11}(MeCN)_3]^{4+}$	3669	$[Bi_{38}O_{45}(NO_3)_{21}(DMSO)_{10}(MeCN)_6(H_2O)]^{3+}$
2729	$[Bi_{38}O_{45}(NO_3)_{20}(DMSO)_{13}]^{4+}$	3678	$[Bi_{38}O_{45}(NO_3)_{21}(DMSO)_{10}(MeCN)_7]^{3+}$
2733	$[Bi_{38}O_{45}(NO_3)_{20}(DMSO)_{13}(H_2O)]^{4+}$	3684	$[Bi_{38}O_{45}(NO_3)_{21}(DMSO)_{10}(MeCN)_7(H_2O)]^{3+}$
2734	$[Bi_{38}O_{45}(NO_3)_{20}(DMSO)_9(MeCN)_8]^{4+}$	3695	$[Bi_{38}O_{45}(NO_3)_{21}(DMSO)_{11}(MeCN)_6(H_2O)]^{3+}$

Table 8.4a: *First part of the ESI-MS data of the hexagonal shaped crystals of* $[Bi_{38}O_{45}(NO_3)_{20}(DMSO)_{28}](NO_3)_4(DMSO)_4$ ***204b*** *- crystallized by diffusion of THF into a DMSO solution of* ***204****.*

m/z	Fragment	*m/z*	Fragment
1814	$[Bi_{38}O_{45}(NO_3)_{18}(DMSO)_{10}(MeCN)_8]^{6+}$	2182	$[Bi_{38}O_{45}(NO_3)_{19}(DMSO)_{10}(MeCN)_7]^{5+}$
1827	$[Bi_{38}O_{45}(NO_3)_{18}(DMSO)_{11}(MeCN)_8]^{6+}$	2177	$[Bi_{38}O_{45}(NO_3)_{19}(DMSO)_9(MeCN)_8(H_2O)]^{5+}$
		2183	$[Bi_{38}O_{45}(NO_3)_{19}(DMSO)_{12}(MeCN)_3(H_2O)]^{5+}$
2049	$[Bi_{38}O_{45}(NO_3)_{19}(DMSO)_5(H_2O)]^{5+}$	2185	$[Bi_{38}O_{45}(NO_3)_{19}(DMSO)_{10}(MeCN)_7](H_2O)]^{5+}$
2065	$[Bi_{38}O_{45}(NO_3)_{19}(DMSO)_6(H_2O)]^{5+}$	2166	$[Bi_{38}O_{45}(NO_3)_{19}(DMSO)_9(MeCN)_7]^{5+}$
2075	$[Bi_{38}O_{45}(NO_3)_{19}(DMSO)_5(MeCN)_3(H_2O)]^{5+}$	2168	$[Bi_{38}O_{45}(NO_3)_{19}(DMSO)_{10}(MeCN)_5(H_2O)]^{5+}$
2080	$[Bi_{38}O_{45}(NO_3)_{19}(DMSO)_7(H_2O)]^{5+}$	2169	$[Bi_{38}O_{45}(NO_3)_{19}(DMSO)_9(MeCN)_7(H_2O)]^{5+}$
2085	$[Bi_{38}O_{45}(NO_3)_{19}(DMSO)_7(MeCN)]^{5+}$	2171	$[Bi_{38}O_{45}(NO_3)_{19}(DMSO)_{13}]^{5+}$
2096	$[Bi_{38}O_{45}(NO_3)_{19}(DMSO)_8(H_2O)]^{5+}$	2173	$[Bi_{38}O_{45}(NO_3)_{19}(DMSO)_{10}(MeCN)_6]^{5+}$
2101	$[Bi_{38}O_{45}(NO_3)_{19}(DMSO)_8(MeCN)]^{5+}$	2174	$[Bi_{38}O_{45}(NO_3)_{19}(DMSO)_{13}(H_2O)]^{5+}$
2112	$[Bi_{38}O_{45}(NO_3)_{19}(DMSO)_9(H_2O)]^{5+}$	2177	$[Bi_{38}O_{45}(NO_3)_{19}(DMSO)_9(MeCN)_8(H_2O)]^{5+}$
2116	$[Bi_{38}O_{45}(NO_3)_{19}(DMSO)_9(MeCN)]^{5+}$	2180	$[Bi_{38}O_{45}(NO_3)_{19}(DMSO)_{11}(MeCN)_5]^{5+}$
2122	$[Bi_{38}O_{45}(NO_3)_{19}(DMSO)_7(MeCN)_5(H_2O)]^{5+}$	2182	$[Bi_{38}O_{45}(NO_3)_{19}(DMSO)_{10}(MeCN)_7]^{5+}$
2124	$[Bi_{38}O_{45}(NO_3)_{19}(DMSO)_{10}]^{5+}$	2183	$[Bi_{38}O_{45}(NO_3)_{19}(DMSO)_{12}(MeCN)_3(H_2O)]^{5+}$
2127	$[Bi_{38}O_{45}(NO_3)_{19}(DMSO)_{10}(H_2O)]^{5+}$	2185	$[Bi_{38}O_{45}(NO_3)_{19}(DMSO)_{10}(MeCN)_7](H_2O)]^{5+}$
2130	$[Bi_{38}O_{45}(NO_3)_{19}(DMSO)_8(MeCN)_4(H_2O)]^{5+}$	2186	$[Bi_{38}O_{45}(NO_3)_{19}(DMSO)_{14}]^{5+}$
2133	$[Bi_{38}O_{45}(NO_3)_{19}(DMSO)_{10}(MeCN)]^{5+}$	2187	$[Bi_{38}O_{45}(NO_3)_{19}(DMSO)_{13}(MeCN)_2]^{5+}$
2138	$[Bi_{38}O_{45}(NO_3)_{19}(DMSO)_8(MeCN)_5(H_2O)]^{5+}$	2189	$[Bi_{38}O_{45}(NO_3)_{19}(DMSO)_{10}(MeCN)_8]^{5+}$
2140	$[Bi_{38}O_{45}(NO_3)_{19}(DMSO)_{11}]^{5+}$	2191	$[Bi_{38}O_{45}(NO_3)_{19}(DMSO)_{12}(MeCN)_4(H_2O)]^{5+}$
2143	$[Bi_{38}O_{45}(NO_3)_{19}(DMSO)_{11}(H_2O)]^{5+}$	2193	$[Bi_{38}O_{45}(NO_3)_{19}(DMSO)_{10}(MeCN)_8(H_2O)]^{5+}$
2145	$[Bi_{38}O_{45}(NO_3)_{19}(DMSO)_8(MeCN)_6(H_2O)]^{5+}$	2196	$[Bi_{38}O_{45}(NO_3)_{19}(DMSO)_{12}(MeCN)_5]^{5+}$
2149	$[Bi_{38}O_{45}(NO_3)_{19}(DMSO)_{10}(MeCN)_3]^{5+}$	2198	$[Bi_{38}O_{45}(NO_3)_{19}(DMSO)_{14}(MeCN)(H_2O)]^{5+}$
2150	$[Bi_{38}O_{45}(NO_3)_{19}(DMSO)_8(MeCN)_7]^{5+}$	2200	$[Bi_{38}O_{45}(NO_3)_{19}(DMSO)_{11}(MeCN)_7(H_2O)]^{5+}$
2153	$[Bi_{38}O_{45}(NO_3)_{19}(DMSO)_9(MeCN)_5(H_2O)]^{5+}$	2202	$[Bi_{38}O_{45}(NO_3)_{19}(DMSO)_{15}]^{5+}$
2156	$[Bi_{38}O_{45}(NO_3)_{19}(DMSO)_{11}(MeCN)_2]^{5+}$	2205	$[Bi_{38}O_{45}(NO_3)_{19}(DMSO)_{12}(MeCN)_6]^{5+}$
2158	$[Bi_{38}O_{45}(NO_3)_{19}(DMSO)_8(MeCN)_8]^{5+}$	2206	$[Bi_{38}O_{45}(NO_3)_{19}(DMSO)_{15}(H_2O)]^{5+}$
2159	$[Bi_{38}O_{45}(NO_3)_{19}(DMSO)_{12}(H_2O)]^{5+}$	2208	$[Bi_{38}O_{45}(NO_3)_{19}(DMSO)_{12}(MeCN)_6(H_2O)]^{5+}$
2161	$[Bi_{38}O_{45}(NO_3)_{19}(DMSO)_9(MeCN)_6(H_2O)]^{5+}$	2211	$[Bi_{38}O_{45}(NO_3)_{19}(DMSO)_{14}(MeCN)_3]^{5+}$
2164	$[Bi_{38}O_{45}(NO_3)_{19}(DMSO)_{11}(MeCN)_3]^{5+}$	2214	$[Bi_{38}O_{45}(NO_3)_{19}(DMSO)_{14}(MeCN)_3(H_2O)]^{5+}$
2166	$[Bi_{38}O_{45}(NO_3)_{19}(DMSO)_9(MeCN)_7]^{5+}$		
2168	$[Bi_{38}O_{45}(NO_3)_{19}(DMSO)_{10}(MeCN)_5(H_2O)]^{5+}$	2616	$[Bi_{38}O_{45}(NO_3)_{20}(DMSO)_7(H_2O)]^{4+}$
2169	$[Bi_{38}O_{45}(NO_3)_{19}(DMSO)_9(MeCN)_7(H_2O)]^{5+}$	2629	$[Bi_{38}O_{45}(NO_3)_{20}(DMSO)_5(MeCN)_5(H_2O)]^{4+}$
2171	$[Bi_{38}O_{45}(NO_3)_{19}(DMSO)_{13}]^{5+}$	2631	$[Bi_{38}O_{45}(NO_3)_{20}(DMSO)_8]^{4+}$
2173	$[Bi_{38}O_{45}(NO_3)_{19}(DMSO)_{10}(MeCN)_6]^{5+}$	2635	$[Bi_{38}O_{45}(NO_3)_{20}(DMSO)_8(H_2O)]^{4+}$
2174	$[Bi_{38}O_{45}(NO_3)_{19}(DMSO)_{13}(H_2O)]^{5+}$	2645	$[Bi_{38}O_{45}(NO_3)_{20}(DMSO)_5(MeCN)_7]^{4+}$
2180	$[Bi_{38}O_{45}(NO_3)_{19}(DMSO)_{11}(MeCN)_5]^{5+}$	2648	$[Bi_{38}O_{45}(NO_3)_{20}(DMSO)_6(MeCN)_5(H_2O)]^{4+}$

Table 8.4b: *Second part of the ESI-MS data of the hexagonal shaped crystals of* $[Bi_{38}O_{45}(NO_3)_{20}(DMSO)_{28}](NO_3)_4(DMSO)_4$ ***204b*** *- crystallized by diffusion of THF into a DMSO solution of* ***204****.*

m/z	Fragment	*m/z*	Fragment
2651	$[Bi_{38}O_{45}(NO_3)_{20}(DMSO)_9]^{4+}$	2693	$[Bi_{38}O_{45}(NO_3)_{20}(DMSO)_8(MeCN)_6]^{4+}$
2655	$[Bi_{38}O_{45}(NO_3)_{20}(DMSO)_5(MeCN)_8]^{4+}$	2695	$[Bi_{38}O_{45}(NO_3)_{20}(DMSO)_{11}(H_2O)]^{4+}$
2658	$[Bi_{38}O_{45}(NO_3)_{20}(DMSO)_6(MeCN)_6(H_2O)]^{4+}$	2697	$[Bi_{38}O_{45}(NO_3)_{20}(DMSO)_8(MeCN)_6(H_2O)]^{4+}$
2664	$[Bi_{38}O_{45}(NO_3)_{20}(DMSO)_6(MeCN)_7]^{4+}$	2701	$[Bi_{38}O_{45}(NO_3)_{20}(DMSO)_{10}(MeCN)_3]^{4+}$
2667	$[Bi_{38}O_{45}(NO_3)_{20}(DMSO)_7(MeCN)_5(H_2O)]^{4+}$	2704	$[Bi_{38}O_{45}(NO_3)_{20}(DMSO)_{11}(MeCN)(H_2O)]^{4+}$
2669	$[Bi_{38}O_{45}(NO_3)_{20}(DMSO)_6(MeCN)_7(H_2O)]^{4+}$	2708	$[Bi_{38}O_{45}(NO_3)_{20}(DMSO)_8(MeCN)_7(H_2O)]^{4+}$
2672	$[Bi_{38}O_{45}(NO_3)_{20}(DMSO)_9(MeCN)_2]^{4+}$	2710	$[Bi_{38}O_{45}(NO_3)_{20}(DMSO)_{12}]^{4+}$
2673	$[Bi_{38}O_{45}(NO_3)_{20}(DMSO)_7(MeCN)_6]^{4+}$	2714	$[Bi_{38}O_{45}(NO_3)_{20}(DMSO)_{12}(H_2O)]^{4+}$
2675	$[Bi_{38}O_{45}(NO_3)_{20}(DMSO)_6(MeCN)_8]^{4+}$	2717	$[Bi_{38}O_{45}(NO_3)_{20}(DMSO)_9(MeCN)_6(H_2O)]^{4+}$
2678	$[Bi_{38}O_{45}(NO_3)_{20}(DMSO)_7(MeCN)_6(H_2O)]^{4+}$	2721	$[Bi_{38}O_{45}(NO_3)_{20}(DMSO)_{11}(MeCN)_3]^{4+}$
2682	$[Bi_{38}O_{45}(NO_3)_{20}(DMSO)_9(MeCN)_3]^{4+}$	2725	$[Bi_{38}O_{45}(NO_3)_{20}(DMSO)_{11}(MeCN)_3(H_2O)]^{4+}$
2684	$[Bi_{38}O_{45}(NO_3)_{20}(DMSO)_7(MeCN)_7]^{4+}$	2729	$[Bi_{38}O_{45}(NO_3)_{20}(DMSO)_{13}]^{4+}$
2688	$[Bi_{38}O_{45}(NO_3)_{20}(DMSO)_7(MeCN)_7(H_2O)]^{4+}$	2734	$[Bi_{38}O_{45}(NO_3)_{20}(DMSO)_9(MeCN)_8]^{4+}$
2690	$[Bi_{38}O_{45}(NO_3)_{20}(DMSO)_{11}]^{4+}$	2740	$[Bi_{38}O_{45}(NO_3)_{20}(DMSO)_{12}(MeCN)_3]^{4+}$

Table 8.5a: *First part of the ESI-MS data of the hexagonal shaped crystals of* $[Bi_{38}O_{45}(NO_3)_{20}(DMSO)_{28}](NO_3)_4(DMSO)_4$ ***204c*** *- crystallized by diffusion of acetone into a DMSO solution of* ***204****.*

m/z	Fragment	*m/z*	Fragment
1202	$[Bi_{38}O_{45}(NO_3)_{15}(DMSO)_{15}(MeCN)(H_2O)]^{9+}$	1395	$[Bi_{38}O_{45}(NO_3)_{16}(DMSO)_{18}(MeCN)_2(H_2O)]^{8+}$
1203	$[Bi_{38}O_{45}(NO_3)_{15}(DMSO)_{14}(MeCN)_3(H_2O)]^{9+}$	1399	$[Bi_{38}O_{45}(NO_3)_{16}(DMSO)_{19}(MeCN)(H_2O)]^{8+}$
1209	$[Bi_{38}O_{45}(NO_3)_{15}(DMSO)_{15}(MeCN)_3]^{9+}$	1409	$[Bi_{38}O_{45}(NO_3)_{16}(DMSO)_{20}(MeCN)(H_2O)]^{8+}$
1211	$[Bi_{38}O_{45}(NO_3)_{15}(DMSO)_{16}(MeCN)(H_2O)]^{9+}$		
1218	$[Bi_{38}O_{45}(NO_3)_{15}(DMSO)_{16}(MeCN)_3]^{9+}$	1796	$[Bi_{38}O_{45}(NO_3)_{18}(DMSO)_{11}(MeCN)_3(H_2O)]^{6+}$
1220	$[Bi_{38}O_{45}(NO_3)_{15}(DMSO)_{16}(MeCN)_3(H_2O)]^{9+}$	1805	$[Bi_{38}O_{45}(NO_3)_{18}(DMSO)_9(MeCN)_8(H_2O)]^{6+}$
1223	$[Bi_{38}O_{45}(NO_3)_{15}(DMSO)_{15}(MeCN)_6]^{9+}$	1809	$[Bi_{38}O_{45}(NO_3)_{18}(DMSO)_{12}(MeCN)_3(H_2O)]^{6+}$
1227	$[Bi_{38}O_{45}(NO_3)_{15}(DMSO)_{16}(MeCN)_5]^{9+}$	1815	$[Bi_{38}O_{45}(NO_3)_{18}(DMSO)_{13}(MeCN)_2(H_2O)]^{6+}$
1230	$[Bi_{38}O_{45}(NO_3)_{15}(DMSO)_{15}(MeCN)_7(H_2O)]^{9+}$	1820	$[Bi_{38}O_{45}(NO_3)_{18}(DMSO)_{12}(MeCN)_5]^{6+}$
1232	$[Bi_{38}O_{45}(NO_3)_{15}(DMSO)_{15}(MeCN)_8]^{9+}$	1822	$[Bi_{38}O_{45}(NO_3)_{18}(DMSO)_{13}(MeCN)_3(H_2O)]^{6+}$
1241	$[Bi_{38}O_{45}(NO_3)_{15}(DMSO)_{16}(MeCN)_8]^{9+}$	1823	$[Bi_{38}O_{45}(NO_3)_{18}(DMSO)_{12}(MeCN)_5(H_2O)]^{6+}$
		1825	$[Bi_{38}O_{45}(NO_3)_{18}(DMSO)_{15}]^{6+}$
1366	$[Bi_{38}O_{45}(NO_3)_{16}(DMSO)_{15}(MeCN)_2(H_2O)]^{8+}$	1827	$[Bi_{38}O_{45}(NO_3)_{18}(DMSO)_{11}(MeCN)_8]^{6+}$
1376	$[Bi_{38}O_{45}(NO_3)_{16}(DMSO)_{16}(MeCN)_2(H_2O)]^{8+}$	1828	$[Bi_{38}O_{45}(NO_3)_{18}(DMSO)_{15}(H_2O)]^{6+}$
1385	$[Bi_{38}O_{45}(NO_3)_{16}(DMSO)_{17}(MeCN)_2(H_2O)]^{8+}$	1833	$[Bi_{38}O_{45}(NO_3)_{18}(DMSO)_{13}(MeCN)_5]^{6+}$

Table 8.5b: *Second part of the ESI-MS data of the hexagonal shaped crystals of* $[Bi_{38}O_{45}(NO_3)_{20}(DMSO)_{28}](NO_3)_4(DMSO)_4$ ***204c*** *- crystallized by diffusion of acetone into a DMSO solution of* ***204****.*

m/z	**Fragment**	*m/z*	**Fragment**
1835	$[Bi_{38}O_{45}(NO_3)_{18}(DMSO)_{15}(MeCN)(H_2O)]^{6+}$	2770	$[Bi_{38}O_{45}(NO_3)_{20}(DMSO)_{14}(MeCN)_2]^{4+}$
1836	$[Bi_{38}O_{45}(NO_3)_{18}(DMSO)_{14}(MeCN)_3(H_2O)]^{6+}$	2778	$[Bi_{38}O_{45}(NO_3)_{20}(DMSO)_{15}(MeCN)]^{4+}$
1838	$[Bi_{38}O_{45}(NO_3)_{18}(DMSO)_{16}]^{6+}$	2782	$[Bi_{38}O_{45}(NO_3)_{20}(DMSO)_{15}(MeCN)(H_2O)]^{4+}$
1840	$[Bi_{38}O_{45}(NO_3)_{18}(DMSO)_{16}(H_2O)]^{6+}$	2784	$[Bi_{38}O_{45}(NO_3)_{20}(DMSO)_{13}(MeCN)_5(H_2O)]^{4+}$
1845	$[Bi_{38}O_{45}(NO_3)_{18}(DMSO)_{16}(MeCN)]^{6+}$	2787	$[Bi_{38}O_{45}(NO_3)_{20}(DMSO)_{16}]^{4+}$
1846	$[Bi_{38}O_{45}(NO_3)_{18}(DMSO)_{14}(MeCN)_5]^{6+}$	2789	$[Bi_{38}O_{45}(NO_3)_{20}(DMSO)_{15}(MeCN)_2]^{4+}$
1849	$[Bi_{38}O_{45}(NO_3)_{18}(DMSO)_{13}(MeCN)_7(H_2O)]^{6+}$	2790	$[Bi_{38}O_{45}(NO_3)_{20}(DMSO)_{13}(MeCN)_6]^{4+}$
1851	$[Bi_{38}O_{45}(NO_3)_{18}(DMSO)_{16}(MeCN)_2]^{6+}$	2793	$[Bi_{38}O_{45}(NO_3)_{20}(DMSO)_{15}(MeCN)_2(H_2O)]^{4+}$
1854	$[Bi_{38}O_{45}(NO_3)_{18}(DMSO)_{16}(MeCN)_2(H_2O)]^{6+}$	2798	$[Bi_{38}O_{45}(NO_3)_{20}(DMSO)_{16}(MeCN)]^{4+}$
1867	$[Bi_{38}O_{45}(NO_3)_{18}(DMSO)_{17}(MeCN)_2(H_2O)]^{6+}$	2802	$[Bi_{38}O_{45}(NO_3)_{20}(DMSO)_{16}(MeCN)(H_2O)]^{4+}$
2229	$[Bi_{38}O_{45}(NO_3)_{19}(DMSO)_{16}(MeCN)(H_2O)]^{5+}$	2807	$[Bi_{38}O_{45}(NO_3)_{20}(DMSO)_{17}]^{4+}$
2245	$[Bi_{38}O_{45}(NO_3)_{19}(DMSO)_{17}(MeCN)(H_2O)]^{5+}$	2809	$[Bi_{38}O_{45}(NO_3)_{20}(DMSO)_{16}(MeCN)_2]^{4+}$
2261	$[Bi_{38}O_{45}(NO_3)_{19}(DMSO)_{18}(MeCN)(H_2O)]^{5+}$	2811	$[Bi_{38}O_{45}(NO_3)_{20}(DMSO)_{17}(H2O)]^{4+}$
2268	$[Bi_{38}O_{45}(NO_3)_{19}(DMSO)_{16}(MeCN)_6]^{5+}$	2814	$[Bi_{38}O_{45}(NO_3)_{20}(DMSO)_{15}(MeCN)_4(H_2O)]^{4+}$
2278	$[Bi_{38}O_{45}(NO_3)_{19}(DMSO)_{18}(MeCN)_3(H_2O)]^{5+}$	2818	$[Bi_{38}O_{45}(NO_3)_{20}(DMSO)_{17}(MeCN)]^{4+}$
2284	$[Bi_{38}O_{45}(NO_3)_{19}(DMSO)_{20}(H_2O)]^{5+}$	2831	$[Bi_{38}O_{45}(NO_3)_{20}(DMSO)_{18}(H2O)]^{4+}$
2300	$[Bi_{38}O_{45}(NO_3)_{19}(DMSO)_{21}(H_2O)]^{5+}$	2834	$[Bi_{38}O_{45}(NO_3)_{20}(DMSO)_{16}(MeCN)_4(H_2O)]^{4+}$
		2838	$[Bi_{38}O_{45}(NO_3)_{20}(DMSO)_{18}(MeCN)]^{4+}$
2590	$[Bi_{38}O_{45}(NO_3)_{20}(DMSO)_3(MeCN)_5(H_2O)]^{4+}$	2858	$[Bi_{38}O_{45}(NO_3)_{20}(DMSO)_{19}(MeCN)]^{4+}$
2610	$[Bi_{38}O_{45}(NO_3)_{20}(DMSO)_4(MeCN)_5(H_2O)]^{4+}$		
2630	$[Bi_{38}O_{45}(NO_3)_{20}(DMSO)_5(MeCN)_5(H_2O)]^{4+}$	3599	$[Bi_{38}O_{45}(NO_3)_{21}(DMSO)_7(MeCN)_7]^{3+}$
2650	$[Bi_{38}O_{45}(NO_3)_{20}(DMSO)_6(MeCN)_5(H_2O)]^{4+}$	3616	$[Bi_{38}O_{45}(NO_3)_{21}(DMSO)_9(MeCN)_4(H_2O)]^{3+}$
2670	$[Bi_{38}O_{45}(NO_3)_{20}(DMSO)_7(MeCN)_5(H_2O)]^{4+}$	3619	$[Bi_{38}O_{45}(NO_3)_{21}(DMSO)_7(MeCN)_8(H_2O)]^{3+}$
2677	$[Bi_{38}O_{45}(NO_3)_{20}(DMSO)_8(MeCN)_4(H_2O)]^{4+}$	3625	$[Bi_{38}O_{45}(NO_3)_{21}(DMSO)_8(MeCN)_7]^{3+}$
2691	$[Bi_{38}O_{45}(NO_3)_{20}(DMSO)_{10}(MeCN)_2]^{4+}$	3638	$[Bi_{38}O_{45}(NO_3)_{21}(DMSO)_8(MeCN)_8]^{3+}$
2697	$[Bi_{38}O_{45}(NO_3)_{20}(DMSO)_9(MeCN)_4(H_2O)]^{4+}$	3643	$[Bi_{38}O_{45}(NO_3)_{21}(DMSO)_{10}(MeCN)_4(H_2O)]^{3+}$
2703	$[Bi_{38}O_{45}(NO_3)_{20}(DMSO)_8(MeCN)_7]^{4+}$	3647	$[Bi_{38}O_{45}(NO_3)_{21}(DMSO)_{12}(MeCN)]^{3+}$
2711	$[Bi_{38}O_{45}(NO_3)_{20}(DMSO)_{11}(MeCN)_2]^{4+}$	3651	$[Bi_{38}O_{45}(NO_3)_{21}(DMSO)_9(MeCN)_7]^{3+}$
2724	$[Bi_{38}O_{45}(NO_3)_{20}(DMSO)_{12}(MeCN)(H_2O)]^{4+}$	3664	$[Bi_{38}O_{45}(NO_3)_{21}(DMSO)_9(MeCN)_8]^{3+}$
2730	$[Bi_{38}O_{45}(NO_3)_{20}(DMSO)_{12}(MeCN)_2]^{4+}$	3668	$[Bi_{38}O_{45}(NO_3)_{21}(DMSO)_{11}(MeCN)_4(H_2O)]^{3+}$
2744	$[Bi_{38}O_{45}(NO_3)_{20}(DMSO)_{12}(MeCN)_3(H_2O)]^{4+}$	3670	$[Bi_{38}O_{45}(NO_3)_{21}(DMSO)_9(MeCN)_8(H_2O)]^{3+}$
2746	$[Bi_{38}O_{45}(NO_3)_{20}(DMSO)_{10}(MeCN)_7(H_2O)]^{4+}$	3673	$[Bi_{38}O_{45}(NO_3)_{21}(DMSO)_{13}(MeCN)]^{3+}$
2750	$[Bi_{38}O_{45}(NO_3)_{20}(DMSO)_{13}(MeCN)_2]^{4+}$	3677	$[Bi_{38}O_{45}(NO_3)_{21}(DMSO)_{10}(MeCN)_7]^{3+}$
2759	$[Bi_{38}O_{45}(NO_3)_{20}(DMSO)_{13}(MeCN)_3]^{4+}$	3679	$[Bi_{38}O_{45}(NO_3)_{21}(DMSO)_{13}(MeCN)(H_2O)]^{3+}$
2763	$[Bi_{38}O_{45}(NO_3)_{20}(DMSO)_{14}(MeCN)(H_2O)]^{4+}$	3683	$[Bi_{38}O_{45}(NO_3)_{21}(DMSO)_{10}(MeCN)_7(H_2O)]^{3+}$

Table 8.5c: *Third part of the ESI-MS data of the hexagonal shaped crystals of* $[Bi_{38}O_{45}(NO_3)_{20}(DMSO)_{28}](NO_3)_4(DMSO)_4$ ***204c*** *- crystallized by diffusion of acetone into a DMSO solution of* ***204****.*

m/z	**Fragment**	*m/z*	**Fragment**
3689	$[Bi_{38}O_{45}(NO_3)_{21}(DMSO)_{11}(MeCN)_6]^{3+}$	3711	$[Bi_{38}O_{45}(NO_3)_{21}(DMSO)_{15}]^{3+}$
3691	$[Bi_{38}O_{45}(NO_3)_{21}(DMSO)_{10}(MeCN)_8]^{3+}$	3716	$[Bi_{38}O_{45}(NO_3)_{21}(DMSO)_{11}(MeCN)_8]^{3+}$
3695	$[Bi_{38}O_{45}(NO_3)_{21}(DMSO)_{11}(MeCN)_6(H_2O)]^{3+}$	3726	$[Bi_{38}O_{45}(NO_3)_{21}(DMSO)_{14}(MeCN)_3]^{3+}$
3699	$[Bi_{38}O_{45}(NO_3)_{21}(DMSO)_{14}(MeCN)]^{3+}$	3728	$[Bi_{38}O_{45}(NO_3)_{21}(DMSO)_{13}(MeCN)_5]^{3+}$
3701	$[Bi_{38}O_{45}(NO_3)_{21}(DMSO)_{13}(MeCN)_3]^{3+}$	3734	$[Bi_{38}O_{45}(NO_3)_{21}(DMSO)_{13}(MeCN)_5(H_2O)]^{3+}$
3703	$[Bi_{38}O_{45}(NO_3)_{21}(DMSO)_{11}(MeCN)_7]^{3+}$	3738	$[Bi_{38}O_{45}(NO_3)_{21}(DMSO)_{16}]^{3+}$
3706	$[Bi_{38}O_{45}(NO_3)_{21}(DMSO)_{13}(MeCN)_3(H_2O)]^{3+}$	3743	$[Bi_{38}O_{45}(NO_3)_{21}(DMSO)_{16}(H_2O)]^{3+}$
3709	$[Bi_{38}O_{45}(NO_3)_{21}(DMSO)_{11}(MeCN)_7](H_2O)^{3+}$	3770	$[Bi_{38}O_{45}(NO_3)_{21}(DMSO)_{16}(MeCN)_2(H_2O)]^{3+}$

$[Bi_{38}O_{45}(OH)_2(pTsO)_8(NO_3)_{12}(DMSO)_{24}](NO_3)_2(DMSO)_4(H_2O)_2$ **205**

3.00 mg (0.22804 mmol) $[Bi_{38}O_{45}(OH)_2(pTsO)_8(NO_3)_{12}(DMSO)_{24}](NO_3)_2(DMSO)_4(H_2O)_2$ **205** were suspended in 0.3 ml DMSO and heated for 5 min at 70 °C. The resulting solution was cooled to room temperature and diluted with 1.7 ml acetonitrile which yielded in a solution of **205** with a concentration of 115 µmol/L. This solution was used for the ESI MS experiments.

$C_{112}H_{230}O_{143}N_{14}S_{36}Bi_{38}$ 13155.4 g/mol

Table 8.6a: *First part of the ESI-MS data of* $[Bi_{38}O_{45}(OH)_2(pTsO)_8(NO_3)_{12}(DMSO)_{24}](NO_3)_2(DMSO)_4(H_2O)_2$ ***205****.*

m/z	**Fragment**	*m/z*	**Fragment**
2180	$[Bi_{38}O_{46}(pTsO)_5(NO_3)_{12}(DMSO)_8]^{5+}$	2308	$[Bi_{38}O_{46}(pTsO)_8(NO_3)_9(DMSO)_{12}]^{5+}$
2187	$[Bi_{38}O_{46}(pTsO)_6(NO_3)_{11}(DMSO)_7]^{5+}$	2312	$[Bi_{38}O_{46}(pTsO)_6(NO_3)_{11}(DMSO)_{15}]^{5+}$
2193	$[Bi_{38}O_{46}(pTsO)_7(NO_3)_{10}(DMSO)_6]^{5+}$	2315	$[Bi_{38}O_{46}(pTsO)_4(NO_3)_{13}(DMSO)_{18}]^{5+}$
2196	$[Bi_{38}O_{46}(pTsO)_5(NO_3)_{12}(DMSO)_9]^{5+}$	2318	$[Bi_{38}O_{46}(pTsO)_7(NO_3)_{10}(DMSO)_{14}]^{5+}$
2202	$[Bi_{38}O_{46}(pTsO)_6(NO_3)_{11}(DMSO)_8]^{5+}$	2321	$[Bi_{38}O_{46}(pTsO)_5(NO_3)_{12}(DMSO)_{16}]^{5+}$
2208	$[Bi_{38}O_{46}(pTsO)_7(NO_3)_{10}(DMSO)_7]^{5+}$	2324	$[Bi_{38}O_{46}(pTsO)_8(NO_3)_9(DMSO)_{13}]^{5+}$
2212	$[Bi_{38}O_{46}(pTsO)_5(NO_3)_{12}(DMSO)_{10}]^{5+}$	2327	$[Bi_{38}O_{46}(pTsO)_6(NO_3)_{11}(DMSO)_{16}]^{5+}$
2215	$[Bi_{38}O_{46}(pTsO)_8(NO_3)_9(DMSO)_6]^{5+}$	2330	$[Bi_{38}O_{46}(pTsO)_4(NO_3)_{13}(DMSO)_{19}]^{5+}$
2218	$[Bi_{38}O_{46}(pTsO)_6(NO_3)_{11}(DMSO)_9]^{5+}$	2333	$[Bi_{38}O_{46}(pTsO)_7(NO_3)_{10}(DMSO)_{15}]^{5+}$
2221	$[Bi_{38}O_{46}(pTsO)_4(NO_3)_{13}(DMSO)_{12}]^{5+}$	2337	$[Bi_{38}O_{46}(pTsO)_5(NO_3)_{12}(DMSO)_{17}]^{5+}$
2224	$[Bi_{38}O_{46}(pTsO)_7(NO_3)_{10}(DMSO)_8]^{5+}$	2340	$[Bi_{38}O_{46}(pTsO)_8(NO_3)_9(DMSO)_{14}]^{5+}$
2227	$[Bi_{38}O_{46}(pTsO)_5(NO_3)_{12}(DMSO)_{11}]^{5+}$	2343	$[Bi_{38}O_{46}(pTsO)_6(NO_3)_{11}(DMSO)_{17}]^{5+}$
2230	$[Bi_{38}O_{46}(pTsO)_8(NO_3)_9(DMSO)_7]^{5+}$	2346	$[Bi_{38}O_{46}(pTsO)_4(NO_3)_{13}(DMSO)_{20}]^{5+}$
2234	$[Bi_{38}O_{46}(pTsO)_6(NO_3)_{11}(DMSO)_{10}]^{5+}$		
2237	$[Bi_{38}O_{46}(pTsO)_4(NO_3)_{13}(DMSO)_{13}]^{5+}$	2702	$[Bi_{38}O_{46}(pTsO)_5(NO_3)_{13}(DMSO)_6]^{4+}$
2240	$[Bi_{38}O_{46}(pTsO)_7(NO_3)_{10}(DMSO)_9]^{5+}$	2706	$[Bi_{38}O_{46}(pTsO)_8(NO_3)_{10}(DMSO)_2]^{4+}$
2243	$[Bi_{38}O_{46}(pTsO)_5(NO_3)_{12}(DMSO)_{12}]^{5+}$	2710	$[Bi_{38}O_{46}(pTsO)_6(NO_3)_{12}(DMSO)_5]^{4+}$
2246	$[Bi_{38}O_{46}(pTsO)_8(NO_3)_9(DMSO)_8]^{5+}$	2714	$[Bi_{38}O_{46}(pTsO)_4(NO_3)_{14}(DMSO)_8]^{4+}$
2249	$[Bi_{38}O_{46}(pTsO)_6(NO_3)_{11}(DMSO)_{11}]^{5+}$	2717	$[Bi_{38}O_{46}(pTsO)_7(NO_3)_{11}(DMSO)_4]^{4+}$
2252	$[Bi_{38}O_{46}(pTsO)_4(NO_3)_{13}(DMSO)_{14}]^{5+}$	2721	$[Bi_{38}O_{46}(pTsO)_5(NO_3)_{13}(DMSO)_7]^{4+}$
2255	$[Bi_{38}O_{46}(pTsO)_7(NO_3)_{10}(DMSO)_{10}]^{5+}$	2725	$[Bi_{38}O_{46}(pTsO)_8(NO_3)_{10}(DMSO)_3]^{4+}$
2258	$[Bi_{38}O_{46}(pTsO)_5(NO_3)_{12}(DMSO)_{13}]^{5+}$	2729	$[Bi_{38}O_{46}(pTsO)_6(NO_3)_{12}(DMSO)_6]^{4+}$
2261	$[Bi_{38}O_{46}(pTsO)_8(NO_3)_9(DMSO)_9]^{5+}$	2733	$[Bi_{38}O_{46}(pTsO)_4(NO_3)_{14}(DMSO)_9]^{4+}$
2265	$[Bi_{38}O_{46}(pTsO)_6(NO_3)_{11}(DMSO)_{12}]^{5+}$	2737	$[Bi_{38}O_{46}(pTsO)_7(NO_3)_{11}(DMSO)_5]^{4+}$
2268	$[Bi_{38}O_{46}(pTsO)_4(NO_3)_{13}(DMSO)_{15}]^{5+}$	2741	$[Bi_{38}O_{46}(pTsO)_5(NO_3)_{13}(DMSO)_8]^{4+}$
2271	$[Bi_{38}O_{46}(pTsO)_7(NO_3)_{10}(DMSO)_{11}]^{5+}$	2745	$[Bi_{38}O_{46}(pTsO)_8(NO_3)_{10}(DMSO)_4]^{4+}$
2274	$[Bi_{38}O_{46}(pTsO)_5(NO_3)_{12}(DMSO)_{14}]^{5+}$	2749	$[Bi_{38}O_{46}(pTsO)_6(NO_3)_{12}(DMSO)_7]^{4+}$
2277	$[Bi_{38}O_{46}(pTsO)_8(NO_3)_9(DMSO)_{10}]^{5+}$	2753	$[Bi_{38}O_{46}(pTsO)_4(NO_3)_{14}(DMSO)_{10}]^{4+}$
2280	$[Bi_{38}O_{46}(pTsO)_6(NO_3)_{11}(DMSO)_{13}]^{5+}$	2756	$[Bi_{38}O_{46}(pTsO)_7(NO_3)_{11}(DMSO)_6]^{4+}$
2283	$[Bi_{38}O_{46}(pTsO)_4(NO_3)_{13}(DMSO)_{16}]^{5+}$	2760	$[Bi_{38}O_{46}(pTsO)_5(NO_3)_{13}(DMSO)_9]^{4+}$
2287	$[Bi_{38}O_{46}(pTsO)_7(NO_3)_{10}(DMSO)_{12}]^{5+}$	2764	$[Bi_{38}O_{46}(pTsO)_8(NO_3)_{10}(DMSO)_5]^{4+}$
2290	$[Bi_{38}O_{46}(pTsO)_5(NO_3)_{12}(DMSO)_{15}]^{5+}$	2768	$[Bi_{38}O_{46}(pTsO)_6(NO_3)_{12}(DMSO)_8]^{4+}$
2293	$[Bi_{38}O_{46}(pTsO)_8(NO_3)_9(DMSO)_{11}]^{5+}$	2772	$[Bi_{38}O_{46}(pTsO)_4(NO_3)_{14}(DMSO)_{11}]^{4+}$
2296	$[Bi_{38}O_{46}(pTsO)_6(NO_3)_{11}(DMSO)_{14}]^{5+}$	2776	$[Bi_{38}O_{46}(pTsO)_7(NO_3)_{11}(DMSO)_7]^{4+}$
2299	$[Bi_{38}O_{46}(pTsO)_4(NO_3)_{13}(DMSO)_{17}]^{5+}$	2780	$[Bi_{38}O_{46}(pTsO)_5(NO_3)_{13}(DMSO)_9]^{4+}$
2302	$[Bi_{38}O_{46}(pTsO)_7(NO_3)_{10}(DMSO)_{13}]^{5+}$	2784	$[Bi_{38}O_{46}(pTsO)_8(NO_3)_{10}(DMSO)_5]^{4+}$
2305	$[Bi_{38}O_{46}(pTsO)_5(NO_3)_{12}(DMSO)_{15}]^{5+}$	2788	$[Bi_{38}O_{46}(pTsO)_6(NO_3)_{12}(DMSO)_8]^{4+}$

Table 8.6b: *Second part of the ESI-MS data of* $[Bi_{38}O_{45}(OH)_2(pTsO)_8(NO_3)_{12}(DMSO)_{24}](NO_3)_2(DMSO)_4(H_2O)_2$ ***205****.*

m/z	**Fragment**	*m/z*	**Fragment**
2792	$[Bi_{38}O_{46}(pTsO)_4(NO_3)_{14}(DMSO)_{12}]^{4+}$	3659	$[Bi_{38}O_{46}(pTsO)_6(NO_3)_{13}(DMSO)_6]^{3+}$
2796	$[Bi_{38}O_{46}(pTsO)_7(NO_3)_{11}(DMSO)_8]^{4+}$	3663	$[Bi_{38}O_{46}(pTsO)_5(NO_3)_{14}(DMSO)_7(MeCN)]^{3+}$
2799	$[Bi_{38}O_{46}(pTsO)_5(NO_3)_{13}(DMSO)_{11}]^{4+}$	3670	$[Bi_{38}O_{46}(pTsO)_7(NO_3)_{12}(DMSO)_5]^{3+}$
2803	$[Bi_{38}O_{46}(pTsO)_8(NO_3)_{10}(DMSO)_7]^{4+}$	3675	$[Bi_{38}O_{46}(pTsO)_5(NO_3)_{14}(DMSO)_8]^{3+}$
2807	$[Bi_{38}O_{46}(pTsO)_6(NO_3)_{12}(DMSO)_{10}]^{4+}$	3679	$[Bi_{38}O_{46}(pTsO)_4(NO_3)_{15}(DMSO)_9(MeCN)]^{3+}$
2811	$[Bi_{38}O_{46}(pTsO)_4(NO_3)_{14}(DMSO)_{13}]^{4+}$	3685	$[Bi_{38}O_{46}(pTsO)_6(NO_3)_{13}(DMSO)_7]^{3+}$
2815	$[Bi_{38}O_{46}(pTsO)_7(NO_3)_{11}(DMSO)_9]^{4+}$	3691	$[Bi_{38}O_{46}(pTsO)_4(NO_3)_{15}(DMSO)_{10}]^{3+}$
2819	$[Bi_{38}O_{46}(pTsO)_5(NO_3)_{13}(DMSO)_{12}]^{4+}$	3696	$[Bi_{38}O_{46}(pTsO)_7(NO_3)_{12}(DMSO)_6]^{3+}$
2823	$[Bi_{38}O_{46}(pTsO)_8(NO_3)_{10}(DMSO)_8]^{4+}$	3701	$[Bi_{38}O_{46}(pTsO)_5(NO_3)_{14}(DMSO)_9]^{3+}$
2827	$[Bi_{38}O_{46}(pTsO)_6(NO_3)_{12}(DMSO)_{11}]^{4+}$	3706	$[Bi_{38}O_{46}(pTsO)_8(NO_3)_{11}(DMSO)_5]^{3+}$
2831	$[Bi_{38}O_{46}(pTsO)_4(NO_3)_{14}(DMSO)_{14}]^{4+}$	3712	$[Bi_{38}O_{46}(pTsO)_6(NO_3)_{13}(DMSO)_8]^{3+}$
2835	$[Bi_{38}O_{46}(pTsO)_7(NO_3)_{11}(DMSO)_{10}]^{4+}$	3715	$[Bi_{38}O_{46}(pTsO)_5(NO_3)_{14}(DMSO)_9(MeCN)]^{3+}$
2839	$[Bi_{38}O_{46}(pTsO)_5(NO_3)_{13}(DMSO)_{13}]^{4+}$	3722	$[Bi_{38}O_{46}(pTsO)_7(NO_3)_{12}(DMSO)_7]^{3+}$
2842	$[Bi_{38}O_{46}(pTsO)_8(NO_3)_{10}(DMSO)_9]^{4+}$	2725	$[Bi_{38}O_{46}(pTsO)_6(NO_3)_{13}(DMSO)_7(MeCN)]^{3+}$
2846	$[Bi_{38}O_{46}(pTsO)_6(NO_3)_{12}(DMSO)_{12}]^{4+}$	3732	$[Bi_{38}O_{46}(pTsO)_8(NO_3)_{11}(DMSO)_6]^{3+}$
2850	$[Bi_{38}O_{46}(pTsO)_4(NO_3)_{14}(DMSO)_{15}]^{4+}$	3737	$[Bi_{38}O_{46}(pTsO)_6(NO_3)_{13}(DMSO)_9]^{3+}$
2854	$[Bi_{38}O_{46}(pTsO)_7(NO_3)_{11}(DMSO)_{11}]^{4+}$	3743	$[Bi_{38}O_{46}(pTsO)_4(NO_3)_{15}(DMSO)_{12}]^{3+}$
2858	$[Bi_{38}O_{46}(pTsO)_5(NO_3)_{13}(DMSO)_{14}]^{4+}$	3748	$[Bi_{38}O_{46}(pTsO)_7(NO_3)_{12}(DMSO)_8]^{3+}$
2862	$[Bi_{38}O_{46}(pTsO)_8(NO_3)_{10}(DMSO)_{10}]^{4+}$	3751	$[Bi_{38}O_{46}(pTsO)_6(NO_3)_{13}(DMSO)_9(MeCN)]^{3+}$
2866	$[Bi_{38}O_{46}(pTsO)_6(NO_3)_{12}(DMSO)_{13}]^{4+}$	3757	$[Bi_{38}O_{46}(pTsO)_4(NO_3)_{15}(DMSO)_{12}(MeCN)]^{3+}$
2870	$[Bi_{38}O_{46}(pTsO)_4(NO_3)_{14}(DMSO)_{16}]^{4+}$	3762	$[Bi_{38}O_{46}(pTsO)_7(NO_3)_{12}(DMSO)_8(MeCN)]^{3+}$
2874	$[Bi_{38}O_{46}(pTsO)_7(NO_3)_{11}(DMSO)_{12}]^{4+}$	3767	$[Bi_{38}O_{46}(pTsO)_5(NO_3)_{14}(DMSO)_{11}(MeCN)]^{3+}$
2878	$[Bi_{38}O_{46}(pTsO)_5(NO_3)_{13}(DMSO)_{15}]^{4+}$	3772	$[Bi_{38}O_{46}(pTsO)_8(NO_3)_{11}(DMSO)_7(MeCN)]^{3+}$
2881	$[Bi_{38}O_{46}(pTsO)_8(NO_3)_{10}(DMSO)_{11}]^{4+}$	3777	$[Bi_{38}O_{46}(pTsO)_6(NO_3)_{13}(DMSO)_{10}(MeCN)]^{3+}$
2885	$[Bi_{38}O_{46}(pTsO)_6(NO_3)_{12}(DMSO)_{14}]^{4+}$	3783	$[Bi_{38}O_{46}(pTsO)_4(NO_3)_{15}(DMSO)_{13}(MeCN)]^{3+}$
2889	$[Bi_{38}O_{46}(pTsO)_4(NO_3)_{14}(DMSO)_{17}]^{4+}$	3788	$[Bi_{38}O_{46}(pTsO)_7(NO_3)_{12}(DMSO)_9(MeCN)]^{3+}$
2893	$[Bi_{38}O_{46}(pTsO)_7(NO_3)_{11}(DMSO)_{13}]^{4+}$	3793	$[Bi_{38}O_{46}(pTsO)_5(NO_3)_{14}(DMSO)_{12}(MeCN)]^{3+}$
2897	$[Bi_{38}O_{46}(pTsO)_5(NO_3)_{13}(DMSO)_{16}]^{4+}$	3798	$[Bi_{38}O_{46}(pTsO)_8(NO_3)_{11}(DMSO)_8(MeCN)]^{3+}$
2901	$[Bi_{38}O_{46}(pTsO)_8(NO_3)_{10}(DMSO)_{12}]^{4+}$	3803	$[Bi_{38}O_{46}(pTsO)_6(NO_3)_{13}(DMSO)_{11}(MeCN)]^{3+}$
2905	$[Bi_{38}O_{46}(pTsO)_6(NO_3)_{12}(DMSO)_{15}]^{4+}$	3809	$[Bi_{38}O_{46}(pTsO)_4(NO_3)_{15}(DMSO)_{14}(MeCN)]^{3+}$
2909	$[Bi_{38}O_{46}(pTsO)_4(NO_3)_{14}(DMSO)_{18}]^{4+}$	3814	$[Bi_{38}O_{46}(pTsO)_7(NO_3)_{12}(DMSO)_{10}(MeCN)]^{3+}$
2913	$[Bi_{38}O_{46}(pTsO)_7(NO_3)_{11}(DMSO)_{14}]^{4+}$	3819	$[Bi_{38}O_{46}(pTsO)_5(NO_3)_{14}(DMSO)_{13}(MeCN)]^{3+}$

$[Bi_{38}O_{45}(C_4H_7SO_3)_x(NO_3)_y(DMSO)_z]$ **206** (x + y = 24)

This $Bi_{38}O_{45}$-cluster contains an unknown composition of counter anions and DMSO molecules. The amounts used were calculated for 24 nitrate ions (x = 24; y = 0). The number of DMSO molecules was set to 24 (z =24). Based on these settings, 3.00 mg (0.24952 mmol) $[Bi_{38}O_{45}(C_4H_7SO_3)_x(NO_3)_y(DMSO)_z]$ **206** were suspended in 0.3 ml DMSO and heated for 5 min at 70 °C. After cooling to room temperature, the solution was diluted with 1.7 ml acetonitrile which yielded in a solution of **206** with a concentration of 125 µmol/L. This solution was used for the ESI MS experiments.

$C_{48}H_{144}O_{141}N_{24}S_{24}Bi_{38}$ 12023.1 g/mol (x = 24; y = 0; z =24)

$C_{144}H_{312}O_{141}S_{48}Bi_{38}$ 13779.6 g/mol (x = 0; y = 24; z =24)

Table 8.7: *ESI-MS data of $[Bi_{38}O_{45}(C_4H_7SO_3)_x(NO_3)_y(DMSO)_z]$ **206** (x + y = 24).*

m/z	**Fragment**	*m/z*	**Fragment**
2220	$[Bi_{38}O_{45}(C_4H_7SO_3)_{14}(NO_3)_5(DMSO)_3]^{5+}$	2771	$[Bi_{38}O_{45}(C_4H_7SO_3)_{13}(NO_3)_7(DMSO)_3]^{4+}$
2221	$[Bi_{38}O_{45}(C_4H_7SO_3)_{13}(NO_3)_6(DMSO)_4]^{5+}$	2773	$[Bi_{38}O_{45}(C_4H_7SO_3)_{12}(NO_3)_8(DMSO)_4]^{4+}$
2235	$[Bi_{38}O_{45}(C_4H_7SO_3)_{14}(NO_3)_5(DMSO)_4]^{5+}$	2778	$[Bi_{38}O_{45}(C_4H_7SO_3)_8(NO_3)_{12}(DMSO)_8]^{4+}$
2236	$[Bi_{38}O_{45}(C_4H_7SO_3)_{13}(NO_3)_6(DMSO)_5]^{5+}$	2779	$[Bi_{38}O_{45}(C_4H_7SO_3)_7(NO_3)_{13}(DMSO)_9]^{4+}$
2237	$[Bi_{38}O_{45}(C_4H_7SO_3)_{12}(NO_3)_7(DMSO)_6]^{5+}$	2780	$[Bi_{38}O_{45}(C_4H_7SO_3)_6(NO_3)_{14}(DMSO)_{10}]^{4+}$
2242	$[Bi_{38}O_{45}(C_4H_7SO_3)_7(NO_3)_{12}(DMSO)_{11}]^{5+}$	2781	$[Bi_{38}O_{45}(C_4H_7SO_3)_5(NO_3)_{15}(DMSO)_{11}]^{4+}$
2243	$[Bi_{38}O_{45}(C_4H_7SO_3)_6(NO_3)_{13}(DMSO)_{12}]^{5+}$	2791	$[Bi_{38}O_{45}(C_4H_7SO_3)_{13}(NO_3)_7(DMSO)_4]^{4+}$
2252	$[Bi_{38}O_{45}(C_4H_7SO_3)_{13}(NO_3)_6(DMSO)_6]^{5+}$	2791	$[Bi_{38}O_{45}(C_4H_7SO_3)_{12}(NO_3)_8(DMSO)_5]^{4+}$
2253	$[Bi_{38}O_{45}(C_4H_7SO_3)_{12}(NO_3)_7(DMSO)_7]^{5+}$	2797	$[Bi_{38}O_{45}(C_4H_7SO_3)_8(NO_3)_{12}(DMSO)_9]^{4+}$
2256	$[Bi_{38}O_{45}(C_4H_7SO_3)_9(NO_3)_{10}(DMSO)_{10}]^{5+}$	2799	$[Bi_{38}O_{45}(C_4H_7SO_3)_7(NO_3)_{13}(DMSO)_{10}]^{4+}$
2257	$[Bi_{38}O_{45}(C_4H_7SO_3)_8(NO_3)_{11}(DMSO)_{11}]^{5+}$	2816	$[Bi_{38}O_{45}(C_4H_7SO_3)_9(NO_3)_{11}(DMSO)_9]^{4+}$
2258	$[Bi_{38}O_{45}(C_4H_7SO_3)_7(NO_3)_{12}(DMSO)_{12}]^{5+}$	2817	$[Bi_{38}O_{45}(C_4H_7SO_3)_8(NO_3)_{12}(DMSO)_{10}]^{4+}$
2259	$[Bi_{38}O_{45}(C_4H_7SO_3)_6(NO_3)_{13}(DMSO)_{13}]^{5+}$		
2271	$[Bi_{38}O_{45}(C_4H_7SO_3)_9(NO_3)_{10}(DMSO)_{11}]^{5+}$	3648	$[Bi_{38}O_{45}(C_4H_7SO_3)_7(NO_3)_{14}(DMSO)_6]^{3+}$
2272	$[Bi_{38}O_{45}(C_4H_7SO_3)_8(NO_3)_{11}(DMSO)_{12}]^{5+}$	3650	$[Bi_{38}O_{45}(C_4H_7SO_3)_6(NO_3)_{15}(DMSO)_7]^{3+}$
		3651	$[Bi_{38}O_{45}(C_4H_7SO_3)_5(NO_3)_{16}(DMSO)_8]^{3+}$
2734	$[Bi_{38}O_{45}(C_4H_7SO_3)_{12}(NO_3)_8(DMSO)_2]^{4+}$	3658	$[Bi_{38}O_{45}(C_4H_7SO_3)(NO_3)_{20}(DMSO)_{12}]^{3+}$
2735	$[Bi_{38}O_{45}(C_4H_7SO_3)_{11}(NO_3)_9(DMSO)_3]^{4+}$	3664	$[Bi_{38}O_{45}(C_4H_7SO_3)_{13}(NO_3)_8(DMSO)]^{3+}$
2750	$[Bi_{38}O_{45}(C_4H_7SO_3)_{14}(NO_3)_6(DMSO)]^{4+}$	3672	$[Bi_{38}O_{45}(C_4H_7SO_3)_8(NO_3)_{13}(DMSO)_6]^{3+}$
2752	$[Bi_{38}O_{45}(C_4H_7SO_3)_{13}(NO_3)_7(DMSO)_2]^{4+}$	3674	$[Bi_{38}O_{45}(C_4H_7SO_3)_7(NO_3)_{14}(DMSO)_7]^{3+}$
2753	$[Bi_{38}O_{45}(C_4H_7SO_3)_{12}(NO_3)_8(DMSO)_3]^{4+}$	3675	$[Bi_{38}O_{45}(C_4H_7SO_3)_6(NO_3)_{15}(DMSO)_8]^{3+}$
2760	$[Bi_{38}O_{45}(C_4H_7SO_3)_7(NO_3)_{13}(DMSO)_8]^{4+}$	3697	$[Bi_{38}O_{45}(C_4H_7SO_3)_9(NO_3)_{12}(DMSO)_6]^{3+}$
2761	$[Bi_{38}O_{45}(C_4H_7SO_3)_6(NO_3)_{14}(DMSO)_9]^{4+}$	3698	$[Bi_{38}O_{45}(C_4H_7SO_3)_8(NO_3)_{13}(DMSO)_7]^{3+}$
2770	$[Bi_{38}O_{45}(C_4H_7SO_3)_{14}(NO_3)_6(DMSO)_2]^{4+}$	3700	$[Bi_{38}O_{45}(C_4H_7SO_3)_7(NO_3)_{14}(DMSO)_8]^{3+}$

$[Bi_{38}O_{45}(C_6H_{13}SO_3)_x(NO_3)_y(DMSO)_z]$ **207** (x + y = 24)

For this $Bi_{38}O_{45}$-cluster which contains an unknown composition of counter anions and DMSO molecules, the amounts used were calculated for 24 nitrate ions as counter anions (x = 24; y = 0). The number of DMSO molecules was set to 24 (z =24). Based on these settings, 3.00 mg (0.24952 mmol) $[Bi_{38}O_{45}(C_6H_{13}SO_3)_x(NO_3)_y(DMSO)_z]$ **207** were suspended in 0.3 ml DMSO and heated for 5 min at 70 °C. The resulting solution was cooled to room temperature and diluted with 1.7 ml acetonitrile which yielded in a solution of **[B4]** with a concentration of 125 µmol/L. This solution was used for the ESI MS experiments.

$\mathbf{C_{48}H_{144}O_{141}N_{24}S_{24}Bi_{38}}$	12023.1 g/mol (x = 24; y = 0; z =24)
$\mathbf{C_{192}H_{456}O_{141}S_{48}Bi_{38}}$	14500.8 g/mol (x = 0; y = 24; z =24)

Table 8.8a: *First part of the ESI-MS data of bismuth-oxido cluster **207**.*

m/z	**Fragment**	*m/z*	**Fragment**
2298	$[Bi_{38}O_{45}(C_6H_{13}SO_3)_{13}(NO_3)_6(DMSO)_4]^{5+}$	2856	$[Bi_{38}O_{45}(C_6H_{13}SO_3)_{14}(NO_3)_6(DMSO)]^{4+}$
2298	$[Bi_{38}O_{45}(C_6H_{13}SO_3)_{16}(NO_3)_3]^{5+}$	2862	$[Bi_{38}O_{45}(C_6H_{13}SO_3)_{15}(NO_3)_5]^{4+}$
2304	$[Bi_{38}O_{45}(C_6H_{13}SO_3)_{14}(NO_3)_5(DMSO)_3]^{5+}$	2865	$[Bi_{38}O_{45}(C_6H_{13}SO_3)_6(NO_3)_{14}(DMSO)_{12}]^{4+}$
2309	$[Bi_{38}O_{45}(C_6H_{13}SO_3)_{15}(NO_3)_4(DMSO)_2]^{5+}$	2869	$[Bi_{38}O_{45}(C_6H_{13}SO_3)_{13}(NO_3)_7(DMSO)_3]^{4+}$
2314	$[Bi_{38}O_{45}(C_6H_{13}SO_3)_{13}(NO_3)_6(DMSO)_5]^{5+}$	2871	$[Bi_{38}O_{45}(C_6H_{13}SO_3)_7(NO_3)_{13}(DMSO)_{11}]^{4+}$
2314	$[Bi_{38}O_{45}(C_6H_{13}SO_3)_{16}(NO_3)_3(DMSO)]^{5+}$	2876	$[Bi_{38}O_{45}(C_6H_{13}SO_3)_{14}(NO_3)_6(DMSO)_2]^{4+}$
2319	$[Bi_{38}O_{45}(C_6H_{13}SO_3)_{17}(NO_3)_2]^{5+}$	2878	$[Bi_{38}O_{45}(C_6H_{13}SO_3)_5(NO_3)_{15}(DMSO)_{14}]^{4+}$
2324	$[Bi_{38}O_{45}(C_6H_{13}SO_3)_{15}(NO_3)_4(DMSO)_3]^{5+}$	2882	$[Bi_{38}O_{45}(C_6H_{13}SO_3)_{15}(NO_3)_5(DMSO)]^{4+}$
2329	$[Bi_{38}O_{45}(C_6H_{13}SO_3)_{16}(NO_3)_3(DMSO)_2]^{5+}$	2884	$[Bi_{38}O_{45}(C_6H_{13}SO_3)_3(NO_3)_{17}(DMSO)_{17}]^{4+}$
2330	$[Bi_{38}O_{45}(C_6H_{13}SO_3)_{10}(NO_3)_9(DMSO)_{10}]^{5+}$	2888	$[Bi_{38}O_{45}(C_6H_{13}SO_3)_{16}(NO_3)_4]^{4+}$
2336	$[Bi_{38}O_{45}(C_6H_{13}SO_3)_{11}(NO_3)_8(DMSO)_9]^{5+}$	2890	$[Bi_{38}O_{45}(C_6H_{13}SO_3)_7(NO_3)_{13}(DMSO)_{12}]^{4+}$
2341	$[Bi_{38}O_{45}(C_6H_{13}SO_3)_{12}(NO_3)_7(DMSO)_8]^{5+}$	2895	$[Bi_{38}O_{45}(C_6H_{13}SO_3)_{14}(NO_3)_6(DMSO)_3]^{4+}$
2346	$[Bi_{38}O_{45}(C_6H_{13}SO_3)_{13}(NO_3)_6(DMSO)_7]^{5+}$	2897	$[Bi_{38}O_{45}(C_6H_{13}SO_3)_5(NO_3)_{15}(DMSO)_{15}]^{4+}$
2351	$[Bi_{38}O_{45}(C_6H_{13}SO_3)_{11}(NO_3)_8(DMSO)_{10}]^{5+}$	2902	$[Bi_{38}O_{45}(C_6H_{13}SO_3)_{12}(NO_3)_8(DMSO)_6]^{4+}$
2357	$[Bi_{38}O_{45}(C_6H_{13}SO_3)_9(NO_3)_{10}(DMSO)_{13}]^{5+}$	2904	$[Bi_{38}O_{45}(C_6H_{13}SO_3)_3(NO_3)_{17}(DMSO)_{18}]^{4+}$
2362	$[Bi_{38}O_{45}(C_6H_{13}SO_3)_{10}(NO_3)_9(DMSO)_{12}]^{5+}$	2908	$[Bi_{38}O_{45}(C_6H_{13}SO_3)_{13}(NO_3)_7(DMSO)_5]^{4+}$
2366	$[Bi_{38}O_{45}(C_6H_{13}SO_3)_{11}(NO_3)_8(DMSO)_{11}]^{5+}$	2915	$[Bi_{38}O_{45}(C_6H_{13}SO_3)_{11}(NO_3)_9(DMSO)_8]^{4+}$
		2916	$[Bi_{38}O_{45}(C_6H_{13}SO_3)_8(NO_3)_{12}(DMSO)_{12}]^{4+}$
2830	$[Bi_{38}O_{45}(C_6H_{13}SO_3)_{13}(NO_3)_7(DMSO)]^{4+}$	2922	$[Bi_{38}O_{45}(C_6H_{13}SO_3)_{12}(NO_3)_8(DMSO)_7]^{4+}$
2837	$[Bi_{38}O_{45}(C_6H_{13}SO_3)_{14}(NO_3)_6]^{4+}$	2924	$[Bi_{38}O_{45}(C_6H_{13}SO_3)_3(NO_3)_{17}(DMSO)_{19}]^{4+}$
2843	$[Bi_{38}O_{45}(C_6H_{13}SO_3)_{12}(NO_3)_8(DMSO)_3]^{4+}$	2928	$[Bi_{38}O_{45}(C_6H_{13}SO_3)_{13}(NO_3)_7(DMSO)_6]^{4+}$
2850	$[Bi_{38}O_{45}(C_6H_{13}SO_3)_{13}(NO_3)_7(DMSO)_2]^{4+}$	2934	$[Bi_{38}O_{45}(C_6H_{13}SO_3)_{14}(NO_3)_6(DMSO)_5]^{4+}$

Table 8.8b: *Second part of the ESI-MS data of bismuth-oxido cluster* ***207****.*

m/z	**Fragment**	*m/z*	**Fragment**
2941	$[Bi_{38}O_{45}(C_6H_{13}SO_3)_{12}(NO_3)_8(DMSO)_8]^{4+}$	3846	$[Bi_{38}O_{45}(C_6H_{13}SO_3)_{13}(NO_3)_8(DMSO)_3]^{3+}$
2947	$[Bi_{38}O_{45}(C_6H_{13}SO_3)_{13}(NO_3)_7(DMSO)_7]^{4+}$	3849	$[Bi_{38}O_{45}(C_6H_{13}SO_3)_4(NO_3)_{17}(DMSO)_{15}]^{3+}$
2949	$[Bi_{38}O_{45}(C_6H_{13}SO_3)_7(NO_3)_{13}(DMSO)_{15}]^{4+}$	3855	$[Bi_{38}O_{45}(C_6H_{13}SO_3)_{11}(NO_3)_{10}(DMSO)_6]^{3+}$
2953	$[Bi_{38}O_{45}(C_6H_{13}SO_3)_{14}(NO_3)_6(DMSO)_6]^{4+}$	3857	$[Bi_{38}O_{45}(C_6H_{13}SO_3)_5(NO_3)_{16}(DMSO)_{14}]^{3+}$
2960	$[Bi_{38}O_{45}(C_6H_{13}SO_3)_{15}(NO_3)_5(DMSO)_5]^{4+}$	3864	$[Bi_{38}O_{45}(C_6H_{13}SO_3)_{12}(NO_3)_9(DMSO)_5]^{3+}$
2966	$[Bi_{38}O_{45}(C_6H_{13}SO_3)_{16}(NO_3)_4(DMSO)_4]^{4+}$	3865	$[Bi_{38}O_{45}(C_6H_{13}SO_3)_9(NO_3)_{12}(DMSO)_9]^{3+}$
		3872	$[Bi_{38}O_{45}(C_6H_{13}SO_3)_{13}(NO_3)_8(DMSO)_4]^{3+}$
3797	$[Bi_{38}O_{45}(C_6H_{13}SO_3)_4(NO_3)_{17}(DMSO)_{13}]^{3+}$	3881	$[Bi_{38}O_{45}(C_6H_{13}SO_3)_{14}(NO_3)_7(DMSO)_3]^{3+}$
3805	$[Bi_{38}O_{45}(C_6H_{13}SO_3)_5(NO_3)_{16}(DMSO)_{12}]^{3+}$	3890	$[Bi_{38}O_{45}(C_6H_{13}SO_3)_{12}(NO_3)_9(DMSO)_6]^{3+}$
3812	$[Bi_{38}O_{45}(C_6H_{13}SO_3)_{12}(NO_3)_9(DMSO)_3]^{3+}$	3898	$[Bi_{38}O_{45}(C_6H_{13}SO_3)_{13}(NO_3)_8(DMSO)_5]^{3+}$
3814	$[Bi_{38}O_{45}(C_6H_{13}SO_3)_3(NO_3)_{18}(DMSO)_{15}]^{3+}$	3900	$[Bi_{38}O_{45}(C_6H_{13}SO_3)_7(NO_3)_{14}(DMSO)_{13}]^{3+}$
3821	$[Bi_{38}O_{45}(C_6H_{13}SO_3)_{19}(NO_3)_{11}(DMSO)_6]^{3+}$	3907	$[Bi_{38}O_{45}(C_6H_{13}SO_3)_{11}(NO_3)_{10}(DMSO)_8]^{3+}$
3824	$[Bi_{38}O_{45}(C_6H_{13}SO_3)_4(NO_3)_{17}(DMSO)_{14}]^{3+}$	3916	$[Bi_{38}O_{45}(C_6H_{13}SO_3)_{12}(NO_3)_9(DMSO)_7]^{3+}$
3830	$[Bi_{38}O_{45}(C_6H_{13}SO_3)_{11}(NO_3)_{10}(DMSO)_5]^{3+}$	3924	$[Bi_{38}O_{45}(C_6H_{13}SO_3)_{13}(NO_3)_8(DMSO)_6]^{3+}$
3832	$[Bi_{38}O_{45}(C_6H_{13}SO_3)_5(NO_3)_{16}(DMSO)_{13}]^{3+}$	3943	$[Bi_{38}O_{45}(C_6H_{13}SO_3)_{12}(NO_3)_9(DMSO)_8]^{3+}$
3838	$[Bi_{38}O_{45}(C_6H_{13}SO_3)_{12}(NO_3)_9(DMSO)_4]^{3+}$	3950	$[Bi_{38}O_{45}(C_6H_{13}SO_3)_{13}(NO_3)_8(DMSO)_7]^{3+}$
3840	$[Bi_{38}O_{45}(C_6H_{13}SO_3)_6(NO_3)_{15}(DMSO)_{12}]^{3+}$	3958	$[Bi_{38}O_{45}(C_6H_{13}SO_3)_{14}(NO_3)_7(DMSO)_6]^{3+}$

$[Bi_{38}O_{45}(C_8H_{17}SO_3)_x(NO_3)_y(DMSO)_z]$ **208** (x + y = 24)

For this $Bi_{38}O_{45}$-cluster which contains an unknown composition of counter anions and DMSO molecules, the amounts used were calculated for 24 nitrate ions as counter anions (x = 24; y = 0). The number of DMSO molecules was set to 24 (z =24). Based on these settings, 3.00 mg (0.24952 mmol) $[Bi_{38}O_{45}(C_8H_{17}SO_3)_x(NO_3)_y(DMSO)_z]$ **208** were suspended in 0.3 ml DMSO and heated for 5 min at 70 °C. The resulting solution was cooled to room temperature and diluted with 1.7 ml acetonitrile which yielded in a solution of **208** with a concentration of 125 µmol/L. This solution was used for the ESI MS experiments.

$C_{48}H_{144}O_{141}N_{24}S_{24}Bi_{38}$ 12023.1 g/mol (x = 24; y = 0; z =24)

$C_{240}H_{552}O_{141}S_{48}Bi_{38}$ 15174.5 g/mol (x = 0; y = 24; z =24)

Table 8.9: *ESI-MS data of* $[Bi_{38}O_{45}(C_8H_{17}SO_3)_x(NO_3)_y(DMSO)_z]$ ***208*** *(x + y = 24).*

m/z	**Fragment**	*m/z*	**Fragment**
2954	$[Bi_{38}O_{45}(C_8H_{17}SO_3)_{11}(NO_3)_9(DMSO)_6]^{4+}$	3898	$[Bi_{38}O_{45}(C_8H_{17}SO_3)_{12}(NO_3)_9(DMSO)_2]^{3+}$
2960	$[Bi_{38}O_{45}(C_8H_{17}SO_3)_{13}(NO_3)_7(DMSO)_3]^{4+}$	3907	$[Bi_{38}O_{45}(C_8H_{17}SO_3)_{11}(NO_3)_{10}(DMSO)_4]^{3+}$
2967	$[Bi_{38}O_{45}(C_8H_{17}SO_3)_{12}(NO_3)_8(DMSO)_5]^{4+}$	3916	$[Bi_{38}O_{45}(C_8H_{17}SO_3)_{13}(NO_3)_8(DMSO)]^{3+}$
2973	$[Bi_{38}O_{45}(C_8H_{17}SO_3)_{14}(NO_3)_6(DMSO)_2]^{4+}$	3925	$[Bi_{38}O_{45}(C_8H_{17}SO_3)_{12}(NO_3)_9(DMSO)_3]^{3+}$
2979	$[Bi_{38}O_{45}(C_8H_{17}SO_3)_{10}(NO_3)_{10}(DMSO)_9]^{4+}$	3933	$[Bi_{38}O_{45}(C_8H_{17}SO_3)_{14}(NO_3)_7]^{3+}$
2986	$[Bi_{38}O_{45}(C_8H_{17}SO_3)_{12}(NO_3)_8(DMSO)_6]^{4+}$	3942	$[Bi_{38}O_{45}(C_8H_{17}SO_3)_{13}(NO_3)_8(DMSO)_2]^{3+}$
2993	$[Bi_{38}O_{45}(C_8H_{17}SO_3)_{14}(NO_3)_6(DMSO)_3]^{4+}$	3950	$[Bi_{38}O_{45}(C_8H_{17}SO_3)_{12}(NO_3)_9(DMSO)_4]^{3+}$
3000	$[Bi_{38}O_{45}(C_8H_{17}SO_3)_{16}(NO_3)_4]^{4+}$	3960	$[Bi_{38}O_{45}(C_8H_{17}SO_3)_{14}(NO_3)_7(DMSO)]^{3+}$
3006	$[Bi_{38}O_{45}(C_8H_{17}SO_3)_{12}(NO_3)_8(DMSO)_7]^{4+}$	3969	$[Bi_{38}O_{45}(C_8H_{17}SO_3)_{13}(NO_3)_8(DMSO)_3]^{3+}$
3013	$[Bi_{38}O_{45}(C_8H_{17}SO_3)_{14}(NO_3)_6(DMSO)_4]^{4+}$	3976	$[Bi_{38}O_{45}(C_8H_{17}SO_3)_{12}(NO_3)_9(DMSO)_5]^{3+}$
3019	$[Bi_{38}O_{45}(C_8H_{17}SO_3)_{13}(NO_3)_7(DMSO)_6]^{4+}$	3977	$[Bi_{38}O_{45}(C_8H_{17}SO_3)_{15}(NO_3)_6]^{3+}$
3026	$[Bi_{38}O_{45}(C_8H_{17}SO_3)_{15}(NO_3)_5(DMSO)_3]^{4+}$	3986	$[Bi_{38}O_{45}(C_8H_{17}SO_3)_{14}(NO_3)_7(DMSO)_2]^{3+}$
3032	$[Bi_{38}O_{45}(C_8H_{17}SO_3)_{14}(NO_3)_6(DMSO)_5]^{4+}$	3994	$[Bi_{38}O_{45}(C_8H_{17}SO_3)_{13}(NO_3)_8(DMSO)_4]^{3+}$
3033	$[Bi_{38}O_{45}(C_8H_{17}SO_3)_{17}(NO_3)_3]^{4+}$	4003	$[Bi_{38}O_{45}(C_8H_{17}SO_3)_{15}(NO_3)_6(DMSO)]^{3+}$
3039	$[Bi_{38}O_{45}(C_8H_{17}SO_3)_{13}(NO_3)_7(DMSO)_7]^{4+}$	4012	$[Bi_{38}O_{45}(C_8H_{17}SO_3)_{14}(NO_3)_7(DMSO)_3]^{3+}$
3046	$[Bi_{38}O_{45}(C_8H_{17}SO_3)_{15}(NO_3)_5(DMSO)_4]^{4+}$	4020	$[Bi_{38}O_{45}(C_8H_{17}SO_3)_{13}(NO_3)_8(DMSO)_4]^{3+}$
3052	$[Bi_{38}O_{45}(C_8H_{17}SO_3)_{14}(NO_3)_6(DMSO)_6]^{4+}$	4029	$[Bi_{38}O_{45}(C_8H_{17}SO_3)_{15}(NO_3)_6(DMSO)_2]^{3+}$
3065	$[Bi_{38}O_{45}(C_8H_{17}SO_3)_{15}(NO_3)_5(DMSO)_5]^{4+}$	4038	$[Bi_{38}O_{45}(C_8H_{17}SO_3)_{14}(NO_3)_7(DMSO)_4]^{3+}$
		4047	$[Bi_{38}O_{45}(C_8H_{17}SO_3)_{16}(NO_3)_5(DMSO)]^{3+}$
3889	$[Bi_{38}O_{45}(C_8H_{17}SO_3)_{10}(NO_3)_{11}(DMSO)_5]^{3+}$	4056	$[Bi_{38}O_{45}(C_8H_{17}SO_3)_{15}(NO_3)_6(DMSO)_3]^{3+}$
3890	$[Bi_{38}O_{45}(C_8H_{17}SO_3)_{13}(NO_3)_8]^{3+}$	4077	$[Bi_{38}O_{45}(C_8H_{17}SO_3)_3(NO_3)_{18}(DMSO)_{24}]^{3+}$

$[Bi_{38}O_{45}(BOC\text{-}Val)_{22}(OH)_2]$ **209**

3.00 mg (0.22300 mmol) $[Bi_{38}O_{45}(BOC\text{-}Val)_{22}(OH)_2]$ **209** were dissolved in 2 ml ethanol and sonicated for 5 min at room temperature. The resulting solution had a concentration of 110 µmol/L **209**. This solution was used for the ESI MS experiments.

$C_{220}H_{398}O_{135}N_{22}Bi_{38}$ 13452.8 g/mol

Table 8.10: *ESI-MS data of* $[Bi_{38}O_{45}(BOC\text{-}Val)_{22}(OH)_2]$ ***209***.

m/z	classification
3082	$[Bi_{38}O_{45}(OH)_2(Val)_{18}(BOC)_{15}(EtOH)]^{4+}$
3089	$[Bi_{38}O_{45}(OH)_2(Val)_{18}(BOC)_{15}(EtOH)_2 - H_2O]^{4+}$
3097	$[Bi_{38}O_{45}(OH)_2(Val)_{18}(BOC)_{16}]^{4+}$
3099	$[Bi_{38}O_{45}(OH)_2(Val)_{18}(BOC)_{15}(EtOH)_2(H_2O)]^{4+}$
3108	$[Bi_{38}O_{45}(OH)_2(Val)_{18}(BOC)_{16}(EtOH)]^{4+}$
3115	$[Bi_{38}O_{45}(OH)_2(Val)_{18}(BOC)_{16}(EtOH)_2 - H_2O]^{4+}$
3122	$[Bi_{38}O_{45}(OH)_2(Val)_{18}(BOC)_{17}]^{4+}$
3136	$[Bi_{38}O_{45}(OH)_2(Val)_{18}(BOC)_{16}(EtOH)_3(H_2O)]^{4+}$
3143	$[Bi_{38}O_{45}(OH)_2(Val)_{18}(BOC)_{17} - H_2O]^{4+}$
3158	$[Bi_{38}O_{45}(OH)_2(Val)_{18}(BOC)_{18}(EtOH)]^{4+}$
3161	$[Bi_{38}O_{45}(OH)_2(Val)_{18}(BOC)_{17}(EtOH)_3(H_2O)]^{4+}$
3165	$[Bi_{38}O_{45}(OH)_2(Val)_{18}(BOC)_{18}(EtOH)_2 - H_2O]^{4+}$
3172	$[Bi_{38}O_{45}(OH)(Val)_{19}(BOC)_{18}]^{4+}$
3193	$[Bi_{38}O_{45}(OH)_2(Val)_{18}(BOC)_{18}(EtOH)_4]^{4+}$
3197	$[Bi_{38}O_{45}(OH)(Val)_{19}\ (BOC)_{19}]^{4+}$
3204	$[Bi_{38}O_{45}(OH)_2(Val)_{18}(BOC)_{18}(EtOH)_5]^{4+}$
3222	$[Bi_{38}O_{45}(Val)_{20}\ (BOC)_{19}]^{4+}$
3247	$[Bi_{38}O_{45}(Val)_{20}\ (BOC)_{20}]^{4+}$
4183	$[Bi_{38}O_{45}(OH)_2(Val)_{19}(BOC)_{16}(EtOH)]^{3+}$
4206	$[Bi_{38}O_{45}(Val)_{21}(BOC)_{15}(EtOH)_3(H_2O)]^{3+}$
4265	$[Bi_{38}O_{45}(OH)(Val)_{20}(BOC)_{17}(EtOH)_2]^{3+}$
4293	$[Bi_{38}O_{45}(OH)_2(Val)_{19}(BOC)_{19}(EtOH)_2 - H_2O]^{3+}$
4329	$[Bi_{38}O_{45}(OH)_2(Val)_{19}(BOC)_{19}(EtOH)_4]^{3+}$
4401	$[Bi_{38}O_{45}(Val)_{21}(BOC)_{21}]^{3+}$
4488	$[Bi_{38}O_{45}(Val)_{21}(BOC)_{21}(EtOH)_6 - H_2O]^{3+}$

$[Bi_{38}O_{45}(BOC\text{-}Phe)_{22}(OH)_2]$ **210**

3.00 mg (0.20676 mmol) $[Bi_{38}O_{45}(BOC\text{-}Phe)_{22}(OH)_2]$ **210** were dissolved in 0.4 ml DMSO and sonicated for 5 min at room temperature. The resulting solution was diluted with 1.6 ml acetonitrile which yielded in a solution of **210** with a concentration of 100 µmol/L. This solution was used for the ESI MS experiments.

$\mathbf{C_{308}H_{398}O_{135}N_{22}Bi_{38}}$ 14509.9 g/mol

Table 8.11: *ESI-MS data of* $[Bi_{38}O_{45}(BOC\text{-}Phe)_{22}(OH)_2]$ ***210****.*

m/z	**classification**
3360	$[Bi_{38}O_{45}(OH)_2(Phe)_{18}(BOC)_{14}(DMSO)_5]^{4+}$
3380	$[Bi_{38}O_{45}(OH)_2(Phe)_{18}(BOC)_{14}(DMSO)_6]^{4+}$
3385	$[Bi_{38}O_{45}(OH)_2(Phe)_{18}(BOC)_{15}(DMSO)_5]^{4+}$
3410	$[Bi_{38}O_{45}(OH)_2(Phe)_{18}(BOC)_{16}(DMSO)_5]^{4+}$
3436	$[Bi_{38}O_{45}(OH)_2(Phe)_{18}(BOC)_{17}(DMSO)_5]^{4+}$
3453	$[Bi_{38}O_{45}(OH)(Phe)_{19}(BOC)_{17}(DMSO)_4]^{4+}$
3461	$[Bi_{38}O_{45}(OH)_2(Phe)_{18}(BOC)_{18}(DMSO)_5]^{4+}$
3476	$[Bi_{38}O_{45}(OH)_2(Phe)_{18}(BOC)_{18}(DMSO)_6 - H_2O]^{4+}$
3481	$[Bi_{38}O_{45}(OH)_2(Phe)_{18}(BOC)_{18}(DMSO)_6]^{4+}$
3503	$[Bi_{38}O_{45}(OH)(Phe)_{19}(BOC)_{19}(DMSO)_4]^{4+}$
3507	$[Bi_{38}O_{45}(OH)(Phe)_{19}(BOC)_{19}(DMSO)_4(H_2O)]^{4+}$
3525	$[Bi_{38}O_{45}(OH)(Phe)_{19}(BOC)_{16}(DMSO)_9]^{4+}$
3531	$[Bi_{38}O_{45}(OH)(Phe)_{19}(BOC)_{17}(DMSO)_8]^{4+}$
3550	$[Bi_{38}O_{45}(OH)(Phe)_{19}(BOC)_{17}(DMSO)_9]^{4+}$
3554	$[Bi_{38}O_{45}(Phe)_{20}(BOC)_{18}(DMSO)_6]^{4+}$
3573	$[Bi_{38}O_{45}(Phe)_{20}(BOC)_{18}(DMSO)_7]^{4+}$
3578	$[Bi_{38}O_{45}(Phe)_{20}(BOC)_{19}(DMSO)_6]^{4+}$
3596	$[Bi_{38}O_{45}(OH)(Phe)_{19}(BOC)_{19}(DMSO)_9 - H_2O]^{4+}$
3604	$[Bi_{38}O_{45}(Phe)_{20}(BOC)_{20}(DMSO)_6]^{4+}$
3620	$[Bi_{38}O_{45}(OH)(Phe)_{19}(BOC)_{19}(DMSO)_{10}]^{4+}$
3626	$[Bi_{38}O_{45}(Phe)_{20}(BOC)_{20}(DMSO)_7(H_2O)]^{4+}$
3650	$[Bi_{38}O_{45}(OH)(Phe)_{19}(BOC)_{18}(DMSO)_{13} - H_2O]^{4+}$
3668	$[Bi_{38}O_{45}(OH)(Phe)_{19}(BOC)_{17}(DMSO)_{15}]^{4+}$
3673	$[Bi_{38}O_{45}(OH)(Phe)_{19}(BOC)_{18}(DMSO)_{14}]^{4+}$
3674	$[Bi_{38}O_{45}(OH)(Phe)_{19}(BOC)_{19}(DMSO)_{13} - H_2O]^{4+}$
4632	$[Bi_{38}O_{45}(OH)(Phe)_{19}(BOC)_{13}(DMSO)_{10}]^{3+}$
4665	$[Bi_{38}O_{45}(OH)(Phe)_{19}(BOC)_{14}(DMSO)_{10}]^{3+}$
4689	$[Bi_{38}O_{45}(OH)_2(Phe)_{19}(BOC)_{18}(DMSO)_6 - H_2O]^{4+}$
4702	$[Bi_{38}O_{45}(OH)(Phe)_{19}(BOC)_{19}(DMSO)_5]^{3+}$
4724	$[Bi_{38}O_{45}(OH)(Phe)_{20}(BOC)_{18}(DMSO)_5 + H_2O]^{4+}$
4733	$[Bi_{38}O_{45}(OH)(Phe)_{120}(BOC)_{20}(DMSO)_3]^{3+}$
4759	$[Bi_{38}O_{45}(OH)(Phe)_{120}(BOC)_{20}(DMSO)_4]^{3+}$
4765	$[Bi_{38}O_{45}(OH)(Phe)_{20}(BOC)_{20}(DMSO)_4 + H_2O]^{4+}$
4787	$[Bi_{38}O_{45}(OH)_2(Phe)_{19}(BOC)_{19}(DMSO)_8 + H_2O]^{4+}$
4798	$[Bi_{38}O_{45}(OH)_2(Phe)_{19}(BOC)_{18}(DMSO)_{10}]^{4+}$

[$Bi_{22}O_{26}(HSal)_{14}$] **211** (and [$Bi_{34}O_{40}(HSal)_{22}$] **212**)

2.00 mg (0.28849 mmol) [$Bi_{22}O_{26}(HSal)_{14}$] **211** were dissolved in 0.4 ml DMSO and sonicated for 5 min at room temperature. The resulting solution was diluted with 2.6 ml acetonitrile which yielded in a solution of **211** with a concentration of 96 µmol/L. This solution was used for the ESI MS experiments. Surprisingly, also fragments of a [$Bi_{34}O_{40}(HSal)_{22}$] **212** cluster were observed in the ESI mass spectrum.

$C_{98}H_{70}O_{68}Bi_{22}$ 6932.8 g/mol

$C_{154}H_{110}O_{106}Bi_{34}$ 10761.79 g/mol

Table 8.12a: *1. part of the MS data of [$Bi_{22}O_{26}(HSal)_{14}$] **211** and [$Bi_{34}O_{40}(HSal)_{22}$] **212**.*

m/z	**classification**	*m/z*	**classification**
1826	$[Bi_{22}O_{26}(HSal)_{10}(DMSO)_6(MeCN)_{11}]^{4+}$	1955	$[Bi_{22}O_{26}(HSal)_{10}(DMSO)_{11}(MeCN)_{13}]^{4+}$
1836	$[Bi_{22}O_{26}(HSal)_{10}(DMSO)_6(MeCN)_{12}]^{4+}$		
1845	$[Bi_{22}O_{26}(HSal)_{10}(DMSO)_7(MeCN)_{11}]^{4+}$	2299	$[Bi_{22}O_{26}(HSal)_{11}(DMSO)_3(MeCN)_3(H_2O)]^{3+}$
1847	$[Bi_{22}O_{26}(HSal)_{10}(DMSO)_6(MeCN)_{13}]^{4+}$	2339	$[Bi_{22}O_{26}(HSal)_{11}(DMSO)_4(MeCN)_4(H_2O)]^{3+}$
1856	$[Bi_{22}O_{26}(HSal)_{10}(DMSO)_7(MeCN)_{12}]^{4+}$	2351	$[Bi_{22}O_{26}(HSal)_{11}(DMSO)_5(MeCN)_3(H_2O)]^{3+}$
1857	$[Bi_{22}O_{26}(HSal)_{10}(DMSO)_6(MeCN)_{14}]^{4+}$	2364	$[Bi_{22}O_{26}(HSal)_{11}(DMSO)_5(MeCN)_4(H_2O)]^{3+}$
1865	$[Bi_{22}O_{26}(HSal)_{10}(DMSO)_8(MeCN)_{11}]^{4+}$	2379	$[Bi_{22}O_{26}(HSal)_{11}(DMSO)_5(MeCN)_5(H_2O)]^{3+}$
1866	$[Bi_{22}O_{26}(HSal)_{10}(DMSO)_7(MeCN)_{13}]^{4+}$	2391	$[Bi_{22}O_{26}(HSal)_{11}(DMSO)_5(MeCN)_6(H_2O)]^{3+}$
1875	$[Bi_{22}O_{26}(HSal)_{10}(DMSO)_8(MeCN)_{12}]^{4+}$	2404	$[Bi_{22}O_{26}(HSal)_{11}(DMSO)_6(MeCN)_5(H_2O)]^{3+}$
1876	$[Bi_{22}O_{26}(HSal)_{10}(DMSO)_7(MeCN)_{14}]^{4+}$	2417	$[Bi_{22}O_{26}(HSal)_{11}(DMSO)_7(MeCN)_4(H_2O)]^{3+}$
1885	$[Bi_{22}O_{26}(HSal)_{10}(DMSO)_9(MeCN)_{11}]^{4+}$	2429	$[Bi_{22}O_{26}(HSal)_{11}(DMSO)_8(MeCN)_3(H_2O)]^{3+}$
1886	$[Bi_{22}O_{26}(HSal)_{10}(DMSO)_8(MeCN)_{13}]^{4+}$	2443	$[Bi_{22}O_{26}(HSal)_{11}(DMSO)_8(MeCN)_4(H_2O)]^{3+}$
1895	$[Bi_{22}O_{26}(HSal)_{10}(DMSO)_9(MeCN)_{12}]^{4+}$	2456	$[Bi_{22}O_{26}(HSal)_{11}(DMSO)_8(MeCN)_5(H_2O)]^{3+}$
1896	$[Bi_{22}O_{26}(HSal)_{10}(DMSO)_8(MeCN)_{14}]^{4+}$	2469	$[Bi_{22}O_{26}(HSal)_{11}(DMSO)_9(MeCN)_4(H_2O)]^{3+}$
1905	$[Bi_{22}O_{26}(HSal)_{10}(DMSO)_9(MeCN)_{13}]^{4+}$	2484	$[Bi_{22}O_{26}(HSal)_{11}(DMSO)_9(MeCN)_5(H_2O)]^{3+}$
1906	$[Bi_{22}O_{26}(HSal)_{10}(DMSO)_8(MeCN)_{15}]^{4+}$	2495	$[Bi_{22}O_{26}(HSal)_{11}(DMSO)_{10}(MeCN)_4(H_2O)]^{3+}$
1915	$[Bi_{22}O_{26}(HSal)_{10}(DMSO)_{10}(MeCN)_{12}]^{4+}$	2502	$[Bi_{22}O_{26}(HSal)_{11}(DMSO)_{10}(MeCN)_5]^{3+}$
1916	$[Bi_{22}O_{26}(HSal)_{10}(DMSO)_9(MeCN)_{14}]^{4+}$	2509	$[Bi_{22}O_{26}(HSal)_{11}(DMSO)_{10}(MeCN)_5(H_2O)]^{3+}$
1919	$[Bi_{22}O_{26}(HSal)_{10}(DMSO)_{10}(MeCN)_{12}(H_2O)]^{4+}$	2515	$[Bi_{22}O_{26}(HSal)_{11}(DMSO)_{11}(MeCN)_4]^{3+}$
1920	$[Bi_{22}O_{26}(HSal)_{10}(DMSO)_9(MeCN)_{14}(H_2O)]^{4+}$	2521	$[Bi_{22}O_{26}(HSal)_{11}(DMSO)_{11}(MeCN)_4(H_2O)]^{3+}$
1925	$[Bi_{22}O_{26}(HSal)_{10}(DMSO)_{11}(MeCN)_{11}]^{4+}$	2527	$[Bi_{22}O_{26}(HSal)_{11}(DMSO)_{12}(MeCN)_3]^{3+}$
1926	$[Bi_{22}O_{26}(HSal)_{10}(DMSO)_{10}(MeCN)_{13}]^{4+}$	2533	$[Bi_{22}O_{26}(HSal)_{11}(DMSO)_{12}(MeCN)_3(H_2O)]^{3+}$
1934	$[Bi_{22}O_{26}(HSal)_{10}(DMSO)_{11}(MeCN)_{12}]^{4+}$	2541	$[Bi_{22}O_{26}(HSal)_{11}(DMSO)_{12}(MeCN)_4]^{3+}$
1935	$[Bi_{22}O_{26}(HSal)_{10}(DMSO)_{10}(MeCN)_{13}]^{4+}$	2547	$[Bi_{22}O_{26}(HSal)_{11}(DMSO)_{12}(MeCN)_4(H_2O)]^{3+}$
1954	$[Bi_{22}O_{26}(HSal)_{10}(DMSO)_{12}(MeCN)_{12}]^{4+}$	2554	$[Bi_{22}O_{26}(HSal)_{11}(DMSO)_{12}(MeCN)_5]^{3+}$

Table 8.12b: *2. part of the MS data of* $[Bi_{22}O_{26}(HSal)_{14}]$ ***211*** *and* $[Bi_{34}O_{40}(HSal)_{22}]$ ***212****.*

m/z	**classification**	***m/z***	**classification**
2561	$[Bi_{22}O_{26}(HSal)_{11}(DMSO)_{12}(MeCN)_5(H_2O)]^{3+}$	2830	$[Bi_{34}O_{40}(HSal)_{18}(DMSO)_{11}(MeCN)_6]^{4+}$
2567	$[Bi_{22}O_{26}(HSal)_{11}(DMSO)_{13}(MeCN)_4]^{3+}$	2834	$[Bi_{34}O_{40}(HSal)_{18}(DMSO)_{11}(MeCN)_6(H_2O)]^{4+}$
2673	$[Bi_{22}O_{26}(HSal)_{11}(DMSO)_{13}(MeCN)_4(H_2O)]^{3+}$	2843	$[Bi_{34}O_{40}(HSal)_{18}(DMSO)_{12}(MeCN)_5(H_2O)]^{4+}$
2681	$[Bi_{22}O_{26}(HSal)_{11}(DMSO)_{13}(MeCN)_5]^{3+}$	2844	$[Bi_{34}O_{40}(HSal)_{18}(DMSO)_{11}(MeCN)_7(H_2O)]^{4+}$
2687	$[Bi_{22}O_{26}(HSal)_{11}(DMSO)_{13}(MeCN)_5(H_2O)]^{3+}$	2849	$[Bi_{34}O_{40}(HSal)_{18}(DMSO)_{12}(MeCN)_6]^{4+}$
2594	$[Bi_{22}O_{26}(HSal)_{11}(DMSO)_{13}(MeCN)_6]^{3+}$	2854	$[Bi_{34}O_{40}(HSal)_{18}(DMSO)_{12}(MeCN)_6(H_2O)]^{4+}$
2600	$[Bi_{22}O_{26}(HSal)_{11}(DMSO)_{13}(MeCN)_6(H_2O)]^{3+}$	2864	$[Bi_{34}O_{40}(HSal)_{18}(DMSO)_{12}(MeCN)_7(H_2O)]^{4+}$
2607	$[Bi_{22}O_{26}(HSal)_{11}(DMSO)_{14}(MeCN)_5]^{3+}$	2868	$[Bi_{34}O_{40}(HSal)_{18}(DMSO)_{13}(MeCN)_6]^{4+}$
2613	$[Bi_{22}O_{26}(HSal)_{11}(DMSO)_{14}(MeCN)_5(H_2O)]^{3+}$	2883	$[Bi_{34}O_{40}(HSal)_{18}(DMSO)_{13}(MeCN)_7(H_2O)]^{4+}$
2619	$[Bi_{22}O_{26}(HSal)_{11}(DMSO)_{15}(MeCN)_4]^{3+}$	2903	$[Bi_{34}O_{40}(HSal)_{18}(DMSO)_{14}(MeCN)_7(H_2O)]^{4+}$
2633	$[Bi_{22}O_{26}(HSal)_{11}(DMSO)_{15}(MeCN)_5]^{3+}$		
		3490	$[Bi_{22}O_{26}(HSal)_{12}(DMSO)_2(MeCN)_4]^{2+}$
2693	$[Bi_{34}O_{40}(HSal)_{18}(DMSO)_4(MeCN)_6]^{4+}$	3524	$[Bi_{22}O_{26}(HSal)_{12}(DMSO)_5]^{2+}$
2712	$[Bi_{34}O_{40}(HSal)_{18}(DMSO)_5(MeCN)_6]^{4+}$	3550	$[Bi_{22}O_{26}(HSal)_{12}(DMSO)_3(MeCN)_5]^{2+}$
2732	$[Bi_{34}O_{40}(HSal)_{18}(DMSO)_6(MeCN)_6]^{4+}$	3554	$[Bi_{22}O_{26}(HSal)_{12}(DMSO)_5(MeCN)(H_2O)]^{2+}$
2736	$[Bi_{34}O_{40}(HSal)_{18}(DMSO)_6(MeCN)_6(H_2O)]^{4+}$	3563	$[Bi_{22}O_{26}(HSal)_{12}(DMSO)_6]^{2+}$
2741	$[Bi_{34}O_{40}(HSal)_{18}(DMSO)_7(MeCN)_5]^{4+}$	3568	$[Bi_{22}O_{26}(HSal)_{12}(DMSO)_4(MeCN)_4]^{2+}$
2746	$[Bi_{34}O_{40}(HSal)_{18}(DMSO)_7(MeCN)_5(H_2O)]^{4+}$	3570	$[Bi_{22}O_{26}(HSal)_{12}(DMSO)_3(MeCN)_6]^{2+}$
2752	$[Bi_{34}O_{40}(HSal)_{18}(DMSO)_7(MeCN)_6]^{4+}$	3576	$[Bi_{22}O_{26}(HSal)_{12}(DMSO)_4(MeCN)_4(H_2O)]^{2+}$
2756	$[Bi_{34}O_{40}(HSal)_{18}(DMSO)_7(MeCN)_6(H_2O)]^{4+}$	3588	$[Bi_{22}O_{26}(HSal)_{12}(DMSO)_4(MeCN)_5]^{2+}$
2761	$[Bi_{34}O_{40}(HSal)_{18}(DMSO)_7(MeCN)_7]^{4+}$	3597	$[Bi_{22}O_{26}(HSal)_{12}(DMSO)_4(MeCN)_5(H_2O)]^{2+}$
2766	$[Bi_{34}O_{40}(HSal)_{18}(DMSO)_7(MeCN)_7(H_2O)]^{4+}$	3602	$[Bi_{22}O_{26}(HSal)_{12}(DMSO)_7]^{2+}$
2770	$[Bi_{34}O_{40}(HSal)_{18}(DMSO)_9(MeCN)_4]^{4+}$	3608	$[Bi_{22}O_{26}(HSal)_{12}(DMSO)_4(MeCN)_6]^{2+}$
2771	$[Bi_{34}O_{40}(HSal)_{18}(DMSO)_8(MeCN)_6]^{4+}$	3615	$[Bi_{22}O_{26}(HSal)_{12}(DMSO)_5(MeCN)_4(H_2O)]^{2+}$
2775	$[Bi_{34}O_{40}(HSal)_{18}(DMSO)_9(MeCN)_4(H_2O)]^{4+}$	3617	$[Bi_{22}O_{26}(HSal)_{12}(DMSO)_4(MeCN)_6(H_2O)]^{2+}$
2776	$[Bi_{34}O_{40}(HSal)_{18}(DMSO)_8(MeCN)_6(H_2O)]^{4+}$	3623	$[Bi_{22}O_{26}(HSal)_{12}(DMSO)_7(MeCN)]^{2+}$
2780	$[Bi_{34}O_{40}(HSal)_{18}(DMSO)_9(MeCN)_5]^{4+}$	3628	$[Bi_{22}O_{26}(HSal)_{12}(DMSO)_5(MeCN)_5]^{2+}$
2785	$[Bi_{34}O_{40}(HSal)_{18}(DMSO)_9(MeCN)_5(H_2O)]^{4+}$	3636	$[Bi_{22}O_{26}(HSal)_{12}(DMSO)_5(MeCN)_5(H_2O)]^{2+}$
2790	$[Bi_{34}O_{40}(HSal)_{18}(DMSO)_{10}(MeCN)_4]^{4+}$	3642	$[Bi_{22}O_{26}(HSal)_{12}(DMSO)_8]^{2+}$
2791	$[Bi_{34}O_{40}(HSal)_{18}(DMSO)_9(MeCN)_6]^{4+}$	3648	$[Bi_{22}O_{26}(HSal)_{12}(DMSO)_5(MeCN)_6]^{2+}$
2795	$[Bi_{34}O_{40}(HSal)_{18}(DMSO)_9(MeCN)_6(H_2O)]^{4+}$	3662	$[Bi_{22}O_{26}(HSal)_{12}(DMSO)_8(MeCN)]^{2+}$
2800	$[Bi_{34}O_{40}(HSal)_{18}(DMSO)_{10}(MeCN)_5]^{4+}$	3668	$[Bi_{22}O_{26}(HSal)_{12}(DMSO)_5(MeCN)_7]^{2+}$
2803	$[Bi_{34}O_{40}(HSal)_{18}(DMSO)_{11}(MeCN)_3(H_2O)]^{4+}$	3675	$[Bi_{22}O_{26}(HSal)_{12}(DMSO)_6(MeCN)_5(H_2O)]^{2+}$
2805	$[Bi_{34}O_{40}(HSal)_{18}(DMSO)_{10}(MeCN)_5(H_2O)]^{4+}$	3695	$[Bi_{22}O_{26}(HSal)_{12}(DMSO)_6(MeCN)_6(H_2O)]^{2+}$
2809	$[Bi_{34}O_{40}(HSal)_{18}(DMSO)_{11}(MeCN)_4]^{4+}$	3707	$[Bi_{22}O_{26}(HSal)_{12}(DMSO)_6(MeCN)_7]^{2+}$
2810	$[Bi_{34}O_{40}(HSal)_{18}(DMSO)_{10}(MeCN)_6]^{4+}$	3716	$[Bi_{22}O_{26}(HSal)_{12}(DMSO)_6(MeCN)_7(H_2O)]^{2+}$
2815	$[Bi_{34}O_{40}(HSal)_{18}(DMSO)_{10}(MeCN)_6(H_2O)]^{4+}$	3722	$[Bi_{22}O_{26}(HSal)_{12}(DMSO)_9(MeCN)_2]^{2+}$
2819	$[Bi_{34}O_{40}(HSal)_{18}(DMSO)_{11}(MeCN)_5]^{4+}$	3740	$[Bi_{22}O_{26}(HSal)_{12}(DMSO)_{10}(MeCN)]^{2+}$
2824	$[Bi_{34}O_{40}(HSal)_{18}(DMSO)_{11}(MeCN)_5(H_2O)]^{4+}$		

$[Bi_{38}O_{45}(HSal)_{22}(OH)_2]$ **213**

3.00 mg (0.23006 mmol) $[Bi_{38}O_{45}(HSal)_{22}(OH)_2]$ **213** were dissolved in 0.4 ml DMSO and sonicated for 5 min at room temperature. The resulting solution was diluted with 1.6 ml acetonitrile which yielded in a solution of **213** with a concentration of 115 µmol/L. This solution was used for the ESI MS experiments.

$C_{188}H_{214}O_{130}S_{17}Bi_{38}$ 13040.0 g/mol

Table 8.13: *ESI-MS data of $[Bi_{38}O_{45}(HSal)_{22}(OH)_2]$* ***213****.*

m/z	**classification**
3544	$[Bi_{38}O_{46}(HSal)_{19}(DMSO) - 2\ H_2O - 5\ H_2Sal]^{3+}$
3550	$[Bi_{38}O_{46}\ (HSal)_{19}(DMSO) - H_2O - 5\ H_2Sal]^{3+}$
3570	$[Bi_{38}O_{46}(HSal)_{19}(DMSO)_2 - 2\ H_2O - 5\ H_2Sal]^{3+}$
3576	$[Bi_{38}O_{46}(HSal)_{19}(DMSO)_2 - \ H_2O - 5\ H_2Sal]^{3+}$
3596	$[Bi_{38}O_{46}(HSal)_{19}(DMSO)_3 - 2\ H_2O - 5\ H_2Sal]^{3+}$
3602	$[Bi_{38}O_{46}(HSal)_{19}(DMSO)_3 - H_2O - 5\ H_2Sal]^{3+}$
3616	$[Bi_{38}O_{46}(HSal)_{19}(DMSO)_2 - 2\ H_2O - 4\ H_2Sal]^{3+}$
3622	$[Bi_{38}O_{46}(HSal)_{19}(DMSO)_2 - H_2O - 4\ H_2Sal]^{3+}$
3628	$[Bi_{38}O_{46}(HSal)_{19}(DMSO)_2 - 4\ H_2Sal]^{3+}$
3642	$[Bi_{38}O_{46}(HSal)_{19}(DMSO)_3 - 2\ H_2O - 4\ H_2Sal]^{3+}$
3648	$[Bi_{38}O_{46}(HSal)_{19}(DMSO)_3 - H_2O - 4\ H_2Sal]^{3+}$
3668	$[Bi_{38}O_{46}(HSal)_{19}(DMSO)_2 - H_2O - 3\ H_2Sal]^{3+}$
3688	$[Bi_{38}O_{46}(HSal)_{19}(DMSO)_3 - 2\ H_2O - 3\ H_2Sal]^{3+}$
3694	$[Bi_{38}O_{46}(HSal)_{19}(DMSO)_3 - H_2O - 3\ H_2Sal]^{3+}$
3714	$[Bi_{38}O_{46}(HSal)_{19}(DMSO)_2 - H_2O - 2\ H_2Sal]^{3+}$

8.8 Data of the Crystal Structures

8.8.1 1,3-bis(2-methylpyridin-3yl)urea **163**

Table 8.14: *Data of the crystal structure of ligand **163**.*

Formula	$C_{13}H_{14}N_4O$
Formula weight	242.28
Crystal system	monoclinic
Space group	$P\ 2_1/c$
a / Å	12.0896(2)
b / Å	4.5931(1)
c / Å	21.5276(5)
α / °	90
β / °	96.920(1)
γ / °	90
V / Å^3	1186.69(4)
Z	4
$D_{calc.}$ / g cm^{-3}	1.356
μ /mm^{-1}	0.091
θ range / °	3.40 - 25.00
Coll. Refl. no.	13848
Indept. refl. No./$R_{Int.}$	2093/0.0459
Refl. No. $I \geq 2\sigma(I)$	1769
Data/Restr/Param	2093/0/165
S	1.058
R [$I \geq 2\sigma(I)$] / R [all data]	0.0372/0.0467
wR [$I \geq 2\sigma(I)$] / wR [all data]	0.0954/0.1020
Res. el. dens./e Å^{-3}	0.187/-0.209

8.8.2 1,3-bis(4-methylpyridin-3yl)urea **164**

Table 8.16: *Data of the crystal structure of ligand **164** cocrystallized with imidazole.*

Formula	$C_{16}H_{20}N_6O_2$
Formula weight	328.38
Crystal system	monoclinic
Space group	$P\ 2_1/c$
a / Å	8.4693(4)
b / Å	13.3280(6)
c / Å	15.0145(8)
α / °	90
β / °	103.537(4)
γ / °	90
V / Å^3	1647.7(1)
Z	4
$D_{calc.}$ / g cm^{-3}	1.324
μ /mm^{-1}	0.092
θ range / °	2.47 - 24.99
Coll. Refl. no.	20238
Indept. refl. No./$R_{Int.}$	2890/0.1289
Refl. No. $I \geq 2\sigma(I)$	1850
Data/Restr/Param	2890/2/227
S	1.055
R [$I \geq 2\sigma(I)$] / R [all data]	0.0631/0.1132
wR [$I \geq 2\sigma(I)$] / wR [all data]	0.1380/0.1616
Res. el. dens./e Å^{-3}	0.269/-0.223

8.8.3 1,3-bis(5-methylpyridin-3yl)urea **165**

Table 8.17: *Data of the crystal structure of ligand **165**.*

Formula	$C_{13}H_{14}N_4O$
Formula weight	242.28
Crystal system	orthorhombic
Space group	$P\ c\ 2_1\ b$
a / Å	8.3854(6)
b / Å	11.5346(5)
c / Å	12.4219(9)
α / °	90
β / °	90
γ / °	90
V / Å^3	1201.5(1)
Z	4
$D_{calc.}$ / g cm^{-3}	1.34
μ /mm^{-1}	0.090
θ range / °	2.93 - 25.00
Coll. Refl. no.	7208
Indept. refl. No./$R_{Int.}$	1113/0.0871
Refl. No. $I \geq 2\sigma(I)$	961
Data/Restr/Param	1113/1/165
S	1.025
R [$I \geq 2\sigma(I)$] / R [all data]	0.0494/0.0618
wR [$I \geq 2\sigma(I)$] / wR [all data]	0.1157/0.1234
Res. el. dens./e Å^{-3}	0.185/-0.204

8.8.4 1,3-bis(6-methylpyridin-3yl)urea **166**

Table 8.18: *Data of the crystal structure of ligand **166**.*

Formula	$C_{13}H_{14}N_4O$
Formula weight	242.28
Crystal system	monoclinic
Space group	$P\ 2_1/c$
a / Å	7.3328(3)
b / Å	8.3915(3)
c / Å	19.4357(6)
α / °	90
β / °	91.223(2)
γ / °	90
V / Å^3	1195.7(1)
Z	4
$D_{calc.}$ / g cm^{-3}	1.346
μ /mm^{-1}	0.090
θ range / °	3.21 - 24.98
Coll. Refl. no.	14382
Indept. refl. No./$R_{Int.}$	2093/0.0731
Refl. No. $I \geq 2\sigma(I)$	1603
Data/Restr/Param	2093/0/165
S	1.043
R [$I \geq 2\sigma(I)$] / R [all data]	0.0563/0.0785
wR [$I \geq 2\sigma(I)$] / wR [all data]	0.1429/0.1578
Res. el. dens./e Å^{-3}	0.215/-0.218

8.8.5 M_2L_2 complex $[((en)Pd)_2(\mathbf{165})_2](NO_3)_2$ **171**

Table 8.19: *Data of the crystal structure of complex **171**.*

Formula	$C_{30}H_{50}N_{16}O_{17}$
Formula weight	1119.66
Crystal system	monoclinic
Space group	$P\ 2_1/c$
a / Å	13.577(4)
b / Å	15.891(5)
c / Å	20.526(6)
α / °	90
β / °	91.995(7)
γ / °	90
V / Å^3	4426 (2)
Z	4
$D_{calc.}$ / g cm^{-3}	1.680
μ /mm^{-1}	0.900
θ range / °	1.65 – 25.00
Coll. Refl. no.	45167
Indept. refl. No./$R_{Int.}$	7747/0.032
Refl. No. $I \geq 2\sigma(I)$	7096
Data/Restr/Param	7747/608/42
S	1.09
R [$I \geq 2\sigma(I)$] / R [all data]	0.069/0.0739
wR [$I \geq 2\sigma(I)$] / wR [all data]	0.1857/0.1890
Res. el. dens./e Å^{-3}	4.419/-1.255

8.8.6 M_2L_2 complex $[((dppp)Pd)_2(\mathbf{162})_2](OTf)_2$ **174a**

Table 8.20: *Data of the crystal structure of complex* ***174a****.*

Formula	$C_{80}H_{72}F_{12}N_8O_{14}P_4Pd_2S_4$
Formula weight	2062.38
Crystal system	triclinic
Space group	$P\ \bar{1}$
a / Å	15.7089(3)
b / Å	16.7004(3)
c / Å	34.7739(6)
α / °	85.194(1)
β / °	82.836(1)
γ / °	88.750(1)
V / Å^3	9019.1(3)
Z	4
$D_{calc.}$ / g cm^{-3}	1.519
μ /mm^{-1}	0.651
θ range / °	0.59 - 25.00
Coll. Refl. no.	75806
Indept. refl. No./$R_{Int.}$	31694/0.0543
Refl. No. $I \geq 2\sigma(I)$	19752
Data/Restr/Param	31694/269/2233
S	1.175
R [$I \geq 2\sigma(I)$] / R [all data]	0.1103/0.1532
wR [$I \geq 2\sigma(I)$] / wR [all data]	0.3137/0.3438
Res. el. dens./e Å^{-3}	4.215/-2.411

8.8.7 M_2L_2 complex $[((dppp)Pd)_2(\mathbf{164})_2](OTf)_2$ **175a**

Table 8.21: *Data of the crystal structure of complex* ***175a****.*

Formula	$C_{95}H_{108}F_{12}N_{11}O_{18.50}P_4Pd_2S_4$
Formula weight	2392.84
Crystal system	triclinic
Space group	$P\ \bar{1}$
a / Å	16.3896(2)
b / Å	18.3213(2)
c / Å	21.5285(3)
α / °	87.680(1)
β / °	78.927(1)
γ / °	71.110(1)
V / Å^3	6000.9(1)
Z	2
$D_{calc.}$ / g cm^{-3}	1.324
μ /mm^{-1}	0.503
θ range / °	2.67 - 25.00
Coll. Refl. no.	71355
Indept. refl. No./$R_{Int.}$	21076/0.050
Refl. No. $I \geq 2\sigma(I)$	16013
Data/Restr/Param	21076/116/1347
S	0.965
R [$I \geq 2\sigma(I)$] / R [all data]	0.0678/0.0896
wR [$I \geq 2\sigma(I)$] / wR [all data]	0.2207/0.2417
Res. el. dens./e Å^{-3}	1.242/-1.086

8.8.8 M_2L_2 complex $[((dppp)Pd)_2(\mathbf{168})_2](OTf)_2$ **178**

Table 8.21: *Data of the crystal structure of complex **178**.*

Formula	$C_{85.50}H_{85}Cl_3F_{12}N_8O_{16}P_4Pd_2S_4$
Formula weight	2279.89
Crystal system	monoclinic
Space group	$P\ 2_1/n$
a / Å	23.0442(5)
b / Å	19.7734(4)
c / Å	25.6540(5)
α / °	90
β / °	106.841(1)
γ / °	90
V / Å^3	11188.2(4)
Z	4
$D_{calc.}$ / g cm^{-3}	1.354
μ /mm^{-1}	0.603
θ range / °	1.94 – 25.00
Coll. Refl. no.	778452
Indept. refl. No./$R_{Int.}$	19696/0.058
Refl. No. $I \geq 2\sigma(I)$	13377
Data/Restr/Param	19696/1354/33
S	0.877
R [$I \geq 2\sigma(I)$] / R [all data]	0.0916/0.1261
wR [$I \geq 2\sigma(I)$] / wR [all data]	0.2551/0.2785
Res. el. dens./e Å^{-3}	2.76/-1.26

9. References

1 J.-M. Lehn, *Supramolecular Chemistry: Concepts and Perspectives*, VCH, Weinheim **1995**.

2 (a) F. Vögtle, *Supramoleculare Chemie*, Teubner, Stuttgart **1992**; (b) B. Dietrich, P. Viout, J.-M. Lehn, *Macrocyclic Chemistry: Aspects of Organic and Inorganic Supramolecular Chemistry*, VCH, Weinheim **1993**; (c) *Comprehensive Supramolecular Chemistry*, J.-M. Lehn, J. L. Atwood, J. E. D. Davis, D. MacNicol, F. Vögtle (eds.), Pergamon, Oxford **1996**; (d) H.-J. Schneider, A. Yatsimirski, *Principles and Methods in Supramolecular Chemistry*, Wiley, New York **2000**; (e) H. Dodziuk, *Introduction to Supramolecular Chemistry*, Kluwer Academic Publishers, Dordrecht **2002**; (f) *Encyclopedia of Supramolecular Chemistry*, J. W. Steed, J. L. Atwood (eds.), Marcel Dekker, New York **2004**; (g) J. W. Steed, D. R. Turner, K. J. Wallace, *Core Concepts in Supramolecular Chemistry and Nanochemistry*, Wiley, Chichester **2007**; (h) J. W. Steed, J. L. Atwood, *Supramolecular Chemistry*, Wiley, Chichester **2009**.

3 IUPAC, *Pure Appl. Chem.* **1999**, *71*, 1919-1981.

4 IUPAC, *Compendium of Chemical Terminology*, 2nd ed. (the "Gold Book"), compiled by A. D. McNaught and A. Wilkinson, Blackwell Scientific Publications, Oxford **1997**. XML on-line corrected version: http://goldbook.iupac.org (**2006**-) created by M. Nic, J. Jirat, B. Kosata; updates compiled by A. Jenkins. ISBN 0-9678550-9-8. doi:10.1351/goldbook.

5 A. Werner, *Z. Anorg. Chem.* **1893**, *3*, 267-330.

6 E. Fischer, *Ber. Deutsch. Chem. Ges.* **1894**, *27*, 2985-2993.

7 (a) *Principles of Molecular Recognition*, A. D. Buckingham, A. C. Legon, S. M. Roberts (eds.), Blackie Academic & Professional, Glasgow **1993**; (b) *Supramolecular Chemistry I – Directed Synthesis and Molecular Recognition*, E. Weber (ed.), *Top. Curr. Chem.* **1993**, *165*; (c) *Supramolecular Chemistry II – Directed Synthesis and Molecular Recognition*, E. Weber (ed.), *Top. Curr. Chem.* **1995**, *175*; (d) *Protein-Ligand Interactions – From Molecular Recognition to Drug Design*, H.-J. Böhm, G. Schneider (eds.), Wiley-VCH, Weinheim **2003**; (e) *Molecular Recognition and Polymers: Control of Polymer Structure and Self-Assembly*, V. Rotello, S. Thayumanavan (eds.), Wiley, Hoboken **2008**.

8 (a) P. Ehrlich, *Studies on Immunity*, Wiley, New York **1906**; see also: (b) F. Sörgel, C. Landersdorffer, J. Bulitta, B. Keppler, *Nachr. Chem.* **2010**, *52*, 777-782.

9 *Analytical Methods in Supramolecular Chemistry*, C. A. Schalley (ed.), Wiley-VCH, Weinheim **2007**.

10 A. J. Goshe, J. D. Crowley, B. Bosnich, *Helv. Chim. Acta* **2001**, *84*, 2971-2985.

11 (a) L. H. Gade, *Koordinationschemie*, Wiley-VCH, Weinheim **1996**; (b) J. Ribas Gispert, *Coordination Chemistry*, Wiley-VCH, Weinheim **2008**.

12 (a) S. Richards, B. Pedersen, J. V. Silverton, J. L. Hoard, *Inorg. Chem.* **1964**, *3*, 27-33; (b) M. D. Lind, M. J. Hamor, T. A. Hamor, J. L. Hoard, *Inorg. Chem.* **1964**, *3*, 34-43; (c) G. H. Cohen, J. L. Hoard, *J.*

Am. Chem. Soc. **1964**, *86*, 2749-2750; (d) M. D. Lind, B. Lee, J. L. Hoard, *J. Am. Chem. Soc.* **1965**, *87*, 1611-1612; (d) J. L. Hoard, B. Lee, M. D. Lind, *J. Am. Chem. Soc.* **1965**, *87*, 1612-1613.

13 R. Alsfasser, C. Janiak, T. M. Klapötke, H.-J. Meyer, *Moderne Anorganische Chemie*, E. Riedel (ed.), de Gruyter, Berlin **2007**.

14 I. Fleming, *Grenzorbitale und Reaktionen organischer Verbindungen*, VCH, Weinheim **1979**.

15 (a) J. Huheey, E. Keiter, R. Keiter, *Anorganische Chemie: Prinzipien von Struktur und Reaktivität*, de Gruyter, Berlin **1995**; (b) A. F. Hollemann, E. Wiberg, N. Wiberg, *Lehrbuch der Anorganischen Chemie*, de Gruyter, Berlin **1995**; (c) C. Elschenbroich, *Organometallchemie*, Teubner, Stuttgart **2003**.

16 B. J. Coe, S. J. Glenwright, *Coord. Chem. Rev.* **2000**, *203*, 5-80.

17 A. Pidcock, R. E. Richards, L. M. Venanzi, *J. Chem. Soc. A* **1966**, 1707-1710.

18 (a) D. Bright, J. A. Ibers, *Inorg. Chem.* **1969**, *8*, 709-716; (b) T. G. Appleton, H. C. Clark, L. E. Manzer, *Coord. Chem. Rev.* **1973**, *10*, 335-422; (c) R. G. Pearson, *Inorg. Chem.* **1973**, *12*, 712-714; (d) E. M. Shustorovich, M. A. Porai-Koshits, Y. A. Buslaev, *Coord. Chem. Rev.* **1975**, *17*, 1-98; (e) P. D. Lyne, D. M. P. Mingos, *J. Chem. Soc., Dalton Trans.* **1995**, 1635-1643.

19 F. Basolo, R.G. Pearson, *Prog. Inorg. Chem.* **1962**, *4*, 381-453.

20 L. I. Elding, O. Groning, *Inorg. Chem.* **1978**, *17*, 1872-1880.

21 IUPAC, *Pure Appl. Chem.* **1994**, *66*, 1077-1184.

22 (a) M. T. Rodgers, P. B. Armentrout, *Int. J. Mass Spectrom.* **1999**, 1*85-187*, 359-380; (b) R. Amunugama, M. T. Rodgers, *Int. J. Mass Spectrom.* **2000**, *195/196*, 439-457; (c) M. T. Rodgers, P. B. Armentrout, *Mass Spectrom. Rev.* **2000**, *19*, 215-247; (d) H. Koizumi, P. B. Armentrout, *J. Am. Soc. Mass Spectrom.* **2001**, *12*, 480-489; (e) H. Koizumi, X.-G. Zhang, P. B. Armentrout, *J. Phys. Chem. A* **2001,** *105*, 2444-2452; (f) N. S. Rannulu, M. T. Rodgers, *J. Phys. Chem. A* **2007**, *111*, 3465-3479.

23 (a) A. Miller, *Self-assembly*, in: *The development Biology of Plants and Animals*, C. F. Graham, P. F. Wareing (eds.), Blackwell Scientific Publications, Oxford **1976**; (b) A. B. Sendova-Franks, N. R. Franks, *Phil. Trans. R. Soc. B* **1999**, *354*, 1395-1405; (c) L. f. Lindoy, I. M. Atkinson, *Self-Assembly in Supramolecular Systems*, The Royal Society of Chemistry, Cambridge **2000**; (d) C. Anderson, G. Theraulaz, J.-L. Deneubourg, *Insect. Soc.* **2002**, *49*, 99-101; (e) G. M. Whitesides, B. Grzybowski, *Science* **2002**, *295*, 2418-2421; (f) K. Ariga, J. P. Hill, M. V. Lee, A. Vinu, R. Charvet, S. Acharya, *Sci. Technol. Adv. Mater.* **2008**, *9*, 014109.

24 (a) G. Nicolis, I. Prigogine, *Self-Organization in Non-Equilibrium Systems*, Wiley, New York **1977**; (b) M. Eigen, P. Schuster, *The Hypercycle: A Principle of Natural Self-Organization*, Springer, Berlin **1979**; (c) W, Krohn, G. Küppers, *Selbstorganisation: Aspekte einer wissenschaftlichen Revolution*, Vieweg, Wiesbaden **1990**; (d) F. Cramer, *Chaos and Order, The Complex Structure of Living Systems*, VCH, Weinheim **1993**; (e) S. Kauffman, *Origins of Order: Self-Organization and Selection in Evolution*, Oxford University Press, Oxford **1993**; (f) M. L. Estep, *Self-Organizing Natural Intelligence: Issues of Knowing, Meaning and Complexity*, Springer, Berlin **2006**.

25 J. D. Halley, D. A. Winkler, *Complexity* **2008**, *14*, 10-17.

26 T. Misteli, *J. Cell Biol.* **2001**, *155*, 181-185.

27 (a) J. S. Lindsey, *New. J. Chem.***1991**, *15*, 153-180; (b) G. M. Whitesides, J. P. Mathias, C. T. Seto, *Science* **1991**, *254*, 1312-1319; (c) D. Philp, J. F. Stoddart, *Angew. Chem.* **1996**, *108*, 1242-1286; *Angew. Chem. Int. Ed.* **1996**, *35*, 1155-1196; (d) C. A. Schalley, A. Lützen, M. Albrecht, *Chem. Eur. J.* **2004**, *10*, 1072-1080.

28 For example: (a) S. Tashiro, M. Tominaga, T. Kusukawa, M. Kawano, S. Sakamoto, K. Yamaguchi, M. Fujita, *Angew. Chem.* **2003**, *115*, 3389-3392; *Angew. Chem. Int. Ed.* **2003**, *42*, 3267-3270; (b) A. Hori, K. Yamaguchi, M. Fujita, *Angew. Chem.* **2004**, *116*, 5126-5129; *Angew. Chem. Int. Ed.* **2004**, *43*, 5016-5019.

29 Some examples for self-assembly via hydrogen bonds: (a) P. Gilli, V. Bertolasi, V. Feretti, G. Gilli, *J. Am. Chem. Soc.* **1994**, *116*, 909-915; (b) D. Braga, A. Angeloni, F. Grepioni, E. Tagliavini, *Chem. Commun.* **1997**, 1447-1448; (c) D. Braga, L. Maini, F. Grepioni, A. DeCian, O. Felix, J. Fischer, M. W. Hosseini, *New J. Chem.* **2000**, *24*, 547-553; (d) M. Hosseini, *Coord. Chem. Rev.* **2003**, *240*, 157-166; (e) T. Friscic, L. R. MacGillivray, *Croat. Chim. Acta* **2006**, *79*, 327-333.

30 M. J. Zaworotko, *Chem. Commun.* **2001**, 1-9.

31 D. J. Duchamp, R. E. Marsh, *Acta Crystallogr. B* **1969**, *25*, 5-19.

32 F. H. Herbstein, M. Kapon, G. M. Reisner, *J. Inclusion Phenom.* **1987**, *5*, 211-214.

33 Reviews on metallo-supramolecular complexes, see for example: (a) M. Albrecht, *Chem. Rev.* **2001**, *101*, 3457-3498; (b) F. A. Cotton, C. Lin, C. A. Murillo, *Acc. Chem. Res.* **2001**, *34*, 759-771; (c) S.-S. Sun, A. J. Lees, *Coord. Chem. Rev.* **2002**, *230*, 170-191; (d) F. Würthner, C.-C. You, C. R. Saha-Möller, *Chem. Soc. Rev.* **2004**, *33*, 133-146; (e) H. Hofmeier, U. S. Schubert, *Chem. Soc. Rev.* **2004**, *33*, 373-399; (f) M. Fujita, M. Tominaga, A. Hori, B. Therrien, *Acc. Chem. Res.* **2005**, *38*, 369-378; (g) A. Kaiser, P. Bäuerle, P. *Top. Curr. Chem.* **2005**, *249*, 127-201; (h) C.-C. You, R. Dobrawa, C. R. Saha-Möller, F. Würthner, *Top. Curr. Chem.* **2005**, *258*, 39-82; (i) J. R. Nitschke, *Acc. Chem. Res.* **2007**, *40*, 103-112; (j) C. P. Pradeep, L. Cronin, *Annu. Rep. Prog. Chem., Sect. A* **2007**, *103*, 287-332; (k) I. G. Georgiev, L. R. MacGillivray, *Chem. Soc. Rev.* **2007**, *36*, 1239-1248; (l) T. Gunnlaugsson, F. Stomeo, *Org. Biomol. Chem.* **2007**, *5*, 1999-2009; (m) M. A. Pitt, D. W. Johnson, *Chem. Soc. Rev.* **2007**, *36*, 1441-1453; (n) J. Cookson, P. D. Beer, *Dalton Trans.* **2007**, 1459-1472; (o) S. J. Lee, W. Lin, *Acc. Chem. Res.* **2008**, *41*, 521-537; (p) S. J. Dalgarno, N. P. Power, J. L. Atwood, *Coord. Chem. Rev.* **2008**, *252*, 825-841; (q) E. C. Constable, *Coord. Chem. Rev.* **2008**, *252*, 842-855; (r) A. Kumara, S.-S. Suna, A. J. Lees, *Coord. Chem. Rev.* **2008**, *252*, 922-939; (s) C. R. K. Glasson, L. F. Lindoy, G. V. Meehan, *Coord. Chem. Rev.* **2008**, *252*, 940-963; (t) G. Aromí, P. Gamez, J. Reedijk, *Coord. Chem. Rev.* **2008**, *252*, 964-989; (u) B. H. Northrop, H.-B. Yang, P. J. Stang, *Chem. Commun.* **2008**, 5896-5908; (v) P. J. Lusby, *Annu. Rep. Prog. Chem. A* **2009**, *105*, 323-347; (w) B. H. Northrop, Y.-R. Zheng, K.-W. Chi, P. J. Stang, *Acc. Chem. Res.* **2009**, *42*, 1554-1563; (x) Y.-F. Han, W.-G. Jia, W.-B. Yu, G.-X. Jin, *Chem. Soc. Rev.* **2009**, *38*, 3419-3434; (y) S. De, K. Mahata, M. Schmittel, *Chem. Soc. Rev.* **2010**, *39*, 1555-1575.

34 S. Leininger, B. Olenyuk, P. J. Stang, *Chem. Rev.* **2000**, *100*, 853-908.

35 B. J. Holliday, C. A. Mirkin, *Angew. Chem.* **2001**, *113*, 2076-2097; *Angew. Chem., Int. Ed.* **2001**, *40*, 2022-2043.

36 Some examples for hierarchical self-assembly: (a) I. S. Choi, N. Bowden, G. M. Whitesides, *Angew. Chem.* **1999**, *111*, 3265-3268; *Angew. Chem. Int. Ed.* **1999**, *38*, 3078-3081; (b) L. A. Cuccia, E. Ruiz, J.-M. Lehn, J.-C. Homo, M. Schmutz, *Chem. Eur. J.* **2002**, *8*, 3448-3457; (c) H. Wu, V. R. Thalladi, S. Whitesides, G. M. Whitesides, *J. Am. Chem. Soc.* **2002**, *124*, 14495-14502; (d) J. A. A. W. Elemans, A. E. Rowan, R. J. M. Nolte, *J. Mat. Chem.* **2003**, *13*, 2661-2670; (e) M. Ruben, U. Ziener, J.-M. Lehn, V. Ksenofontov, P. Gütlich, G. B. M. Vaughan, *Chem. Eur. J.* **2005**, *11*, 94-100; (f). M. Ikeda, T. Nobori, M. Schmutz, J.-M. Lehn, *Chem. Eur. J.* **2005**, *11*, 662-668; (g) H. M. Keizer, R. P. Sijbesma, *Chem. Soc. Rev.* **2005**, *34*, 226-234; (h) S.-I. Sakurai, K. Okoshi, J. Kumaki, E. Yashima, *Angew. Chem.* **2006**, *118*, 1267-1270; *Angew. Chem. Int. Ed.* **2006**, *45*, 1245-1248; (i) M. Albrecht, M. Baumert, J. Klankermayer, M. Kogej, C. A. Schalley, R. Fröhlich, *Dalton Trans.* **2006**, 4395-4400; (j) N. S. S. Kumar, S. Varghese, G. Narayan, S. Das, *Angew. Chem.* **2006**, *118*, 6465-6469; *Angew. Chem. Int. Ed.* **2006**, *45*, 6317-6321; (k) Y. Yan, N. A. M. Besseling, A. de Keizer, A. T. M. Marcelis, M. Drechsler, M. A. Cohen Stuart *Angew. Chem.* **2007**, *119*, 1839-1841; *Angew. Chem. Int. Ed.* **2007**, *46*, 1807-1809; (l) H. Wei, B. Li, Y. Du, S. Dong, E. Wang, *Chem. Mater.* **2007**, *19*, 2987-2993; (m) A. Langner, S. L. Tait, N. Lin, R. Chandrasekar, M. Ruben, K. Kern, *Angew. Chem.* **2008**, *120*, 8967-8970; *Angew. Chem. Int. Ed.* **2008**, *47*, 8835-8838; (n) M. Baumert, M. Albrecht, H. D. F. Winkler, C. A. Schalley, *Synthesis* **2010**, 953-958; (o) J. K. Clegg, S. S. Iremonger, M. J. Hayter, P. D. Southon, R. B. Macquart, M. B. Duriska, P. Jensen, P. Turner, K. A. Jolliffe, C. J. Kepert, G. V. Meehan, L. F. Lindoy, *Angew. Chem.* **2010**, *122*, 1093-1096; *Angew. Chem. Int. Ed.* **2010**, *49*, 1075-1078; (p)J. K.-H. Hui, P. D. Frischmann, C.-H. Tso, C. A. Michal, M. J. MacLachlan, *Chem. Eur. J.* **2010**, *16*, 2453-2460; (q) H. Fenton, I. S. Tidmarsh M. D. Ward, *Dalton Trans.* **2010**, *39*, 3805-3815; (r) M. Albrecht, M. Baumert, H. D. F. Winkler, C. A. Schalley, R. Fröhlich, *Dalton Trans.* **2010**, *39*, 7220-7222.

37 (a) H. T. Baytekin, B. Baytekin, A. Schulz, C. A. Schalley, *Small* **2009**, *5*, 194-197; (b) H. T. Baytekin, B. Baytekin, A. Schulz, A. Springer, T. Gross, W. Unger, M. Artamonova, S. Schlecht, D. Lentz, C. A. Schalley, *Chem. Mater.* **2009**, *21*, 2980-2992.

38 M. Albrecht, S. Mirtschin, M. de Groot, I. Janser, J. Runsink, G. Raabe, M. Kogej, C. A. Schalley, *J. Am. Chem. Soc.* **2005**, *127*, 10371-10387.

39 T. D. Hamilton, L. R. MacGillivray, Self-Assembly in Biochemistry, in: *Ecyclopedia of Supramolecular Chemistry*, J. L. Atwood, J. W. Steed (eds.), Marcel Dekker, New York **2004**.

40 (a) A. Klug, *Angew. Chem.* **1983**, *95*, 579-596; *Angew. Chem. Int. Ed.* **1983**, *22*, 565-582; (b) A. Klug, *Phil. Trans. R. Soc. Lond. B* **1999**, *354*, 531-535; (c) P. J. Butler, *Phil. Trans. R. Soc. Lond. B* **1999**, *354*, 537-550.

41 A. X. Wu, L. Isaacs, *J. Am. Chem. Soc.* **2003**, *125*, 4831-4835.

42 P. Mukhopadhyay, A.-X. Wu, L. Isaacs, *J. Org. Chem.* **2004**, *69*, 6157-6164.

43 Y. Rudzevich, V. Rudzevich, F. Klautzsch, C. A. Schalley, V. Böhmer, *Angew. Chem.* **2009**, *121*, 3925-3929; *Angew. Chem. Int. Ed.* **2009**, *48*, 3867-3871.

44 K. Mahata, M. Schmittel, *J. Am. Chem. Soc.* **2009**, *131*, 16544-16554.

45 (a) A. X. Wu, A. Chakraborty, J. C. Fettinger, R. A. Flowers, L. Isaacs, *Angew. Chem.* **2002**, *114*, 4200-4203; *Angew. Chem. Int. Ed.* **2002**, *41*, 4028-4031; (b) S. Gosh, A. X. Wu, J. C. Fettinger, P. Y. Zavalij, L. Isaacs, *J. Org. Chem.* **2008**, *73*, 5915-5925.

46 (a) S. M. Liu, C. Ruspic, P. Mukhopadhyay, S. Chakrabarty, P. Y. Zavalij, L. Isaacs, *J. Am. Chem. Soc.* **2005**, *127*, 15959-15967; (b) P. Mukhopadhyay, P. Y. Zavalij, L. Isaacs, *J. Am. Chem. Soc.* **2006**, *128*, 14093-14112.

47 (a) D. Braekers, C. Peters, A. Bogdan, Y. Rudzevich, V. Böhmer, J. F. Desreux, *J. Org. Chem.* **2008**, *73*, 701-706; (b) Y. Rudzevich, Y. Cao, V. Rudzevich, V. Böhmer, *Chem. Eur. J.* **2008**, *14*, 3346-3354.

48 (a) W. Jiang, H. D. F. Winkler, C. A. Schalley, *J. Am. Chem. Soc.* **2008**, *130*, 13852-13853; (b) W. Jiang, C. A. Schalley, *Proc. Natl. Acad. Sci. USA* **2009**, *106*, 10425-10429; (c) W. Jiang, P. C. Mohr, A. Schäfer, C. A. Schalley, *J. Am. Chem. Soc.* **2010**, *132*, 2309-2320; (d) W. Jiang, C. A. Schalley, *J. Mass Spectrom.* **2010**, *45*, 788-798; (e) W. Jiang, Q. Wang, I. Linder, F. Klautzsch, C. A. Schalley, *Chem. Eur. J.* **2011**, *17*, 2344-2348.

49 (a) S. Ulrich, J.-M. Lehn, *J. Am. Chem. Soc.* **2009**, *131*, 5546-5559; (b) S. Ulrich, J.-M. Lehn, *Chem. Eur. J.* **2009**, 15, 5640-5645.

50 (a) A. Rang, M. Engeser, N. M. Maier, M. Nieger, W. Lindner, C.A. Schalley, *Chem. Eur. J.* **2008**, *14*, 3855-3859; (b) A. Rang, M. Nieger, M. Engeser, A. Lützen, C. A. Schalley, *Chem. Commun.* **2008**, 4789-4791.

51 (a) C. Addicott, N. Das, P. J. Stang, *Inorg. Chem.* **2004**, *43*, 5335-5338; (b) K.-W. Chi, C. Addicott, A. M. Arif, P. J. Stang, *J. Am. Chem. Soc.* **2004**, *126*, 16569-16574; (c) L. Z. Zhao, B. H. Northrop, Y.-R. Zheng, H.-B. Yang, H. J. Lee, Y. M. Lee, J. Y. Park, K.-W. Chi, P. J. Stang, *J. Org. Chem.* **2008**, *73*, 6580-6586; (d) B. H. Northrop, H.-B. Yang, P. J. Stang, *Inorg. Chem.* **2008**, *47*, 11257-11268; (e) Y.-R. Zheng, H.-B. Yang, K. Ghosh, L. Zhao, P. J. Stang, *Chem. Eur. J.* **2009**, *15*, 7203-7214.

52 J. Lee, K. Ghosh, P. J. Stang, *J. Am. Chem. Soc.* **2009**, *131*, 12028-12029.

53 (a) M. Schmittel, K. Mahata, *Inorg. Chem.* **2009**, *48*, 822-824; (b) M. Schmittel, K. Mahata, *Chem. Commun.* **2010**, 4163-4165; (c) K. Mahata, M. Lal Saha, M. Schmittel, *J. Am. Chem. Soc.* **2010**, *132*, 15933-15935.

54 (a) M. Albrecht, *Chem. Soc. Rev.* **1998**, *27*, 281-288; (b) D. Caulder, K. Raymond, *Acc. Chem. Res.* **1999**, *32*, 975-982; (c) D. Caulder, K. Raymond, *J. Chem. Soc., Dalton Trans.* **1999**, 1185-1200; (d) M. Albrecht, *J. Inclusion Phenom. Macrocyc. Chem.* **2000**, *36*, 127-151.

55 For an overview about templates see: (a) *Templated Organic Synthesis*, F. Diederich, J. P. Stang (eds.), Wiley-VCH, Weinheim **2000**; (b) *Templates in Chemistry I*, C. A. Schalley, F. Vögtle, K. H. Dötz (eds.), *Top. Curr. Chem.* **2004**, *248*; (c) *Templates in Chemistry II*, C. A. Schalley, F. Vögtle, K. H.

Dötz (eds.), *Top. Curr. Chem.* **2005**, *249*; (d) *Templates in Chemistry III*, P. Broeckmann, K. H. Dötz, C. A. Schalley (eds.), *Top. Curr. Chem.* **2009**, *287*.

56 Some examples for metallo-supramolecular helicates formed by the *Symmetry-Interaction Strategy*: (a) E. Enemark, T. Stack, *Angew. Chem.* **1998**, *110*, 977-981; *Angew. Chem. Int. Ed.* **1998**, *37*, 932-935; (b) M. Albrecht, M. Schneider, H. Röttele, *Angew. Chem.* **1999**, *111*, 512-515; *Angew. Chem. Int. Ed.* **1999**, *38*, 557-559; (c) M. Albrecht, O. Blau, J. Zauner, *Eur. J. Org. Chem.* **1999**, *1999*, 3165-3169; (d) C. R. Rice, S. Worl, J. C. Jeffery, R. L. Paul, M. D. Ward, *Chem. Commun.* **2000**, 1529-1530; (e) N. Yoshida, K. Ichikawa, M. Shiro, *J. Chem. Soc., Perkin Trans. 2* **2000**, 17-26; (f) S. L. James, E. Lozano, M. Nieuwenhuyzen, *Chem. Commun.* **2000**, 617-618; (g) C. P. Iglesias, M. Elhabiri, M. Hollenstein, J.-C. G. Bünzli, C. Piguet, *J. Chem. Soc., Dalton Trans.* **2000**, 2031-2043; (h) S. Rigault, C. Piguet, J.-C. G. Bünzli, *J. Chem. Soc., Dalton Trans.* **2000**, 2045-2053; (i) J. Hamblin, L. J. Childs, N. W. Alcock, M. J. Hannon, *J. Chem. Soc., Dalton Trans.* **2001**, 164-169; (j) P. E. Kruger, N. Martin, M. Nieuwenhyzen, *J. Chem. Soc., Dalton Trans.* **2001**, 1966-1970; (k) J. Hamblin, A. Jackson, N. W. Alcock, M. J. Hannon, *J. Chem. Soc., Dalton Trans.* **2002**, 1636-1641; (l) A. Lavalette, J. Hamblin, A. Marsh, D. M. Haddleton, M. J. Hannon, *Chem. Commun.* **2002**, 3040-3041; (m) F. Tuna, M. R. Lees, G. J. Clarkson, M. J. Hannon, *Chem. Eur. J.* **2004**, *10*, 5737-5750; (n) M. Vázquez, M. R. Bermejo, M. Licchelli, A. M. González-Noya, R. M. Pedrido, C. Sanregorio, L. Sorace, A. M. García-Deibe, J. Sanmartin, *Eur. J. Inorg. Chem.* **2005**, 3479-3490; (o) L. Allouche, A. Marquis, J.-M. Lehn, *Chem. Eur. J.* **2006**, *12*, 7520-7525; (p) J. Hamblin, F. Tuna, S. Bunce, L. J. Childs, A. Jackson, W. Errington, N. W. Alcock, H. Nierengarten, A. Van Drosselaer, E. Leize-Wagner, M. J. Hannon, *Chem. Eur. J.* **2007**, *13*, 9286-9296; (q) T. Haino, H. Shio, R. Takano, Y. Fukazawa, *Chem. Commun.* **2009**, 2481-2483; (r) Y. Morita, Y. Yakiyama, S. Nakazawa, T. Murata, T. Ise, D. Hashizume, D. Shiomi, K. Sato, M. Kitagawa, K. Nakasuji, T. Takui, *J. Am. Chem. Soc.* **2010**, *132*, 6944-6946; (s) R. Pedrido, M. Vázquez-López, L. Sorace, A. M. González-Noya, M. Cwiklinska, V. Suárez-Gómez, G. Zaragoza, M. R. Bermejo, *Chem. Commun.* **2010**, 4797-4799.

57 Some examples for metallo-supramolecular tetrahedra formed by the *Symmetry-Interaction Strategy*: (a) T. Beissel, R. Powers, T. Parac, K. Raymond, *J. Am. Chem. Soc.* **1999**, *121*, 4200-4206; (b) T. N. Parac, M. Scherer, K. N. Raymond, *Angew. Chem.* **2000**, *112*, 1288-1291; *Angew. Chem. Int. Ed.* **2000**, *39*, 1239-1242.

58 Reviews of metallo-supramolecular grids: (a) L. K. Thompson, *Coord. Chem. Rev.* **2002**, *233-234*, 193-206; (b) M. Ruben, J. Rojo, F. J. Romero-Salguero, L. H. Uppadine, J.-M. Lehn, *Angew. Chem.* **2004**, *116*, 3728-3747; *Angew. Chem. Int. Ed.* **2004**, *43*, 3644-3662; (c) L. K. Thompson, *Canad. J. Chem.* **2005**, *83*, 77-92; (d) L. N. Dawe, K. V. Shuvaev, L. K. Thompson, *Chem. Soc. Rev.* **2009**, *38*, 2334-2359; (e) A.-M. Stadler, *Eur. J. Inorg. Chem.* **2009**, 4751-4770.

59 (a) M. Tominaga, K. Suzuki, M. Kawano, T. Kusukawa, T. Ozeki, S. Sakamoto, K. Yamaguchi, M. Fujita, *Angew. Chem.* **2004**, *116*, 5739-5743; *Angew. Chem. Int. Ed.* **2004**, *43*, 5621-5625; (b) S. Sato, J. Iida, K. Suzuki, M. Kawano, T. Ozeki, M. Fujita, *Science* **2006**, *313*, 1273-1276; (c) T. Murase, S.

Sato, M. Fujita, *Angew. Chem.* **2007**, *119*, 1101-1103; *Angew. Chem. Int. Ed.* **2007**, *46*, 1083-1085; (d) K. Suzuki, M. Kawano, M. Fujita, *Angew. Chem.* **2007**, *119*, 2877-2880; *Angew. Chem. Int. Ed.* **2007**, *46*, 2819-2822; (e) K. Suzuki, J. Iida, S. Sato, M. Kawano, M. Fujita, *Angew. Chem.* **2008**, *120*, 5864-5866; *Angew. Chem. Int. Ed.* **2008**, *47*, 5780-5782.

60 N. Gianneschi, M. Masar, C. A. Mirkin, *Acc. Chem. Res.* **2005**, *38*, 825-837.

61 M. J. Wiester, C. A. Mirkin, *Inorg. Chem.* **2009**, *48*, 8054-8056.

62 (a) J. R. Farrell, C. A. Mirkin, I. A. Guzei, L. M. Liable-Sands, A. L. Rheingold, *Angew. Chem.* **1998**, *110*, 484-487; *Angew. Chem. Int. Ed.* **1998**, *37*, 465-467; (b) J. R. Farrell, A. H. Eisenberg, C. A. Mirkin, I. A. Guzei, L. M. Liable-Sands, C. D. Incarvito, A. L. Rheingold, C. L. Stern, *Organometallics* **1999**, *18*, 4856-4868; (c) B. J. Holliday, J. R. Farrell, C. A. Mirkin, K.-C. Lam, A. L. Rheingold, *J. Am. Chem. Soc.* **1999**, *121*, 6316-6317; (d) F. M. Dixon, A. H. Eisenberg, J. R. Farrell, C. A. Mirkin, L. M. Liable-Sands, A. L. Rheingold, *Inorg. Chem.* **2000**, *39*, 3432-3433; (e) A. H. Eisenberg, F. M. Dixon, C. A. Mirkin, C. L. Stern, C. D. Incarvito, A. L. Rheingold, *Organometallics* **2001**, *20*, 2052-2058; (f) X. Liu, A. H. Eisenberg, C. L. Stern, C. A. Mirkin, *Inorg. Chem.* **2001**, *40*, 2940-2941; (g) A. H. Eisenberg, F. M. Dixon, C. A. Mirkin, C. L. Stern, C. D. Incarvito, A. L. Rheingold, *Organometallics* **2002**, *21*, 4889-4889; (h) X. Liu, A. H. Eisenberg, C. L. Stern, C. A. Mirkin, *J. Am. Chem. Soc.* **2003**, *125*, 2836-2837.

63 (a) A. W. Maverick, F. F. Klavetter, *Inorg. Chem.* **1984**, *23*, 4129-4130; b) A. W. Maverick, S. C. Buckingham, Q. Yao, J. R. Bradbury, G. G. Stanley, *J. Am. Chem. Soc.* **1986**, *108*, 7430-7431.

64 (a) M. Fujita, S. Nagao, M. Iida, K. Ogata, K. Ogura, *J. Am. Chem. Soc.* **1993**, *115*, 1574-1576; (b) M. Fujita, J. Yazaki, T. Kuramochi, K. Ogura, *Bull. Chem. Soc. Jpn.* **1993**, *66*, 1837-1839.

65 (a) M. Fujita, F. Ibukuro, H. Hagihara, K. Ogura, *Nature* **1994**, *367*, 720-723; (b) M. Fujita, F. Ibukuro, H. Seki, O. Kamo, M. Imanari, K. Ogura, *J. Am. Chem. Soc.* **1996**, *118*, 899-900.

66 M. Fujita, F. Ibukuro, K. Yamaguchi, K. Ogura, *J. Am. Chem. Soc*. **1995**, *117*, 4175-4176.

67 M. Fujita, M. Aoyagi, F. Ibukuro, K. Ogura, K. Yamaguchi, *J. Am. Chem. Soc.* **1998**, *120*, 611-612.

68 M. Fujita, M. Aoyagi, K. Ogura, *Inorg. Chim. Acta* **1996**, *246*, 53-57.

69 R. Schneider, M. W. Hosseini, J. M. Planeix, A. DeCian, J. Fischer, *Chem. Commun.* **1998**, 1625-1626.

70 G. Ma, Y. S. Yung, D. S. Chung, J. I. Hong, *Tet. Lett.* **1999**, *40*, 531-534.

71 M. Schmitz, S. Leininger, J. Fan, P. J. Stang, *Organometallics* **1999**, *18*, 4817-4824.

72 Some examples for M_2L_2 complexes with *cis*-blocked square-planar metal centers: (a) T. W. Kim, M. S. Lah, J.-I. Hong, *Chem. Commun.* **2001**, 743-744; (b) D. K. Chand, M. Fujita, K. Biradha, S. Sakamoto, K. Yamaguchi, *Dalton Trans.* **2003**, 2750-2756; (c) B. Chatterjee, J. C. Noveron, M. J. E. Resendiz, J. Liu, T. Yamamoto, D. Parker, M. Cinke, C. V. Nguyen, A. M. Arif, P. J. Stang, *J. Am. Chem. Soc.* **2004**, *126*, 10645-10656; (d) L.-C. Song, G.-X. Jin, W.-X. Zhang, Q.-M. Hu, *Organometallics* **2005,** *24*, 700-706; (e) Y. Liu, *Tetrahedron Lett.* **2007**, *48*, 3871-3874; (f) M. Capó, J. Benet-Buchholz, P. Ballester, *Inorg. Chem.* **2008**, *47*, 10190-10192; (g) G. Koshkakaryan, K. Parimal, J. He, X. Zhang, Z. Abliz, A. H. Flood, Y. Liu, *Chem. Eur. J.* **2008**, *14*, 10211-10218; (h) V. Blanco, D.

Abella, E. Pía, C. Platas-Iglesias, C. Peinador, J. M. Quintela, *Inorg. Chem.* **2009**, *48*, 4098-4107; (i) P. Teo, L. L. Koh, T. S. A. Hor, *Dalton Trans.* **2009**, 5637-5646; (j) J. Lu, D. R. Turner, L. P. Harding, L. T. Byrne, M. V. Baker, S. R. Batten, *J. Am. Chem. Soc.* **2009**, *131*, 10372-10373; (k) C. Peinador, E. Pía, V. Blanco, M. D. García, J. M. Quintela, *Org. Lett.* **2010**, *12*, 1380-1382.

73 (a) T. Weilandt, U. Kiehne, G. Schnakenburg, A. Lützen, *Chem. Commun.* **2009**, 2320-2322; (b) T. Weilandt, U. Kiehne, J. Bunzen, G. Schnakenburg, A. Lützen, *Chem. Eur. J.* **2010**, *16*, 2418-2426.

74 (a) P. J. Stang, B. Olenyuk, K. Chen, *Synthesis* **1995**, 937-938; (b) P. J. Stang, K. Chen, *J. Am. Chem. Soc.* **1995**, *117*, 1667-1668; (c) P. J. Stang, K. Chen, A. M. Arif, *J. Am. Chem. Soc.* **1995**, *117*, 8793-8797; (d) B. Olenyuk, J. A. Whiteford, P. J. Stang, *J. Am. Chem. Soc.* **1996**, *118*, 8221-8230.

75 Recent examples for M_2L_2 complexes with other metal centers: (a) Y. Qi, Y. Che, J. Zheng, *J. Mol. Struct.* **2008**, *891*, 98-102; (b) C.-L. Chen, Z.-Q. Yu, Q. Zhang, M. Pan, J.-Y. Zhang, C.-Y. Zhao, C.-Y. Su, *Cryst. Growth Des.* **2008**, *8*, 897-905; (c) U. Kiehne, T. Weilandt, A. Lützen, *Eur. J. Org. Chem.* **2008**, *12*, 2056-2064; (d) G. B. Guseva, N. A. Dudina, E. V. Antina, A. I. V'yugin, A. S. Semeikin, *Russ. J. Coord. Chem.* **2009**, *35*, 65-73; (e) Y. Ma, A.-L. Cheng, C.-Y. Tian, H. Tian, E.-Q. Gao, *J. Mol. Struct.* **2009**, *935*, 129-135; (f) H.-K. Liu, Y. Cai, W. Luo, F. Tong, C. You, S. Lü, X. Huang, H.-Y. Ye, F. Su, X. Wang, *Inorg. Chem. Commun.* **2009**, *12*, 457-460; (g) H.-Y. Deng, J.-R. He, M. Pan, L. Lia, C.-Y. Su, *Cryst. Eng. Comm* **2009**, *11*, 909-917; (h) S. Zhang, Y. Tang, Y. Su, J. Lan, R. Xie, J. You, *Inorg. Chim. Acta* **2009**, *362*, 1511-1518; (i) L.-j. Liu, F. Wang, M. Shi, *Eur. J. Inorg. Chem.* **2009**, 1723-1728; (j) J. Bunzen, T. Bruhn, G. Bringmann, A. Lützen *J. Am. Chem. Soc.* **2009**, *131*, 3621-3630; (k) J. Bunzen, M. Hapke, A. Lützen, *Eur. J. Org. Chem.* **2009**, 3885-3894; (l) J. Bunzen, R. Hovorka, A. Lützen, *J. Org. Chem.* **2009**, *74*, 5228-5236; (m) S. J. Bullock, C. E. Felton, R. V. Fennessy, L. P. Harding, M. Andrews, S. J. A. Pope, C. R. Rice, T. Riis-Johannessen, *Dalton Trans.* **2009**, 10570-10573; (n) N. Dalla Favera, U. Kiehne, J. Bunzen, S. Hytteballe, A. Lützen, C. Piguet, *Angew. Chem.* **2010**, *122*, 129-132; *Angew. Chem. Int. Ed.* **2010**, *49*, 125-128; (o) J.-A. Zhang, M. Pan, R. Yang, Z.-G. She, W. Kaim, Z.-J. Fan, C.-Y. Su, *Polyhedron* **2010**, *29*, 581-591; (p) Q. Zhang, J. Zhang, Q.-Y. Yu, M. Pan, C.-Y. Su, *Cryst. Growth Des.* **2010**, *10*, 4076-4084.

76 R. V. Slone, D. I. Yoon, R. M. Calhoun, J. T. Hupp, *J. Am. Chem. Soc.* **1995**, *117*, 11813–11814.

77 P. Diaz, J. A. Tovilla, P. Ballester, J. Benet-Buchholz, R. Vilar, *Dalton Trans.* **2007**, 3516-3525.

78 (a) M. Fujita, J. Yazaki, K. Ogura, *J. Am. Chem. Soc.* **1990**, *112*, 5645-5647; (b) M. Fujita, J. Yazaki, K. Ogura, *Chem. Lett.* **1991**, *20*, 1031-1032; (c) M. Fujita, J. Yazaki, K. Ogura, *Tetrahedron Lett.* **1991**, *32*, 5589-5592.

79 (a) P. J. Stang, V. V. Zhdankin, *J. Am. Chem. Soc.* **1993**, *115*, 9808-9809; (b) P. J. Stang, D. H. Cao, *J. Am. Chem. Soc.* **1994**, *116*, 4981-4982.

80 (a) A. Rang, *Darstellung funktionalisierter Quadrate für einen supramolekularen Rezeptorbaukasten*, diploma thesis, Universität Bonn **2003**; (b) T. Weilandt, *Hierarchische Selbstorganisation funktionalisierter supramolekularer Quadrate*, diploma thesis, Universität Bonn **2004**.

81 R. W. Troff, *Supramolekulare Metall-Komplexe auf der Basis von Dipyridylharnstoffen*, diploma thesis, Universität Bonn **2006**.

82 A. Rang, *Self-Assembled Supramolecular Squares from Chiral [4,4']-Bipyridines and Mass Spectrometric Investigations of Oligothiophene-Based Catenates and Catenanes*, PhD thesis, Universität Bonn **2008**.

83 T. Weilandt, *Neue Chemische Template: Funktionale Metallosupramolekulare Rauten, Dreiecke und Quadrate und Massenspektrometrische Untersuchungen Metall- und Elementorganischer Verbindungen*, PhD thesis, Universität Bonn **2009**.

84 (a) C. Safarowsky, L. Merz, A. Rang, P. Broekmann, B. A. Hermann, C. A. Schalley, *Angew. Chem.* **2004**, *116*, 1311-1314; *Angew. Chem. Int. Ed.* **2004,** *43*, 1291-1294; (b) C. Safarowsky, A. Rang, C. A. Schalley, K. Wandelt, P. Broekmann, *Electrochim. Acta* **2005**, *50*, 4257-4268.

85 Q.-H. Yuan, L.-J. Wan, H. Jude, P. Stang, *J. Am. Chem. Soc.* **2005**, *127*, 16279-16286.

86 (a) F. Würthner, A. Sautter, *Chem. Commun.* **2000**, 445-446; (b) F. Würthner, A. Sautter, D. Schmid, P. J. A. Weber, *Chem. Eur. J.* **2001**, *7*, 894-902; (c) F. Würthner, A. Sautter, *Org. Biomol. Chem.* **2003**, *1*, 240-243; (d) C.-C. You, F. Würthner, *J. Am. Chem. Soc.* **2003**, *125*, 9716-9725; (e) C.-C. You, C. Hippius, M. Grüne, F. Würthner, *Chem. Eur. J.* **2006**, *12*, 7510-7519.

87 L. Zhao, B. H. Northrop, Y.-R. Zheng, H.-B. Yang, H. J. Lee, Y. M. Lee, J. Y. Park, K.-W. Chi, P. J. Stang, *J. Org. Chem.* **2008**, *73*, 6580-6586.

88 S. Ghosh, D. R. Turner, S. R. Batten, P. S. Mukherjee, *Dalton Trans.* **2007**, 1869-1871.

89 some examples: (a) P. J. Stang, B. Olenyuk, *Angew. Chem.* **1996**, *108*, 797-802; *Angew. Chem. Int. Ed.* **1996**, *35*, 732-736; (b) S.-S. Sun, A. Lees, *Inorg. Chem.* **2001**, *40*, 3154-3160; (c) S. Lee, J. Kim, W. Lin, *Inorg. Chem.* **2004**, *43*, 6579-6588; (d) D. E. Janzen, K. N. Patel, D. G. VanDerveer, G. J. Grant, *Chem. Commun.* **2006**, 3540-3542; (e) T. M. Fyles, C. C. Tong, *New J. Chem.* **2007**, *31*, 296-304; (f) T. M. Fyles, C. C. Tong, *New J. Chem.* **2007**, *31*, 655-661; (g) M. Mounir, J. Lorenzo, M. Ferrer, M. J. Prieto, O. Rossell, F. X. Aviles, V. Moreno, *J. Inorg. Biochem.* **2007**, *101*, 660-666; (h) R. Kieltyka, P. Englebienne, J. Fakhoury, C. Autexier, N. Moitessier, H. F. Sleiman, *J. Am. Chem. Soc.* **2008**, *130*, 10040-10041; (i) P. J. Lusby, P. Müller, S. J. Pike, A. M. Z. Slawin, *J. Am. Chem. Soc.* **2009**, *131*, 16398-16400; (j) J. Y. Balandier, M. Chas, S. Goeb, P. I. Dron, D. Rondeau, A. Belyasmine, N. Gallego, M. Sallé, *New J. Chem.* **2011**, *35*, 165-168; (k) V. Vajpayee, H. Kim, A. Mishra, P. S. Mukherjee, P. J. Stang, M. H. Lee, H. K. Kim, K.-W. Chi, *Dalton Trans.* **2011**, *40*, 3112-3115.

90 H. T. Baytekin, M. Sahre, A. Rang, M. Engeser, A. Schulz, C. A. Schalley, *Small* **2008**, *4*, 1823-1834.

91 (a) A. Khutia, P. J. Sanz Miguel, B. Lippert, *Chem. Eur. J.* **2011**, *17*, 4195-4204; (b) A. Khutia, P. J. Sanz Miguel, B. Lippert, *Chem. Eur. J.* **2011**, *17*, 4205-4216.

92 (a) R. Slone, J. T. Hupp, C. Stern, T. Albrecht-Schmitt, *Inorg. Chem.* **1996**, *35*, 4096-4097; (b) R. Slone, J. T. Hupp, *Inorg. Chem.* **1997**, *36*, 5422-5423; (c) K. F. Czaplewski, J. T. Hupp, R. Q. Snurr, *Adv. Mater.* **2001**, *13*, 1895-1897.

93 F. A. Cotton, C. Lin, C. A. Murillo, *Inorg. Chem.* **2001**, *40*, 478-484.

94 S.-S. Sun, J. Anspach, A. Lees, *Inorg. Chem.* **2002**, *41*, 1862-1869.

95 (a) C. M. Drain, J.-M. Lehn, *J. Chem. Soc., Chem. Commun.* **1994**, 2313-2315; (b) K. F. Cheng, N. A. Thai, L. C. Teague, K. Grohmann, C. M. Drain, *Chem. Commun.* **2005**, 4678-4680.

96 (a) R.-D. Schnebeck, L. Randaccio, E. Zangrando, B. Lippert, *Angew. Chem.* **1998**, *110*, 128-130; *Angew. Chem. Int. Ed.* **1998**, *37*, 119-121; (b) R.-D. Schnebeck, E. Freisinger, F. Glahe, B. Lippert, *J. Am. Chem. Soc.* **2000**, *122*, 1381-1390; (c) R.-D. Schnebeck, E. Freisinger, B. Lippert, *Eur. J. Inorg. Chem.* **2000**, *2000*, 1193-1200.

97 (a) F. A. Cotton, L. Daniels, C. Lin, C. A. Murillo, *J. Am. Chem. Soc.* **1999**, *121*, 4538-4539; (b) F. A. Cotton, C. Lin, C. A. Murillo, *Acc. Chem. Res.* **2001**, *34*, 759-771; (c) J. Bera, P. Angaridis, F. A. Cotton, M. Petrukhina, P. Fanwick, R. Walton, *J. Am. Chem. Soc.* **2001**, *123*, 1515-1516; (d) F. A. Cotton, C. A. Murillo, X. Wang, R. Yu, *Inorg. Chem.* **2004**, *43*, 8394-8403; (e) F. A. Cotton, C. A. Murillo, S.-E. Stiriba, X. Wang, R. Yu, *Inorg. Chem.* **2005**, *44*, 8223-8233; (f) F. A. Cotton, C. Y. Liu, C. A. Murillo, X. Wang, *Inorg. Chem.* **2006**, *45*, 2619-2626; (g) F. A. Cotton, C. A. Murillo, R. Yu, *Dalton Trans.* **2006**, 3900-3905; (h) F. A. Cotton, C. A. Murillo, R. Yu, *Inorg. Chim. Acta* **2006**, *359*, 4811-4820; (i) F. A. Cotton, C. Y. Liu, C. A. Murillo, Q. Zhao, *Inorg. Chem.* **2006**, *45*, 9480-9486.

98 Some examples for metallo-supramolecular triangles containing metal centers at the corners: (a) R.-D. Schnebeck, E. Freisinger, B. Lippert *Chem. Commun.* **1999**, 675-676; (b) S.-W. Lai, M. C.-W. Chan, S.-M. Peng, C.-M. Che, *Angew. Chem.* **1999**, *111*, 708-710; *Angew. Chem. Int. Ed.* **1999**, *38*, 669-671; (c) T. Habereder, M. Warchhold, H. Nöth, K. Severin, *Angew. Chem.* **1999**, *111*, 3422-3425; *Angew. Chem. Int. Ed.* **1999**, *38*, 3225-3228; (d) S.-S. Sun, A. J. Lees, *Inorg. Chem.* **1999**, *38*, 4181-4182; (e) S.-S. Sun, A. J. Lees, *J. Am. Chem. Soc.* **2000**, *122*, 8956-8967; (f) M. Schweiger, S. R. Seidel, A. M. Arif, P. J. Stang, *Angew. Chem.*, **2001**, *113*, 3575-3577; *Angew. Chem. Int. Ed.*, **2001**, *40*, 3467-3469; (g) S. J. Lee, A. Hu, W. Lin, *J. Am. Chem. Soc.* **2002**, *124*, 12948-12949; (h) J. Fornies, J. Gomez, E. Lalinde, M. T. Moreno, *Chem. Eur. J.* **2004**, *10*, 888-898; (i) J. K. Clegg, L. F. Lindoy, B. Moubaraki, K. S. Murray, J. C. McMurtrie, *Dalton Trans.* **2004**, 2417-2423; (j) S. Derossi, M. Casanova, E. Iengo, E. Zangrando, M. Stener, E. Alessio, *Inorg. Chem.* **2007**, 46, 11243-11253; (k) S. A. Willison, J. A. Krause, W. B. Connick, *Inorg. Chem.* **2008**, *47*, 1258-1260; (l) P. Teo, L. L. Koh, T. S. A. Hor, *Inorg. Chem.* **2008**, *47*, 6464-6474; (m) B.-C. Tzeng, J.-H. Kuo, Y.-C. Lee, G.-H. Lee, *Inorg. Chim. Acta* **2008**, *361*, 2515-2521.

99 (a) P. Mukherjee, N. Das, Y. Kryschenko, A. Arif, P. Stang, *J. Am. Chem. Soc.* **2004**, *126*, 2464-2473; (b) G. Tarkanyi, H. Jude, G. Palinkas, P. Stang, *Org. Lett.* **2005**, *7*, 4971-4973; (c) H. Jude, H. Disteldorf, S. Fischer, T. Wedge, A. Hawkridge, A. Arif, M. Hawthorne, D. Muddiman, P. Stang, *J. Am. Chem. Soc.* **2005**, *127*, 12131-12139; (d) H. Jude, D. Sinclair, N. Das, M. Sherburn, P. Stang, *J. Org. Chem.* **2006**, *71*, 4155-4163; (e) B. H. Northrop, D. Chercka, P. J. Stang, *Tetrahedron* **2008**, *64*, 11495-11503.

100 U. Maran, D. Britt, C. B. Fox, J. M. Harris, A. M. Orendt, H. Conley, R. Davis, V. Hlady, P. J. Stang, *Chem. Eur. J.* **2009**, *15*, 8566-8577.

101 (a) F. M. Romero, R. Ziessel, A. Dupont-Gervais, A. J. van Dorsselaer, *J. Chem. Soc., Chem. Commun.* **1996**, 551-553; (b) H. Dias, C. Gamage, J. Keltner, H. Diyabalanage, I. Omari, Y. Eyobo, N. Dias, N. Roehr, L. McKinney, T. Poth, *Inorg. Chem.* **2007**, *46*, 2979-2987; (c) G.-H. Ning, T.-Z. Xie, Y.-J. Pan, Y.-Z. Li, S.-Y. Yu, *Dalton Trans.* **2010**, 3203-3211.

102 T. Megyes, H. Jude, T. Grosz, I. Bako, T. Radnai, G. Tarkanyi, G. Palinkas, P. J. Stang, *J. Am. Chem. Soc.* **2005**, *127*, 10731-10738.

103 Some examples: (a) S. B. Lee, S. Hwang, D. S. Chung, H. Yun, J.-I. Hong, *Tetrahedron Lett.* **1998**, *39*, 873-876; (b) R.-D. Schnebeck, E. Freisinger, B. Lippert, *Eur. J. Inorg. Chem.* **2000**, 1193-1200; (c) A. Sautter, D. G. Schmid, G. Jung, F. Würthner, *J. Am. Chem. Soc.* **2001**, *123*, 5424-5430; (d) L. Zhang, Y.-H. Niu, A. K.-Y. Jen, W. Lin, *Chem. Commun.* **2005**, 1002-1004; (e) F. A. Cotton, C. A. Murillo, R. Yu, *Dalton Trans.* **2006**, 3900-3905; (f) K. Uehara, K. Kasai, N. Mizuno, *Inorg. Chem.* **2007**, *46*, 2563-2570.

104 (a) R.-D. Schnebeck, E. Freisinger, B. Lippert, *Eur. J. Inorg. Chem.* **2000**, 1193-1200; (b) A. Sautter, D. G. Schmid, G. Jung, F. Würthner, *J. Am. Chem. Soc.* **2001**, *123*, 5424-5430; (c) M. Ferrer, M. Mounir, O. Rossell, E. Ruiz, M. A. Maestro, *Inorg. Chem.* **2003**, *42*, 5890-5899; (d) L. Zhang, Y.-H. Niu, A. K.-Y. Jen, W. Lin, *Chem. Commun.* **2005**, 1002-1004; (e) M. Ferrer, A. Gutierrez, M. Mounir, O. Rossel, E. Ruiz, A. Rang, M. Engeser, *Inorg. Chem.* **2007**, *46*, 3395-3406; (f) S. Ghosh, P. S. Mukherjee, *Inorg. Chem.* **2009**, *48*, 2605-2613; (g) K. Uehara, K. Kasai, N. Mizuno, *Inorg. Chem.* **2010**, *49*, 2008-2015.

105 C. A. Schalley, T. Müller, P. Linnartz, M. Witt, M. Schäfer, A. Lützen, *Chem. Eur. J.* **2002**, *8*, 3538-3551.

106 T. Weilandt, R. W. Troff, H. Saxell, K. Rissanen, C. A. Schalley, *Inorg. Chem.* **2008**, *47*, 7588-7598.

107 O. Mamula, F. J. Monlien, A. Porquet, G. Hopfgartner, A. E. Merbach, A. von Zelewsky, *Chem. Eur. J.* **2001**, *7*, 533-539.

108 T. Bark, M. Düggeli, H. Stoeckli-Evans, A. von Zelewsky, *Angew. Chem.* **2001**, *113*, 2924-2927; *Angew. Chem. Int. Ed.* **2001**, *40*, 2848-2851.

109 D. Chand, K. Biradha, M. Kawano, S. Sakamoto, K. Yamaguchi, M. Fujita, *Chem. Asian J.* **2006**, *1-2*, 82-90.

110 B. Hasenknopf, J.-M. Lehn, B. O. Kneisel, G. Baum, D. Fenske, *Angew. Chem.* **1996**, *108*, 1987-1990; *Angew. Chem. Int. Ed.* **1996**, *35*, 1838-1840.

111 B. Hasenknopf, J.-M. Lehn, N. Boumediene, A. Dupont-Gervais, A. Van Dorsselaer, B. Kneisel, D. Fenske, *J. Am. Chem. Soc.* **1997**, *119*, 10956-10962.

112 For example: (a) I. M. Müller, D. Möller, K. Föcker, *Chem. Eur. J.* **2005**, *11*, 3318; (b) A. Hori, T. Sawada, K.-i. Yamashita, M. Fujita, *Angew. Chem.* **2005**, *117*, 4974-4977; *Angew. Chem. Int. Ed.* **2005**, *44* (31), 4896-4899; (c) H.-B. Yang, A. Hawkridge, S. Huang, N. Das, S. Bunge, D. Muddiman, P. Stang, *J. Am. Chem. Soc.* **2007**, *129*, 2120-2129; (d) R. John, M. Park, D. Moon, K. Lee, S. Hong, Y. Zou, C. Hong, M. Lah, *J. Am. Chem. Soc.* **2007**, *129*, 14142-14143; (e) H.-B. Yang, K. Ghosh, B.

Northrop, Y.-R. Zheng, M. Lyndon, D. Muddiman, P. Stang, *J. Am. Chem. Soc.* **2007**, *129*, 14187-14189; (f) H.-B. Yang, K. Ghosh, Y. Zhao, B. Northrop, M. Lyndon, D. Muddiman, H. White, P. Stang, *J. Am. Chem. Soc.* **2008**, *130*, 839-841; (g) W. Liu, K. Lee, M. Park, R. P. John, D. Moon, Y. Zou, X. Liu, H.-C. Ri, G. H. Kim, M. S. Lah, *Inorg. Chem.* **2008**, *47*, 8807-8812; (h) L. Zhao, B. H. Northop, P. J. Stang, *J. Am. Chem. Soc.* **2008**, *130*, 11886-11888; (i) Y.-T. Chan, X. Li, M. Soler, J.-L. Wang, C. Wesdemiotis, G. R. Newcome, *J. Am. Chem. Soc.* **2009**, *131*, 16395-16397; (j) Y.-R. Zheng, M. Wang, S. Kabayashi, P. J. Stang, Tetrahedron Lett. **2011**, *52*, 2188-2191.

113 (a) N. Matsumoto, Y. Motoda, T. Matsuo, T. Nakashima, N. Re, F. Dahan, J. P. Tuchagues, *Inorg. Chem.* **1999**, *38*, 1165-1173; (b) T. Yamamoto, A. Arif, P. Stang, *J. Am. Chem. Soc.* **2003**, *125*, 12309-12317.

114 Some reviews of MOFs: (a) Y.-G. Huang, F.-L. Jiang, M.-C. Hong, *Coord. Chem. Rev.* **2009**, *253*, 2814-2834; (b) R. Yu, X.-F. Kuang, X.-Y. Wu, C.-Z. Lu, J. P. Donahue, *Coord. Chem. Rev.* **2009**, *253*, 2872-2890; (c) S. Qiu, G. Zhu, *Coord. Chem. Rev.* **2009**, *253*, 2891-2911; (d) V. I. Isaeva, L. M. Kustov, *Petroleum Chemistry* **2010**, *50*, 167-180; (e) O. K. Farha, J. T. Hupp, *Acc. Chem. Res.* **2010**, *43*, 1166-1175; (f) M. Meilikhov, K. Yusenko, D. Esken, St. Turner, G. Van Tendeloo, R. A. Fischer, *Eur. J. Inorg. Chem.* **2010**, 3701-3714; (g) J. Della Rocca, W. Lin, *Eur. J. Inorg. Chem.* **2010**, 3725-3734; (h) A. Corma, H. García, F. X. Llabrés i Xamena, *Chem. Rev.* **2010,** *110*, 4606-4655; (i) A. C. McKinlay, R. E. Morris, P. Horcajada, G. Férey, R. Gref, P. Couvreur, C. Serre, *Angew. Chem.* **2010**, *122*, 6400-6406; *Angew. Chem. Int. Ed.* **2010**, *49*, 6260-6266;

115 P. Jin, S. J. Dalgarno, J. L. Atwood, *Coord. Chem. Rev.* **2010**, *254*, 1760-1768.

116 K. Suzuki, M. Kawano, M. Fujita, *Angew. Chem.* **2007**, *119*, 2877-2880; *Angew. Chem. Int. Ed.* **2007**, *46*, 2819-2822.

117 G. H. Clever, S. Tashiro, M. Shionoya, *J. Am. Chem. Soc.* **2010**, *132*, 9973-9975.

118 Recent examples: (a) H.-K. Liu, Y. Cai, W. Luo, F. Tong, C. You, S. Lu, X. Huang, H.-Y. Ye, F. Su, X. Wang, *Inorg. Chem. Commun.* **2009**, *12*, 457-460; (b) J. D. Crowley, E. L. Gavey, *Dalton Trans.* **2010**, *39*, 4035-4037; (c) P. Liao, B. W. Langloss, A. M. Johnson, E. R. Knudsen, F. S. Tham, R. R. Julian, R. J. Hooley, *Chem. Commun.* **2010**, *46*, 4932-4934.

119 (a) M. Hong, Y. Zhao, W. Su, R. Cao, M. Fujita, Z. Zhou, A. S. C. Chan, *J. Am. Chem. Soc.* **2000**, *122*, 4819-4820; (b) H.-K. Liu, X. Tong, *Chem. Commun.* **2002**, 1316-1317; (c) D. K. Chand, K. Biradha, M. Fujita, S. Sakamoto, K. Yamaguchi, *Chem. Commun.* **2002**, 2486-2487; (d) I. M. Müller, S. Spillmann, H. Franck, R. Pietschnig, *Chem. Eur. J.* **2004**, *10*, 2207-2213; (e) D. K. Chand, R. Manivannan, H. S. Sahoo, K. Jeyakumar, *Eur. J. Inorg. Chem*. **2005**, 3346-3352; (f) R. M. McKinlay, P. K. Thallapally, G. W. V. Cave, J. L. Atwood, *Angew. Chem.* **2005**, *117*, 5879-5882; *Angew. Chem. Int. Ed.* **2005**, *44*, 5733-5736; (g) R. M. McKinlay, G. W. V. Cave, J. L. Atwood, *Proc. Natl. Acad. Sci. U.S.A* **2005**, *102*, 5944-5948; (h) Y. Liu, V. C. Kravtsov, D. A. Beauchamp, J. F. Eubank, M. Eddaoudi, *J. Am. Chem. Soc.* **2005**, *127*, 7266-7267; (i) Y. Wang, P. Cheng, Y. Song, D.-Z. Liao, S.-P. Yan, *Chem. Eur. J.* **2007**, *13*, 8131-8138; (j) T. K. Ronson, J. Fisher, L. P. Harding, M. J. Hardie,

Angew. Chem. **2007**, *119*, 9244-9246; *Angew. Chem. Int. Ed.* **2007**, *46*, 9086-9088; (k) O. Ugono, J. P. Moran, K. T. Holman, *Chem. Commun.* **2008**, 1404-1406.

120 K. Suzuki, M. Tominaga, M. Kawano, M. Fujita, *Chem. Commun.* **2009**, 1638-1640.

121 M. Tominaga, K. Suzuki, M. Kawano, T. Kusukawa, T. Ozeki, S. Sakamoto, K. Yamaguchi, M. Fujita, *Angew. Chem.* **2004**, *116*, 5739-5743; *Angew. Chem. Int. Ed.* **2004**, *43*, 5621-5625.

122 (a) M. Ikemi, T. Kikuchi, S. Matsumura, K. Shiba, S. Sato, M. Fujita, *Chem. Sci.* **2010**, *1*, 68-71; (b) T. Kikuchi, S. Sato, M. Fujita, *J. Am. Chem. Soc.* **2010**, *132*, 15930-15932.

123 L. Zhao, K. Ghosh, Y.-R. Zheng, P. J. Stang, *J. Org. Chem.* **2009**, *74*, 8516-8521.

124 Some examples: (a) M. Tominaga, K. Suzuki, T. Murase, M. Fujita, *J. Am. Chem. Soc.* **2005**, *127*, 11950-11951; (b) S. Sato, J. Iida, K. Suzuki, M. Kawano, T. Ozeki, M. Fujita, *Science* **2006**, *313*, 1273-1276; (c) T. Murase, S. Sato, M. Fujita, *Angew. Chem.* **2007**, *119*, 1101-1103; *Angew. Chem. Int. Ed.* **2007**, *46*, 1083-1085; (d) T. Murase, S. Sato, M. Fujita, *Angew. Chem.* **2007**, *119*, 5225-5228; *Angew. Chem. Int. Ed.* **2007**, *46*, 5133-5136; (e) N. Kamiya, M. Tominaga, S. Sato, M. Fujita, *J. Am. Chem. Soc.* **2007**, *129*, 2816-3817; (f) K. Suzuki, M. Kawano, S. Sato, M. Fujita, *J. Am. Chem. Soc.* **2007**, *129*, 10652-10653; (g) T. Kikuchi, T. Murase, S. Sato, M. Fujita, *Supramol. Chem.* **2008**, *20*, 81-94; (h) K. Suzuki, J. Iida, S. Sato, M. Kawano, M. Fujita, *Angew. Chem.* **2008**, *120*, 5864-5866; *Angew. Chem. Int. Ed.* **2008**, *47*, 5780-5782; (i) N. K. Al-Rasbi, I. S. Tidmarsh, S. P. Argent, H. Adams, L. P. Harding, M. D. Ward, *J. Am. Chem. Soc.* **2008**, *130*, 11641-11649; (j) S. Sato, Y. Ishido, M. Fujita, *J. Am. Chem. Soc.* **2009**, *131*, 6064-6065.

125 Q.-F. Sun, J. Iwasa, D. Ogawa, Y. Ishido, S. Sato, T. Ozeki, Y. Sei, K. Yamaguchi, M. Fujita, *Science* **2010**, *328*, 1144-1147.

126 A. C. Schulze, K. Föcker, I. M. Oppel, *Nachr. Chem.* **2009**, *57*, 507-514.

127 R. W. Saalfrank, A. Stark, K. Peters, H. G. von Schnering, *Angew. Chem.* **1988**, *100*, 878-880; *Angew. Chem. Int. Ed. Engl.* **1988**, *27*, 851-853.

128 D. L. Caulder, R. E. Powers, T. N. Parac, K. N. Raymond, *Angew. Chem.* **1998**, *110*, 1940-1943; *Angew. Chem. Int. Ed.* **1998**, *37*, 1840-1843.

129 (a) T. Beissel, R. E. Powers, K. N. Raymond, *Angew. Chem.* **1996**, *108*, 1166-1168; *Angew. Chem. Int. Ed. Engl.* **1996**, *35*, 1084-1086; (b) D. L. Caulder, K. N. Raymond, *Dalton Trans.* **1999**, 1185-1200; (c) M. Scherer, D. L. Caulder, D. W. Johnson, K. N. Raymond, *Angew. Chem.* **1999**, *111*, 1690-1694; *Angew. Chem. Int. Ed.* **1999**, *38*, 1588-1592; (d) T. Beissel, R. E. Powers, T. N. Parac, K. N. Raymond, *J. Am. Chem. Soc.* **1999**, *121*, 4200-4206; (e) A. J. Terpin, M. Ziegler, D. W. Johnson, K. N. Raymond, *Angew. Chem.* **2001**, *113*, 161-164; *Angew. Chem. Int. Ed.* **2001**, *40*, 157-160; (f) D. W: Johnson, K. N. Raymond, *Inorg. Chem.* **2001**, *40*, 5157-5161; (g) A. V. Davis, R. M. Yeh, K. N. Raymond, *Proc. Natl. Acad. Sci. U.S.A* **2002**, *99*, 4793-4796; (h) S. M. Biros, R. M. Yeh, K. N. Raymond, *Angew. Chem.* **2008**, *120*, 6151-6153; *Angew. Chem. Int. Ed.* **2008**, *47*, 6062-6064.

130 (a) D. H. Leung, R. G. Bergman, K. N. Raymond, *J. Am. Chem. Soc.* **2007**, *129*, 2746-2747; (b) S. M. Biros, R. G. Bergman, K. N. Raymond, *J. Am. Chem. Soc.* **2007**, *129*, 12094-12095; (c) M. D. Pluth, R. G. Bergman, K. N. Raymond, *J. Org. Chem.* **2008**, *73*, 7132-7136.

131 For example: (a) U. N. Andersen, G. Seeber, D. Fiedler, K. N. Raymond, D. Lin, D. Harris, *J. Am. Soc. Mass. Spectrom.* **2006**, *17*, 292-296; (b) M. D. Pluth, R. G. Bergman, K. N. Raymond, *J. Am. Chem. Soc.* **2008**, *130*, 6362-6366; (c) M. D. Pluth, D. W. Johnson, G. Szigethy, A. V. Davis, S. J. Teat, A. G. Oliver, R. G. Bergman, K. N. Raymond, *Inorg. Chem.* **2009**, *48*, 111-120.

132 Some examples: (a) R. W. Saalfrank, B. Demleitner, H. Glaser, H. Maid, S. Reihs, W. Bauer, M. Maluenga, F. Hampel, M. Teichert, H. Krautscheid, *Eur. J. Inorg. Chem.* **2003**, 822-829; (b) Y. Bai, D. Guo, C. Duan, D. Dang, K. Pang, Q. Meng, *Chem. Commun.* **2004**, 186-187; (c) J. K. Clegg, L. F. Lindoy, B. Moubaraki, K. S. Murray, J. C. McMurtrie, *Dalton Trans.* **2004**, 2415-2423; (d) I. S. Lee, J. R. Long, *Dalton Trans.* **2004**, 3434-3436; (e) P. Cai, M. Li, C. Duan, F. Lu, Q. Meng, *Eur. J. Inorg. Chem.* **2005**, 2581-2585; (f) S. P. Argent, T. Riis-Johannessen, J. C. Jeffery, L. P Harding, M. D. Ward, *Chem. Commun.* **2005**, 4647-4649; (g) N. K. Al-Rasbi, C. Sabatini, F. Barigelletti, M. D. Ward, *Dalton Trans.* **2006**, 4769-4772; (h) S. P. Argent, H. Adams, T. Riis-Johannessen, J. C. Jeffery, L. P Harding, W. Clegg, R. W. Harrington, M. D. Ward, *Dalton Trans.* **2006**, 4996-5013; (i) R. Frantz, C. S. Grange, N. K. Al-Rasbi, M. D. Ward, J. Lacour, *Chem. Commun.* **2007**, 1459-1461; (j) C. R. K. Glasson, G. V. Meehan, J. K. Clegg, L. F. Lindoy, P. Turner, M. B. Duriska, R. Willis, *Chem. Commun.* **2008**, 1190-1192; (k) I. S. Tidmarsh, B. F. Taylor, M. J. Hardie, L. Russo, W. Clegg, M. D. Ward, *New. J. Chem.* **2009**, *33*, 366-375.

133 Some examples: (a) R. W. Saalfrank, H. Glaser, B. Demleitner, F. Hampel, M. M. Chowdhry, V. Schünemann, A. X. Trautwein, G. B. M. Vaughan, R. Yeh, A. V. Davis, K. N. Raymond, *Chem. Eur. J.* **2002**, *8*, 493-497; (b) M. Albrecht, I. Janser, S. Meyer, P. Weis, R. Fröhlich, *Chem. Commun.* **2003**, 2854-2855; (c) M. Albrecht, I. Janser, J. Runsik, G. Raabe, P. Weis, R. Fröhlich, *Angew. Chem.* **2004**, *116*, 6832-6836; *Angew. Chem. Int. Ed.* **2004**, *43*, 6662-6666; (d) M. Albrecht, I. Janser, R. Fröhlich, *Chem. Commun.* **2005**, 157-165; (e) S. Hiraoka, K. Harano, M. Shiro, M. Shionoya, *Angew. Chem.* **2005**, *117*, 2787-2791; *Angew. Chem. Int. Ed.* **2005**, *44*, 2727-2731; (f) R. M. Yeh, J. Xu, G. Seeber, K. N. Raymond, *Inorg. Chem.* **2005**, *44*, 6228-6239; (g) C. J. Sumby, M. J. Hardie, , *Angew. Chem.* **2005**, *117*, 6553-6557; *Angew. Chem. Int. Ed.* **2005**, *44*, 6395-6399; (h) J. Zhang, P. W. Miller, M. Nieuwenhuyzen, S. L. James, *Chem. Eur. J.* **2006**, *12*, 2448-2453; (i) M. Albrecht, I. Janser, S. Burk, P. Weis, *Dalton Trans.* **2006**, 2875-2880; (j) M. Albrecht, R. Fröhlich, *Bull. Chem. Soc. Jpn.* **2007**, *80*, 797-808; (k) M. Albrecht, S. Burk, R. Stoffel, A. Lüchow, R. Fröhlich, M. Kogej, C. A. Schalley, *Eur. J. Inorg. Chem.* **2007**, 1361-1372; (l) J. Hamacek, G. Bernadinelli, Y. Filinchuk, *Eur. J. Inorg. Chem.* **2008**, 3419-3422.

134 M. Fujita, D. Oguro, M. Miyazawa, H. Oka, K. Yamaguchi, K. Ogura, *Nature* **1995**, *378*, 469-471.

135 H. Ito, T. Kusukawa, M. Fujita, *Chem. Lett.* **2000**, 598-599.

136 (a) M. Yoshizawa, Y. Takeyama, T. Kusukawa, M. Fujita, *Angew. Chem.* **2002**, 114, 1403-1405; *Angew. Chem. Int. Ed.* **2002**, *41*, 1347-1349; (b) M. Yoshizawa, Y. Takeyama, T. Okano, M. Fujita, *J. Am. Chem. Soc.* **2003**, *125*, 3243-3247.

137 (a) T. Kusukawa, M. Fujita, *Angew. Chem.* **1998**, *110*, 3327-3329; *Angew. Chem. Int. Ed.* **1998**, *37*, 3142-3144; (b) T. Kusukawa, M. Fujita, *J. Am. Chem. Soc.* **1999**, *121*, 1397-1398; (c) T. Kusukawa, M. Yoshizawa, M. Fujita, *Angew. Chem.* **2001**, *113*, 1931-1936; *Angew. Chem. Int. Ed.* **2001**, *40*, 1879-1884; (d) T. Kusukawa, M. Fujita, *J. Am. Chem. Soc.* **2002**, *124*, 13576-13582.

138 (a) T. Beissel, R. E. Powers, K. N. Raymond, *Angew. Chem.* **1996**, *108*, 1166-1168; *Angew. Chem., Int. Ed. Engl.* **1996**, *35*, 1084-1086; (b) C. M. Hartshorne, P. J. Steel, *Chem. Commun.* **1997**, 541-542; (c) P. J. Stang, B. Olenyuk, D. C. Muddiman, R. D. Smith, *Organometallics* **1997**, *16*, 3094-3096; (d) M. Schweiger, T. Yamamoto, P. J. Stang, D. Blaser, R. Boese, *J. Org. Chem.* **2005**, *70*, 4861-4864.

139 B. Brusilowskij, S. Neubacher, C. A. Schalley, *Chem. Commun.* **2009**, 785-787.

140 (a) I. M. Müller, R. Robson, F. Separovic, *Angew. Chem.* **2001**, *113*, 4519-4520; *Angew. Chem. Int. Ed.* **2001**, *40*, 4385-4386; (b) I. M. Müller, D. Möller, C. A. Schalley, *Angew. Chem.* **2005**, *117*, 485-488; *Angew. Chem. Int. Ed.* **2005**, *44*, 480-484; (c) I. M. Oppel, K. Föcker, *Angew. Chem.* **2008**, *120*, 408-411; *Angew. Chem. Int. Ed.* **2008**, *47*, 402-405.

141 (a) S. Hiraoka, K. Harano, M. Shiro, Y. Ozawa, N. Yasuda, K. Toriumi, M. Shionoya, *Angew. Chem.* **2006**, *118*, 6638-6641; *Angew. Chem. Int. Ed.* **2006**, *45*, 6488-6491, (b) S. Hiraoka, K. Harano, M. Shiro, M. Shionoya, *J. Am. Chem. Soc.* **2008**, *130*, 14368-14369.

142 S. Roche, C. Haslam, S. L. Heath, J. A. Thomas, *Chem. Commun.* **1998**, 1682-1683.

143 (a) J. L. Heinrich, P. A. Berseth, J. R. Long, *Chem. Commun.* **1998**, 1681-1682; (b) P. A. Berseth, J. J. Sokol, M. P. Shores, J. L. Heinrich, J. R. Long, *J. Am. Chem. Soc.* **2000**, *122*, 9655-9662; (c) Z. R. Bell, L. P. Harding, M. D. Ward, *Chem. Commun.* **2003**, 2432-2433; (d) S. C. N. Hsu, M. Ramesh, J. H. Espenson, T. B. Rauchfuss, *Angew. Chem.* **2003**, *115*, 2767-2770; *Angew. Chem. Int. Ed.* **2003**, *42*, 2663-2666; (e) M. L. Kuhlman, T. B. Rauchfuss, *Inorg. Chem.* **2004**, *43*, 430-435; (f) M. L. Kuhlman, H. Yao, T. B. Rauchfuss, *Chem. Commun.* **2004**, 1370-1371; (g) Y. Liu, V. Kravtsov, R. D. Walsh, P. Poddar, H. Srikanth, M. Eddaoudi, *Chem. Commun.* **2004**, 2806-2807; (h) E. J. Schelter, A. V. Prosvirin, K. R. Dunbar, *J. Am. Chem. Soc.* **2004**, *126*, 15004-15005; (i) I.-W. Hwang, T. Kamada, T. K. Ahn, D. M. Ko, T. Nakamura, A. Tsuda, A. Osuka, D. Kim, *J. Am. Chem. Soc.* **2004**, *126*, 16187-16198; (j) S. P. Argent, H. Adams, L. P. Harding, M. D. Ward, *Dalton Trans.* **2006**, 542-544; (k) D. Li, R. Clérac, O. Roubeau, E. Harté, C. Mathoniére, R. Le Bris, S. M. Holmes, *J. Am. Chem. Soc.* **2008**, *130*, 252-258; (l) M. Nihei, M. Ui, N. Hoshino, H. Oshio, *Inorg. Chem.* **2008**, *47*, 8126-8133; (m) M.-L. Cao, H.-G. Hao, W.-X. Zhang, B.-H. Ye, *Inorg. Chem.* **2008**, *47*, 8126-8133.

144 (a) K. K. Klausmeyer, T. B. Rauchfuss, S. R. Wilson, *Angew. Chem.* **1998**, *110*, 1808-1810; *Angew. Chem. Int. Ed.* **1998**, *37*, 1694-1696; (b) K. K. Klausmeyer, S. R. Wilson, T. B. Rauchfuss, *J. Am. Chem. Soc.* **1999**, *121*, 2705-2711; (c) J.-P. Lang, Q.-F. Xu, Z.-N. Chen, B. F. Abrahams, *J. Am. Chem. Soc.* **2003**, *125*, 12682-12683.

145 (a) S. C. Johannessen, R. G. Brisbois, J. P. Fischer, P. A. Grieco, A. E. Counterman, D. E. Clemmer, *J. Am. Chem. Soc.* **2001**, *123*, 3818-3819; (b) R. Natarajan, G. Savitha, J. N. Moorthy, *Cryst. Growth Des.* **2005**, *5*, 69-72; (c) D. C. Caskey, T. Yamamoto, C. Addicott, R. K. Shoemaker, J. Vacek, A. M. Hawkridge, D. C. Muddiman, G. S. Kottas, J. Michl, P. J. Stang, J. *Am. Chem. Soc.* **2008**, *130*, 7620-7628.

146 (a) A. J. Amoroso, J. C. Jefferey, P. L. Jones, J. A. McCleverty, P. Thornton, M. D. Ward, *Angew. Chem.* **1995**, *107*, 1577-1580; *Angew. Chem. Int. Ed. Engl.* **1995**, *34*, 1443-1446; (b) B. Olenyuk, J. A. Whiteford, A. Fechtenkötter, P. J. Stang, *Nature* **1999**, *398*, 796-799; (c) S. Aoki, M. Shiro, E. Kimura, *Chem. Eur. J.* **2002**, *8*, 929-939.

147 B. Olenyuk, M. D. Levin, J. A. Whiteford, J. E. Shield, P. J. Stang, *J. Am. Chem. Soc.* **1999**, *121*, 10434-10435.

148 T. Brasey, R. Scopelliti, K. Severin, *Chem. Commun.* **2006**, 3308-3310.

149 (a) O. D. Fox, J. F.-Y. Leung, J. M. Hunter, N. K. Dalley, R. G. Harrison, *Inorg. Chem.* **2000**, *39*, 783-790; (b) R. G. Harrison, O. D. Fox, M. O. Meng, N. K. Dalley, L. J. Barbour, *Inorg. Chem.* **2002**, *41*, 838-843.

150 (a) C. J. Sumby, M. J. Hardie, *Angew. Chem.* **2005**, *117*, 6553-6555; *Angew. Chem. Int. Ed.* **2005**, *44*, 6395-6399; (b) C. J. Sumby, M. J. Carr, A. Franken, J. D. Kennedy, C. A. Kilner, M. J. Hardie, *New J. Chem.* **2006**, *30*, 1390-1396.

151 For example: (a) R. M. McKinlay, P. K. Thallapally, G. W. V. Cave, J. L. Atwood, *Angew. Chem.* **2005**, *116*, 5879-5882; *Angew. Chem. Int. Ed.* **2005**, *44*, 5733-5736; (b) R. M. McKinlay, P. K. Thallapally, J. L. Atwood, *Chem. Commun.* **2006**, 2956-2958; (c) N. P. Power, S. J. Dalgarno, J. L. Atwood, *New J. Chem.* **2007**, *31*, 17-20; (d) S. J. Dalgarno, N. P. Power, J. L. Atwood, *Chem. Commun.* **2007**, 3447-3449; (e) S. J. Dalgarno, N. P. Power, J. E. Warren, J. L. Atwood, *Chem. Commun.* **2008**, 1539-1541.

152 B. Brusilowskij, *Studien zur Entschlüsselung von Komplexität in Supramolekularen Architekturen*, PhD thesis, Freie Universität Berlin **2010**.

153 B. H. Northrop, H.-B. Yang, P. J. Stang, *Chem. Commun.* **2008**, 5896-5908.

154 (a) K.-W. Chi, C. Addicott, P. J. Stang, *J. Org. Chem.* **2004**, *69*, 2910-2912; (b) F. Huang, H.-B. Yang, N, Das, U Maran, A. M. Arif, H. W. Gibson, P. J. Stang, *J. Org. Chem.* **2006**, *71*, 6623-6625.

155 P. J. Stang, D. H. Cao, K. Chen, G. M. Gray, D. C. Muddiman, R. D. Smith, *J. Am. Chem. Soc.* **1997**, *119*, 5163-5168.

156 M. J. E. Resendiz, J. C. Noveron, H. Disteldorf, S. Fischer, P. J. Stang, *Org. Lett.* **2004**, *6*, 651-653.

157 B. Brusilowskij, C. A. Schalley, *Eur. J. Org. Chem.* **2011**, 469-477.

158 B. Brusilowskij, E. V. Dzyuba, R. W. Troff, C. A. Schalley, *Chem. Commun.* **2011**, *47*, 1830-1832.

159 B. Brusilowskij, E. V. Dzyuba, R. W. Troff, C. A. Schalley, *Dalton Trans.* **2011**, in press.

160 K. Suzuki, S. Sato, M. Fujita, *Nature Chem.* **2010**, *2*, 25-29.

161 K. Ghosh, H.-B. Yang, B. H. Northrop, M. M. Lyndon, Y.-R. Zheng, D. C. Muddiman, P. J. Stang, *J. Am. Chem. Soc.* **2008**, *130*, 5320-5334.

162 Recent examples for *exo*-functionalized metallo-supramolecular complxes: (a) H.-B. Yang, B. H. Northrop, Y.-R. Zheng, K. Ghosh, M. M. Lyndon, D. C. Muddiman, P. J. Stang, *J. Org. Chem.* **2009**, *74*, 3524-3527; (b) K. Ghosh, J. Hu, H.-B. Yang, B. H. Northrop, H. S. White, P. J. Stang, *J. Org. Chem.* **2009**, *74*, 4828-4833; (c) H.-B. Yang, B. H. Northrop, Y.-R. Zheng, K. Ghosh, P. J. Stang, *J. Org. Chem.* **2009**, *74*, 7067-7074; (d) Y.-R. Zheng, K. Ghosh, H.-B. Yang, P. J. Stang, *Inorg. Chem.* **2010**, *49*, 4747-4749; (e) G.-Z. Thao, L.-J. Chen, C.-H. Wang, H.-B. Yang, K. Ghosh, Y.-R. Zheng, M. M.Lyndon, D. C. Muddiman, P.J. Stang, *Organometallics* **2010**, *29*, 6137-6140; (f) X.-D. Xu, H.-B. Yang, Y.-R. Zheng, K. Ghosh, M. M. Lyndon, D. C. Muddiman, P. J. Stang, *J. Org. Chem.* **2010**, *75*, 7373-7380; (g) M. Wang, Y.-R. Zheng, T. R. Cook, P. J. Stang, *Inorg. Chem.* **2011**, *50*, 6107-6113.

163 A. von Zelewsky, *Stereochemistry of Coordination Compounds*, John Wiley & Sons, New York, **1996**.

164 K. S. Jeong, S. Y. Kim, U.-S. Shin, M. Kogej, N. T. M. Hai, P. Broekmann, N. Jeong, B. Kirchner, M. Reiher, C. A. Schalley, *J. Am. Chem. Soc.* **2005**, *127*, 17672-17685.

165 T. W. Kim, M. S. Lah, J.-I. Hong, *Chem. Commun.* **2001**, 743-744.

166 (a) C. Piguet, G. Bernardinelli, G. Hopfgartner, *Chem. Rev.* **1997**, *97*, 2005-2062; (b) M. Albrecht, *Chem. Rev.* **2001**, *101*, 3457-3498; (c) C. R. Glasson, G. Meehan, J. Clegg, L. Lindoy, J. Smith, F. R. Keene, C. Motti, *Chem. Eur. J.* **2008**, *14*, 10535-10538; (d) J. Malina, M. Hannon, V. Brabec, *Chem. Eur. J.* **2008**, *14*, 10408-10414.

167 P. N. W. Baxter, J.-M. Lehn, K. Rissanen, *J. Chem. Soc., Chem. Commun.* **1997**, 1323-1324.

168 (a) G. Baum, E. C. Constable, D. Fenske, C. E. Housecroft, T. Kulke, *Chem. Commun.* **1999**, 195-196 (b) R. Annunziata, M. Benaglia, M. Cinquini, F. Cozzi, C. Woods, J. Siegel, *Eur. J. Org. Chem.* **2001**, *2001*, 173-180; (c) R. Prabaharan, N. C. Fletcher, M. Nieuwenhuyzen, *J. Chem. Soc., Dalton Trans.* **2002**, 602-608; (d) O. Mamula, A. von Zelewsky, *Coord. Chem. Rev.* **2003**, *242*, 87-95; (e) M. Albrecht, I. Janser, J. Fleischhauer, Y. Wang, G. Raabe, R. Fröhlich, *Mendeleev Commun.* **2004**, *14*, 250-253.

169 (a) A. Lützen, M. Hapke, J. Griep-Raming, D. Haase, W. Saak, *Angew. Chem.* **2002**, *114*, 2190-2194; *Angew. Chem. Int. Ed.* **2002**, *41*, 2086-2089; (b) U. Kiehne, T. Weilandt, A. Lützen, *Org. Lett.* **2007**, **9**, 1283-1286; (c) U. Kiehne, A. Lützen, *Org. Lett.* **2007**, *9*, 5333-5336; (d) U. Kiehne, A. Lützen, *Eur. J. Org. Chem.* **2007**, *2007*, 5703-5711; (e) U. Kiehne, T. Weilandt, A. Lützen, *Eur. J. Org. Chem.* **2008**, *2008*, 2056-2064.

170 For example: (a) D. Fiedler, D. Pagliero, J. Brumaghim, R. G. Bergman, K. N. Raymond, *Inorg. Chem.* **2004**, *43*, 846-848; (b) D. Fiedler, D. H. Leung, R. G. Bergman, K. N. Raymond, *J. Am. Chem. Soc.* **2004**, *126*, 3674-3675; (c) D. Fiedler, D. H. Leung, R. G. Bergman, K. N. Raymond, *Acc. Chem. Res.* **2005**, *38*, 349-358.

171 S. M. Biros, R. G. Bergman, K. N. Raymond, *J. Am. Chem. Soc.* **2007**, *129*, 12094-12095.

172 K. Kumazawa, K. Biradha, T. Kusukawa, T. Okano, M. Fujita, *Angew. Chem.* **2003**, *115*, 4039-4043; *Angew. Chem. Int. Ed.* **2003**, *42*, 3909-3913.

173 Recent examples: (a) K. Ono, M. Yoshizawa, M. Akita, T. Kato, Y. Tsunobuchi, S.-i. Ohkoshi, M. Fujita, *J. Am. Chem. Soc.* **2009**, *131*, 2782-2783; (b) Y. Ozaki, M. Kawano, M. Fujita, *Chem. Commun.* **2009**, 4245-4247; (c) Y. Yamauchi, M. Yoshizawa, M. Akita, M. Fujita, *Proct. Natl. Acad. Sci. USA* **2009**, *106*, 10435-10437; (d) K. Ono, J. K. Klosterman, M. Yoshizawa, K. Sekiguchi, T. Tahara, M. Fujita, *J. Am. Chem. Soc.* **2009**, *131*, 12526-12527; (e) Y. Yamaguchi, M. Yoshizawa, M. Akita, M. Fujita, *J. Am. Chem. Soc.* **2010**, *132*, 960-966; (f) S. Sato, O. Morohara, D. Fujita, Y. Yamaguchi, K. Kato, M. Fujita, *J. Am. Chem. Soc.* **2010**, *132*, 3670-3671; (g) T. Murase, K. Otsuka, M. Fujita, *J. Am. Chem. Soc.* **2010**, *132*, 7864-7865; (h) Y. Yamauchi, Y. Hanaoka, M. Yoshizawa, M. Akita, T. Ichikawa, M. Yoshio, T. Kato, M. Fujita, *J. Am. Chem. Soc.* **2010**, *132*, 9555-9557; (i) M. Kiguchi, T. Takahashi, Y. Takahashi, Y. Yamauchi, T. Murase, M. Fujita, T. Tada, S. Watanabe, *Angew. Chem.* **2011**, *123*, 5826-5829; *Angew. Chem. Int. Ed.* **2011**, *50*, 5708-5711.

174 J. K. Klosterman, Y. Yamauchi, M. Fujita, *Chem. Soc. Rev.* **2009**, *38*, 1714-1725.

175 P. Mal, B. Breiner, K. Rissanen, J. R. Nitschke, *Science* **2009**, *324*, 1697-1699.

176 M. Yoshizawa, J.K. Klosterman, M. Fujita, *Angew. Chem.* **2009**, *121*, 3470-3490; *Angew. Chem. Int. Ed*. **2009**, *48*, 3418-3438.

177 (a) D. Fiedler, R. G. Bergman, K. N. Raymond, *Angew. Chem.* **2004**, *116*, 6916-6919; *Angew. Chem. Int. Ed.* **2004**, *43*, 6748-6751; (b) D. H. Leung, D. Fiedler, R. G. Bergman, K. N. Raymond, *Angew. Chem.* **2004**, *116*, 981-984; *Angew. Chem. Int. Ed*. **2004**, *43*, 963-966; (c) D. H. Leung, R. G. Bergman, K. N. Raymond, J. *Am. Chem. Soc.* **2006**, *128*, 9781-9797; (d) A. V. Davis, D. Fiedler, G. Seeber, A. Zahl, R. van Eldik, K. N. Raymond, *J. Am. Chem. Soc.* **2006**, *128*, 1324-1333; (e) D. Leung, R. Bergman, K. Raymond, *J. Am. Chem. Soc.* **2007**, *129*, 2746-2747; (f) M. Pluth, R. Bergman, K. Raymond, *Angew. Chem.* **2007**, *119*, 8741-8743; *Angew. Chem. Int. Ed.* **2007**, *46*, 8587-8589; (g) M. D. Pluth, R. G. Bergman, K. N. Raymond, *J. Am. Chem. Soc.* **2008**, *130*, 6362-6366; (h) M. D. Pluth, R. G. Bergman, K. N. Raymond, *J. Org. Chem.* **2008**, *73*, 7132-7136; (i) C. J. Hastings, D. Fiedler, R. G. Bergman, K. N. Raymond, *J. Am. Chem. Soc.* **2008**, *130*, 10977-10983.

178 (a) M. D. Pluth, R. G. Bergman, K. N. Raymond, *Science* **2007**, *316*, 85-88; (b) M. Pluth, R. Bergman, K. Raymond, *Angew. Chem.* **2007**, *119*, 8741-8743; *Angew. Chem. Int. Ed.* **2007**, *46*, 8587-8589.

179 M. Yoshizawa, Y. Takeyama, T. Okano, M. Fujita, *J. Am. Chem. Soc.* **2003**, *125*, 3243-3247.

180 T. Kusukawa, T. Nakai, Okano, M. Fujita, *Chem. Lett.* **2003**, *32*, 284-285.

181 M. Yoshizawa, M. Tamura, M. Fujita, *J. Am. Chem. Soc.* **2004**, *126*, 6846-6847.

182 M.Yoshizawa, N. Sato, M. Fujita, *Chem. Lett.* **2005**, *34*, 1392-1393.

183 (a) M. Fujita, S.-Y. Yu, T. Kusukawa, H. Funaki, K. Ogura, K. Yamaguchi, *Angew. Chem.* **1998**, *110*, 2192-2196; *Angew. Chem. Int. Ed.* **1998**, *37*, 2082-2085; (b) S.-Y. Yu, T. Kusukawa, K. Biradha, M. Fujita, *J. Am. Chem. Soc.* **2000**, *122*, 2665-2666.

184 (a) R. V. Slone, J. T. Hupp, *Inorg. Chem.* **1997**, *36*, 5422-5423; (b) S. J. Lee, K. L. Mulfort, X. Zuo, A. J. Goshe, P. J. Wesson, S. T. Nguyen, J. T. Hupp, D. M. Tiede, *J. Am. Chem. Soc.* **2008**, *130*, 836-838.

185 Recent examples: (a) M. D. Pluth, R. G. Bergman, K. N. Raymond, *J. Org. Chem.* **2009**, *74*, 58-63; (b) M. D. Pluth, R. G. Bergman, K. N. Raymond, *Acc. Chem. Res.* **2009**, *42*, 1650-1659; (c) Y. Furutani, H. Kandori, M. Kawano, K. Nakabayashi, M. Yoshizawa, M. Fujita, *J. Am. Chem. Soc.* **2009**, *131*, 4764-4768; (d) C. J. Brown, R. G. Bergman, K. N. Raymond, *J. Am. Chem. Soc.* **2009**, *131*, 17530-17531; (e) T. Kawamichi, Y. Inokuma, M. Kawano, M. Fujita, *Angew. Chem.* **2010**, *122*, 2425-2427; *Angew. Chem. Int. Ed.* **2010**, *49*, 2375-2377; (f) T. Murase, S. Horiuchi, M. Fujita, *J. Am. Chem. Soc.* **2010**, *132*, 2866-2867; (g) S. Horiuchi, Y. Nishioka, T. Murase, M. Fujita, *Chem. Commun.* **2010**, *46*, 3460-3462; (h) K. Ohara, Y. Inokuma, M. Fujita, *Angew. Chem.* **2010**, *122*, 5639-5641; *Angew. Chem. Int. Ed.* **2010**, *49*, 5507-5509; (i) K. Ikemoto, Y. Inokuma, M. Fujita, *Angew. Chem.* **2010**, *122*, 5886-5888; *Angew. Chem. Int. Ed.* **2010**, *49*, 5750-5752; (j) Y. Yamauchi, M. Fujita, *Chem. Commun.* **2010**, *46*, 5897-5899; (k) C. J. Hastings, M. D. Pluth, R. G. Bergman, K. N. Raymond, *J. Am. Chem. Soc.* **2010**, *132*, 6938-6940; (l) Z. J. Wang, C. J. Brown, R. G. Bergman, K. N. Raymond, F. D. Toste, *J. Am. Chem. Soc.* **2010**, *132*, 7358-7360; (m) Y. Inokuma, S. Yoshioka, M. Fujita, *Angew. Chem.* **2010**, *122*, 9096-9098; *Angew. Chem. Int. Ed.* **2010**, *49*, 8912-8914; (n) T. Murase, S. Peschard, S. Horiuchi, Y. Nishioka, M. Fujita, *Supamol. Chem.* **2011**, *23*, 199-208; (o) K. Suzuki, K. Takao, S. Sota, M. Fujita, *Angew. Chem.* **2011**, *122*, 4960-4963; *Angew. Chem. Int. Ed.* **2011**, *50*, 4858-4861; (p) S. Horiuchi, T. Murase, M. Fujita, *Chem. Asian. J.* **2011**, *6*, 1839-1847.

186 J. H. Gross, *Mass Spectrometry - A Textbook, Springer*, Heidelberg **2004**.

187 C. A. Schalley, A. Springer, *Mass Spectrometry and Gas-Phase Chemistry of Non-Covalent Complexes*, Wiley, Hoboken **2009**.

188 K. A. Jolliffe, M. C. Calama, R. Fokkens, N. M. M. Nibbering, P. Timmerman, D. N. Reinhoudt, *Angew. Chem.* **1998**, *110*, 1294-1297; *Angew. Chem. Int. Ed.* **1998**, *37*, 1247-1251.

189 C. E. H. Dessent, K. Müller-Dethlefs, *Chem. Rev.* **2000**, *100*, 3999-4021.

190 (a) F. Sobott, A. Wattenberg, H. D. Barth, B. Brutschy, *Int. J. Mass. Spectrom.* **1999**, *187*, 271-279; (b) A. Wattenberg, F. Sobott, H. D. Barth, B. Brutschy, *Int. J. Mass. Spectrom.* **2000**, *203*, 49-57; (c) N. Morgner, T. Kleinschroth, H. D. Barth, B. Ludwig, B. Brutschy, J. *Am. Soc. Mass. Spectrom.* **2007**, *18*, 1429-1438.

191 M. Dole, L. L. Mack, R. L. Hines, R. C. Mobley, L. D. Ferguson, M. B. Alice, *J. Chem. Phys.* **1968**, *49*, 2240-2249

192 (a) J. B. Fenn, M. Mann, C. K. Meng, S. F. Wong, C. M. Whitehouse, *Science* **1989**, *246*, 64-71; (b) J. B. Fenn, M. Mann, C. K. Meng, S. F. Wong, C. M. Whitehouse, *Mass Spectrom. Rev.* **1990**, *9*, 37-70; (c) P. Kebarle, L. Tang, *Anal. Chem.* **1993**, *65*, A972-A986; (d) S. J. Gaskell, *J. Mass Spectrom.* **1997**, 32, 677-688; (e) J. B. Fenn, Angew. Chem. **2003**, *115*, 3999-4024; *Angew. Chem. Int. Ed.* **2003**, *42*, 3871-3894.

193 H. D. F. Winkler, Freie Universität Berlin, unpublished results.

194 (a) J. V. Iribarne, B. A: Thomson, *J. Chem. Phys.* **1976**, *64*, 2287-2294; (b) B. A. Thomson, J. V. Iribarne, *J. Chem. Phys.* **1979**, *71*, 4451-4463; (c) J. B. Fenn, J. Rosell, C. K. Meng, *J. Am. Soc. Mass Spectrom.* **1997**, *8*, 1147-1157.

195 P. Kebarle, G. Peschke, *Anal. Chim. Acta* **2000**, *406*, 11-35.

196 E. O. Lawrence, M. S. Livingston, *Phys. Rev.* **1932**, *40*, 19-35.

197 (a) L. G. Smith, *Rev. Sci. Instrum.* **1951**, *22*, 115-116; (b) H. Sommer, H. A. Thomas, J. A. Hipple, *Phys. Rev.* **1951**, *82*, 697-702; (c) J. D. Baldeschwieler, *Science* **1968**, *159*, 263-273.

198 (a) M. B. Comisarow, A. G. Marshall, *Chem. Phys. Lett.* **1974**, *25*, 282-283; (b) M. B. Comisarow, A. G. Marshall, *J. Chem. Phys.* **1976**, *64*, 110-119; (c) M. B. Comisarow, *J. Chem. Phys.* **1978**, *69* , 4097-4104; (d) M. B. Comisarow, V. Grassi, G. Parisod, *Chem. Phys. Lett.* **1978**, *57*, 413-416; (e) A. G. Marshall, P. B. Grosshans, *Anal. Chem.* **1991**, *63*, 215A-229A; (f) M. B. Comisarow, A. G. Marshall, *J. Mass Spectrom.* **1996**, *31*, 581-585; (g) A. G. Marshall, *Acc. Chem. Res.* **1996**, *29*, 307-316; (h) A. G. Marshall, C. L. Hendrickson, G. S. Jackson, *Mass Spectrom. Rev.* **1998**, *17*, 1-35; (i) F. He, C. L. Hendrickson, A. G. Marshall, *Anal. Chem.* **2001**, *73*, 647-650; (j) R. E. Bossio, A. G. Marshall, *Anal. Chem.* **2002**, *74*, 1674-1679; (k) A. G. Marshall, C. L. Hendrickson, *Int. J. Mass Spectrom.* **2002**, *215*, 59-75.

199 J. W. Larson, T. B. McMahon, *J. Am. Chem. Soc.* **1982**, *104*, 6255-6261.

200 C. Spickermann, T. Felder, C. A. Schalley, B. Kirchner, *Chem. Eur. J.* **2008**, *14*, 1216-1227.

201 H. Wang, E. N. Kitova, J. S. Klassen, *J. Am. Chem. Soc.* **2003**, *125*, 13630-13631.

202 K. Vékey, *J. Mass Spectrom.* **1996**, *31*, 445-463.

203 R. C. Dunbar, *Mass Spectrom. Rev.* **1992**, *11*, 309-339.

204 J. Laskin, C. Lifshitz, *J. Mass Spectrom.* **2001**, *36*, 459-478.

205 L. Sleno, D. A. Volmer, *J. Mass Spectrom.* **2004**, *39*, 1091-1112.

206 J. Laskin, J. H. Futrell, *Mass Spectrom. Rev.* **2005**, *24*, 135-167.

207 (a) D. P. Weimann, H. D. F. Winkler, J. A. Falenski, B. Koksch, C. A. Schalley, *Nature Chem.* **2009**, *1* 573-577; (b) H. D. F. Winkler, D. P. Weimann, A. Springer, C. A. Schalley, *Angew. Chem.* **2009**, *121*, 7382-7386; *Angew. Chem. Int. Ed.* **2009**, *48*, 7246-7250; (c) H. D. F. Winkler, E. V. Dzyuba, J. A. W. Sklorz, N. K. Beyeh, K. Rissanen, C. A. Schalley, *Chem. Sci.* **2011**, *2*, 615-624; (d) for a review see: H. D. F. Winkler, E. V. Dzyuba, C. A. Schalley, *New J. Chem.* **2011**, *35*, 529-541.

208 For reviews see: (a) S. Meyer and J. O. Metzger, *Anal. Bioanal. Chem.* **2003**, *377*, 1108-1114. (b) L. S. Santos, L. Knaak and J. O. Metzger, *Int. J. Mass. Spectrom.* **2005**, *246*, 84-104.

209 Some examples: (a) A. A. Sabino, A. H. L. Machado, C. R. D. Correia and M. N. Eberlin, *Angew. Chem.* **2004**, *116*, 2568–2572; *Angew. Chem. Int. Ed.* **2004**, *43*, 2514-2518. (b) S. Fürmeier, J. Griep-Raming, A. Hayen and J. O. Metzger, *Chem. Eur. J.* **2005**, *11*, 5545-5554. (c) W. Schrader, P. P. Handayani, C. Burstein and F. Glorius, *Chem. Commun.* **2007**, 716-718. (d) L. S. Santos and J. O. Metzger, *Rapid Commun. Mass Spectrom.* **2008**, *22*, 898-904.

210 (a) C. A. Schalley, J. Hoernschemeyer, X. Li, G. Silva, P. Weis, Int. *J. Mass Spectrom.* **2003**, *228*, 373-388; (b) C. A. Schalley, P. Ghosh, M. Engeser, *Int. J. Mass Spectrom.* **2004**, *232*, 249-258.

211 (a) H. Mansikkamäki, C. A. Schalley, M. Nissinen, K. Rissanen, *New J. Chem.* **2005**, *29*, 116-127; (b) H. Mansikkamäki, C. A. Schalley, M. Nissinen, K. Rissanen, *New J. Chem.* **2005**, *29*, 116-127; (c) T. Becherer, D. Meshcheryakov, A. Springer, V. Böhmer, C. A. Schalley, *J. Mass Spectrom.* **2009**, *44* 1338-1347, (d) K. Salorinne, D. P. Weimann, C. A. Schalley, M. Nissinen, *Eur. J. Org. Chem.*, **2009**, 6151-6159; (e) R. E. Dawson, A. Hennig, D. P. Weimann, D. Emery, V. Ravikumar, J. Montenegro, T. Takeuchi, S. Gabutti, M. Mayor, J. Mareda, C. A. Schalley, S. Matile, *Nature Chem.* **2010**, *2*, 533-538.

212 (a) T. Felder, C. A. Schalley, H. Fakhrnabavi, O. Lukin, *Chem. Eur. J.* **2005**, *11*, 5625-5636; (b) B. Baytekin, N. Werner, F. Luppertz, M. Engeser, J. Brüggemann, S. Bitter, R. Henkel, T. Felder, C. A. Schalley, *Int. J. Mass Spectrom.* **2006**, *249*, 138-148; (c) O. Lukin, V. Gramlich, R. Kandre, I. Zhun, T. Felder, C. A. Schalley, G. Dolgonos, *J. Am. Chem. Soc.* **2006**, *128*, 8964-8974; (d) C. A. Schalley, B. Baytekin, H. T. Baytekin, M. Engeser, T. Felder, A. Rang, *J. Phys. Org. Chem.* **2006**, *19*, 479-490; (e) D. Schubert, M. Corda, O. Lukin, B. Brusilowskij, E. Fiskin, C. A. Schalley, *Eur. J. Org. Chem.* **2008**, 4148-4156; (f) B. Baytekin, H. T. Baytekin, U. Hahn, W. Reckien, B. Kirchner, C. A. Schalley, *Chem. Eur. J.* **2009**, *15*, 7139-7149; (g) M. Albrecht, M. Baumert, H. D. F. Winkler, C. A. Schalley, R. Fröhlich, *Dalton Trans.* **2010**, *39*, 7220-7222; (h) Z. Qi, C. A. Schalley, *Supramol. Chem.* **2010**, *22*, 672-682.

213 Y.-R. Zheng, P. J. Stang, *J. Am. Chem. Soc.* **2009**, *131*, 3487-3489.

214 M. Engeser, A. Rang, M. Ferrer, A. Gutiérrez, H. T. Baytekin, C. A. Schalley, *Int. J. Mass Spectrom.* **2006**, *255*, 185-194.

215 (a) T. G. Apleton, M. A. Bennett, I. B. Tomkins, *J. Chem. Soc., Dalton Trans.* **1976**, 439-446; (b) P. J. Stang, D. H. Cao, S. Saito, A. M. Arif, *J. Am. Chem. Soc.* **1995**, *117*, 6273-6283.

216 I want to thank Dipl.-Chem. Maurice Taszarek for the ligands he offered me to use for metallo-supramolecular self-assembly reactions. The syntheses of these ligands refer to: M. Taszarek, unpublished results.

217 (a) Y. Cohen, L. Avram, L. Frish, *Angew. Chem.* **2005**, *117*, 524-560; *Angew. Chem., Int. Ed*. **2005**, *44*, 520-554; (b) Y. Cohen, L. Avram, T. Evan-Salem, L. Frish, Diffusion NMR in Supramolecular Chemistry, in: *Analytical Methods in Supramolecular Chemistry*; C. A. Schalley, Ed.; Wiley-VCH: Weinheim **2007**; (c) A. Macchioni, G. Ciancaleoni, C. Zuccaccia, D. Zuccaccia, *Chem. Soc. Rev.* **2008**, *37*, 479-489.

218 *CACHE 5.0 for Windows*; Fujitsu Ltd.: Krakow, Poland, **2001**.

219 (a) P. K. Tikoo, R. D. Singh, *Electrochim. Acta* **1981**, *26*, 1057-1063; (b) S. Taniewska-Osinska, A. Piekarska, A. Kacperska, *J. Solution Chem.* **1983**, *12*, 717-727; (c) G. Chen, Y. Hou, H. Knapp, *J. Chem. Eng. Data* **1995**, *40*, 1005-1010; (d) A. Ali, A. K. Nain, M. Kamil, *Thermochimica Acta* **1996**, *274*, 209-221; (e) Y. Zhao, J. Wang, X. Xuan, J. Lu, J. *J. Chem. Eng. Data* **2000**, *45*, 440-444; (f) M. Cocchi, M. Manfredini, D. Manzini, A. Marchetti, S. Sighinolfi, L. Tassi; A. Ulrici, M. Vignali, P.

Zannini, *J. Molecul. Liquids* **2003**, *102*, 309-345; (g) N. G. Tsierkezos, A. C. Filippou, *J. Chem. Thermodynamics* **2006**, *38*, 952-961.

220 M. Schweiger, S. R. Seidel, A. M. Arif, P. J. Stang, *J. Inorg. Chem.* **2002**, *41*, 2556-2559.

221 M. Fujita, O. Sasaki, T. Mitsuhashi, T. Fujita, J. Yzaki, K. Yamaguchi, K. Ogura, *Chem. Commun.* **1996**, 1535-1536.

222 (a) K. P. C. Vollhardt, N. E: Shore, *Organische Chemie*, Volume 3, Wiley-VCH, Weinheim **2000**; (b) E. Breitmaier, G. Jung, *Organische Chemie*, Volume 4, Thieme, Stuttgart **2001**.

223 For example: (a) E. Ohlsson, *Chem. Ber.* **1916**, *49*, 1341-1344; (b) D. B. Grotjahn, C. Joubran, *Tetrahedron: Asymmetry* **1995**, *6*, 745-752.

224 (a) L. S. Reddy, S. Basavoju, V. R. Vangala, A. Nangia, *Cryst. Growth Des.* **2006**, *6*, 161-173; (b) R. Custelcean, B. A. Moyer, V. S. Bryantsev, B. P. Hay, *Cryst. Growth Des.* **2006**, *6*, 555-563.

225 (a) D. K. Kumar, D. A. Jose, A. Das, P. Dastidar, *Chem. Commun.* **2005**, 4059-4061; (b) N. N. Adarsh, D. K. Kumar, P. Dastidar, *Tetrahedron* **2007**, *63*, 7386-7396.

226 F. H. Allen, *Acta Crystallogr.* **2002**, *B58*, 380-388.

227 *CACHE 5.0 for Windows*; Fujitsu Ltd.: Krakow, Poland, **2001**.

228 (a) P. K. Tikoo, R. D. Singh, *Electrochim. Acta* **1981**, *26*, 1057-1063; (b) S. Taniewska-Osinska, A. Piekarska, A. Kacperska, *J. Solution Chem.* **1983**, *12*, 717-727; (c) G. Chen, Y. Hou, H. Knapp, *J. Chem. Eng. Data* **1995**, *40*, 1005-1010; (d) A. Ali, A. K. Nain, M. Kamil, *Thermochimica Acta* **1996**, *274*, 209-221; (e) Y. Zhao, J. Wang, X. Xuan, J. Lu, J. *J. Chem. Eng. Data* **2000**, *45*, 440-444; (f) M. Cocchi, M. Manfredini, D. Manzini, A. Marchetti, S. Sighinolfi, L. Tassi; A. Ulrici, M. Vignali, P. Zannini, *J. Molecul. Liquids* **2003**, *102*, 309-345; (g) N. G. Tsierkezos, A. C. Filippou, *J. Chem. Thermodynamics* **2006**, *38*, 952-961.

229 C. A. Hunter, *Angew. Chem.* **2004**, *116*, 5424-5439; *Angew. Chem. Int. Ed.* **2004**, *43*, 5310-5324.

230 (a) R. V. Slone, D. I. Yoon, R. M. Calhoun, J. T. Hupp, *J. Am. Chem. Soc.* **1995**, *117*, 11813-11814. (b) S. Serroni, S. Campagna, F. Puntoriero, C. Di Pietro, N. D. McClenaghan, F. Loiseau, *Chem. Soc. Rev.* **2001**, *30*, 367-375. (c) P. de Wolf, S. L. Heath, J. A. Thomas, *Chem. Commun.* **2002**, 2540-2541. (e) P. de Wolf, P. Waywell, M. Hanson, S. L. Heath, A. J. H. M. Meijer, S. J. Teat, J. A. Thomas, *Chem. Eur. J.* **2006**, *12*, 2188-2195; (f) Y.-Z. Zhang, Z.-M. Wang, S. Gao, *Inorg. Chem.* **2006**, *45*, 5447-5454; (g) F. N. Shi, L. Cunha-Silva, M. J. Hardie, T. Trindade, F. A. A. Paz, J. Rocha, *Inorg. Chem.* **2007**, *46*, 6502-6515.

231 For examples, see: (a) D. L. Caulder, K. N. Raymond, *Angew. Chem.* **1997**, *109*, 1508-1510; *Angew. Chem. Int. Ed.* **1997**, *36*, 1439-1442; (b) M. Fujita, N. Fujita, K. Ogura, K. Yamaguchi, *Nature* **1999**, *400*, 52-55; (c) G. F. Swiegers, T. J. Malefetse, *Chem. Rev.* **2000**, *100*, 3483-3537; (d) R. Pinalli, V. Cristini, V. Sottili, S. Geremia, M. Campagnolo, A. Caneschi, E. Dalcanale, *J. Am. Chem. Soc.* **2004**, *126*, 6516-6517; (e) T. Kamada, N. Aratani, T. Ikeda, N. Shibata, Y. Higuchi, A. Wakamiya, S. Yamaguchi, K. S. Kim, Z. S. Yoon, D. Kim, A. Osuka, *J. Am. Chem. Soc.* **2006**, *128*, 7670-7678; (f) Y.-M. Legrand, A. Lee, M. Barboiu, *Inorg. Chem.* **2007**, *46*, 9540-9547; (g) E. Zangrando, M.

Casanova, E. Alessio, *Chem. Rev.* **2008**, *108*, 4979-5013; (h) A. K. Bar, R. Chakrabarty, K-W. Chi, S. R. Batten, P. S. Mukherjee, *Dalton Trans.* **2009**, 3222-3229.

232 (a) S. Hiraoka, T. Tanaka, M. Shionoya, *J. Am. Chem. Soc.* **2006**, *128*, 13038-13039; (b) S. Hiraoka, M. Goda, M. Shionoya, *J. Am. Chem. Soc.* **2009**, *131*, 4592-4593; (c) M. Albrecht, Y. Liu, S. S. Zhu, C. A. Schalley, R. Fröhlich, *Chem. Commun.* **2009**, 1195-1197.

233 (a) V. C. M. Smith, J.-M. Lehn, *Chem. Commun.* **1996**, 2733-2734; (b) C. Piguet, G. Hopfgartner, B. Bocquet, O. Schaad, A. F. Williams, *J. Am. Chem. Soc.* **1994**, *116*, 9092-9102; (c) C. Piguet, G. Bernardinelli, J.-C. G. Bünzli, S. Petoud, G. Hopfgartner, *J. Chem. Soc., Chem. Commun.* **1995**, 2575-2577; (d) C. Piguet, C. Edder, S. Rigault, G. Bernardinelli, J.-C. G. Bünzli, G. Hopfgartner, *J. Chem. Soc., Dalton Trans.* **2000**, 3999-4006; (e) C. Edder, C. Piguet, J.-C. G. Bünzli, G. Hopfgartner, *Chem. Eur. J.* **2001**, ***7***, 3014-3024.

234 M. Albrecht, O. Ossetzka, R. Fröhlich, J.-C. G. Bünzli, A. Aebischer, F. Gumy and J. Hamacek, *J. Am. Chem. Soc.* **2007**, *129*, 14178-14179.

235 (a) M. Albrecht, R. Fröhlich, *J. Am. Chem. Soc.* **1997**, *119*, 1656-1661; (b) F. E. Hahn, M. Offermann, C. Schulze-Isfort, T. Pape, R. Fröhlich, *Angew. Chem.* **2008**, *120*, 6899-6902; *Angew. Chem. Int. Ed.* **2008**, *47*, 6794-6797.

236 (a) G. P. C. M. Dekker, C. J. Elsevier, K. Vrieze, P. W. N. M. van Leeuwen, C. F. Roobeek, *J. Organomet. Chem.* **1992**, *430*, 357-372; (b) F. Fochi, P. Jacopozzi, E. Wegelius, K. Rissanen, P. Cozzini, E. Marastoni, E. Fisicaro, P. Manini, R. Fokkens, E. Dalcanale, *J. Am. Chem. Soc.* **2001**, *123*, 7539-7552.

237 P. de Wolf, S. L. Heath, J. A. Thomas, *Inorg. Chim. Acta*, **2003**, *355*, 280-285.

238 A similar observation has been made with a different Schiff-base ligand: E. Holló-Sitkei, G. Szalontai, I. Lois, À. Gömöry, F. Pollreisz, L. Párkányi, H. Jude, G. Besenyei, *Chem. Eur. J.* **2009**, *15*, 10620-10633.

239 (a) Z Qin, M. C. Jennings, R. J. Puddephatt, *Inorg Chem.* **2003**, *42*, 1956-1965; (b) A. Kaiser, P. Bäuerle, *Top. Curr. Chem.* **2005**, *249*, 127-201.

240 I want to thank my Dr. Boris Brusilowskij and Dipl.-Chem. Egor V. Dzyuba for the syntheses of the ligands used within this study.

241 For examples of kinetically controlled self-assembly, see: (a) N. Fatin-Rouge, S. Blanc, E. Leize, A. Van Dorsselaer, P. Baret, J. L. Pierre, A. M. Albrecht-Gary, *Inorg. Chem.* **2000**, *39*, 5771-5778; (b) N. Fatin-Rouge, S. Blanc, A. Pfeil, A. Rigault. A. M. Albrecht-Gary, *Helv. Chim. Acta* **2001**, *84*, 1694-1711; (c) C. J. Kuehl, S. D. Huang, P. J. Stang, *J. Am. Chem. Soc.* **2001**, *123*, 9634-9641.

242 For example: (a) U. Belluco, L. Cattalini, F. Basolo, R. G. Pearson, A. Turco, *J. Am. Chem. Soc.* **1965**, *87*, 241-246; (b) L. Cattalini, A. Orio, M. L. Tobe, *J. Am. Chem. Soc.* **1967**, *89*, 3130-3134; (c) R. G. Pearson, H. R. Sobel, J. Songstad, *J. Am. Chem. Soc.* **1968**, *90*, 319-326; (d) G. Faraone, V. Ricevuto, R. Romeo, M. Trozzi, *Inorg. Chem.* **1970**, *9*, 1525-1528; (e) S. C. Chan, S. B. Tong, *Inorg. Chim. Acta* **1971**, *5*, 634-636; (f) V. Ricevuto, R. Romeo, M. Trozzi, *J. Chem. Soc., Dalton Trans.* **1972**, 1857-

1862; (g) L. Canovese, M. Cusumano, A. Giannetto, *J. Chem. Soc., Dalton Trans.* **1983**, 195-198; (h) E. Rotondo, F. C. Priolo, *Inorg. Chim. Acta* **1984**, *85*, 111-115; (i) R. Romeo, A. Grassi, L. Monsu Scolaro, *Inorg. Chem.* **1992**, *31*, 4383-4390; (j) B. Pitteri, G. Marangoni, L. Cattalili, T. Bobbo, *J. Chem. Soc., Dalton Trans.* **1994**, 169-174; (k) R. Romeo, G. Arena, L. Monsu Scolaro, M. R. Plutino, *Inorg. Chim. Acta* **1995**, *240*, 81-92; (l) F. Basolo, *Coord. Chem. Rev.* **1996**, *154*, 151-161; (m) L. Canovese, F. Visentin, P. Uguagliata, F. Di Bianca, A. Fontana, B. Crociani, *J. Organomet. Chem.* **1996**, *525*, 43-48; (n) R. Romeo, N. Nastasi, L. Monsu Scolaro, M. R. Plutino, A. Albinati, A. Macchioni, *Inorg. Chem.* **1998**, *37*, 5460-5466; (o) A. Hofmann, L. Dahlenburg, R. van Eldik, *Inorg. Chem.* **2003**, *42*, 1688-1700; (p) C. F. Weber, R. van Eldik, *Eur. J. Inorg. Chem.* **2005**, 4755-4761; (q) N. Summa, W. Schiessl, R. Puchta, N. van Eikema Hommes, R. van Eldik, *Inorg. Chem.* **2006**, *45*, 2948-2959; (r) S. Jafar Hoseini, S. Masoud Nabavizadeh, S. Jamali, M. Rashidi, *J. Organomet. Chem.* **2007**, *692*, 1990-1996; (s) H. Ertuerk, R. Puchta, R. van Eldik, *Eur. J. Inorg. Chem.* **2009**, 1331-1338; (t) J. Bogojeski, Z. D. Bugarcic, R. Puchta, R. van Eldik, *Eur. J. Inorg. Chem.* **2010**, 5439-5445.

243 (a) M.-F. Ng, S. Yokojima, D. Zhou, G. Chen, *Chem. Phys. Lett.* **2000**, *327*, 374-380; (b) A. H. Göller, U.-W. Grummt, *Chem. Phys. Lett.* **2002**, *345*, 233-242.

244 M. A. Balbo, C. Kaiser, A. Khan, S. Hecht, *Top. Curr. Chem.* **2005**, *245*, 89-150.

245 (a) C. A. Schalley, *Mass Spectrom. Rev.* **2001**, *20*, 253-309; (b) B. Baytekin, H. T. Baytekin, C. A. Schalley, *Org. Biomol. Chem.* **2006**, *4*, 2825-2841.

246 (a) J. Poppenberg, *Untersuchung metallo-supramolekularer Komplexe mittels FTICR-Massenspektrometrie*, Bachelor thesis, Freie Universität Berlin **2007**; (b) S. Richter, *Massenspektrometrie als Methode zur Reaktivitätsuntersuchung von supramolekularen Metallkomplexen*, Bachelor thesis, Freie Universität Berlin **2007**.

247 (a) J. Hamacek, M. Borkovec and C. Piguet, *Dalton Trans.* **2006**, 1473-1490. (b) Z. Chen, A. Lohr, C. R. Saha-Möller and F. Würthner, *Chem. Soc. Rev.* **2009**, 38, 564-584.

248 A. Y. Tsivadze, G. V. Ionova, V. K. Mikhalko and Y. N. Kostrubov, *Russ. Chem. Rev.* **2007**, *76*, 213-233.

249 S. Serefis, *Arch. Dermatol. Syph.* **1934**, *171*, 1-98.

250 Y. M. Yukhin, T. V. Daminova, L. I. Afonina, B. B. Bokhonov, O. A. Logutenko, A. I. Aparnev, K. Y. Mikhailov, T. A. Udalova, V. I. Evseenko, *Chem. Sustain. Develop.* **2004**, *12*, 395-401.

251 (a) C. Silvestru, H. J. Breunig, H. Althaus, *Chem. Rev.* **1999**, *99*, 3277-3328; (b) N. Yang, H. Sun, *Coord. Chem. Rev.* **2007**, *251*, 2354- 2366; (c) H. R. Kricheldorf, *Chem. Rev.* **2009**, *109*, 5579-5594; (d) M. A. Malik, M. Afzaal, P. O'Brien, *Chem. Rev.* **2010**, *110*, 4417-4446.

252 M. Mehring, *Coord. Chem. Rev.* **2007**, *251*, 974-1006.

253 I want to thank Dipl.-Chem. Linda Miersch, Dipl.-Chem. Maik Schlesinger, Dr. Dirk Mansfeld and Dipl.-Chem. Tony Böhle for providing me with the bismuth-oxido clusters which were studied within my thesis.

254 L. Miersch, M. Schlesinger, R. W. Troff, C.A. Schalley, T. Rüffer, H. Lang, D. Zahn, M. Mehring, *Chem. Eur. J.* **2011**, *17*, 6985-6990.

255 For example: (a) M. Mehring, M. Schürmann, *Chem. Commun.* **2001**, 2354-2355; (b) D. Mansfeld, M. Mehring, M. Schürmann, *Angew. Chem.* **2005**, *117*, 250-254, *Angew. Chem. Int. Ed.* **2005**, *44*, 245-249; (c) M. Mehring, S. Paalasmaa, M. Schürmann, *Eur. J. Inorg. Chem.* **2005**, 4891-4901; (d) M. Mehring, D. Mansfeld, S. Paalasmaa, M. Schürmann, *Chem. Eur. J.* **2006**, *12*, 1767-1781; (e) A. Auer, D. Mansfeld, C. Nolde, W. Schneider, M. Schürmann, M. Mehring, *Organometallics* **2009**, *28*, 5405-5411; (f) L. Miersch, T. Rüffer, H. Lang, S. Schulze, M. Hietschold, D. Zahn, M. Mehring, *Eur. J. Inorg. Chem.* **2010**, 4763-4769.

256 (a) J. Opitz-Coutureau, A. Fielicke, B. Kaiser, K. Rademann, *Phys. Chem. Chem. Phys.* **2001**, *3*, 3034-3041; (b) A. Fielicke, B. Kaiser, K. Rademann, *Chem. Phys. Lett.* **2002**, *359*, 360-366 .

257 For example: (a) L. Vila-Nadal, A. Rodriguez-Fortea, L. Yan, E. F. Wilson, L. Cronin, J. M. Poblet, *Angew. Chem.* **2009**, *121*, 5560-5564; *Angew. Chem. Int. Ed.* **2009**, *48*, 5452-5456; b) S. Kang, C. Jolley, L. Liepold, M. Young, T. Douglas, *Angew. Chem.* **2009**, *121*, 4866-4870; *Angew. Chem. Int. Ed.* **2009**, *48*, 4772-4776.

258 (a) P. D. Beer, C. A. P. Dickson, N. C. Fletcher, A. J. Goulden, A. Grieve, J. Hodacova, T. Wear, *Chem. Commun.* 1**993**, 828-830; (b) P. D. Beer, N. C. Fletcher, T. Wear, *Polyhedron* **1996**, *15*, 1339-1347; (c) N. C. Baker, N. McGaughey, N. C. Fletcher, A. V. Chernikov, P. N. Horton, M. B. Hursthouse, *Dalton Trans.* **2009**, 965-972.

259 See for example: (a) G. M. Meyer, *Inorg. Chem.* **2005**, *44*, 6852-6864; (b) J. G. Vos, J. M. Kelly, *Dalton Trans.* **2006**, 4869-4883; (c) M. Ryan, *Platinum Metals Rev.* **2009**, *53*, 216-218.

260 K. Szacilowski, M. Macyk, A. Drzewiecka-Matuszek, M. Brindell, G. Stochel, *Chem. Rev.* **2005**, *105*, 2647-2694.

10. Acknowledgements

I am deeply indebted to my PhD supervisor *Prof. Dr. Christoph A. Schalley* who offered me the opportunity to join his research group and gave me the freedom to elaborate my own scientific ideas resulting in my PhD thesis. I appreciated the long and fruitful discussions which helped me to solve many problems emerging during my PhD thesis.

I want to express my gratitude to *Prof. Dr. Rainer Haag* for being my second supervisor and spending his valuable time on reading and reviewing my PhD thesis.

All former and current group members of the Schalley group are acknowledged for their help and the fruitful discussions during my time in this group. They made me feel welcome and created a great atmosphere for scientific research. They are (in a non specific order) *Dr. Thorsten Felder, Dr. Jens Illigen, Dr. Michael Kogej, Dr. Alexander Rang, Dr. Torsten Weilandt, Dr. Sascha Shuxia Zhu, Dr. Bilge Baytekin, Dr. Tarik Baytekin, Dr. Domononkos Fehér, Dr. Andreas Springer, Dr. Boris Brusilowskij, Dr. Wei Jiang, Dr. Henrik Winkler, Dr. Rainer Brehme, Andrea Schulz, Dominik Weimann M. Sc., Dominik Sattler M. Sc., Qi Wang M. Sc., Dipl.-Chem. Egor Dzyuba, Marc Driessen M. Sc., Johannes Poppenberg M. Sc., Sebastian Richter M. Sc., Lena Kaufmann M. Sc., Karol Nowosinski M. Sc., Zhenhui Qi M. Sc., Christoph Traulsen M. Sc., Igor Linder M. Sc., Maria Tatzke M. Sc., Sophia Möhl M. Sc., Elisa Kanaki M. Sc., Lee Garret M. Sc., Dorian Grothe M. Sc., Matthias Grabowski M. Sc., Daniel Wachs M. Sc., Ina Pumpe M. Sc., Dipl-Chem. Christian Timper* and *Michael Thiele*.

I want to express my gratitude to *Dr. Andreas Springer*, *Dr. Henrik Winkler*, *Dipl.-Ing. Fabian Klautsch, Thomas Kolrep* and *Ursula Ostwald* for their advice and help in performing mass spectrometric experiments.

I would like to thank *Dr. Andreas Schäfer, Dr. Parveen Mohr, Anja Peuker, Gabriele Kahn, Bettina Zeisig, Claus Schmidt* and *Ulrike Weynand* for their scientific help in performing NMR spectroscopic experiments.

I am grateful to my cooperation partners for the fruitful scientific cooperations which enabled us to reveal many interesting aspects discovered within my thesis. They are *Prof. Dr. Kari Rissanen, Prof. Dr. Michael Mehring, Prof. Dr. Hans-Ulrich Reißig, Prof. Dr. Dieter Lenz,*

Prof. Dr. Dirk Zahn, Prof. Dr. Iris Oppel, Dr. Heidi Saxell, Dr. Martin Nieger, Dr. Dirk Mansfeld, Dr. Kirsten Föcker, Dr. Maurice Taszarek, Dr. Torsten Weilandt, Dr. Boris Brusilowskij, Dr. Tarik Baytekin, Dr. Bilge Baytekin, Dipl.-Chem. Egor Dzyuba, Dipl.-Chem. Maik Schlesinger, Dipl.-Chem. Linda Miersch, Dipl.-Chem. Tony Böhle, Dipl.-Chem. Rainer Hovorka, Maria Tatzke M. Sc., Johannes Poppenberg M. Sc. and *Sebastian Richter M. Sc.*.

I want to thank all students I supervised during their bachelor's theses or practical courses for their scientific help. *Johannes Poppenberg M. Sc., Sebastian Richter M. Sc., Marc Driessen M. Sc., Maria Tatzke M. Sc., David Nicolson B. Sc., Sissy Lorenz B. Sc.* and *Ömer Erdogan B. Sc.* are gratefully acknowledged.

I am grateful to the Freie Universität Berlin, the Deutsche Forschungsgemeinschaft (DFG), the Deutscher Akademischer Austausch Dienst (DAAD) and the Center for Supramolecular Interactions (CSI) for funding during my PhD thesis.

During my PhD thesis, I got to know many new persons whereof some became good friends. I thank all my old and new friends from Berlin, Bonn, Jyväskylä, Leer and all over the world for their friendship and the pleasant time.

I am deeply indebted to my family – most of all my parents *Wilhelm Troff* and *Magret Troff* – who always believed in me and supported me to achieve my own goals.

Finally, I would like to thank the reader for reading my thesis.

11. Curriculum Vitae

Due to data protection, the curriculum vitae is not shown in the online version.

Aus Datenschutzgründen wird der Lebenslauf in der Online-Version nicht veröffentlicht

Due to data protection, the curriculum vitae is not shown in the online version.

Aus Datenschutzgründen wird der Lebenslauf in der Online-Version nicht veröffentlicht

12. Publications and Presentations

Publications

1. *Metallo-Supramolecular Self-Assembly: the Case of Triangle-Square Equilibria*
   T. Weilandt, R. W. Troff, H. Saxell, K. Rissanen, C. A. Schalley, *Inorg. Chem.* **2008**, *47*, 7588-7598. DOI: 10.1021/ic800334k

2. *Thermodynamically controlled self-sorting of hetero-bimetallic metallo-supramolecular macrocycles: What a difference a methylene group makes!*
   B. Brusilowskij, E. V. Dzyuba, R. W. Troff, C. A. Schalley, *Chem. Commun.* **2011**, *47*, 1830-1832. DOI: 10.1039/C0CC04476H

3. *Hydrolysis of a Basic Bismuth Nitrate - Formation and Stability of Novel Bismuth Oxido Clusters*
   L. Miersch, M. Schlesinger, R. W. Troff, C. A. Schalley, T. Rüffer, H. Lang, D. Zahn, M. Mehring, *Chem. Eur. J.* **2011**, *17*, 6985-6990. DOI: 10.1002/chem.201100673

4. *Effects of subtle differences in ligand constitution and conformation in metallo-supramolecular self-assembled polygons*
   B. Brusilowskij, E. V. Dzyuba, R. W. Troff, C. A. Schalley, *Dalton Trans.* **2011**, *Dalton Trans.* **2011**, *40*, 12089-12096. DOI: 10.1039/C1DT10621J.

5. *From $\{Bi_{22}O_{26}\}$ to Chiral Ligand-Protected $\{Bi_{38}O_{45}\}$-Based Bismuth Oxido Clusters*
   D. Mansfeld, L. Miersch, T. Rüffer, D. Schaarschmidt, H. Lang, T. Böhle, R. W. Troff, C. A. Schalley, J. Müller, M. Mehring, *Chem. Eur. J.* **2011**, *17*, 14805-14810. DOI: 10.1002/chem.201102437

Poster Presentations

1. *Kinetically Controlled Self-Assemblies in a Dynamic Combinatorial Library of Metallo-Supramolecular Cages*
   R. W. Troff, J. Poppenberg, S. Richter, C. A. Schalley, *Tag der Chemie*, Berlin (Germany), 27. June **2007**.

2. *Kinetically Controlled Self-Assemblies in a Dynamic Combinatorial Library of Metallo-Supramolecular Cages*
   R. W. Troff, J. Poppenberg, S. Richter, C. A. Schalley, *Nanoscience Days 2007*, Jyväskylä (Finland), 25.-26. October **2007**.

3. *Kinetically Controlled Self-Assemblies of Metallo-Supramolecular Cages*
   R. W. Troff, J. Poppenberg, K. Rissanen, C. A. Schalley, *ORCHEM 2008*, Weimar (Germany), 01.-03. September **2008**.

4. *The Mass Spectrometric Double Syringe Experiment – A Useful Tool for Mechanistics in Metallo-Supramolecular Self Assembly*
   R. W. Troff, J. Poppenberg, S. Richter, C. A. Schalley, *ORCHEM 2008*, Weimar (Germany), 01.-03. September **2008**.

5. *Self-Assembly of Metallo-Supramolecular Cages – an Easy Way to Nanoscale Structures*
   R. W. Troff, B. Brusilowskij, Q. Wang, C. A. Schalley, *Nanoscience Days 2008*, Jyväskylä (Finland), 23.-24. October **2008**.

6. *Self-Assembly of Metallo-Supramolecular Complexes*
   R. W. Troff, Q. Wang, K. Rissanen, C. A. Schalley, *1st Doctoral Students' Workshop DRS Molecular Science*, Berlin (Germany), 17. February **2009**.

7. *Strukturaufklärung von Supramolekülen und Clustern*
   W. Jiang, R. W. Troff, A. Springer, C. A. Schalley, *Fachgruppentreffen FTMS der DGMS*, Mühlheim (Germany), 01.-03. September **2010**.

8. *ESI MS and Tandem MS of Bismuth-Oxido Clusters*
   R. W. Troff, L. Miersch, D. Mansfeld, M. Schlesinger, M. Mehring, C. A. Schalley, *Jahrestagung der DGMS 2011*, Dortmund (Germany), 28. February **2011**.

9. *Behavior of supramolecules in the gas ghase: From H/D exchange to IRMPD fragmentation reactions*
   E. V. Dzyuba, H. D. F. Winkler, B. Brusilowskij, R. W. Troff, C. A. Schalley, 6th *International Symposium on Macrocyclic & Supramolecular Chemistry (ISMSC)*, Brighton (United Kingdom), 03.-07. July **2011**.

Oral Presentations

1. *Metallo-Supramolecular Cages*
   R. W. Troff, *G4-Workshop 2007 (Albrecht/Engeser/Lützen/Schalley)*, Berlin 11.-14. August **2007**.

2. *Mechanisms in Metallo-Supramolecular Chemistry – A Mass Spectrometric Approach*
   R. W. Troff, *G4-Workshop 2008 (Albrecht/Engeser/Lützen/Schalley)*, Aachen 08.-10. July **2008**.

3. *A Mixed-Flow Technique for Mass Spectrometric Analysis of Self-Assembly Mechanisms*
   R. W. Troff, *SFB 765 Symposium*, Rheinsberg 07.-09. September **2009**.

4. *Diffusion NMR Spectroscopy – An interesting non-invasive analytical method to study molecular and supramolecular particles*
   R. W. Troff, *SFB 765 graduate school lecture series*, 10. February **2011**.